Hydrogeochemical controls on rare earth element behaviour in an acidic metal mine-impacted stream

Xiaotong Huang

Thesis submitted in fulfilment of the requirements for the degree of

Doctor of Philosophy

School of Engineering

Newcastle University

June 2019

Abstract

Due to the high value of rare earth elements (REEs) and their significant pathogenic potential, understanding the sources, fate and transport of REE in aqueous systems is of increasing interest. The behaviour of REE in mine water polluted streams has been well investigated in America, European countries and China. Very few studies of REE transport and fate in watercourses receiving mine water in the UK have been undertaken.

The Woodend low level mine water, from the abandoned Threlkeld mine, discharges to the Gate Gill with a pH of ~3.5, and contains high concentration of Zn, Pb, Al, Mn. The Gate Gill was selected for the detailed investigation of REE source, transport and fate, with the aim of understanding (1) the behaviour of REE in watercourses downstream of a mine discharge under varied hydrological conditions; and (2) the factors that influence REE transformation and fractionation in freshwater.

ICP-MS was adopted for measuring REE concentration in waters due to its high sensitivity and very low detection limits. However, Ba can cause significant oxide interference on Eu during sample measurement, due to the generally low abundance of REE in nature compared with Ba. In addition, the lanthanide has the strongest metal oxide bond among all the metals, and the lighter rare earth elements oxides formed can cause interferences on the heavier rare earth elements (the mass of which is 16amu more than the interfering lighter REE).

To ensure the accuracy of measurement, a mathematical correction method was developed to remove the polyatomic interferences on measured REE isotope. This was based on the signal of the interfering element in the sample and the correction factor of each interference species' intensity to the interfering element intensity. The interference of BaO on Eu was quite serious on specific samples and the highest error induced was more than 50%. The error was reduced to less 6% after adopting the developed BaO correction equations. The interference of lighter REE on heavier REE was determined to be negligible. This was due to the relatively small concentration difference between the interfering REE and interfered REE analytes.

Threlkeld mine is the main source of REE content in the Gate Gill, but the contribution of REE from Threlkeld mine to the River Glenderamackin, into which Gate Gill flows, is rather limited.

pH is a master control on REE transformation from truly dissolved (<0.005μm) to (suspended) solid phase and there is an inverse relationship between pH and the degree of REE transformation degree. The transformation of REE from truly dissolved (<0.005μm) to suspended solid phase is strongly inhibited when pH is ≤ ≈ 4.5. A higher degree of REE transformation from truly dissolved (< 0.005μm) to suspended solid is likely to occur when pH in water reaches ≈ 5. Fe and Al flocs/ oxyhydroxides are likely to be the main materials scavenging REE from the truly dissolved phase.

At sampling sites on the Gate Gill downstream of the mine water the main REE species in water are free REE ions and REE sulphate complexes. Solution chemistry-related processes (especially surface complexation) begin to fractionate REE during the transformation process when pH in the water reaches around pH 5. HREE have greater affinity for the Fe, Al flocs and/ or secondary Fe, Al precipitates which are remobilised from the stream bed relative to MREE and LREE during the REE adsorption process.

In the River Glenderamackin, which has a much higher pH (mean pH of 6.05) relative to Gate Gill, the main REE species are free REE ions and REE carbonates. Solution chemistry-related processes (especially solution complexation) results in LREE having a greater affinity for the Fe, Al flocs and/ or secondary Fe, Al precipitates during the REE adsorption process.

But source-related processes still have a dominant control on the REE distribution pattern at all downstream sampling sites of mine discharge.

Acknowledgement

Firstly I would like to thank my parents Mr Zhenying Huang and Mrs Lijing Ding who gave me significant support for my PhD study. Especially, I would like to thank my husband Dr Yuyuan Zhang for his company with me during these four years' life time in UK.

Secondly I would like to thank my first supervisor Dr Adam Jarvis and my second supervisor Dr Catherine Gandy, who helped me a lot for my work.

Next, I would like to thank the technicians for their help with my experiments.

Finally I would like to thank my colleagues, who also gave me lots of help when I got stuck during my work.

Table of Contents

List of Tables

List of Figures

Chapter 1 Introduction

1.1 Background and scope

Rare earth elements (REE) are a group of metals with similar chemical and physical characteristics, which includes scandium (Sc), yttrium (Y) and lanthanides (BGS, 2011). There has been a sharp increase in the use of hi-tech material-REE in the electronics, magnetic, optical and catalytic industries over the last few decades due to their critical role in digital technologies, environmental protection and energy efficiency improvements in many sectors. REE are used in a very wide range of products when compared to other groups of elements (Castor and Hedrick, 2006; BGS, 2011). REE (including the 15 lanthanides, yttrium and scandium) were defined as critical raw materials by the European Commission in 2017 due to their high supply risk and their economic importance (European Commission, 2017).

The rapidly growing demand for REE has resulted in an expansion of mining and processing of REE in recent years (Kulaksız and Bau, 2013; Gao and Zhou, 2011). REE leaching from operational and abandoned mine sites (particularly due to acid mine drainage) can result in elevated REE concentrations in the surrounding waters and soils (Medas et al. 2013; Anawar et al. 2012; Li et al. 2010; Zhao et al. 2007).

The eco-toxicological behaviour of other metals and metalloids (e.g. Hg, As, Pb, Cd, Cu, Cr) leached from waste and discharged in mine waters, and the impact of them on aquatic ecosystems has been well documented (Cobelo-García et al. 2015; Protano & Riccobono, 2002). Relevant environmental regulations and standards (WHO Drinking Water Guidelines, EU Water Framework Directive and Groundwater Directive) have been set for these dangerous elements and their chemical species, and aqueous emissions are therefore controlled (Cobelo-García et al. 2015). In contrast, REE have usually been regarded as being of minor environmental concern (Bowen, 1979) and threshold values for emissions of REE to the environment have not been set yet. Understanding of REE eco-toxicity and bioaccumulation, and the risks of anthropogenic emissions of REE to human health, are quite limited (Herrmann et al. 2016; Gonzalez et al. 2014).

Even though the available toxicity data for REE are mainly confined to Ce, La and Gd, it has been found that REE can accumulate in specific tissues and cause damage to many organs and the immune response system (based on animal studies at high REE concentrations condition; Pagano et al. 2015b). Some toxicological studies (Xia et al. 2012; Zhang et al. 1994) indicate

that waters and soils with high concentrations of REE will be harmful to human beings, animals and plants. What is more, the eco-toxicity effect of REE is enhanced at low pH. REE pollution is therefore a serious environmental concern, particularly in locations where acid mine discharge contaminates rivers and mine spoils contaminate soils (Pagano et al. 2015a).

Due to the high value of REEs and their significant pathogenic potential, understanding the sources, fate and transport of REE in aqueous systems is of increasing interest. Such an understanding is the foundation for then addressing possible low cost remediation technologies to recover REE.

To date studies undertaken in UK waters have investigated the behaviour and attenuation of the REE from coastal peaty soil areas in estuaries (alkaline water), where REE-enriched river water mixes with sea water (Hoyle *et al*. 1984; Elderfield *et al*. 1990), and the geochemistry of REE from their bedrock/ host rock in shallow groundwater (Smedley, 1991). Also, research has focused on the anomalous behavior of anthropogenic sources of REE in streams from Wastewater Treatment Plant effluent in London, and its consequence effect on the relatively high Gd concentration in London's drinking water (Kulaksiz and Bau, 2011).

1.1.1 Research gap

The fate and attenuation of REE in mine waters has been well investigated in America, European countries and China (Verplanck 2013; Romero *et al*., 2010; Medas *et al*. 2013; Ferreira da Silva *et al*. 2009; Leybourne & Johannesson, 2008; Zhao *et al*. 2007; Verplanck *et al*. 2004; Protano & Riccobono, 2001; Verplanck *et al*. 1999). Some research has been done to investigate the concentrations of REE in UK freshwaters, in particular, for example their general correlation with Fe, and the occurrence of REE in some mine water sites in eastern UK (Neal & Davies, 2003; Neal, 2007). However, there has been no systematic investigation of the extent to which drainage from abandoned mines contributes to the overall REE burden of freshwaters, what the downstream fate of these REE is, or whether there may be a possibility to recover REE from these waters.

1.2 Aim and objectives

1.2.1 Aim

The overall aim of this study was to understand the transport and fate in surface waters of REE discharged in metal mine drainage, and to quantify the variability of REE flux under different hydrological conditions. The objectives set to fulfil this aim are described below.

1.2.2 Objectives

1. Identify a suitable mine discharge and stream with elevated REE concentrations, via review of existing water quality databases;

2. Design a monitoring programme to understand the transport, fate and fractionation of REE from the mine discharge and down the stream;

3. Collect water quality samples and flow data over at least one year to understand variability of REE, and other metal, concentrations and flux across varying hydrological conditions;

4. Develop a method for REE analysis on the ICP-MS at Newcastle University;

5. Undertake geochemical modelling to help understand the fractionation of REE in the receiving watercourse.

1.3 Site selection and investigation

There has been no systematic investigation of the extent to which drainage from abandoned mines contributes to the overall REE burden of freshwaters, and higher content of REE is possible to present in the discharges with relatively low pH value and high Fe, Si, Al, Zn, Cu, Pb concentration, as mentioned by Johannesson et al. (1994a).

In order to identify an appropriate study site, a mine water database, containing physico-chemical data for UK metal mine drainage, was set up. This included location data, as well as chemical data for mine discharges, such as pH, metals concentrations and flow-rate. The database used data from Newcastle University, Environment Agency and literature. The drainage from coal mine sites were not considered as potential sampling sites and not included in the database because the most significant abandoned coal mine discharges are now treated through an existing programme of the UK Coal Authority (Johnston & Rolley, 2008).

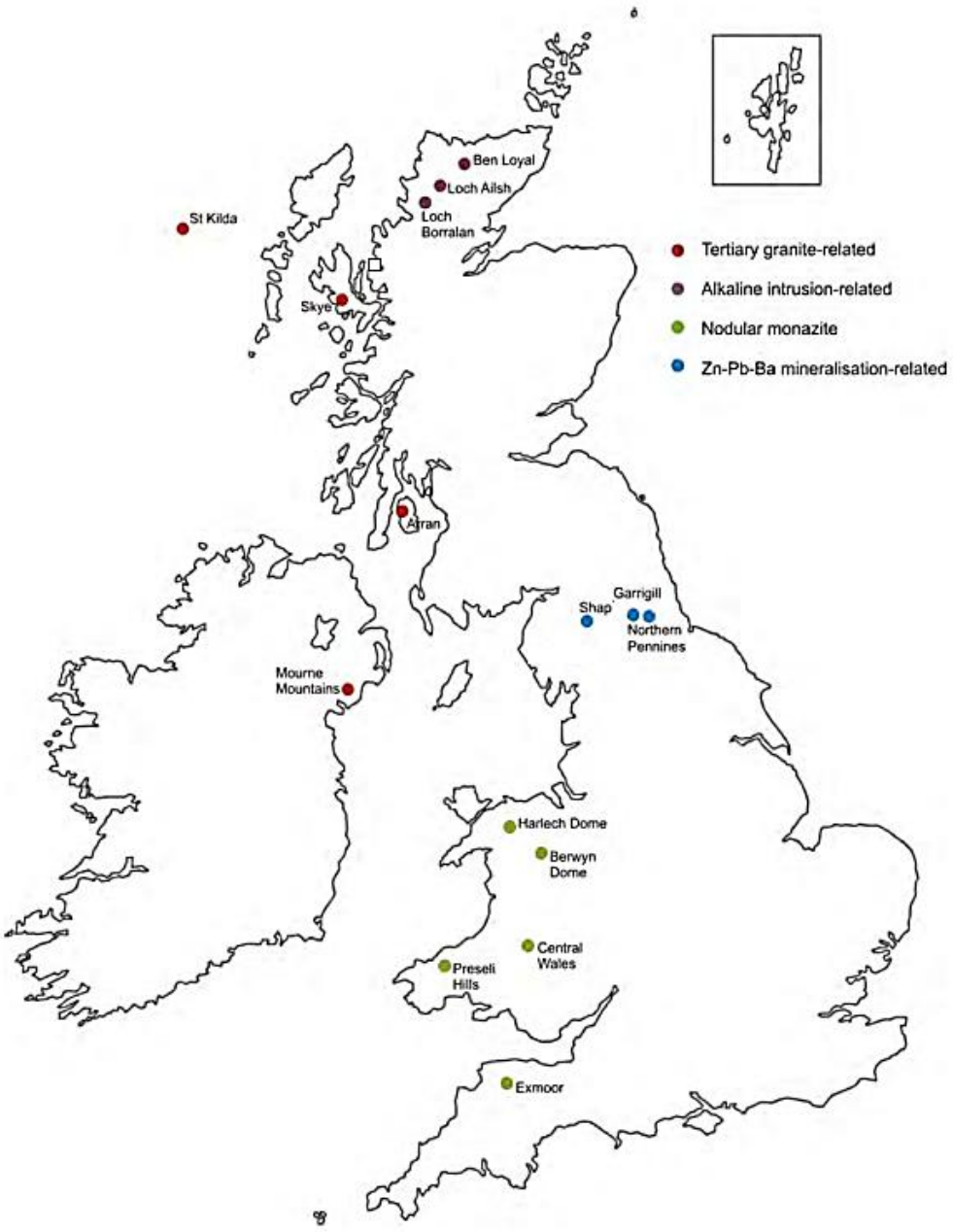

Figure 1.1: Occurrence of REE-bearing minerals in UK (BGS, 2011)

The occurrences of REE-bearing minerals are another consideration when selecting the suitable sampling sites. Even though there are no large occurrences with economic potential in the UK, few REE resources are found to occur in four geological settings with the locations displayed in Figure 1.1 (BGS, 2011):

1. Nodular monazites in Lower Palaeozoic sedimentary rocks of central Wales and in Variscan sedimentary succession of south west England

2. Alkaline igneous rocks with associated REE bearing minerals from north-west Scotland

3. REE-bearing minerals within Tertiary granites from the British Tertiary Igneous Province

4. Synchysite and other REE mineral in the lead-zinc-fluorite-barite veins of the Alston Block, North Pennines

Since REE (and other metals) are typically present at higher concentrations in waters with low pH, these discharges were a focus of the review. Approximately 110 discharges with pH < 7 were identified. These were also sites where flow measurement appeared feasible, for the purposes of quantifying REE flux. However, the majority of these are located in Wales and the southwest of England, and therefore regular visits (to capture a range of hydrological conditions) was not deemed feasible. Therefore, sites in northern England, close enough to Newcastle to allow a sampling visit in one day, were the focus. With that in mind a regional sampling of suitable mine sites in northern England was undertaken instead.

1.4 Regional sampling sites

Most discharges from mine sites in northern England have a neutral to slightly alkaline pH (due to the presence of limestone strata in the discharge flowing path), just two discharges have pH < 7. When pH is above 7, REE concentrations in waters will be very low according to the literature (Medas et al., 2013; Verplanck et al., 2004; Protano and Riccobono, 2002), and may be below the detection limit of analytical equipment. Therefore just those discharges with the lowest pH in northern England were selected for sampling. Figure 1.2 and Figure 1.3 shows the locations of the mine discharges sampled. One sampling site is located at Keswick, in the Lake District National Park, Cumbria, whilst the others are all in the North Pennines. The Woodend low level or Gate Gill mine discharge near Keswick is strongly acidic, with low pH. In the North Pennines, the Sharnberry Gill mine water discharge has a pH of 6.53, while the other discharges are all within a pH range of 7.08- 7.66 on the sampling date of 06/04/2017.

The Woodend low level mine discharge with pH of ≈3.5 and high concentrations of Zn, Pb, Al, Mn was selected as the sites for detailed investigation. Specific areas of the research were:

1. the fate and transport of REE in downstream watercourses of mine discharge

2. the factors (e.g. pH, other metal concentrations) that influence the REE concentration and distribution pattern in waters, and

3. the mechanisms of REE attenuation and fractionation in freshwater.

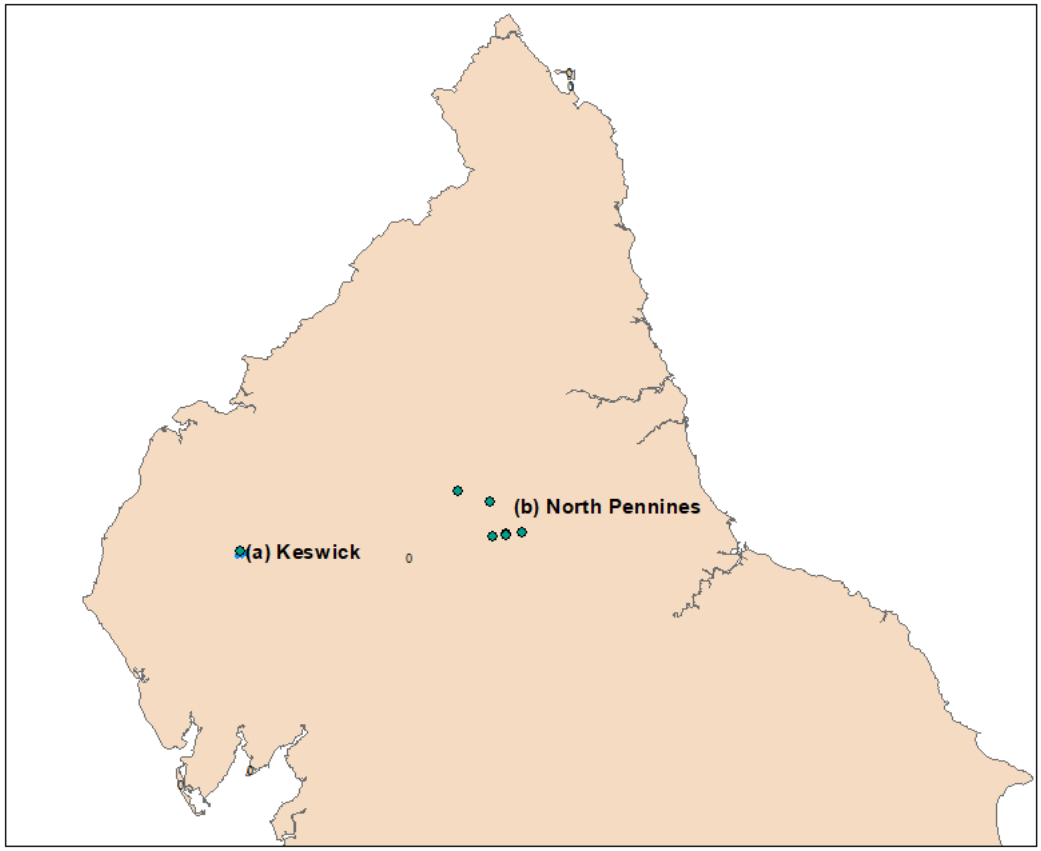

Figure 1.2: Locations of regional mine discharge sampling sites at northern England

Although the iron concentration in Woodend low level mine discharge is not very high and there is not a perfect pH gradient in-stream, which means this site may not be ideal for understanding the behaviour of REE in water as iron and pH play important roles on the REE attenuation. The location of Gate Gill makes it appropriate as the detailed sampling site since it is feasible to visit on a regular base from Newcastle University without taking considerable time. As noted above, other metal mine discharges with low pH and high iron concentrations are mostly located in Wales, and are not logistically feasible to visit periodically.

The sites in the North Pennines are not selected for the detailed investigation. This is because REE concentrations of mine discharge at these sites are quite low, especially for REE with heavier atomic weight. The concentrations of a few heavier atomic number REE in samples collected from North Pennines sites were below the instrument detection limits. Since one important aspect of this study is to understand the fractionation of individual REE along the mine water receiving streams and REE fractionation influencing factors, the site at Keswick is more suitable for performing detailed investigation.

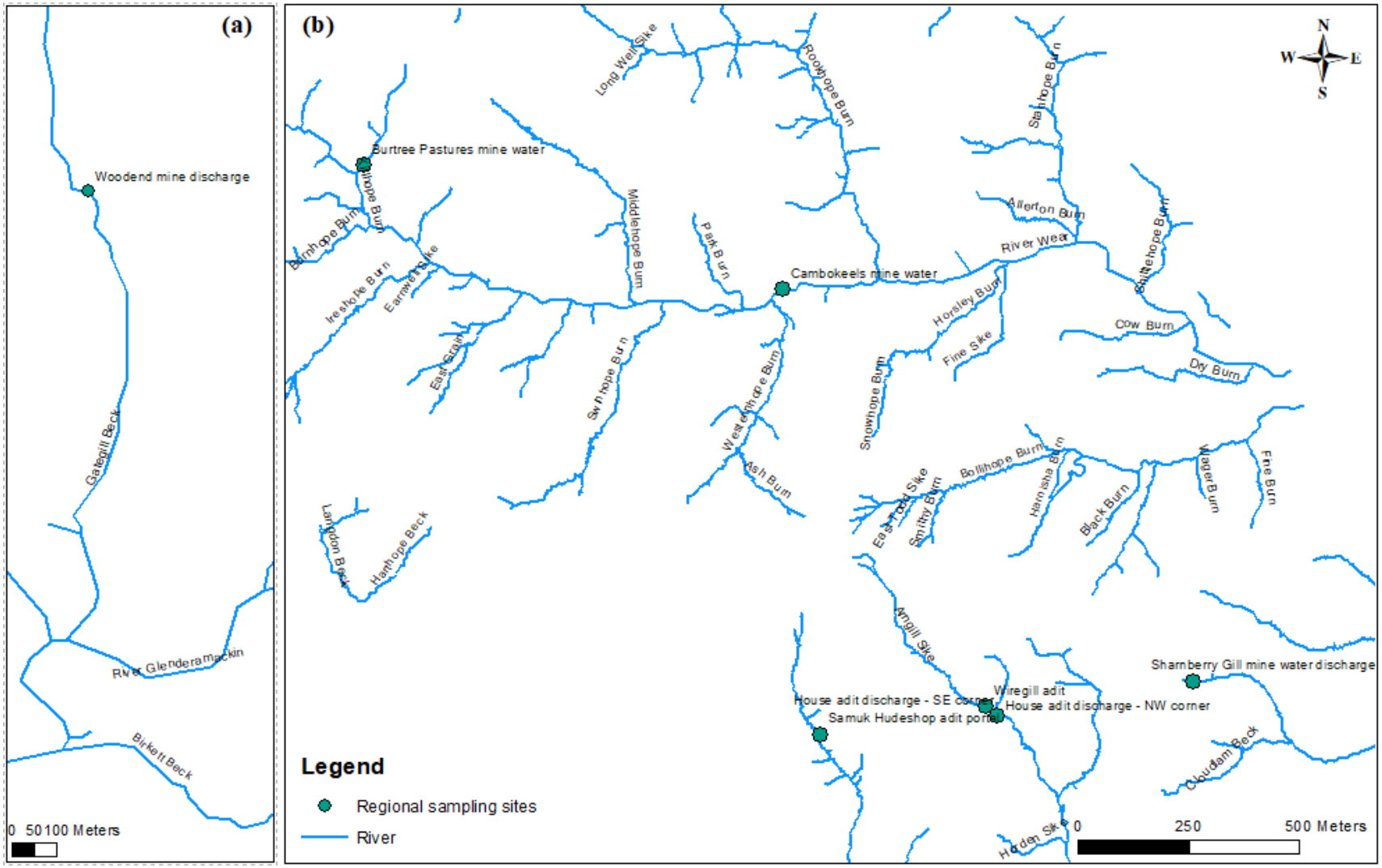

Figure 1.3: (a) Mine water discharge location at Gate Gill study site, near Keswick; (b) Mine water discharge locations in the North Pennines

1.5 Gate Gill study site

Threlkeld mine actually consists of two mines -Woodend Mine and Gate Gill Mine. They are approximately 6 kilometres northwest of Keswick, above the village of Threlkeld. The lower Woodend Mine worked lead and zinc veins, and yielded galena, zinc blende and iron pyrites; while the higher workings of Gate Gill Mine worked lead veins and produced mainly galena (Cameron and Withey, 2017; CAT, 2013). Those two mines were connected underground. Gate Gill mine was worked during the 17th century, prior to the use of gunpowder. Woodend mine was very productive between the late 19th century and early 20th century, and was finally closed in 1928 (Woodhall, 2000a). Woodend mine was located at Hall's Fell and extended for 1.5 km under the mountain Blencathra (Figure 1.4). Large underground stopes were created within the flanks of Blencathra (Cameron and Withey, 2017).

The point source mine water pollution at Woodend low level is the main metal pollution source at Woodend mine. Environment Agency (EA) data, collected since 2010 (Restore case study, 2017), shows that the Woodend low level is one of the most polluting metal mine discharge in the UK. EA monitoring data shows that the zinc and cadmium concentrations of the mine discharge receiving point at Gate Gill are up to 1770 and 525 times the EQS (Environmental quality standard) for zinc and cadmium respectively, depending on the flow rate of the Gill. The zinc and cadmium concentrations of the River Glenderamackin, into which Gate Gill flows, also fails to meet the EQS, with up to 30 and 10 times the EQS for Zn and Cd respectively. Further downstream the River Derwent and Bassenthwaite Lake are also influenced by the Woodend mine water pollution (Bailey, 2016), and even these two waterbodies fail to reach the EQS for Zn and Cd (Restore case study, 2017).

The mine water flow rate at Woodend low level adit is approximately 6 L/s, which is relatively low. However, the zinc loading is extremely high, ranging from 15.9 to 19.2 kg/d, and iron loading ranges from 1.7 to 2 kg/d (URS, 2014).

Besides the Woodend low level mine discharge, the waste spoil heaps at the mine site are a potential diffuse source of pollution and may contribute metals to downstream watercourses under during rainfall events (Restore case study, 2017).

1.5.1 Geology of study site

Figure 1.4 shows the overall geology around Threlkeld mine, including the type of bedrock, superficial deposits, and the location of mineral veins and faults. To clearly display the bedrock and superficial deposits types at Woodend mine, Figure 1.5 (a) shows just the bedrock geology at study site, whilst Figure 1.5 (b) shows the superficial deposits geology.

The bedrock at Hall's Fell is 1500 to 2500 metres thick distal turbidites made up of laminated dark grey mudstone and siltstone (Kirk stile formation) of the Skiddaw group deposited between Arenig and basal Llanvirn age (Woodhall, 2000a; Woodhall, 2000b). The Kirk Stile Formation is the main formation of the Skiddaw Group at Northern Fells belt. These mudstone and siltstone came from the far south of Gondwana ancient continental-arc volcanic rocks and deposited in deep water as siliciclastic turbidites on passive oceanward northern margin of Gondwana before/ during the Eastern Avalonian which is a micro-continent (Woodhall, 2000a; Cooper et al., 1993; Cooper et al., 1995).

The superficial deposits formed during the Quaternary glacial stages as a result of glaciation. The glacial erosion modified upland by removing its unconsolidated deposits and soil. The lowland was mainly modified through the deposition of large amounts of debris which derived from the uplands. The deposition of glacial sediment mantle causing the superficial deposits at Blencathra consist of undifferentiated rock fragments mixture which may from many source areas (BGS, 1992).

1.5.2 Mineralization of study site

The north-south orientated lead-zinc veins contain large amounts of galena (PbS) and sphalerite (ZnS) minerals formed during the early Carboniferous age. A small amount of chalcopyrite ($CuFeS_2$) is also present in the vein. Quartz is the main gangue mineral, and the other gangue minerals include pyrite, baryte, calcite and dolomite. The galena- sphalerite veins formed from highly saline brines at about 110 to 130 degree centigrade (Woodhall, 2000a; Stanley and Vanghan, 1982). The metals in the veins may come from the lower Palaeozoic sedimentary rocks and the basement granites (BGS, 1992).

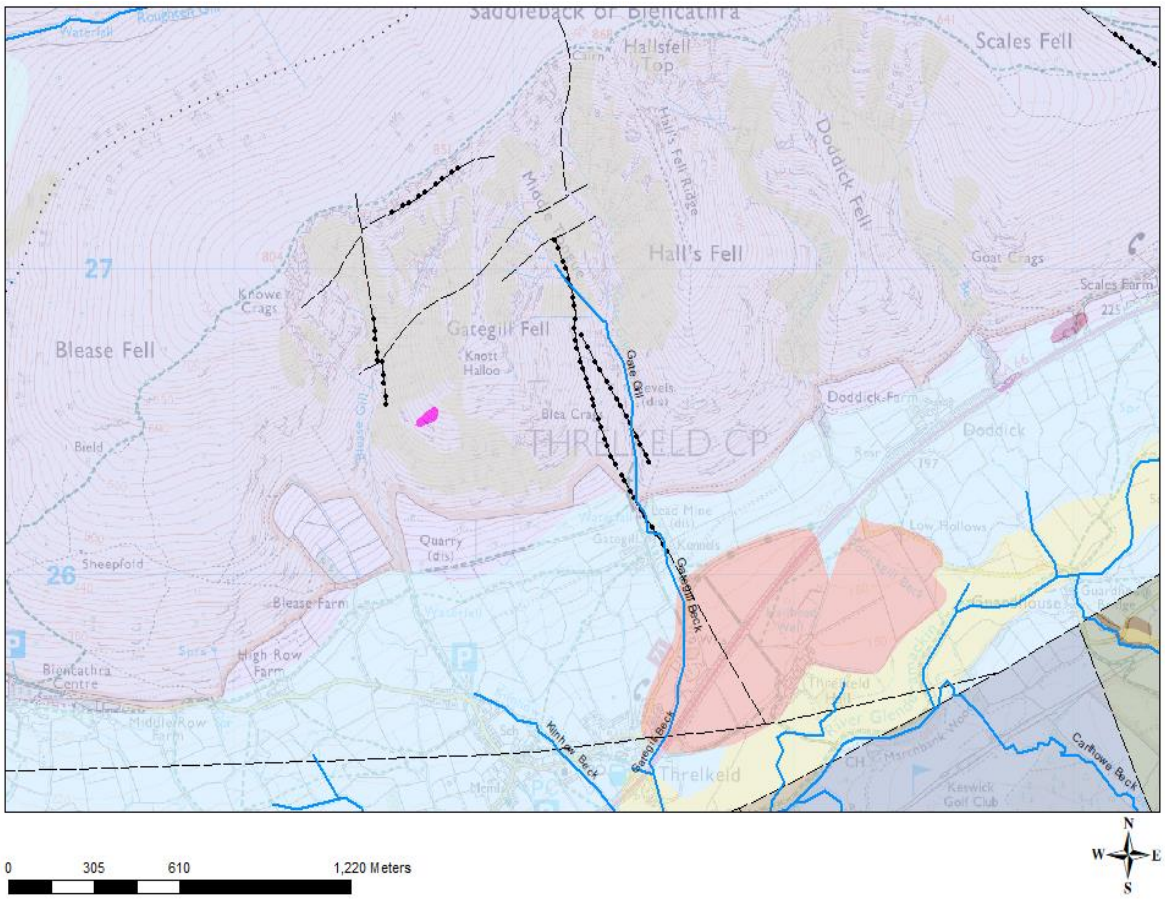

Bedrock

- Bassenthwaite Diorite Intrusions - Diorite (BADIN-DI)
- Lake District Ordovician Minor Intrusion Suite - Microgabbro (LDOMI-MCGB)
- Tarn Moor Formation - Mudstone (TMF-MDST)
- Buttermere Formation - Mudstone (BUF-MDST)
- Kirk Stile Formation - Mudstone And Siltstone (KST-MDSI)

Superficial Deposits

- Alluvial Fan Deposits - Sand And Gravel (ALF-XSV)
- Talus - Rock Fragments, Angular, Undifferentiated Source Rock (TALU-RFA)
- Till, Devensian - Diamicton (TILLD-DMTN)
- Alluvium - Clay, Silt, Sand And Gravel (ALV-XCZSV)

Linear Features

- Fault
- Mineral vein

Figure 1.4: Geology of study site and surrounding area

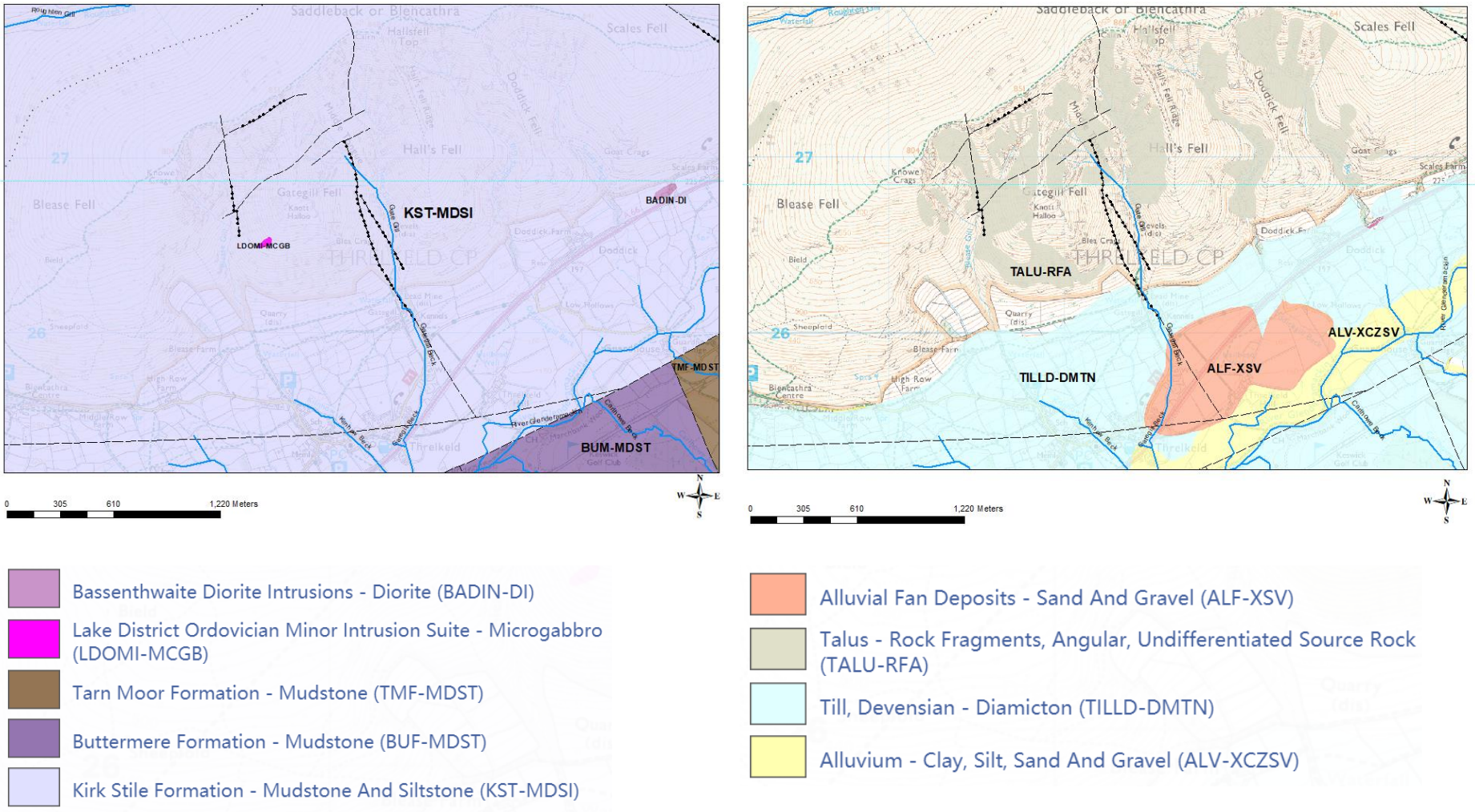

Figure 1.5: Bedrock type (a) and superficial deposits type (b) around study site

1.5.3 Location of routine sampling sites

After a preliminary site reconnaissance survey at Gate Gill study site, 5 sites along Gate Gill from upstream of the mine discharge to the confluence with the River Glenderamakin, were selected. In addition the River Glenderamackin itself was sampled upstream (only for the first 2 sampling occasions) and downstream of the confluence with the Gate Gill. Sampling was undertaken regularly over a period from February 2016 and September 2017. The selection of the sampling sites was based on: 1) The appropriateness of locations for demonstrating the fate and distribution pattern of REE down the length of the stream and 2) The feasibility for undertaking flow measurement.

Figure 1.6 shows the location of Gate Gill study site and the 7 sampling locations at study site. Photographs of each site are shown in Figure 1.7. Detailed information about each sampling site on Figure 1.6 is provided in Section 3.2.

1.6 Thesis structure

The thesis is structured as follows:

- Chapter 1 describes the motivation for this study and the study sites selected to fulfil the aim and objectives

- Chapter 2 first presents the REE characteristics, geology setting and mineralisation of main REE deposits in both the world and UK, and the current knowledge with regards to REE eco-toxicity. The main part of Chapter 2 is the review of the geochemical process involved during REE attenuation and/ or transformation and fractionation in aqueous systems and the role that REE source rock plays in the REE distribution patterns in streams, mainly based on the studies undertaken in North America and Europe.

- Chapter 3 provides a description of the field and laboratory methods employed, including analytical methods for *in situ* and laboratory analysis, and flow measurement techniques. Chapter 3 also indicates the thermodynamic data added to the original WATEQ4F database to form a new database which was used to calculate REE speciation in water samples. The newly developed database includes the stability constants of REE for all the relevant REE inorganic complexation reactions.

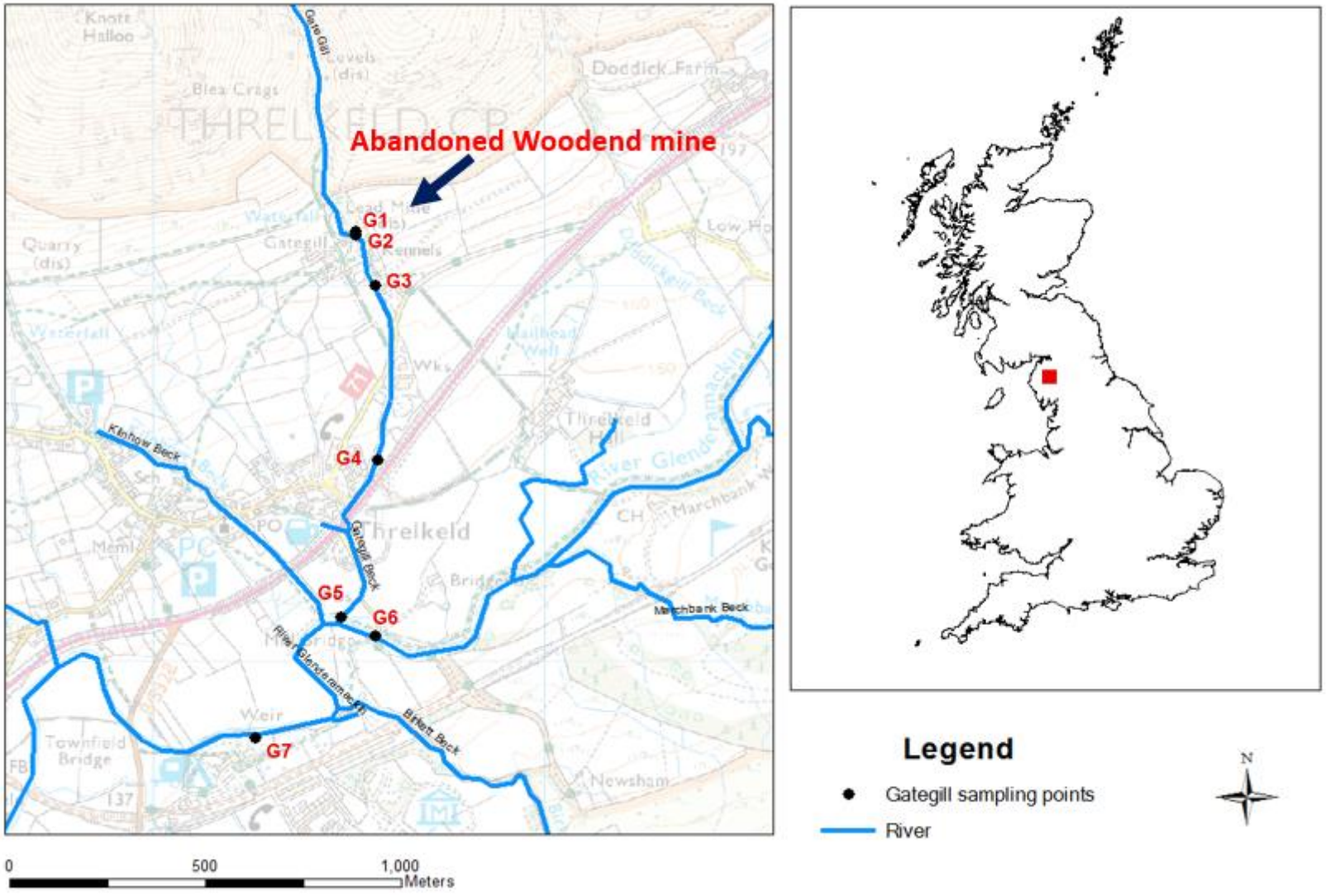

Figure 1.6: Location of Gate Gill study site (on the right) and sampling sites location at study site (on the left)

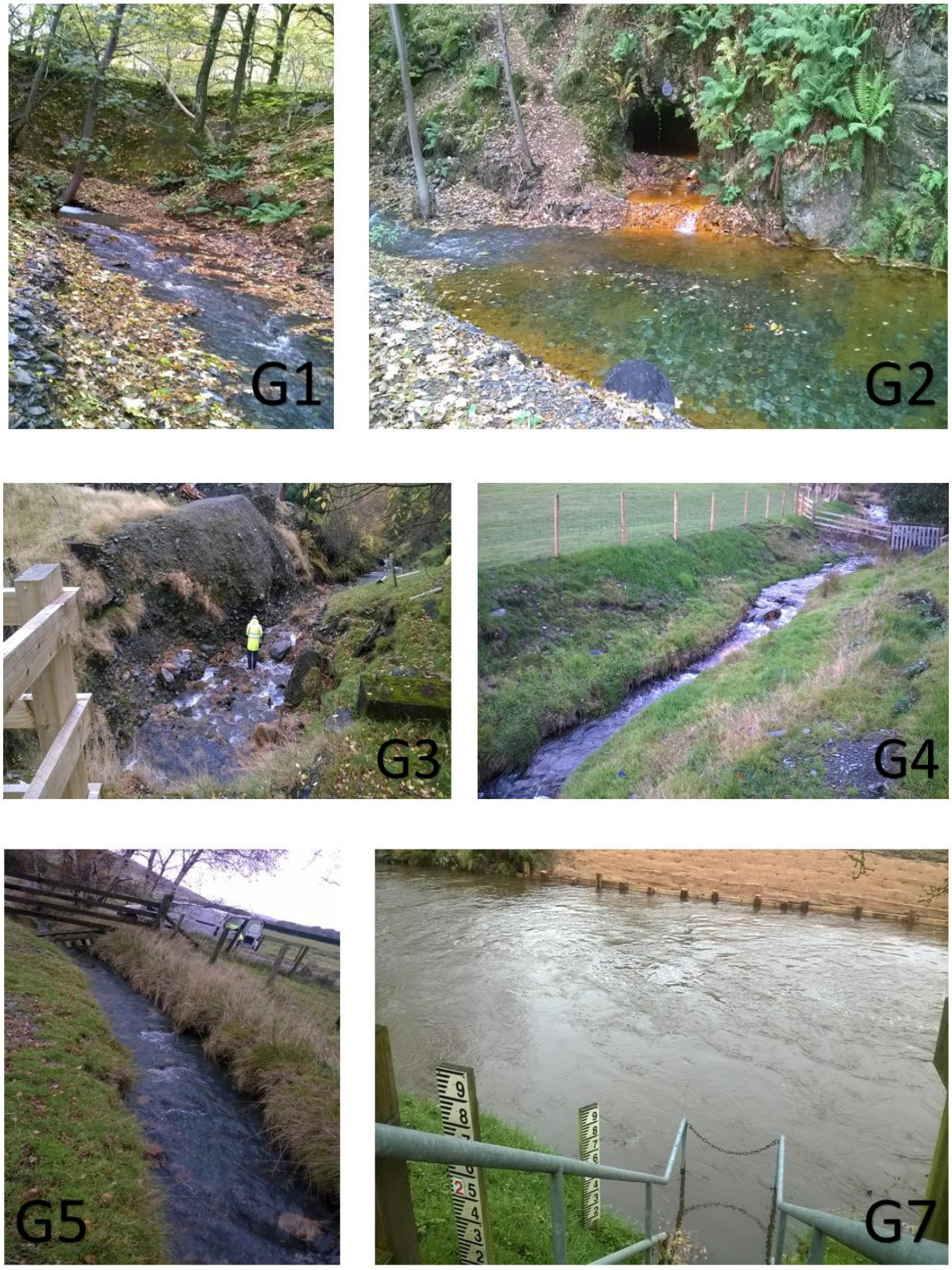

Figure 1.7: Sampling site pictures, taken on 10th, November, 2016

- Chapter 4 details the method developed with respect to the determination of REE by ICP-MS. This chapter demonstrates the selection criteria of REE measuring isotope, all the potential spectral interferences on the measuring analyte isotope, the procedure employed to remove the polyatomic interference and the evaluation of the method used.

- Chapter 5 is one of two Results and Discussion chapters. It mainly discusses the factors that control REE transformation along the Gate Gill and River Glenderamackin.

- Chapter 6 displays the variation of REE distribution pattern in different phases along the Gate Gill and River Glenderamackin under different hydrological conditions. The influence of in-stream processes and source-related processes on REE fractionation and REE anomalies is then discussed.

- The conclusions and achievements of this study and recommended future work are summarised in Chapter 7.

Chapter 2 Literature review

2.1 REE definition and characteristics

Rare earth elements (REE) including scandium (Sc, atomic number 21), yttrium (Y, atomic number 39) and 15 lanthanides (from lanthanum, atomic number 57 to lutetium, atomic number 71) are a group of 17 metals with the similar chemical and physical characteristic (Spedding, 1978). Table 2.1 below shows the elements in REE group and the general property of REE. The REE electronic configuration is not shown with 100% certainty due to the significant electronic spectra complexity of these elements.

Table 2.1: General property of rare earth elements (Gupta and Krishnamurthy, 2005).

Element	Symbol	Atomic number	Atomic weight	Electronic configuration of REE atom	Electronic configuration of REE^{3+}	Radius (M^{3+})
Scandium	Sc	21	44.95	$3d4s^2$		0.68
Yttrium	Y	39	88.90	$4d5s^2$		0.88
Lanthanum	La	57	138.90	$5d6s^2$		1.061
Cerium	Ce	58	140.11	$4f^15d^16s^2$	4f	1.034
Praseodymium	Pr	59	140.90	$4f^36s^2$	$4f^2$	1.013
Neodymium	Nd	60	144.24	$4f^46s^2$	$4f^3$	0.995
Promethium*	Pm	61	145.00	$4f^56s^2$	$4f^4$	0.979
Samarium	Sm	62	150.36	$4f^66s^2$	$4f^5$	0.964
Europium	Eu	63	151.96	$4f^76s^2$	$4f^6$	0.95
Gadolinium	Gd	64	157.25	$5f^75d6s^2$	$4f^7$	0.938
Terbium	Tb	65	158.92	$4f^96s^2$	$4f^8$	0.923
Dysprosium	Dy	66	162.5	$4f^{10}6s^2$	$4f^9$	0.908
Holmium	Ho	67	164.93	$4f^{11}6s^2$	$4f^{10}$	0.894
Erbium	Er	68	167.26	$4f^{12}6s^2$	$4f^{11}$	0.881
Thulium	Tm	69	168.93	$4f^{13}6s^2$	$4f^{12}$	0.869
Ytterbium	Yb	70	173.04	$4f^{14}6s^2$	$4f^{13}$	0.858
Lutetium	Lu	71	174.97	$4f^{14}5d6s^2$	$4f^{14}$	0.848

Note: *Pm is an element with radioactivity and not naturally contained in the earth's crust

It can be seen from Table 2.1, with the increase of REE atomic number, the electron is gradually filled into the 4f subshell and the valance electrons configuration of all REE outermost shell are consequently the same. The progressively filling of electron into 4f subshell cause the chemical coherence of REE (Quinn, 2006).

Table 2.1 also shows that with the increase of atomic number from La to Lu, there is a steady decrease of REE ions radius, this phenomenon is called the lanthanide contraction. This contraction trend of REE is also demonstrated in Figure 2.1. The highly directional 4f electrons and the orbitals shape induces a significantly imperfect shielding of atomic nucleus on one electron by another in 4f subshell. An continuous increase of effective nuclear charge

experienced by the 4f electron with the increasing of lanthanide atomic number then causes the successive decrease of REE size or 4f subshell size, which is the lanthanide contraction (Gupta and Krishnamurthy, 2005; Linnen and Samson, 2005). Although the atomic number of Y is much smaller than the lanthanides, the contraction effect causing the radius of heavier REE (to be more specific Ho-Er region) decrease to that similar as Y. The chemical characteristic of Y is therefore similar as that of the heavier lanthanides. On the other hand, the contraction effect is not sufficient to reduce the lanthanide radius to reach the value similar as that of Sc, the chemical property of Sc then differs from the rest of REE (Gupta and Krishnamurthy, 2005).

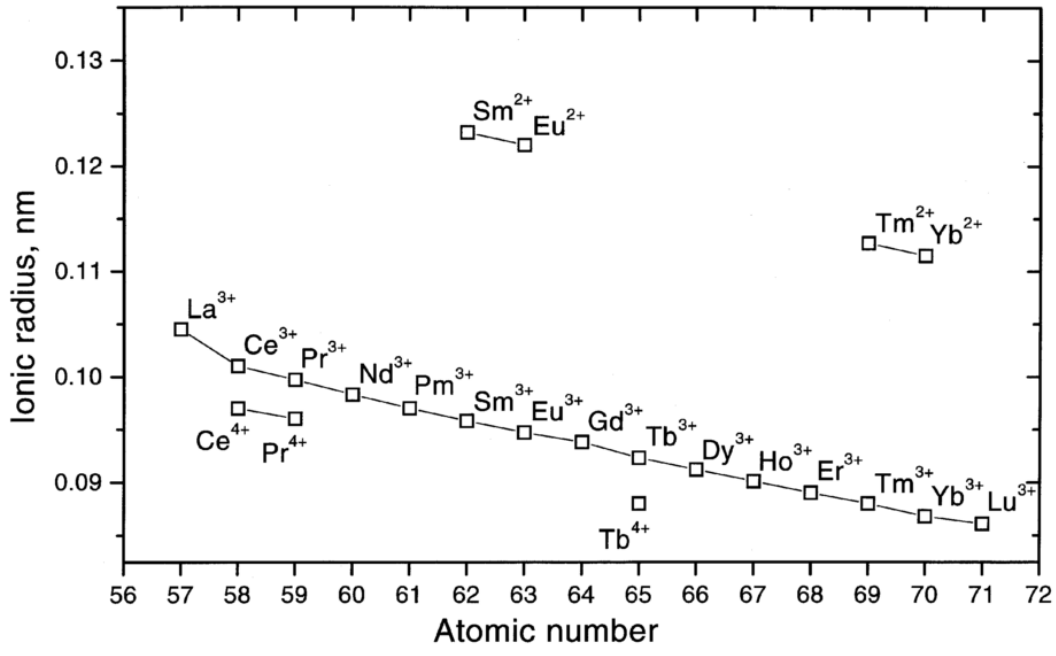

Figure 2.1: Radius decrease of lanthanide ions with the increase of atomic number (Gupta and Krishnamurthy, 2005)

Although REE have similar chemical and geochemical property, the steady decrease of REE radius with the increase of atomic number causing the geochemical behaviour differs slightly across REE group and the change of chemical characteristic across the group is predictable (Verplanck et al. 1999; Aide and Aide, 2012). As a consequence of the lanthanide contraction, lighter REE and heavier REE appear in different minerals. For example, the smaller size heavier REE like Lu can substitute the element in minerals where the available sites are not large while the lighter REE like La cannot (Geological society, 2011).

Due to the large radius of REE ions, there is only a limited number of REE complexes and the species that can complex with REE normally have small size, large charge and complexation ability. The formation of REE complexes depends on pH and the complexes stability associated with the ionic radius of REE (Gupta and Krishnamurthy, 2005).

Trivalent is the main REE oxidation state in solution at 25 degree (Protano and Riccobono, 2002). While trivalent Ce can be oxidized to tetravalent Ce under oxidizing conditions, and trivalent Eu Sm and Yb can be reduced to divalent states under extremely reduction conditions (Henderson, 1984; Medas et al., 2013). The only stable tetravalent REE specie in both solutions and solid phase is Ce as Ce^{4+} has the stable empty 4f shell ($4f^0$) (Moeller 1967). Eu^{2+} is stable in solution and the oxidizing process is quite slow. Sm^{2+}, Yb^{2+}, Eu^{2+} can be rapidly oxidized to trivalent states in acid waters exposed to air, and the oxidation speed of Sm^{2+} Yb^{2+} is much faster than Eu^{2+} (Gupta and Krishnamurthy, 2005).

Based on the weight of REE, REE are commonly classified into light rare earth elements (LREE) including element from La to Eu, and heavy rare earth elements (HREE), including element from Gd to Lu and Y (Castor and Hendrick, 2006). Y is classed into HREE group due to its similar chemistry and geochemistry as HREE, as mentioned before. Besides LREE and HREE, middle REE which includes elements from Eu to Dy can sometimes be added into the classification group. The classification is actually a bit arbitrary and different people may classify them differently (Samson and Wood, 2004). Geological Society (2011), Protano and Rccobono (2002) and Sholkovitz (1995) classify La to Sm as LREE, Eu to Lu as HREE. For a further classification, Nd to Gd can be regarded as MREE, according to Sholkovitz (1995). While Seredin and Dai (2012) describes La to Sm as LREE, Eu to Dy and Y as MREE and Ho to Lu as HREE. It is more suitable to classify REE into LREE, MREE and HREE group in order to better describe the distribution of REE in minerals.

The very similar ionic radius of trivalent state Y and Ho makes them behave in a similar way (Bau et al., 1996). When plotting the distribution pattern of REE, Y is normally put next to Ho (between Dy and Ho) (Bau et al., 1996). It needs to note that due to the large radius difference between Sc and the lanthanides, the chemical and geochemical behaviour of Sc differs enough from that of the other REE. Most literature does not include it when describing REE behaviours and only paying attention on the lanthanides and Y (Geological society, 2011).

Unlike their name, rare earth elements are relatively plentiful in nature with an overall crustal abundance of 9.2ppm in the crust (Rudnick and Gao, 2003). However, REE are normally less concentrated in nature compared with other metals, even though they are quite frequent in occurrence in the crust (EPA, 2012). REE overall abundance are similar as that of lots of important elements like germanium with overall abundance of 1.3ppm, tin with overall abundance of 1.7ppm and uranium with overall abundance of 1.3ppm (Geological society, 2011). However, the abundance of individual REE varies significantly one and another. The most abundant individual REE cerium is at 43ppm while the least abundant REE thulium is at 0.28ppm (Rudnick and Gao, 2003; Taylor and Mclennan, 1985). This is due to the Oddo-Harkins effect, which causes the even atomic number lanthanides are more abundant than the odd atomic number lanthanides next to them (Piper and Bau, 2013; BGS, 2011). In addition, the smaller radius of HREE causes them to be more compatible than LREE, as a result, LREE are more concentrated in the earth crust than HREE (BGS, 2011). The small difference in REE ionic radius causes the deposits which are enriched in REE are either enriched in LREE or enriched in HREE (Castor and Hedrick, 2006).

2.2 Sources of Rare Earth Elements (REE) in freshwater

2.2.1 Geological and mineralogical sources

International REE mineral deposits

Even though REE are relatively abundant in the crust, they do not concentrate in pure ore deposit as other metals (EPA, 2012). Due to the large ionic radius of REE, REE prefer to enrich in upper mantle or crustal origin melts (Möller, 1986). They present in lots of different mineral types, like carbonates, oxides, silicates, phosphate and halides and they substitute for the major ions with similar ionic radius in the rock-forming minerals (Medas et al. 2013). Most of REE are contained in REE-bearing minerals but with different concentration for individual element, and the minerals are normally enriched in either LREE or HREE. REE are known to occur in about 200 minerals, with only a few minerals contain high content of REE which may have the economic value. The chemical symbol following the REE-bearing mineral is normally the most abundant REE in that mineral (BGS, 2011). Table 2.2 shows commercially significant REE-bearing minerals and the content of REO in each mineral (BGS, 2011). Major REE resources are related to three minerals- Bastnäsite, monazite and xenotime, with the former two minerals enriched in LREE (Ce, La and Nd) and the latter one enriched in HREE (Y, Dy, Er, Yb and Ho) (Harben, 2002).

Table 2.2: Commercially significant REE-bearing minerals (BGS, 2011)

Mineral	REO (%)	Mineral	REO (%)	Mineral	REO (%)	Mineral	REO (%)
Aeschynite-(Ce)	32	Eudialyte	9	Loparite	30	Cebaite-(Ce)	32
Allanite-(Ce)	38	Euxenite-(Y)	24	Monazite-(Ce)	65	Florencite-(Ce)	32
Apatite	19	Britholite-(Ce)	32	Parisite-(Ce)	61	Synchysite-(Ce)	51
Bastnäsite-(Ce)	75	Fergusonite-(Ce)	53	Xenotime	61	Samarskite-(Y)	24
Brannerite	9	Gadolinite-(Ce)	60	Yttrocerite	53	Huanghoite-(Ce)	39
Britholite-(Ce)	32	Kainosite-(Y)	38	Knopite	Na		

There are two deposit categories for the REE minerals:

(1) primary deposits: formed as a consequence of magmatic and hydrothermal processes and normally occur in the quartz and fluorite bearing veins, skarns, pegmatites and breccia;

(2) secondary deposits: formed from the sedimentary and weathering processes of the primary deposits.

Table 2.3 describes the characteristic of main deposit types that REE mineral associated with for both primary and secondary deposit category and the typical REO content in each deposit (BGS, 2011). The global distribution of the main REE deposit mentioned in Table 2.3 is displayed in Figure 2.2.

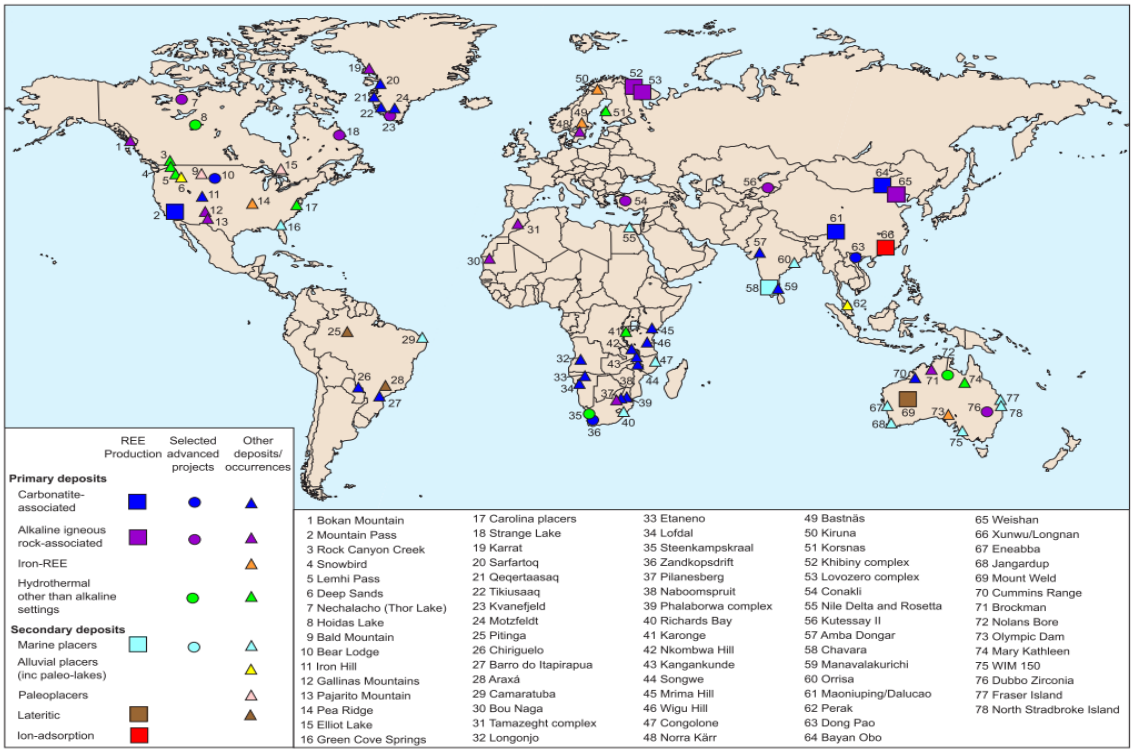

Figure 2.2: Occurrence of major REE deposits in the world (BGS, 2011).

Table 2.3: Characteristics of main REE deposit types (BGS, 2011)

Primary deposit			
Type	Characteristics	REE grade	Example
Carbonatite-related	-deposits associated with carbonatite igneous rocks which occur at alkaline igneous areas and major faulting places -carbonatite enriched in CO_2, Ca, Mg, Fe, REE, Ba, Sr, F, P, Nb, U and Th (Rankin, 2004) -mainly LREE enriched minerals, bastnäsite, allanite, apatite, monazite presenting in carbonatite (Gupta and Krishnamurthy, 2005)	0.1-10% REO	Mountain Pass, USA; Bayan Obo, China; Okorusu, Namibia; Amba Dongar, India; Barra do Itapirapuã carbonatites, Brazil
Alkaline igneous rocks -related	-deposits associated with alkaline igneous rocks -composition of alkaline igneous rocks varies from ultramafic to felsic -alkaline rocks enriched in alkali metals, Zr, Ti, Y, Nb, REE -alkaline rocks containing low grade of REE, mainly enriched in Y and HREE (Castor and Hedrick, 2006)	Less than 5% REO	Llimaussaq, Greenland; Khibina and Lovozero, Russia; Thor Lake and Strange Lake, Canada; Weishan, China; Brockman, Australia; Pajarito Mountain, USA
Iron-REE deposits	-also called iron-oxide-copper-gold deposits or Olympic Dam type -contain significant amount of magnetite and hematite -also contain quartz, apatite, REE minerals (bastnäsite, monazite, xenotime, allanite, parasite and apatite), uraninite and thorite	0.3295% REO	Olympic Dam, Australia; Pea Ridge, USA
Hydrothermal deposits which are not related to alkaline igneous rocks	Normally contain quartz, fluorite, polymetallic veins and a variety of origin pegmatites	Normally 0.5-4% REO, but can reach up to 12% occasionally	Karonge, Burundi; Naboomspruit and Steenkampskraal, South Africa; Lemhi Pass and Snowbird and Bear Lodge, USA; Hoidas Lake, Canada
Secondary deposit			
Type	Characteristics	REE grade	Example
Marine placer	-deposited resistant and heavy minerals accumulation by coastal processes -located close to current coastlines -abundant in Ti and Zr	Less than 0.1% monazite	Eneabba, Jangardup, Capel, WIM 150, North Stradbroke Island, Australia; Green Cove Springs, USA; Richards Bay, South Africa; Chavara, India
Alluvial placer	Deposit resistant and heavy minerals by river processes	Less than 0.1% monazite	Perak, Malaysia; Chavara, India; Carolina monazite belt and Horse Creek, USA; Guangdong, China Elliot
Paleoplacer	-Older placer deposits -cemented and consolidated	Less than 0.1% REO	Elliot Lake, Canada; Bald Mountain, USA
Lateritic deposits (residual weathering)	-Formed by depositing REE released/leached from chemical weathering of REE enriched parent rock -typical high REO grade	0.1-10% REO	Mount Weld, Australia; Araxá, Brazil; Kangankunde, Malawi
Ion-adsorption clay	-REE released from granites weathering and adsorbed by clay minerals -HREE enrichment (Chi and Tian, 2008)	0.03-0.35% REO	Longnan, Xunwu, China

REE mineral occurrence in UK

There are few REE resources in UK and they present in the following four geological settings (BGS, 2011):

(1) Occurrence of nodular monazites in Lower Palaeozoic sedimentary rocks of Welsh Basins and in Variscan sedimentary succession of south west England:

These nodules in panned stream sediment concentrates of Wales and south west England contain high level of REE (more than 5000ppm Ce), displaying zonation of LREE and HREE. The streams which drain Welsh Basin Ordovician and Silurian sedimentary rocks in south central Wales are the most extensive high Ce contained zone (Cooper and Read, 1983).

These nodules are secondary REE mineralisation formed by diagenesis during sediment dewatering compaction and then be concentrated as placers in alluvial sediments (BGS, 2011; Milodowski and Zalaciewicz, 1991).

(2) Caledonian alkaline igneous intrusion associated REE bearing minerals from north-west Highlands, Scotland

Cnoc nan Cuilean intrusion of the Loch loyal complex which is mafic syenite altered by hydrothermal processes has 2% REO (Walters et al. 2013). REE minerals occur in Ben Loyal area are allanite, ancylite, betafite and rhabdophane (Shaw and Gunn, 1993). Up to 739 ppm of Ce, 1764 ppm of Ce, 986 ppm of Y amd 2% of apatite are contained in Loch Borralan complex. Loch Ailsh Complex contains 0.7% La plus Ce (Shaw and Gunn, 1993).

(3) REE-bearing minerals within Tertiary granites

(4) Lead-zinc-fluorite-barite veins associated synchysite and other REE mineral occurrences in the Alston Block, North Pennines

Synchysite, very small amount of monazite, xenotime and adularia intergrown with bismuthinite in the bismuthinite-bearing quartz veins which close to Stanhope and Rookhope (Ixer et al. 1996). Fluorite in Northern Pennine Orefield contains high REE content (up tp 1888ppm for Ce, La and Y in total), which either comes from the Weardale granite underneath, or due to an inclusion of REE mineral within the fluorite (Smith, 1974).

Tynebottom mine located around Garrigill also contains synchysite (Ixer and Stanley, 1987).

2.3 REE eco-toxicity

The broad spectrum applications of REE in clean energy, agriculture, electronic, industrial and medical areas induce REE enrichment in the aqueous systems, soils, vegetables, even human hair in China as a result of anthropogenic activities e.g. mining activities, wastewater treatment plant of hospital zones (González et a. 2015; Li et al. 2013; Wei at al. 2013). Li et al. (2010) notes that human activities can increase the REE content in soils 5-10 times than its normal content.

Pagano et al. (2015a) notes that redox reactivity, ROS formation, lipid peroxidation and antioxidant activity modulation are the action mechanisms that REE associated with.

2.3.1 Environmental exposures effect

Human body can uptake REE through dermal contact, inhalation and ingestion, REE accumulate in human organs which induces some diseases after a long-term environmental exposures to REE (Wei et al. 2013). The study from Wei et al. (2013) shows that the residents from Inner Mongolia REE mining area, China are found to have accumulated higher level of REE in their hair compared with the residents from normal areas. In addition, the serum total protein and levels of globulin of residents in REE mining areas contaminated with HREE or LREE are much lower than the controls (Zhu et al. 2005).

Long-term of low dose REE intake due to the environmental exposure causes intelligence quotient, lung capacity, blood pressure and IgM immune proteins decline for children, central nervous conduction bioelectricity speed decrease and dramatically rise of the biochemical indicators for adult (Xia et al. 2012; Zhu et al. 1996).

2.3.2 Toxicity of REE on plants, animals and human body

The health effect regards to REE shows a hermetic concentration-related trend, which means REE has stimulatory effect at low dose but toxicity effect at high concentration condition. The concentration of individual REE which induces inhibition effect varies with the plant, animal types (Pagano et al. 2015a). Pagano et al. (2015a) reviewed the papers related to the hermetic concentration-related REE toxicity on life and the reviewed data are shown in Table 2.4. All the test objects listed in Table 2.4 display a hermesis-related trend in the noted REE concentration range.

Table 2.4: Hermetic concentration-related REE toxicity

Element	Concentration range		Test object	References
	Stimulatory	Inhibition		
14 lanthanides	1-10μM	50-100μM	matrix metalloproteinase-1 and cell proliferation of human keratinocytes	Jenkins et al. (2011)
Y (III)	11-56μM		SOD activity, glutathione content of Nymphoides peltata	Fu et al. (2014)
La (III)	0.1nM-0.1μM	0.1μM-1mM	cell proliferation, osteogenic differentiation of murine preosteoblast cell line	Liu et al. (2012)
	2- 480μM		catalase, guaiacol peroxidase, ascorbate peroxidase activities of vicia faba seedlings	Wang et al. (2011)
	0.1- 50μM		calcium deposition, β-glycer-ophosphate-induced alkaline phosphatase activity, apoptosis of bovine vascular smooth muscle cells	Zhao et al. (2012)
$nCeO_2$	0.3- 3mM		lipid peroxidation, fatty acid and lignin content, electrolyte leakage of rice seedlings	Rico et al. (2013)
	0.1- 1.6mM		Na+/K+-ATPase induction of Carassius auratus	Xia et al. (2013)
	0.17- 17μM		photosynthesis and ROS formation of algae	Rodea-Palomares et al. (2012)
Ce (III)	10 to 80 μM		membrane proteins and plasma membrane structure of Horseradish seedlings	Yang et al. (2012)
Gd	10 μM-1 mM		human dermal fibroblast	Edward et al. (2010); Bleavins et al. (2012)
Ho(III)	10 μM to 1 mM		V. faba root tips	Qu et al. (2004)

Under the similar conditions of experiment, the eco-toxicity of REE is generally lower than that of the traditional heavy metals like Cd, Pb. In the absence of ligands like phosphate which can induce the precipitation of REE, the toxicity of REE increases with the increase of atomic number, but the increased degree is not known precisely due to the limited experimental data (González et al. 2015; Gonzalez et al. 2014). There is not a clear conclusion regards to the trend in bioaccumulation across the REE group, with the increase of REE atomic number, the study from Weltje et al. (2002) notices a decrease trend in the bioaccumulation decreases, while Tsuruta (2006) discovers a increase trend.

2.3.3 Proposed EQS value for La

Herrmann et al. (2016) suggests a water quality criterion of 4 μg/l for La based on the no observed effect concentration (NOEC) value of 0.04mg/l for Daphnia carinata (Barry and Meehan, 2000), an assessment factor of 10. The threshold value of 36.9mg/kg for La in

sediment is also suggested by Herrmann et al. (2016). However, there is no suggested EQS values for other rare earth elements as there is scarce data available for deriving quality criteria for the other REE. In addition, the threshold values for La were calculated based on the limited available data, these standards are therefore should be used as the preliminary criteria, as suggested by Herrmann et al. (2016).

2.4 REE aqueous geochemical process

2.4.1 REE normalisation

To show the concentration variation across REE group in natural waters and rocks induced by the different geochemical behaviour of individual REE, REE distribution pattern can be demonstrated by plotting the relative concentrations of REE against their atomic number (Protano and Riccobono, 2002). The relative concentration of REE is used instead of the actual measured REE concentration to eliminate fractionation of REE caused by the Oddo-Harkins effect, which causes a more abundant even atomic numbered REE than the odd atomic numbered REE and will produce a zigzag pattern if the actual REE concentrations are used (Quinn, 2006; Coryell *et al*., 1963; Masuda, 1962). The Oddo-Harkins effect is the result of nucleosynthesis as the stability of nucleus is strongly related to the odevity of the proton and neutron number. The stability of nucleus is most enhanced when both the proton number and neutron number are even while the stability of nucleus is most reduced when both the proton number and neutron number are odd (Henderson, 1984).

The relative concentration of REE can be obtained by dividing the REE concentration in natural samples by that in the reference materials, on element by element basis. The process to obtain the relative REE concentration is called REE normalization and the normalized REE distribution pattern is a generally smooth curve. The reference materials normally used are:

1. Post-Archean average Australian Shale (PAAS), which is the average values obtained from 23 Australian shales (McLennan, 1989; Taylor and McLennan, 1985; Nance and Taylor, 1976);

2. North American Shale Composite (NASC), which is the mean values of 40 North American (mainly from) shales (Haskin *et al*., 1966; Gromet *et al*. 1984);

3. Mean shales, the averaged values of North American, European and Russian shale composite (Haskin and Haskin, 1966; Piper, 1974a; de Baar *et al*., 1985);

4. Chondritic meteorites, with reported values differ significantly in literature (Korotev, 2009): (i) 9 chondrites composite (Haskin *et al*. 1968); (ii) mean values of 10 most representative ordinary chondrites according to Nakamura (1974); (iii) Leedey chondritic meteorite, with the most representative REE contents according to Masuda *et al*. (1973). However, Nakamura (1974) mentions that REE distribution of chondritic meteorite Leedey shows some degree of fractionation regards to the mean value of 10 ordinary chondrites in his work although the REE concentrations of chondritic meteorite Leedey are very similar to the averaged REE concentrations of 10 ordinary chondrites; (iv) Calculated volatile free carbonaceous (CI) chondrites (Korotev, 2009), obtained from multiplying CI chondrites values of Anders and Grevesse (1989) by a normalization factor 1.36; (v) Calculated volatile free CI chondrites (Boynton, 1984), based on the original CI chondrites values of Evensen et al. (1978) and a normalization factor. Both (iv) and (v) transfer the values of CI chondrites to that of volatile-free CI chondrites is to keep consistency with the other literature reported ordinary chondrites values.

Table 2.5: REE concentrations in PAAS (McLennan, 1989), NASC (Haskin et al*., 1966), mean shale (Haskin and Haskin, 1966), averaged values of 10 ordinary chondrites (OC) (Nakamura, 1974), Leedey chondrite (Masuda* et al*., 1973), composite of 9 chondrites (Haskin* et al*. 1968), calculated volatile free CI chondrites (vf CI) (Korotev, 2009) based on the data from Anders and Grevesse (1989), calculated volatile free CI chondrites (Boynton, 1984) based on CI chondrites values from Evensen et al. (1978)*

Element	PAAS (ppm)	NASC (ppm)	Mean Shale (ppm)	Averaged 10 OC (ppm)	Leedey Chondrite (ppm)	9 chondrites Composite (ppm)	vf CI (ppm)	
							Korotev (2009)	Boynton (1985)
Y	27	27	36		-		2.12	
La	38.2	32	41	0.329	0.378	0.330	0.319	0.310
Ce	79.6	73	83	0.865	0.976	0.88	0.820	0.808
Pr	8.83	7.9	10.1		-	0.112	0.121	0.122
Nd	33.9	33	38	0.630	0.716	0.60	0.615	0.600
Sm	5.55	5.7	7.5	0.203	0.230	0.181	0.2000	0.195
Eu	1.08	1.24	1.61	0.0770	0.0866	0.069	0.0761	0.0735
Gd	4.66	5.2	6.35	0.276	0.311	0.249	0.267	0.259
Tb	0.774	0.85	1.23		-	0.047	0.0493	0.0474
Dy	4.68	5.8	5.50	0.343	0.390	-	0.330	0.322
Ho	0.991	1.04	1.34		-	0.070	0.0755	0.0718
Er	2.85	3.4	3.75	0.225	0.255	0.200	0.216	0.210
Tm	0.405	0.50	0.63		-	0.030	0.0329	0.0324
Yb	2.82	3.1	3.53	0.220	0.249	0.200	0.221	0.209
Lu	0.433	0.48	0.61	0.0339	0.0387	0.034	0.0330	0.0322

The REE abundances in the reference materials normally used in literature to do the samples normalization are noted in Table 2.5. PAAS, NASC, mean shale are the sedimentary rocks

with different ages of geology and represent felsic siliciclastic-source-rocks, while chondrite represents ultramafic siliciclastic-source-rocks (Piper and Bau, 2013).

Haskin and Gehl (1962) notes that different kinds of sedimentary rocks, the main rock type that experiences weathering on the continents, have the shale pattern. Shale is therefore the representative of upper continental crust characteristic (Taylor and McLennan, 1985). The weathering of continental source materials and then transporting REE from continental crust sources into the oceans through the rivers and estuaries is the main input of REE in the sea. Although there are some degree of fractionation during weathering, the relatively inert property of REE during subaerial weathering causes the rivers and estuaries entering into the oceans also have the similar REE pattern as shale (Piper, 1974a; Piper, 1974b). The marine components like seawater, marine sediments then have the similar REE distribution pattern as shales (Elderfield, 1988; Taylor and McLennan, 1985; Piper, 1974a), but significantly differs from chondrites REE pattern (Piper, 1974a; Piper, 1974b). The normalization of seawater components is then based on shale to demonstrate any fractionation that occurs during weathering, transportation and water-solid interaction (Piper, 1974a).

On the other hand, the terrestrial waters may react with different rock types whose REE compositions are different to that of shales or weathering modified shale-pattern rocks (Elderfield et al. 1990; Johannesson et al., 1996a). A uniform normalization reference standard for the terrestrial waters does not exist as the standard needs to represent the REE composition in the rocks that water samples reacted with and therefore the standard depends on the source rocks type of water samples (Johannesson et al. 1996a). Protano and Riccobono (2002), Quinn (2006) suggest that chondrites, which represent the REE abundances of the earth's parental material, might be used instead as the reference materials when normalizing the terrestrial waters and rocks (Castor and Hendrick, 2006; Masuda *et al*. 1973). Particularly, they are more suitable to be used for samples with the mafic and ultramafic source rocks (Piper and Bau, 2013). When a flat REE distribution pattern is obtained after normalizing the REE abundance in water samples to the chondrite, it means that REE signature in the source rock of water samples is quite similar as that in the earth parental material (Gosselin et al. 1992).

Piper and Bau (2013) mentions that the selected reference material needs to have the similar REE distribution as the samples collected. Then after normalization, the fractionation induced by the different valence state (regards to trivalent state) REE, minor difference in ionic radius

and electron structure of individual REE, stability of formed REE-complexes can be demonstrated.

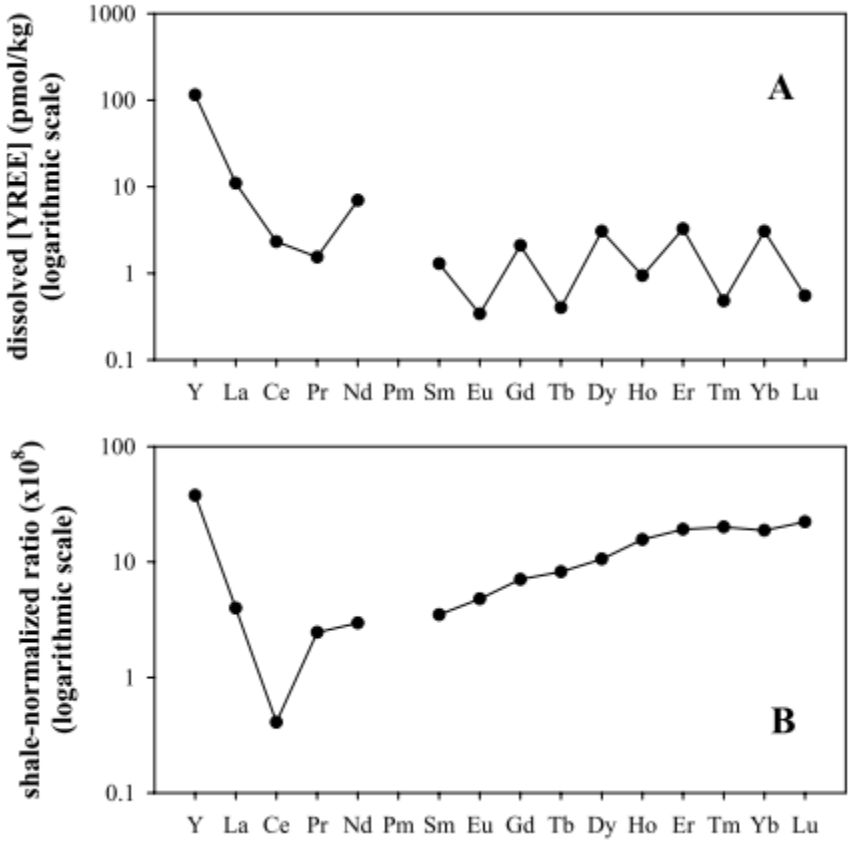

Figure 2.3: (A) REE concentrations of seawater sample collected from Pacific Ocean at 689m depth (Zhang and Nozaki, 1996); (B) PAAS (McLennan, 1989) normalized REE distribution pattern of (A) sample

Shale can be used as the normalization material when the source rocks are felsic (Piper and Bau, 2013). Therefore, shale is the most suitable normalization reference material for water samples whose source rock are mainly composed of sandstones, siltstones, mudstones, clays and shales as them are fine grained clastic sediments (Liu et al. 2014). It needs to note that Goldstein and Jacobsen (1988a) note that PAAS represents composition of the average post-Archean shales and is not able to show the erosion of continental crustal surface during the Phanerozoic, which means PAAS is not the best reference material to show the composition of modern continental crustal surface. In addition, they also mention that NASC cannot represent the modern upper crust as NASC is a mixture of uncommon sedimentary and metamorphic rocks obtained from a wide range of geographic places. Goldstein and Jacobsen (1988a) collect a series of samples which are suitable for producing a reference standard representing the modern upper crust REE composition. However, as the values of Pr, Tb, Ho,

Tm are not contained in the standard of Goldstein and Jacobsen (1998a), their standard is not shown in Table 2.5 and consequently not used as the normalization reference standard in this study.

An example showing the REE distribution pattern before and after normalization and the importance of normalization is demonstrated in Figure 2.3.

2.4.2 REE attenuation and fractionation

Definition of attenuation and "in-stream" process- related fractionation (or called solution chemistry-related)

Attenuation of REE in stream means the mass load decrease for REE in water column, and the mass loss transforms to solid phase in the sediment. The behaviour of REE may be uniform or fractionated during the REE attenuation under different circumstance. To be more specific, attenuation means that REE are regarded as a whole group, only the general trend of this group's mass load (∑REE) (transport from water column to solid phase) under different circumstances e.g. solution chemistry, solid composition along the stream and the effects of each circumstances on ∑REE mass load (transport from water column to solid phase) is taken into account. In-stream process related fractionation is a more detail discussion along with the REE attenuation. This is because it focus on analysing which elements among the group are more prone to attenuate compared to others and the reason causing that, through analysing the variation of normalized REE value across REE group under each circumstances.

This in-stream process related REE fractionation is due to the ionic radius and electron structure difference between individual REE and the oxidation states of individual REE (Byrne and Sholkovitz, 1996). If no in-stream process related REE fractionation occurs, REE distribution pattern after normalizing to a suitable reference materials which can represent REE pattern of study site's source rock should be a flat line (when REE are not fractionated during weathering) and there will have no obvious normalized concentration variation across REE series. This means all the elements have the same attenuation degree under the circumstances. If in-stream process related fractionation of REEs occurs, it can be categorised as LREE, MREE, HREE enrichment and the positive/ negative abundance peaks of certain element (e.g. Eu, Ce, Gd) in water/ solid phase.

In-stream process related MREE enrichment means the intermediate atomic numbers or masses REE are enriched when compared to LREE and HREE on the REE distribution

pattern after normalizing to source rock (of study site) representative reference material (when REE are not fractionated during weathering). This type of enrichment is also called roof-shaped enrichment (Protano & Riccobono, 2002). MREE enrichment in water (induced by in-stream process related fractionation) means the LREE and HREE are more prone to be scavenged by solid phase compared with MREE. Same, in-stream process related LREE enrichment in water means that REE with smaller atomic numbers and masses are enriched in water compared to MREE and HREE, and LREE are more stable and prone to remain in solution. HREE enrichment in water (induced by in-stream process related fractionation) means that REE with larger atomic numbers and masses are enriched in water relative to LREE and MREE, and HREE are more prone to remain in solution compared with other two types.

De Baar et al. (1985) notes that using La_n/Yb_n, Tb_n/La_n, Tb_n/Yb_n (subscript n means suitable reference materials normalized value of each element) parameters for both water and solid samples is another method to indicate the fractionation of LREE, MREE and HREE at each sampling point (in water or solid phase). To be more specific, La_n/Yb_n represents the comparison between LREE and HREE, and can indicate which type of REE prefers to enrich relative to the other one. Tb_n/La_n and Tb_n/Yb_n respectively shows the comparison between MREE and LREE, and the comparison between MREE and HREE. Johannesson and Lyons (1995) use Gd_n instead of Tb_n (Gb_n/La_n and Gb_n/Yb_n) to describe MREE enrichment. In addition, the comparison of MREE/ LREE and MREE/ HREE ratios can show the enrichment difference of MREE over LREE and HREE (Johannesson & Lyons, 1995; Johannesson et al. 1996a).

As in-stream process related fractionation is a more detail analysis of attenuation and they are related to each other, they will be discussed together in those sections below.

Importance of filter pore size

Verplanck (2013); Verplanck et al. (2004); Nelson et al. (2003); Smedley (1991) and Elderfield et al. (1990) all describe REE in rivers (unfiltered or called total phase) are accounted for dissolved phase, colloidal phase and particulates. REE in particulates can be removed by 0.45µm filter, and particulates REE is the difference between the acidified unfiltered and acidified 0.45µm filtered water. Truly dissolved and colloidal REE are present in 0.45µm filtrate, and the difference between the acidified 0.45µm filtered and ultra-filtered

sample is REE in colloidal phase (Verplanck, 2013). Elderfield et al. (1990) mentions that a large proportion of REE is present in the colloidal phase in most rivers.

For study related to the metals behaviour in natural water, the common assumption is that all fresh solid phases are removed by the filtration and the filtrate represents the truly dissolved phase. 0.45μm filtration is normally adopted and the metals concentrations of the filtrates (<0.45μm) are regarded as the dissolved metals concentrations in most metals behaviour study (Verplanck, 2013). However, this is not suitable for REE study due to the need of understanding the mechanism of REE fractionation at sampling sites. Some misinterpretations may be induced when using the mixture of truly dissolved phase and colloids/ colloids plus particulates as the dissolved phase to understand the source-related and process-related process influence on REE fractionation. Verplanck et al. (2004) notes that it is critical to obtain the truly dissolved REE in order to understand the in-stream process related partition between dissolved and fresh solid phase across REE group.

To be more specific, when the REE fractionation is entirely controlled by source-related process, the REE in the truly dissolved phase and in the fresh solids will have the identical normalized distribution pattern, which is their source-rocks pattern. But when the solution chemistry starts to fractionate REE, the normalized REE distribution pattern in the fresh solid begins to differ from that in truly dissolved phase. If the solution chemistry has the dominated control on REE fractionation, the normalized distribution pattern of REE in truly dissolved will be significantly different from that in corresponding solid phase (Verplanck, 2013; Elderfield et al. 1990; Goldstein and Jacobsen, 1988a). When the truly dissolved water sample has the similar REE distribution pattern as its corresponding solid phase, source-related signatures may be predominantly reflected (Verplanck et al. 1999). More details about process-related and source-related fractionation are shown in the following part of this section- current issue for fractionation mechanism. The following examples demonstrate the importance of undertaking ultra-filtration on water when discussing the influence process on REE fractionation.

Based on the works of Hoyle et al. (1984) and Goldstein and Jacobsen (1988a), before large amount of sediments formed, using either unfiltered or coarser filtered water sample as the dissolved REE pattern will demonstrate a source-related pattern. Although in-stream process has a large influence on the truly dissolved REE pattern in their studies, the overall source-

related pattern for unfiltered or coarsely filtered “dissolved” sample leads to a misunderstanding of the mechanism for REE fractionation at sampling sites.

Nelson et al. (2003) finds a contrary normalized REE distribution pattern for the dissolved water fraction and colloids/ particulate fraction when the in-stream process plays an important role on REE fractionation. And the difference between the dissolved phase and colloids phase is smaller than the difference between the dissolved phase and particulate phase. This also shows the importance of undertaking ultrafiltration for analysing the dissolved REE pattern, as adding colloids and particulates will influence the pattern of truly dissolved REE, and consequently misinterpret the in-stream process induced REE fractionation pattern.

The study from Protano and Riccobono (2002) shows that using 0.45µm filtered water sample instead of ultrafiltered water sample as the dissolved phase leads to a positive anomaly of Ce presenting on the normalized REE distribution pattern. But this figure does not show on the normalized REE distribution pattern of ultrafiltered water phase. This is because relative to the adjacent element of Ce, Ce prefers to be oxidised to the tetravalent state under oxidation condition, which will then have the greater affinity for the (fresh) solid phase. It prefers to be removed from the truly dissolved phase compared to its neighbouring elements and the colloidal phase in solution has a positive Ce anomaly.

Bau (1999) notes that even for water passing through 0.2 µm filter, fine colloids will still contain in the filtrate. Nelson et al. (2003) concludes that the positive Ce anomaly on the normalized distribution pattern of filtrate from 0.1µm filtration may because the Ce^{4+} are incorporated into small colloidal particles. This means although element has been removed from truly dissolved phase and serves as the fresh solid, it may still be regarded as dissolved phase and add the extra concentrations for the truly dissolved part when ultra-filtration is not undertaken. This indicates that even 0.1µm filter is still not able to remove the smaller colloidal particles. The solution chemistry-related fractionation pattern is misinterpreted when using 0.1 µm filtered water samples instead of the truly dissolved samples to show the normalized REE distribution pattern in the dissolved phase (Nelson et al. 2003).

Therefore, performing ultra-filtration on total water to obtain the truly dissolved REE pattern is essential for REE fractionation study. To ensure obtain the truly dissolved REE sample, Verplanck (2013) performs tangential ultrafiltration with 10kDa molecular weight membranes (pore size of ~0.005 µm) for the collected river water samples. Protano and Riccobono (2002) also collected ultra-filtration water samples at downstream of the mine discharge to obtain the

truly dissolved REE amount. The REE species in the truly dissolved phase is free REE ions, REE-inorganic complexes and lower molecular weight organic complexes of the REE (Goldstein and Jacobsen, 1988a).

Debate for fractionation mechanism

Parent rocks pattern, water-rock interaction along the flow path and the in-stream solution chemistry control concentration and fractionation of REE in natural water. The potential processes occur from REE host rocks to the sampling sites are dissolution and precipitation of mineral, oxidation and reduction reactions, solution complexation with inorganic and organic ligands, adsorption/desorption onto the suspended flocs and/or secondary minerals (Tang and Johannesson, 2006; Verplanck et al. 1999). However, the REE distribution pattern (when normalized to the traditional reference materials i.e. NASC, PAAS instead of the real source rock of sampling waters) that observed in water course is the result mainly related to source rock or process is a much debated question (Medas et al. 2013; Protano and Riccobono, 2002). The explanations of source-related and process-related are shown as follows:

- source-related fractionation

The whole REE series is typically present in minerals, but the abundance of individual REE varies with minerals type and different minerals in source rocks are enriched in different types of REE, either LREE or HREE, as a result of mineral formation (BGS, 2011; Nesbitt, 1979). There may be significant variation in the REE distribution pattern for major minerals, secondary minerals and accessory phases in the source rock (Biddau et al., 2009; Fee et al., 1992). The REE distribution pattern released to water is controlled by the following factors: (1) the solubility of minerals when interacting with aqueous fluids during the weathering/dissolution process; (2) the abundance and distribution of the various minerals in the host rocks; (3) the aqueous fluids chemistry; and (4) capture of REE removed from the unweathered parent rock by the secondary minerals formed as weathering product (Johannesson and Zhou, 1999; Nance and Taylor, 1977; Haskin and Schimitt, 1967). Traditionally, the source-related fractionation means REE are not fractionated relative to REE pattern of bulk rock during and since released from their host rock to water. That is to say, the distribution pattern of REE in stream inheriting the bulk rock REE signature (or called parent rocks or source rocks) rather than the pattern of some specific minerals within the parent rocks which differs from pattern of bulk rock, and REE are not fractionated during the

formation of weathering residual materials and during their transport along the water flow pathway (Biddau et al., 2009; Johannesson and Zhou, 1999; Fee et al., 1992; Smedley, 1991; Banner et al., 1989).

As noted above, whether the source rock is the ultimate source of REE fractionation in stream is an argumentative question, and the adverse hypothesis is the impacts of solution chemistry (Protano & Riccobono, 2002). It should be noted that the stability and abundance of different minerals within the host rocks and the chemistry of aqueous fluids may cause the distribution pattern of released REE differing from their whole parent rocks (Nesbitt, 1979; Nance & Taylor, 1977). This is because released REE pattern from host rocks inherits only the characteristics of some readily leachable minerals phase within the host rocks, but these phase cannot represent the signature of whole host-rocks (Medas et al. 2013; Protano and Riccobono, 2002; Johannesson and Zhou, 1997), and/ or some host rocks released REE are preferentially captured by the weathering residues relative to other REE. In this sense, REE are actually fractionated during the dissolution/ releasing process by the solution chemistry, and the REE fractionation pattern in water is not entirely source-related. Fractionation of REE induced during the dissolution of their source rocks is categorised into the process-related fractionation group (the following part of this section).

- process-related fractionation

Both the ligands in water and the solid phase (suspended solid or solid) have the ability to complex with truly dissolved REE. REE can be kept staying in water phase by complexing with ligands due to the formation of stable solution complexes, especially when strong REE complexes dominate REE species. Whilst, the complexation of REE with solid surface leads to the removal of REE from water phase. Therefore, the competition between solution complexation and surface complexation is the main mechanism that controls the in-stream process-related REE distribution pattern/ fractionation (Verplanck, 2013; Verplanck, et al. 2004).

The competition result between solution and surface complexation is controlled by the pH, temperature, Eh conditions of water, concentration of inorganic and organic ligands (Tang and Johannesson, 2006; Sholkovitz, 1995; Moller and Bau, 1993; Gosselin et al., 1992; Fee et al., 1992; Smedley, 1991; Elderfield et al., 1990), the formation of REE scavenging solids and the composition of solids (Verplanck, 2013; Quinn et al. 2006b; Quinn et al. 2006a; Quinn,

2006; Quinn et al. 2004). The reactions involved during the competition between solution and surface complexation for dissolved REE include REE speciation, oxidation and reduction reactions and adsorption reaction (Verplanck, et al. 2004). The ultimate mechanism that leads to the in-stream process related fractionation as a results of competition between solution and surface complexation is the variation of ionic radius and electron structure across REE group (Byrne and Sholkovitz, 1996).

- Debate for fractionation mechanism

Although several authors have attempted to figure out the mechanism of REE distribution pattern in fresh water, there is still not a clear answer for this.

The study of Keasler and Loveland (1982) shows that REE distribution pattern in the northwest seawater in Pacific mimics their sedimentary parent rocks, suggesting that source-related fractionation controls the REE distribution pattern in water phase.

Johannesson et al. (1997a, b) and Fee et al., (1992) notice that REE pattern in groundwater is similar as REE signature of the aquifer rocks that groundwater flows through. Smedley (1991) also notes that REE pattern in ground waters with pH in the range of 5.1 to 6.8 inherits from its source rocks. However, Tang and Johannesson (2005) and Leybourne et al. (2000) describe that the solution chemistry-related process can modify the REE distribution pattern of groundwater, which leads to the REE pattern of the groundwater differing from the source rocks.

Hall et al. (1995) notes that REE distribution pattern of lake water, associated sediments and the parent rocks of lake is very similar. Sholkovitz (1995) also mentions that the surface waters can inherit the REE signature of their source rocks. However, the study from Sholkovitz (1995); Moller and Bau (1993); Elderfield et al. (1990); Goldstein and Jacobsen (1988a) show that REE distribution pattern in surface water is mainly influenced by the solution chemistry instead of parent rocks.

Leybourne et al. (2000) describes that these inconsistency conclusion with regards to the main control on REE distribution pattern in water from different studies is because different authors undertook their study in different scale natural water. To be more specific, when samples are collected from large scale rivers, the large scale watersheds will average different bedrocks input and the catchment rock type has minor influence on REE distribution pattern. The small

scale of river on the other hand normally shows the basin bedrock REE signature. The REE pattern of major rivers are relatively uniform since the pattern variations of small rivers are averaged in major rivers (Goldstein and Jacobsen, 1988a).

Some studies (Sun et al. 2011; Protano & Riccobono, 2002; Johannesson et al. 1996) suggest that source-related and process-related fractionation inextricably coexist and they together influence the REE distribution pattern in natural water. Sun et al. (2011) and Biddau et al. (2009) suggest that REE distribution pattern in natural water is controlled by the rocks that (ground)water flows over, pH, Eh of water, solution complexation and fresh solid/precipitates composition. They suggest that REE pattern in water may be influenced by the following factors together: (1) REE pattern of parent rocks and water rock interaction; (2) competition between solution and surface complexation; (3) co-precipitation of REE with Fe, Mn or Al oxides/oxyhydroxides; (4) REE phosphate and/or REE carbonate precipitation (Sun et al. 2011; Tang and Johannesson, 2006). The study from Moller and Bau (1993) shows that both source and process-related mechanisms influence the concentration and distribution pattern of REE in waters: the negative Eu anomaly is related to the source, whereas the pattern of other elements is process-related.

Smedley (1991), Elderfield et al. (1990) and Goldstein and Jacobsen (1988a) use another way to demonstrate the relevance of source rocks and solution chemistry on fractionation. Before large amount of sediments formed, the REE distribution pattern in total (dissolved plus fresh particles- colloids and particulates) river waters is similar as the bulk composition of parent rocks, if little fractionation occurs during the water- rock interaction. The demonstrated dissolved and fresh particles pattern is a combination of process-related and source-related process effects, whether dissolved and fresh particles shows a different or similar REE pattern depends on which process predominate the major control. If possible, source rock REE pattern (whole rock REE profiles) or REE abundances in the "world average" source type rock (if source rock pattern is not achieved) should also be investigated to further indicate the mechanism of REE fractionation in stream.

Therefore, the relationship between the source-related and process-related process could be thought as below. When the released REE mainly inherit its source rock pattern, source rocks dominate the major control on the overall REE distribution pattern which means the dissolved plus corresponding (fresh) solid REE phase (when no REE fractionation occurs during the water-rock interaction). But the solution chemistry has some influences (or play a major role

sometimes) on the dissolved REE distribution pattern (other effects are caused by source rocks) when solution chemistry has the ability to fractionate REE (Goldstein and Jacobsen, 1988a; Elderfield et al., 1990).

2.4.3 Source-related process and fractionation

Some REE anomalies on the distribution pattern of water are the typical source-related fractionation and can be used as an indicator to point out the type of their host rock or at least show which mineral is present in their host rock. Sometimes a positive Ce anomaly with low sum REE concentration can be observed in water (Worral, 1999; Nesbit, 1979). This positive Ce anomaly is a typical source-related fractionation, and its source rock is the residual weathering products. This residual weathering products normally formed in the presence of oxygen, Ce was oxidised from relatively mobile trivalent state to relatively insoluble tetravalent state while other REE stayed in trivalent state. Other REE besides Ce were therefore substantial dissolved/released from rock during weathering process, but the relatively insoluble Ce^{4+} barely released to the solution. The residual weathering products therefore contain highly positive Ce anomaly (Worral, 1999; Nesbit, 1979).

Another source-rock related fractionation is positive Eu anomaly on distribution pattern in water. Positive Eu anomaly is a common figure in plagioclase. Under reduced magmatic systems, Eu can be partially reduced from trivalent state to divalent state, which leads it mobilizing from igneous rocks and then easily substituting for Ca in plagioclase feldspar (Krauskopf and Bird, 1995; Johannesson & Lyons, 1994; Henderson, 1984). Positive Eu anomaly is normally noticed in stream whose host rocks have high content of plagioclase (Drysdale, 2008).

Whether the REE pattern in sampling water is source-related can be checked by analysing REE pattern of whole parent rocks. If the REE pattern of source rocks is similar as that observed in sampling water, REE pattern in water is controlled by its bulk source rocks (Medas et al. 2013; Biddau et al. 2009; Protano & Riccobono, 2002; Zhou et al. 1995; Smedley, 1991). In addition, leaching experiments for the source rock can also be undertaken and the REE pattern in the leachate compared to the REE signature in the source rock and also to the REE distribution pattern in the stream to determine whether the fractionation observed in the stream is due to the source rock signature (Protano & Riccobono, 2002; Johannesson & Zhou, 1997). If the REE distribution pattern in the leachate is similar to that in the source

rocks, the readily leachable fraction in the source rocks must control the REE concentrations, i.e. the REE pattern in the leachate is entirely controlled by source-related fractionation.

If the leachate REE pattern differs from that in the source rocks, the amorphous fraction in the source rock, which is most easily leached, must not control the REE pattern of source rock (Johannesson & Zhou, 1999). The situation may occur when pH of interacting water is not low. Since under not low pH condition, only the readily leached phases like plagioclase, K-feldspar and apatite (Middelburg et al., 1988) is dissolved, and the resistant minerals (if also present in parent rocks) like zircon, monazite, xenotime, sphene, allanite (Smedley, 1991) which are rich in REE may not be able to release REE to water. In this case, solution chemistry must influences the REE distribution pattern even before the leachates drain into the sampling streams. This means that even though the REE distribution pattern of the sampling stream might mimic the leachate pattern, the sampling stream REE pattern is controlled by the solution chemistry (Protano & Riccobono, 2002; Johannesson & Zhou, 1999).

However, this method is only suitable when the parent/ source rocks are indicated and the rock collections are approachable. If source rock pattern is not achieved, REE abundances in the "world average" source type rock could also be used for indicating the REE fractionation. But when the REE pattern in sampling water differs from that in "world average" source rocks, it is difficult to say whether the different pattern is due to the process-related fractionation or the fractionation of the real source rocks of sampling waters relative to "world average" source rocks (Keasler and Loveland, 1982). Smedley (1991) notes that the suitable study sites for the investigations of REE geochemistry in waters should have many information related to the hydrogeology and hydrogeochemistry of the REE source rocks. Sun et al. (2011) and Elderfield et al. (1990) also state that the influence of the source rock pattern on the REE distribution pattern in rivers cannot be known unless the dissolution reactions of the source rock are examined in detail.

2.4.4 Process-related attenuation and fractionation

The water chemistry and composition change with the water flowing down-gradient along the flow path, as a result of chemical weathering, “in-stream” process occurring in the groundwater and surface water systems (Edmunds et al., 2003; Hamlin, 1988). Consequently, the REE concentration and distribution pattern in different phases may be changed. The attenuation/ transformation between different phase (truly dissolved, colloids, particulates)

and process-related fractionation of REE occurring in the aqueous system between the source and discharge zone has the similar mechanism as part of the geochemical process occurred in stream. The process-related fractionation pattern is the change of REE distribution pattern relative to the pattern of bulk source rock (Johannesson and Zhou, 1999).

Under acidic conditions, a large amount of REE can be released from host rocks and the surface of particles. Natural water under low pH condition normally has elevated dissolved REE concentration. Free REE ions and REE sulphate complexes are commonly the most important REE species in acidic condition water (Gammons et al., 2005; Verplanck et al., 2004; Astrom, 2001; Johannesson and Zhou, 1999; Johannesson and Lyons, 1995).

As water flowing down gradient, dissolved REE concentration decreases with the increase of pH. This may due to: (1) the adsorption of REE onto suspended Fe and/or Al oxyhydroxides and/or secondary Fe/Al precipitation, and/or co-precipitation of REE with the precipitation of Fe/Al (Medas et al. 2013); (2) precipitation or co-precipitation of REE bearing phases; (3) dilution effect due to inputs of ground/surface water (Verplanck et al., 2004). To eliminate the possibility of dilution effect induced decrease of REE concentration along the ground/surface water flow path, REE mass loads at each sampling site (REE concentration multiply by flowrate) is suggested to use by Verplanck et al. (2004). This is because the change of REE mass loads (in different phase e.g. truly dissolved, unfiltered phase) along the flow path can indicate whether dissolved REE concentration decrease along the flow path is due to the attenuation or dilution effect.

In addition, the concentration/ load of REE in fresh precipitates which is the concentration/ load difference between unfiltered and truly dissolved REE phase at each sampling point with different water chemistry and composition can also help to understand the influence of water parameters change on (1) REE transformation between different phase (e.g. truly dissolved, colloids and particulates) and (2) process-related fractionation (Verplanck et al., 2004). Medas et al. (2013) also collects the solid samples (sediment) at the same sampling sites where water samples, and the collection of solid and water samples are undertaken at the same time. Astrom et al. (2012) notes that REE fractionation pattern controlled by the solution chemistry can be obtained by analysing which type of REE (LREE or MREE or HREE) or individual REE have the greater affinity for the solid phase (either suspended Fe/Al flocs or secondary Fe/Al precipitates). Verplanck et al. (1999) describes that when normalized REE distribution pattern in dissolved phase is largely different from that in corresponding solid phase,

normalized REE distribution pattern is mainly controlled by in-stream process rather than source-related process.

It needs to note that the reference material used for dissolved and (suspended) solid REE normalization has a large influence on demonstrating the process-related fractionation. If REE pattern of reference material differs significantly from source rocks REE pattern of sampling water, the process-related fractionation may not be easily noticed on normalized REE distribution pattern for the dissolved and (suspended) solid phase, even though the solution chemistry fractionation degree is not low. But when the reference material has very similar REE pattern as the source rocks, the in-stream related fractionation can then be easily observed on the normalized REE distribution pattern for the dissolved and corresponding solid phase, even when the solution chemistry has small influence on REE fractionation.

Therefore, for the purpose of demonstrating any solution chemistry-related fractionation occurring at the downstream of discharge zone, the REE distribution pattern in total water phase at the discharge zone can be regarded as the source pattern and used for downstream dissolved and solid phase REE normalization if the source rocks are not achievable in the study (Goldstein and Jacobsen, 1988a).

The following sections describe REE behaviour across REE group in waters with the change of pH, major ligands types and concentration, Eh, the concentration of metals (Fe, Al, Mn, Pb, Zn) that control REE sorption.

pH

pH has the master control on the concentration and process-related fractionation pattern of REE in dissolved phase (Verplanck et al., 2004; Protano & Riccobono, 2002). With the acidic surface water flowing down gradient along the flow path, pH of water increases progressively by reacting with carbonate rocks in the streambed and/ or due to the input of the clean tributaries and groundwater along the stream (Protano & Riccobono, 2002). There is a negative correlation between the dissolved REE concentration and pH. The mobility of REE progressively decrease with the pH of water increase (Cao et al. 2001; Landa et al., 2000; Leybourne et al., 2000; Johannesson et al., 1996a; Gimeno et al., 1996).

Verplanck et al. (2004) notes that when pH is less than 5.1, no REE are removed from dissolved phase, although a large amount of Fe and Al hydroxides flocs forms. Fe and Al

flocs are effective REE scavenging materials, especially Fe flocs (HFOs). The adsorption of REE onto Fe and Al flocs is well-known, and REE can also co-precipitate with the precipitation of Fe and Al hydroxides from total water column. When pH increases from 5.13 to 6.62, significantly amount of REE are removed from dissolved phase and present in the colloidal phase due to the scavenging of Fe and Al flocs (Verplanck et al., 2004). Smedley (1991) mentions the dissolved REE concentration is restricted to low level when pH increases to 6. Protano and Riccobono (2002) also notes that REE adsorption degree (onto freshly formed Fe and Al flocs) is very high when pH increases from 6 to 7. Medas et al. (2013) notes that even under neutral pH condition, dissolved REE concentration dramatically decreases with a small increase of pH.

REE are fractionated during the process of continuous removal of REE from truly dissolved phase with pH increase from 5 to above neutral condition. The fractionation pattern of REE normally depends on pH, Eh and the composition of REE scavenging materials in water, but is fundamentally due to the characteristics of REE themselves (Verplanck, 2013).

With the increase of pH from 5.13 to 6.62, Verplanck et al. (2004) notices an attenuation-induced (process-related) increase of colloidal REE concentration (after normalization) with the increase of REE atomic number. HREE enrichment pattern in the colloidal phase becomes apparent with the increase of pH suggests that HREE has larger partition tendency to the solid phase relative to LREE when pH is between 5.13 and 6.62. This fractionation pattern is mainly induced by the surface complexation and controlled by the characteristics of REE (Verplanck et al., 2004). To be more specific, Verplanck et al. (2004) notes that no strong REE complexes are present in their samples due to the lower pH (5.13- 6.62), the ionic radius and electron configuration of individual REE leads to the observed fractionation pattern. In addition, sorption modelling undertaken by different studies (Tang and Johannesson, 2010b; Quinn et al. 2006a; Tang and Johannesson, 2005; Quinn et al. 2004; Ohta and Kawabe, 2001; Bau, 1999; Kawabe et al., 1999b; De Carlo et al., 1998) using different substrates all shows that in the absence of strong complexes (REE-carbonate complexes and REE-organic complexes), with the pH increasing from 4 to 9, HREE are preferentially removed compared with LREE at each pH.

When pH of water is at neutral to alkaline condition, LREE generally have greater affinity for the colloidal phase relative to HREE, and there is an increase of normalized REE concentration with the increase of REE atomic number for the dissolved phase (Verplanck,

2013). The phenomenon that REE mobility increases with the increase of atomic number across REE group has been noticed in high pH water like alkaline surface water and seawater (Johannesson et al., 1994; Johannesson and Lyons, 1994; Moller and Bau, 1993). The HREE enrichment degree relative to LREE in dissolved phase increases with the increase of pH. This fractionation pattern under high pH condition is induced by the solution complexation due to the presence of strong REE-carbonates complexes in neutral to alkaline natural water (Verplanck, 2013).

Eh

As described in the previous section, REE mobility and fractionation pattern is influenced by pH. Eh is another chemical parameter that has the ability to fractionate certain REE and also influence the solubility of certain REE (Smedley, 1991).

As noted in Section 2.4.3, Eu is present in divalent state under high temperature reducing condition and fractionates from its neighbouring elements. Eh is the main reason that induces the fractionation of Eu. However, temperature has the major control on Eu redox equilibrium (McLennan, 1989). Eu reduction can only occur under conditions of low oxygen concentration when both temperature and pressure are high, such as in hydrothermal fluids (Klinkhammer et al., 1994; German et al., 1990; Michard et al., 1983). Bau (1991) and Sverjensky (1984) show that in the hydrothermal solution with high temperature (reducing condition), Eu^{2+} shows greater stability than Eu^{3+}. When temperature is below 100^{o}C, Eu cannot be reduced to divalent state and will stay in trivalent state (McLennan, 1989). Sverjensky (1984) also mentions that Eu^{3+} and trivalent Eu complexes are the dominated species in low temperature water. So Eh induced Eu anomaly in natural water system, to be more specific, for groundwater typically with higher temperature and under reducing condition will not occur (Sverjensky, 1984).

In natural water systems, Ce is the only element that can be influenced by Eh and can fractionate from its neighbouring elements (Moffett, 1994a). But similar as the other REE, Ce mainly occurs in trivalent state in the continental sedimentary and igneous rocks (Piper, 1974b).This is because besides Ce, other REE are present in trivalent state in natural waters system under no matter oxidising or reducing condition. But Ce can be oxidised to tetravalent state under oxidising condition in natural water (BGS, 2011). The change of valence state is the change of ionic radius. The change of ionic radius is the ultimate mechanism that leads to the fractionation/ anomaly of Ce (Dia et al., 2000; Bau, 1999). The ionic radius for Ce

decreases around 15% when Ce^{3+} is oxidised to Ce^{4+}, which leads to an increase of surface reactivity for Ce. A depletion of Ce in dissolved phase is normally noticed in oxygenated water due to the greater affinity of Ce^{4+} for (fresh) solid phase and Ce^{4+} is relatively insoluble due to the enhanced bonding between Ce^{4+} and (fresh) solid phase (Medas et al. 2013; Protano & Riccobono, 2002; Bau, 1999). The preferential removal of Ce figure is usually noticed in groundwater under oxidising condition and open ocean waters (Sholkovitz, 1992; Smedley, 1991).

Besides the typical process-related Ce fractionation described in the last paragraph (oxidation of Ce^{3+} to Ce^{4+} by dissolve oxygen in water and preferential complexing of Ce^{4+} with solid phase subsequently), oxidation of Ce can also occur on the surface of the scavenging material if the scavenging material has the oxidation ability (Bau, 1999; De Carlo et al. 1998). This will lead to a further removal of Ce from dissolved phase. To be more specific, since not all Ce^{3+} ions in water are oxidised to Ce^{4+}, during the scavenging process of REE, some Ce^{3+} ions also absorb onto solid phase. If the scavenging solids have the oxidation ability, the absorbed Ce^{3+} can be partially oxidised to Ce^{4+}, which reduce the their tendency for partition back to dissolved water phase (Bau, 1999). Mn oxyhydroxides is a strong oxidising agent, the depletion of Ce in dissolved phase is distinctive in the presence of Mn oxyhydroxides even though no dissolved oxygen is present in water (Ohta and Kawabe, 2001; De Carlo et al. 1998). Fresh Fe oxyhydroxides also has the oxidation ability for Ce under atmospheric conditions, but the oxidation ability of suspended Fe flocs on Ce is much lower than Mn oxyhydroxides (Ohta and Kawabe, 2001; Bau, 1999).

The process-related Ce fractionation is a function of pH in water, however, different studies show a contrary pattern for this. The study from Smedley (1991); Elderfield et al. (1990); Goldstein and Jacobsen (1988a) and Elderfield and Sholkovitz (1987) all show that the depletion degree of Ce in dissolved phase is positively correlated to pH, and Ce fractionation is most pronounced in alkaline water with high pH condition. They suggest that the lack of Ce depletion in many natural water is because the oxidation of Ce is suppressed by the lower pH condition, and Ce^{3+} is more stable than Ce^{4+} at low pH condition.

However, the study from Medas et al. (2013); Davranche et al. (2004) and Bau (1999) show that the affinity of Ce for Mn and Fe hydroxides decreases with the increase of pH under oxidising condition. Bau (1999) mentions that the positive Ce anomaly on Fe oxides is only obvious when pH is below 5, where REE attenuation degree is quite low and other REE

removal amount is quite small. When pH increases to above 5, the removal amount of other REE increases significantly due to the high attenuation degree. Although Ce on Fe oxides is still in tetravalent state, its greater affinity for solid phase is hidden in the high attenuation degree on other REE. Ohta and Kawabe (2001) mentions that greater affinity of Ce for Mn oxides relative to its neighbouring elements is distinctive when pH is between 4.7 and 6.5, but starts to decrease when pH is above 6.5, due to the steep increase of La and Pr removal amount. The pH range inducing different degree of positive Ce anomaly for Mn oxyhydroxides is different as that for Fe oxyhydroxides. This is because for Mn oxyhydroxides, steeply adsorption occurs at pH > 6. While for Fe oxyhydroxides, steeply adsorption starts at pH >5, when other REE also be significantly removed and the difference removal between Ce and other REE is small (De Carlo et al. 1998).

Under strong alkaline aerobic water with very high pH (>9.8) and carbonate concentration, a positive anomaly of Ce can be noticed in the dissolved phase (Moller and Bau, 1993). Although Smedley (1991) notes that a depletion of dissolved Ce should be noticed in high pH aerobic water, due to the formation of relatively insoluble tetravalent Ce. Under very high pH condition, the very high level of carbonate in water will complex with formed Ce^{4+} in water to form the stable pentacarbonato- Ce^{IV}- complexes ($Ce^{IV}(CO_3)_5^{6-}$), which will enhance the mobility of Ce and prevent the adsorption of Ce^{IV}. In addition, this strong pentacarbonato-Ce^{IV}- complexes can also lead to desorption of Ce which has already absorbed onto the solid phase.

Surface complexation

Sorption is an important process that controls REE concentration in solid phase, and consequently influences REE concentration in dissolved phase, according to many REE aqueous geochemistry studies (Medas et al. 2013; Bau, 1999; Johannesson et al. 1999; Sholkovitz et al., 1994; Koeppenkastrop and De Carlo, 1992).

The most effective scavenging material for REE in solution is Fe oxyhydroxides due to their large surface area (Bau, 1999). Dzombak and Morel (1990) also notes that HFOs which are a mixture of hydrous ferric oxides normally precipitating from mine discharge have the largest scavenging capacity for any environmental materials. The synthetic HFOs (like schwertmannite) precipitating in natural have greater sorption capacity than pure HFOs (Carlson et al., 2002; Webster et al., 1998). The sorption study undertaken by Quinn et al. (2004) shows that Fe hydroxides particles has the main control on REE scavenging in

seawater. Protano and Riccobono (2002) also mentions that Fe oxides/ oxyhydroxides in sampling stream are enriched in REE and have the dominated control on REE concentration in stream. Besides Fe oxyhydroxides, Mn oxyhydroxides also have a large control on REE adsorption. Adsorption of REE onto suspended Fe-Mn oxyhydroxides and Fe-Mn oxyhydroxides sediments is the main REE removal process in seawater (Ohta and Kawabe, 2001; 2000). REE concentration is also strongly influenced by Al oxyhydroxides (Quinn, 2006). Protano and Riccobono (2002) mentions that Fe oxyhydroxides has a larger control on REE removal when compare to Al oxyhydroxides.

As noted in the pH part of this section, the removal of REE by Fe and Al oxyhydroxides can only occur when pH in water reaches 5. When pH increases from 5 to neutral condition, REE starts to absorb onto the freshly formed Fe and Al flocs and are then removed from water column with the aggregating precipitation of Fe and Al flocs (Zanker et al., 2003). With the continuous increase of pH from neutral to slightly alkaline condition, Fe concentration in stream is nearly below the detective limit, REE then adsorb onto the freshly formed Zn and Pb oxyhydroxides flocs. REE concentration in dissolved water and in stream are consequently controlled by Zn and Pb in water (Medas et al. 2012; Zussas and Podda, 2005).

It needs to note that normally, during the interaction with freshly formed other metal oxyhydroxides (e.g. Fe, Al, Mn), besides sorption, another removal process- coprecipitation of REE with freshly formed metal oxyhydroxides will also occur during the precipitation of these suspended metal oxyhydroxides flocs (Medas et al. 2013; Zhao et al. 2007; Bau, 1999). However, it is difficult to distinguish the major attenuation of REE process- sorption and co-precipitation during the precipitation of Fe, Al, Mn oxyhydroxides from water phase along the stream from the mine discharge zone. This is because they normally occur together during Fe, Mn or Al oxyhydroxides precipitation (Bau, 1999; Ohta and Kawabe, 2000; Quinn, 2006). Ohta and Kawabe (2001) notes that the REE partition coefficient for REE adsorption is not systematic different from that for REE co-precipitation with Fe oxyhydroxides and the coordination state of REE co-precipitated with Fe oxyhydroxides are the same as that of REE adsorbed onto Fe oxyhydroxides. As co-precipitation of REE with fresh formed secondary mineral is based on REE sorption, this subsection will mainly discuss sorption but will also refer this co-precipitation process. For the sorption, it could be caused either by columbic attractions between the REE species and surface sites or the simply surface complexation with the surface sites. In addition, REE will also absorb onto the pre-formed solid phases, like sediments, but the sorption degree will be lower compared with the freshly formed solids.

Different scavenging materials have different characteristics, which lead them to have different fractionation capacity when complexing with REE on their surface (Quinn, 2006). Fe and Mn oxyhydroxides can both fractionate REE during the adsorption process and induce the partition coefficient of REE group on the (fresh) solid phase displaying M-type tetrad pattern in the absence of strong REE complexes in solution (Quinn et al., 2004; Ohta and Kawabe 2000, 2001; Bau, 1999; Bau, 1996). As defined by Gosselin et al. (1992), the partition coefficient equals REE ion activity in the solid phase divided by REE ion activity in the solution phase. But with the increase of REE atomic number, a general increase of REE partition coefficient onto Fe oxyhydroxides is noticed (Figure 2.4 a), and a general decrease of REE partition coefficient onto Mn oxyhydroxides is observed (Figure 2.4 b) (Quinn et al., 2004; Ohta and Kawabe 2000, 2001; Bau, 1999). Sorption experiments undertaken by Quinn et al. (2004) shows that at pH of 6 and in the absence of strong REE complexes, the partition coefficient of REE onto Al oxyhydroxides smoothly and strongly increases with the increase of REE atomic number. Protano and Riccobono (2002) also notices a smooth increase of REE removal degree with REE atomic number increasing when Al oxyhydroxides is the main scavenging material in their study.

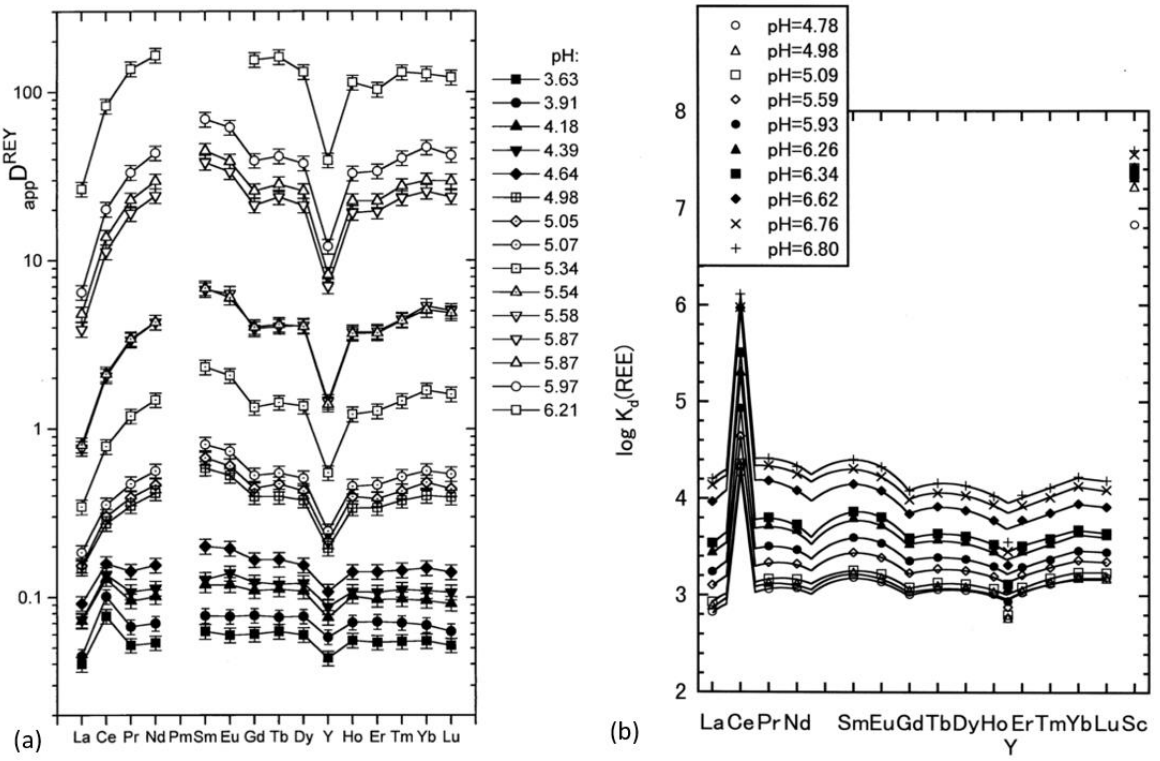

Figure 2.4: REE partition coefficient distribution pattern at different pH condition when the scavenging material is (a) Fe oxyhydroxides (Bau, 1999) and (b) Mn oxyhydroxides (Ohta and Kawabe, 2001)

It should be noted that the surface complexation induced REE fractionation pattern mentioned above will only occur with the lack of strong REE complexes in solution. Since in the absence of ligands which can form strong REE complexes, there is no strong competition between solution complexation and surface complexation for dissolved REE, surface complexation will then control the process-related fractionation of REE.

In the absence of strong REE complexes, the progressively decrease of REE ionic radius with increasing REE atomic number/ mass leads to a progressively increased affinity of REE for scavenging solids phase with the increase of atomic number across REE series (Tang and Johannesson, 2005). Therefore, it is expected to have a smooth and progressive increase of REE removal degree in the absence of strong REE complexes. But this fractionation pattern is only noticed when Al oxyhydroxides control the adsorption of REE. This is because besides the ionic radius, the variation of electron structure of REE group can also induce the fractionation during the adsorption process, and this fractionation is related to the characteristics of absorbing solid (Bau, 1999).

As shown in Figure 2.4 (a), the distribution pattern of REE partition coefficient on Fe oxyhydroxides in the absence of strong complexes at different pH values is a four upward-curved segment (M-type tetrad pattern) with a general increase of partition coefficient with the increase of REE atomic number. The four segments are 1: La to Nd, 2: Nd to Gd, 3: Gd to Ho; 4: Ho to Lu (Quinn et al., 2004; Ohta and Kawabe 2000, 2001), which produces a negative anomaly of La, Y, Gd and Lu in the distribution pattern of REE partition coefficient on Fe oxyhydroxides. Y is placed next to Ho on the distribution pattern due to their very similar ionic radius and consequently very similar chemical and geochemical behaviours, Y and Ho are called geochemical twins (Bau, 1999). The electron structures of four elements Y, La, Gd and Lu lead to their anomalies on the distribution pattern of REE partition coefficient on Fe oxyhydroxides (Bau, 1999).

Since the bonding is influenced by the 4f orbitals of the REE, the delocalization of electrons in REE 4f orbitals when interacting with more covalent ligands/ soft ligands induces an enhanced covalency of other REE compared with Y. Y therefore behaves as a LREE when the interaction between Y and solid phase is comparatively covalent (Borkowski and Siekierski, 1992; Siekierski, 1981). But Y has a similar chemical behaviour to Ho when interacting with more ionic ligands/ hard ligands and consequently behaves as a HREE (Martell and Hancock, 1996; Liu and Byrne, 1995). Quinn et al. (2004) notes that the interaction between Y and Fe

oxyhydroxides is comparatively covalent, the surface reactivity of Y is between that of La and Ce, and is therefore weaker than most of the LREE and all the MREE and HREE. While the interaction between Y and Al oxyhydroxides is comparatively ionic, Y behaves as the HREE and has a greater partition tendency for the solid phase relative to MREE and LREE.

The anomaly of La, Gd and Lu is not observed in the REE partition coefficient distribution pattern for the adsorption of REE onto Al oxyhydroxides. Since no fractionation is induced by the electron structure of REE during their interaction with Al oxyhydroxides, the variation of REE ionic radius then controls the REE fractionation during the scavenging process in the absence of strong REE complexes. Therefore, a progressive increase in the degree of adsorption onto Al oxyhydroxides with increasing atomic number across the REE group can be observed in the absence of strong REE complexes in solution (Quinn et al. 2004).

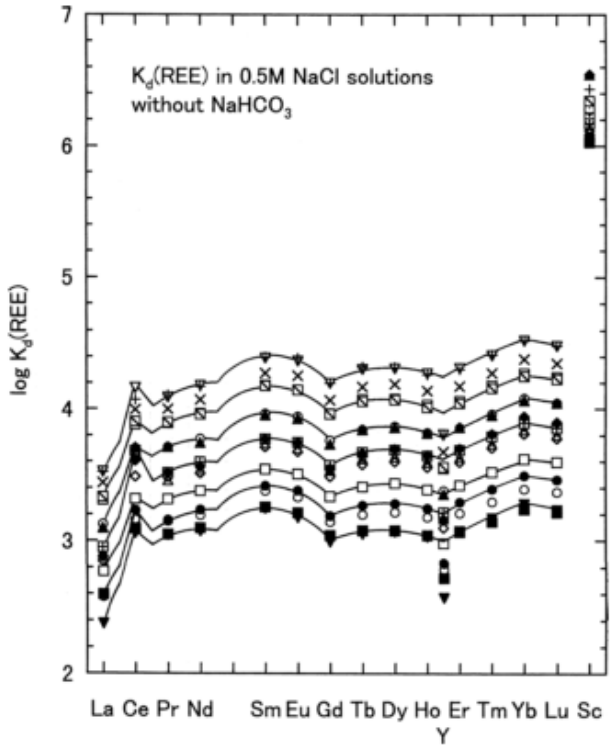

Figure 2.5: Partition coefficient of REE for Fe oxyhydroxides with increasing pH from 5.6 to 6.6 in the absence of strong complexes (Ohta and Kawabe, 2000).

Bau (1999) notes that pH controls the fractionation degree of REE during the complexation with Fe hydroxides in the absence of strong complexes. To be more specific, a relatively flat REE distribution coefficient pattern on Fe hydroxides was seen when pH was below 4.64, whilst a more pronounced M-type lanthanide tetrad effect was observed when pH increased from 4.64 to 6.2, as shown in Figure 2.4 (a) (Bau, 1999; Figure 2.4 a).

In the absence of strong complexes, Ohta and Kawabe (2000, 2001) also notices a pronounced lanthanide tetrad effect in REE distribution coefficient pattern on Fe hydroxides in their experiments with pH range of 5.6- 6.6, although the adsorption of each REE increases with pH, the REE fractionation trends are parallel to one another. Ohta and Kawabe (2001) mentions that changing from a flatter distribution to a remarkable tetrad effect with the increase of pH is not observed in their experiment due to the experiment is undertaken within a relatively higher pH range. The experimental results of Ohta and Kawabe (2001) are shown in Figure 2.5. The work from Quinn et al. (2006a) demonstrates a general good agreement with the work of Bau (1999) and Ohta and Kawabe (2000, 2001) for the distribution coefficient patterns obtained at pH > 5.0.

The distribition coefficient pattern of REE onto Mn oxyhydroxides in the absence of strong REE complexes also shows convex tetrad curves but accompanied by LREE enrichment relative to HREE (Ohta and Kawabe, 2001). To be more specific, in the absence of strong REE complexes, with pH increases from 4.7 to 6.8, the fractionation trend of REE becomes more obvious, adsorption of each REE increases but the increase degree of LREE is much larger than that of HREE. In addition, the fractionation trends of REE are not parallel one to another and the fractionation pattern of REE at lower pH of 4.7 to 5.09 is flatter (Ohta and Kawabe, 2001). The results of studies of Ohta and Kawabe (2001) is shown in Figure 2.4 (b). De Carlo et al. (1998) also mentions that under their experiment with pH from 4 to 9 in the absence of large amount of strong complexes, the LREE prefer to be removed by Mn oxyhydroxides compared with HREE, whereas HREE prefer to be removed by Fe oxyhydroxides compared with LREE (HREE>MREE>LREE). But the convex tetrad curves are the common features for Mn and Fe oxyhydroxides (Ohta and Kawabe, 2001).

De Carlo et al. (1998) mentions that the REE adsorption onto Mn oxyhydroxides is stronger than onto Fe oxyhydroxides at low pH. To be more specific, REE start adsorbing onto Fe oxyhydroxides when pH is above 5, while 20% of REE have already adsorbed onto Mn oxyhydroxides under pH of 4. This is because the characteristics of surface charge for these two solids are different (Quinn et al. 2006a). The solid surface is mainly consisted of negatively charged Mn oxyhydroxides before pH reaches 4, while positively charged Fe oxyhydroxides dominates the solid surface when water is below neutral condition (Parks, 1965). The negatively charged surface of Mn oxyhydorixdes at low pH can induce the physical adsorption of cationic REE species, which leads to the adsorption of REE onto Mn oxyhydroxides begins even when pH is below 4.

De Carlo et al. (1998) and Ohta and Kawabe (2001) also shows that the adsorption of each REE for Mn oxyhydroxides smoothly increases with pH increasing from 4 to 6, and the adsorption edge occurs when pH >6. For Fe oxyhydroxides, there is also an increasing trend of REE uptake from pH of 4 to 8, under pH of 5, the adsorption amount increases slightly with increasing pH, when pH is above 5, REE adsorption increases significantly with pH increasing (De Carlo et al. 1998). Bau (1999) also notes that when pH increases to 4.6, only 10% of REE are scavenged by freshly precipitated Fe phase, when pH increase to 6, 90% of REE are removed. But HREE are preferentially removed by Fe oxyhydroxides relative to LREE, while LREE are preferentially absorb onto Mn oxyhydroxides compared to HREE at higher pH in the absence of strong REE complexes (Ohta and Kawabe, 2001).

Solution complexation

Trivalent REE ions are hard ions, and will preferentially complex with hard ligands which contain highly electronegative donor atoms (Pearson, 1963). REE in water can mainly complex with halides, sulphate, phosphate, hydroxides, carbonate and organic ligands through the solution complexation process (Lewis et al. 1998). Among these ligands species, carbonate, phosphate and organic ligands can form strong complexes with REE (Leybourne et al., 2000; Lewis et al., 1998; Takahashi et al., 1997; Millero, 1992; Wood, 1990).

The formation of strong REE-complexes reduces the partition tendency of those complexed REE for the scavenging solids, like Fe, Mn oxyhydroxides and enhances the mobility of REE (Johannesson & Hendry, 2000; Ohta and Kawabe, 2000; Kawabe et al. 1999b). However, there is one exception: although the stability constant of REE-phosphate complexes is in the similar magnitude to that of some REE-carbonate complexes (Lee and Byrne, 1993; 1992). Phosphate actually promotes the removal of REE from dissolved phase through the precipitation of REE phosphate salts rather than keep REE staying in the dissolved phase (the role that carbonate and organic complexes plays), based on the equilibrium calculations (Johannesson et al., 1995; Byrne and Kim, 1993). Therefore, strong REE-complexes/ solution complexation related fractionation refers to species of REE-carbonate complexes and REE-organic complexes.

When strong REE complexes are the important species in water, the variation of strong REE-complexes stability constant across REE group may have a significant influence on the process-related REE fractionation pattern. The strong REE complexes/ solution complexation will normally have a dominated control on process-related REE fractionation pattern, and

REE fractionation pattern in scavenging solid phase will then be controlled by the stability constant of strong REE complexes for each individual REE on most conditions. (The only exception condition is when REE carbonate complexes [$Ln(CO)_3^+$] is the most important species but REE surface complexation is mainly based on the strong surface sites of solids. The reason is explained in the below paragraphs.)

The proportion of REE complexes decreases with the increase of ionic strength, while free REE ions proportion increases with the increase of ionic strength in water. This is because the increase in ionic strength leads to an increase in the formation of major cations e.g. Ca^{2+}, Mg^{2+} and major anions ion pairs/complexes (Nordstrom and Munoz, 1994; Morel and Hering, 1993). Less free ligands are available in solution after ion pairing with major cations, therefore less REE-complexes are formed and the percentage of free REE ions increases. Since ionic strength increases with decreasing pH, the formation of REE-complexes is suppressed in water with low pH, and free REE ions are commonly the predominated species in low pH natural water (Johannesson et al., 1996a; Wood, 1990; Lee and Byrne, 1992). The formations of REE carbonate complexes and REE organic complexes are suppressed at low pH condition, but the formation of sulphate complexes is normally inhibited by the high pH (Gosselin et al. 1992). REE sulphate complexes is not a strong solution complexes species.

Therefore, the fractionation of REE induced by the competition of dissolved REE between solution complexation and solid complexation is largely controlled by pH. That is to say, strong REE complexes will be absent under lower pH condition, fractionation pattern of REE is entirely controlled by the property of main scavenging material for REE, which is ultimately related to the characteristics of REE group (ionic radius and electron configuration of individual REE). Under higher pH condition where a large amount of strong-REE complexes forms, fractionation pattern of REE can be significantly influenced by the variation of strong REE complexes stability constant across REE series. The concentration of strong ligands is also a key factor that influences the proportion of strong REE complexes in water, and consequently influences the fractionation of REE (Tang and Johannesson, 2005). Generally speaking, the process-related fractionation of REE is controlled by pH of water, carbonate and organic matter concentration in water and scavenging material composition (Quinn et al. 2006b; 2004).

- REE inorganic complexes

In acidic water condition, free REE ions and REE sulphate complexes will be the dominated species in water (Wood, 1990). Acid mine drainage (AMD) normally contains high SO_4^{2-} concentration which is from the oxidation of acid-forming metal sulfides e.g. pyrite that contained in the ore body. For acidic natural water which is highly polluted by the AMD, the proportion of sulphate complexes will be relatively high (Zhao et al. 2007). The stability constant of REE sulphate complexes demonstrate very small change with the increase of REE atomic number, and the not strong complexes species- REE sulphate complexes does not induce solution complexation related fractionation of REE (Verplanck et al. 2004; Wood, 1990).

In near neutral to alkaline water condition, strong complexes species- REE carbonate and di-carbonate complexes are the predominated inorganic species in water (Lee and Byrne, 1993; Wood, 1990; Goldstein and Jacobsen, 1988a). Wood (1990) notes that carbonate species are the most important inorganic species when pH of water is above 6. Without the consideration of organic species, the increase of stability constant of both REE carbonate ($LnCO_3^+$) and REE di-carbonate complexes [$Ln\text{-}(CO_3)_2^-$] with the increase of REE atomic number reduces the activities of HREE relative to LREE and leads to the HREE are more difficult to be removed from dissolved phase relative to LREE (Byrne and Kim, 1993; Wood, 1990). Consequently, in neutral to alkaline water where carbonate species control the solution complexation, a LREE enrichment pattern will be noticed in the solid phase and a HREE enrichment pattern will be shown in the dissolved phase when discussing the process-related fractionation (Quinn et al., 2006b; Kawabe et al., 1999b). But the stability constant difference between HREE and LREE for $Ln\text{-}(CO_3)_2^-$ is greater than that for $LnCO_3^+$, and $Ln\text{-}(CO_3)_2^-$ is much stronger complexes than $LnCO_3^+$. The (di)carbonate complexes induced fractionation degree of REE can be influenced by the proportion of carbonate and di-carbonate species for individual REE which is controlled by the carbonate concentration and pH in water (Tang and Johannesson, 2010b). Without the consideration of organic species, the concentration of REE in dissolved phase can also be affected by the carbonate and dicarbonate complex concentration (Sun et al. 2011). It should be noted that the preferential removal of LREE will not be shown when $LnCO_3^+$ is the most important species for dissolved REE and surface complexation is mainly based on the strong sites on solids surface (which are discussed into details below).

Sun et al. (2011) calculates REE speciation in neutral to slightly alkaline water with pH ranging from 7.14 to 8.2 (without the consideration of organic matter). Under neutral pH condition, the $LnCO_3^+$ species is more important for HREE relative to MREE and LREE. This is because carbonate prefers to complex with higher atomic number REE first, then with the low atomic number REE. With the increase of pH from 7.14 to 8.2, carbonate concentration in water also increases, carbonate ions continue complexing with $LnCO_3^+$ and form $Ln(CO_3)_2^-$. But carbonate still complexes with HREE-CO_3^+ first, then with MREE-CO_3^+ and at last with LREE-CO_3^+. In general, LREE form strong REE carbonate complexes ($LnCO_3^+$) and HREE tend to be completed as REE di-carbonate complexes [$Ln(CO_3)_2^-$] with pH increasing from neutral to slightly alkaline (Johannesson et al., 1996). When pH continues increasing from slightly alkaline (8.36 to 8.78) to alkaline enriched water, REE di-carbonate complexes is the dominated species. Over 80% of dissolved LREE are REE di-carbonate complexes, and over 90% of dissolved MREE and HREE are REE di-carbonate complexes. There is a positive correlation between pH and proportion of $Ln(CO_3)_2^-$ and a negative correlation between pH and $LnCO_3^+$ when pH increases from slightly alkaline to alkaline condition (Sun et al. 2011).

The similar results have also been found by Tang and Johannesson (2006) for neutral to alkaline groundwater (without the consideration of organic matter). Their speciation modelling results show that the proportion of free REE ions decreases with the increase of pH from 6.13 to 8.68, but the proportion of REE di-carbonate complexes increases with the increase of pH. When pH is below 7, the proportion of free REE ions decreases with the increase of REE atomic number, whilst the proportion of both carbonate and di-carbonate complexes increases with the increase of REE atomic number. When pH increases to above neutral level (pH>7), the proportion of carbonate complexes decreases with the increase of REE atomic number, but the proportion of di-carbonate complexes increases with the increase of atomic number across REE group. Di-carbonate complexes are the most important species when pH increases to above 8 and free REE ions then becomes negligible.

Johannesson and Zhou (1997) notes that for neutral pH condition water, REE carbonate complexes is the dominated REE species, while for alkaline water, REE di-carbonate complexes is the predominated species (without the consideration of organic matter). Tang and Johannesson (2006) also notes that in general, carbonate complexes (REE-CO_3^+) are predominate at pH between 6.5 and 7.5, and dicarbonate complexes (REE-$[CO_3]^{2-}$) are predominate at pH above 8.0 (without the consideration of organic matter). The REE speciation results in natural water under near neutral to alkaline condition from other studies

(Leybourne et al., 2000; Johannesson et al., 1996; Johannesson and Lyons, 1994; Lee and Byrne, 1993; Millero, 1992) show the similar conclusions (without the consideration of organic matter).

In addition, if continue increasing carbonate concentration and pH, polycarbonato-complexes with much more strong stability constant compared to carbonate and di-carbonate complexes may also forms. The formation of polycarbonato-complexes makes REE quite difficult to be removed from dissolved phase (Sun et al. 2011).

Although in the subsection of surface complexation, in order to understand REE fractionation pattern induced only by the surface complexation, the formations of strong REE-carbonate and di-carbonate complexes are carefully avoided when performed pH is high in the sorption modelling study like De Carlo et al. (1998). Normally for waters with neutral or alkaline pH, the absence of carbonate ions in waters is not possible, and the carbonate concentration will increase with pH increase.

The experiments from Kawabe et al. (1999b) and Ohta and Kawabe (2000) both show that LREE prefer to absorb onto the amorphous ferric hydroxide on performed pH condition (7.6 to 8.7) when carbonate is not removed from the system (without the consideration of organic species). The sorption modelling undertaken by Quinn et al. (2006a) at pH of 7.6, 7.9 and 8.2 in the presence of carbonate ligands shows that LREE have greater affinity for ferric hydroxides compared to HREE at each pH and also with the increase of pH from 7.6 to 8.2 (Figure 2.6). A preferential scavenging of LREE pattern for REE sorption from alkaline water/ seawaters (carbonate and di-carbonate species control the solution complexation related fractionation) by Fe and Mn oxyhydroxides have been noticed (De Carlo, 1992; Koeppenkastrop et al., 1991). The formation of more stable HREE-(di)carbonate complexes relative to LREE-(di)carbonate complexes, and the preferential removal of LREE compared to HREE lead to HREE is more difficult to be scavenged by fresh Fe flocs/ Fe and Mn oxyhydroxides (Ohta and Kawabe, 2000; De Carlo et al. 2000; Kawabe et al. 1999b; De Baar et al., 1988). HREE enrichment pattern in the dissolved phase is a common figure in high pH condition natural waters (Johannesson et al., 1994; Johannesson and Lyons, 1994; Moller and Bau, 1993).

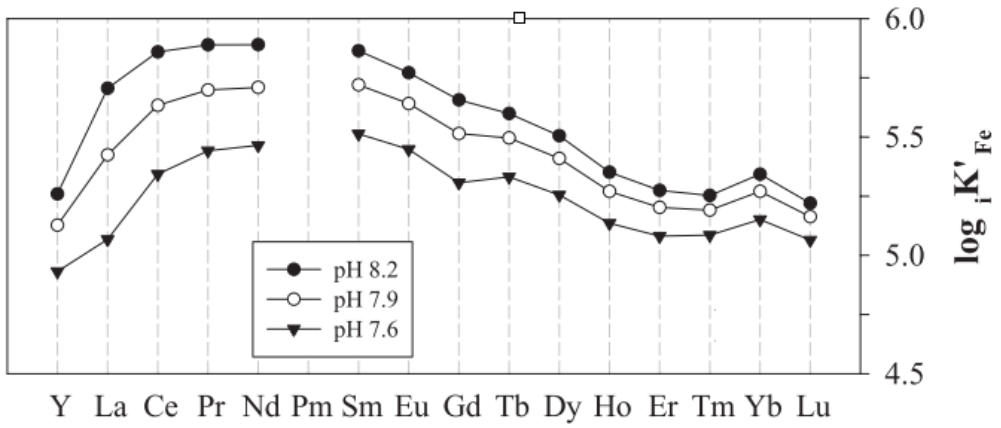

Figure 2.6: pH dependence of predicted REE distribution coefficient for ferric hydroxides in the presence of carbonate ions (Quinn et al. 2006a)

Surface complexing sites type can influence the competition result between solution complexation and surface complexation in the presence of REE (di)carbonate complexes. Tang and Johannesson (2005) mentions that there are two site types- high-affinity sites and low-affinity sites (can also be referred to as "strong sites" and "weak sites") on oxides/oxyhydroxides surface which can complex with REE. The surface complexation is also called the chemical adsorption, which is much stronger than the electrostatic attraction between REE species and negative (for most REE species) charges dominated solid surface (Hall, 1998).

The sorption modelling results from Tang and Johannesson (2005) indicate that strong surface complexing sites of oxides/oxyhydroxides can outcompete carbonate complexes but not di-carbonate complexes for the dissolved REE (Ln^{3+}). Moller and Bau (1993) also notes that although the progressive decrease in ionic radius with increasing atomic number across REE group should enhance the surface reactivity of HREE and lead to an increase of surface complexation from the LREEs to the HREEs, di-carbonate complexation dominates over surface reactivity. This means that when strong sites of oxides/ oxyhydroxides surface have the main responsibility for complexing with REE, dissolved REE then dissociate from REE carbonate complexes and being sorbed as the free REE ions onto the strong sites on solid surface (Tang and Johannesson, 2005). However, dissolved REE (especially HREE) will complex with di-carbonate ions rather than with the strong surface sites of oxides/ oxyhydroxides. Even though adsorption occurs, the strong sites on oxides/ oxyhydroxides surface may only complex with the whole REE (especially HREE) di-carbonate complexes as REE (especially HREE) di-carbonate complexes cannot release the free REE ions for

absorbing onto the solid phases (Tang and Johannesson, 2010b; Tang and Johannesson, 2005; Quinn et al., 2004).

When there are sufficient strong sites on oxides/oxyhydroxides (not Mn oxides/oxyhydroxides) surface available for complexing with REE, and REE carbonate complexes [$Ln(CO_3)^+$] is the most important strong complexes species, a preferential removal of HREE instead of LREE will be observed. This is because that carbonate ligands cannot effectively compete with the strong sites on the solid surface and free REE ions are the adsorbing species. In addition, this suggests that the surface complexation dominates the process-related fractionation during the REE removal process. The variation of ionic radius of REE group leads to a preferential removal of HREE (Tang and Johannesson, 2005). However, when REE di-carbonate complexes is the dominated species, di-carbonate ions can outcompete strong surface sites on solids especially for dissolved HREE, which leads to a preferential removal of LREE from dissolved phase (Tang and Johannesson, 2010b).

Weak sites of oxides/oxyhydroxides surface are ineffective competitors against both carbonate ligands and di-carbonate ligands for dissolved REE. Therefore, weak surface sites are only able to complex with the REE carbonate complexes and di-carbonate complexes (Tang and Johannesson, 2010b). Since the stability constant of both REE carbonate and di-carbonate complexes increases with the increase of REE atomic number, a LREE enrichment pattern should be observed on the weak surface sites without the consideration of organic species influence. Weak surface sites are more important when REE concentration in water is not low, which means the number of strong surface sites that can complex with REE is quite small relative to the adsorbing REE number (Tang and Johannesson, 2010b).

Strong and weak sites together control the surface complexation and influence the competition results between (di)carbonate complexation and surface complexation for dissolved REE, which consequently influences REE fractionation pattern in water phase (Tang and Johannesson, 2010b).

The difference between REE carbonate complexes and REE di-carbonate complexes is due to carbonate and di-carbonate ions have different complexation ability (Johannesson and Hendry, 2000). The stability constant of REE carbonate species is 4 orders of magnitude weaker than that of REE di-carbonate species (Johannesson et al., 1994). The formation of very strong REE di-carbonate complexes means the removal of REE from dissolved phase is more difficult. The adsorption degree of REE decreases with the increase of REE di-carbonate

complexes proportion (Tang and Johannesson, 2010b; Quinn et al. 2006b). Experiment results from Sun et al. (2011) also show that for either neutral to slightly alkaline water or high alkaline enriched water, the REE concentration in water increases with the increase of bicarbonate complexes proportion. Dissolved REE concentrations in the higher alkalinity and pH waters are therefore higher than that in the lower alkalinity and pH waters (Johannesson et al., 1994). In addition, the (di)carbonate complexes induced HREE enrichment degree relative to LREE increases when the proportion of $Ln(CO_3)_2^-$ increases (Quinn et al. 2006a).

In addition, the physical adsorption or non-specific adsorption also plays an important role on the overall REE adsorption when the negatively charged sites dominate the solid surface. The dominated charge of hydrous oxides on the solid surface is a function of pH. Hall (1998) notes that when pH is above 8 (the exact pH value depends on the solid composition), the negatively charged sites dominate on the solid surfaces of newly formed Fe and Al oxyhydroxides (while the pH for Mn oxides or clays with substantial negatively charged sites is much lower). Under alkaline waters condition where most of Fe and Al oxyhydroxides surface sites are negatively charged, physical adsorption also contributes to the LREE enrichment pattern on these oxyhydroxides surface (Sun et al. 2011).

To be more specific, under slightly alkaline water condition, although carbonate complexes is the dominate the REE speciation (without the consideration of organic species), MREE and HREE tend to be completed as $Ln(CO_3)_2^-$ while LREE mainly form $LnCO_3^+$ (Medas et al. 2013; Johannesson et al., 1996). The positively charged species LREE-CO_3^+ can easily adsorb onto negative charges dominated oxyhydroxides surface, the negatively charged species MREE- and HREE-$(CO_3)_2^-$ on the other hand will be stabilized in water (Sun et al. 2011; Tang and Johannesson, 2006). HREE are therefore more difficult to be removed from water phase under slightly alkaline condition from the physical adsorption aspect (carbonate/di-carbonate complexes related REE fractionation).

For the high alkaline water, although di-carbonate species is the dominated REE species (without the consideration of organic species), the proportion of di-carbonate complexes increases with the increase of atomic number across REE group. The proportion of REE $Ln(CO_3)_2^-$ for HREE and MREE is larger than that for LREE (Sun et al. 2011; Tang and Johannesson, 2006). LREE therefore have greater affinity for the negatively charged oxyhydroxides surface relative to HREE under high alkaline condition (carbonate/di-carbonate complexes related REE fractionation). Since $Ln(CO_3)_2^-$ is the predominated species

for dissolved REE, significant fractionation caused by physical adsorption will not occur. Thus, chemical adsorption (e.g. the stability constant of di-carbonate) is the main reason for HREE enrichment in high alkaline waters (Johannesson and Lyons, 1994; Johannesson et al., 1994; Moller and Bau, 1993). In addition, the higher proportion of ∑REE di-carbonate complexes under high alkaline condition compared to low alkaline condition leads to a higher concentration of ∑REE in high alkaline water than low alkaline water (Sun et al., 2011).

- REE organic complexes

Organic matter is mainly comprised of humic substance (HS) which consists of humic acids (HA) and fulvic acids (FA) which in natural water can complex with REE to form strong REE complexes (Pourret et al., 2007; Sonke and Salters, 2006; Tang and Johannesson, 2003). Thurman (1985) notes that humic acids with a high molecular weight and low solubility is the humic type organic fraction; while fulvic acids with low molecular weight and higher solubility is the fulvic type organic fraction. pH, concentration of dissolved organic matter, ionic strength and competitive cations together control the complexation of humic substances with REE, and the dominant controlling factor is pH and dissolved organic matter concentration.

The modelling undertaken by Tang and Johannesson (2003) which includes the stability constant of both REE inorganic complexes and REE organic complexes to predict REE speciation as a function of pH based on the world average concentration of dissolved organic carbon (DOC) of groundwater and river water shows: (1) REE organic complexes are unimportant in acidic water and the dominant species in acidic water are free REE ions and REE sulphate complexes; (2) REE carbonate/ dicarboante complexes are the dominant species in alkaline waters; (3) organic complexes can outcompete the carbonate for the dissolved REE and REE organic complexes is the dominated species in near neutral pH waters when the dissolved organic carbon (DOC) concentration is higher than 0.7ppm; (4) REE organic complexes are much less important when the concentration of organic matter is low.

Takahashi et al. (1997) notes that the stability constant of divalent metals with HS is generally smaller than that for trivalent metals, and the relative strength of the stability constant of Fe/Al with HS is greater than that for REE. Therefore, Fe and Al in natural waters can strongly compete with REE for the sites on HS during the formation of HS complexes, which decrease the REE amount complexed with HS (Tang and Johannesson, 2003). The REE

fractionation pattern induced by the strong organic complexes depends on the type of HS (strong or weak) that the majority of REE binds to (Tang and Johannesson, 2010a).

The affinity of REE to the strong site of HS increases with increasing atomic number across the REE series and consequently the stability constant of REE-HS complexes increase with increasing atomic number. The lanthanide contraction is responsible for the affinity change of REE to strong sites of HS across the REE group (Sonke and Salters, 2006). When the molar ratios of REE/DOC is low (less than $3.5x10^{-4}$) and the competition of other metals with REE for the complexing site of HS is at quite low degree, strong sites of HS have the main responsibility for binding REE (Marsac et al., 2010; Stern et al., 2007; Sonke and Salters, 2006). The affinity of REE to the weak sites of HS decreases in the order of MREE>HREE>LREE. The weak sites of HS are the main binding sites for REE when the REE/DOC molar ratio is high (10^{-3} to 1.5×10^{-2}) (Marsac et al., 2010; Yamamoto et al., 2010, 2005), or when there is strong competition of Fe, Al and other metals with REE for the strong sites of HS even though the REE/DOC molar ratio is low (between 5×10^{-6} to 3×10^{-4}) (Tang and Johannesson, 2010a).

The competition ability of Fe and Al relative to REE for the available HS sites is significantly strong between a pH of 4 and 9 (Tipping et al., 2002). In natural waters, the common trace metals (e.g. Fe, Al) are more abundant than REE and the relative strength of the stability constant of Fe/Al with HS is greater than that for REE. This leads to the strong sites of HS being saturated with the common trace metals like Fe, Al and other cations, thus leaving the weak sites of HS available for binding REE. Without the consideration of other strong REE complexes (REE carbonate complexes), the MREE enrichment pattern is normally induced by the REE organic complexes in natural waters even though the REE/DOC molar ratio is quite low (Tang and Johannesson, 2010a). Overall, the REE/DOC molar ratio in natural water is not important and the stability constant of REE-HS complexes in natural water decreases in the order of MREE>HREE>LREE (Tang and Johannesson, 2010a).

Similar to REE carbonate complexes, REE organic complexes are also strong complexes. In the presence of carbonate ions, there is competition between HS and carbonate for complexing with REE in water. The process-related REE fractionation in natural water especially at around neutral pH is the result of competition between HS and carbonate for complexing with REE. HS is composed of FA and HA, FA cannot compete with carbonate for binding REE particularly for HREE, but HA can outcompete with carbonate for binding

with REE (Tang and Johannesson, 2010a). This is because REE-HA complexes are stronger than REE-FA complexes (Sonke and Salters, 2006). Therefore, the result of competition between HS and carbonate for REE depends on concentration and the dominant form (HA or FA) of DOC, and pH (Tang and Johannesson, 2010a).

When low molecular weight DOC like FA is the main composition of DOC, the complexation ability of carbonate with REE is stronger than that of FA with REE even in neutral pH river water, a HREE enrichment pattern is then induced by the carbonate complexation in water phase during the in-stream process (Tang and Johannesson, 2010; Pokrovsky et al., 2006). On the other hand, when DOC in neutral river waters is mainly in the form of HA, process-related fractionation of MREE enrichment pattern should be observed in water phase since the organic complexes have the dominant control on the solution complexation (Tang and Johannesson, 2010a). This is because, when organic complexes have the main control on the REE fractionation pattern, the decrease in stability constant of strong REE-HA (weak sites) complexes in the order of MREE>HREE>LREE leads to a decrease in REE affinity to scavenging materials in the order of MREE>HREE>LREE. A MREE enrichment relative to HREE and LREE and HREE enrichment relative to LREE should be shown in water phase as the results of strong REE-organic complexes induced fractionation.

Precipitation and co-precipitation of REE

Besides the main REE attenuation process- chemical adsorption (maybe also co-precipitation with the precipitation of scavenging materials if the degree of REE removal is quite high), precipitation and/or co-precipitation of REE salts is another process that influences REE concentrations in water under suitable conditions, which is mainly in seawater (Byrne and Kim, 1993; Jonasson et al. 1985). This is because similar to the precipitation manner of other metals, REE have high solubility and the REE sulphate, carbonate and phosphate precipitates are under-saturated in the acidic waters (Johannesson et al, 1996; Johannesson et al., 1995; Johannesson and Lyons, 1994; Johannesson et al. 1994).

Due to the low solubility of REE-phosphate, precipitation and co-precipitation of REE phosphate are important processes for REE attenuation in seawater and neutral to alkaline terrestrial water with quite high concentration of phosphate (Zhu et al. 2006; Lewis et al. 1998; Johannesson et al., 1995; Byrne and Kim, 1993). REE-phosphate co-precipitation results in mixed REE phosphate precipitates. A very small proportion of formed REE phosphate complexes can result in alkaline waters saturated with freshly formed precipitates

and co-precipitation of REE phosphate and lead to REE settled from total water phase as REE-phosphate salts. But phosphate cannot outcompete carbonates for REE in water phase, phosphate complexes is normally not an important REE species compared to REE carbonate complexes in alkaline waters (Johannesson et al. 1995; Johannesson et al. 1994). When the precipitation and co- precipitation of REE phosphate occurs, enrichment of HREE will be observed in water as the LREE phosphates are less soluble than the HREE phosphates (Byrne and Kim, 1993; Firsching and Brune, 1991).

Although the carbonate concentration in neutral to alkaline water is normally quite high and REE carbonate complexes are normally the dominant species in water, the formation of REE carbonate precipitates is expected to be negligible and the removal of REE by the precipitation of REE carbonates in natural neutral to alkaline waters is unlikely (Johannesson et al. 1995). This is because elevated carbonate in neutral to alkaline water complexes with REE to form stable REE-carbonate/dicarbonate complexes and consequently REE remain in the water phase rather than being removed (Johannesson and Lyons, 1994; Johannesson et al, 1994). The formation of carbonate precipitates or co-precipitation [e.g. $Ln_2(CO_3)_3 \cdot nH_2O$] will only occur in waters with very high REE concentrations and also high pH and carbonate concentrations (Tang and Johannesson, 2010b).

Johannesson et al. (1995) mentions that precipitates of both REE sulphates and REE carbonates are normally extremely undersaturated in alkaline waters.

2.5 Chapter summary

- There are no large occurrences of REE-bearing minerals with economic potential in the UK. Some relatively minor REE resources occur in central Wales, south west England, north-west Scotland, British Tertiary Igneous Province, and the Alston Block of North Pennines.

- The eco-toxicity of REE are generally lower than that of the other heavy metals, such as Cd and Pb. Nevertheless, the limited experimental data available suggest that REE may have toxic effects on plants, animals and humans at high concentrations. Relevant environmental regulations and standards have not set the threshold values for REE emissions to the environment. Only La has a suggested threshold value of 4μg/l for water and 36.9mg/kg for sediment (Herrmann et al., 2016).

- The mobility of REE progressively decreases with an increase of pH. The possible reasons for the decreased mobility at higher pH are: (1) the adsorption of REE onto suspended Fe, Al, Zn, Mn oxyhydroxides and/ or secondary Fe, Al, Zn, Mn oxyhydroxides; (2) co-precipitation of REE with the precipitation of Fe, Al, Zn, Mn oxyhhydroxides; (3) precipitation or co-precipitation of REE bearing phases.

- There is a steady decrease of REE ion radius with the increase of atomic number from La to Lu, which is called the lanthanide contraction. The lanthanide contraction is the root cause of the slightly varying geochemical behaviour across the REE group.

- REE fractionation in terrestrial water components can be shown by normalizing actual measured REE concentration to that in the reference materials, such as PAAS, NASC, mean shales and chondritic meteorites. Shales are more suitable to be used for samples with felsic source rocks, while chondrites can be used as the normalization reference material when the source rocks are mafic and ultramafic.

- Source- related processes have the dominant control on REE fractionation when the normalized REE distribution pattern in the dissolved and corresponding (suspended) solid phase is similar to that in the whole parent rocks.

- In-stream processes have a major control on REE fractionation when the normalized REE distribution pattern in the dissolved and corresponding (suspended) solid phase is largely different.

- The solution chemistry-related fractionation of REE is controlled by pH, Eh, ligands concentrations in water and the composition of REE scavenging materials.

Chapter 3 Methodology

3.1 Introduction

The detailed description of routine sampling sites at Gate Gill study site which mentioned in Chapter 1 is shown in Section 3.2. The following Section 3.3 details the field methodology employed at those selected sampling sites, including *in situ* measurement of water chemical parameters; water samples collection and flow measurement. Ultrafilter the collected water samples and laboratory analysis of samples by inductively coupled plasma optical emission spectrometry (ICP-OES), inductively coupled plasma-mass spectrometry (ICP-MS) and Ion Chromatograph (IC) are demonstrated in Section 3.4, and the quality of the laboratory obtained data is then assessed in Section 3.5. It needs to note that this chapter only describes the general analysis method of ICP-MS, a detailed methodology development for ICP-MS interference correction is illustrated in Chapter 4. The speciation calculations applied on either the ultrafiltered or 0.1 μm filtered water samples are detailed in Section 3.6. The standard used for normalizing REE in samples is noted in Section 3.7. The traditional meaning of source-related fractionation and the meaning of source-related fractionation in this study is described in Section 3.8.

3.2 Sampling sites at Gate Gill study site

Global Positioning System (GPS) with spatial reference to British National Gird coordinates and photographic record were used to locate each sampling site (G1-G7) at Gate Gill study site that mentioned in Chapter 1, in order to precisely revisit all sampling sites. The accuracy of the GPS is up to ±3m. Description of each sampling site was demonstrated in Table 3.1 below.

Table 3.1 Routine monitoring sites at Gate Gill study site

Site symbol in Figure 3.1	Site name	OS Grid reference	Flow measurement
G1	Gate Gill upstream Woodend mine water	NY 32516 26144	--
G2	Woodend mine water	NY 32518 26136	--
G3	Gate Gill downstream Woodend mine water	NY 32566 26002	Salt gauging
G4	Gate Gill at Threlkeld	NY 32574 25535	Salt gauging
G5	Gate Gill upstream confluence with River Glenderamackin	NY 32481 25118	Salt gauging
G6	River Glenderamackin upstream Gate Gill	NY 32567 25067	Stage-discharge
G7	River Glenderamackin at Threlkeld gauging station	NY 32260 24795	Salt gauging

The feasibility for undertaking flow measurement is a major consideration on sampling site selection, as the flowrate data at each sampling site is the base for obtaining the fluxes trend of metals in-stream in order to understand the REE behaviours. However, flowrate measurement was not undertaken at the upstream of mine discharge (G1) as no method is suitable for measuring the flow at G1 due to its topography. To be more specific, it is not suitable for using the bucket and stopwatch method to measure the flow directly from the pipe due to the large amount of water draining from pipe each second. In addition, the short distance between the pipe and the next sampling point- Woodend mine water (G2), and the big pool below the pipe make salt gauging method not appropriate to be adopted at G1. But G1 has to be chosen as the mine discharge upstream sampling site since the next further upstream site that can take samples is far from mine drainage and not suitable to be the blank control to show how the mine discharge affects its downstream water quality.

Flow data was not recorded at G2, although there is a sharp-crested V-notch weir at G2 that can measure the mine discharge flow rate. However, the build-up ochre in the mine drainage receiving v-notch weir induces the v-notch weir drowned during sampling period of this study and an accurate flowrate was therefore not able to obtain. In addition, the water flowing from the pipe is too fast to be measured accurately by the bucket and stop-watch method.

Salt gauging method was adopted at the three downstream sampling points (G3, G4, G5) of mine discharge on Gate Gill on most sampling occasions and at the upstream of Gate Gill confluence with River Glenderamackin (G6) on the first sampling event. It needs to note that sampling was not continued undertaking at G6 after the first two times fieldwork. This is because it is not suitable to use either salt gauging or velocity-area method to measure the flow at such a big river like River Glenderamackin.

It should be noted that ideally the sampling point in the Gate Gill immediately downstream (G3) of the Woodend low level mine water discharge would be just below the mixing zone. However, the recently renovated “yellow dam” is approximately 75m downstream of the mine water discharge point, which causes the Gate Gill to form a deep pool at the point where it would be best to monitor flow and water quality, as can be seen from Figure 3.1. The large pool in the Gate Gill downstream of the mine discharge made this location inappropriate for salt injection (see Section 3.3.3 for salt dilution method). In order to obtain a suitable reach

for undertaking flow measurement, the sampling point of G3 was therefore selected at downstream of the dam.

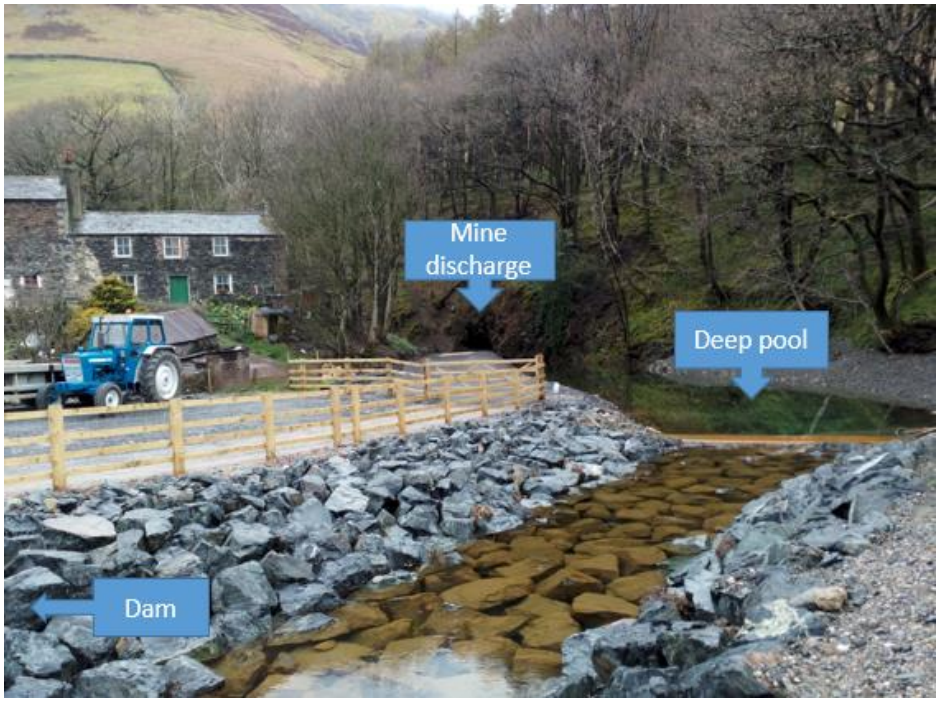

Figure 3.1: Large pool area between the dam and the confluence point of mine discharge and Gategill Beck (photo taken on 13/04/2016)

The downstream sampling point of Gate Gill confluence was located at G7 where Environment Agency gauging station are present as the gauging station has good access facility and routine flowrate could be obtained safely. No other sampling sites were selected between G5 and G7 although the pH increased directly from less than 5 at G5 to above 6 at G7 on many sampling occasions and there was not a good pH gradient from G5 to G7 on such sampling occasions. Since it is better to have a nice pH gradient particularly between the value of 5 (when REE starts to attenuate) and 6.5 (when REE are mostly removed from the water phase) in order to demonstrate the behaviour of REE during the progressive removal from dissolved phase process (Verplanck et al., 2004). But Gate Gill has much smaller volume of water than River Glenderamackin which with a near neutral pH on these sampling occasions, and pH will be increased immediately at the confluence. A pH measurement was undertaken on 13rd October, 2016 at where Gate Gill just confluence with River Glenderamackin, however the pH of the water was very similar to that of G7. Also, it is better to take sample at place with a distance from the confluence to obtain a well-mixed river water sample.

3.3 Fieldwork

The fieldwork includes water sample collection and flow measurement, the collected water samples were used for water quality analysis including *in situ* and lab work data collection. To be more specific, *in situ* data collection was to record water quality data that can only be recorded accurately *in situ*; lab work data collection was to obtain the concentration of total metal, filtered metal and anions in samples. The fieldwork process follows British Standard ISO 5667-1: 2006 "Water quality- Sampling- Part 1: Guidance on the design of sampling programmes and sampling techniques" and British Standard ISO 5667-6:2016 "Water quality — Sampling Part 6: Guidance on sampling of rivers and streams". The measured flow data was used along with metal concentrations to show metals flux trend in-stream.

3.3.1 In situ *measurement of water sample parameter*

In order to keep the accuracy of measured results and prevent any degradation or changes of samples occurring during transportation, some chemical parameters of river water: pH, temperature, conductivity, Eh (oxidation reduction potential) and alkalinity were measured *in situ*.

The Ultrameter, Model 6P II, produced by Myron L Company with two probes which can measure the pH, temperature, conductivity and Eh of river water was used to display digital readings. These water parameters were measured at the same place where water samples were collected.

Measured Eh value was converted to pe value by the equation below (Appelo and Postma, 2005) and then input in PHREEQC in order to calculate the speciation of redox element:

$$pe = \frac{F}{2.303RT} Eh$$

where: F = Faraday Constant = 96.42 kJ/volt gram equivalent;

R = universal gas (molar) constant = 8.314x10-3 KJ/deg/mol;

T = temperature in Kelvin (Kelvin = oC + 273.15)

Alkalinity of river water was determined by using a Hach Digital Titrator, Model AL-DT, which involves titrating 100ml of water sample with 0.1600N sulphuric acid and using bromcresol green/methyl red as an indicator which can identify a colour change from green to

permanent pink at endpoint of pH 4.5. The digits of alkalinity provided on titrator is the alkalinity when use 1.600N sulphuric acid to titrate the samples. As 0.1600N sulphuric acid was used in the titrations, the alkalinity in water samples was 0.1 times the reading provided on the screen of titrator, with a unit of mg/l $CaCO_3$. The reason for using 0.1600N sulphuric acid instead of 1.600N sulphuric acid for all sampling sites is that samples collected have lower alkalinity, so using 0.1600N sulphuric acid in practice could obtain more accurate results. The alkalinity was measured immediately after sample retrieval, to avoid carbon dioxide degassing (Appelo & Postma, 2005). Table 3.2 below shows the units of in situ measured water parameters and accuracy of the measurement equipments.

Table 3.2: Summary of Summary of in situ measured sample parameters

Parameter	Unit	Analysis machine	Accuracy of measurement (±)	Comments
pH	---	Ultrameter, Model 6P II, Myron L Company	0.01	
Conductivity	µS/cm		0.01	
Temperature	°C		0.1	
Eh (Oxidation reduction potential)	mV		1	
Alkalinity	mg/l CaCO3	Hach Digital Titrator	---	Multiplied digits by 0.1 to obtain the sample alkalinity as 0.1600N sulphuric acid was used

The measured alkalinity equals to the carbonate ions concentration (HCO_3^- and CO_3^{2-}), although the alkalinity means the equivalents number of all dissociated weak acids in water, other weak acids except carbonate species are quantitatively negligible. As pH in the samples were all below 8.3, no more than 1% of the carbonic acid is present as carbonate, the contribution to alkalinity is initially assumed from bicarbonate only. The bicarbonate concentration then equals to 1.2192 times the measured alkalinity concentration with a unit of mg/l $CaCO_3$ (Appelo and Postna, 2005). The figure 1.2192 is the ratio of the equivalent weights of HCO_3^- to $CaCO_3$. The alkalinity in the unit of mg/l HCO_3^- was then inputted into PHREEQC along with other chemical parameters of each modelled sample for determining the amount of REE bicarbonate complexes and REE carbonate complexes in samples to understand the REE distribution pattern.

Ideally, the ultra-filtered water sample should be used for the alkalinity measurement in order to obtain the concentration of carbonate species in truly dissolved phase. As it is not able to

do the ultrafiltration in the field, the alkalinity of the water filtered through 0.1μm filter was regarded as the alkalinity in truly dissolved phase and then compared with the alkalinity in unfiltered water sample to test whether some of carbonate species are present in colloids and particulates. Four fieldwork tests have been undertaken at G7, covering the flowrate from low to high condition. No tests were undertaken at other sampling sites since their pH are all below ~5, and both carbonate and bicarbonate are not the dominant species complexing with REE in this pH range, as noted in Section 2.4.4. After the comparison, the alkalinity differences between unfiltered water sample and the 0.1um filtered water sample were all less than 0.5 mg $CaCO_3$/l. These tiny differences indicate that the carbonate species in colloids and particulates were negligible. So the calculation of carbonate species concentration were based on the alkalinity in unfiltered water samples.

3.3.2 River water sampling

Water samples were collected (by a sampling pole when the flowrate was high) from a flowing section as close to the centre of stream to be as representative as possible of the sampling stream.

For the first 6 times sampling occasions at Gate Gill study site, three cation water samples – total, 0.45 μm filtered, 0.1 μm filtered water samples were collected at each sampling site for metal analysis by using 30ml polypropylene bottles. Total water sample is unfiltered water sample for metal analysis, which includes the concentration of dissolved metals and metals bound in the particulate fraction. The 0.45 μm filtered water sample is water filtered through a 0.45 μm pore-size membrane, which includes the REE and other metal concentration in both dissolved and colloidal phase. The 0.1 μm filtered water sample is water filtered through a 0.1 μm pore-size membrane, which includes the REE and other metal concentration in both dissolved and very fine colloidal phase. A separate, inacidified sample for anions analysis was collected at each sampling site in using 30ml polypropylene bottle. Anion samples were filtered through 0.2 μm filter before injecting into the Ion Chromatography equipment used to measure the anion concentrations.

For the last 7 monitoring campaigns at Gate Gill study site, another 2L water sample was also collected using clean 1L polypropylene bottles at each sampling site besides total, 0.45 μm filtered, 0.1 μm filtered water, anion (0.2 μm filtered) samples. The 2L water sample was then filtered through a 10 KDa molecular-weight membranes (0.005 μm equivalent pore size)

in the laboratory. Unlike the 0.1 µm pore-size membrane, the 10 KDa membrane can prevent the very fine colloids in the size range of ~0.005 to 0.1 µm passing through the membrane. The ultrafiltrates can represent the truly dissolved metal and anion concentrations (Alpers et al. 2000). The ultrafiltrates used for analysing anion was not acidified and the analysed results were anions in truly dissolved phase. This ultrafiltered anion results were compared with the results from 0.2 µm filtered anions to see whether some anions were present in the colloidal phase.

All cation samples were acidified in the laboratory prior to analysis with Merck ultra-pure concentrated nitric acid (60%) and Merck ultra-pure concentrated hydrochloric acid (30%) or Fisher chemical optima grade concentrated hydrochloric acid (32-35%) to form 2% v/v nitric acid and 1% (v/v) hydrochloric acid in samples. Acidification lowers sample pH to less than 2 which prevents any adsorption or precipitation of metals during storage. Samples were then stored at 4^{o}C until analysis. Fisher chemical optima grade concentrated hydrochloric acid (32-35%) was used between October, 2016 and April, 2017 as Merck one was out of stock during that period.

It should be noted that for the first 6 sampling occasions, the metals results from 0.1 µm filtered samples were used for the speciation calculation, while ultra-filtered samples results were used instead for the last 7 times samplings. The errors of REE speciation results caused by using 0.1 µm filtered metals concentrations instead of ultra-filtered metals concentrations for the first 6 times fieldwork are expected to be quite small. This is because REE speciation results obtained by using the 0.1 µm filtered metals concentrations is similar as that obtained by using ultra-filtered metals concentrations for the last 7 times fieldwork. The detailed results and discussions are shown in Section 6.2.

The location of water sample collection used for water quality analysis at three downstream sites on Gate Gill was taken place at the downstream point where the conductivity probe was placed to record the measured flow rate in order to analyse the fluxes of metal in that specific location. At each of these three sites, beside the location of collected water sample used for water quality analysis, another location of water sample collection used for calibrating the value k was at the upstream where the salt solution was injected for measuring flow. All water samples at these three downstream sampling points were collected before pouring the salt solution.

3.3.3 Flow measurement

Adopting the salt gauging method at G3 to G5 is due to the irregular channel cross-section and the discontinuous, turbulent flow at downstream of the mine discharge on Gate Gill (G3 to G5). Herschy (2009); Moore (2004a); Day (1977) and Elder *et al*. (1990) all note that the salt dilution method is the most appropriate and satisfactory method to measure the flowrate in mountain or upland stream with turbulence flow, high gradient, bouldery, rock-strewn shallow channel. And the velocity-area method is only suitable to be adopted at site with a well-defined channel with low turbulence (Hiscock, 2005).

In this study, the procedure detailed in BS 3680-2A (1995) was followed when undertaking the salt dilution gauging at G3 to G5. In summary, a salt solution with a known concentration and volume was injected into the stream at the selected upstream point which is also the beginning of the flow measurement reach. The conductivity in stream was recorded at the selected downstream point where the injected salt solution can mix with stream water uniformly (the place that water samples were collected). The conductivity meter was used to record the EC changes in stream at each 2s interval from the background level until the entire tracer wave had passed the recording point. The calibration value used to obtain the discharge value, was determined in the laboratory.

In situ conductivity recording

The conductivity meter was placed at the selected recording point first before the salt solution was injected into the stream to record the background conductivity and water temperature at G3 to G5. The conductivity probe was placed in the main flow of the channel and away from the turbulent areas to ensure that air bubbles did not get entrained through the probe, since the air bubbles can result a temporary decrease in conductivity.

The selected salt solution injection point for performing the salt dilution gauging of G3 was at the dam itself, where the flow is quite turbulence. The selected salt solution injection point for G4 and G5 has a constricted flow, where flow narrows down channel because of the surrounding boulder. The narrow channel and turbulent flow at injection point of G3 to G5 can promote a rapid mixing between the injected salt solution and stream water in lateral dimension. The salt solution was injected instantaneously at the centre of channel (which is also the main flow part) without cause splashing of the stream water.

The length between the salt solution injection point and the conductivity recording point at each sampling point of G3 to G5 was around 25 times the channel width, which is sufficient to allow complete mixing between the salt solution and stream water occurring in lateral dimension (Day, 1977). After the complete mixing in lateral dimension occurs, the discharge measured at any point of the cross-section (the conductivity recording point) is then the same. Since the vertical mixing is faster than that lateral mixing, the complete mixing length in lateral dimension is therefore the complete mixing length required for salt solution uniformly mixing with stream water (Spitzer, 1991; Day, 1977). Figure 3.2 below shows the change of salt wave from injection point to where lateral mixing completes, from alteration of longitudinal, lateral dispersion and the peak concentration/ conductivity aspects.

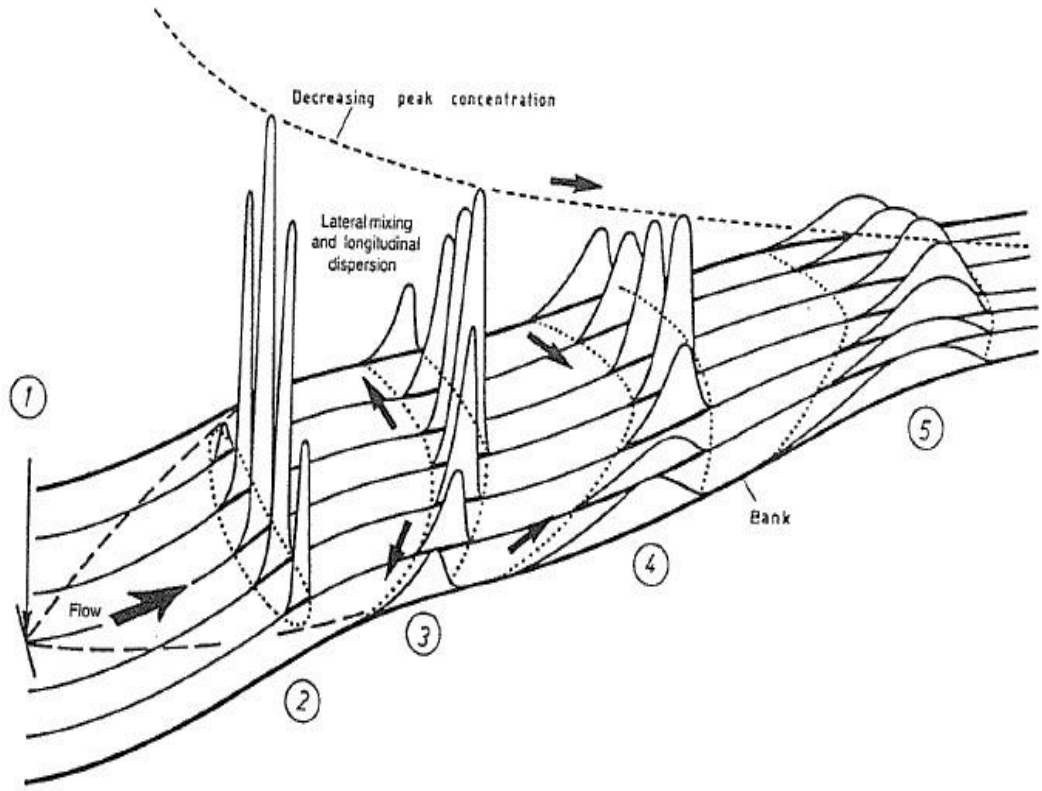

Figure 3.2: The salt solution mixing model from injection point to lateral mixing complete for a slug injection (Benischke and Harum, 1990)

Annotation: (1) Upstream injection point; (2) The distribution of salt wave just downstream the injection point; (3) The moment when salt just reach the channel banks; (4) subsequent mixing in lateral and longitudinal dimension during backward flow direction from banks to channel centre; (5) Complete mixing in lateral dimension.

The mixing length depends on several factors, like channel width, depth and morphology, mean velocity of water of channel cross-section and injection location (Spitzer, 1991; Day, 1977). The channel width of a stream is the most important factor that can influence the mixing length. A distance between the injection point and conductivity recording point longer than the theoretical mixing length (25 times the channel width) is not suggested by several authors. Because a longer distance will induce more longitudinal dispersion and increase the error induced by the tracer loss (Dingman, 1994; Day, 1977).

The peak conductivity value recorded during the salt wave passing by needs to be suitably higher than the stream background conductivity, which can then minimize the error caused by the tracer loss and ensure providing an accurate flow result (Elder et al. 1990). The EC increased degree (for the peak) relative to background as salt wave passing by depends on the salt solution concentration, the injection volume of salt solution and the stream mixing characteristics which may vary with flow condition and channel morphologies. With the consideration of the solubility of salt in water, 7L of water is required for dissolving each 1kg of salt when making the salt solution. An additional 0.32L is generated after dissolving 1kg of salt in 7L of water.

It should be noted that there is a large pool at the bottom of the spillway, which is unavoidable when selecting the reach to perform the salt dilution at G3 (Figure 3.3). The pool within the reach can cause losses of tracer during measurement. To be more specific, the salt can be retained in the pool areas with only slow release to the flowing portion of the stream. This may significantly increase the time required for measurement, to ensure all salt has passed the recording point (Moore, 2005). This can also increase the longitudinal dispersion of the salt wave, lower the peak EC and lead to a higher degree of tracer loss. To reduce the measurement error that can be caused by having a large pool within the reach of G3, a larger volume of salt solution (2kg salt in 14L stream water) was injected into the stream at G3 to increase the peak EC to a higher level above the background EC. This can reduce the influence of increased longitudinal dispersion of the salt wave and to some degree to mitigate against tracer loss due to the pool, and increase the accuracy of the salt dilution method (Elder *et al*. 1990). In addition, it should also be noted that some of the water from the injection point at the dam appears to flow in the subsurface (under the dam) (Figure 3.3). The water leaching from the dam causes some unavoidable tracer losses, this may lead to some errors of calculated flowrate at G3.

At G4 and G5, there is no large pool or backwater existing within the reach selected for performing salt dilution at G4 and G5, and the channel within the reach is narrow. A small volume of salt solution (1kg salt in 7L stream water) was normally injected into stream when measuring flow at G4 and G5.

Because 60ml of salt solution was extracted in situ and used for calibration (described in more detail in the following section), the injected volume of salt solution used for calculating the flowrate is the volume of the stream water used for mixing the salt plus the additional volume that generated by the salt, minus the extracted 60ml of salt solution used for calibration.

Figure 3.3: Gate Gill physical characteristics at partial mixing reach of G3 (photo taken on 27/10/2016)

Obtaining calibration k value in the laboratory

For the purpose of obtaining calibration value k, at each sampling site of G3 to G5:

1. two 30ml samples were extracted from the prepared salt solution before injecting the salt solution into the stream and preserved in glass bottles to avoid the salt absorbing onto the surface of plastic wall;

2. two 1L samples of stream water were collected from the conductivity recording point.

These samples were preserved under the same conditions as other samples during transport and then preserved in a dark cold room with a temperature of 4°C before doing the calibration in laboratory.

The method of Moore (2004b) was used to determine the calibration value in the laboratory. Firstly, a secondary solution was created by mixing 500ml stream water with a certain volume of salt solution. As the secondary solution is used for mixing with the stream water collected in the field to generate a series of conductivity that covers the recorded conductivity range during the salt wave passing by period in the field. The volume of salt solution used for making secondary solution depends on the recorded peak EC in the field. The relative concentration of secondary solution equals salt solution volume used for making the secondary solution dividing by the volume of secondary solution (which is the sum of 500ml stream water and salt solution volume used for making the secondary solution):

$$RC_{sec} = \frac{\text{Salt solution volume used for making the secondary solution}}{\text{Volume of secondary solution}}$$

Secondly, 900L of stream water was injected into the calibration bottle and the conductivity probe was placed in the bottle to record the conductivity of stream water. The recorded value was set as the initial EC which corresponds to an initial relative concentration of solution of zero. After that, known increments of created secondary solution were injected into calibration bottle successively to generate a series of relative concentration values corresponding to different conductivity values in the calibration bottle. The conductivity value finally generated in calibration bottle was ensured to be higher than the peak EC recorded in the field.

The relative concentration of solution in calibration vessel after each injection of secondary solution can be calculated as below:

$$RC = \frac{RC_{sec} \sum y}{(V_c + \sum y)}$$

Where: The RC_{sec} is the relative concentration of secondary solution;

$\sum y$ is the cumulative volume of secondary solution injected into the calibration tank;

V_c is the volume of stream water in the calibration tank, which should be 900mL here.

Then, these generated relative concentration values (y axis) against their corresponding EC values (x axis) in calibration tank were plotted in a graph (calibration curve of G5 on sampling date-10/11/2016 is shown in Figure 3.4 as an example). The slope of every two successive points was the calibration factor achieved from each injection of secondary solution. The averaged slope value was used as the calibration value to calculate the discharge at G3 to G5.

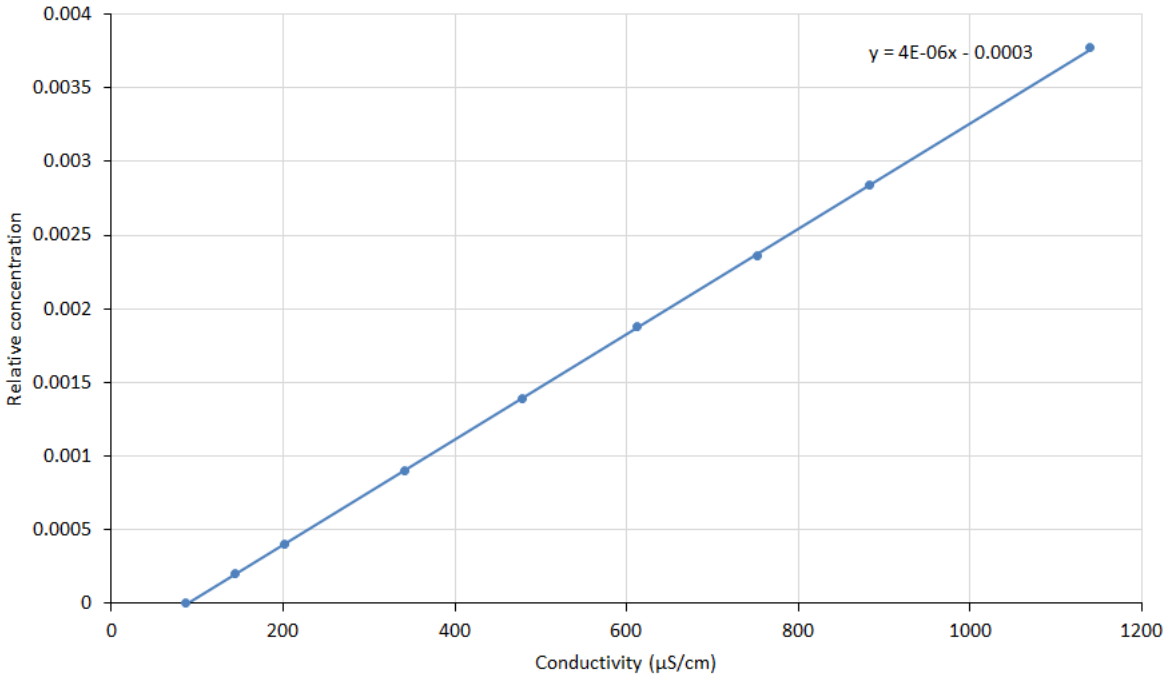

Figure 3.4: Calibration curve obtained for G5 on sampling date of 10/11/2016

Calculate flowrate at sampling site

The discharge calculation including the effect caused by the injected salt solution volume can be calculated from the following formula, based on the principle of mass balance (Moore, 2005):

$$Q = \frac{V}{k\Delta t \sum_{n} [EC(t) - EC_{bg}]}$$

Where: Q is the discharge including the effect caused by the injected salt solution volume (L/s);

V is the salt solution volume that injected in upstream;

k is the calibration constant value;

EC_{bg} is the background electrical conductivity in stream, EC (t) is the electrical conductivity at time t;

n is the times that diver detect the EC during the period that salt wave passing through;

Δt is the interval that diver measure EC, and it was 2s for the diver used in this study

In addition, the additional flow rate caused by the injected volume of salt solution was subtracted from the calculated flow rate to receive the stream flow rate.

3.4 Laboratory work

Details of the laboratory work includes the ultrafiltration procedure (Section 3.4.1), and analysis of cation and anion concentrations by ICP-OES and ICP-MS (Section 3.4.2), and IC (Section 3.4.3) respectively.

3.4.1 Ultrafiltration

Tangential ultrafiltration of water samples was undertaken on the last six field work visits to obtain the operationally defined truly dissolved phase. Sartorius Vivaflow 200 crossflow cassette with 10kDa molecular weight cutoff (MWCO) polyethersulfone (PES) membrane (~0.005 µm equivalent pore size) was employed for sample ultrafiltration. 10kDa MWCO membrane was chosen as its pore size is proven to be the most suitable one to produce the truly dissolved concentrations (Alpers *et al*. 2000). Sample was pumped by the peristaltic pump to pass through the ultrafilter and the ultrafiltrate was collected subsequently. The separation between filtrate and retentate were induced by the system back pressure which is generated from the flow restrictor at the retentate tubing. The system was set up as shown in Figure 3.5.

The system was pre-cleaned before doing sample ultrafiltration by first pumping deionised water through the ultrafilter until 400ml of filtrate had been collected. 1L of 1% HCl solution (AnalaR grade of concentrated HCl in deionised water) was then pumped through the ultrafilter to remove any metal contamination in the system from previous operations. After this, 1L 10mM EDTA Na salt solution (in deionised water) was then pumped through as an extra rinsing solution to bind any remaining metal (complexes) contamination residues in the systems (Croot, 2016). The system was finally rinsed with deionised water to wash out the HCl and EDTA Na salt solution remaining in the system. The system was then ready for the ultrafiltration.

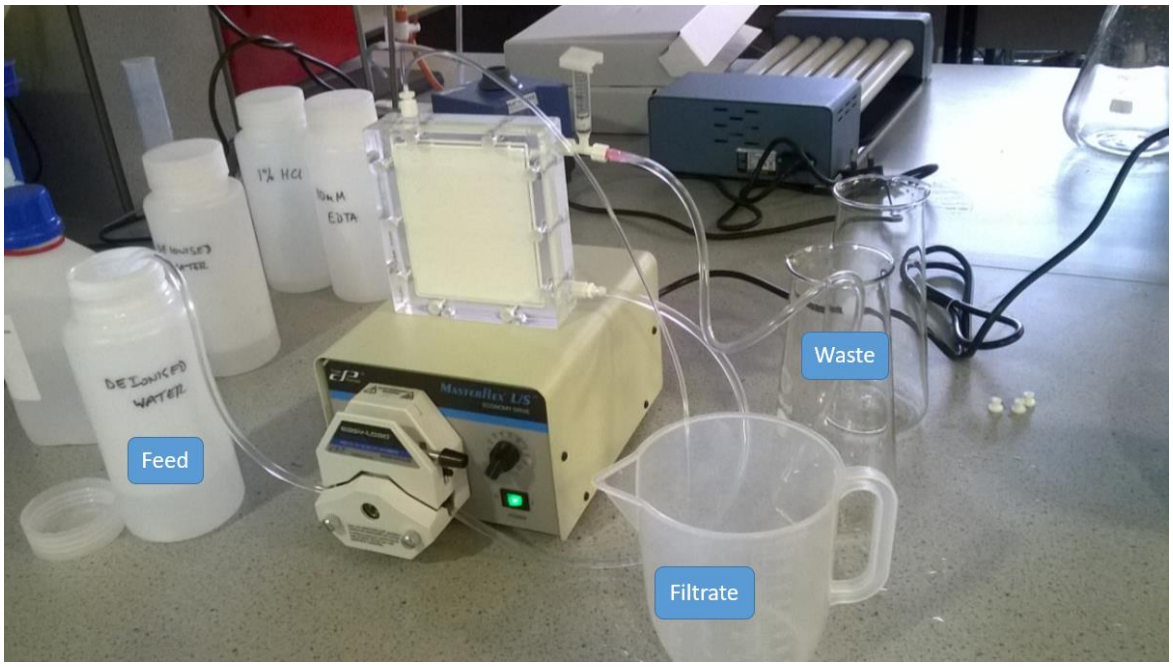

Figure 3.5: Sartorius vivaflow 200 ultrafiltration system

2L of each sampling site sample was pumped through the system one by one in the order of least contaminated to the most contaminated and only the filtrate from the last 400ml of each sampling site sample was collected as the ultrafiltered metal sample and anion sample. Deionised water was pumped through the system between different sampling sites samples to clean the system and avoid the cross-contamination during sample ultrafiltration. The operating condition of ultrafiltration system during pre-cleaning and subsequent ultrafilteration period is shown in Table 3.3.

Table 3.3: Vivaflow 200 operating condition during cleaning period before sample ultrafiltration and sample ultrafiltration period

Operating conditions	
Retentate flow rate	250 ml/min
System back pressure	2.25 bar
Pump dial reading	5-5.5

As mentioned in Section 3.3.2, the ultrafiltered metal sample was then acidified with 6 drops of ultrapure concentrated HNO_3 (Merck) and 3 drops of ultrapure concentrated HCl (Merck/ Fisher chemical) to form 2% HNO_3 and 1% HCl in sample. Ultrafiltered anion samples were not acidified and analysed directly by IC.

For the reuse purpose, the ultrafilter was cleaned after doing the ultrafiltration for each time fieldwork samples. The ultrafilter was first flushed by the deionised water to wash out the sample water remained in the system. The system was then recirculated with 0.5M NaOH at pump flow rate of 80 ml/min for 40 minutes to remove the particles remained in the ultrafilter from sample ultrafiltration. NaOH was then drained from the system and the system was recirculated with deionised water at flow rate of 80 ml/min for 10 minutes. The system was drained and cleaned again by flushing with the deionised water. Ultrafilter was then reserved by filling with 10% ethanol and refrigerating at 4^{o}C to prevent the bacterial growth before next time usage (Sartorius, 2016). The operating condition of the ultrafiltration system during this cleaning period was shown in the following Table 3.4.

Table 3.4: Vivaflow 200 operating condition during cleaning period after ultrafiltration

Operating conditions	
Pump flow	80 ml/min
System back pressure	2 bar
Pump dial reading	1.5

3.4.2 Cations analysis

Cation analysis was undertaken in the laboratory of Devonshire Building, Newcastle University. Cations were analysed within one month of sample collection by Inductively Coupled Plasma-Optical Emission Spectrometer (ICP-OES) and Inductively Coupled Plasma-Mass Spectrometry (ICP-MS). To be more specific, cations with concentration more than 100ppb were measured by ICP-OES, while cations with concentration less than 100ppb were measured by ICP-MS.

ICP-OES

The concentrations of 18 analytes were determined by ICP-OES on ultrafiltered, 0.1 µm membrane filtered, 0.45 µm membrane filtered and unfiltered water samples. The analytes were: calcium, magnesium, sodium, potassium, zinc, lead, aluminium, iron, manganese, cadmium, nickel, copper, arsenic, chromium, barium, strontium, silicon, sulphur. The procedure of the analysis follows that described in BS ISO 11885: 2009. The selected wavelengths of each element used for analysis have minimal spectral line overlap from other elements. After analysis, the elements with concentration less than 0.1ppm were analysed

again by ICP-MS to obtain more accurate results as ICP-MS is more suitable for analysing elements with lower concentration.

A calibration blank which contains 1% (v/v) HNO_3 and three calibration standards each containing certain amount of analyte in a 1% (v/v) HNO_3 matrix were used to calibrate the instrument prior to sample analysis. The calibration blank was made up from traceable grade concentrated nitric acid (69%) (Fisher Scientific) and 18.2Ω MilliQ deionised water, using glass volumetric flask. Each calibration standard was made up from VWR/ Fisher Scientific/ Merck 1000mg/l single element stock solutions (traceable to NIST), traceable grade concentrated nitric acid (69%) (Fisher Scientific) and 18.2Ω MilliQ deionised water, using glass volumetric flask. Calibration blank and standards were prepared monthly and stored in polypropylene bottles at 4ºC. The concentration of the three standards used for each element are shown in Table 3.5.

Table 3.5: Metal concentrations of ICP-OES calibration standards

Element	Symbol	Std 1 (mg/l)	Std 2 (mg/l)	Std 3 (mg/l)	Detection limit (mg/l)
Calcium	Ca	10	20	30	0.03
Magnesium	Mg	5	10	15	0.05
Sodium	Na	5	10	15	0.002
potassium	K	10	20	30	0.1
iron	Fe	2	4	6	0.005
Manganese	Mn	2	4	6	0.003
Aluminium	Al	2	4	6	0.06
Zinc	Zn	2	4	6	0.005
lead	Pb	0.2	0.5	1	0.02
Copper	Cu	0.2	0.5	1	0.008
Arsenic	As	0.5	1	2	0.2
Cadmium	Cd	0.1	0.2	0.3	0.004
Nickel	Ni	0.2	0.5	1	0.01
Chromium	Cr	0.1	0.2	0.3	0.01
Barium	Ba	0.2	0.5	1	0.003
Strontium	Sr	0.2	0.5	1	0.01
Sulphur	S	30	50	100	0.7
Silicon	Si	5	10	15	0.05

Samples were diluted appropriately (2 times, 5 times and 10 times) with 1% (v/v) HNO_3 where necessary to keep the analyte concentration within the calibration range. Calibration standard 2 was measured after every nine sample measurements to ensure no instrument drift influenced the analytical accuracy and precision of measurement. The instrument was recalibrated when the measured concentration of standard 2 was not within a deviation of 5% the standard 2 known concentration. The precision of the instrument was ensured by

analysing individual samples in triplicate. The repeatability of the machine was determined by measuring the reference sample several times under the same operating condition.

Samples were measured in the order from the least contaminated to the most contaminated to avoid cross-contamination. A blank sample of 1% (v/v) HNO_3 was used each time after instrument drift check to avoid the standard 2 contaminating the following sample measurement.

The quantitative detection limits of the instrument were calculated as 10 times the standard deviation for each analyte (measured at the same wavelength as that used for sample measurement) of 10 calibration blank replicates. The detection limits of the instrument are also described in Table 3.2. For the measured element result below the detection limit, half of the detection limit was used as the concentration of that element (Cidu and Biddau, 2007).

ICP-MS

Both the filtered and unfiltered water samples were normally measured twice by Agilent 7700x ICP-MS, once for the REE analysis, and once for the environmental elements with concentration less than 0.1ppm, as determined via ICP-OES analysis. The ICP-MS analytical procedure is that of BS ISO 17294-1:2006 and BS ISO 17294-2:2016. The obtained environmental elements results from ICP-MS were subsequently used to replace that values obtained from ICP-OES. As ICP-MS has much higher sensitivity and lower detection limit than ICP-OES, it is capable of detecting elements at low concentrations and provide more accurate results for them.

The principle of determining analytes in sample is to nebulize the sample solution and introduce the fine resulting aerosol droplet by argon gas into the plasma torch. The high temperature in the plasma induces the desolvation, decomposition of the aerosol droplets and the analyte species are then atomized and ionized by removing one electron from each atom. The ions from the plasma are extracted to pass through a vacuum system with integrated ion optics and then separated by the mass spectrometer based on their mass-to-charge ratios and detected by the electron multiplier (EPA, 6020A). Figure 3.6 below demonstrates the ICP-MS principle components.

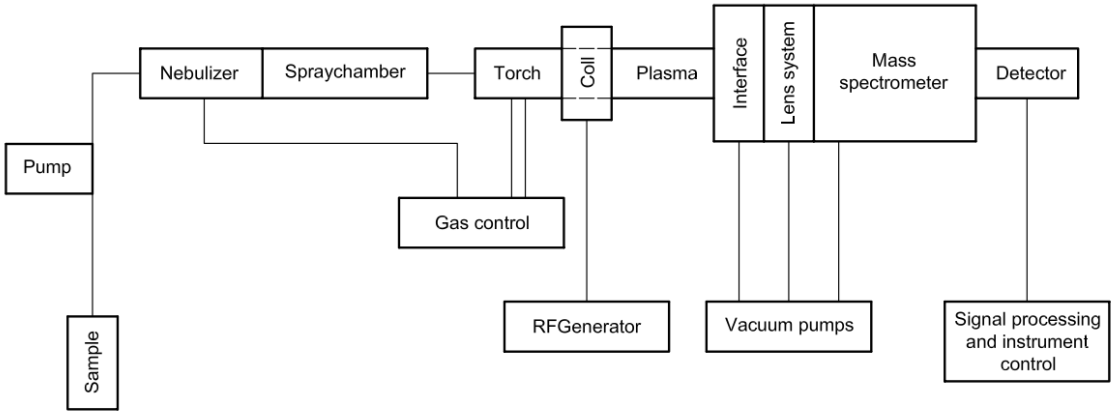

Figure 3.6: ICP-MS components diagram (British Standard ISO 17294-1:2006)

Spectral interference from polyatomic ions can lead to non-analyte peak in the mass spectrum and is the main problem that influences the accuracy of results (Agilent Technologies, 2005). Octopole Reaction System (ORS) that operates in both normal/no gas mode and Helium (He) gas mode was applied during analysis, with the latter one used for reducing the isobaric polyatomic interference on analytes. While the result from normal mode is the sum of both the analyte and interfering ions. The operating conditions of the ICP-MS during this work are shown in Table 3.6.

Table 3.6: 7700x ICP-MS operating conditions

Plasma parameters	
RF power	1550W
Carrier gas flow	1.05L/min
Nebulizer pump	0.1rps
Sampling depth	8mm
Sample uptake rates	0.4ml/min
Internal standard uptake rates	0.02ml/min
Plasma mode	Low matrix
Cell parameters	
He flow	4.3ml/min
Energy Discrimination	3V
Acquisition settings of mass spectrometer	
Points per peak	1
Replicates	3
Sweep/Replicate	100
Detector mode	dual

Although the interference removal rate reached an optimal and acceptable level by using Helium (He) collision mode, the concentration difference between the interfered and interfering element can significantly influence the data quality. Correction check solutions which mimic the concentration of interfered and interfering elements were used to assess the

He mode result quality. Correction equations were applied where necessary to further reduce the interference on analytes in addition to the application of the collision mode. The interference level during analysis and the detailed method to remove the interference and ensure the quality of data are discussed in the Chapter 4.

Machine was optimized and tuned with tuning solution containing 1ppb of Ce, Co, Li, Y, Tl in a 1% (v/v) HNO_3 matrix prior to the calibration process. Li, Y, Tl in solution was used for optimizing the machine response and establishing good sensitivity for low, mid and high mass range. The signal stability was ensured by optimizing the sensitivity RSD of ^{7}Li, ^{89}Y, ^{205}Tl to less than 5%. For the purpose of minimising the spectral interference on the analytes, Ce is presented in solution to establish the oxides level based on the ratio of $^{156}CeO^{+}$ to $^{140}Ce^{+}$ and the doubly charged ions level according to $^{70}Ce^{2+}/^{140}Ce^{+}$ result. Ce is used as the oxide interferences indicator since the high Ce-oxygen bond strength makes Ce has one of the highest oxide production rates (Agilent Technologies, 2005). Also, Ce is more prone to form doubly charged ion than other metals. Ce oxides and doubly charged level are optimized to an acceptable low level which are <1.2% and <2% respectively under no gas mode, and are as half of the no gas mode oxides ratio and similar to the no gas mode doubly charged ratio respectively under He mode. Tuning solution was prepared from Agilent Technologies ICP-MS 10ppm tuning stock solution, ultrapure grade concentrated nitric acid (60%) (Merck) and 18.2Ω MilliQ deionised water, using plastic volumetric flask.

Instrument calibration and sample measurement was all undertaken in both no gas and He mode. Isobaric elemental interference is another type of spectral interference that induces the additive signal on the analytical mass and was eliminated by carefully selecting the analyte isotope used for measurement. The selected analyte isotope and the selection criteria are described in Chapter 4.

To correct the non-spectral interference, eliminate the signal drift and ensure the machine stability during analysis (Vaughan and Horlick, 1989), internal standard was in-line added to the calibration blank, standards, all unknown samples, reference samples, single interfering element solutions and correction check solutions by mixing tee during measurement. Internal standard was diluted about 20 times by the sample/calibration standard after mixing.

As the internal standard was used as a reference to normalize matrix effects of the instrument, the element in the internal standard needs to have the same relative signal response shift as its

assigned analytes (Dams et al. 1995; Vaughan and Horlick, 1989). The selected internal standard elements also need to have negligible concentration in the measuring samples and negligible interference on analytes (British Standard ISO 17294-1:2006). Also, the internal standard itself does not suffer from spectral interference during analysis (Prohaska et al. 1999). Due to the mass based function of matrix effects, the internal standard is selected to closely match the mass number and IP of analyte to ensure an accurate drift correction and improve the precision (Agilent Technologies, 2012, Vanhaecke et al. 1992; Dohorty, 1989; Vaughan and Horlick, 1989).

Although ^{103}Rh, ^{115}In and ^{209}Bi were the suggested internal standard elements for non-spectral interference correction on REE according to Agilent Technologies, the study of Prohaska et al. (1999) shows that ^{115}In matches the signal response behaviour of REE more closely than other elements. ^{115}In is more suitable for internal standardization and was therefore used as the assigned internal standard for REE during the experiment. For matrix variation effects correction on environmental elements, three elements ^{45}Sc, ^{72}Ge, ^{115}In were used as the internal standard, each was assigned to the analytes in its surrounding mass range. The internal standards were made up with Merck 1000mg/l single element stock solutions, Merck ultra-pure concentrated nitric acid (60%), Merck ultra-pure concentrated hydrochloric acid (30%) or Fisher chemical optima grade concentrated hydrochloric acid (32-35%) (As noted in Section 3.3.2, Fisher HCl was used between October, 2016 and April, 2017 while Merck one was used in the other period) and deionised water. Table 3.7 indicates the analytes assigned to each internal standard element and the concentration of prepared internal standard elements. The internal standard recovered from standards and samples relative to that obtained from calibration blank during measurement was within 80% to 120%, meeting the internal standard performance criteria.

Table 3.7: Assigned internal standard to analytes

Element	REE	Environmental element		
	Sc, Y, lanthanides	Al, Cr, Mn, Fe, Ni, Cu	Zn, As	Cd, Ba, Pb
Internal standard	^{115}In	^{45}Sc	^{72}Ge	^{115}In
Concentration	100ppb	100pbb	100ppb	100ppb

Before analysis the machine was calibrated with a calibration blank containing 2% (v/v) HNO_3 and 1% (v/v) HCl, and five calibration standards each with a known concentration of REE/ environmental elements stabilized with 2% (v/v) HNO_3 and 1% (v/v) HCl. The acids

used in the preparation of calibration blank and standards were the same as that used in the internal standard preparation and sample acidification. The calibration blank was prepared by diluting required amount of concentrated acids with 18.2Ω MilliQ deionised water. Besides acids and deionised water, the stock solution used for making REE calibration standards was Agilent Technologies 10mg/l multi-element calibration standard containing Sc, Y and 14 lanthanides, while Agilent Technologies multi-enviromental calibration standard which contains 1000mg/l Fe and 10mg/l other analytes (Al, Cr, Mn, Fe, Ni, Cu, Zn, As, Cd, Ba, Pb) was used for preparing environmental calibration standards. All the ICP-MS calibration blank and standards were prepared weekly by using plastic volumetric flask instead of glass volumetric flask and stored in polypropylene bottles at 4^{o}C.

Table 3.8 shows the concentration of REE and environmental elements in five calibration standards respectively. The calibration curve is plotted based on the ratio of the analyte signal to its assigned internal standard signal against the calibration standards concentrations. A six-point calibration curve spanning concentrations from 0ppb (calibration blank) to 100ppb was used for environmental elements measurement. Although calibrating machine to 100ppb for all analytes was suggested by Agilent Technologies. Since the concentrations of all individual REE in the samples were below 30ppb, 50ppb was used as the maximum REE calibration standard to improve the accuracy of measurement. Each analyte concentration in sample was produced by comparing the ratio of the analyte signal to internal standard signal in sample to that of the calibration curve.

Table 3.8: ICP-MS calibration standard values for REE and Environmental elements

	REE (ug/l)	**Environmental elements**	
	Sc, Y, La, Ce, Pr, Nd, Sm, Eu, Gd, Tb, Dy, Ho, Er, Tm, Yb, Lu	Al, Cr, Mn, Ni, Cu, Zn, As, Cd, Ba, Pb (ug/l)	Fe (ug/l)
Standard 1	0.1	0.1	10
Standard 2	1	1	100
Standard 3	5	10	1000
Standard 4	20	50	5000
Standard 5	50	100	---

To ensure no systematic errors occur due to the interferences and evaluate the accuracy of quantitative REE measurements, two REE standard reference water samples- PPREE and SCREE were analyzed after calibrating the instrument. PPREE is the acid mine discharge from Paradise Portal, San Juan Mountains, Colorado, USA and SCREE is the partially treated acid mine discharge from the Spring Creek Debris Dam, West Shasta mining district,

California, USA (Verplanck et al. 2001). The difference between the certified values and measured values were within 10% for all 16 REE analytes.

Samples were run from the least contaminated to the most contaminated in order to avoid cross-contamination. Calibration standard 3 was run as a quality control solution after every 9 sample measurements to ensure the analytical accuracy and the precision of measurement. The instrument was recalibrated when the difference between the prepared and the measured analytes concentration was more than 10%. A blank containing the sample matrix as the calibration blank was measured after each time analysing the quality control solution to flush the system and remove any memory interferences that may be induced by standard 3.

As the machine uses an autosampler to introduce samples, standards, etc., the probe and instrument were rinsed automatically between samples to flush any residues from previous measurement out of the system. The peri-pump parameters set to control the rinsing process and to introduce samples, standards, etc. are specified in Table 3.9.

Table 3.9: Peri-pump parameters of instrument

Pre-run task	Time (seconds)	Speed (rps)
Sample uptake	60	0.3
Stabilise	40	0.3
Post-run task	Time (seconds)	Speed (rps)
Probe rinse by deionised water (sample)	10	0.3
Probe rinse by deionised water (standard)	10	0.3
Acid rinse (2% (v/v) HNO_3 and 1% (v/v) HCl)	60	0.3

Besides calibration blank and standards, other solutions including reference samples, single interfering solutions, correction check solution were all in a 2% (v/v) HNO_3 and 1% (v/v) HCl matrix to match the unknown water samples.

The plastic volumetric flasks were soaked in 10% (v/v) HNO_3 and 5% (v/v) HCl (prepared with AnalaR grade concentrated acids) overnight after using for standard and tuning solution preparation to clean the glassware and plastics thoroughly and ensure reliable solutions were made up for use in subsequent analyses.

The quantitative detection limits of the instrument were calculated as ten times the standard deviation of seven replicate blanks containing 2% (v/v) HNO_3 and 1% (v/v) HCl. The REE and environmental elements detection limits are shown in Table 3.10.

Table 3.10: ICP-MS detection limits for different analytes

Analyte	Detection limits (ppb)	Analyte	Detection limits (ppb)
Sc	0.019	Yb	0.004
Y	0.004	Lu	0.003
La	0.003	Al	0.5
Ce	0.003	Cr	0.02
Pr	0.002	Mn	0.06
Nd	0.005	Fe	0.4
Sm	0.004	Ni	0.04
Eu	0.004	Cu	0.02
Gd	0.004	Zn	0.5
Tb	0.002	As	0.04
Dy	0.004	Cd	0.009
Ho	0.002	Ba	0.03
Er	0.003	Pb	0.03
Tm	0.002		

3.4.3 Anions analysis

Anions analysis of samples was undertaken in the Cassie Building laboratory, Newcastle University. Anions were analysed within one month of sample collection using a Dionex ICS-1000 Ion Chromatograph (IC) with an AS40 auto sampler. 8.0mM Na_2CO_3/1.0mM $NaHCO_3$ solution was used as eluent to carry the sample through the guard and the separator column at a flow rate of 1ml/min, and to help to with ion separation. The column used was an Ionpac AS14A, 4x250mm analytical column. The interaction difference of anions with the ion exchange site induces a specific rate for each anion migrating through the column, which is the separation principle. A suppressor is then used to enhance the conductivity of sample anions and reduce the eluent conductivity for the sample anions able to be detected by the conductivity detector.

The analysis procedure follows the guide of BS ISO 10304-1:2009.

The standard used to calibrate the machine was prepared monthly with VWR chemicals multi-component anion mix ion chromatography standard and deionised water. The concentrations of each anion in the calibration standard and the stock solution are described in Table 3.11. Samples were diluted with deionised water where necessary to keep the anions concentration below 40ppm which is the upper limit for machine to analyse sample

accurately. The standard was measured after every six samples analysis for the quality control purpose and the machine was recalibrated when the difference between the measured result and the actual value was more than 10%.

Table 3.11: Anions concentration in standard and stock solution

Anion	Calibration standard (ppm)	VWR multi-anion stock solution (ppm)
F^-	5	100
Cl^-	10	200
SO_4^{2-}	20	400
Br^-	20	400
NO_3^-	20	400
PO_4^{3-}	30	600

3.5 Quality Assurance and Quality Control (QA/QC)

Since all the aqueous solutions are electrically neutral, the sum of the positive charges (meq/L) equals the sum of the negative charges (meq/L) in water (Parkhurst and Appelo, 2005). The analytical accuracy of samples were checked by the Charge Balance Error (CBE) in PHREEQC, which includes the complexes of measured element and the free ions of element in the calculation and provides a more accurate result. The difference of up to ±10% is normally acceptable for analytical accuracy. The equation the applied in the PHREEQC to calculate the CBE is as following:

$$\text{CBE (\%)} = 100 \times \frac{(\sum m_c z_c - \sum m_a z_a)}{(\sum m_c z_c + \sum m_a z_a)}$$

Where: m_c = molality of the cations

m_a = molality of the anions

z_c = valence of the cations

z_a = valence of the anions

3.6 Speciation modelling

Rare earth element speciation calculations can be performed using PHREEQC code (version 3.3.3, Parkhurst and Appelo, 2013) and its ion association model at the *in situ* measured chemical and physical conditions with the LLNL database directly which contains the thermodynamic data of REE. LLNL database was adopted by several authors (Inguaggiato et al. 2015; Yuan et al. 2014; Medas, et al. 2013; Guo et al. 2010; Köhler et al. 2005) for doing

the speciation modelling, but it should be noted that the thermodynamic data in LLNL database lacks internal consistency, which lowers the quality of the database. However, to review the data and correct the inconsistency data is a difficult and time-consuming process (Wolery and Jové-Colón, 2017).

Therefore, WATEQ4F database which contains good quality base data was used, as part of this research, was updated to include recent published the infinite dilution stability constants of REE from Schijf and Byrne (2004) for sulfate ($LnSO_4^+$) complexes, from Luo and Byrne (2004) for carbonate ($LnCO_3^+$, $Ln(CO_3)_2^-$) and bicarbonate ($LnHCO_3^{2+}$), from Klungness and Byrne (2000) for hydrolysis ($LnOH^{2+}$), from Luo and Byrne (2000) for fluoride (LnF^{2+}), and from Millero (1992) for chloride ($LnCl_2^+$) complexes to calculate REE speciation in waters. Phosphate complexes were not considered in the modelling due to no detectable phosphate in most of the samples.

Table 3.12: REE inorganic complexation reactions inputted into the original WATEQ4F database of PHREEQC for the purpose of REE speciation modelling

REE-complexes	Reaction	Formular of stability constant
$LnSO_4^+$	$Ln^{3+} + SO_4^{2-} <=> LnSO_4^+$	$K=\frac{[LnSO_4^+]}{[Ln^{3+}][SO_4^{2-}]}$
$LnCO_3^+$	$Ln^{3+} + HCO_3^- <=> LnCO_3^+ + H^+$	$K=\frac{[LnCO_3^+][H^+]}{[Ln^{3+}][HCO_3^-]}$
$Ln(CO_3)_2^-$	$Ln^{3+} + 2HCO_3^- <=> Ln(CO_3)_2^- + 2H^+$	$K=\frac{[Ln(CO_3)_2^-][H^+]^2}{[Ln^{3+}][HCO_3^{2-}]^2}$
$LnHCO_3^{2+}$	$Ln^{3+} + HCO_3^- <=> LnHCO_3^{2+}$	$K=\frac{[LnHCO_3^{2+}]}{[Ln^{3+}][HCO_3^-]}$
$LnOH^{2+}$	$Ln^{3+} + H_2O <=> LnOH^{2+} + H^+$	$K=\frac{[LnOH^{2+}][H^+]}{[Ln^{3+}]}$
LnF^{2+}	$Ln^{3+} + F^- <=> LnF^{2+}$	$K=\frac{[LnF^{2+}]}{[Ln^{3+}][F^-]}$
$LnCl^{2+}$	$Ln^{3+} + Cl^- <=> LnCl^{2+}$	$K=\frac{[LnCl^{2+}]}{[Ln^{3+}][Cl^-]}$

Table 3.12 and /deg/mol respectively show each REE complexation reaction, and the stability constants of REE inorganic complexes used in the modelling. As the ionic strength of the samples were all below 0.01, the activity coefficients of individual ion was calculated using the Davies equation, which is applicable for solutions with ionic strength below 0.5, according to Appelo and Postma (2005). The Davies equation has been adopted by Zhao et al. (2007); Verplanck et al. (2004); Gammons et al. (2003) and Gimeno Serrano et al. (2000) in the REE speciation modelling.

Table 3.13: Formation constants (log_K) of REE inorganic species at 25°C and zero ionic strength inputted into the original WATEQ4F database of PHREEQC for the purpose of REE speciation modelling

	$LnSO_4^+$	$LnCO_3^+$	$Ln(CO_3)_2^-$	$LnHCO_3^{2+}$	$LnOH^{2+}$	LnF^{2+}	$LnCl^{2+}$
Y	3.5	-2.85	-8.03	2.32	-7.8	4.46	---
La	3.61	-3.6	-9.36	2.34	-8.81	3.62	0.29
Ce	3.61	-3.27	-8.9	2.31	-8.34	3.86	0.31
Pr	3.62	-3.1	-8.58	2.25	-8.32	3.84	0.32
Nd	3.6	-3.05	-8.49	2.28	-8.18	3.82	0.32
Sm	3.63	-2.87	-8.13	2.34	-7.84	4.15	0.3
Eu	3.64	-2.85	-8.03	2.47	-7.76	4.27	0.28
Gd	3.61	-2.94	-8.18	2.36	-7.83	4.24	0.28
Tb	3.59	-2.87	-7.88	2.46	-7.64	4.37	0.27
Dy	3.57	-2.77	-7.75	2.5	-7.59	4.39	0.27
Ho	3.54	-2.78	-7.66	2.46	-7.56	4.28	0.27
Er	3.51	-2.72	-7.54	2.49	-7.52	4.27	0.28
Tm	3.48	-2.65	-7.39	2.52	-7.39	4.29	0.27
Yb	3.46	-2.53	-7.36	2.53	-7.24	4.39	0.16
Lu	3.44	-2.58	-7.29	2.49	-7.27	4.25	-0.03

The calculations were performed at 25°C not the field temperature condition, as the uncertainty due to the temperature correction to the log K by the use of delta_H is expected to be small for this study (*personal communication*, Dr. David Parkhurst, USGS, 31st March, 2017). The formation constant of complexes at the field temperature can be calculated through van's Hoff equation below based on delta_H and the stability constant at standard condition (Appelo and Postma, 2005):

$$\log K_r = logK_0 + \frac{\Delta H_r^0}{2.303R}\left(\frac{1}{T_{k_0}} - \frac{1}{T_k}\right)$$

Where: K_r =stability constant at field temperature

K_0 =stability constant at standard condition

ΔH_r^0=standard reaction enthalpy

T_k =field temperature in Kelvin

T_{k_0}=temperature in Kelvin, where ΔH_r^0 was obtained

R = universal gas (molar) constant = 8.314×10^{-3} KJ/deg/mol

3.7 REE normalization standard

The distribution pattern of REE is shown by plotting the concentrations of REE against their atomic number. As described in Section 2.4.2, the Oddo-Harkins effect results in more

abundant even numbered REE than odd numbered elements (Quinn, 2006; Coryell *et al.*, 1963; Masuda, 1962). To eliminate the natural fractionation of REE caused by the Oddo-Harkins effect on the distribution pattern of the sampling waters at Gate Gill study site, the concentrations of each individual REE in the samples were normalized to those in the reference materials (PAAS in this study). The relative (i.e. normalized) concentration of each individual REE was then plotted against its atomic number to form a normalized REE distribution pattern. The concentration variation across the REE group in the Gate Gill samples, relative to the PAAS reference material, can be displayed in the normalized REE distribution pattern.

Ideally, the reference material used for normalizing REE in samples needs to represent the REE composition in the source rocks. Then the normalized REE distribution pattern at the sampling sites is able to show any fractionation occurring during interaction between the source rock and aqueous fluids (process-related fractionation), and during REE removal process. When the reference material has the same/similar REE pattern as the source rock, Tang and Johannesson (2006) and Verplanck et al. (1999) state that the normalised REE distribution pattern displayed in streams is related to the interaction between the host/source rocks and water passing the host rocks together with the in-stream solution chemistry.

As noted in Section 1.5.1, the bedrock around Gate Gill consists of laminated mudstone and siltstone of the Skiddaw group. Quartz is the main gangue mineral for the lead-zinc veins of Threlkeld mine. Shales, which are sedimentary rocks and represent felsic siliciclastic-source-rocks (Piper and Bau, 2013), are more suitable to use as the reference materials in this study, when compared with chondrite which represents ultramafic siliciclastic-source-rocks. As described in Section 2.4.2, Liu et al. (2014) notes that when the source rock is composed mainly of sandstones, siltstones, mudstones and clays, shale is the most suitable normalization reference material. Post-Archean average Australian Shale (PAAS), which is the average value obtained from 23 Australian shales, is used as the reference material for REE normalization in this study.

However, REE pattern of Gate Gill source rock may be different to the PAAS pattern, in which case the PAAS normalized REE distribution pattern at the sampling site will show the source rock-related fractionation relative to PAAS and the solution chemistry induced fractionation. The solution-chemistry induced fractionation includes the fractionation due to

source rock- aqueous fluids interaction and the fractionation during transport of the REE along sampling sites.

3.8 Source-related fractionation in this study

As described in Section 2.4.2, source-related fractionation traditionally means that the distribution pattern of REE in streams inherit the REE characteristics of the parent rocks and no fractionation occurs during and after the source rock dissolution/weathering process (Biddau et al., 2009; Fee et al., 1992). REE released from source rocks may not have the exact same distribution pattern as that in the source rocks themselves, since the readily leachable minerals in the source rocks may not control the REE patterns (Medas et al. 2013; Protano and Riccobono, 2002).

As mentioned in Section 2.4.2, the precise and convincible method to test whether the fractionation in a stream is source-related is to collect several parent/ source rocks and analyse the normalized REE distribution pattern of source rocks and source rocks' leachate (Medas et al. 2013; Protano & Riccobono, 2002). The normalized REE distribution pattern here means normalizing the REE concentration of the whole rock or source rocks' leachate to the reference material used for water samples. Whether the leachate REE closely resembles the REE signature in parent rock and REE pattern in sampling streams entirely inherits source rock REE pattern can then be demonstrated.

However, this method is only suitable when the parent/ source rocks are known and the collection of rock samples is possible. The source rocks of the Woodend mine discharge are not accessible, since they are underground and flooded, leaching experiments on the source rocks were not undertaken. Therefore, there is no way to know whether the PAAS normalized REE pattern in the mine leachates draining into the Gate Gill is entirely related to the source rocks or whether the solution chemistry of the aqueous fluid fractionated the REE pattern during dissolution of the source rocks. If the latter occurred, the PAAS normalized REE pattern in the mine leachates must be related to both the source rocks and the solution chemistry of the aqueous fluid that interacts with the source rocks. The PAAS normalized REE pattern of the leachates from the source rocks has to be regarded as the source-related fractionation pattern (although it may not have a similar pattern to the real source pattern) when discussing the source-related and in-stream process related controls on the REE distribution pattern at Gate Gill in this study.

3.9 Chapter summary

- Gate Gill was sampled 13 times for synchronous flow measurement and water quality monitoring between February 2016 and September 2017.
- The salt dilution method was used for determining flow rate at G3 to G5, and the flow rate at G7 was obtained from an Environment Agency gauging station.
- Environmental elements with concentration less than 100ppb and REE were measured by ICP-MS. ICP-OES was used for environmental elements with concentrations greater than 100ppb. Analysis of anions was performed using IC.
- REE speciation modelling was performed through PHREEQC. The base database WATEQ4F was used and updated to include the thermodynamic data of REE from the most recent published papers to calculate REE speciation in waters.
- Sample analytical accuracy was ensured by checking the Charge Balance Error (CBE) in PHREEQC.
- PAAS is selected as the reference material for REE normalization of all the samples.
- The source-related fractionation pattern in this study means PAAS normalized REE pattern of the leachates from the source rocks.

Chapter 4 Method development and evaluation

4.1 Introduction

ICP-MS is suitable for measuring the concentration of multi ultra-trace elements due to the high sensitivity and very low detection limit of the machine. In addition, sample analysis time is short (Liu et al. 2014; Lichte et al., 1987). However, attention needs to be paid to the potential interferences that may occur during analysis. This chapter describes the major interferences that can influence the accuracy of measurement of REE in particular, and the associated approaches to reducing these interferences. The interference level and the interference removal methods were then evaluated during analysis.

Section 4.2 shows the spectral interferences that may occur during ICP-MS measurement. The general methods used to remove or reduce the polyatomic interferences in the literature, the method developed and adopted in this study were described in Section 4.3. The application of developed correction equation to remove the polyatomic interference on REE are demonstrated in Section 4.4 and 4.5.

4.2 ICP-MS spectral interferences

The elements or analytes in ICP-MS mainly form singly charged ions M^+ some of them may form polyatomic ions e.g. MO^+, MOH^+, doubly charged ions M^{2+}. Singly charged ions M^+ are the specie that required in the measurement. The other three species types MO^+, MOH^+, M^{2+} may respectively cause isobaric elemental, isobaric polyatomic interference and doubly charged interference on other analytes.

4.2.1 Isobaric elemental interference

Isobaric elemental interference means the overlap on the analyte isotope that is caused by the isotope of a (or several) different element(s) with the same nominal mass as the analyte isotope. The interference level mainly depends on the analyte concentration and the sample matrix (Agilent Technologies, 2012). Normally the most abundant isotope of an element is selected for analysis in order to obtain sufficient sensitivity during measurement, particularly when the analyte in samples is at the ultra-trace level, as can be the case with REEs. The preferred isotope of the analyte should have the least possible interference from other element isotopes to avoid, or at least minimise, the elemental interference during analysis (Palmieri et al. 2011). When concentrations of the interferent is many times lower than the analyte, or the

interfering isotope is of low abundance and the interferent is at relatively low concentration compared to the analyte concentration, then interference can be deemed negligible and no correction is required during measurement (Agilent Technologies, 2012). In addition, free of polyatomic interference on analyte isotope is another important consideration in the selection criteria.

The selected REE isotopes for analysis were ^{89}Y, ^{139}La, ^{140}Ce, ^{141}Pr, ^{146}Nd, ^{147}Sm, ^{153}Eu, ^{157}Gd, ^{159}Tb, ^{163}Dy, ^{165}Ho, ^{166}Er, ^{169}Tm, ^{172}Yb, ^{175}Lu. The isotopes selected for environmental elements were ^{27}Al, ^{52}Cr, ^{55}Mn, ^{56}Fe, ^{60}Ni, ^{63}Cu, ^{66}Zn, ^{75}As, ^{111}Cd, ^{137}Ba, ^{208}Pb. For each analyte, the selected isotope is the most abundant one among all isotopes that meets the following two criteria:

(1) no isobaric elemental overlap;

(2) polyatomic interference which is either negligible, or requires less correction steps, and is easy to correct (Agilent Technologies, 2005; Lee et al. 2000b).

The natural abundance of selected REE and environmental element isotope (Lide, 2005) is shown in Table 4.1.

Table 4.1 Natural abundance of selected analyte isotope (Lide, 2005)

Analyte isotope	Natural abundance (atomic %)	Analyte isotope	Natural abundance (atomic %)
^{45}Sc	100.00	^{172}Yb	21.83
^{89}Y	100.00	^{175}Lu	97.41
^{139}La	99.91	^{27}Al	100
^{140}Ce	88.45	^{52}Cr	83.79
^{141}Pr	100.00	^{55}Mn	100
^{146}Nd	17.2	^{56}Fe	91.75
^{147}Sm	14.99	^{60}Ni	26.22
^{153}Eu	52.19	^{63}Cu	69.17
^{157}Gd	15.65	^{66}Zn	27.90
^{159}Tb	100.00	^{75}As	100
^{163}Dy	24.90	^{111}Cd	12.80
^{165}Ho	100.00	^{137}Ba	11.23
^{166}Er	33.61	^{208}Pb	52.4
^{169}Tm	100.00		

As each of the analyte isotopes selected for this study is free of elemental interference, no correction was undertaken for this type of interference. The paragraphs below briefly describe the common method used to correct the elemental interference if this type of interference needs to take into account.

When a higher abundance isotope with isobaric elemental interference is selected to ensure a greater sensitivity of measurement, or all the analyte isotopes have some degree of atomic interference, a mathematical equation method is normally used for correction. To be more specific, the correct concentration of interfered analyte isotope is obtained by subtracting the signal contributed by the interfering isotope from the total signal of the relevant analyte isotope mass. The signal of the interfering isotope is calculated based on the signal of another isotope of interfering element which is ideally free of interference and the natural abundance ratio of interfering isotope to another isotope of interfering element. The natural abundance ratio here can be regarded as a conversion factor. To obtain the correct signal of the interfering isotope, it is preferable for the other isotope of the interfering element to not have any interferences and to have a relatively high natural abundance. If all the other isotopes of the interfering element are not free of interferences, the interferences must be corrected first and only the real signal of the other isotope of the interfering element can be used in the analyte correction equation (British Standard ISO 17294-2:2016; EPA, 200.8; EPA, 6020A).

The accuracy of the natural abundances ratio of the interfering element is another important factor in the correction process. Normally the tabulated theoretical abundance ratio is used in the calculation, Garbarino and Taylor (1987) mentions that the traditional method (by using theoretical abundance ratio) may not be accurate enough due to the difference between the experimental abundance ratio and the theoretical abundance ratio.

This method is only valid when the element involved has a fixed natural abundance ratio. This method is not suitable for elements such as Pb, which have a variable natural abundances ratio. As natural abundances ratio of Pb is not uniform over the crust of earth, Agilent Technologies pre-programmed correction equation which sums the signal of all Pb isotopes on the measuring Pb isotope was applied in the calibration and subsequent samples measurement process to eliminate any error that may related to Pb isotope abundance.

4.2.2 Isobaric polyatomic interference

The interfering signal on the analyte mass induced by polyatomic species derived and formed from the sample matrix, solvent and plasma gas during analysis is called the isobaric polyatomic interference. The overlap of polyatomic ions on the preferred isotope of the analyte being determined is the main problem with ICP-MS analysis (Agilent Technologies, 2009). The categories of polyatomic ions are (1) oxides and (2) argides. These induce

interference on elements with masses of 16 amu and 40amu greater than the interferent element respectively. Chlorides, sulfates and phosphates can also sometimes cause severe interference depending on the matrix of samples (Agilent Technologies, 2012).

Oxygen has another two isotopes (^{17}O and ^{18}O) in addition to ^{16}O. Although metals may also form oxides with ^{17}O and ^{18}O, the interferences caused by these oxides are normally negligible due to the extremely low natural abundance of ^{17}O (0.038%) and ^{18}O (0.2%) (Dulski, 1994). Therefore, only interferences caused by oxides and hydroxides of ^{16}O (natural abundance of 99.76%) are considered in the correction process.

The potential oxides, hydroxides and chloride interferences on REE analysis by ICP-MS analysis have been identified by a number of researchers (Chien et al., 2006; May and Wiedmeyer, 1998; Dulski, 1994; Vaughan and Horlick, 1990b; Longerich et al. 1987; Vaughan and Horlick, 1986). The main interference species in the REE mass range are the oxides (Longerich et al, 1987; Dulski, 1994). Because the lanthanides have the strongest metal oxide bond among all the metals, the lighter rare earth element oxides can cause interferences on the heavier rare earth elements whose mass is 16 amu more than the interfering lighter REE (Sugiyama and Woods, 2012; Kajiya, et al. 2004). Since the light REE are naturally more abundant in the lanthanide group and the abundance of REE with even atomic number is higher than that with odd atomic number, the analysis of some heavier REE with low abundance may be influenced significantly (Shaw et al. 2003; Lee et al. 2000b; Lichte et al. 1987). Barium is the main matrix related metal that can cause significant oxides interference on some REE, which is because of the generally low abundance of REE in nature compared to Ba (Sugiyama, 2012).

Table 4.2 shows the potential interferences on REE which have been identified in literature (British Standard ISO 17294-1:2006; Chien *et al*., 2006; Kajiya *et al.*, 2004; Merten and Büchel, 2004; Cao *et al*., 2001; Lee *et al*., 2000b; Prohaska *et al*., 1999; May and Wiedmeyer, 1998; Dulski, 1994). Some of these may be negligible in practise like the REE-hydroxides and some REE-oxides, unexpected level of interference may present for samples with certain matrix. It is important to check the degree of interference in samples when the REE concentrations in the sample vary over orders of magnitude and the interference level depends on the ratio of interfering element to interfered analyte. Y, La, Ce, Pr are free of metal oxide/hydroxide interferences though (Lee *et al*. 2000b). Although the main issue of

some REE analysis is the spectral overlap of the polyatomic ions noted in Table 4.2, the formation of REEO or REEOH may also reduce the sensitivity of interfering REE.

Table 4.2: Potential polyatomic interferences during analysis of individual REE

Analyte isotope used for analysis	Potential molecular interference
^{89}Y	
^{139}La	
^{140}Ce	
^{141}Pr	
^{146}Nd	$^{130}BaO^{+}$
^{147}Sm	$^{130}BaOH^{+}$
^{153}Eu	**$^{137}Ba^{16}O^{+}$(11.232%)**, $^{136}Ba^{16}OH^{+}$, $^{136}CeOH^{+}$
^{157}Gd	**$^{141}Pr^{16}O^{+}$(100%)**, $^{140}Ce^{16}OH^{+}$
^{159}Tb	**$^{143}Nd^{16}O^{+}$(12.2%)**, $^{142}NdOH^{+}$, $^{142}CeOH^{+}$
^{163}Dy	**$^{147}Sm^{16}O^{+}$(14.99%)**, $^{146}NdOH^{+}$
^{165}Ho	**$^{149}Sm^{16}O^{+}$(13.82%)**, $^{148}NdOH^{+}$, $^{148}SmOH^{+}$
^{166}Er	**$^{150}SmO^{+}$(7.38%), $^{150}NdO^{+}$(5.6%),** $^{149}SmOH^{+}$
^{169}Tm	**$^{153}Eu^{16}O^{+}$(52.19%)**, $^{152}SmOH^{+}$, $^{152}GdOH^{+}$
^{172}Yb	**$^{156}GdO^{+}$(20.47%)**, $^{156}Dy^{16}O$, $^{155}GdOH^{+}$
^{175}Lu	**$^{159}TbO^{+}$(100%),** $^{158}GdOH^{+}$, $^{158}Dy^{16}OH$

Notes:

(1) Earth's crust does not naturally contain Promethium (Pm) which is therefore are not included in the table and sample analysis;

(2) Species in bold are those for which the interference may need correcting; the level of interference level due to these species was checked during analysis;

(3) The natural abundance of the main interferent isotopes (in bold) are indicated in brackets after the species.

The species causing polyatomic interference on environmental elements are not shown in this chapter because identification of interference species is only necessary when a mathematical equation is being applied for the correction. In this research the polyatomic interferences on elements As and Cd were corrected by the correction equations that were pre-programmed by Agilent Technologies in the software of the ICP-MS used in the research. No other correction equations were applied for removal of interferences on any other environmental elements in this study. This is because the number of interference species on environmental elements is too many to use the correction equation method. The mathematical method is not effective when the correction requires multiple complex equations. A detailed description of the correction equation method is shown in Section 4.3.3. Interferences on environmental elements were mainly removed by the use of the collision mode. More details about the collision mode are provide in Section 4.3.2.

4.2.3 Doubly-charged interference

As elements are separated and measured based on their mass to charge ratio (m/z) and all the analytes are ionised by losing only one electron from each atom in the plasma, the detected signal at each m/z is actually at each analyte mass. Elements which have a low second ionization potential tend to continue losing a second electron in the ionisation process (M^{2+}) and are detected at half of their mass. This causes doubly-charged ions interference for elements with mass that is half of the interferent mass (Agilent Technologies, 2012; Agilent Technologies, 2005). Elements with second ionization potentials which are less than the argon first ionization potential can form doubly charged ions (Garbarino and Taylor, 1987). Normally only a very small proportion of doubly charged ions forms in the plasma.

There are no doubly charge ions interferences on REE, but some REE like Ce, Sm, Eu can easily form doubly charge ions and certain isotopes of them will then interfere with the middle mass analytes when the concentrations of these REE in the samples are quite high. Ba can also form doubly charged ions (Thomas, 2008). Thomas (2008) describes some doubly charged interference species and the analyte isotopes that may be interfered by them, and these are shown in Table 4.3 as an example.

Table 4.3: Doubly charged ions species and the interfered ions (Thomas, 2008)

Interfering ions	Interfered ions
$^{138}Ba^{2+}$	$^{69}Ga^{+}$
$^{140}Ce^{2+}$	$^{70}Ge^{+}$, $^{70}Zn^{+}$
$^{151}Eu^{2+}$	$^{75}As^{+}$
$^{152}Sm^{2+}$	$^{76}Ge^{+}$, $^{76}Se^{+}$

As noted in Section 3.4.2, the doubly charged ions ratio was optimized to an acceptable low level which is less than 2% for Ce doubly charged ratio ($^{70}Ce^{2+}/^{140}Ce^{+}$) during the tuning process. In addition, REE and Ba concentrations in samples were at a relatively low level compared with that of the middle mass analytes that may be interfered by doubly charged REE ions. The doubly charged ions interference were then not considered as a problem in this study.

4.3 Polyatomic ions interferences removal approaches

4.3.1 Instrument optimization

As noted in Section 3.4.2, the machine was optimized and tuned before analysis to reduce polyatomic interference and maintain the sensitivity of analysis. The machine operating conditions can significantly affect the rate of polyatomic ion formation (Prohaska et al. 1999; Garbarino and Taylor, 1987). The operating conditions that were used in this study are shown in Table 3.6. The reasons for setting up the parameters as detailed in Table 3.6 are explained in the following paragraphs.

- ICP power

Plasma power plays an important role on the oxide production rate. The production rate decreases with the increase of ICP power when the carrier gas flow and sample uptake rate operated by the nebulizer are kept constant (Vanhaecke et al. 1992; Lichte et al. 1987; Longerich et al., 1987). In this study a high RF power of 1550W was used. This maintains a higher plasma temperature for efficiently decomposing the sample matrix, whilst minimizing the cooling effect on plasma caused by the sample aerosol and carrier gas. In this way the level of molecular interference due to oxides and hydroxides, for example, were reduced significantly (Agilent Technologies, 2005). It is important to note that the doubly charged production rate may increase at a hotter plasma condition, but the production rate of doubly charged ions is acceptable at the RF power used in this study.

- Carrier gas flow and sample introduction rate

There is a positive relationship between the sample introduction rate and the sensitivity of measurement (Lichte et al. 1987). However, at a given RF power, a high sample uptake rate and carrier gas flow can have a cooling effect on the plasma and induce a higher production rate of oxides, and even hydroxides (Agilent Technologies, 2005; Vaughan and Horlick, 1986). In contrast a low sample uptake and nebulizer gas flow rate increases the sample residence time in the plasma, helps further decompose the sample, and reduces the polyatomic ion production rate at the given ICP power (Aries et al. 2000). The nebulizer sample uptake rate and nebulizer gas flow were set at approximately 0.4ml/min and 1.05L/min respectively so that:

1. the samples were decomposed efficiently

2. sample load and carrier gas do not cause a decrease of the plasma temperature and also

3. the high sensitivity of measurement is maintained.

The parameters of carrier gas flow and sample introduction rate were established along with the ICP power parameter in order to obtain the optimal compromise between maximising the analyte signal and minimising the polyatomic ions production rate.

As noted in Section 3.4.2, the optimized machine was then tuned by running the tuning solution which contains 1ppb of Ce. This is because the oxide production rate of Ce is one of the highest among metals and the polyatomic ion production rate can be checked by the ratio of cerium oxide to cerium. The interference level during sample analysis can be dramatically reduced when the machine is tuned to form very low levels of CeO, and this avoids the need to apply many correction equations on interfering elements (Agilent Technologies, 2005).

4.3.2 Application of collision cell

The octopole Reaction System (ORS) of the ICP-MS is located in the intermediate stage of the process, just behind the main ion lens. It can be operated in no gas mode and collision/reaction mode. ORS acts only as the ion guide for shaping the ion beam, and separating the neutrals, under no gas mode and no polyatomic interferences are removed in the cell. For either collision or reaction mode, the cell is filled with a gas to effectively reduce the molecular interference through the corresponding mechanism.

The reaction mode is use H_2 or other type of gas to react with the interferents and convert them to different species to avoid them causing overlaps on the analytes. The collision mode uses He gas to remove the polyatomic interferences based on either kinetic energy discrimination (KED) or collision induced dissociation (CID). Under this mode, the He gas distributes in the cell in a random motion at low kinetic energy and collides with the defined trajectory ion beam which has greater energy. A very small portion of molecules with weak bonds are dissociated during the collision with He. The majority of the polyatomic ions that survive from CID are removed through the KED process. As the cross section of the polyatomic ions are larger than the monatomic analyte ions they interfere with, polyatomic ions collide more frequently with the He gas than the analyte. Consequently the molecules

undergo more energy loss and the polyatomic species with lower energy are then separated by energy discrimination from analytes with higher energy (Agilent Technologies, 2012). Collision mode was applied instead of reaction mode in this study for the following reasons:

(1) In collision mode the energy discrimination is specifically targeting all matrix- and plasma- related polyatomic interferences at the analyte mass and removes them from the ion beam, leaving only the analytes present at the measuring mass (Agilent Technologies, 2009). The plasma- related interferences can be reduced to ppt level by applying He mode (Agilent Technologies, 2005). Collision mode is suitable for analysing complex and variable samples to remove different or unknown polyatomic interferences on multi- analytes (Agilent Technologies, 2012; Agilent Technologies, 2009; Agilent Technologies, 2005). The composition of samples has no influence on the effectiveness of interference removal or efficiency of He mode (Agilent Technologies, 2005).

On the other hand, reaction gas mode is proved to be less effective for multi-element measurement of unknown samples. This is because (1) different analytes have different polyatomic interferences and they may not all react with the chosen gas type, and (2) the reaction gas will fail to react with some specific matrix-based interferences of unknown samples. Both conditions leave some unreacted interfering species present in the ion beam and influence the accuracy of results (Agilent Technologies, 2009). It is appropriate to use reaction gas mode only for certain samples with specific analytes and known, consistent interferences (Agilent Technologies, 2005).

(2) The removal process in collision mode is based on either the physical sizes of interfering ions and analytes or the chemical bond strength of molecules, and He is an inert gas. No chemical reaction occurs between these interfering ions and He gas and therefore no new interfering species are produced in the cell (Agilent Technologies, 2005, 2012).

In contrast, the reaction gas can react with not only the interferences but also the analytes and matrix, creating some new species. These newly formed interferences may induce some overlaps on other analytes, and the produced species and the interference degree of them vary depending on the matrix of samples. Therefore, some new interferences can be introduced into the ion beam in the removal process of existing interferences (Agilent Technologies, 2009).

(3) The reaction between the reaction gas and the analytes leads to the analyte signal loss and a degradation of the detection limits (Agilent Technologies, 2009). On the other hand, Yamanaka and Wilbur (2013) notes that there is an improvement of the analytes detection limits at the He mode.

Analyte ions in the ion beam also experience energy loss during the collision with He gas. There is an increasing signal loss of the analytes with the increase of the cell gas flow (Agilent Technologies, 2012). To ensure the system can effectively remove the molecular ions without losing the analyte ions it is important to control the cell parameters. In this study He gas flow rate was set to 4.3ml/min and the energy discrimination was set to 3.0V, as noted in Table 3.6. The instrument was tuned and the interference removal effect of the collision mode was ensured by checking the oxide production ratio on the tune report with the operating criteria under He gas mode, as described in Section 3.4.2.

Agilent Technologies suggests using He mode results only for analytes with mass between 25 and 80. This is because the middle mass elements normally suffer from significant plasma-based and matrix-related interferences. Applying a series of mathematical correction equations on the analyte which is overlapped by many different complex interferences may not lead to an accurate result. Depending on the complexity of the correction equations applied the error caused by the correction equations themselves on the analyte's result may be relatively large. The details of the correction equation method are shown in Section 4.3.3.

The application of collision mode for complex interferences removal can be more effective than the traditional correction equation method. Agilent Technologies does not suggest to use He mode on the light and heavy elements. As the light elements do not have interferences from argon or oxides, and may be subject to 'blow away' by the gas, there is a substantial signal loss of the low mass analytes when applying the collision mode on them. The sensitivity reduction effect becomes increasingly obvious with the decrease of analyte mass. Interferences on heavier elements are not severe since they only suffer oxide interferences and no gas mode has higher sensitivity than He mode. In this study, the lightest element analysed was Al (with a mass of 27). Most of the heavy elements analysed were REE, which can easily form REEO compared to other metals. Since some of the REEO formed can cause interference on other REE the results from He mode were used for all analytes.

4.3.3 Application of interference equation

The classic method used to correct the spectral interference is to use mathematical equations on the measured results. Machine parameters such as RF power, sample uptake rate, sampling depth and setting of ion lens is optimized, all in an effort to reduce interference. In addition collision mode is applied during the analysis, and analyte isotopes with minimal interference are employed to reduce the interferences. Nevertheless, polyatomic species cannot be removed completely and there might still be spectral interferences on analytes mass. Whilst some of these may be negligible, whether there is a need to employ correction equations depends on the concentration of the interferents and analytes in samples and the polyatomic ions production rate. The remaining interference on analyte isotope can be further corrected by the correction equation. Aries et al. (2000) mentions that there is no need to apply the correction equations when the contribution of interferences is less than 5% compared with the contribution of analyte.

The foundation of the mathematical correction is to obtain the signal of the interference which has the same mass to charge ratio as the selected analyte isotope and remove it from the total signal obtained at the measured analyte mass. There are two approaches to obtain the interference intensity:

1. based on the natural abundance of interfering element isotopes and the intensity of another isotope of interfering element oxide which does not interfere with the selected analyte isotope;

2. based on the interfering element oxide (hydroxide) production rate and the interfering element signal in sample.

Each method has its own benefits and drawbacks and they are discussed in Section 4.3.3. The comparison between two methods and the method selected in this study are described in Section 4.3.3.

Correction based on the natural abundance of interfering element

For the interfering element with more than one isotope, the isotope that combines with the oxygen or other element(s) to form oxide or other polyatomic ions with the same mass to charge ratio as the measured analyte isotope is called the interfering isotope. The isotope that

forms a polyatomic ion with a different mass compared to the selected analyte's isotope is called the non-interfering isotope. As the natural abundance of the interfering and non-interfering isotopes are fixed values, the non-interfering isotope forming oxide is proportional to the interfering isotope forming oxide. The intensity of the interference on the sample analyte can then be calculated based on the signal of the non-interfering isotope forming oxide in the sample and the abundance ratio of the interfering and non-interfering isotopes. The net analyte signal in the sample can then be obtained by subtracting the interference signal from the apparent signal at the analyte mass (EPA, 6020A).

For mono isotope interfering element, this approach can still work as long as the other element besides the interfering element in the molecular component has more than one isotopes. The correction can then be built up based on the signal of non-analyte interfering polyatomic ion which is comprised of the mono isotope interfering element and the non-interfering isotope of the other element, and the natural abundance of interfering and non-interfering isotope of the other element.

The natural abundance of the isotope used must be high enough to be able to produce an accurate signal in the measured samples, because this is the foundation of an accurate correction equation. In the case of oxide interference, although oxygen has three isotopes, if the interfering element M has only one isotope and the interfering oxygen is ^{16}O, this method may not be suitable due to the very low natural abundance of ^{17}O and ^{18}O.

Accurately establishing the abundances of interfering element isotopes is a precondition of applying this correction method (EPA, 200.8; EPA, 6020A). The abundances used can either be published theoretical values (e.g. Lide, 2005) or the measured result of a solution containing the interfering element. The values from the latter method are more accurate (De Boer, 2000).

The benefit of this approach is that changing operating conditions with time does not influence the accuracy of the correction, as the principle of this method is to obtain the interference signal based on each sample and remove them subsequently. In contrast the effectiveness of the second approach (see Section 4.3.3) can be strongly affected by changing operating conditions.

As the correction requires an accurate signal of the non-analyte interfering molecular, this method is not appropriate to use when all the available and suitable non-interfering isotope molecules suffer some degree of complex interferences from a series of interferents. The complex interferences here means the relevant ion B (non-analyte interfering molecule) used for obtaining the analyte interference signal A is also interfered by another ion C, and the other ion D used for obtaining the signal of another ion C is however, overlapped by a species E. A, B, C, D, E mentioned above are the representative symbols of different species and each species has non-negligible interference on the correction related ion. If there is also a non-negligible interference on species E, correction will be further confounded unless an interference-free correction related specie is found (or the interference is within an acceptable range). In such a case numerous associated equations need to be applied in order to obtain the signal of the non-analyte interfering molecule.

In such circumstances it is essential to ensure the accuracy of the initial equation which is based on the species not subject to interference, since all subsequent equations are based upon that result. Even in a situation in which all of the potential interferences that may cause non-negligible error are considered there is still some degree of error after the correction, and the corrected result cannot be assumed to be 100% accurate. In the common correction criteria, the correction is regarded as satisfactory when the interference level is reduced to less than 5%. However, errors may be compounded where multiple equations are required.

Besides Ba-oxides, the other interferences on REE are mainly the LREE-oxides on MREE and HREE, and the MREE-oxides on HREE. Due to the very low abundance of ^{17}O and ^{18}O, the non-interfering isotope of interfering element-LREE and MREE should be selected to use in the correction equation. However, some interfering REEs only have one isotope, like ^{141}Pr and ^{163}Dy, and therefore the interfering oxide of them ($^{141}Pr^{16}O^{+}$, $^{159}Tb^{16}O^{+}$), which affects the measured analytes ^{157}Gd and ^{175}Lu respectively, cannot be accurately removed if using the correction method described above.

For the other interfering REE with more than one isotope, the non-interfering isotope oxides have complex interferences at their mass. This is because REE is a group of elements with the mass range from 139 to 175. Consequently, suitable non-interfering isotope oxides that can be used for obtaining the signal of the interfering isotope oxide at the measured isotope mass of one analyte normally have the same mass as the isotope of that analyte not selected

for use in the correction (or the selected or not selected isotope of a different analyte). There are also some other REE forming oxides that have the same mass as the non-interfering isotope oxides required for the correction. For this reason the correction can be very complicated and time consuming.

For example, the signal of $^{153}Eu^{16}O^{+}$ interference in this study selected analyte isotope ^{169}Tm (see Table 4.2 for the interference species on REE), which can be obtained from the signal of $^{151}Eu^{16}O^{+}$, but $^{151}Eu^{16}O^{+}$ has the same mass as the ^{167}Er. To obtain and then remove the signal of ^{167}Er at 167 amu, the signal of another Er isotope is required. If ^{166}Er is selected, which is also a measured analyte isotope in this study, the net signal of ^{166}Er cannot be obtained unless the interferences of $^{150}Sm^{16}O^{+}$ and $^{150}Nd^{16}O^{+}$ are removed from 166 amu. $^{147}Sm^{16}O^{+}$ can be used to get the $^{150}Sm^{16}O^{+}$ signal, and $^{150}Nd^{16}O^{+}$ signal can be obtained from the intensity of $^{146}Nd^{16}O^{+}$. However, $^{147}Sm^{16}O^{+}$ is interfered by the selected analyte isotope ^{163}Dy, while the unselected analyte isotope ^{162}Dy causes interference on $^{146}Nd^{16}O^{+}$. To obtain the signal of ^{163}Dy and ^{162}Dy, another isotope signal of Dy is needed, but each of two suitable Dy isotopes (^{161}Dy and ^{163}Dy) have oxide interferences on their mass, and therfefore correction has to continue until a correction related species which is not subject to interference is found. The complete steps of this particular correction are not described here, as the description above is sufficient to illustrate the complexity of correcting the interferences on REE.

There are also many different non-interfering isotope oxides and other isotopes of the analyte that can be used in the correction process besides the species selected in this example. The species selected in the example are mostly the ones noted in Table 4.2 for the purpose of demonstrating the correction in an easy and clear way. Similar numbers of correction equations would be needed if other available species were used.

Correction based on the polyatomic production rate

The magnitude of polyatomic interference in samples relates to the interferent element concentration, the natural abundance of the interfering isotope of interferent and the formation rate of the interfering element polyatomic ions (Garbarino and Taylor, 1987). This correction method is based on the fact that regardless of matrix variation of samples a constant fraction of the interfering element forms the interfering molecules when the plasma operating condition remains the same (British Standard ISO 17294-1:2006). This fixed fraction is the oxide or hydroxide production rate and it is also the correction factor used in

the correction equation. Lee *et al*. (2000a) examined the oxide production rate of Ba and interfering REE with changing interfering element concentration from 1 ppb to 100 ppb; the resulting correction factor (CF) remained almost constant, irrespective of concentration, when the machine operating conditions remained the same.

Prohaska et al. (1999) noted that the correction factor can be obtained by running the solution containing only the pure single interfering element (M) at a concentration which is high enough to produce a corresponding interfering element oxide (MO^+) or hydroxide (MOH^+) with sufficient sensitivity. Due to the very low formation rate of MOH^+, the MOH^+ interference is normally negligible in a sample (Jarvis, 1989) unless the interfering element in the sample is at an extremely high level and the interfered analyte is present at a very low level. Because no analyte element is present in the single interferent element solution, the signal obtained at the selected analyte isotope mass will be from the interferent element forming polyatomic ion only (Agilent Technologies, 2009). Based on the interferent element and polyatomic interference intensity of the single interfering element solution, the correction factor (CF) can then be calculated according to the equation below.

$$CF = \frac{\text{the gross intensity of interfering element oxide at the monitored analyte isotope mass}}{\text{the intensity of the selected interfering element isotope}}$$

When the samples and single interfering element solution are measured under the same or very similar operating conditions, the interference intensity in the sample equals the interfering element signal in the sample multiplied by the CF obtained from the single element solution. The correct analyte signal can then be calculated from the following equation:

Analyte isotope signal= Apparent intensity at selected analyte isotope mass - CF x intensity of the selected interfering element isotope in sample

The specific interfering element isotope that combines with the oxygen or hydroxide to form the polyatomic interference on the measured analyte isotope does not have to be the isotope monitored for obtaining the CF of the single interfering element solution. The isotope with higher natural abundance and consequently higher sensitivity among all the interfering element isotopes is normally selected for improving the accuracy of the CF. The non-

interfering isotope can also be used for determining the CF because there is a fixed abundance ratio between the non-interfering and the interfering isotope. Therefore the CF obtained based on the non-interfering isotope is a fixed fraction of the CF obtained based on the interfering isotope. The CF obtained based on two different isotopes and the relationship between them are shown in the equations below. As long as the isotope of the interfering element being measured in samples is the same as the one used for obtaining the CF the validity of using a non-interfering isotope to obtain the CF and correct the interference in samples can be guaranteed.

$$CF_{\text{non-interfering isotope}} = \frac{\text{signal of interfering isotope oxide at analyte mass}}{\text{signal at non} - \text{interfering isotope mass}}$$

$$CF_{\text{interfering isotope}} = \frac{\text{signal of interfering isotope oxide at analyte mass}}{\text{signal at interfering isotope mass}}$$

$$CF_{\text{non-interfering isotope}} = CF_{\text{interfering isotope}} * \frac{\text{signal at interfering isotope mass}}{\text{signal at non} - \text{interfering isotope mass}}$$

$$= CF_{\text{interfering isotope}} * \frac{\text{interfering isotope natural abundance}}{\text{non} - \text{interfering isotope natural abundance}}$$

As the CF calculation is based on the net signal of the interfering element and the interfering element oxide in the single interfering element solution, to obtain an accurate CF it is critical that no analyte contamination is present in the solution (British Standard ISO 17294-1:2006). De Boer (2000) notes that it is not possible to make the single element solution with zero concentration of analytes, and subtraction of analyte signal from the interfering element oxide mass should be performed when calculating the CF. Another isotope of the analyte that is not selected for the quantification purpose should be used as a control isotope to obtain the signal of the analyte at the interfering element oxide mass (De Boer, 2000). However, this may not be necessary for the REE interference correction, as the interfered analytes of- REE are normally present at an extremely low level in the solution e.g. acid, stock solution used for single element solution preparation or DI water. More importantly, the interfering element concentration in the single element solution is required to be at a high level and the produced

oxide concentration will then be much higher than the potential analyte REE concentration in the solution. Therefore, the analyte REE in the single element solution will have negligible influence on the CF result even though the signal of analyte is not removed in the CF calculation.

British Standard ISO 17294-1 (2006) and De Boer (2000) recommend eliminating the background noise interference and obtaining more accurate results by subtracting the blank signal from both (1) the single interfering element solutions when calculating the correction factor and (2) the measured samples when correcting the interference on the analytes. The blank signal then needs to be removed when generating the calibration curve. However, the calibration curve commonly plotted is based on the sum of the background and standard signal at the analyte mass, which was the approach adopted in this work (as suggested by Agilent Technologies and described in Section 3.4.2). However, ultrapure DI water and acids were used in the blank preparation for this study, as described in Section 3.4.2, and it was concluded that the background interferences would be negligible compared to the net signal of the measured species in the single interferent solution and the net signal of the interfering element in the samples. The background noise issue was therefore disregarded when applying this correction method.

To ensure the CF determined from the high concentration single element solution is applicable to the sample with different concentrations of interfering element, it is better to measure another single interfering element solution with the same concentration as in sample, as suggested by specialist at Agilent Technologies (*personal communication*, Maryanne Thomsen, Agilent Technologies, 27th May, 2016).

As the CF in the correction equation is dependent on the plasma operating conditions (Vaughan and Horlick, 1986), the CF keeps constant when the plasma operating conditions stay the same every day. The CeO/Ce ratio can be used as the indicator to check whether there is a variation of instrument operating conditions. As suggested by the specialist at Agilent Technologies (*personal communication*, Maryanne Thomsen, Agilent Technologies, 14th June, 2016), when the Ce oxide production rate measured during the tuning process is similar to that measured previously (within a small tolerance) there is no need to re-run the single interfering element solutions before sample measurement and the CF obtained from the previous experiment can be used directly in the correction equation.

For the purpose of obtaining a more accurate CF, even though the single element solution is measured as a routine procedure every day when the CeO/Ce is similar day to day, EPA (6020A) suggests not to use the obtained CF directly in the sample interference correction. The reason is that there is a drift of the operating condition during sample measurement as the sample matrix starts to deposit on the sample and skimmer cones with the increase in measuring time, which gradually reduces the orifice size of the cones and causes a variation in polyatomic production rate (Prohaska *et al*. 1999; Lichte *et al*. 1987). Lichte *et al*. (1987) showed that the drift of CF can be nearly 100% after three hours of sample measurement. Therefore, the CF obtained at the beginning of the analysis may not be suitable for application to samples measured at a later time. Applying the CF obtained at the beginning of the experiment to the correction of all samples is based on the assumption that CF neither varies with time or matrix (Aries et al. 2000).

Aries et al. (2000) suggests calculating the interfering polyatomic production rate in each sample instead to overcome matrix and time dependence problems. EPA (6020A) notes that an element with the similar oxide forming behaviour as the interfering element can be used as the oxide internal standard to adjust the CF variation with regards to the measuring time. At the given plasma condition, the internal standard oxide production rate undergoes a similar drift as the interfering element oxide production rate, so the internal standard oxide production rate normalized CF remains invariant with the changing of time (Lichte *et al*. 1987). It should be noted that this normalized CF can remain constant only when the drift of CF is less than 50%. When the CF drifts to a higher level, second order equations will need to be applied to ensure the accuracy of the correction (Lichte *et al*. 1987). When the internal standard has a similar first ionisation energy to the interfering element, the CF after normalization is also independent of sample composition. The hydroxide production rate of the interfering element is also independent of time and sample matrix after normalizing to a suitable internal standard hydroxide production rate (Aries et al. 2000).

The internal element selected for normalization needs to have a strong bond with the oxygen and be able to produce the oxide with sufficient sensitivity when the normalizing element in solution is at a suitably high concentration. In addition, the normalizing element and its oxide must not suffer from any spectral interferences (Aries et al. 2000). Th (atomic mass 232) is normally used as the normalization element for REE analysis to adjust the variation of REE oxide or hydroxide production rate during sample measurement (Lichte *et al*., 1987). When

use M^+ to represent the interfering element, the oxide production rate of the interfering element is MO^+/M^+, and the ratio of $(MO^+/M^+)/(ThO^+/Th^+)$ stays constant during sample measurement (Lichte *et al*., 1987).

The steps to obtain the interfering oxide or hydroxide signal in each sample are as follows:

1. Add thorium to each single interfering element solution and sample, and ensure the concentration of Th added is high enough to produce the ThO with sufficient sensitivity

2. Obtain the constant value of $(MO^+/M^+)/(ThO^+/Th^+)$ based on the intensity at the mass of the interfering element oxide MO^+, and of the interfering elements M^+, ThO^+ and Th^+ in the single interfering element solution

3. Determine the signal at mass of M^+, ThO^+ and Th^+ in measured sample

4. The interfering oxide in each sample can be calculated based on the constant $(MO^+/M^+)/(ThO^+/Th^+)$ value obtained from single interfering element solution, and M^+, ThO^+ and Th^+ in sample through the equation below:

MO^+ signal in sample= $(MO^+/M^+)/(ThO^+/Th^+)$ of single interfering element solution * (ThO^+/Th^+) value in sample * M^+ signal in sample

It should be noted that all of the signal or intensity mentioned above is the ratio of the signal at measured mass to the signal of the internal standard that is assigned to that measured mass.

According to the interference species shown in Table 4.2, when ignoring negligible species (the species not in bold), all the MREE and most of the HREE only have one interference species. As each interfering LREE which combines with the oxygen to form the interference on MREE and one HREE (Ho in this case) does not suffer from interference itself, only one correction equation is required to correct the interference on the interfered MREE and Ho when the correction method described in this section is adopted. For HREE (Er) with two different LREE-oxide interferences, two correction equations are required, but they are not associated with each other and the compound error mentioned in Section 4.3.3 will not occur. For the rest of the HREE subject to interference by the MREE-oxide, two equations (one based on the other) are required for the correction. The first is to remove LREE-oxide interference on interfering MREE, and then the corrected signal of the interfered HREE can be obtained based on the net signal of the interfering MREE. As the number of equations is

only two for these HREE corrections the compound error caused in this case will be quite small and much less than when using the first method.

However, obtaining the CF may not be straightforward when different isotopes of the same interferent element each combines with a different element to form different species with exactly the same mass to charge ratio. To distinguish the signal of two different interference species and obtain the CF for each of them it is necessary to determine one of the interference species signals first, based on the abundance ratio of one of the interference component element isotopes (Aries et al. 2000). This situation occurs with REE interference correction. For example, two isotopes of interfering element Nd, ^{143}Nd and ^{142Nd}, can respectively form $^{143}Nd^{16}O^{+}$ and $^{142}NdOH^{+}$ interference on ^{159}Tb. Since the hydroxide formation rate is normally 10% of the oxide formation rate (Prohaska *et al*., 1999), the hydroxide interferences are normally negligible for REE measurement unless the interfering element is present at a relatively high level compared to the interfered element. The hydroxide interferences were not considered in this work based on the concentrations of interfering and interfered REE in the samples.

Correction approach adopted in this study

As noted in Section 4.3.3, time independent and individual sample-based correction is the main advantage of the first method, which is based on the signal of non-analyte interfering polyatomic ions in the sample. Although the main weakness of the original second correction method based only on the CF of single interfering element solution is that the correction effectiveness declines with time, the CF drift problem can be overcome by applying an internal standard. In this sense, the second approach can have the same time independent benefit as the first method.

The main drawback of the first method compared with the second method for REE interference correction is that the correction equations involved in the first method are very complicated and consequently the accuracy of correction decreases substantially due to the accumulation of errors induced by those equations. On the other hand, the correction equation number required is reduced significantly when the second method is applied and the accuracy of the correction is improved, and so the second method is more suitable to use in this respect.

However, there are some unavoidable drawbacks in the correction process no matter which method is used:

The first issue is that the whole correction process is time consuming. For the first correction method, the removal of REE interference requires application of numerous correction equations on the mass of non-interfering isotope oxide (in respect to the specific analyte that is overlapped by the interfering isotope oxide) before then applying the formal correction equation on that analyte. This is a time-consuming process In addition, to obtain the non-analyte interfering molecular signal requires additional measurements of the mass of non-analyte interfering molecule and all the related species that are needed for obtaining the non-analyte interfering molecular signal. Those additional measurements then increase the time needed for analysis. For the second method, the measurement of all single interfering element solutions significantly increases the analysis time.

The second drawback is that some unexpected correction errors may occur when the unknown sample has an unusual complex matrix, even though both correction methods consider all the potentially non-negligible interference species mentioned in literature. This is because only the common interferences that may occur in different types of water samples have been described in the literature. If an unusual interferent is present at a relatively high concentration in the sample, the interferent forming interference may become the non-negligible interference species when the interfered element is present at a low concentration.

To be more specific, for the first method, the errors may occur when the unexpected interference species overlaps with analyte or all the correction-related species that are required to obtain the analyte signal. For the second method, the net signal of the interfering element in the sample is another important factor to make sure the correction on interfered analyte is accurate. Therefore, besides the errors caused by failing to remove unexpected interference species on the analyte, Agilent Technologies (2005) mentions that errors may also occur when an unknown sample with complex matrix composition causes some unexpected interferences on the interfering element mass. As a result the intensity of the interfering element mass may not be noticed, and the sum of the interfering element and the unexpected interferences signal are erroneously used in the correction equation.

After the comparison between two methods, it is clear that the second method is the best option to use in the correction process. In this study, correction mostly followed the

procedure noted in Section 4.3.3. It should be noted that the correction equation method is not suitable for removing the interferences on environmental elements as mentioned in Section 4.2.2. Irrespective of whether the first or the second method is selected, a series of associated equations are required in the correction process. The accumulated errors caused by those equations can still lead to an erroneous result after correction. Therefore, Section 4.3.3 and the following section regards to the mathematical correction only targets the interferences removal on REE.

There were two aspects that required attention in applying the second method:

The first one is there was a small variation of the Ce oxide production rate from day to day in this study, because the operating conditions were shown not to be the same every day. As the CF value strongly depends on the instrument operating conditions, the single interfering solutions were run each day before sample measurement to ensure the CF accuracy.

The second issue was that the application of the internal standard oxide production rate is recommended when adopting the correction factor method (EPA, 6020A; De Boer, 2000; Aries *et al*., 2000). Th was not added to each of the single interferent element solutions, calibration standards and measured samples in the experiments. Rather, the single interferent element solution contained only the interfering element itself, and the CF obtained from the single interfering element solution was applied directly to the measured samples to remove the interferences. This is because the drift of the CF was within the acceptable range during the period that the samples requiring correction were measured. A more detailed explanation is provided in Section 4.4.4.

As suggested by Lee *et al*. (2000b), the analysis was undertaken in the order of measuring calibration blank, four REE calibration standards, each single interferent element solution, and finally the samples. To ensure the accuracy of the CF obtained from the single interfering element solution, interference correction check solutions which contained only the interferent element and the interfered analyte, at a concentration similar to that in the samples, were measured before sample analysis. The mathematical equations applied in the experiments, based on the second method, are shown in Section 4.4 below.

4.4 Correction of BaO, LREEO and MREEO interference on REE

4.4.1 Single interfering element solutions used in this study

Different isotopes of barium form a series of Ba-oxides with different mass overlapping on different REE. Based on the mass of selected REE isotopes in this study, ^{146}Nd and ^{153}Eu were interfered by $^{130}BaO^+$ and $^{137}Ba^{16}O^+$ respectively. Due to the low natural abundance of ^{130}Ba (0.106%) the interference on ^{146}Nd should be negligible. But special attention needed to be paid to the $^{137}Ba^{16}O^+$ interference on ^{153}Eu due to the much higher concentration of Ba compared to Eu in natural waters (Shaw et al. 2003) and the higher natural abundance of ^{137}Ba (11.232%). When the concentration difference between Ba and Eu is extremely large, the $^{137}Ba^{16}O^+$ interference can have a serious influence on the accuracy of Eu measurement if no correction equation is applied to the measured results.

Table 4.4: Composition of pure single interfering element solution measured in this study

Element contained in the solution(1)	Solution number	Single element concentration in solution
Pr	1	50ppb
	2	100ppb
Nd	1	50ppb
	2	100ppb
Sm	1	50ppb
	2	100ppb
Eu	1	50ppb
	2	100ppb
Gd	1	50ppb
	2	100ppb
Tb	1	50ppb
	2	100ppb
Ba	1	10ppb(2)
	2	50ppb(3)/100ppb(4)
	3	100ppb(3)/1ppm(4)

Notes:

(1) Only single Ba solutions were measured on each occasion when undertaking REE analysis experiments from September 2016, while the single REE solutions were only measured in the REE analysis experiment in September 2016;

(2) Concentration of single Ba solution used in the REE analysis from September 2016 to June, 2017;

(3) Single Ba solution concentration used only in the REE analysis experiment in September 2016;

(4) Single Ba solution concentration used in the REE analysis experiments after September 2016.

Table 4.4 shows the concentration of single interfering element solutions used in this study to obtain the correction factors for $^{137}Ba^{16}O^{+}$ interference on ^{153}Eu, LREEO interference on MREE, and the LREEO and MREEO interference on HREE. Single element solutions of seven different interferents were required in this study: Ba, Pr, Nd, Sm, Eu, Gd, Tb. Single Ba solution was made up with VWR 1000 ppm single Ba standard solution for ICP (traceable to NIST), Merck ultra-pure concentrated nitric acid (60%), Merck ultra-pure concentrated hydrochloric acid (30%) and 18.2Ω MilliQ deionised water. Each single interfering REE solution was prepared with 10 ppm Fisher Chemical mono-element standard solution, and the same acid and DI water used for preparing the single Ba solution. Each single interfering element solution was prepared to form a required concentration of interfering element solution in 2% (v/v) HNO_3 and 1% (v/v) HCl matrix.

For each interferent REE, two single element solutions, one with concentration of 50 ppb and another with concentration of 100 ppb were measured. 100 ppb of interfering element was selected to ensure an accurate signal of the interfering element oxide was determined. Although the specialist at Agilent Technologies (*personal communication,* Maryanne Thomsen, Agilent Technologies, 27th May, 2016) suggested measurement of another single element solution with an interfering element concentration similar to that in the samples, to verify that the CF obtained from high concentration single element solution was suitable to use in the measured samples. However, interfering REE concentrations in the samples of this study were at a quite low level and the CF obtained, based on such a low concentration of single element solution, may not be that reliable. 50 ppb of interfering element was therefore selected instead to check whether the CF obtained from the single element solution with lower concentration (which can still maintain a sufficient sensitivity obtained at the interfering element oxide mass) was similar to that in the 100 ppb single element solution. The correction factors of the two single element solutions were very similar and the averaged value of two solutions was used as the CF for interference correction in samples.

The single interfering REE solutions were only measured once for the samples collected in September 2016. This is because after applying the obtained CF to the measured samples the contributions of LREEO and MREEO interferences to the analyte's mass were found to be negligible (<5% error); the concentration differences between the interfering and interfered elements were small. The interfering and interfered element concentration differences of samples collected from the fieldwork after September 2016 were all similar to that from

September 2016. Therefore, the single interfering REE solutions were not measured again and the LREEO and MREEO interference in samples were not corrected. Section 4.5 shows the CF for each interfering REE oxide, the concentration differences between the interfering and interfered REE, the results of interfered REE obtained before and after correction, and the error caused by the interferences.

The situation for BaO interference on Eu was totally different. Although BaO interference in the samples collected from G2 to G5 was negligible, its interference in G1 and G7 samples was much more serious based on the correction results from September 2016 to September 2017. Therefore, measurement of single Ba solutions and the correction of BaO interference on Eu for the samples was undertaken from September 2016. In the experiment undertaken in September 2016, three single Ba solutions with concentrations of 10 ppb, 50 ppb, 100 ppb were measured. Three single Ba solutions with concentration of 10 ppb, 100 ppb and 1 ppm were used for obtaining the CF in the experiments undertaken from October 2016 to June 2017. The last experiment only used two single Ba solutions, one containing 100 ppb Ba and the other 1 ppm Ba in solution.

The reason for discontinuing measurement of the 10 ppb Ba solution in the last experiment was that the previous experiments showed that the RSD of the BaO signal obtained from the 10 ppb single Ba solution was sometimes high, indicating that 10 ppb of Ba was not high enough to produce the oxide with sufficient sensitivity. In addition, previous experiments also showed that the CF obtained from the 10 ppb single Ba solution was sometimes not similar to that obtained from 100 ppb and 1 ppm single Ba solutions. The original reason for measuring the 10 ppb single Ba solution was because it was a similar concentration to that of the actual water samples. However, the results described above illustrated that it was more appropriate to measure the high concentration single interfering REE solutions in the experiments to ensure accuracy of the CF.

The September 2016 showed the importance of correcting BaO interference in samples, and also that the concentration of 10 ppb Ba solution was too low to provide an accurate result. After September 2016 100 ppb and 1 ppm single Ba solutions were used in the experiments, rather than 50 ppb and 100 ppb single Ba solutions. This was to ensure a high sensitivity for BaO, with a lower RSD for the BaO signal from the single Ba solutions, and consequently a more accurate CF value. Section 4.5 shows the CF results from different concentrations of Ba

solutions, the concentration differences between the Ba and Eu in samples, the error caused by BaO interference in samples and the corrected and uncorrected Eu results in samples.

A new clean blank solution containing 2% (v/v) HNO_3 and 1% (v/v) HCl was measured before the single element solution analysis and was measured between the measurements of two different concentrations of single interferent solutions to eliminate instrument memory effects and ensure the measured solution contained only the interferent itself.

4.4.2 CF and correction equations applied on analytes

Correction factor of interference species

Table 4.5 shows the interference species that were checked in this study for their degree of interference on measured REE isotopes, the interfered REE isotope, the isotope of the interfering element used to obtain each interference species CF from the single interferent solution, and the equation for obtaining the CF of each interference.

Table 4.5: Measured isotope of interfering element of single interferent solution, interference species, analyte isotopes that interfering ions acts on and equations used for determining the CF

Single element solution	Measuring Interferent isotopes(1)	Interfering ion(2)	Acting on/Interfered isotopes	Interference correction factor
Ba	^{137}Ba	$^{137}Ba^{16}O^{+}$	^{153}Eu	$^{137}Ba^{16}O^{+}/^{137}Ba$
Pr	^{141}Pr	$^{141}Pr^{16}O^{+}$	^{157}Gd	$^{141}Pr^{16}O^{+}/^{141}Pr$
Nd	^{146}Nd	$^{143}Nd^{16}O^{+}$	^{159}Tb	$^{143}Nd^{16}O^{+}/^{146}Nd$
	^{146}Nd	$^{150}Nd^{16}O^{+}$	^{166}Er	$^{150}Nd^{16}O^{+}/^{146}Nd$
Sm	^{147}Sm	$^{147}Sm^{16}O^{+}$	^{163}Dy	$^{147}Sm^{16}O^{+}/^{147}Sm$
	^{147}Sm	$^{149}Sm^{16}O^{+}$	^{165}Ho	$^{149}Sm^{16}O^{+}/^{147}Sm$
	^{147}Sm	$^{150}Sm^{16}O^{+}$	^{166}Er	$^{150}Sm^{16}O^{+}/^{147}Sm$
Eu	^{153}Eu	$^{153}Eu^{16}O^{+}$ (3)	^{169}Tm	$^{153}Eu^{16}O^{+}/^{153}Eu$
Gd	^{157}Gd	$^{156}Gd^{16}O^{+}$	^{172}Yb	$^{156}Gd^{16}O^{+}/^{157}Gd$
Tb	^{159}Tb	$^{159}Tb^{16}O^{+}$	^{175}Lu	$^{159}Tb^{16}O^{+}/^{159}Tb$

Notes:

(1) Some of the monitoring interferents isotopes e.g. Nd, Sm of the single element solution for obtaining the CF are not the same isotope comprising the interfering molecule e.g. $^{143}Nd^{16}O^{+}$, $^{149}Sm^{16}O^{+}$, but the signal of interfering element oxide is still proportional to the monitoring interferent isotope intensity;

(2) This column shows the interfering isotope of interferent forming oxide which has the same mass to charge ratio as the measured isotope of analyte, and the signal obtained at the interfered analyte isotope mass of single interferent solution was the net signal of interference used to get the CF. The interference species that are not in bold in Table 4.2 are not included in this column due to their negligible contribution at the analytes mass;

(3) Lee et al. (2000b) suggest to ignore $^{153}EuO^{+}$ interference on $^{169}Tm^{+}$ due to the small natural abundance ratio of Eu to Tm and low oxide formation rate of ^{153}Eu.

In Table 4.5, besides Nd and Sm, each interfering element only has one interfering isotope which forms oxide interference of the selected analyte isotope mass. Nd has two interfering isotopes, ^{143}Nd and ^{150}Nd, forming $^{143}Nd^{16}O^{+}$ interference at measured Tb mass, and $^{150}Nd^{16}O^{+}$ interference at measured Er mass respectively. Sm has three interfering isotopes, ^{147}Sm, ^{149}Sm, ^{150}Sm, and their corresponding interfering oxides $^{147}Sm^{16}O^{+}$, $^{149}Sm^{16}O^{+}$, $^{150}Sm^{16}O^{+}$ overlap on ^{163}Dy, ^{165}Ho, ^{166}Er respectively.

For an interferent with mono-interfering isotope (in respect of the measured analyte isotope mass), if using Ba as an example, the calculation of interference (BaO) CF according to the single Ba solutions measurement was based on the ratio of the signal at the selected analyte isotope mass-^{153}Eu which represents the interference $^{137}Ba^{16}O^{+}$ signal to the signal at the measured isotope of interferent-^{137}Ba.

For Nd and Sm, which have more than one interfering isotopes, the CF calculation for each interference specie was the same as the calculation process described in the above paragraph. If using Nd as an example, the CF of $^{143}Nd^{16}O^{+}$ equalled the ratio of the gross signal at m/z 159 amu (mass of Tb isotope selected for sample determination) to the signal of the measured isotope of the interferent which was ^{146}Nd of the single Nd solutions.

Correction equations applied on analytes

To obtain the correct signal of the interfered analytes requires the CF of the interference species, the interfering element, and the interfered analyte concentration in the samples. Based on the experimentally obtained mean CF value from the single interferent solutions for each interference species, the interference species signal and correct signal of interfered analytes ^{153}Eu, ^{157}Gd, ^{159}Tb, ^{163}Dy, ^{165}Ho, ^{166}Er, ^{169}Tm, ^{172}Yb, ^{175}Lu in samples can be determined based on the equations shown in Table 4.6.

As shown in Table 4.6, the net signals of interfered analytes were obtained from two-step equations:

(1) the net signal of the interference of the samples based on the previously derived mean CF and the intensity of the monitored interferent isotope of samples through the equations shown in the first column of Table 4.6;

(2) Obtain the net signal of the interfered analyte isotope based on the net signal of interference of samples through the equations described in the second column of Table 4.6.

Table 4.6: Correction equations for REE isobaric polyatomic interferences

Equations for obtaining net intensities of interference	Net intensity of interfered analyte isotopes
$BaO(153)=^{137}Ba(app.)*[^{137}Ba^{16}O^{+}/^{137}Ba]_m$	**Eu(153)** = ^{153}Eu (app.)-BaO(153)
$PrO(157)=^{141}Pr(app.)*[^{141}Pr^{16}O^{+}/^{141}Pr]_m$	**Gd(157)** = ^{157}Gd (app.)-PrO(157)
$NdO(159)=^{146}Nd(app.)*[^{143}Nd^{16}O^{+}/^{146}Nd]_m$	**Tb(159)** = ^{159}Tb (app.)-NdO(159)
$SmO(163)=^{147}Sm(app.)*[^{147}Sm^{16}O^{+}/^{147}Sm]_m$	**Dy(163)** = ^{163}Dy (app.)-SmO(163)
$SmO(165)=^{147}Sm(app.)*[^{149}Sm^{16}O^{+}/^{147}Sm]_m$	**Ho(165)** = ^{165}Ho (app.)-SmO(165)
$SmO(166)=^{147}Sm(app.)*[^{150}Sm^{16}O^{+}/^{147}Sm]_m$	**Er(166)** =^{166}Er (app.)-SmO(166)-NdO(166)
$NdO(166)=^{146}Nd(app.)*[^{150}Nd^{16}O^{+}/^{146}Nd]_m$	
EuO(169)= **Eu(153)** $*[^{153}Eu^{16}O^{+}/^{153}Eu]_m$	**Tm(169)** =^{169}Tm (app.)-EuO(169)
GdO(172)= **Gd(157)** $*[^{156}Gd^{16}O^{+}/^{157}Gd]_m$	**Yb(172)** =^{172}Yb (app.)- GdO(172)
TbO(175)= **Tb(159)** $*[^{159}Tb^{16}O^{+}/^{159}Tb]_m$	**Lu(175)** = ^{175}Lu (app.)- TbO(175)

Notes:

(1) M(n) means net intensity of specie M at mass of n amu;

(2) (app.) in the equations means the apparent signal at that mass;

(3) $[\ ]_m$ in the first column means the mean CF obtained from single interferent solutions;

(4) The bold REE are the interfered analyte isotope, and the bold REE value used in the equations were the net signal obtained after correction.

Special attention was paid to three interfered analytes: ^{169}Tm, ^{172}Yb and ^{175}Lu. This was because the interference on these analytes is caused by $^{153}Eu^{16}O^{+}$, $^{156}Gd^{16}O^{+}$, and $^{159}Tb^{16}O^{+}$ respectively, and the parent elements of these interferents (Eu, Gd and Tb) also suffer from oxide overlap. The corrected net signal of the parent element Eu, Gd, Tb in samples was used to determine the corresponding oxide $^{153}Eu^{16}O^{+}$, $^{156}Gd^{16}O^{+}$, $^{159}Tb^{16}O^{+}$ signal in samples.

As the REE calibration standards contained both the interfering REE and interfered REE, the MREE and HREE in standards were also affected by the interferences (Garbarino, and Taylor, 1987). As the concentrations of interfering REE and interfered REE in standards were the same, the interference should have negligible influence on the accuracy of results even though mathematical correction was not undertaken. When applying the correction equations onto the batch, a synchronous correction of the minor interferences in the calibration standards and the interferences in the samples was carried out. The correct concentrations of analytes were then obtained based on the corrected analytes' signals and the corrected calibration standard curve.

4.4.3 Performance of obtained CF in the BaO interference correction

As noted in Section 4.4.1, the interferences caused by LREEO and MREEO were negligible in samples, the removal of BaO interference on Eu must be undertaken for samples G1 and G7 due to the relatively large error caused by BaO. Although the CF obtained from single Ba solutions with different concentrations (except 10 ppb) were very similar, it was necessary to verify the CF effectiveness before applying it for correction of concentrations in standards and samples correction.

BaO interference check solution(s) containing only Ba and Eu, with similar concentration ratios of Ba to Eu as samples G1 and/or G7 were prepared and measured before sample analysis. This was to check the effectiveness of the CF. The check solutions were re-analysed either after analysis of all samples, or during sample analysis, to evaluate any drift of CF with time. This was done for experiments undertaken between September 2016 and June 2017. Table 4.7 shows Ba and Eu concentration of the interference check solutions used in the experiments from September 2016 to June 2017. It also shows the results of interfered element Eu in the interference check solutions before and after applying the CF for BaO. The percentage differences between the measured Eu results and prepared Eu concentrations in the interference check solutions before and after correction are also shown in Table 4.7.

Depending on the concentration differences between the interferent Ba and interfered Eu in all the prepared interference check solutions from September 2016 to June 2017, the measured Eu error ranged from 7.46% to 42.8% when the CF was not applied to the measured results of the first check solution. Table 4.7 shows that the percentage differences between the corrected and the "true" Eu concentrations of the first interference check solutions were all reduced to less than 3.79% after the application of the CF, which verified the effectiveness of the CF. As the interference check solutions approximately mimicked the concentration differences between Ba and Eu in samples G1 and/ or G7, effective removal of BaO interference in the interference check solutions after correction shows that the obtained CF can successfully reduce the interference in samples to an acceptable level.

Table 4.7: Composition of BaO interference check solutions used in the experiments and the effectiveness of mathematics correction

Date	No. *	Interference check solution composition	Eu result before correction (ppb)	Concentration difference (%) before correction	Eu result after correction (ppb)	Concentration difference (%) after correction
Sep 2016	1	100ppb Ba, 0.05ppb Eu	0.0599	19.85%	0.0485	-3.04%
		100ppb Ba, 0.1ppb Eu	0.108	8.07%	0.0967	-3.35%
	2	100ppb Ba, 0.05ppb Eu	0.0606	21.30%	0.0491	-1.71%
		100ppb Ba, 0.1ppb Eu	0.108	8.42%	0.0969	-3.06%
Oct 2016	1	20ppb Ba, 0.005ppb Eu	0.0071	42.80%	0.0049	-0.19%
		50ppb Ba, 0.05ppb Eu	0.0544	8.90%	0.049	-1.94%
	2	20ppb Ba, 0.005ppb Eu	0.0069	37.39%	0.0047	-5.73%
		50ppb Ba, 0.05ppb Eu	0.0529	5.71%	0.0474	-5.19%
Nov 2016	1	10ppb Ba, 0.005ppb Eu	0.0063	26.80%	0.0051	2.8%
		10ppb Ba, 0.01ppb Eu	0.0114	14.3%	0.0102	1.9%
	2	10ppb Ba, 0.005ppb Eu	0.0063	26.2%	0.0051	1.6%
		10ppb Ba, 0.01ppb Eu	0.0108	8.1%	0.0096	-4.2%
Nov 2016	1	10ppb Ba, 0.005ppb Eu	0.0065	29.04%	0.0052	3.79%
		10ppb Ba, 0.01ppb Eu	0.0116	15.87%	0.0103	3.46%
	2	10ppb Ba, 0.005ppb Eu	0.0061	22.59%	0.0048	-3.22%
Dec 2016	1	20ppb Ba, 0.005ppb Eu	0.007	40.6%	0.0049	-0.6%
		50ppb Ba, 0.05ppb Eu	0.0549	9.84%	0.0497	-0.64%
	2	50ppb Ba, 0.05ppb Eu	0.0526	5.18%	0.0475	5.06%
June 2017	1	50ppb Ba, 0.05ppb Eu	0.0549	9.88%	0.0508	1.5%
	2	50ppb Ba, 0.05ppb Eu	0.0526	5.12%	0.0484	-3.18%

Note: * The interference check solutions were measured twice. The first measurement was undertaken just after the single interferent solution analysis and before the sample analysis. The second measurement was undertaken after analysis of all samples for the experiments from September 2016 to December, 2016 except the second day measurement on Nov, 2016. The second measurement on the second day analysis of samples collected on Nov, 2016 was performed after half samples measurement (2 hours interval between the first and second time measurement). The second measurement on the June 2017 samples was undertaken just after analysis of samples G7 and G1.

Samples G7 and G1 were measured immediately after the interference check solutions to maximise reduction in CF drift effect on the correction. To ensure the accuracy of corrected Eu results for samples G1 and G7, it is necessary to check the degree of CF drift with time and performance of Eu correction on the measured samples when applying the mean CF obtained from the single Ba solutions at the beginning of the experiment. To fulfil this aim, a second measurement of the interference check solutions was undertaken after hours sample analysis. This was done for analysis of all samples from September 2016 to June 2017 and the results are shown Table 4.7. The discussion of the drift of the CF is described in the Section 4.4.4.

4.4.4 Evaluation of CF drift with time

Table 4.7 shows that the errors of Eu results were a little bit higher after correction (5.73% error maximum) compared with that of the first measurement. The magnitude of error was generally dependent on the time interval between the first and second measurement. The size of error also appeared to be related to the concentration differences between the Ba and Eu in solutions, as shown in Table 4.7.

To better check the degree of CF drift with time, first and second interference check solutions, with the same Ba to Eu concentration ratios, were analysed again but with different time intervals between measurements. Samples from September 2016 to June 2017 were used in this analysis, and the correction performance is shown in Table 4.8. The concentration of the interfering element Ba in all the selected interference check solutions noted in Table 4.8 was 1000 times greater than the interfered element Eu concentration in all solutions.

There relationship between correction performance and time was not entirely clear. For example, the error with three hours between measurements was 5.06% in December 2016, while the error was -4.2% with four hours between measurements in November 2016 (due to the different operating conditions of each time experiment). Nevertheless, when looking at all data Table 4.8 there appears to be a broad trend of increasing CF drift with increasing analysis time.

Table 4.8: Drift of correction effect with time

Date	Interference check solution composition	Interval between first and second time measurement of interference check solutions	Concentration difference (%) of the second time interference check solutions measurement after correction
Sep 2016	100ppb Ba, 0.1ppb Eu	2 hours	-3.06%
Oct 2016	50ppb Ba, 0.05ppb Eu	4 and half hours	-5.19%
Nov 2016	10ppb Ba, 0.01ppb Eu	4 hours	-4.2%
Dec 2016	50ppb Ba, 0.05ppb Eu	3 hours	5.06%
June 2017	50ppb Ba, 0.05ppb Eu	1 and half hours	-3.18%

For the experiments from September 2016 to December 2016, the second measurement was undertaken after analysis of all samples (G7, G1, G5, G4, G3, G2). The maximum error was 5.19% for the second measurement, which was undertaken after 4.5 hours sample analysis in October 2016. Since a 5% error can normally be considered as negligible, this suggests that

even though normalization of CF was not performed to correct the CF drift during the correction process, an effective correction can still be maintained during sample measurement in this study.

Due to the high BaO interference level in samples G1 and G7, for the purposes of checking the correction effect on these highly interfered samples, the second measurement of the interference check solution was undertaken immediately after analysis of samples G7 and G1 in June, 2017. The error was around 3%, indicating that a successful correction could be made of even those samples most influenced by the BaO interference. The interference check solutions were not measured in the last time experiment on September 2017 because the analysis of samples G7 and G1 was undertaken immediately after the single Ba solutions measurement and whole samples analysis was finished within three hours. The CF drift effect can be ignored and the CF determined should be effective for corrections of G1 and G7 analyses, and the correction of all other samples based on the values determined for the September 2016 to June 2017 samples.

Although interferences from BaO on samples G2 to G5 was minimal, the correction equation was applied to them also to remove the signal of BaO on Eu mass. Thus, the approach was consistent to that for samples G1 and G7.

4.5 Oxide interference degree on REE

4.5.1 BaO interference on Eu

Table 4.9 shows the CF applied in the correction equations to obtain the corrected Eu concentration of samples from September 2016 to September 2017. As the measurement of samples collected on November 2017 was performed on two different dates, two CF values for the November analyses were then noted in Table 4.9. The CF values shown in Table 4.9 are based on the signal of interference, not the concentration, and monitoring interferent isotope in the single interferent solutions. Therefore, when applying the CF in the correction equation in the software, the software used the input CF and the signal of interferent isotope in the samples to obtain the interference signal in the samples, and then subtracted the interference signal from the apparent signal obtained at the analyte mass to get the net signal of the analyte. The corrected concentration of analyte in the samples was then obtained based on the calibration curve and the corrected signal of the analyte.

Table 4.9: CF used in the correction equations

Date	BaO correction factor equation	CF value
Sep 2016	$^{137}Ba^{16}O^{+}/^{137}Ba$	0.000968
Oct 2016	$^{137}Ba^{16}O^{+}/^{137}Ba$	0.000926
Nov 2016	$^{137}Ba^{16}O^{+}/^{137}Ba$	0.00102
		0.001065
Dec 2016	$^{137}Ba^{16}O^{+}/^{137}Ba$	0.000905
June 2017	$^{137}Ba^{16}O^{+}/^{137}Ba$	0.000754
Sep 2017	$^{137}Ba^{16}O^{+}/^{137}Ba$	0.001096

For samples G1 and G6 from September 2016 to September 2017, after applying the CF and correction equations (Table 4.9) to the raw data, BaO induced errors on Eu and the concentration differences between interferent Ba and interfered Eu were calculated. The results are shown in Table 4.10. The error in Table 4.10 was calculated based on the concentration of Eu before and after applying the correction equations. The Eu concentration used for calculating the difference between Ba and Eu was the value after correction. The raw Eu data before correction, the Eu concentration after correction and Ba concentration of the G1 and G7 samples collected from September 2016 to September 2017 are listed in Appendix A.

Dulski (1994) suggests that there is no need to subtract the interference from the measured analyte mass when the interference production rate obtained from the single interfering element solution is below 1%. The CF obtained on different dates in this study were all less than 0.11% according to Table 4.9. It can be seen from Table 4.10 that most of the BaO interference induced errors on Eu concentration of samples G1 and G7 were greater than 10% and the highest error was more than 50%. This indicates that the interferences were non-negligible and corrections must be undertaken even though the BaO production rate was less than 0.11%. This is because, as noted before, the magnitude of interference is also sample-related and the concentration of interferent element and interfered element in samples has significant influence on the accuracy of results. As the concentrations of Ba were at least three orders of magnitude greater than that of Eu in most of the collected G1 and G7 samples, a high degree of BaO was generated during measurement when compared with Eu concentration in samples.

Table 4.10: Percentage error on Eu before correction, and the degree of BaO interference in samples G1 and G7

Date	Sample	Error%	Concentration ratio of Ba to Eu	Date	Sample	Error%	Concentration ratio of Ba to Eu
Sep 2016	G1 0.1F	38.88%	3459	15th Nov 2016	G7 0.1F	14.02%	1141
	G1 0.45F	30.03%	2672		G7 0.45F	14.21%	1162
	G1 Tot	34.08%	3032		G7 Tot	13.72%	1119
	G7 0.1F	13.92%	1173		G1 ultra	17.13%	1397
	G7 0.45F	12.19%	1083		G1 0.1F	7.97%	650
	G7 Tot	11.50%	1086		G1 0.45F	7.10%	579
13rd Oct 2016	G1 ultra	36.68%	3294		G1 Tot	5.81%	475
	G1 0.1F	38.51%	3459	Dec 2016	G1 ultra	35.72%	3245
	G1 0.45F	37.35%	3355		G1 0.1F	21.05%	1938
	G1 Tot	33.45%	3004		G1 0.45F	20.29%	1875
	G7 ultra	49.85%	4478		G1 Tot	19.43%	1814
	G7 0.1F	25.83%	2320		G7 ultra	57.49%	5205
	G7 0.45F	21.98%	1975		G7 0.1F	23.68%	2176
	G7 Tot	21.16%	1901		G7 0.45F	22.47%	2020
27th Oct 2016	G1 ultra	39.30%	3531		G7 Tot	22.55%	2044
	G1 0.1F	32.68%	2936	June 2017	G1 ultra	64.62%	7644
	G1 0.45F	33.97%	3051		G1 0.1F	32.09%	3707
	G1 Tot	33.96%	3051		G1 0.45F	31.49%	3724
	G7 ultra	57.14%	5133		G1 Tot	28.26%	3319
	G7 0.1F	23.86%	2143		G7 ultra	33.13%	3918
	G7 0.45F	21.51%	1933		G7 0.45F	18.66%	2215
	G7 Tot	17.56%	1577		G7 Tot	16.99%	1990
10th Nov 2016	G1 ultra	15.18%	1238	Sep 2017	G1 ultra	24.71%	1957
	G1 0.1F	14.50%	1183		G1 0.1F	18.07%	1396
	G1 0.45F	13.93%	1136		G1 0.45F	17.68%	1324
	G1 Tot	14.29%	1166		G1 Tot	17.63%	1331
	G7 ultra	20.02%	1632		G7 ultra	28.03%	2118
	G7 0.1F	9.24%	754		G7 0.1F	12.88%	984
	G7 0.45F	8.76%	715		G7 0.45F	11.95%	931
	G7 Tot	5.60%	458				
15th Nov 2016	G1 ultra	17.81%	1453		G7 Tot	10.45%	786

Note: Ultra, 0.1F, 0.45F in sample column respectively represents the water sample obtained after filtrating through ultrafilter, 0.1 µm pore-size membrane and 0.45 µm filter, while the Tot in sample column means the unfiltered water sample.

On the other hand, a much lower concentration difference between Ba and Eu in samples G2, G3, G4, G5 (from September 2016 to September 2017), combined with the very low BaO production rate, ensured that accurate Eu results could be obtained even though corrections were not undertaken. As the BaO interferences on Eu in samples G2 - G5 (September 2016 to September 2017) were negligible, only the results of samples collected from one fieldwork campaign were recorded in Table 4.11. This is included as an example to show the BaO interference level on Eu and the concentration difference between Ba and Eu. The degree of BaO interference on Eu concentrations of samples G2 - G5 from all other dates, as well as Ba concentrations, and Eu concentrations before and after correction, are shown in Appendix A.

Table 4.11: BaO induced errors on Eu for samples G2, G3, G4, G5 collected on 15th November 2016, and the concentration difference between the interferent Ba and analyte Eu in these samples

Date	Sample	Error%	Concentration ratio of Ba to Eu
Sep, 2017	G2 ultra	0.46%	35
	G2 0.1F	0.46%	36
	G2 0.45F	0.46%	35
	G2 T	0.46%	35
	G3 ultra	3.35%	256
	G3 0.1F	3.10%	238
	G3 0.45F	3.06%	238
	G3 T	3.05%	231
	G4 ultra	4.15%	314
	G4 0.1F	3.81%	296
	G4 0.45F	3.83%	298
	G4 T	3.79%	297
	G5 ultra	10.50%	800
	G5 0.1F	4.92%	378
	G5 0.45F	4.78%	365
	G5 T	4.29%	331

The results of analysis of samples G2 to G5, from September 2017, were selected to demonstrate the degree of interference during measurement. This was because the September 2017 samples produced the largest BaO-induced errors on Eu. It can be seen from Table 4.10 and Table 4.11 that the concentration differences between Ba and Eu for samples G2 to G5 were much smaller than those for samples G1 and G7. Consequently, the BaO interference on Eu was not significant for samples G2 to G5. Table 4.11 shows that, with the exception of sample G5 ultra, the errors of all samples were below 5%. G5 ultra samples collected from other dates were all less than 5.82% (Appendix A). When the error on Eu caused by BaO interference was less than 5%, Kajiya, *et al*. (2004) did not undertake any BaO interference correction on Eu because the influence of interference was deemed negligible. With the exception of sample G5 ultra from September 2017 BaO induced errors on Eu for all G2 to G5 samples were deemed negligible. But BaO interference correction equation was still applied to all the samples collected from Sep, 2016 to Sep, 2017.

4.5.2 LREEO and MREEO interferences

For each analyte isotope subject to interference, Table 4.12 shows the interferent, correction factor and mean CF value. These data are from the measurement of single interferent solutions on September 2016. It can be seen from Table 4.12 that the oxide production rate of

REE (besides Eu) are generally larger than that of Ba (Table 4.9) due to the stronger metal oxide bond of REE.

Table 4.12: MREE and HREE correction factors due to LREEO and MREEO interferents, for samples from September 2016

Date	Interferent	Correction factor equation	CF value	Interfered analyte isotope
Sep 2016	Pr	$^{141}Pr^{16}O^{+}/^{141}Pr$	0.00623	^{157}Gd
	Nd	$^{143}Nd^{16}O^{+}/^{146}Nd$	0.00517	^{159}Tb
		$^{150}Nd^{16}O^{+}/^{146}Nd$	0.00228	^{166}Er
	Sm	$^{147}Sm^{16}O^{+}/^{147}Sm$	0.00111	^{163}Dy
		$^{149}Sm^{16}O^{+}/^{147}Sm$	0.00148	^{165}Ho
		$^{150}Sm^{16}O^{+}/^{147}Sm$	0.00108	^{166}Er
	Eu	$^{153}Eu^{16}O^{+}/^{153}Eu$	0.0002	^{169}Tm
	Gd	$^{156}Gd^{16}O^{+}/^{157}Gd$	0.00434	^{172}Yb
	Tb	$^{159}Tb^{16}O^{+}/^{159}Tb$	0.00388	^{175}Lu

Greater oxide production rates for REE relative to that for Ba are shown in Table 4.12 After applying the correction equation of LREEO and MREEO interference to the interfered REE of the samples, the interfered REE concentrations changed by only a very small amount (less than 3%), as shown in Table 4.12 and Table 4.13. Both Willie and Sturgeon (2001) and Prohaska et al. (1999) mention that no corrections are required when the oxide interferences on REE are less than 5% and the interferences can be considered as negligible. Therefore, with regard to interference of LREEO and MREEO on MREEO and HREEO, no corrections were made on samples collected in this study.

The minor degree of interference on the samples is because the concentration differences between most of the interfering REE and interfered REE of the samples collected from September 2016 were within one order of magnitude of each other (Table 4.14). Kajiya *et al*. (2004) did not perform REEO interference corrections in their study due to the small concentration differences between the interferent and the interfered REE, which were also within one order of magnitude.

The interfered MREE and HREE concentrations of samples collected from September 2016 before and after corrections are noted in Appendix B. Appendix B also shows the concentration differences between the interfering REE and the interfered REE of samples collected after September 2016.

Table 4.13: REEO interference on monitored MREE and HREE isotope

Sample	Percentage error induced by interference on analyte (%)							
	^{157}Gd	^{159}Tb	^{163}Dy	^{165}Ho	^{166}Er	^{169}Tm	^{172}Yb	^{175}Lu
G1 0.1F	0.00%	2.22%	0.01%	0.09%	1.05%	0.02%	0.81%	0.94%
G1 0.45F	0.21%	2.23%	0.03%	0.12%	0.90%	0.03%	0.67%	0.91%
G1 Tot	0.02%	2.34%	0.02%	0.10%	1.01%	0.02%	0.81%	0.84%
G2 0.1F	0.12%	2.72%	0.04%	0.16%	1.76%	0.07%	1.52%	2.08%
G2 0.45F	0.11%	2.73%	0.04%	0.16%	1.76%	0.07%	1.49%	2.08%
G2 T	0.09%	2.67%	0.04%	0.16%	1.77%	0.07%	1.53%	2.25%
G3 0.1F	0.10%	2.64%	0.03%	0.14%	1.68%	0.06%	1.46%	1.90%
G3 0.45F	0.15%	2.66%	0.04%	0.15%	1.70%	0.06%	1.46%	1.96%
G3 T	0.15%	2.60%	0.03%	0.15%	1.71%	0.06%	1.45%	2.09%
G4 0.1F	0.05%	2.55%	0.03%	0.14%	1.58%	0.06%	1.46%	2.13%
G4 0.45F	0.03%	2.53%	0.03%	0.14%	1.60%	0.06%	1.46%	2.00%
G4 T	0.02%	2.60%	0.03%	0.14%	1.59%	0.06%	1.44%	1.96%
G5 0.1F	0.13%	2.60%	0.03%	0.13%	1.68%	0.06%	1.51%	2.01%
G5 0.45F	0.13%	2.59%	0.03%	0.14%	1.63%	0.06%	1.44%	2.02%
G5 T	0.06%	2.44%	0.03%	0.13%	1.60%	0.06%	1.49%	2.02%
G7 0.1F	0.00%	1.45%	0.00%	0.09%	0.62%	0.02%	0.78%	1.00%
G7 0.45F	0.00%	1.48%	0.01%	0.08%	0.70%	0.02%	0.80%	1.14%
G7 Tot	0.00%	1.56%	0.00%	0.09%	0.66%	0.03%	0.79%	1.16%

Table 4.14: Concentration differences between the interferent REE and the interfered REE of samples collected on September 2016

Sample	Concentration ratio of interferent to interfered element								
	Pr/Gd	Nd/Tb	Sm/Dy	Sm/Ho	Nd/Er	Sm/Er	Eu/Tm	Gd/Yb	Tb/Lu
G1 0.1F	0.9	31	1.2	6.1	11	2.3	3.5	3.5	2.7
G1 0.45F	1.1	31	1.6	7.3	9.4	2.8	3.8	3.1	2.7
G1 Tot	1.0	33	1.4	6.6	11	2.4	2.9	3.5	2.6
G2 0.1F	1.0	38	1.6	9.4	18	3.7	8.4	5.8	4.8
G2 0.45F	1.0	38	1.7	9.4	18	3.8	8.6	5.7	4.8
G2 T	1.0	37	1.7	9.5	18	3.8	8.6	5.8	5.1
G3 0.1F	1.0	37	1.5	8.7	17	3.5	7.9	5.6	4.5
G3 0.45F	1.1	37	1.7	9.3	17	3.8	7.9	5.6	4.6
G3 T	1.1	37	1.6	8.9	17	3.7	7.8	5.6	4.8
G4 0.1F	1.0	36	1.5	8.5	16	3.4	7.1	5.6	4.9
G4 0.45F	1.0	36	1.6	8.7	16	3.5	7.5	5.6	4.7
G4 T	1.0	36	1.5	8.3	16	3.3	7.7	5.5	4.6
G5 0.1F	1.0	36	1.5	8.1	17	3.4	7.5	5.7	4.7
G5 0.45F	1.0	36	1.6	8.8	17	3.6	7.2	5.5	4.7
G5 T	1.0	34	1.5	8.1	16	3.4	7.7	5.7	4.7
G7 0.1F	0.6	21	1.1	5.6	6.9	2.0	3.6	3.4	2.8
G7 0.45F	0.6	21	1.1	5.5	7.7	2.1	3.8	3.5	3.1
G7 Tot	0.7	22	1.1	5.6	7.3	2.1	4.0	3.5	3.1

4.6 Chapter summary

- The isotope of each of the REEs analysed were free of elemental interference and the doubly charged interference on each of the REE analytes was negligible

- The operating parameters established on the analytical equipment was designed so as to obtain the optimal compromise between minimizing the polyatomic ion production rate and maximizing the analyte signal. Collision mode was applied to measurement of all analyte isotopes to further remove/ reduce different or unknown plasma- and matrix-based polyatomic interference.

- The potential polyatomic interferences on REE isotope measurements were identified and their influence on the accuracy of REE measurement (collision mode) were checked based on the developed mathematical correction equations and the validated correction factor (obtained from single interferent solution measurement before sample measurement).

- No correction equations were required for removing the LREEO and MREEO interferences on MREE and HREE, due to their negligible interference level.

- BaO interference on Eu for G2 to G5 samples was within the acceptable level (<5%). BaO interference induced error on Eu for G1 and G7 samples was relatively large (from 10% to >50%), which is due to a very large concentration difference between Ba and Eu in G1 and G7 samples.

- BaO interference on Eu for all samples collected from 15/09/2016 to 14/07/2017 was reduced to negligible level after applying the correction equation along with the validated correction factor (obtained from single Ba solution measurement before sample analysis).

Chapter 5 Influence factors on REE transformation

5.1 Introduction

This chapter mainly discusses the REE transformation controlling factors and the suitable conditions for inducing the removal of REE from the truly dissolved phase (0.005µm filtered). Section 5.2 shows the change in REE concentrations and loads in different phases along the sampling sites under different hydrological conditions. The potential sources for REE content downstream of the mine discharge under varying hydrological conditions are identified. Section 5.3 displays the change of pH along the sampling sites under different flow conditions, and the influence of pH on REE transformation. The most likely scavenging substances that control the transport and fate of REE at Gate Gill are discussed in Section 5.4. Section 5.4 also describes the mechanism of REE adsorption which is the main process controlling REE attenuation and the important role that pH plays on REE adsorption.

5.2 Hydrogeochemical characteristics of Gate Gill

5.2.1 Flow rate

As described in Section 3.2, there were seven sampling locations (G1 to G7) in total, but only 4 of these were routinely measured (G3 to G5 and G7) for flow rate. This was because the field conditions at locations G1, G2 and G6 (River Glenderamackin upstream of the Gate Gill) were not suitable for undertaking flow measurements. The Environment Agency, however, have measured the mine water (G2) flow rate at a consistent 6 L/s and this value will therefore be used throughout this chapter.

Figure 5.1 shows the flow rate at G3 to G5 and G7 on each sampling occasion. The flowrate data are provided in Appendix C. G3, G4 and G5 were located on the Gate Gill, downstream of the mine discharge while G7 was located on the River Glenderamackin, downstream of the confluence with the Gate Gill. Due to the significant flowrate difference between G3- G5 and G7, the flowrate at G7 is displayed in a separate graph in Figure 5.1.

Note that the data are displayed in the order of increasing flow at G5, the most downstream sampling location on the Gate Gill. Figure 5.1 shows that the flowrates of G3, G4 and G7 also display a general increasing trend and, therefore, G5 is representative of the flow conditions on each sampling occasion. Sampling at Gate Gill was undertaken across a range

of hydrological conditions, from as low as 5.53 L/s to up to 115.1 L/s at G5 (see flow data in Appendix C). The corresponding flow range for G7 is from 206 to 10,200 L/s.

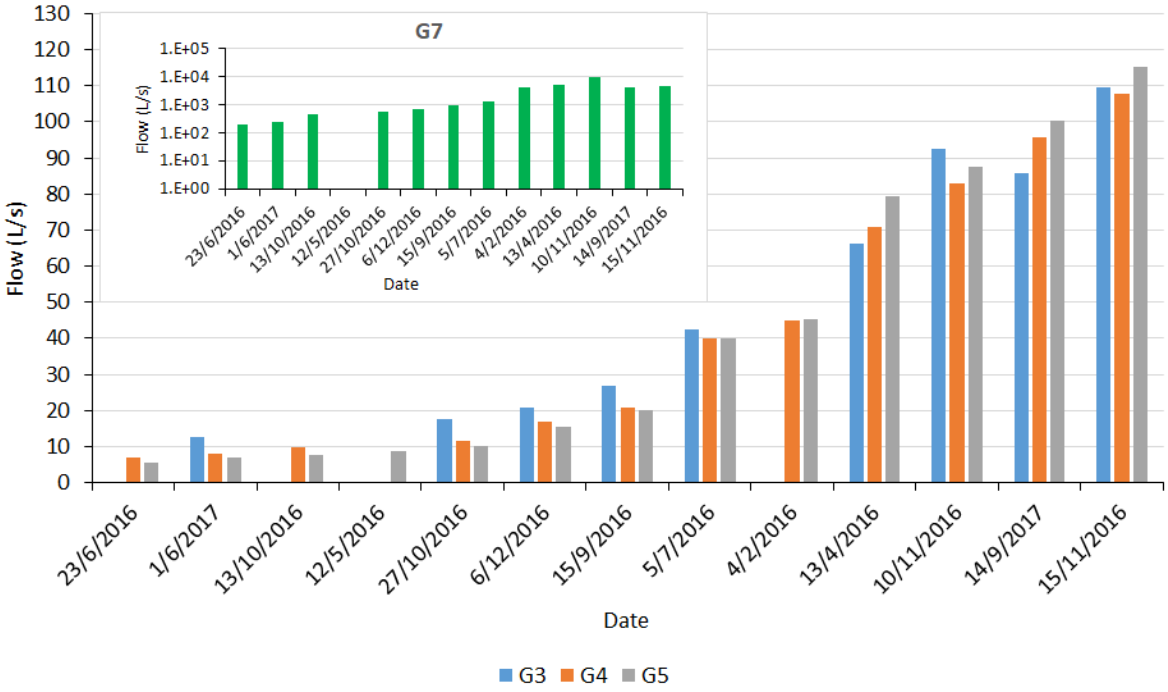

Figure 5.1: Flowrate of G3, G4, G5 and G7 on all sampling occasions. The data are displayed in order of flow at G5, the most downstream sampling location on the Gate Gill

The Gate Gill appears to be a losing stream under lower flow conditions (with flow of G5 ranging from 5.53- 40.1L/s) as indicated by a decrease in flowrate between G3 and G5, with the greatest decrease occurring in the reach G3 to G4 (Figure 5.1). This is likely due to the subsurface-surface water interaction. The position of the surface water body and groundwater flow system, the streambed characteristics and local climatic circumstances control the surface-groundwater interaction (Winter, 1999). To be more specific, the hydraulic head gradients between the groundwater and stream water and the streambed hydraulic conductivity together control the river and aquifer interface flow exchange (Munz et al. 2011). The groundwater and surface water exchange direction depends on the hydraulic head and the flowrate or the exchange intensity related to the hydraulic conductivity of the sediment (Sophocleous, 2002).

Therefore, under lower flow conditions (5.53~40.1L/s at G5), the water table in the underlying aquifer must be lower than the stage of the Gate Gill, at least in some reaches between G3 and G5. The Gate Gill water thus flows downwards through the streambed to the water table, leading to the observed decrease in flowrate from G3 to G4 and from G4 to G5.

In contrast, Figure 5.1 shows that under higher flow conditions (with flow of G5 ranging from 45.42-115.1L/s) the Gate Gill becomes a gaining stream, as indicated by an increase in flow rate between G3 and G5. Since there are no obvious tributaries within this reach, input of surface runoff and/or subsurface infiltration are the likely reasons for the observed increase in flow rate.

Sophocleous (2002) notes that besides the direct flow/event flow (rainfall) entering the stream promptly, subsurface flow/ interflow may also contribute to the stream water in response to a rainfall event. The hydraulic head can be altered during precipitation or storm events and, as a consequence, the groundwater and surface water exchange flow direction will change (Sophocleous, 2002). If the water table increases to a level which is higher than the stream water stage, a hydraulic gradient will develop towards the stream and groundwater infiltration will be induced. Besides the groundwater ridging mechanism just described, which is based on storm magnitude, antecedent soil-moisture conditions and heterogeneity in soil hydraulics properties, subsurface flow entering a stream under high flow conditions may also be the result of one, or a combination, of the following mechanisms: (1) translatory flow/plug flow; (2) macropore flow; (3) return flows (Sklash, 1990; Wood et al. 1990; Beven, 1989).

The groundwater-surface water exchange in the Gate Gill differs to that commonly seen in other perennial streams, which act as gaining streams during low flow conditions and losing streams during high flow conditions. In these streams, under low flows, the lower stream water altitude induces groundwater infiltration whilst, under high flow conditions, the large volume of surface runoff and subsurface interflow leads to the stream water having a higher hydraulic head, which induces recharge to the groundwater system (Munz et al. 2011; Sophocleous, 2002).

It should be noted that a decrease in flow rate between G3 and G4 was observed on two higher flow condition sampling occasions (10/11/2016 and 15/11/2016) (Figure 5.1). It should be noted that a decrease in flow rate between G3 and G4 was observed on two higher flow condition sampling occasions (10/11/2016 and 15/11/2016)

As described in Section 3.3.3, the channel morphology and stream mixing characteristics downstream of the discharge point of the mine water cause some difficulties in accurately determining the flow rate in the Gate Gill immediately downstream of the mine discharge

(G3). Although the dam was the best location for salt injection, some of the water from the injection point appears to flow under the dam. The unavoidable tracer losses caused by the water leaching from the dam can lead to the measured flowrate being higher than the actual flowrate.

5.2.2 REE loads

Flowrate is an important factor to demonstrate the transport of REE along the mine water polluted stream, as it is required to calculate the change in metal loads between different sampling sites. Displaying the REE load along the stream can indicate whether the decreasing REE concentrations are caused by the dilution of stream water by surface and ground water inputs, or the mass loss. In addition, the trend shown by the mass loads can also show whether there are some other REE input sources along the stream besides the mine discharge. Moreover, REE loads under different seasonal conditions can help to determine the potential REE sources and their proportional importance under varying hydrological conditions.

As mentioned in Section 2.4.2, REE may be present in waters in truly dissolved, colloidal and particulate phases. Filtering samples through different pore sizes enables quantification of the different phases, and therefore an improved understanding of REE transformation between different phases and fractionation mechanisms (Verplanck et al., 2004; Nelson et al., 2003; Protano and Riccobono, 2002; Elderfield et al., 1990). Filtering through a 0.45μm pore size membrane filter removes particulates greater than 0.45 μm, leaving the truly dissolved and colloidal phases in the filtrate (Verplanck, 2013; Elderfield et al., 1990). A 0.1 μm filter can remove the larger colloids in waters, leaving very fine colloids and the truly dissolved phase in the filtrate (Nelson et al., 2003). The filtrate obtained from ultrafiltration contains only truly dissolved REE (< 0.005 μm) (Verplanck, 2013; Protano and Riccobono, 2002). The ∑REE loads in ultrafiltered (<0.005μm), <0.1μm, <0.45μm and unfiltered water samples at different sampling locations on Gate Gill under varying hydrological conditions are discussed in this section. The ∑REE concentrations in different phases at different sampling sites under different flow conditions are discussed in the following Section 5.2.3.

Gate Gill (G2- G5)

Figure 5.2 shows the ∑REE loads in the unfiltered phase at G2 on different sampling occasions (based on the flow of 6L/s measured by the Environment Agency) and the variation of ∑REE loads with flow in the unfiltered phase at G3- G5 under all flow conditions (5.53-115.1 L/s for G5). Figure 5.3 shows the ∑REE loads in the < 0.005 µm, < 0.1 µm, < 0.45 µm and unfiltered phases at G3, G4 and G5 under all flow conditions (5.53-115.1 L/s for G5; 6.78-107.7L/s for G4; 12.68-109.5L/s for G3). It should be noted that the < 0.005 µm results are not available for all the flow conditions shown in Figure 5.3, since ultrafiltration was only undertaken on the last 7 sampling occasions. Combining the results from Figure 5.2 and Figure 5.3 can indicate: (1) the importance of the mine discharge as the REE source for Gate Gill under varying hydrological conditions; (2) other potential sources for the REE load in Gate Gill, which may be induced by high flow conditions; (3) the reasons for spatial variation of ∑REE loads along Gate Gill under varying hydrological conditions; (4) the transformation of REE between different phases at G3 to G5 under different flow conditions.

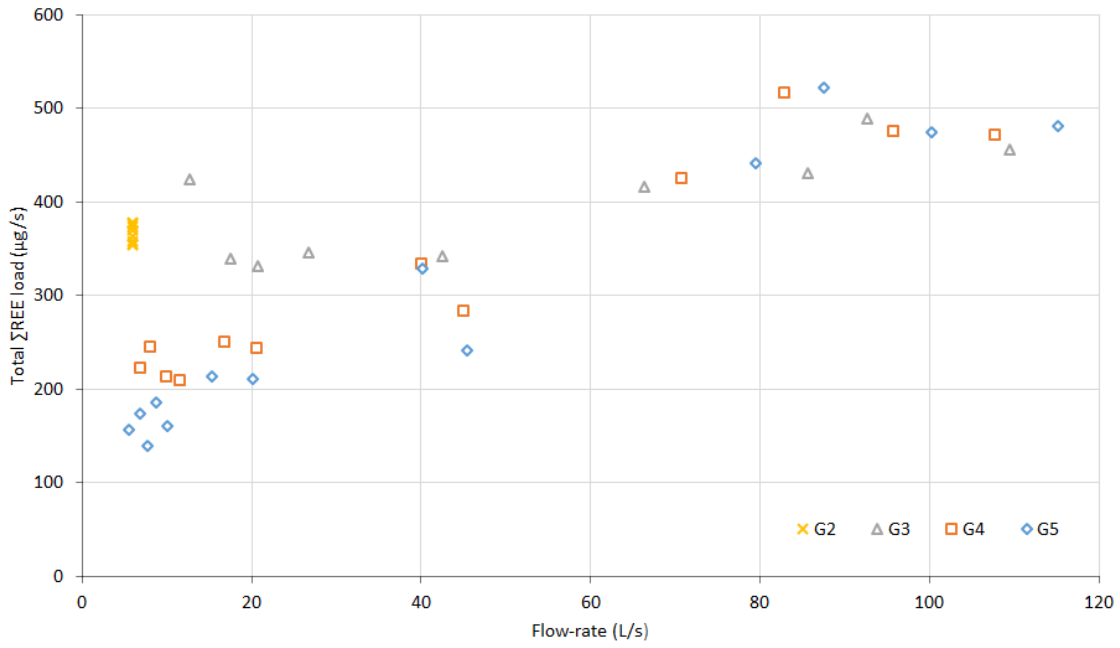

Figure 5.2: ∑REE load in the unfiltered phase at G3 to G5 under all flow conditions and at G2 on different sampling occasions (based on mine discharge flow data from Environment Agency of 6 L/s)

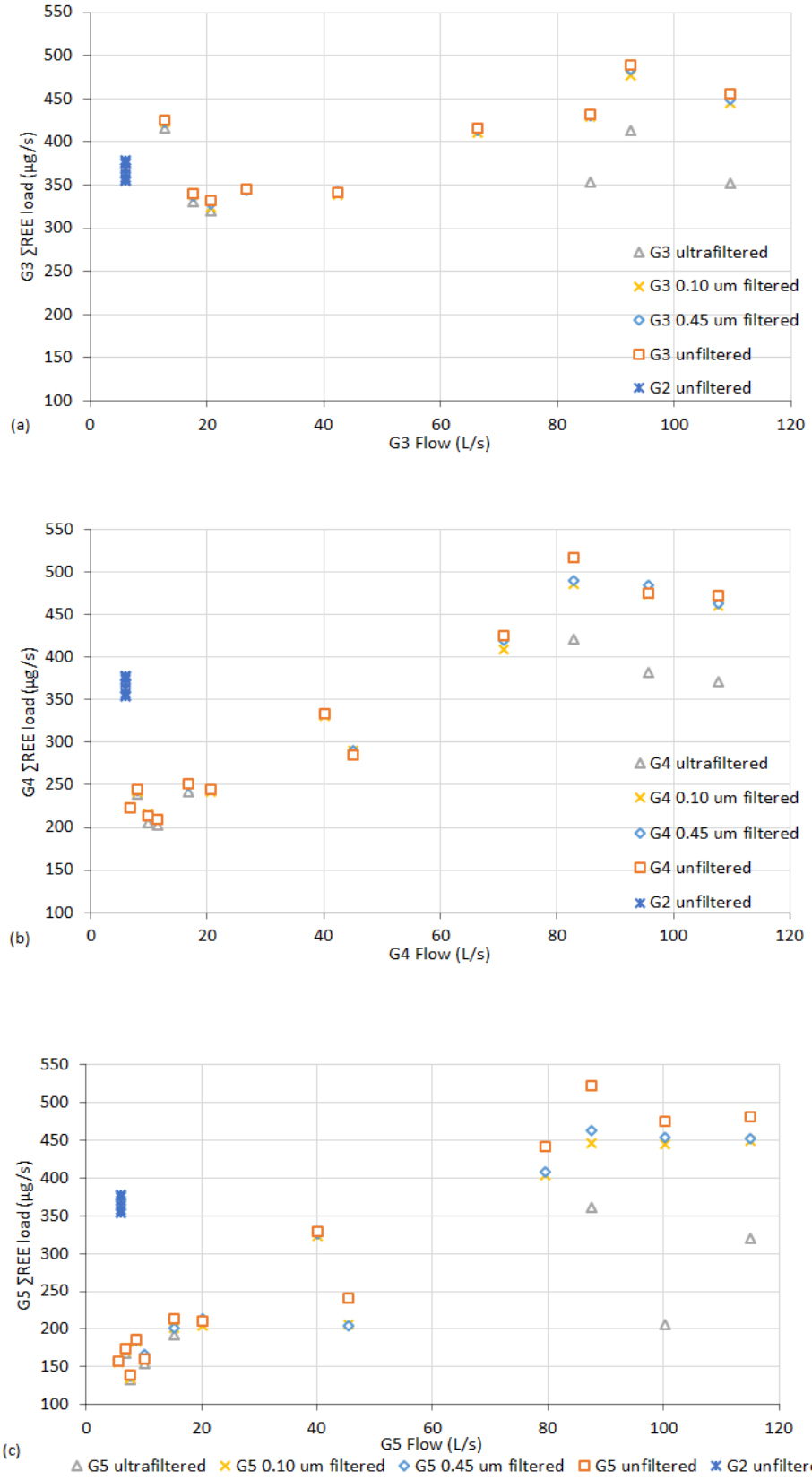

Figure 5.3: ∑REE loads in the unfiltered phase at G2 and ∑REE loads in the < 0.005 µm, < 0.1 µm, < 0.45 µm and unfiltered phases at (a) G3 (b) G4 and (c) G5 under all flow conditions

As can be seen from Figure 5.2, under lower flow conditions (5.53-40.1L/s for G5; 6.78-40.1L/s for G4; 12.68-42.44L/s for G3) when Gate Gill is a losing stream: (1) the ∑REE loads in the unfiltered phase at G3-G5 are lower than that at G2, apart from an exception at G3 at a flow of approximately 15 L/s which has a load of > 400 µg/s; (2) there is a decrease in ∑REE loads in the unfiltered phase from G3 (mean value of 356.5 µg/s) to G4 (mean value of 245.7 µg/s) and to G5 (mean value of 196.4 µg/s); (3) the ∑REE loads in the unfiltered phase at G3 are relatively constant, and the mean ∑REE load at G3 is 356.5 µg/s which is slightly lower than the mean ∑REE load at G2 (367.5 µg/s); (4) ∑REE loads in the unfiltered phase at both G4 (range 209.5-334 µg/s) and G5 (range 139.5-329.5 µg/s) display a general increasing trend with increasing flow.

Figure 5.3 shows that the ∑REE loads in the < 0.005 µm, < 0.1µm, < 0.45µm and unfiltered phases are similar at G3 to G5 under lower flow conditions. This indicates that the ∑REE are present primarily in the < 0.005 µm fraction, resulting in a low particulate fraction under these flow conditions.

The slightly lower ∑REE loads in the unfiltered phase at G3 compared to at G2 and the relatively constant ∑REE loads in the unfiltered phase at G3 under lower flow conditions (12.68-42.44L/s for G3; 5.53-40.1L/s for G5) suggest that the mine discharge is the main REE source for the Gate Gill downstream of G2. But it should be noted that the G3 load is lower than G2 so there must be some loss of load between G2 entering Gate Gill Beck and G3. The gradual decrease in ∑REE load in the unfiltered phase from G3 to G5 under these conditions may in part be the result of some loss of REE from the Gate Gill to the underlying groundwater in the losing reach between G3 and G5 (Section 5.2.1). Figure 5.3 suggests that there is little chemical transformation of REE at each sampling site (G3-G5) under lower flow conditions. This is due to low pH (mean pH of G3, G4 and G5 is 4.09, 4.31 and 4.44 respectively; see Section 5.3 for more details). Therefore, the solution chemistry is not favourable for REE settling from the water column to occur from G3 to G5.

Gate Gill changes from a losing stream to a gaining stream with increasing flow, and the degree of flow loss from surface water to groundwater either between G3 and G4 or between G4 and G5 displays a decreasing trend as flow increases within lower flow conditions (5.53-40.1L/s for G5), as can be seen from Figure 5.4. The progressive increase of flow under lower flow conditions may therefore lead to a decrease in REE loss to the subsurface between

G3 and G5. This may then induce the increase of ∑REE load at both G4 and G5 with increasing flow. The input of REE from other sources is not expected to be the reason for the observed increase in ∑REE load at G4 and G5 with increasing flow as the PAAS normalized REE distribution patterns in the unfiltered phase at G3 to G5 under these lower flow conditions are identical to that at G2, but totally different to that at G1. This suggests that G2 is the main source of REE to the Gate Gill (see Section 6.3.2).

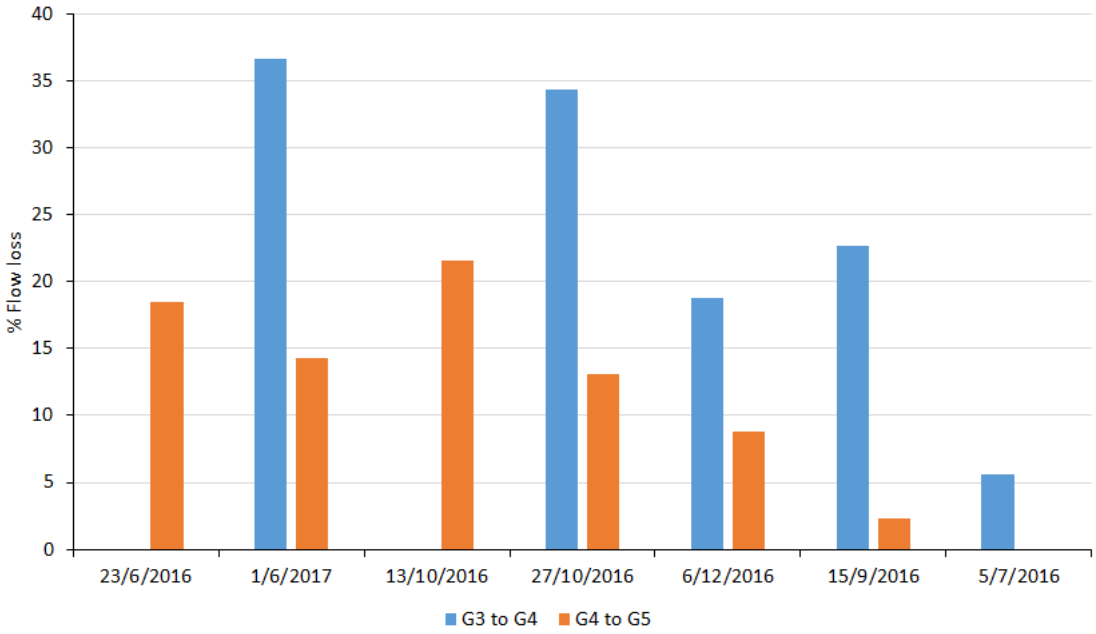

Figure 5.4: Decrease of percentage loss of flow between G3 and G4, and between G4 and G5 as flow increases within lower flow conditions (sampling dates are displayed in the order of increasing flow at G5)

The unfiltered data can be used as representative of the rest of the phases, due to the very similar ∑REE loads in the < 0.005 µm, < 0.1µm, < 0.45µm and unfiltered phases at each sampling site (G3-G5) under lower flow conditions.

According to Figure 5.2, under higher flow conditions (45.42L/s≤G5 flow≤115.1L/s; 44.98L/s≤G4 flow≤107.7L/s; 42.44L/s<G3 flow≤66.4L/s) when Gate Gill becomes a gaining stream, the ∑REE loads in the unfiltered phase at G3- G5 generally increase with increasing flow, and exceed that at G2, at flows greater than approximately 40 L/s.

Figure 5.3 shows that under higher flow conditions (45.42L/s≤G5 flow≤115.1L/s; 44.98L/s≤G4 flow≤107.7L/s; 42.44L/s<G3 flow≤66.4L/s):

(1) the < 0.1µm and < 0.45µm ∑REE loads at G3, G4 and G5 are higher than the unfiltered ∑REE load at G2.

(2) the < 0.1µm, < 0.45µm and the unfiltered phase at G3 and G4 have similar ∑REE loads. The mean ∑REE load of the < 0.1µm, < 0.45µm and the unfiltered phase under higher flow conditions at G3 is respectively 441 µg/s, 444 µg/s and 448 µg/s, at G4 is respectively 424 µg/s, 430 µg/s and 435 µg/s (please note that the ∑REE load at G3 on 4/2/2016 is not available due to the lack of flow data and the flowrate of G4 on 4/2/2016 is 44.98L/s, the mean ∑REE load at G3 is therefore lower than G4). This suggests that only a very small amount of REE are present in the particulate fraction (> 0.45µm) or coarse colloidal fraction (0.45µm- 0.1µm) at both G3 and G4.

(3) At G5, a small proportion of ∑REE is present in the particulates (> 0.45 µm), the mean ∑REE particulate load is 396 µg/s and in the unfiltered phase 432 µg/s.

(4) Under some higher flow conditions (87.59-115.1L/s for G5; 82.85-107.7L/s for G4; 92.63-109.5L/s for G3) with dissolved ∑REE loads available: ∑REE loads in dissolved phase at G3 and G4 are occasionally higher than the mean ∑REE load in unfiltered phase at G2 (367.5 µg/s); ∑REE loads in dissolved phase at G5 are lower than the mean ∑REE load in unfiltered phase at G2; the suspended REE (>0.005µm) are mainly present in the fine colloidal fraction (0.005µm- 0.1µm) at G3 to G5; the proportion of fine colloidal ∑REE at G5 (16.62%- 50.24%) is larger than that at G3 (13.13%- 20.45%) and G4 (12.55%-19.15%).

Comparing the REE data in different phases (Figure 5.3), REE are present in the fine colloidal fraction (0.005µm- 0.1 µm) at G3, G4 and G5 only under higher flow conditions. In addition, REE are present in particulate form (> 0.45 µm) only at G5 under higher flow conditions. The pH of the Gate Gill generally rises with increasing flow, as there is more dilution of the Woodened mine water under higher flow conditions. The mean pH ranges from 4.09 to 4.46 at G3, 4.31 to 4.64 at G4 and 4.4 to 5.11 at G5 as flow increases from lower flow conditions to higher flow conditions. Some REE are likely being chemically transformed from the dissolved (< 0.005 µm) phase to the fine colloidal phase (0.005µm- 0.1 µm) at G3 to G5 in the Gate Gill at higher pH.

In addition, pH generally increases from G3 to G5 under all flow conditions (Section 5.3). This may lead to: (1) a greater degree of chemical transformation of REE from dissolved (<

0.005 µm) to 0.1µm filtered phase at G5 than that at G3 and G4 under higher flow conditions; (2) some REE being chemically transformed from colloidal (0.005µm -0.45µm) to particulate (> 0.45µm) phase at G5 under higher flow conditions. Section 5.3 displays the spatial variation of pH along the sampling sites and the variation of pH at each sampling site (G3-G5 and G7) under varying flow conditions.

What is more, under higher flow conditions, some REE may be mobilised from the sediments on the Gate Gill streambed, contributing to REE loads in the colloidal (0.005µm- 0.45µm) and/ or particulate (> 0.45µm) fraction at G3- G5. But the hydrous ferric oxide (HFO; ochre) sediments below the mine water discharge (G2) should not contribute to the REE content in the suspended solid phase downstream of G2 on Gate Gill even under higher flow conditions when the HFO may be subject to resuspension. Since the HFO sediments below the mine discharge are not expected to be a sink for REE. To be more specific, the ∑REE loads or concentrations in <0.005µm, <0.1µm, <0.45µm and unfiltered phase of mine discharge on each sampling occasion are the same (Appendix C).

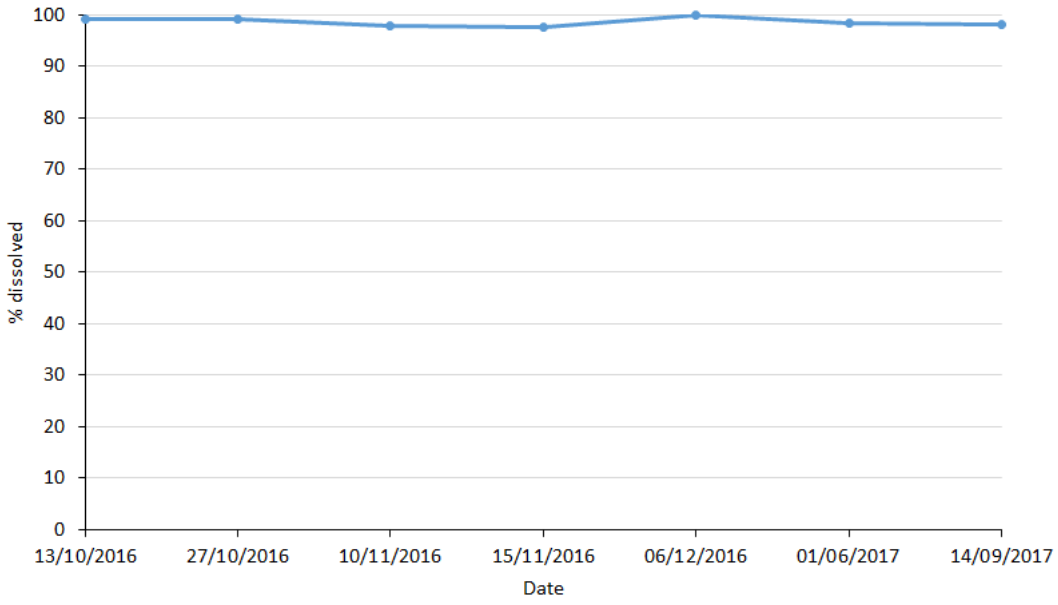

Figure 5.5: Proportion of REE present in dissolved phase (<0.005µm) at G2

Figure 5.5 also shows that the proportions of dissolved REE (<0.005µm) in water column of G2 are nearly 100%. These results suggest that all REE in the water column of mine discharge are present in the dissolved phase. Due to the extremely low pH of mine discharge (range from 3.11- 3.74, mean value of 3.53), the process of chemical transformation of REE

from dissolved to suspended solid or solid phase in mine discharge is mediated (even though a large amount of iron oxyhydroxide forms in mine discharge and iron oxyhydroxide plays an important role on REE scavenging). Therefore, the ochre sediments settled from mine discharge should contain little REE.

On some occasions under higher flow conditions, the dissolved ∑REE loads (<0.005µm) at G3 and G4 are higher than the mean unfiltered ∑REE load at G2. The dissolved ∑REE loads at G5 under higher flow conditions, on the other hand, are all lower than the mean unfiltered ∑REE load at G2. This may be due to the higher degree of chemical transformation of REE from the truly dissolved phase to suspended solids at G5 compared to that at G3 and G4. The higher pH at G3 to G5 under higher flow conditions could induce chemical transformation of some REE from the truly dissolved phase to suspended solids and therefore lower the dissolved ∑REE load. Possible reasons for the increase of ∑REE loads in the unfiltered phase under higher flow conditions at locations G3 to G5 are: (1) the dissolution of REE from new sources (besides the mine discharge); (2) the mobilisation of REE from sediments.

Two potential REE-containing mining-related surface spoils are located in the vicinity of G3, one close to the bottom of the dam which is upstream of G3 (Figure 5.6 a), and the other next to G3 (Figure 5.6 b). The REE in the spoil heaps could potentially be mobilised during rainfall events and then enter the Gate Gill in the vicinity of G3. The spoil heaps may become a possible diffuse source for the additional REE content at G3 to G5 under higher flow conditions.

The majority of suspended REE (>0.005µm) are present in the fine colloidal (0.005µm-0.1µm) fraction at G3 and G4 under higher flow conditions, and most of the suspended REE are present in the fine colloidal fraction at G5. Therefore, little chemical transformation of REE from suspended solids to the sediments at G3 to G5 is likely to occur under higher flow conditions.

Figure 5.6: Location of mine spoil: (a) close to the bottom of the dam (b) besides G3 sampling location (photos taken on 14/09/2017)

River Glenderamackin (G7)

To show the REE input to the River Glenderamackin from the Gate Gill under varying hydrological conditions, Figure 5.7 shows the unfiltered ∑REE loads at G5 and G7 under all flow conditions (5.53-115.1L/s for G5 and 203-10200L/s for G7). As can be seen from Figure 5.7, there is a considerable increase of ∑REE load at G7 with increasing flow in the River Glenderamackin (from 202-37995µg/s as flow increased from 203-10200L/s). However, the importance of the Gate Gill as a REE source to the River Glenderamackin decreases significantly with increasing flow.

To be more specific, under the first two lowest flow (203-253L/s for G7; corresponding 5.53-6.88L/s for G5), 78%-86% of the REE content in the River Glenderamackin is due to the input of REE from the Gate Gill. With the continuous increasing of flow under lower flow condition from 495 to 1380L/s for G7 and corresponding 7.74- 40.1L/s for G5, the contribution of the REE content from the Gate Gill to the River Glenderamackin decreases from ~40% to 13%. Under the higher flow conditions (4160-10200L/s for G7; corresponding 45.42-115.1L/s for G5), only 1.37%-7.22% REE in River Glenderamackin are from Gate Gill.

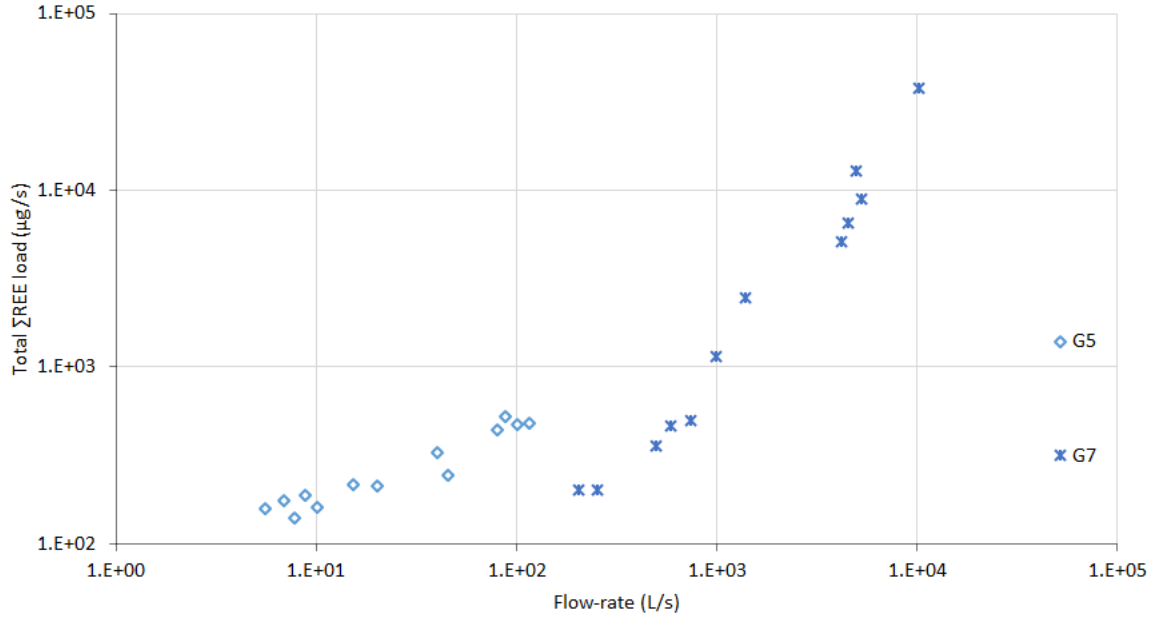

Figure 5.7: Contribution of REE from Gate Gill to River Glenderamackin under all flow conditions (5.53-115.1 L/s for G5; 206-10200 L/s for G7)

Although the unfiltered ∑REE load at G5 also increases with flow, the ∑REE load increase with flow in the Glenderamackin is not due entirely to the equivalent load increase in the Gate Gill at G5. Therefore, the significant increase in REE flux with increasing flow in the River Glenderamackin must be due to additional sources upstream of the confluence with the Gate Gill.

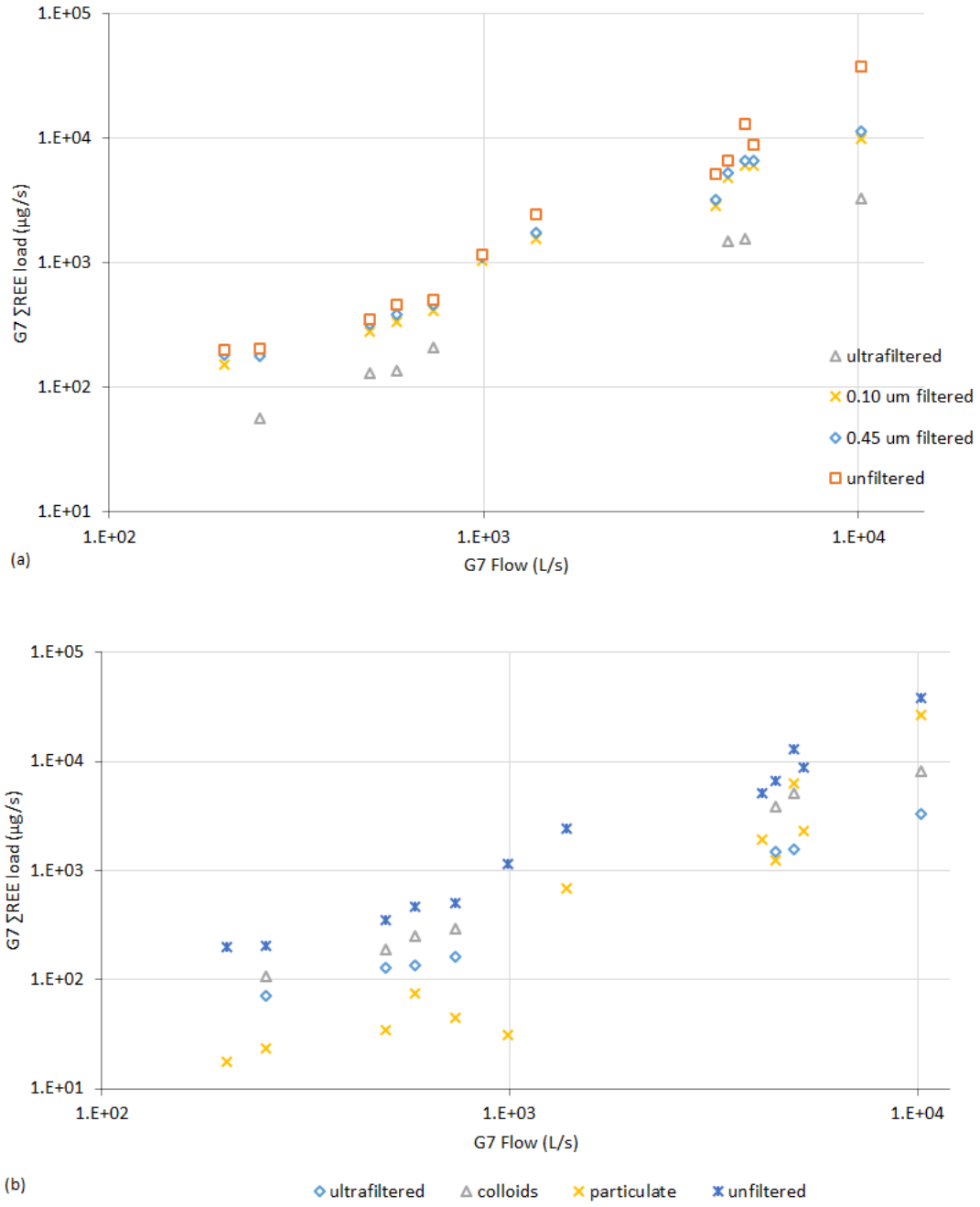

Figure 5.8: ∑REE load at G7 in (a) dissolved, 0.1µm filtered, 0.45µm filtered and unfiltered phase; (b) dissolved, colloidal (0.005µm- 0.45µm), particulate (>0.45µm) and unfiltered phase under all flow conditions (206-10200 L/s)

Figure 5.8 (a) shows the ∑REE load in the < 0.005 µm, < 0.1 µm, < 0.45 µm and the unfiltered phase at G7 under all flow conditions (203-10200L/s for G7; 5.53-115.1L/s for G5). Figure 5.8 (b) displays the variation of ∑REE load in dissolved (< 0.005 µm), colloidal (0.005 µm- 0.45µm), particulate (> 0.45µm) and unfiltered phases under all flow conditions. Since < 0.005 µm data are not available for some sampling occasions, the dissolved and colloidal data are not shown for these occasions in Figure 5.8 (b). As with the variation in the unfiltered ∑REE load shown in Figure 5.7, Figure 5.8 (a) shows that the < 0.005 µm, < 0.1 µm and < 0.45 µm ∑REE loads at G7 also display an increasing trend with flow. In addition, Figure 5.8 (b) shows that the ∑REE loads in both the colloidal and particulate fractions increase with flow.

According to Section 5.3, there is no clear pattern to the pH at G7 as flow increases and pH in the Glenderamackin is relatively constant under different flow conditions (mean value of pH is 6.05). Although the pH of Gate Gill generally rises as flow increases (due to dilution of the mine discharge), the River Glenderamackin is a much bigger river compared to the Gate Gill, and the impact of the Gate Gill on it is rather limited. The River Glenderamackin is therefore unaffected by the polluted Gate Gill in terms of pH. Therefore, the increases of ∑REE loads in the colloidal (0.005 µm - 0.45µm) and particulate (> 0.45µm) fractions as flow increases may largely be due to physical processes associated with changing flow condition. To be more specific, more REE-containing sediments are mobilised from stream bed as flow increases, which can induce an addition of colloidal and particulate REE in the water column. The < 0.1 µm, < 0.45 µm and unfiltered ∑REE loads may largely increase with flow as a consequence.

However, the increase in load with flow is not just associated with suspended solids. The increase in dissolved ∑REE loads as flow increases indicates the introduction of new sources of REE in the upper reaches of the Glenderamackin. Since the abandoned Bannerdale mine is in the River Glenderamackin catchment and located upstream of the confluence with the Gate Gill (Figure 5.9), it might therefore be a potential source of REE content in G7 as flow increases. The Bannerdale lead mine was working for galena and ceased in 1870, leaving a large open cut area, and a small amount of spoils near the base of Bannerdale Crags. Minerals at Bannerdale lead mine are barytes, galena, malachite, linarite, chalcopyrite, sphalerite, graphite (Hewer, 1984).

The dissolution of REE from Bannerdale mine may contribute to the increase in the dissolved ∑REE and may contribute to some degree to the increase in < 0.1 µm, < 0.45 µm and unfiltered ∑REE loads as flow increases. In addition, since the pH (ranging from 5.6-6.88, mean pH is 6.03) at G7 is circum-neutral, it is reasonable to conclude that some REE from Bannerdale mine may be chemically transformed from truly dissolved to the suspended solid phase at G7. This could also contribute, in part, to the increase of ∑REE loads in the colloid and particulate phases at G7 as flow increases.

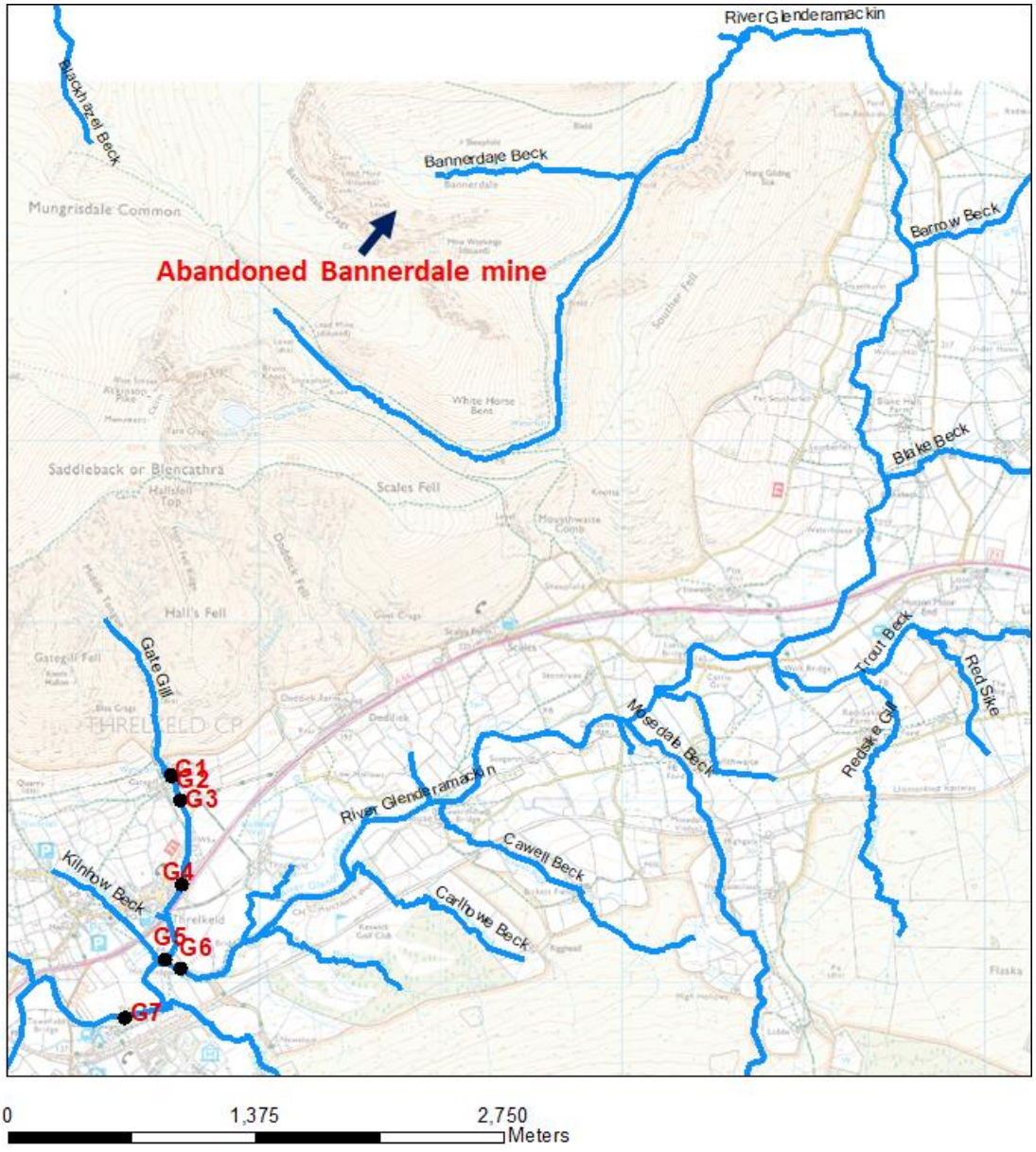

Figure 5.9: Location of abandoned Bannerdale mine relative to the Gate Gill and River Glenderamackin at G7

The higher pH at G7 (ranging from 5.6-6.88, mean pH is 6.03) relative to G5 (ranging from 3.94-5.37; mean pH is 4.69) suggests a higher degree of chemical transformation of REE from dissolved to suspended solid phase at G7 compared to G5 under all flow conditions. Therefore, besides the contribution of the re-suspended sediments at G7, a much higher proportion of colloidal and particulate REE in the River Glenderamackin relative to the Gate Gill under higher flow conditions may also be due to the higher pH of G7. See Section 5.3 for more details.

5.2.3 ∑REE concentrations in different phases

Figure 5.10 shows the variation in unfiltered ∑REE concentration along the Gate Gill and G7 under all flow conditions (5.53-115.1 L/s for G5). Figure 5.11 shows the mean ∑REE concentration in the unfiltered phase for all locations (G1- G7). It should be noted that sampling of the River Glenderamackin upstream of the confluence with the Gate Gill (G6) was undertaken only on the first two sampling occasions which are under the higher flow conditions (the flow of G5 was 45.42L/s and 79.49L/s respectively).

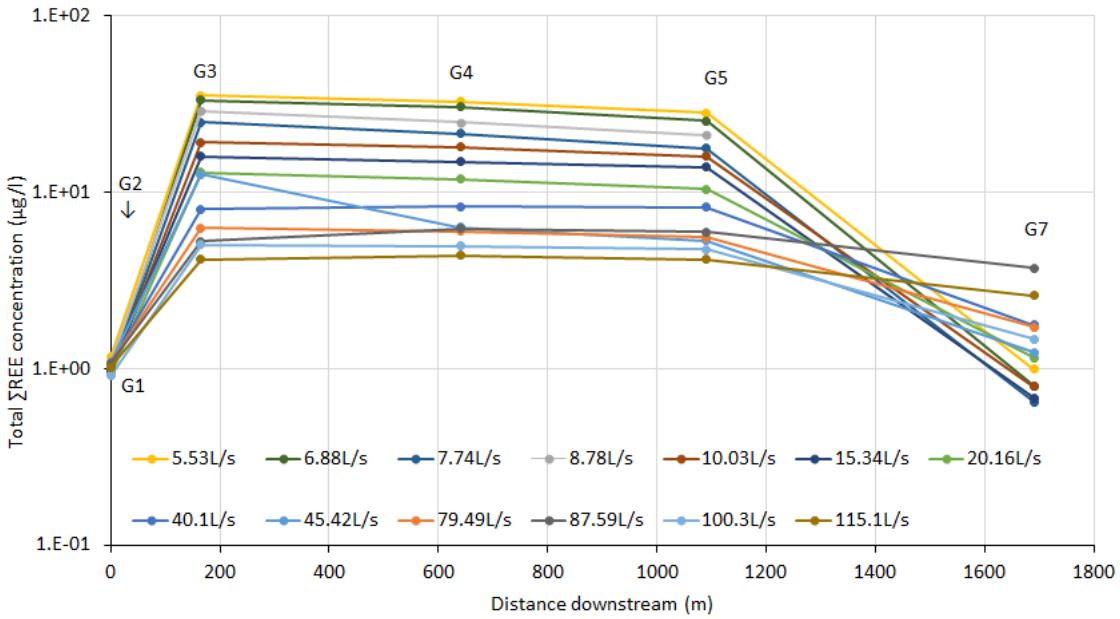

Figure 5.10: Spatial variation of ∑REE concentration in unfiltered phase along the Gate Gill (G1, G3- G5) and River Glenderamackin downstream of the confluence with the Gate Gill (G7) under all flow conditions (flow of G5 is used as the representative for displaying the flow conditions: 5.53-115.1 L/s for G5)

As can be seen from Figure 5.10, the unfiltered ∑REE concentration increases significantly from location G1 (mean value of 1.02 µg/l) to location G3 (mean value of 16.36 µg/l) on the

Gate Gill under all flow conditions. This is because the mine water discharge (G2) with very high REE concentration (mean value of 62.84 µg/l, unfiltered phase) enters the Gate Gill between these two locations, as can be seen from Figure 5.11. REE concentrations and flow of G2 are relatively constant, and the ∑REE concentrations in filtered and unfiltered phases on each sampling occasion are the same. Mixing of the mine discharge with the Gate Gill therefore causes a large increase of ∑REE concentration at G3.

Figure 5.10 also shows that the unfiltered ∑REE concentration decreases gradually downstream from G3 to G4 and to G5 under most of the flow conditions when Gate Gill is a losing stream (5.53-40.1 L/s for G5, Section 5.2.1). As noted in Section 5.2.2, little REE are chemically transformed from total water column to solid phase (sediments) under lower flow conditions. The chemical removal process are not likely to be involved during the gradual decrease of ∑REE concentration in the unfiltered phase as water moves from G3 to G5 under lower flow conditions. Although the flowrate decreases from G3 to G4 and to G5 under these lower flow conditions (as described in Section 5.2.1), there must be some other surface water and / or groundwater with low REE concentration entering Gate Gill between G3 and G4, and between G4 and G5 (for example, there may be some gaining reaches between G3 and G4, and between G4 and G5, and the groundwater with low REE concentration enters Gate Gill in these gaining reaches). The input of these natural waters leads to the decrease of ∑REE concentration in the unfiltered phase from G3 to G4 and to G5.

According to Figure 5.10, there is a general decreasing trend of ∑REE concentration in unfiltered phase from G3 to G5 under most of the higher flow conditions when Gate Gill is a gaining stream (45.42-115.1L/s for G5). The unfiltered ∑REE concentration increases from G3 to G4 on two occasions (flowrate of G5 is 87.59 and 115.1L/s) when flow decreases from G3 to G4 (Section 5.2.1). Since there is a small degree of ∑REE loads increase from G3 to G5 under higher flow conditions and flow generally increases from G3 to G5 under higher flow conditions. The general decrease trend of ∑REE concentration in the unfiltered phase from G3 to G5 is due to a dilution effect. The mean unfiltered ∑REE concentration under all flow conditions shown in Figure 5.11 also decreases from 16.36 µg/l to 14.71 µg/l and to 12.87 µg/l as water moves downstream from G3 to G4 and to G5.

In the River Glenderamackin downstream of the confluence with the Gate Gill (G7), the concentrations in the unfiltered phase are lower relative to those at G5 under all flow

conditions. Even though G5 contains a high concentration of ∑REE (mean value of 12.87 µg/l for unfiltered phase) the impact on the River Glenderamackin downstream of the confluence with Gate Gill (G7, mean ∑REE concentration in unfiltered phase is 1.47 µg/l) appears to be limited. This is a result of dilution, specifically the mixing of the relatively small Gate Gill with the much larger River Glenderamackin.

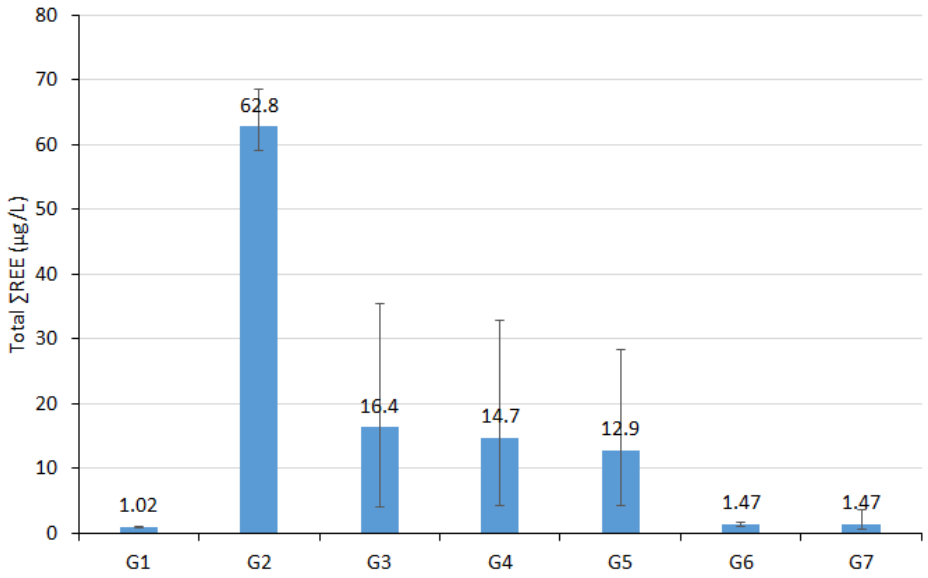

Figure 5.11: Mean ∑REE concentration in unfiltered phase at G1- G7 (based on data from all flow conditions: 5.53-115.1 L/s for G5)

The ∑REE concentration at G6 can illustrate the background ∑REE concentration of the River Glenderamackin and the influence of Gate Gill on the water quality of the River Glenderamackin. The mean unfiltered ∑REE concentrations in the River Glenderamackin upstream (G6) and downstream (G7) of the confluence with the Gate Gill are the same (1.47 µg/l, Figure 5.11). Although the mean ∑REE concentration at G6 is only based on the data from the first two sampling events, ∑REE concentration at G6 under the rest of the flow conditions is expected to be similar as that at G7 under the corresponding flow condition. This is because the unfiltered ∑REE concentrations at G6 and G7 are quite similar on the first two sampling occasions (1.14 µg/l at G6 and 1.23 µg/l at G7; 1.79 µg/l at G6 and 1.73 µg/l at G7) The flow at G5 on these two occasions was 45.42 L/s and 79.49L/s. The similar ∑REE concentration at G6 and G7 further indicates that the Gate Gill has limited influence on the ∑REE concentration in the River Glenderamackin.

Figure 5.12 shows the variation in unfiltered ∑REE concentration downstream of the mine discharge (G3-G5 and G7), with flow (5.53- 115.1L/s for G5; 206- 10200 L/s for G7). The variation in dissolved (< 0.005 µm), < 0.1 µm, < 0.45 µm and unfiltered ∑REE concentrations at G3, G4 and G5 under all flow conditions is shown in Figure 5.13 (a), (b) and (c) respectively and at G7 in Figure 5.14.

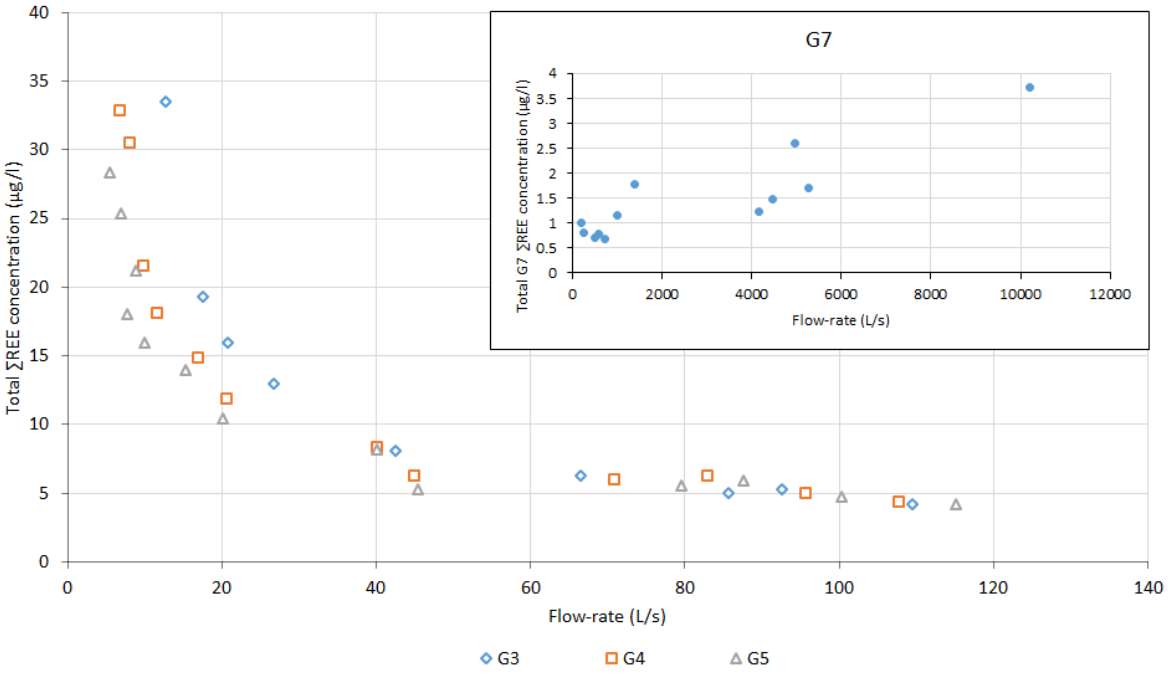

Figure 5.12: ∑REE concentration in unfiltered phase at G3 to G5 and G7 under all flow conditions (5.53-115.1 L/s for G5; 206-10200 L/s for G7)

As can be seen from Figure 5.12 and Figure 5.13, the dissolved (< 0.005 µm), < 0.1 µm, < 0.45 µm and unfiltered ∑REE concentrations at G3, G4 and G5 all display a clear decreasing trend with the increasing flow (from 5.53 to 115.1 L/s for G5; 6.78-107.7L/s for G4; 12.68-109.5L/s for G3). This is due to the dilution effect. Since the ∑REE loads in dissolved, 0.1µm filtered, 0.45µm filtered and unfiltered phases at each sampling site of G3- G5 all display an overall increase pattern as flow increases from lower to higher conditions (as shown in Section 5.2.2). But the additional REE mass introduced to the water column (from Threlkeld mine spoils and re-suspended sediments from Gate Gill streambed) at G3- G5 under higher flow conditions should be at relatively low concentration.

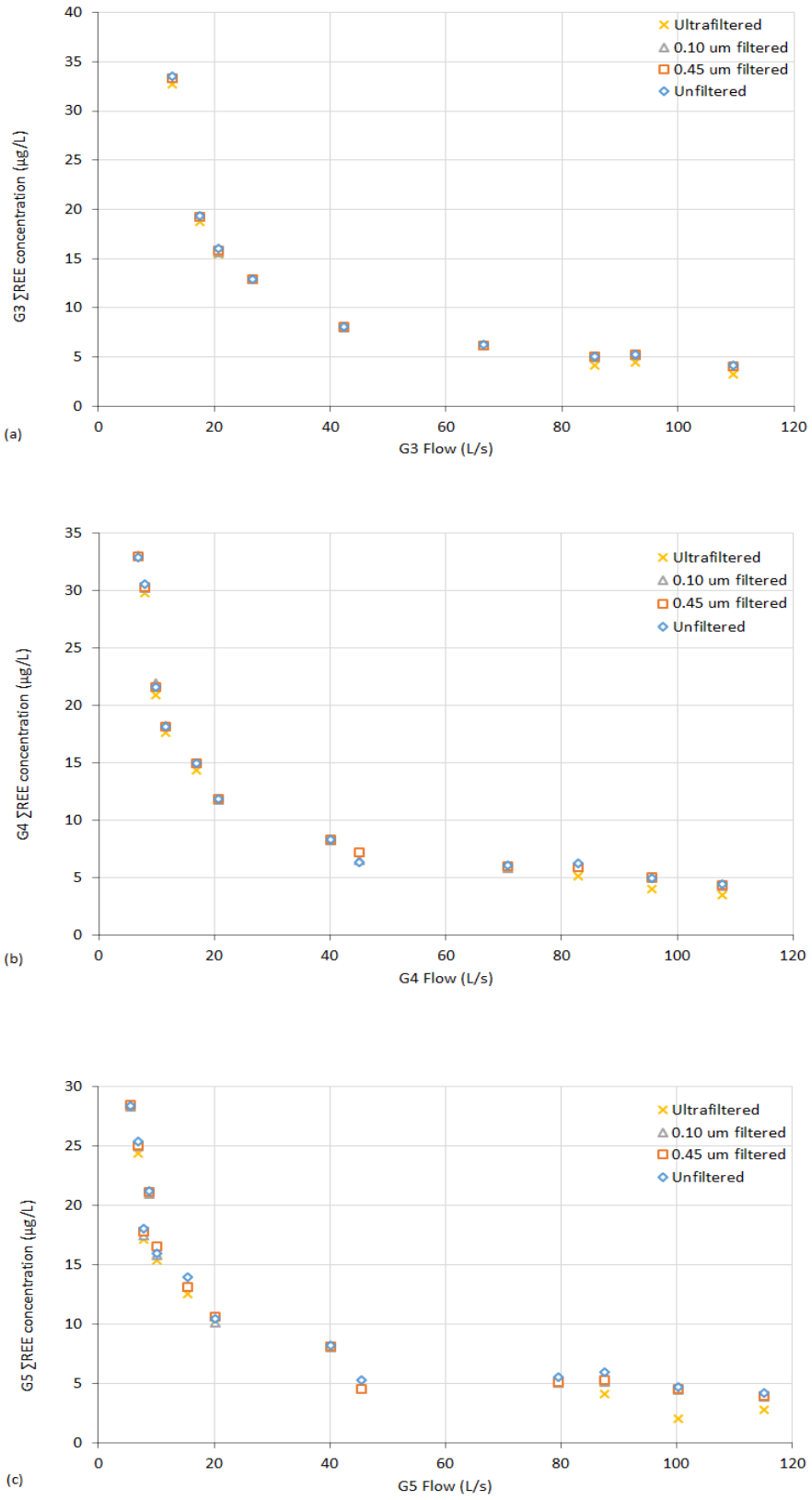

Figure 5.13: ∑REE concentration in < 0.005 µm, < 0.1 µm, < 0.45 µm and unfiltered phases at (a) G3; (b) G4; (c) G5 under all flow conditions (5.53-115.1L/s for G5; 6.78-107.7L/s for G4; 12.68-109.5L/s for G3)

Figure 5.12 and Figure 5.14 show that as flow increases at G7 (734-10200L/s), the < 0.1 µm, < 0.45 µm and unfiltered ∑REE concentrations show a general increasing trend. This may be attributed, in part, to mobilisation of river bed sediments and also to the input of REE from new sources (e.g. Bannerdale mine upstream of the confluence of the River Gleneramackin and the Gate Gill, see Section 5.2.2). A dilution effect is seen at low flow (< 734 L/s). Although there is no clear relationship between dissolved (< 0.005 µm) ∑REE concentration and flow at low flow (< 734L/s), there is a small increase in concentration (0.2816 µg/l - 0.3349 µg/l) at flows greater than 734, which may be due, in part, to additional sources. These variations at G3-G5 and G7 under different flow conditions can also be observed from Figure 5.10.

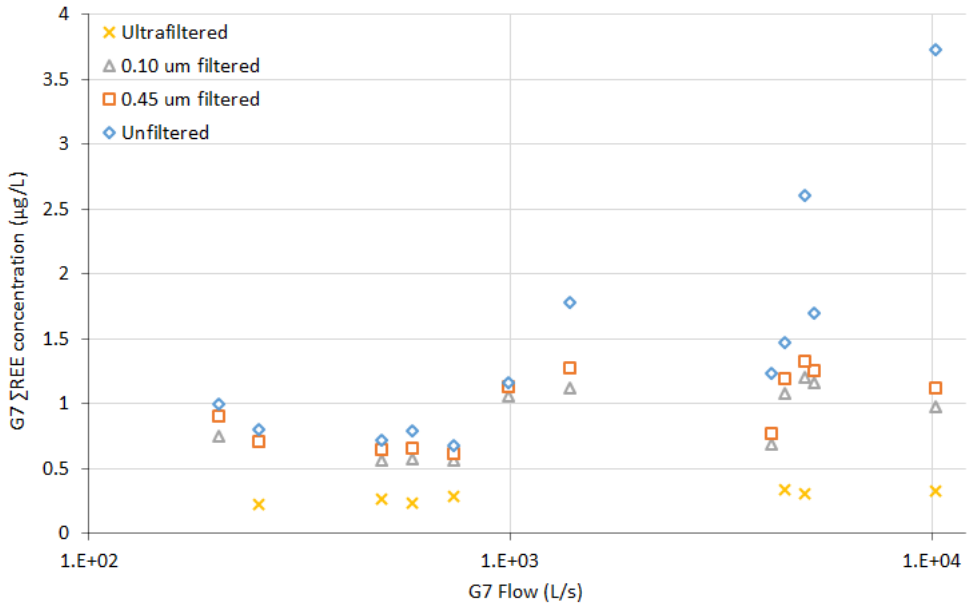

Figure 5.14: ∑REE concentration in < 0.005 µm, < 0.1 µm, < 0.45 µm and unfiltered phases at G7 under all flow conditions (203-10200L/s for G7; corresponding flow range for G5 is 5.53-115.1L/s)

5.3 Influence of pH on REE transformation

The difference in the proportion of total REE present as dissolved REE (<0.005µm) between sampling sites, and at one sampling location under varying hydrological conditions, are useful indicators of the influence of pH on REE dynamics. The discussion in this section is therefore based on the sampling occasions for which dissolved REE data (<0.005µm) are available. Based on the flow range of lower and higher flow condition noted in Section 5.2.1, the lower flow conditions on the sampling occasions with ultrafiltered data (<0.005µm) are

6.88-15.34L/s for G5 and 253-734L/s for G7. The higher flow conditions on the sampling occasions with ultrafiltered data are 87.59-115.1L/s for G5 and 4480-10200L/s for G7.

The mean pH and mean proportion of total REE present in dissolved form from the mine discharge (G2) to the most downstream location (G7) are calculated and displayed in Figure 5.15. The spatial variation in pH and the proportion of total REE present in dissolved form as mine discharge polluted water flows from G3 to G7 under all flow conditions is shown in Figure 5.16 (a) and (b) respectively. The flowrate of G5 is used as a representative to show the change of flow condition in Figure 5.16.

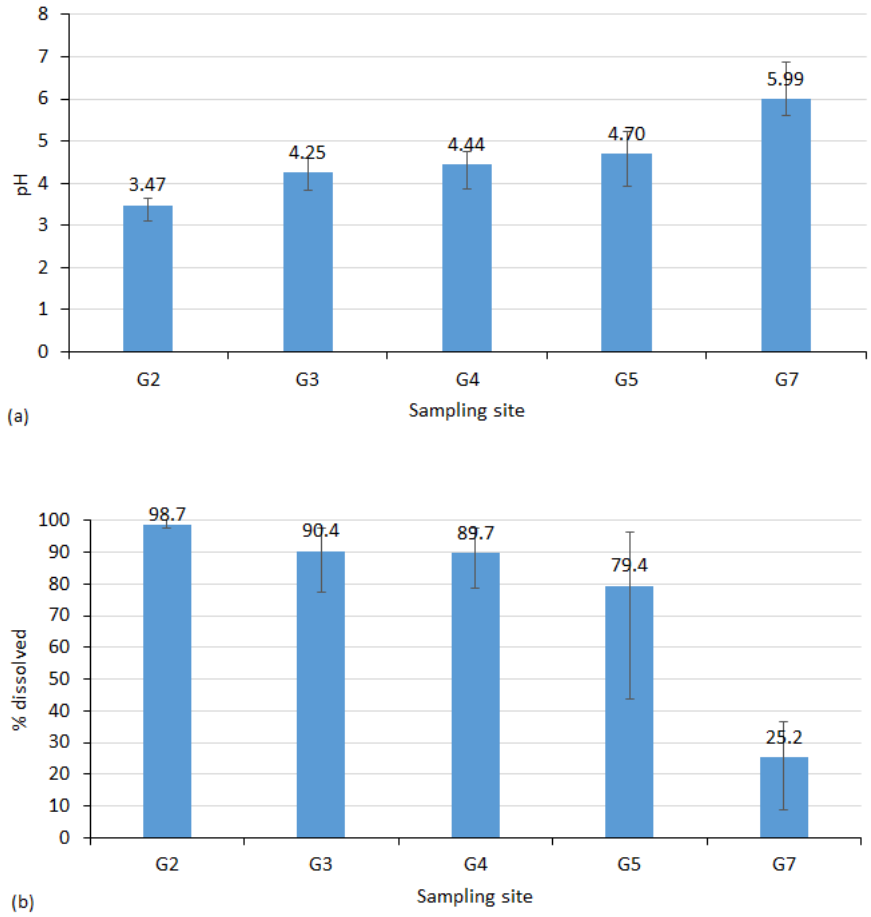

Figure 5.15: Spatial variation of mean value of (a) pH; and (b) dissolved REE proportion in total water column in downstream of G2 based on data from all flow conditions when ultrafiltration was undertaken

Figure 5.15 (a) shows that mean pH displays a small and gradual increase from G2 to G5 (from 3.47 to 4.7), and then shows a relatively larger increase from G5 to G7 (from 4.7 to 5.99). The mean proportion of total REE present as dissolved REE (<0.005µm) shows a small decrease from G2 to G5 (from 98.7%-79.4%), and a large decrease from G5 to G7 (79.4%-

25.2%), according to Figure 5.15 (b). A similar spatial variation of pH and the proportion of total REE present as dissolved REE (<0.005µm) on each sampling occasion can be observed in Figure 5.16 (a) and Figure 5.16 (b) respectively.

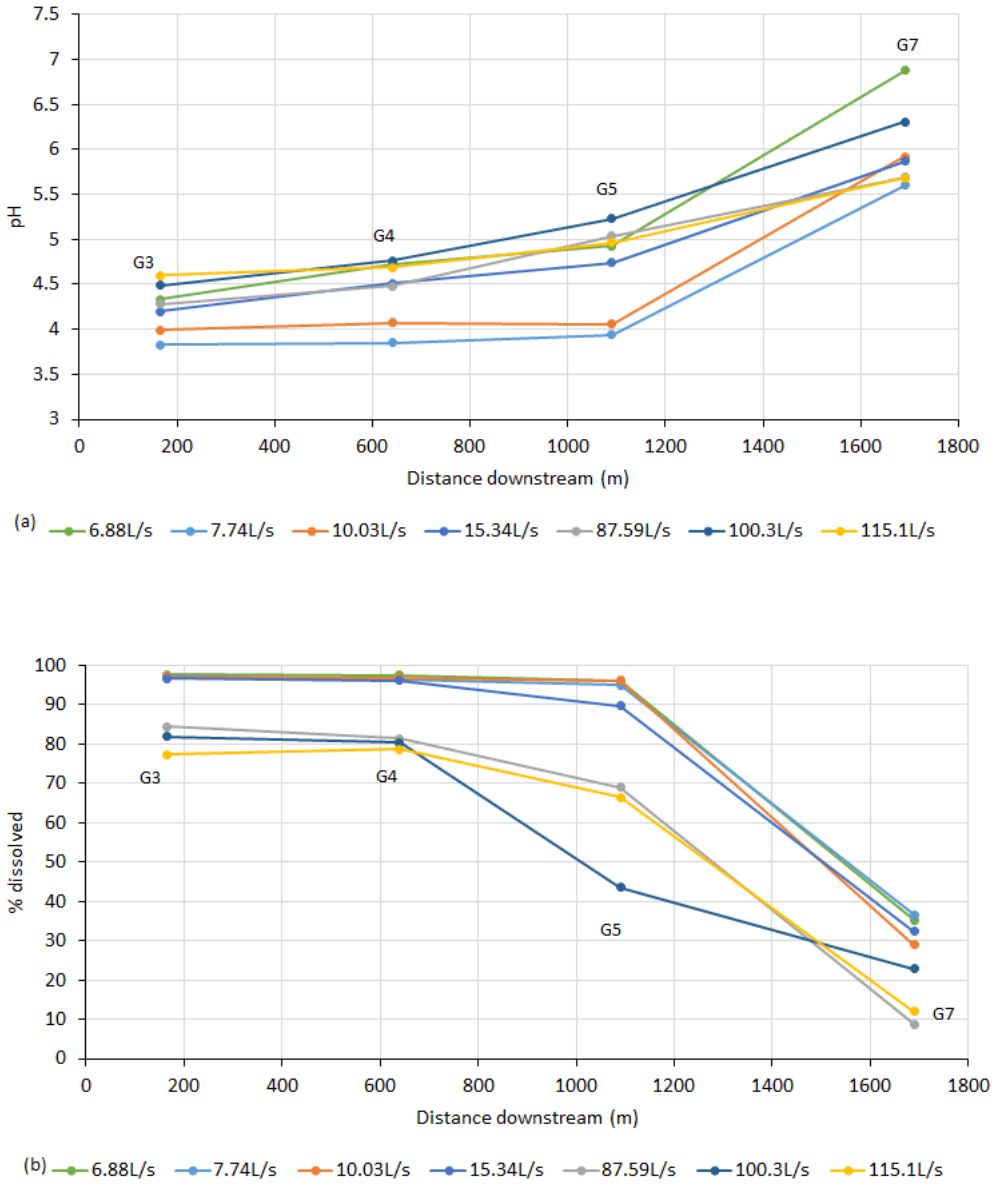

Figure 5.16: Spatial variation of (a) pH; and (b) dissolved REE proportion in total water column downstream of G2 under all flow conditions (flow shown in graphs is based on that at G5)

The continuous increase of pH from the mine discharge (G2) to the most downstream location (G7) may play an important role on the decrease in proportion of total REE present in dissolved phase from G2 to G7. Higher pH can induce more REE to transform from dissolved to (suspended) solids, and REE are more soluble at low pH and more readily

mobilized in acidic water compared with slightly acidic (~6) and near neutral water (~7) (Smedley, 1991; Elderfield et al. 1990; Goldstein and Jacobsen, 1987, 1988a; Keasler and Loveland 1982). The positive relationship between pH and REE transformation from dissolved to suspended solid phase and/ or solid phase (sediments) has been well documented in previous studies of REE behaviour in acidic surface water and groundwater (Cao et al. 2001; Leybourne et al., 2000; Landa et al., 2000; Gimeno et al., 1996; Johannesson et al., 1996a; Johannesson et al., 1995; Johannesson & Lyons, 1995; Sholkovitz, 1995; Johannesson et al. 1994a). It occurs mainly because REE are progressively scavenged by the freshly formed Fe and Al oxyhydroxides as pH increases from acidic to around neutral condition. Given appropriate pH (>7) there may also be quantitative removal of REE from the water column due to precipitation of Fe (and Al) oxyhydroxides (Medas et al. 2013). Scavenging of dissolved REE by fresh Fe and Al oxyhydroxides in this way (through adsorption and/ or co-precipitation processes) is a well-documented phenomenon especially for water with acidic to around neutral pH (e.g. Verplanck et al. 2004; Protano and Riccobono, 2002).

The decrease in proportion of total REE present in the dissolved phase as water flows from G2 to G7 may therefore be at least in part caused by the progressive increase in REE transformation from dissolved to suspended solid phase from G2 to G7. Besides the role of pH, the substantially lower proportion of total REE present as dissolved REE at G7 relative to G5 is likely also due to the resuspension of large amounts of REE-containing riverbed sediments at G7. Although the resuspension of sediments may also occur at G5 under higher flow conditions, since the River Glenderamackin is a much bigger river compared to the Gate Gill, it is likely that G7 has more fine-grained bed sediments than G5.

In addition, as can be seen from Figure 5.16 (b), the proportion of REE present in the dissolved phase (<0.005μm) decreases from G3 to G5 to a greater extent under higher flow conditions (87.59-115.1L/s for G5) than under lower flow conditions (6.88-15.34L/s for G5). To be more specific, as water flows from G3 to G5, the mean proportion of REE present in the dissolved phase only decreases by a value of 3% under lower flow conditions, but decreases by a value of 21.6% under higher flow conditions. This may due to the following two reasons: (1) a generally lower increase in pH from G3 to G5 under lower flow conditions (mean pH increases from 4.08 to 4.41) relative to that under higher flow conditions (mean pH increases from 4.45 to 5.07) (Figure 5.16 a); (2) higher pH on Gate Gill (G3 to G5) under higher flow conditions compared to that under lower flow condition. The degree of REE

adsorption increases with pH, as shown in many studies (e.g. Tang and Johannesson, 2010b; Verplanck et al. 2004; Gammons et al. 2005; Bau, 1999).

Although the increase in pH from G5 to G7 under lower flow conditions (pH increases from 4.45 to 6.07) is higher than that under higher flow conditions (pH increases from 5.07 to 5.89), the decrease in the proportion of total REE present as dissolved REE (<0.005μm) from G5 to G7 under lower flow conditions is less than that under higher flow conditions. This may be due to a dramatic increase of sediment resuspension at G7 with flow.

Figure 5.17 shows the variation in pH and the proportion of total REE present as dissolved at each sampling location of G3 to G5 under all flow conditions. The selected trendline type in Figure 5.17 returns the best value of R^2. At each location, pH displays a general increasing trend with increasing flow, since the rainfall under the higher flow conditions induces more dilution of the Gate Gill mine water and raises the pH. In contrast, the proportion of total REE present as dissolved decreases with increasing flow at each location (Figure 5.17), which may due to: (1) the rise in pH results in some REE that were present as truly dissolved transforming to colloidal / particulate REE; (2) the potential influence of the re-suspended sediments from Gate Gill stream bed under higher flow conditions. The phenomenon that the proportion of REE present in the dissolved phase at G3 to G5 under higher flow conditions (87.59-115.1L/s for G5) is lower than that under lower flow conditions (6.88-15.34L/s for G5) can also be observed in Figure 5.16 (b).

According to Figure 5.17, as flow increases: (1) at G3, the mean pH increases from 4.08 to 4.45 and the mean proportion of REE present in the dissolved phase decreases from 97.3% to 81.2%; (2) at G4, the mean pH increases from 4.28 to 4.63 and the mean proportion of REE present in the dissolved phase decreases from 96.8% to 80.1%; (3) at G5, the mean pH increases from 4.41 to 5.07 and the mean proportion of REE present in the dissolved phase decreases from 94.3% to 59.6%.

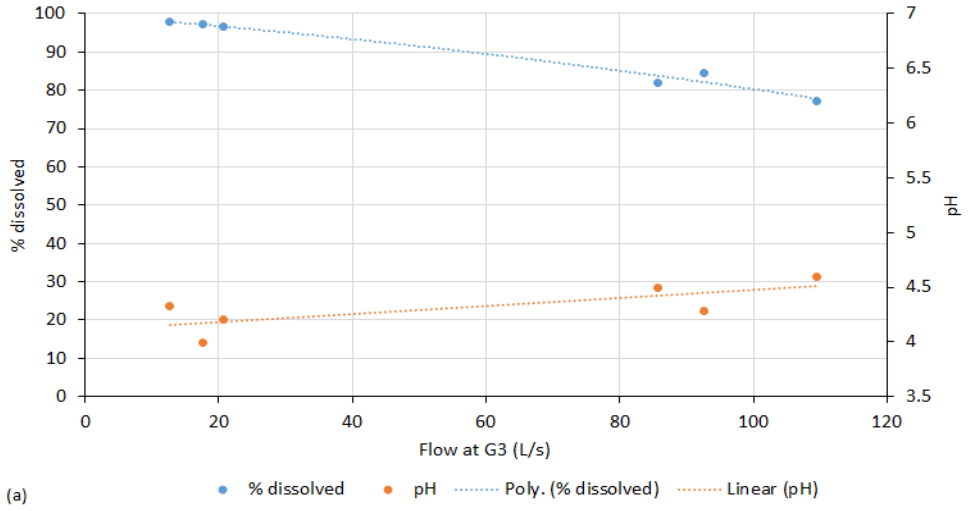

(a)

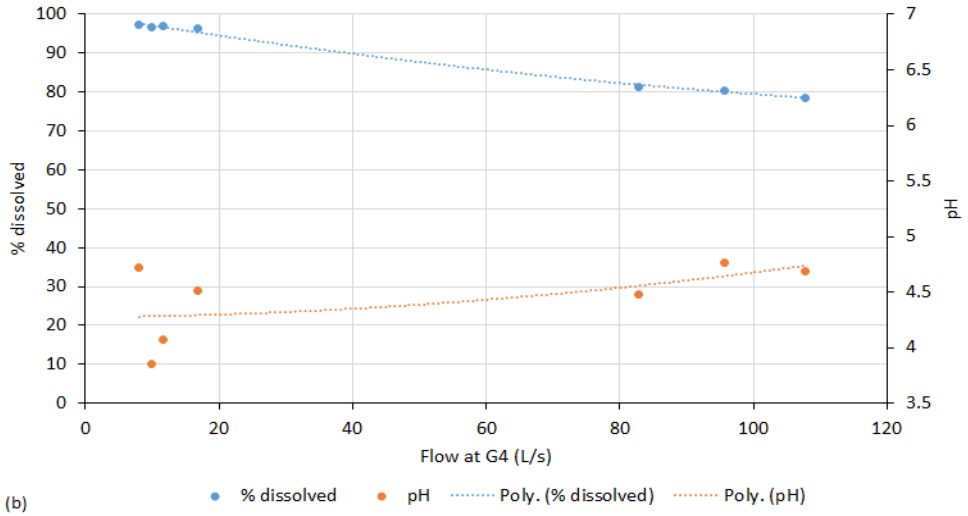

(b)

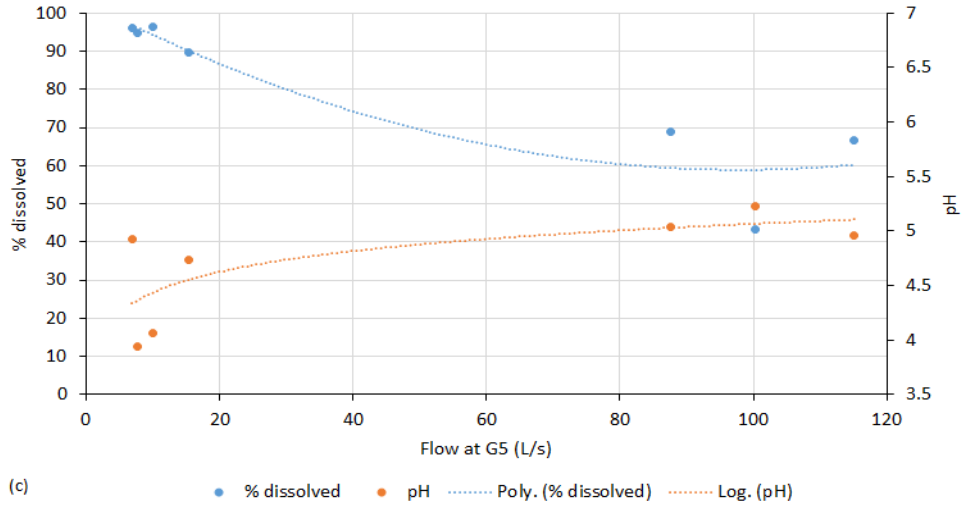

(c)

Figure 5.17: Variation of pH and the proportion of REE present in dissolved phase (<0.005µm) at (a) G3; (b) G4; and (c) G5 under all flow conditions

It should be noted that even though the mean pH at G3 (4.45) under higher flow conditions is very similar to that at G5 (mean pH of 4.41) under lower flow conditions, the mean proportion of REE present in the dissolved phase at G3 (81.2%) under higher flow conditions is lower than that at G5 under lower flow conditions of 13.1%. This suggests that pH has a minor influence on the proportion of REE present in the dissolved phase at G3 (81.2%) under higher flow conditions, compared to the influence of sediment resuspension under higher flow conditions. Although the studies of Tang and Johannesson (2010b), Quinn et al. (2006a) and Bau (1999) all show that REE begin to attenuate even at pH ≈ 4, Tang and Johannesson (2010b) show that there is only a slight increase in adsorption of REE when pH increases from 4 to 5, but adsorption then increases significantly when pH increases from 5 to 7. Bau (1999) draw a similar conclusion to Tang and Johannesson (2010b), showing that a very small amount of REE can adsorb onto Fe oxyhydroxides when pH is less than 4.6, and the degree of REE adsorption gradually increases with the increase in pH from 4.98 to 6.21. Verplanck et al. (2004) and Gammons et al. (2005) both state that the strong partition of REE into the freshly formed HFO occurs when pH is between 5.1 and 6.6. However, Quinn et al. (2006a) observed a linear increase of REE adsorption with increase of pH from 3.9 to 7.1. In addition, Sun et al. (2012) show that the adsorption of REE increases significantly when pH is within the range of 4 to 6.

This study shows that the transformation of REE from dissolved (<0.005µm) to suspended solid (>0.005µm) is strongly inhibited when pH is <~4.4 (< ~5% of total REE are removed from the dissolved phase). Due to the influence of the sediments resuspension under higher flow conditions, it is difficult to point out the trigger pH which can induce a large degree of REE transforming from dissolved phase to suspended solid. However, the studies of Sun et al. (2012), Tang and Johannesson (2010b), Quinn et al. (2006a), Gammons et al. (2005), Verplanck et al. (2004) and Bau (1999) all show that the degree of REE removal is higher when pH reaches ~5. Therefore, the relatively low mean proportion of REE present in the dissolved phase (59.6%) at G5 under higher flow conditions may largely be due to the relatively higher degree of REE transformation from dissolved to suspended solid, since the mean pH at G5 under higher flow conditions (87.59-115.1L/s for G5) is 5.07.

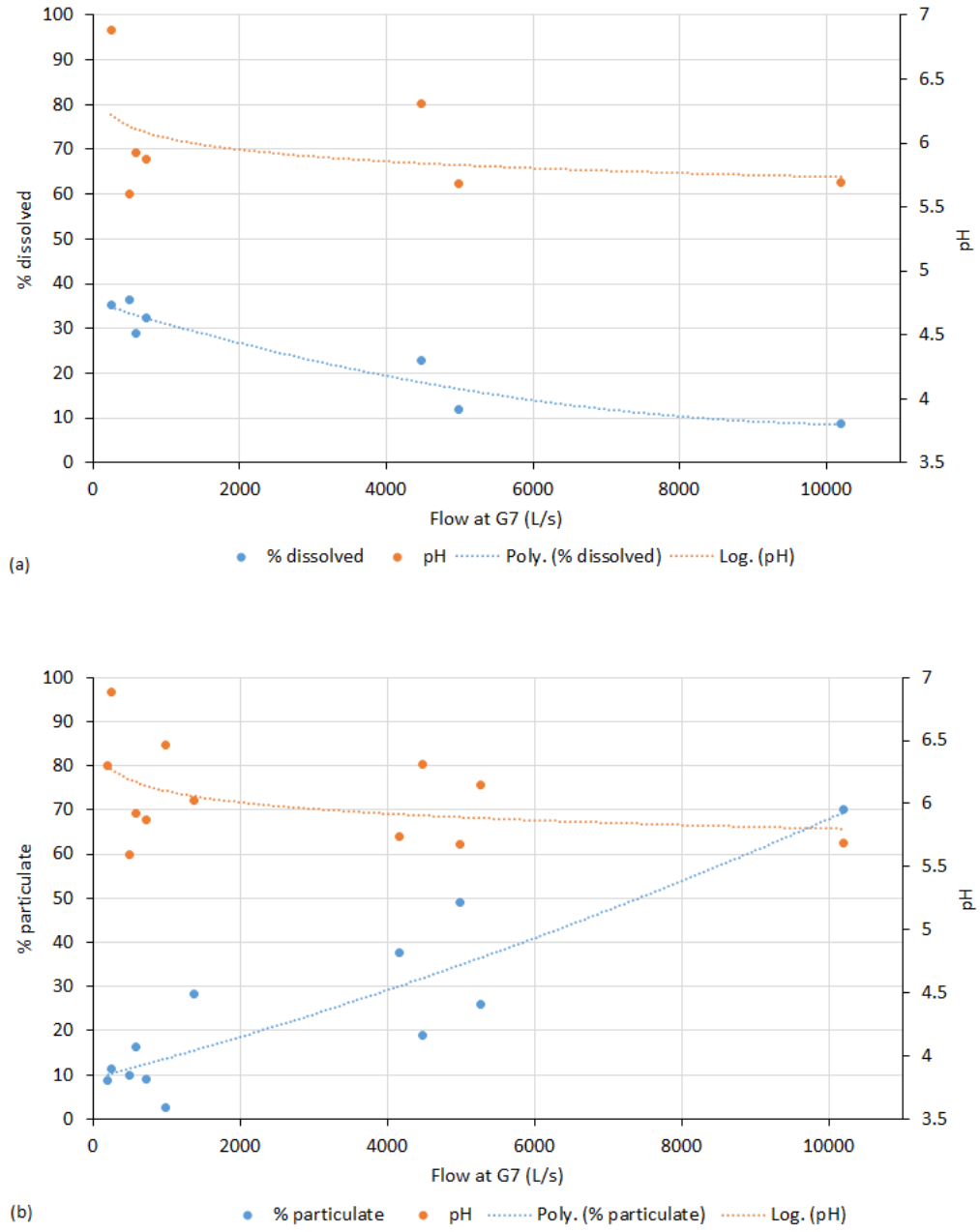

Figure 5.18: (a) variation of pH and the proportion of REE present in dissolved phase (<0.005µm); (b) variation of pH and the proportion of REE present in particulate form (>0.45µm) at G7 under all flow conditions

Figure 5.18 shows the variation in pH, proportion of REE present in dissolved phase and proportion of REE present in particulate form with flow (The selected trendline type returns the best value of R^2). There is no clear increase in pH at G7 with flow, and the mean pH at G7 under lower flow conditions is 6.07 and under higher flow condition is 5.89. The decrease in the proportion of REE present in the dissolved phase with flow at G7 is therefore independent of pH. It may be mainly caused by the increase in degree of sediments

resuspension with flow. The increase in the proportion of total REE present as particulates with flow at G7 (Figure 5.18 b) further indicates that the degree of physical transformation of REE from sediments to the water column increases with flow. However, the much higher pH conditions at G7 under both lower (253-734L/s for G7) to higher conditions (4480-10200L/s for G7) compared to that at Gate Gill suggests that a large amount of REE are chemically transformed from dissolved to suspended solid phases at G7 under all flow conditions.

5.4 Surface complexation/adsorption

The interactions of REE with freshly formed solid phases in the water column, such as adsorption, desorption, co-precipitation and ion exchange, control the REE transformation. This section identifies the metals which appear to play a role in controlling the transport and fate of REE in-stream below the mine discharge. This section then discusses adsorption of REE in detail, as this is a key mechanism controlling REE fate.

5.4.1 Source of other metals in G2

The pyrite and chalcopyrite contained in the mineral veins of Woodend mine is likely the main source of iron in Gate Gill. Where there is oxygen ingress, weathering of pyrite and also chalcopyrite results in ferrous iron (Fe^{2+}) being present in flooded mine workings. The ferrous iron is then oxidized to ferric iron (Fe^{3+}) when contaminated groundwater discharges at the surface as mine drainage, under atmospheric conditions. At the mine discharge, ferric iron (Fe^{3+}) forms ferric oxyhydroxides and precipitates from water rapidly. Acidity is produced during these reactions and therefore pH drops as a consequence. This series of reactions is shown in equations 5.1, 5.2, 5.3 and 5.4 (Mayes et al. 2008; Younger et al. 2002):

$$\text{Pyrite: } FeS_2(s) + 7/2O_2 + H_2O \rightarrow Fe^{2+} + 2SO_4^{2-} + 2H^+ \quad (5.1)$$

$$\text{Chalcopyrite: } CuFeS_2(s) + 4O_2(aq) \rightarrow Cu^{2+} + Fe^{2+} + 2SO_4^{2-} \quad (5.2)$$

$$Fe^{2+} + 1/4O_2 + H^+ \rightarrow Fe^{3+} + 1/2H_2O \quad (5.3)$$

$$Fe^{3+} + 3H_2O \rightleftharpoons Fe(OH)_3(s) + 3H^+ \quad (5.4)$$

Galena and sphalerite in the veins are the source of zinc and lead in Gate Gill. The soluble zinc and lead are released from these two minerals to solution based on the reactions (Younger et al. 2002) shown in equations 5.5 and 5.6:

Galena: $PbS(s) + 2O_2(aq) \rightarrow Pb^{2+} + SO_4^{2-}$ (5.5)

Sphalerite: $ZnS(s) + 2O_2(aq) \rightarrow Zn^{2+} + SO_4^{2-}$ (5.6)

5.4.2 Scavenging of REE by Fe and Al oxyhydroxides

Fe and Al oxyhydroxides are the common scavenging materials that control the fate and transport of REE (Medas et al. 2013; Quinn, 2006; Verplanck et al. 2004; Protano and Riccobono, 2002). The studies from Medas et al. (2013); Ohta and Kawabe (2001) and Ohta and Kawabe (2000) show that Zn and Mn oxyhydroxides can also effectively scavenge REE from the dissolved phase.

Zn and Mn should have little influence on REE fate and transport in stream in this study. This is because trivalent metals normally form hydroxides at a lower pH range, while a higher level of pH is required for divalent metals forming hydroxides. pH at G3 to G5 and G7 on all sampling occasions ranges from 3.88-6.88 (Section 5.3), which was generally within the pH range required for forming Fe and Al oxyhydroxides. To be more specific, a small amount of Fe oxyhydroxides flocs forms even though pH is around 3 and the formation of Al oxyhydroxides flocs begins when pH reaches 4.5- 5 (Younger et al. 2002). The precipitation of Fe and Al oxyhydroxides from total water prevails when pH is between 6 and 8 (Younger et al. 2002).

However pH at G3 to G5 and G7 under all flow conditions (5.53-115.1L/s; 203-10200L/s for G7) is not high enough to induce the formation of the divalent metals- Zn and Mn hydroxides flocs. To be more specific, Zn hydroxides flocs are not expected to form when pH is less than ~7 and Mn hydroxides flocs are not expected to form when pH is less than ~8 (Younger et al. 2002). pH at sampling sites downstream of the Gategill discharge under all flow condition was no more than 6.88, and mostly less than 6.47, divalent metals Zn and Mn are expected to have high solubility at G3 to G7. The precipitation of Zn, Mn oxide/hydroxide solid phase prevails when the pH in the receiving stream largely increases to 9 to 11 (Younger et al. 2002). But before pH reaches circumneutral condition, these divalent metals can absorb onto Fe and Al oxyhydroxides (Gaillardet et al. 2003). Medas et al. (2013) also notes that REE can absorb onto the more abundant hydrozincite particles only under circumneutral condition when most Fe oxyhydroxides flocs have precipitated from the water phase. Mn oxyhydroxides normally play an important role on REE attenuation in seawater (Ohta and

Kawabe, 2001; Ohta and Kawabe, 2000; Elbaz-Poulichet and Dupuy, 1999; Sholkovitz, 1995; Sholkovitz et al., 1994; Elderfield et al., 1990).

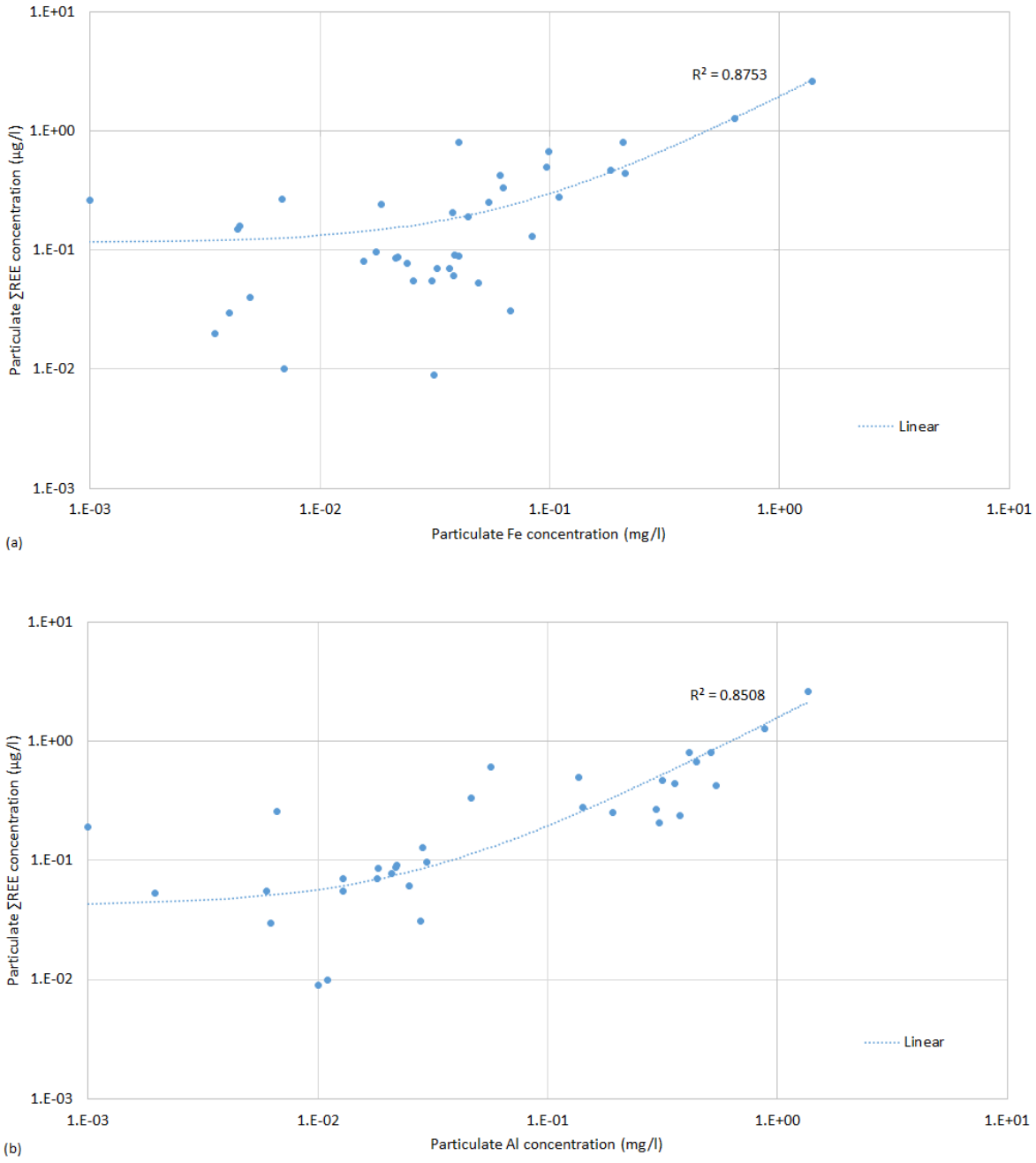

Figure 5.19: Relationship between particulate ∑REE concentration and (a) particulate Fe concentration; and (b) particulate Al concentration at G3 to G5 and G7 under all flow conditions (5.53-115.1L/s for G5; 203-10200L/s for G7)

Figure 5.19 (a) and (b) respectively shows the relationship between particulate ∑REE and Fe concentration, and Al concentration at G3- G5 and G7 under all flow conditions (5.53-115.1L/s for G5; 203-10200L/s for G7). This is to demonstrate whether Fe and/ or Al

oxyhydroxides control the transport and fate of REE downstream of the mine discharge. According to Figure 5.19, there is a strong positive correlation between particulate ∑REE and Fe concentration (R^2=0.88), and between particulate ∑REE and Al concentration (R^2=0.85) at G3- G5 and G7.

This indicates that Fe and Al oxyhydroxides are likely the main materials scavenging REE and they may both play an important role in the REE transformation between dissolved and suspended solid/ solid phase downstream of the mine discharge. Many studies found that iron oxyhydroxides are extremely effective in scavenging REE and controlling REE migration in water due to their high specific surface area and large sorption capacity for metals (Protano and Riccobono, 2002; Bau, 1999). REE can also largely adsorb to Al oxyhydroxides and thus be removed from the truly dissolved phase (Quinn, 2006). Therefore, the REE in the suspended solids at G3 to G5 and G7 under all flow conditions are likely associated with the freshly formed Fe and Al flocs and/ or secondary Fe and Al oxyhydroxides precipitates which are brought into the water column under higher flows.

Figure 5.20 (a) and (b) respectively shows the relationship between particulate (>0.005µm) ∑REE and Fe concentration, and Al concentration at G3 to G5 under all flow conditions (5.53-115.1L/s for G5). There is a moderate positive correlation between particulate ∑REE and Fe concentration (R^2=0.51), and also between particulate ∑REE and Al concentration (R^2=0.55) at Gate Gill (G3 to G5).

As discussed in Section 5.3, negligible to a very small proportion of total REE (< ~5%) is transformed from dissolved (<0.005µm) to suspended solid phase (>0.005µm) at G3 and G4 under all flow conditions (5.53-115.1L/s for G5) with low pH (G3: mean pH is 4.18, pH ranges from 3.83-4.6; mean pH is 4.4, pH ranges from 3.85-4.76), and at G5 under lower flow conditions with low pH (5.53-40.1L/s for G5, mean pH is 4.43). A relatively higher proportion of total REE is expected to be transformed from dissolved to suspended solid at G5 under higher flow conditions with higher pH (45.42-115.1L/s, mean pH is 5.11, pH ranges from 4.94-5.37). But the degree of REE transformation from dissolved to suspended solid at G5 under higher flow conditions (45.42-115.1L/s) is unknown due to the higher flows induced sediments resuspension.

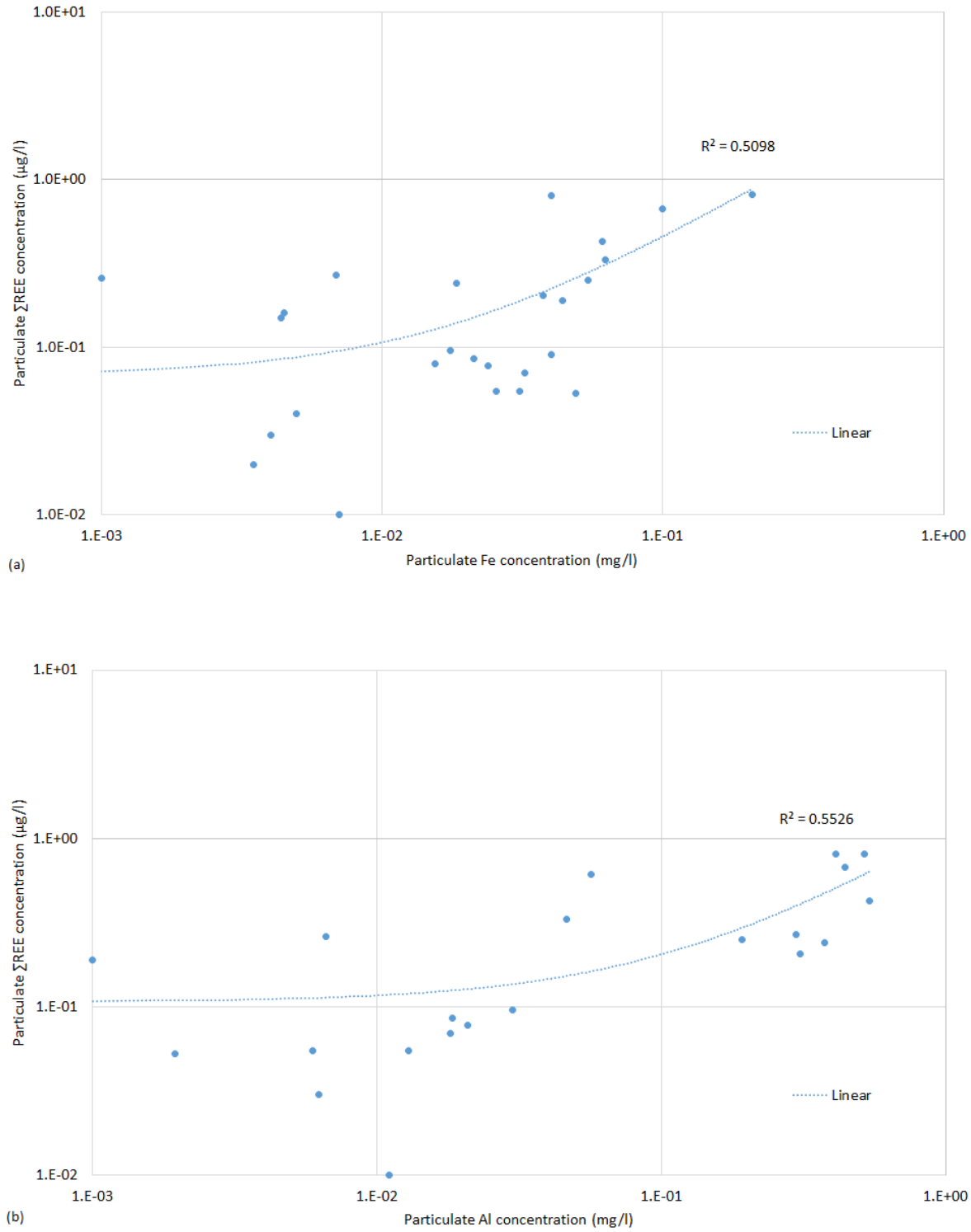

Figure 5.20: The relationship between particulate (>0.45µm) ∑REE concentration and (a) Fe concentration; (b) Al concentration at G3 to G5 under all flow conditions (5.53-115.1L/s for G5)

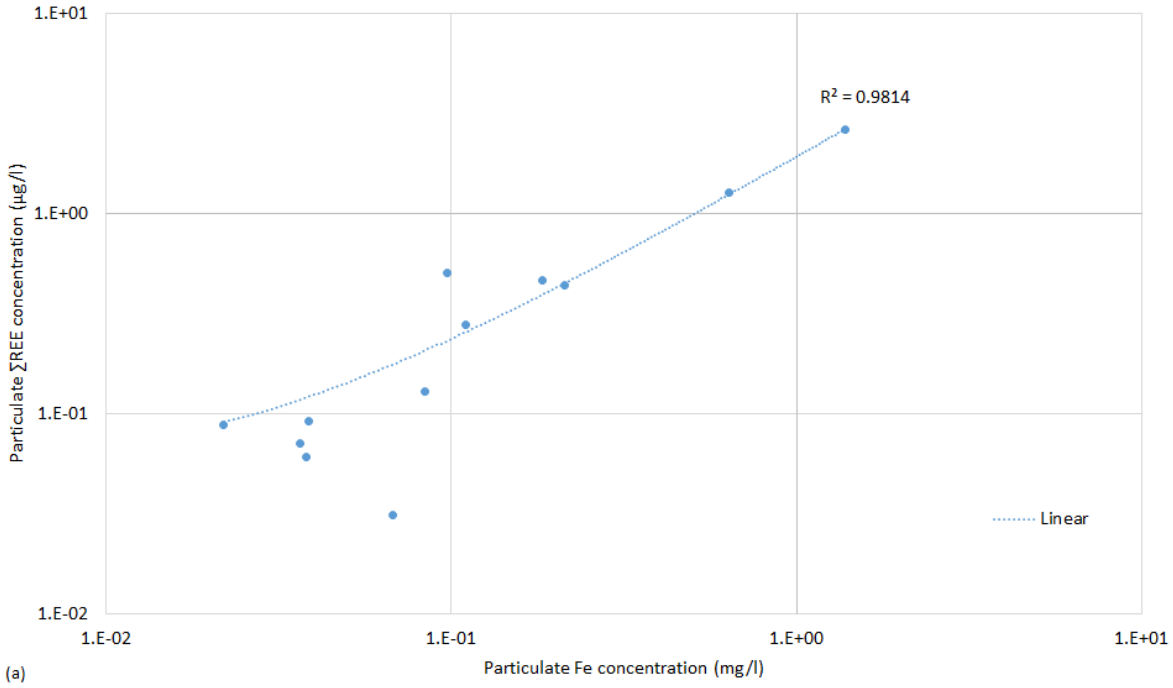

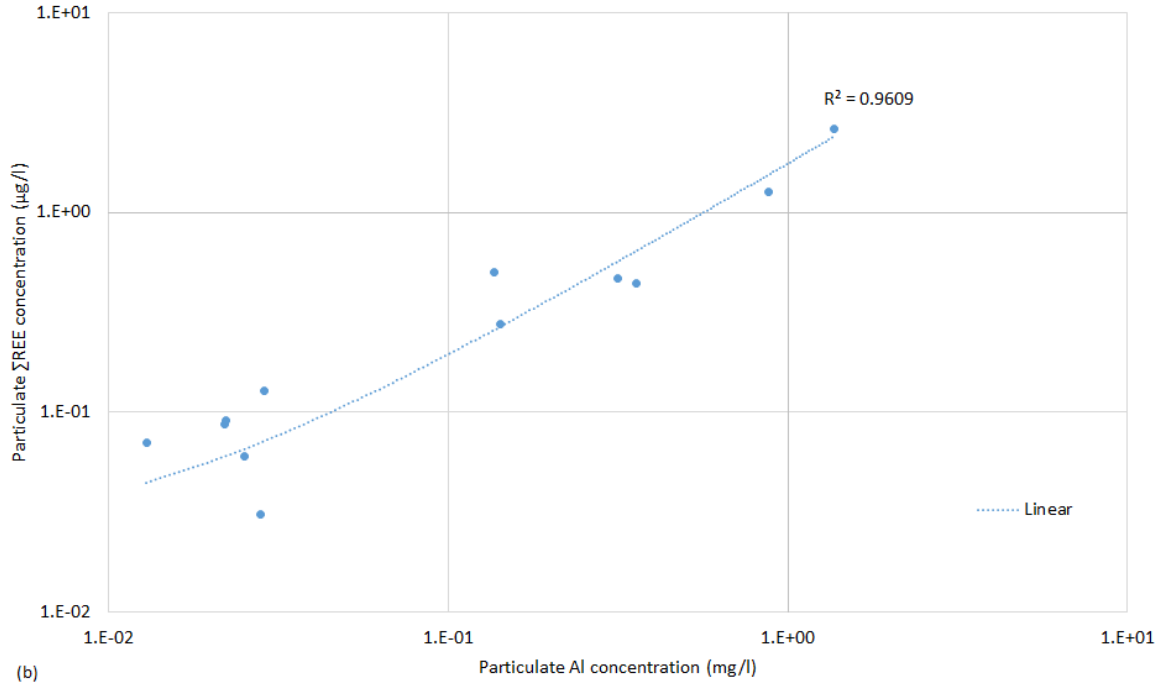

Figure 5.21: The relationship between particulate (>0.45µm) ∑REE and (a) Fe concentration; (b) Al concentration at G7 under all flow conditions (203-10200L/s for G7)

Tang and Johannesson (2010b); Gammons et al. (2005); Verplanck et al. (2004) and Bau (1999) found that the adsorption of REE is pH dependent, which means that adsorption becomes important only if pH in solution is above the 'trigger' pH (~5). Before pH reaches

~5, even though a large amount of Fe and Al flocs formed in the water, the scavenging of REE by the freshly formed Fe and Al flocs is strongly inhibited (Gammons et al., 2005; Verplanck et al., 2004). The moderate positive correlation between particulate ∑REE and Fe/ Al concentration at G3 to G5 under all flow conditions (Figure 5.20) is likely due to the overall low degree of REE adsorption onto Fe and Al oxyhydroxides at G3 to G5.

Figure 5.21 (a) and (b) respectively show the change of particulate ∑REE concentration as a function of particulate Fe concentration and as a function of particulate Al concentration at G7 under all flow conditions (203-10200L/s for G7). At G7, there is a strong positive correlation between particulate ∑REE and Fe concentration (R^2=0.98), and also between particulate ∑REE and Al concentration (R^2=0.96).

As discussed in Section 5.3, the degree of REE transformation from dissolved (<0.005μm) to suspended solid (>0.005μm) at G7 is likely to be quite high (actual degree is not known since REE-containing sediments are likely to be brought into the water column as flow increases), due to the much higher pH at G7 (mean pH is 6.05, pH ranges from 5.6-6.88) compared to G5 under all flow conditions (203-10200L/s for G7). This makes G7 a suitable sampling site to explore the relationship between REE and Fe, Al oxyhydroxides, and specifically whether they control REE fate in stream. REE is expected to be largely scavenged during the coagulation and aggregation of Fe and Al flocs at G7. The high degree of REE adsorption onto Fe and Al oxyhydroxides leads to a strong positive correlation between particulate ∑REE and Fe/ Al concentration at G7.

The surface charge of Fe/ Al hydroxide changes with the change of pH, which is the result of protonated or deprotonated water chemically bound to the Fe/ Al hydroxide surface. When using Fe hydroxide as an example, the reactions of Fe hydroxide surface protonation and deprotonation are shown in equations 5.7 and 5.8 (Dzombak and Morel, 1990). Symbol S-Fe in the equations 5.7 and 5.8 represents an adsorption site on the surface of iron hydroxide. When pH is below 7.29, the sites on Fe hydroxide surface are mainly positively charged. Zero charged/uncharged sites and negatively charged sites on Fe hydroxide surface are negligible under such conditions (Dzombak and Morel, 1990). Similar as Fe hydroxides, the positively charged sites dominate on Al oxides and hydroxides surface when pH is below 7. The point of zero net charge values for oxides and hydroxides of Fe and Al are in the range of 7 to 9 (Huang et al. 2011).

$S\text{-}FeOH_2^+ \rightleftharpoons S\text{-}FeOH + H^+$ $-\log K_1=7.29$ (25^oC, I=0.5M) (5.7)

$S\text{-}FeOH \rightleftharpoons S\text{-}FeO^- + H^+$ $-\log K_2=8.93$ (25^oC, I=0.5M) (5.8)

The pH dependence of REE adsorption onto Fe hydroxides is caused by competition between the protons and REE for the adsorption sites on the Fe hydroxide surface. The surface complexation reaction between REE and Fe hydroxides occurs via exchange of REE ions in solution with protons of Fe hydroxide surface hydroxyl groups, which results in partial formation of covalent bonds (Quinn et al. 2006a). This surface complexation reaction produces protons, but the high proton level at low pH drives the reaction to the left, which causes desorption of REE from Fe hydroxides surface.

The attenuation caused by physical sorption of REE onto Fe flocs is not expected to occur as the important REE species in the Gate Gill are mainly Ln^{3+}, $LnSO_4^+$ and $LnCO_3^+$, which are all positively charged species. The results of REE speciation modelling at Gate Gill is shown in Section 6.2. Given that sorption sites on Fe and Al flocs are dominated by positively charged sites, and that REE species are also positively charged, it seems unlikely that physical sorption of REE to Fe and Al flocs is a likely attenuation mechanism for REE in the Gate Gill and River Glendearmackin.

5.5 Chapter summary

- Gate Gill appears to be a losing stream under lower flow conditions (flowrate of G5: 5.53 - 40.1 L/s) but becomes a gaining stream under higher flow conditions (45.42 - 115.1 L/s).

- The main source of REE content to Gate Gill under all flow conditions is the Woodend mine discharge. Under higher flow conditions, when total REE loads in Gate Gill are higher than that of the Woodend mine discharge, spoil heaps and resuspended REE-containing sediments are likely to contribute to the REE load in Gate Gill.

- Threlkeld mine has quite a limited overall contribution to REE content in the River Glenderamackin downstream (G7) of the confluence with the Gate Gill. Remobilised REE-containing sediments, both upstream of G7 and at G7 itself, appear to contribute substantially to the REE loads at G7 under higher flows. Bannerdale mine may be

another potential source of REE load in the River Glendermackin under higher flows.

- REE transformation from truly dissolved (<0.005μm) to (suspended) solid phase in the Gate Gill and River Glenderamackin is controlled by pH and the formation of Fe and Al oxyhydroxides.

- There is a decrease in the degree of REE transformation from truly dissolved (<0.005μm) to (suspended) solid phase with the increase of pH. Fe and / or Al oxyhydroxides appears to be the main REE scavenging materials at Gate Gill and River Glenderamackin on sampling occasions with pH below neutral conditions (≤6.88).

- The degree of REE adsorption onto Fe and / or Al oxyhydroxides is significantly low (<5%) when pH value is <~4.5 (G3 and G4 under all flow conditions, G5 under lower flow conditions). The degree of REE adsorption is expected to be relatively higher when pH increases to >~5 (G5 under higher flow conditions) and is likely to be much higher at pH of around 6 (G7 under all flow conditions: 203 – 10200 L/s for G7).

Chapter 6 Control of REE fractionation in waters

6.1 Introduction

This chapter describes the influence of source- and solution chemistry-related fractionation in the Gategill mine water discharge and its receiving streams (G3 to G7). In addition, which process (source or solution chemistry) has the dominant control on the PAAS-normalized REE distribution pattern, at G3 to G7 under different hydrological conditions, is discussed in detail.

Section 6.2 displays the main REE species at G1 to G7 under different hydrological conditions. Section 6.3 describes the PAAS-normalized REE distribution pattern in different phases at G1 to G7 under different flow conditions. The source-related fractionation patterns at G1 to G7 under varying hydrological conditions are also shown in Section 6.3. Since solution chemistry may fractionate REE when REE are scavenged by Fe and Al flocs/ precipitates. Section 6.4 discusses the influence of solution chemistry-related fractionation at G3, G4 and G5 under suitable flow and pH conditions when noticeable REE are present in the suspended solid and/ or >0.1μm. A relative large to large proportion of REE are present in suspended solid and/ or >0.1μm at G7 (River Glenderamackin) under all flow conditions (5.53~4980L/s for G5); therefore, the solution chemistry-related fractionation at G7 across the full range of flow conditions is discussed in Section 6.5. Section 6.6 describes the reasons for the MREE enrichment pattern. The anomalies of Eu at G2 to G5 are discussed in section 6.7.

Same as that shown in Chapter 5, the flow of study sites (G1, G3, G4, G5 and G7) are categorised into lower and higher conditions based on the criteria whether the Gate Gill is a losing stream or a gaining stream. The flowrate of G5 is mainly used as the representative to demonstrate the flow range of the lower flow (5.53~40.1L/s for G5, based on all sampling events data) and higher flow (45.42~115.1 L/s for G5, based on all sampling events data) conditions in this chapter since it is the most downstream site of the main study stream (Gate Gill). The flowrate ranges of G7 under lower and higher flow conditions are also shown besides that of G5 when discussing the REE behaviours and REE speciation at G7 under varying hydrological conditions.

6.2 REE speciation at Gategill

Since the data used for speciation modelling should be the concentration of the truly dissolved metals and the anions, the speciation modelling results from sampling occasions when ultrafiltration (0.005µm filtered) was undertaken are mainly shown and discussed into details in this section. The speciation calculation results from sampling occasions when ultrafiltration was not undertaken (0.1µm filtered REE concentrations were used for performing the speciation modelling) are mainly shown in Appendix D and briefly discussed in this section.

6.2.1 Gategill Beck

The speciation modelling results for each individual REE in the ultra (0.005µm) filtered phase at sampling sites located on Gate Gill (G1, G3, G4 and G5) and at mine discharge (G2) are displayed in the graphs in Appendix D. Generally speaking, under both lower flow (6.88~15.34L/s for G5) and higher flow (87.59~115.1 L/s for G5) conditions when ultrafiltration (0.005µm) was undertaken, free REE/lanthanide ions (Ln^{3+}) and REE sulphate complexes ($LnSO_4^+$) are the only important REE species at G1 to G5. As noted in Section 5.3, these sites are all acidic and pH of these sites ranges from 3.11 to 5.23 on occasions when ultra-filtration (0.005µm) was undertaken. The speciation modelling results are similar to those noted by Wood (1990), in which Ln^{3+} and $LnSO_4^+$ were the only important species in an acidic region. Same as the finding from Zhao et al. (2007), under acidic conditions, the percentage of $LnSO_4^+$ shows quite small decrease and the percentage of Ln^{3+} displays quite small increase with the increase in atomic number across the REE group under both lower (6.88L/s~15.34L/s for G5) and higher (87.59~115.1L/s for G5) flow conditions (Appendix D).

Due to the little difference of either Ln^{3+} or $LnSO_4^+$ percentage within REE group, the mean percentage of Ln^{3+} and $LnSO_4^+$ across all elements is used to show the spatial variation of REE species percentage and at Gate Gill under each flow condition, as can be seen from Figure 6.1. In addition, as mentioned in section 2.4.4, $LnSO_4^+$ is not a strong complexes and the solution complexation related fractionation among REE series is not expected to be induced by $LnSO_4^+$ (Verplanck et al. 2004; Wood, 1990). Therefore, it is suitable to use the mean percentage of $LnSO_4^+$ across all elements instead of the percentage of individual $LnSO_4^+$. In Figure 6.1, the mean percentage of REE species is plotted against the distance of

each Gate Gill sampling site (G1, G3, G4 and G5) relative to G1 instead of the site name. In addition, the flowrate of G5 is used as a representative to show the flow condition on each sampling occasion and the flowrate of G5 in the legend is displayed in increasing order. The flow range of G5 for lower flow conditions is 6.88~15.34L/s, and for higher flow conditions is 87.59~115.1 L/s.

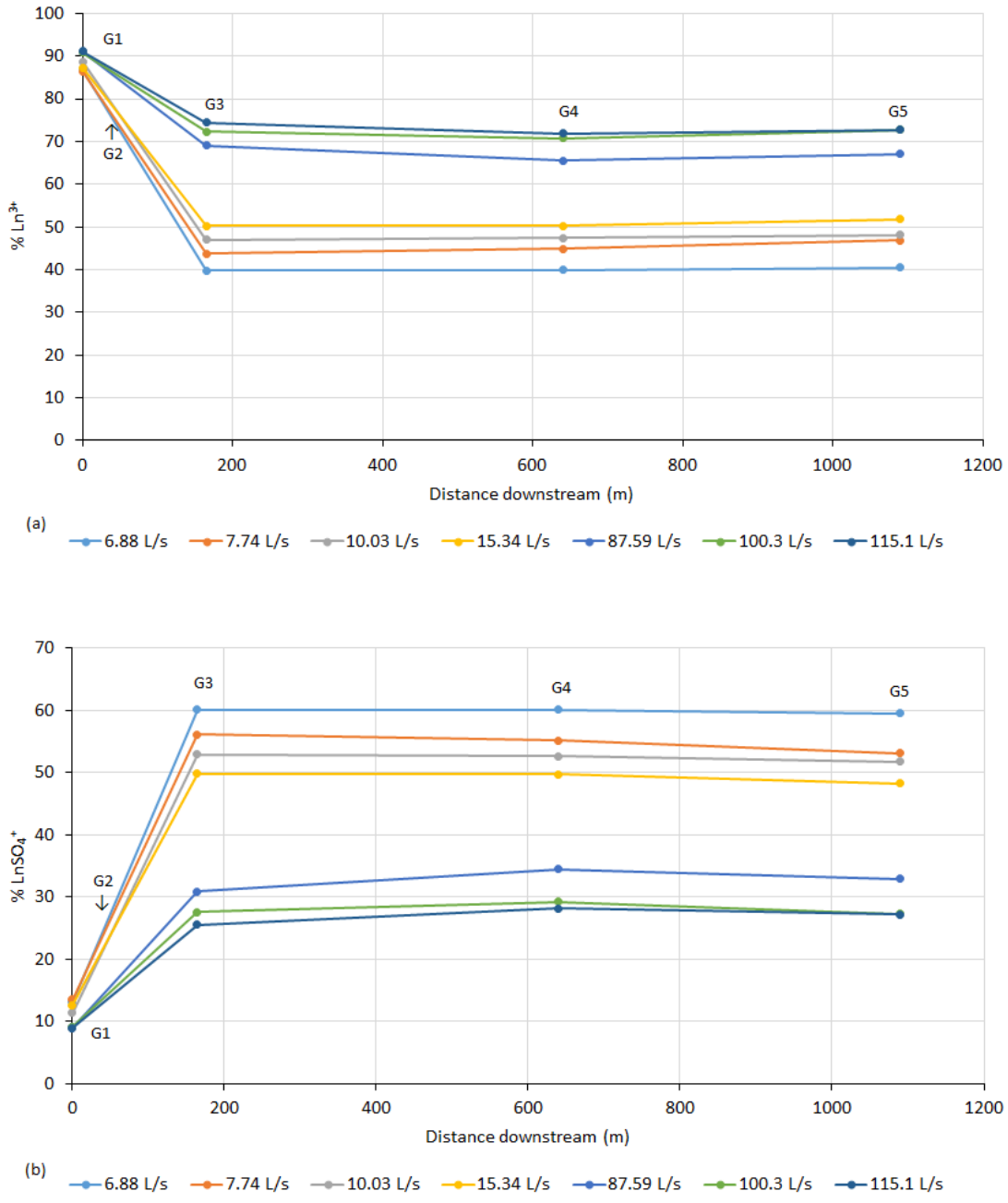

Figure 6.1: Spatial variation of the mean percentage of (a) Ln^{3+} and (b) $LnSO_4^+$ at Gate Gill (G1 is the reference point and the distance of each sampling site relative to G1 is plotted) under different flow conditions (using the flowrate of G5 as the representative) when ultrafiltration (0.005µm) was undertaken

As can be seen from Figure 6.1, under each flow condition, the mean percentage of Ln^{3+} (graph a) is the highest (within the range of 87%- 91%) and the mean percentage of $LnSO_4^+$ (graph b) is the lowest (within the range of 9%-13%) at the upstream of mine discharge (G1). The mean percentages of $LnSO_4^+$ (graph b) at three mine discharge downstream sampling sites- G3 (165m downstream of G1), G4 (640m downstream of G1) and G5 (1090m downstream of G1) are similar and all larger than that at G1 under each flow condition. The mean percentages of Ln^{3+} at G3, G4 and G5 (graph a) are consequently similar and all smaller relative to that at G1.

The input of mine discharge between G1 and G3 leads to the spatial variation of Ln^{3+} and $LnSO_4^+$ along Gate Gill sampling sites. Figure 6.2 shows the averaged value of the mean percentage of $LnSO_4^+$ from all flow conditions (when ultrafiltration was undertaken, flow ranging from 6.88 to 115.1 L/s for G5) at each Gate Gill sampling site (G1, G3, G4 and G5) and at G2. According to Figure 6.2, G2 has the highest value of the averaged mean percentage of $LnSO_4^+$ (69%), which induces the sharp increase in the mean percentage of $LnSO_4^+$ (and consequently a sharp decrease of the mean Ln^{3+} percentage) between G1 and G3.

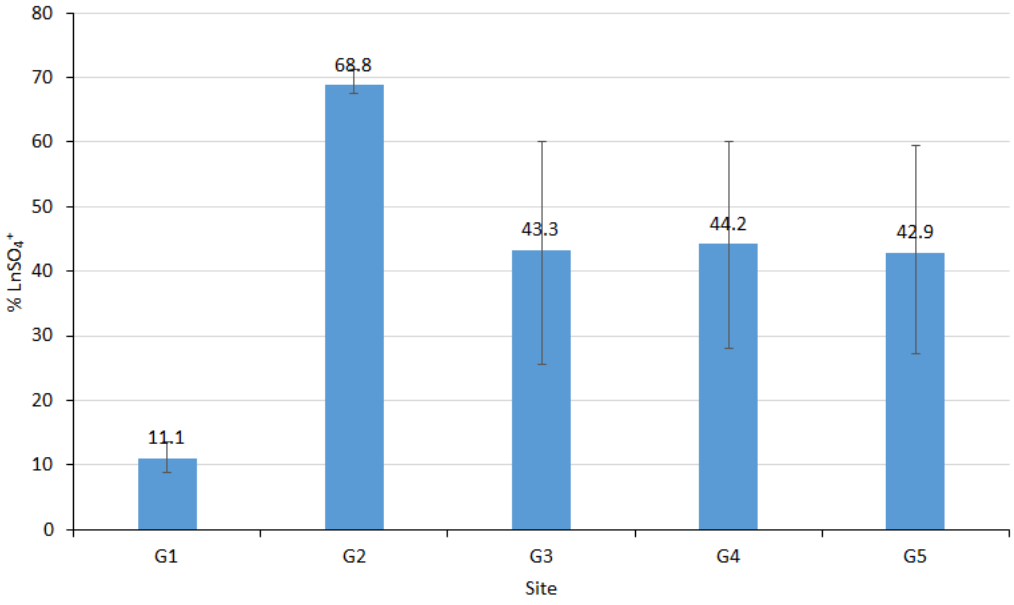

Figure 6.2: Averaged value of the mean percentage of $LnSO_4^+$ from all sampling occasions (when ultrafiltration was undertaken, flow ranging from 6.88 to 115.1 L/s for G5) at G1 to G5

The spatial variation of sulphate concentration (in ultra/0.005µm filtered phase) at Gate Gill sampling sites under each flow condition (the flow of G5 within the range of 6.88-115.1 L/s) shown in Figure 6.3 is similar as that of the mean $LnSO_4^+$ percentage (graph b) shown in Figure 6.1. The average concentration of sulphate from all flow conditions (when ultrafiltration was undertaken, flow ranging from 6.88 to 115.1 L/s for G5) at G1 to G5 is shown in Figure 6.4, and G2 also has the highest mean concentration of sulphate (188 mg/l). These results suggest that the mean percentage of $LnSO_4^+$ percentage (and consequently the mean percentage of Ln^{3+}) at each sampling site (G1 to G5) under each flow condition (when ultrafiltration was undertaken) is influenced by the concentration of sulphate in sampling water.

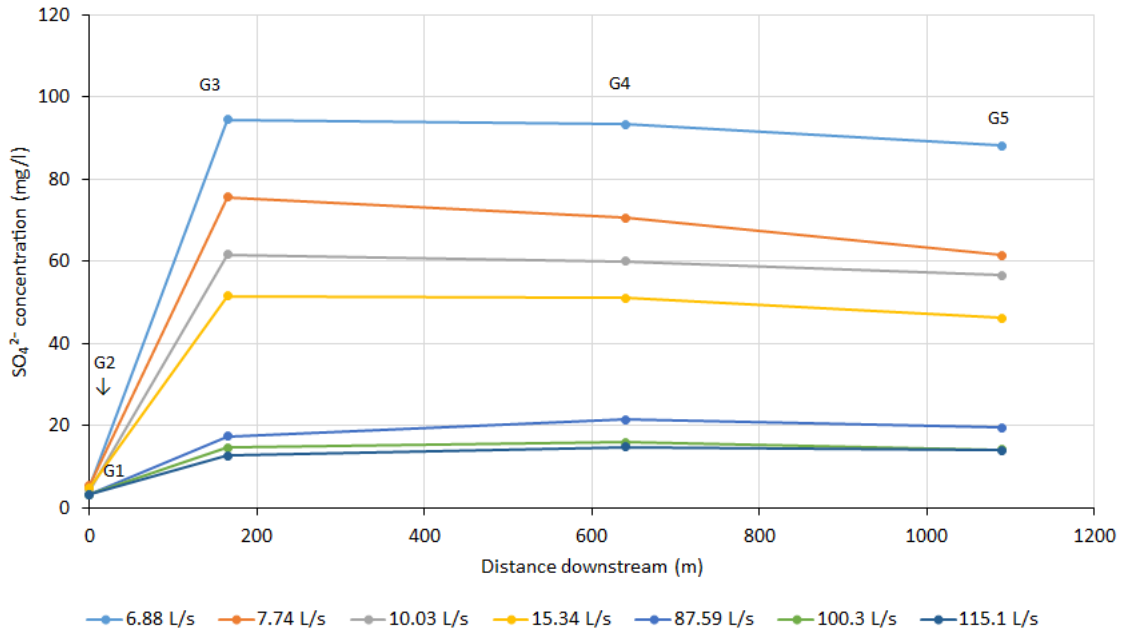

Figure 6.3: Spatial variation of sulphate concentration from G1 to G5 under difference flow conditions when ultrafiltration (0.005µm) was undertaken (the flowrate of G5 is used to show the flow condition)

The very low sulphate concentrations (3.21- 5.55 mg/l) and the acidic conditions at G1 under both lower (6.88~15.34L/s for G5) and higher flow (87.59~115.1 L/s for G5) conditions (shown in Figure 6.3) lead to the mean percentage of Ln^{3+} at G1 within the range of 87%-91% under these flow conditions (shown in graph a of Figure 6.1). Zhao *et al.* (2007) and Verplanck *et al.* (2004) both noted that Ln^{3+} is expected to be the most important species in the acidic natural waters unless the sulphate concentration in waters is at high level. The high sulphate concentrations (177- 212 mg/l) at G2 (shown in Figure 6.4) lead to $LnSO_4^+$ the

dominated species (67%- 70% for the mean percentage of $LnSO_4^+$) at G2 (Figure 6.2). The higher mean $LnSO_4^+$ percentages at G3, G4 and G5 compared to that at G1 under each flow condition, is due to the receiving of high sulphate concentration mine water at Gate Gill. Zhao *et al.* (2007) and Verplanck *et al.* (2004) also found that the percentage of REE sulphate complexes will largely increase when the watercourses are influenced by acidic mine discharges containing high concentration of sulphate. In addition, the similar sulphate concentrations at G3, G4 and G5 under each flow condition lead to the mean $LnSO_4^+$ percentages (and consequently the mean Ln^{3+} percentages) at G3, G4 and G5 are similar under each flow condition.

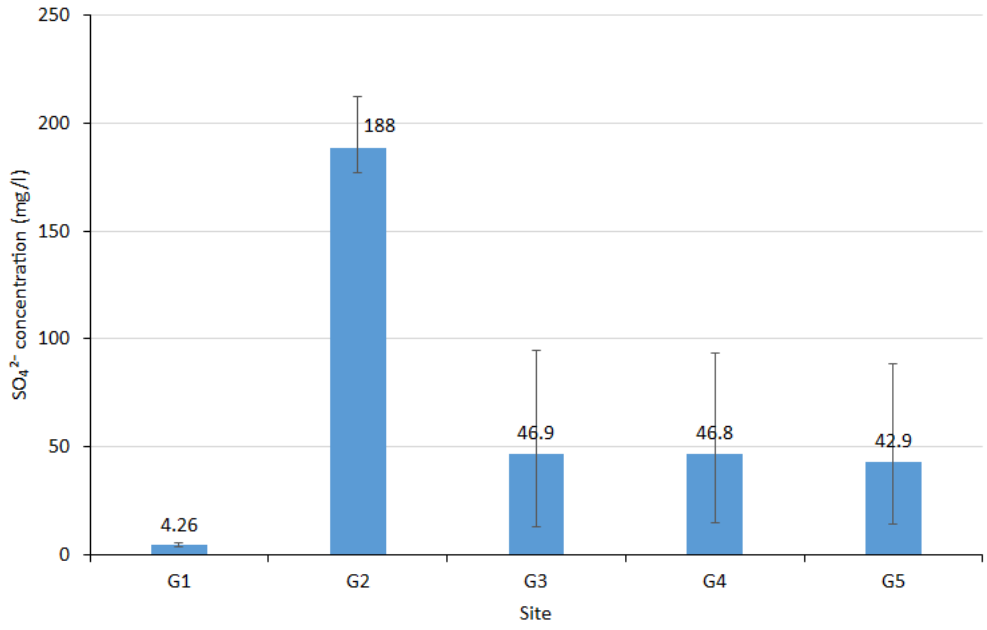

Figure 6.4: Average SO_4^{2-} concentration from all sampling occasions (when ultrafiltration was undertaken, flow ranging from 6.88 to 115.1 L/s for G5) at G1 to G5

In addition, Figure 6.1 also shows that with the flow conditions increasing (from 6.88 L/s to 115.1 L/s for G5), the mean percentage of Ln^{3+} (graph a) and $LnSO_4^+$ (graph b) at G3, G4 and G5 increases and decreases respectively. But the mean percentages of Ln^{3+} and $LnSO_4^+$ at G1 show little temporal variation. Figure 6.5 also plots the mean percentage of Ln^{3+} and $LnSO_4^+$ against the corresponding flowrate at G3, G4 and G5 (for sampling occasions when ultrafiltration was undertaken) to better show the temporal variation of REE species percentages at downstream sampling sites on Gate Gill. According to Figure 6.5, the importance of Ln^{3+} species (graph a) generally increases and the importance of $LnSO_4^+$

species (graph b) generally decreases as flow increasing at each sampling site (G3, G4 and G5).

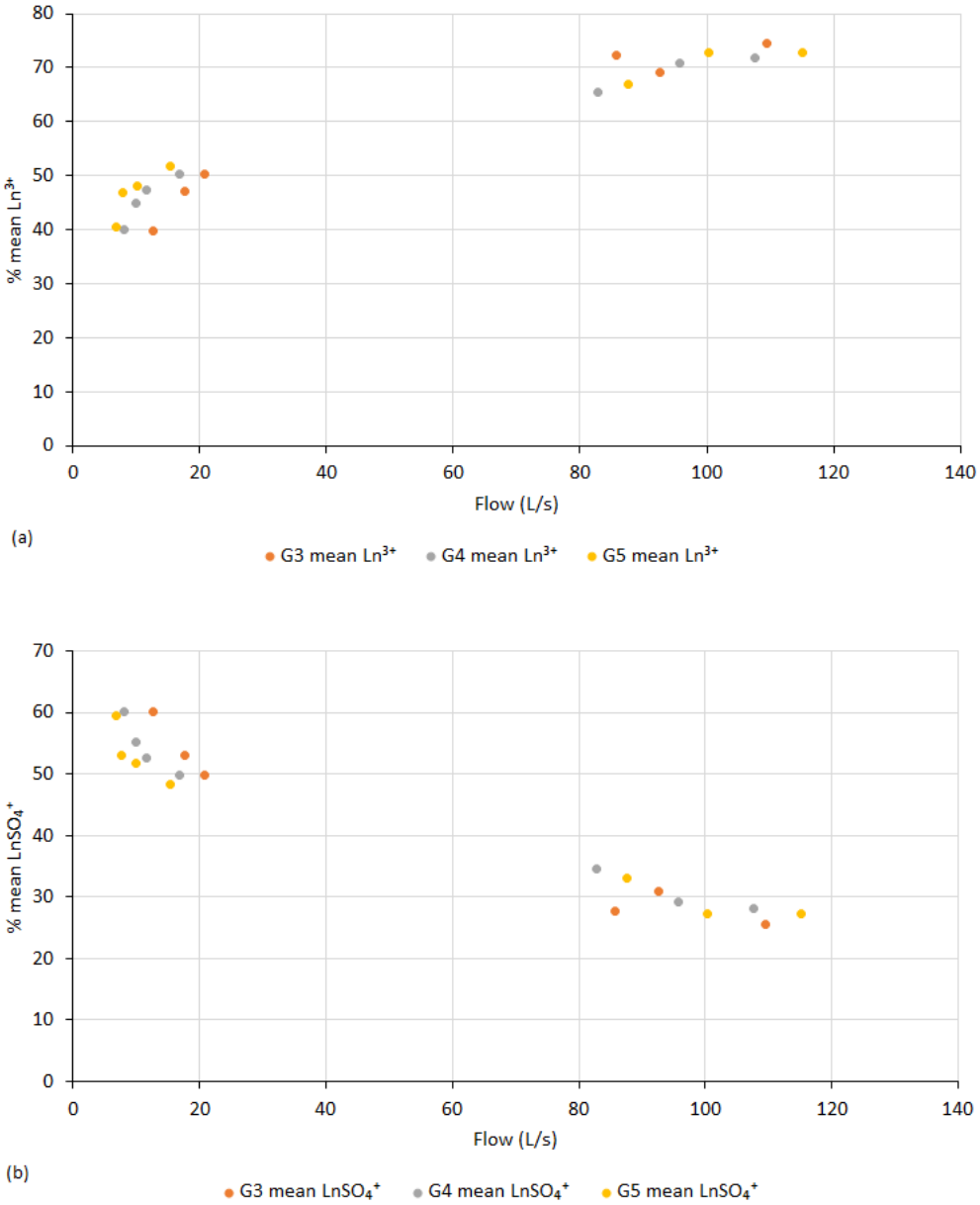

Figure 6.5: (a) The increase of the mean percentage Ln^{3+} and (b) the decrease of the mean percentage of $LnSO_4^+$ with increasing flowrate at G3, G4 and G5 (for sampling occasions when ultrafiltration was undertaken)

The temporal variation of the mean $LnSO_4^+$ percentage and consequently the mean Ln^{3+} percentage) at G3, G4 and G5 under different flow conditions (6.88- 115.1 L/s for G5) may be induced by the temporal variation of sulphate concentration. Since similar as the mean $LnSO_4^+$ percentage, Figure 6.3 shows that the sulphate concentrations (in ultra/ 0.005µm

filtered phase) at G3, G4 and G5 decrease with the increase of flow condition (from 6.88- 115.1 L/s for G5), and the sulphate concentrations at G1 demonstrate very small change.

The temporal variation of sulphate concentrations (in ultra/ 0.005µm filtered phase) at G3, G4 and G5 against their corresponding flow rate is also shown in Figure 6.6. Sulphate concentration generally decreases with the increase of flowrate at each sampling site (G3, G4 and G5), which is the result of dilution. As noted in the above paragraph of this section, the mean $LnSO_4^+$ percentages and sulphate concentrations have the similar spatial variation from G1 to G5 under each flow condition (flow of G5 within the range of 6.88- 115.1 L/s).

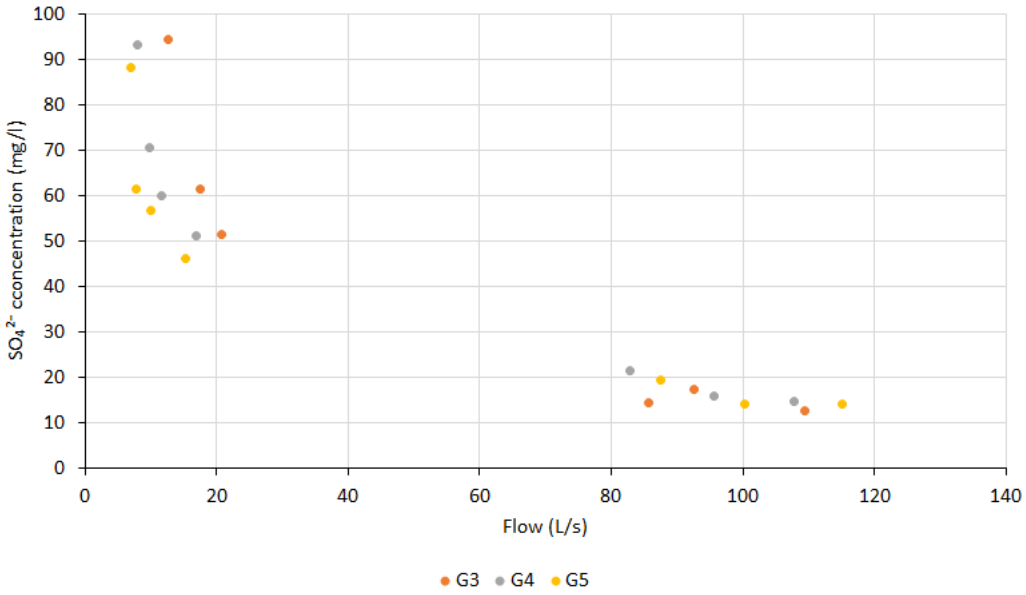

Figure 6.6: SO_4^{2-} concentration under different flow conditions (based on data from sampling occasions when ultrafiltration was undertaken)

To better show the influence of sulphate concentration on the formation of $LnSO_4^+$, the mean $LnSO_4^+$ percentages against sulphate concentrations (in ultra/ 0.005µm filtered phase) at G1 to G5 under different flow conditions (ranging from 6.88- 115.1 L/s for G5) are plotted in Figure 6.7. It is clear that the mean $LnSO_4^+$ percentages at G1 to G5 all increase with the increase of sulphate concentration in waters. Johannesson and Lyons (1995) also note that there is a positive correlation between sulphate concentration and the percentage of REE sulphate complexes. In addition, Figure 6.7 shows that $LnSO_4^+$ becomes a more important species relative to Ln^{3+} when the concentration of SO_4^{2-} in water >50 mg/l.

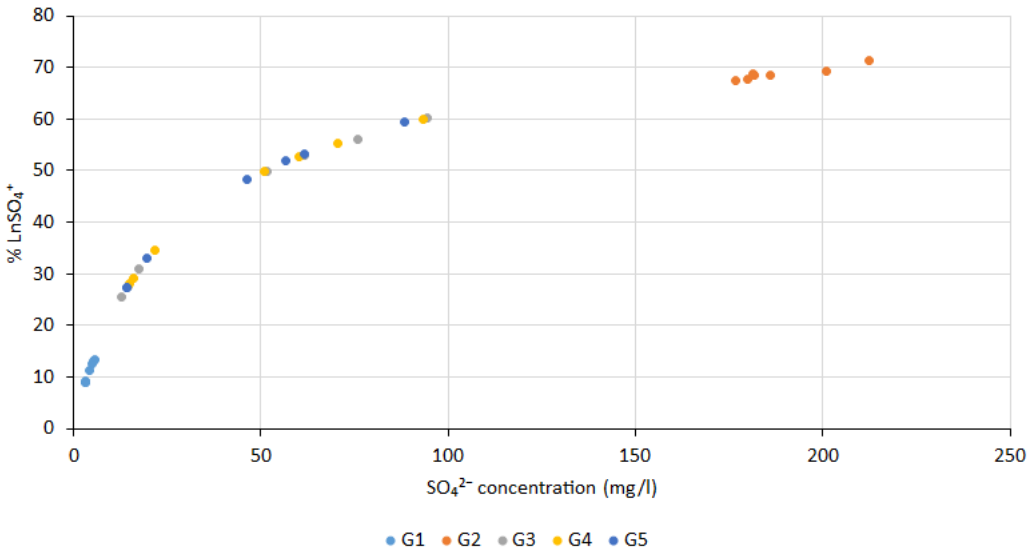

Figure 6.7: The relationship between the mean percentage of $LnSO_4^+$ and SO_4^{2-} concentration (based on data from sampling occasions when ultrafiltration was undertaken)

The speciation results of each individual REE at G1 to G5 which based on the metals concentration in the 0.1µm filtered phase on sampling occasions when ultrafiltration (0.005µm) was not undertaken are shown in Appendix D. These results should not differ much from that obtained based on the truly dissolved (ultra-filtered) metals concentrations if ultra-filtered metals data are available. This is because for the sampling occasions when ultrafiltration (0.005µm) was undertaken, the speciation results obtained from using ultra-filtered data are similar to that from using 0.1µm filtered data. And the speciation results obtained based on 0.1µm filtered data for the sampling occasions when ultrafiltration was undertaken are shown in Appendix D.

The key findings from the speciation results based on 0.1µm filtered data on sampling occasions when ultrafiltration (0.005µm) was not undertaken are generally the same as that (based on 0.005µm/ ultra-filtered data) from sampling occasions when ultrafiltration was undertaken, which are summarised below:

(1) Ln^{3+} and $LnSO_4^+$ are also the dominant species at the G1 to G5 (Appendix D).

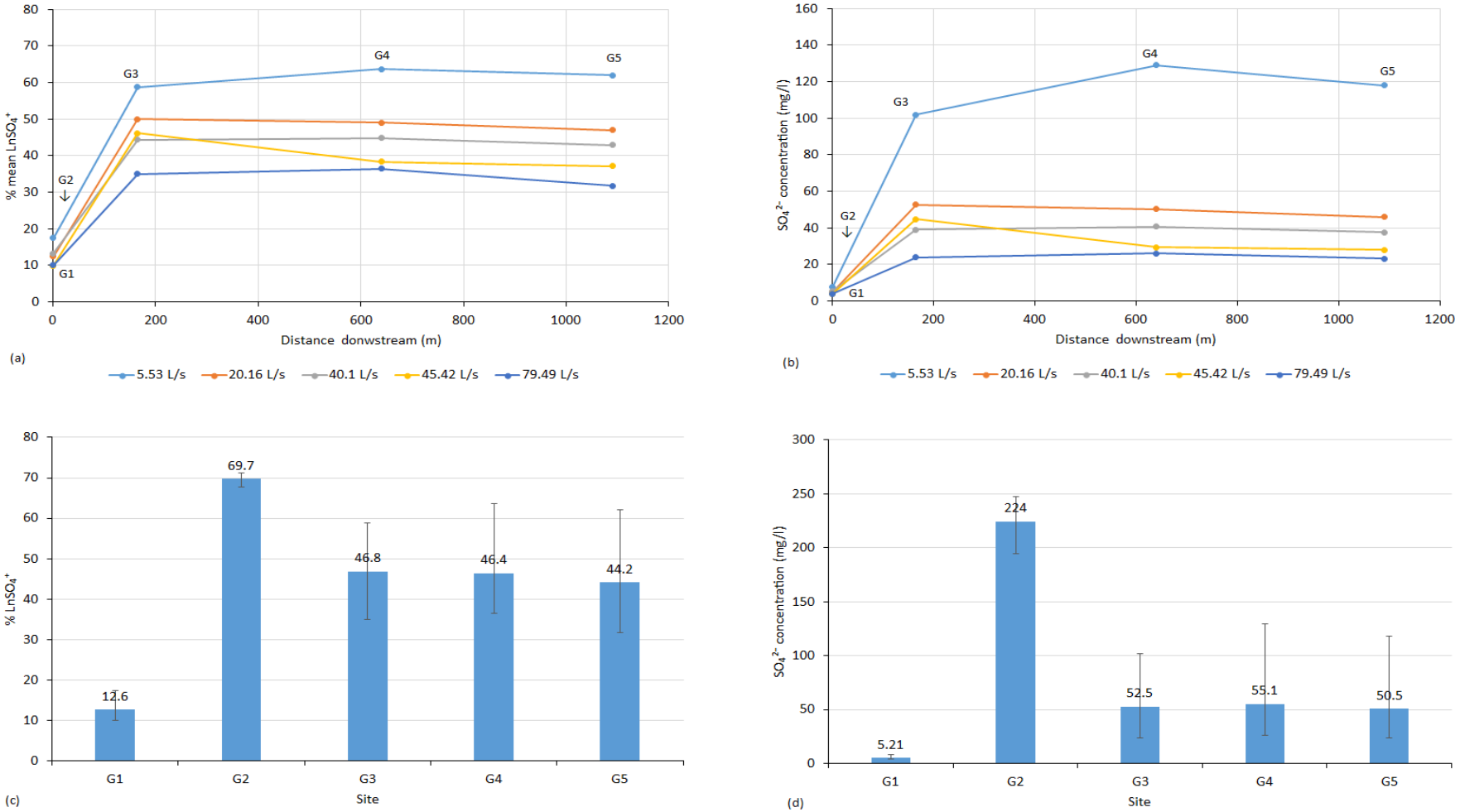

Figure 6.8: Spatial variation of (a) the mean percentage of $LnSO_4^+$ and (b) the concentration of SO_4^{2-} at Gate Gill Sampling site on different flow conditions when ultrafiltration (0.005µm) was not undertaken (flowrate of G5 is used to show the flow condition); the averaged value of (c) the mean percentage of $LnSO_4^+$ and (d) SO_4^{2-} concentration from all flow conditions when ultrafiltration (0.005µm) was not undertaken at G1 to G5

(2) The spatial variation of the mean percentage of $LnSO_4^+$ and SO_4^{2-} concentration from G1 to G5 under each flow condition are similar, as can be seen from Figure 6.8. Ln^{3+} is the most important species at Gate Gill (G1) before the mine water is discharged to Gill. The importance of $LnSO_4^+$ largely increases (relative to G1) at the downstream of Gate Gill (G3, G4 and G5) which is polluted by the mine water containing high SO_4^{2-} concentration.

(3) The temporal variation of the mean percentage of $LnSO_4^+$ and SO_4^{2-} concentration at each sampling site (G1 to G5) under different flow conditions (when ultrafiltration was not undertaken) is also similar. The decrease of SO_4^{2-} concentration with the increase of flowrate at G3, G4 and G5 leads to the subsequent decrease of the mean percentage of $LnSO_4^+$ as flow condition increasing (Figure 6.8).

(4) The importance of $LnSO_4^+$ increases with increasing of sulphate concentration in water. When the sulphate concentration in water increases to >50, $LnSO_4^+$ is a more important species relative to Ln^{3+}, according to Figure 6.9.

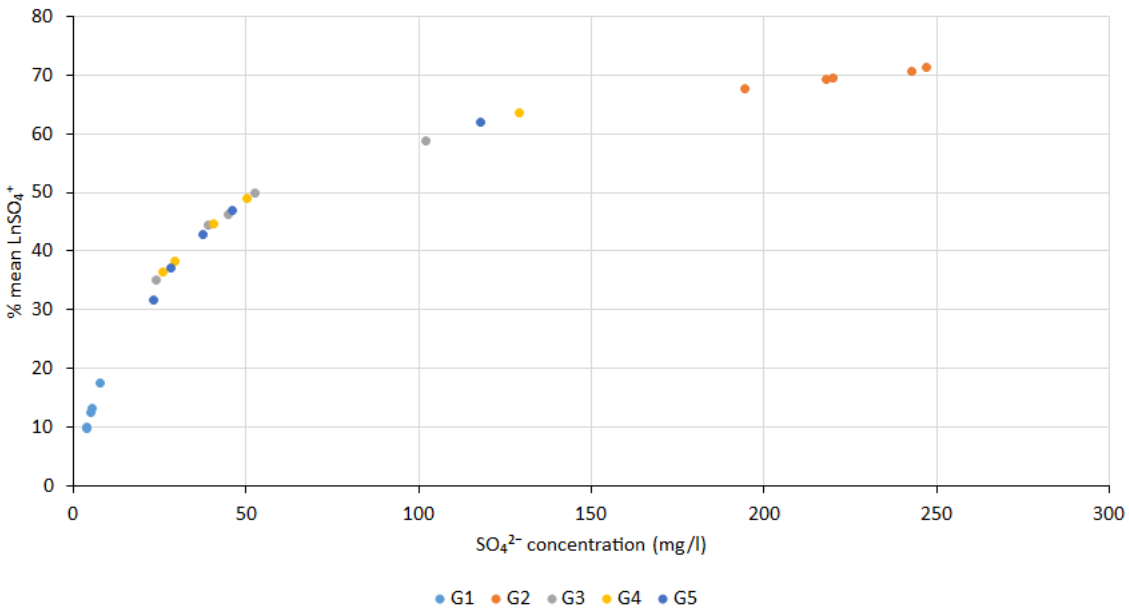

Figure 6.9: The relationship between the mean percentage of $LnSO_4^+$ and the concentration of SO_4^{2-} (based on data from sampling occasions when ultrafiltration was not undertaken)

6.2.2 River Glenderamackin

Figure 6.10 and Figure 6.11 show the speciation results for each individual REE at G7 on occasions when ultrafiltration (0.005µm) was undertaken. These speciation results are displayed in increasing flowrate (of G7) order from the first graph in Figure 6.10 to the last

graph in Figure 6.11. According to Figure 6.10 and Figure 6.11, free REE ions (Ln^{3+}) and REE carbonate complexes ($LnCO_3^+$) are the most important species at G7 under both lower (6.88~15.34L/s for G5; 253~734L/s for G7) and higher flow (87.59~115.1 L/s for G5; 4480~10200L/s for G7) conditions.

The pH, inorganic ligands concentration and alkalinity are the dominant controls on REE speciation in water (Sun et al. 2011; Tang and Johannesson, 2010b; Wood, 1990). As described in Section 2.4.4, REE carbonate complexes formation is supressed under acidic conditions (Gosselin et al. 1992). Therefore, no $LnCO_3^+$ are present at G1 to G5 due to the lower pH (within the range of 3.11~ 5.37 on all sampling occasions, see Section 6.2.1 and Appendix D). At G7, on the other hand, the pH was ≥ 5.6 under all flow conditions/ all sampling occasions (shown in this section and Appendix E), allowing the formation of REE carbonate complexes.

Table 6.1 shows the sulphate concentration in the truly dissolved phase at sites G1 to G7 under lower (6.88~15.34L/s for G5; 253~734L/s for G7) and higher flow (87.59~115.1 L/s for G5; 4480~10200L/s for G7) conditions on occasions when ultrafiltration (0.005µm) was undertaken. The much lower concentration of sulphate at G7 shown in Table 6.1 compared with that at G3, G4 and G5 leads to a much smaller proportion of $LnSO_4^+$ at G7 (Figure 6.10 and Figure 6.11) compared with G3, G4 and G5 (shown in Appendix D and can also be seen based on the mean $LnSO_4^+$ percentage in Figure 6.1 and Figure 6.3). In addition, the proportion of REE sulphate complexes at G7 is also smaller than that at G1 (shown in Appendix D).

Table 6.1: Sulphate concentration in truly dissolved phase at Gategill sampling sites when ultrafiltration (0.005µm) was undertaken

Site	SO_4^{2-} concentration (mg/l) in ultra-filtered water samples						
	Lower flow conditions*				Higher flow conditions*		
	253L/s	495L/s	596L/s	734L/s	4480L/s	4980L/s	10200L/s
G1	5.16	5.55	4.39	4.9	3.34	3.21	3.27
G2	181.6	200.9	186.1	180	176.8	181.3	212.2
G3	94.55	75.75	61.61	51.6	14.60	12.71	17.4
G4	93.38	70.66	60.11	51.1	16.03	14.88	21.57
G5	88.21	61.55	56.71	46.3	14.14	14.07	19.59
G7	5.95	4.25	4.06	6.6	2.35	1.69	1.44

Note: * The flowrate of G7 is shown to here to demonstrate the flow range of lower and higher flow conditions

Figure 6.10 and Figure 6.11 show that the proportion of REE-carbonate complexes increases and the proportion of free REE ions decreases with increasing atomic number across the REE group when pH is within the range of 5.6 to 6.88. Tang and Johannesson (2006) also found that the proportion of Ln^{3+} decreased whilst the proportion of $LnCO_3^+$ increased with increasing REE atomic number when pH was below 7 (no large amount of REE di-carbonate complexes formed). Sun et al. (2011) also noted that the $LnCO_3^+$ species is more important for HREE when compared to MREE and LREE. This is because carbonate prefers to complex with the higher atomic number REE first, then with the lower atomic number REE (Sun et al., 2011).

For the first graph in Figure 6.10 with a near neutral pH value of 6.88 at G7 on sampling occasion, $LnCO_3^+$ is much important than Ln^{3+} in dissolved phase. Tang and Johannesson (2006); Johannesson and Zhou (1997) both noted that $LnCO_3^+$ was the dominant dissolved REE specie in neutral pH waters. When pH is 6.88, the proportion of $LnCO_3^+$ largely exceeds the proportion of Ln^{3+} of that specific element for all REE except La which is the lightest REE. To be more specific, the proportion of $LaCO_3^+$ and La^{3+} is 35% and 51% respectively. The proportion of $CeCO_3^+$ to $LuCO_3^+$ ranges from 53% to 80%, and the proportion of Ce^{3+} to Lu^{3+} is within the range of 10%- 36%. Negligible LREE and MREE form $Ln(CO_3)_2^-$, and around 5% HREE form $Ln(CO_3)_2^-$ when pH at G7 is 6.88.

For the rest of graphs shown in Figure 6.10 and Figure 6.11 with pH $\leq$ 6.31, free REE ions are more important relative to REE carbonate complexes, and no $Ln(CO_3)_2^-$ forms. But under a lower near neutral pH condition with the value of 6.31 (the first graph in Figure 6.11), the proportion of $LnCO_3^+$ is smaller than the proportion of Ln^{3+} of that specific element for all the REEs except the two heaviest REE- Yb (48% for $YbCO_3^+$ and 42% for Yb^{3+}) and Lu (46% for $LuCO_3^+$ and 44% for Lu^{3+}). When pH decreases to $\leq$ 5.92 (the rest of graphs in Figure 6.10 and Figure 6.11 besides the first graph in both Figure 6.10 and Figure 6.11), the proportion of Ln^{3+} exceeds the proportion of $LnCO_3^+$ of that specific element for all REE. These results are contrary to the findings from Wood (1990), showing that carbonate species are the most important inorganic species for waters with pH>6. However, the study from Tang and Johannesson (2006) showed that carbonate complexes (REE-CO_3^+) become the dominate species when pH is between 6.5 and 7.5.

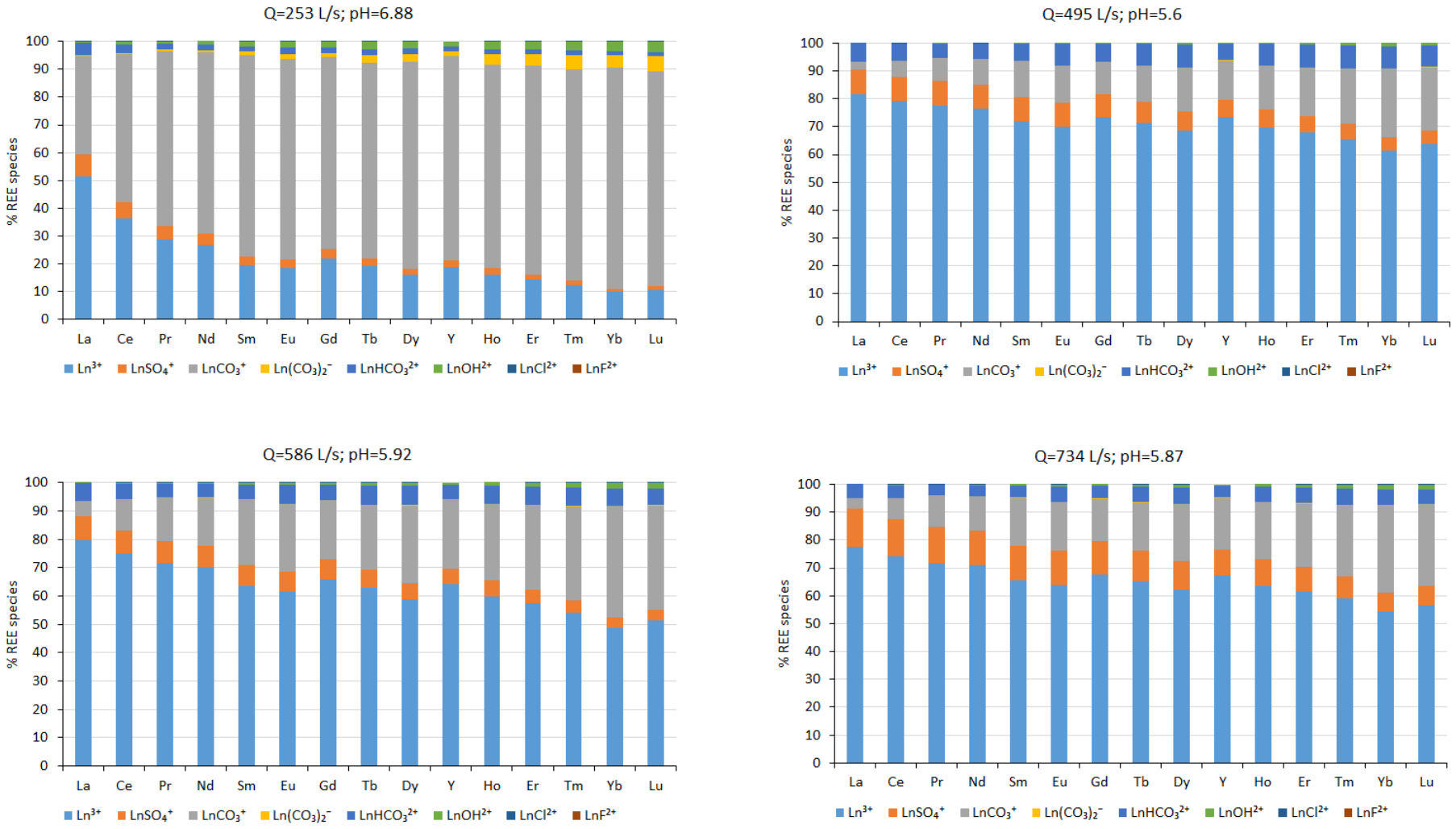

Figure 6.10: REE speciation modelling results at River Glenderamackin (G7) under lower flow condition when ultrafiltration (0.005µm) was undertaken (the speciation modelling was based on 0.005µm filtered cations concentrations)

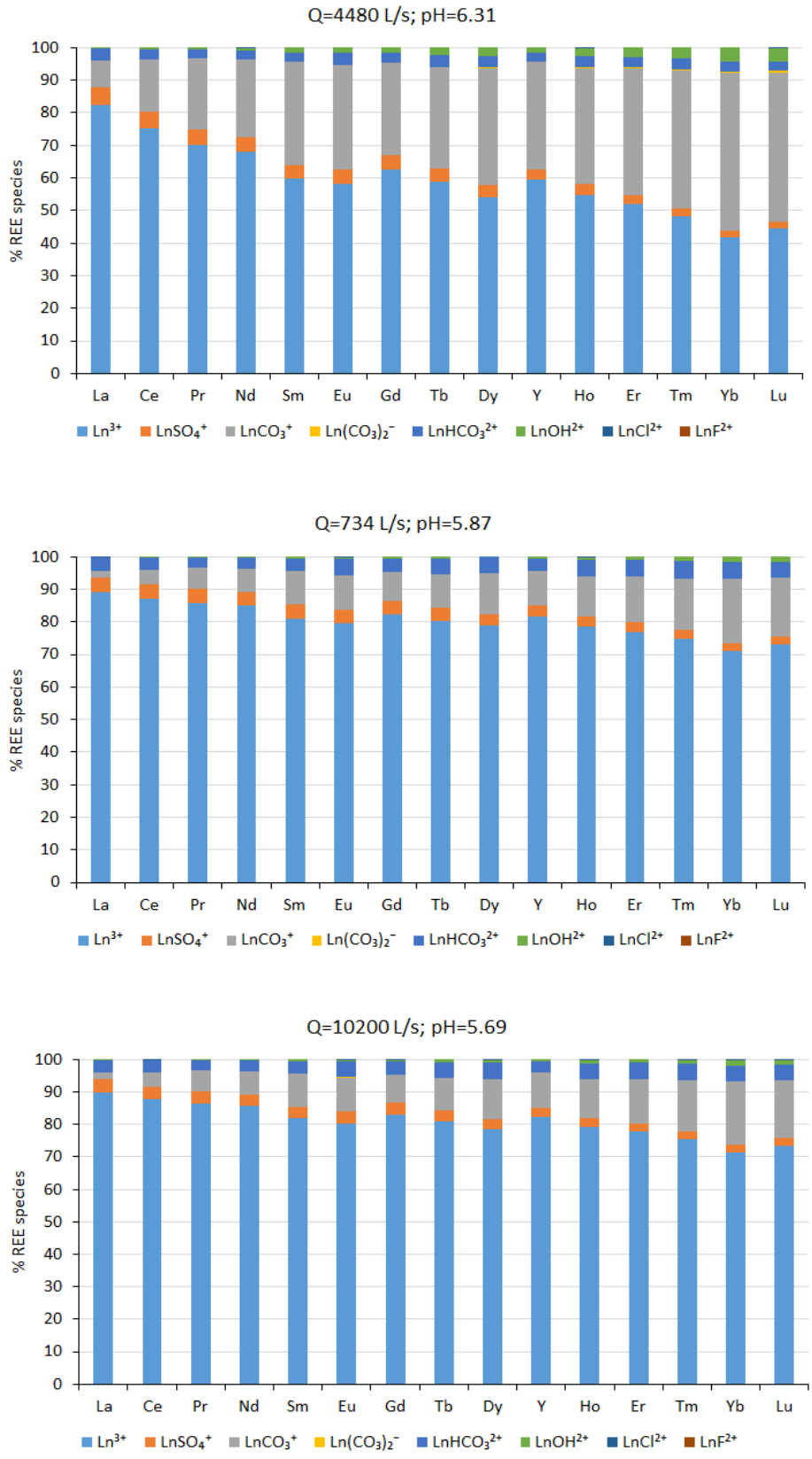

Figure 6.11: REE speciation modelling results at G7 under higher flow condition when ultrafiltration (0.005µm) was undertaken (the speciation modelling was based on 0.005µm filtered cations concentrations)

Based on the results from Figure 6.10 and Figure 6.11, pH (and consequently alkalinity) seems to control the importance of REE carbonate complexes species (and consequently free REE ions species). To show the influence of pH on the importance of $LnCO_3^+$ species (and consequently Ln^{3+} species), the mean $LnCO_3^+$ and Ln^{3+} values against pH value on different sampling occasions (when ultra-filtration was undertaken) are plotted in Figure 6.12. According to Figure 6.12, the mean $LnCO_3^+$ and Ln^{3+} percentage at G7 generally increases and decreases respectively when pH increases from 5.6 to 6.88, suggesting that the importance of REE-carbonate complexes species increases with increasing pH. This results are similar to those found in other studies (Leybourne et al., 2000; Johannesson et al., 1996; Johannesson and Lyons, 1994) for near neutral to neutral groundwater. Tang and Johannesson (2006) noted a positive correlation between pH and proportion of $LnCO_3^+$ and a negative correlation between pH and Ln^{3+} when pH was below neutral. In addition, Figure 6.12 also shows that the percentage of the mean $LnCO_3^+$ increases 21% when pH increases from 5.68 to 6.31, but the increased value of mean $LnCO_3^+$ percentage is 37% when pH increases from 6.31 to 6.88. This suggests that the increased degree of importance of $LnCO_3^+$ species increases with pH increasing from 5.6 to 6.88.

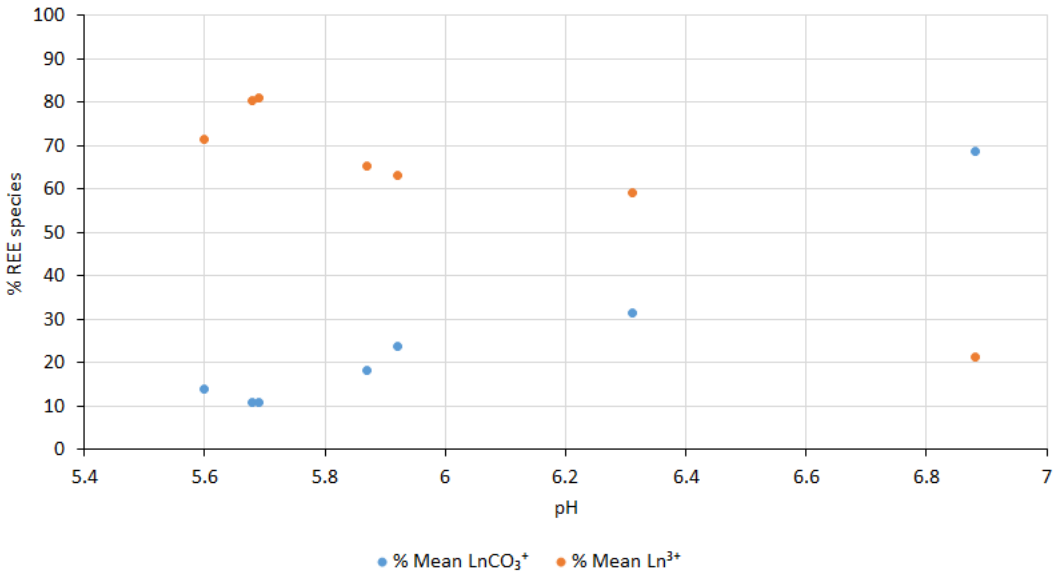

Figure 6.12: Increase of mean $LnCO_3^+$ percentage and decrease of mean Ln^{3+} percentage with pH increasing from 5.6 to 6.88 (based on data from sampling occasions when ultra-filtration was undertaken and the speciation modelling was based on 0.005µm filtered cations concentrations)

Tang and Johannesson (2006) noted that the distribution of $LnCO_3^+$ complexes is controlled by pH and alkalinity of water. To show the pH influence on the variation of $LnCO_3^+$

formation for individual REE, Figure 6.13 displays the percentage of $LnCO_3^+$ for each individual REE (based on <0.005µm data) under different pH values (ranging from 5.6 to 6.88). According to Figure 6.13, although the percentage of $LnCO_3^+$ for each individual REE generally increases with increasing pH, the $LnCO_3^+$ percentage of heavier REE displays a much larger increase than that of lighter REE. This result suggest that the increase in proportion of $LnCO_3^+$ complexes generally increased with the increase in REE atomic number when pH increases from 5.6 to 6.88.

As described in above paragraph, $Ln(CO_3)_2^-$ is a negligible species at G7 on the sampling occasions with pH ≤ 6.88 (based on ultra/ 0.005µm filtered data). This is because the formation of $Ln(CO_3)_2^-$ is through the complexation of carbonate ions and $LnCO_3^+$. The $Ln(CO_3)_2^-$ species starts to become noticeable when pH (and consequently alkalinity/ carbonate concentration) increases to around neutral condition when $LnCO_3^+$ is an important species. But again, carbonate prefers to complex with HREE-CO_3^+ first, then with MREE-CO_3^+ and finally with LREE-CO_3^+ (Sun et al. 2011). Therefore, besides G7 on sampling occasion with an around neutral pH value of 6.88 has ~5% of HREE-$(CO_3)_2^-$, no $Ln(CO_3)_2^-$ presents in truly dissolved phase at G7 on the rest of sampling occasions with pH ≤ 6.31.

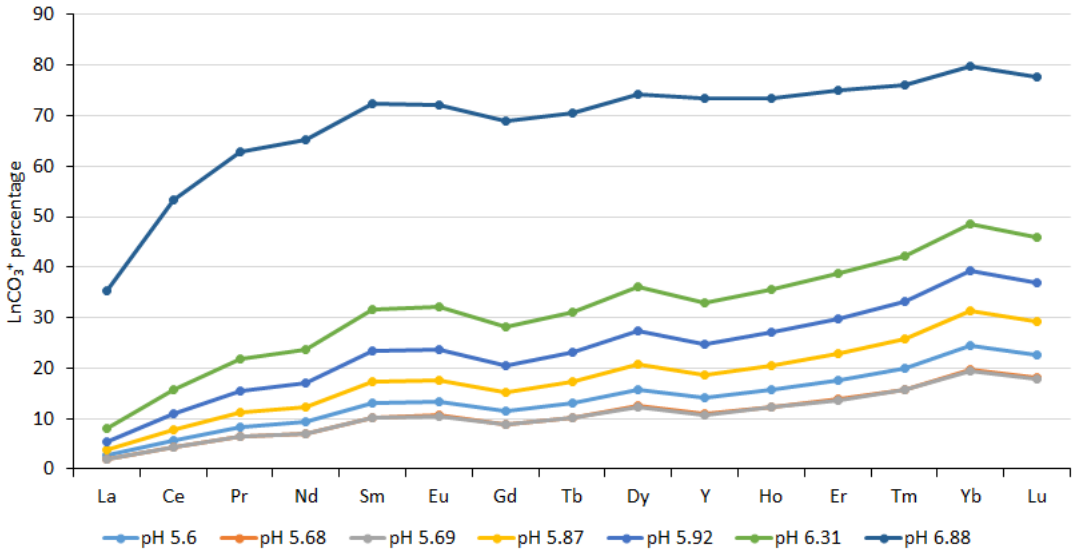

Figure 6.13: The distribution pattern of the $LnCO_3^+$ percentage under different pH conditions ranging from 5.6 to 6.88 at G7 (based on data from sampling occasions when ultrafiltration was undertaken and the speciation modelling was based on 0.005µm filtered data)

The speciation modelling results at G7 from the sampling occasions when ultrafiltration (0.005µm) was not undertaken are mainly displayed in Appendix E, but briefly shown and discussed in this section. Since no truly dissolved REE data are available on these sampling occasions and the REE speciation results based on the 0.1µm filtered samples may not be as-accurate as the speciation results obtained from the sampling occasions when ultrafiltration was undertaken. Similar to the speciation results obtained from sampling occasions when ultrafiltration was undertaken, free REE ions and REE-carbonate complexes are also the dominant species at G7 on sampling occasions when ultrafiltration was not undertaken (based on the 0.1µm filtered data), which are shown in Appendix E.

It should be noted that the speciation results (for the sampling occasions when ultrafiltration was not undertaken) obtained based on 0.1µm filtered REE concentrations are not expected to be largely differed from the results if ultra-filtered REE concentrations are used for the speciation modelling. This is because, no distinctive difference between the speciation results obtained from using the ultra-filtered (0.005µm) REE concentrations and from using 0.1µm filtered REE concentrations for the sampling occasions when ultrafiltration (0.005µm) was undertaken. The speciation results obtained based on 0.1µm filtered REE concentrations for the sampling occasions when ultrafiltration (0.005µm) was undertaken are shown in Appendix E. The influence of pH (alkalinity) on the mean percentage of two main REE species (Ln^{3+} and $LnCO_3^+$) and on the percentage of $LnCO_3^+$ for each individual REE for the sampling occasions when ultrafiltration (0.005µm) was not undertaken is respectively shown in Figure 6.14 and Figure 6.15.

Similar as the conclusions obtained from the sampling occasions when ultrafiltration (0.005µm) was undertaken, the speciation modelling results obtained based on REE concentrations of 0.1µm filtered water samples from the sampling occasions when ultrafiltration was not undertaken show:

(1) According to Figure 6.14:

- the importance of $LnCO_3^+$ and Ln^{3+} generally increases and decreases respectively with the increase of pH from 5.74 to 6.47;
- overall speaking, $LnCO_3^+$ species is a less important species compared to Ln^{3+} when pH is ≤6.3, but $LnCO_3^+$ becomes a slightly more important species when pH is at 6.47;
- the increased degree of $LnCO_3^+$ percentage increases with pH increasing (mean $LnCO_3^+$

percentage increases a value of 14% when pH increases from 5.74 to 6.15, but the increased value of mean $LnCO_3^+$ percentage is 23% for pH increasing from 6.15 to 6.47).

(2) As shown in Figure 6.15:

- the increase of pH (from 5.74 to 6.47) induces a greater increase of the importance of $LnCO_3^+$ species for heavier REE relative to lighter REE;
- $LnCO_3^+$ is a less important species relative to Ln^{3+} for each individual REE when pH is ≤6.3, except for two heaviest REE- Yb and Lu (49% for $YbCO_3^+$ and 38% for Yb^{3+}; 47% for $LuCO_3^+$ and 40% for Lu^{3+}) at pH of 6.3 (details see Appendix E);
- $LnCO_3^+$ is a more important species compared to Ln^{3+} for only for HREE at pH of 6.47 (details see Appendix E).

(3) Appendix E shows that no $Ln(CO_3)_2^-$ species presents even for HREE at G7 on sampling occasions with pH ranging from 5.74 to 6.47, since the pH values were all below neutral conditions.

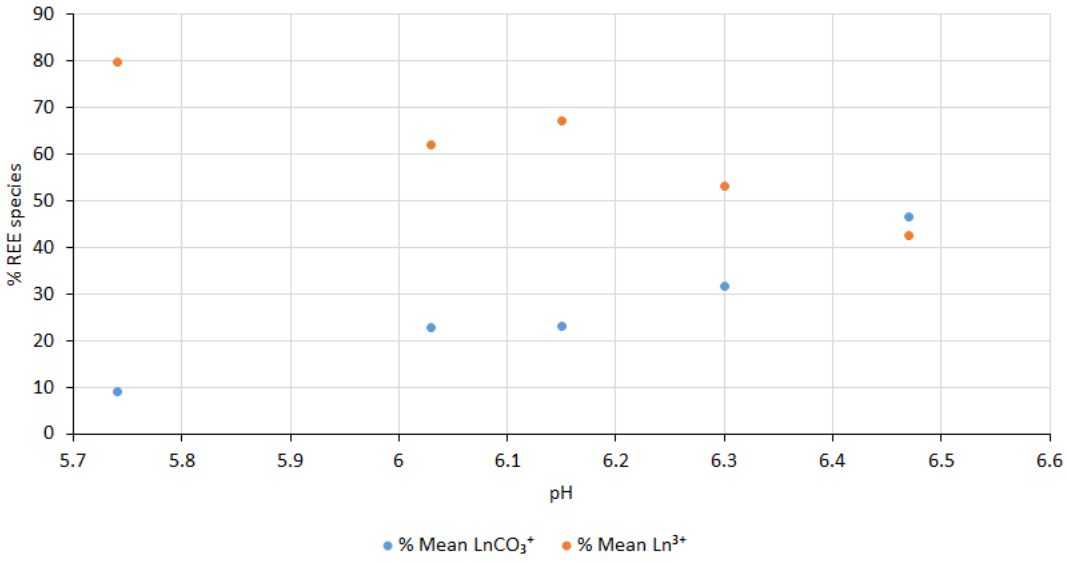

Figure 6.14: Increase of mean $LnCO_3^+$ percentage and decrease of mean Ln^{3+} percentage with pH increasing from 5.74 to 6.47 (based on data from sampling occasions when ultra-filtration was not undertaken and the speciation modelling was based on 0.1µm filtered cations concentrations)

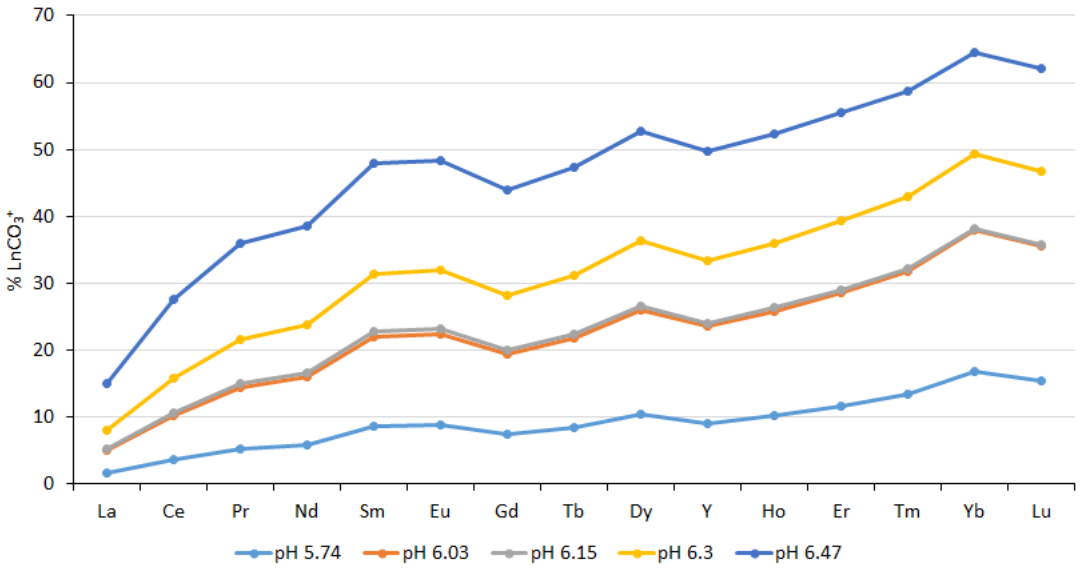

Figure 6.15: The distribution pattern of the $LnCO_3^+$ percentage under different pH conditions ranging from 5.74 to 6.47 at G7 (based on data from sampling occasions when ultra-filtration was not undertaken and the speciation modelling was based on 0.1µm filtered cations concentrations)

6.2.3 Other ligands complexes

The REE fluoride complexes are negligible at all sampling sites under all flow conditions, due to the generally very low concentration of fluoride. REE fluoride complexes are only important when the fluoride concentration in water is extremely high due to natural or anthropogenic factors (Wood, 1990). Although REE phosphate complexes play an important role in REE attenuation (as described in Section 2.4.4), the phosphate concentration in samples is not detectible and negligible REE phosphate complexes are present at sampling sites.

The REE chloride complexes and REE nitrate complexes are also negligible at all sampling sites. Wood (1990, 1979) noted that REE chloride complexes are not expected to be an important species in most surface and ground waters. REE chloride complexes may only become important in brines with extremely high concentrations of chloride and a relatively low pH (Gosselin et al. 1992; Wood, 1990). REE nitrate complexes are negligible in most natural waters even water that is artificially polluted and contains high concentrations of nitrate (Wood, 1990).

6.3 REE fractionation pattern relative to PAAS at Gate Gill

As discussed in Section 5.4, the transformation of REE between dissolved and (suspended) solid phase is strongly associated with Fe and Al oxyhydroxides. In-stream processes mainly influence REE fractionation through competition between solution complexation of REE with ligands and surface complexation of REE (REE complexes as well sometimes) with Fe and Al oxyhydroxides. Unlike the source-rock related fractionation, in-stream fractionation of REE may only occur during the chemical transformation of REE from dissolved (<0.005µm) phase to either fresh precipitates (>0.005µm) in the stream or to solid phases in the sediment. If no chemical transformation of REE occurs, the PAAS normalized REE distribution pattern in waters will entirely inherit the REE fractionation pattern of the source rock leachates, which means that source-related fractionation controls the PAAS-normalized REE distribution pattern in stream waters. As mentioned in Section 3.8, the source-related fractionation in this study refers to REE patterns of source rocks leachates.

As noted in Section 2.4.2 and Section 2.4.3, it is critical to use the truly dissolved phase REE concentrations when discussing the source- and process-related fractionation in streams (Verplanck et al. 2013; 2004). This is because the solution chemistry-related fractionation may lead to a REE distribution pattern in the fine colloids that differs from that in the truly dissolved phase (Nelson et al., 2003).

0.1µm filtered water contains both truly dissolved REE (that filtered through 10kDa (0.005µm) filter) and fine colloidal REE (0.005µm- 0.1µm). It is not ideal to use the normalized distribution pattern of 0.1µm filtered water as the dissolved REE distribution pattern. Neither is it appropriate to regard the suspended solid REE distribution pattern as the difference between the unfiltered and 0.1µm filtered fractions. Therefore discussion of the PAAS-normalized REE distribution pattern in this section focuses on those sampling dates when ultrafiltered (0.005µm) concentration data are available.

In this study, light rare earth elements (LREE) refer to elements from La to Nd, middle rare elements (MREE) refer to elements from Sm to Dy, and heavy rare earth elements (HREE) refer to elements from Ho to Lu plus Y. Y is classified as a HREE due to its similar chemical characteristics to the HREE. The very similar ionic radius of trivalent Y and trivalent Ho makes Y and Ho geochemical twins (Bau, 1999). Y is therefore placed between Dy and Ho in the PAAS normalized distribution pattern in this study.

6.3.1 PAAS-normalized REE distribution pattern

As discussed in Section 5.2 and 5.3, under lower flow conditions (6.88-15.34L/s for G5), little REE (proportion of total REE present in suspended solid is <5%) are transformed from dissolved (<0.005µm) to suspended solid phase (>0.005µm), and consequently no REE should be removed from water column at G3 to G5. Also, no sediments are resuspended into the water column at G3 to G5 under these lower flow conditions.

Under higher flow conditions (87.59-115.1L/s for G5), a very small proportion of REE is expected to be scavenged by Fe and Al flocs from dissolved phase at G3 (~5%) and G4 (might be slightly larger than that at G3). A larger proportion of REE (relative to that at G3 and G4) is likely to be chemically transformed from dissolved to suspended solid phase at G5 under these higher flow conditions. Some sediments are possibly mobilised from the stream bed and are brought into the water column at G3 to G5 under these higher flow conditions. At G7 under all flow conditions (lower flow conditions: 253-734L/s for G7; higher flow conditions: 4480-10200L/s for G7), a relatively large degree of REE (compared to that at G5 under higher flow conditions) is expected to be scavenged by the Fe and Al flocs from the dissolved phase (<0.005µm). The sediments resuspension degree increases significantly with the increase of flow at G7.

When truly dissolved and (suspended) solid REE have a similar distribution pattern, the source-related process may largely control the REE fractionation. When solution chemistry related process has the dominant control on REE fractionation, the truly dissolved and (suspended) solid REE will have quite different distribution pattern (Verplanck, 2013; Verplanck et al. 1999; Elderfield et al. 1990; Goldstein and Jacobsen, 1988a). In addition, before a large degree of REE transformation between water (unfiltered phase) and solid (e.g. sediments) occurs, the unfiltered phase can be regarded as having a source-related REE distribution pattern (source-rock leachates) (Goldstein and Jacobsen, 1988a; Hoyle et al. 1984).

In order to understand the influence of source-rocks and solution chemistry on REE distribution patterns in the Gate Gill (G3 to G7) below the mine water discharge, the discussion below is mainly based on the following data:

(1) unfiltered phase at G1 under all flow conditions when ultrafiltration was undertaken

(2) truly dissolved (<0.005µm) and unfiltered phase at G2 to G7 under all flow conditions, and

(3) suspended solids (>0.005µm) at G3 to G5 under higher flow conditions (87.59~115.1L/s for G5, since only noticeable REE are present in suspended solid phase under such flow conditions: the proportion of REE present in suspended phase at G3, G4 and G5 is 15.6%-22.7%, 18.6%-21.4% and 31%-56.6% respectively), and at G7 under all flow conditions when ultrafiltration was undertaken.

Under either the lower (6.88~15.34 L/s for G5) or the higher (87.59~115.1L/s for G5) flow conditions the spatial variation of PAAS normalized REE concentration distribution pattern in the unfiltered phase from G1 to G7, and in dissolved (< 0.005µm) and in 0.1µm filtered phase from G2 to G7, are very similar. The PAAS normalized REE concentration distribution pattern in unfiltered phase at G1, and different phases (< 0.005µm, < 0.01µm and unfiltered) at G2 to G7, from one example from lower flow conditions (flow at G5 of 10.03L/s) and one example from higher flow conditions (flow at G5 of 100.3L/s) are shown in Figure 6.16 and Figure 6.17 respectively. The results from other lower (6.88~15.34L/s at G5) and higher (87.59~115.1L/s at G5) flow conditions are displayed in Appendix F.

Comparing the results of 0.1µm filtered and truly dissolved (< 0.005µm) phase in Figure 6.16 and Figure 6.17 (with additional data shown in Appendix F) for G3 to G7 under varying flow conditions provides an indication as to whether the results of 0.1µm filtered phase, from sampling occasions when ultrafiltration was not undertaken, can be used to qualitatively show the REE distribution pattern in truly dissolved phase at G3 to G7.

PAAS normalized REE concentration distribution pattern in suspended solids (>0.005µm, which is likely to include REE associated with the freshly formed Fe and Al precipitates and with secondary Fe and Al precipitates that re-suspended from the river bed) at G7 under all flow conditions is also shown in Figure 6.16, Figure 6.17 and Appendix F. The spatial variations of PAAS normalized REE concentration distribution pattern in suspended solids from G3 to G7 under higher flow conditions are displayed in Figure 6.17 and Appendix F.

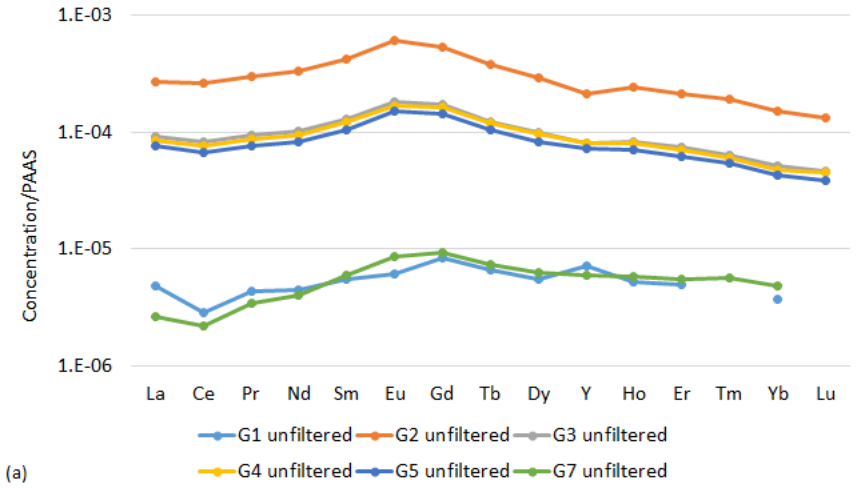

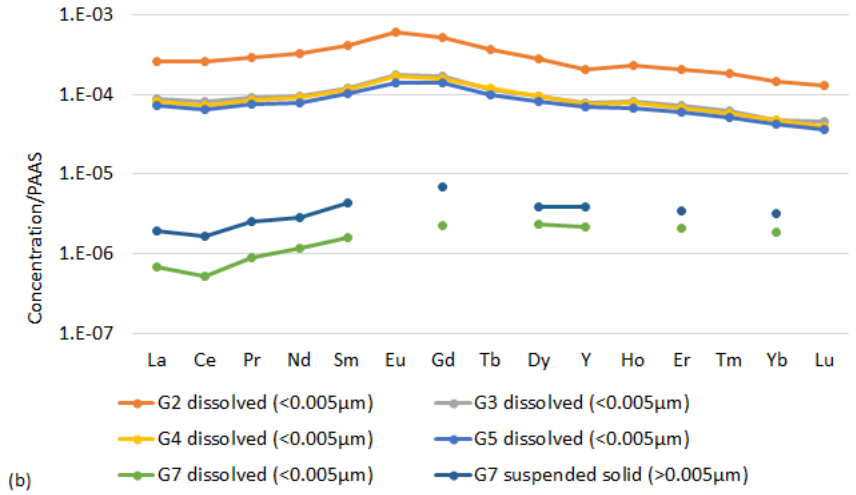

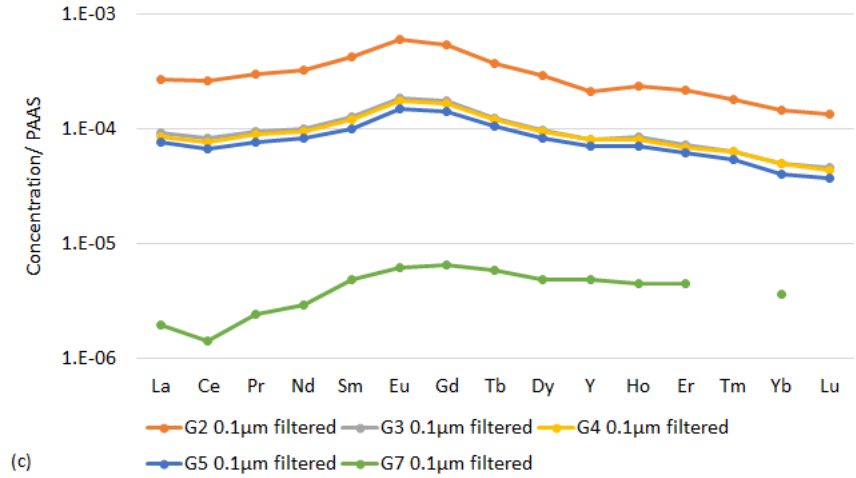

Figure 6.16: PAAS normalized REE concentration distribution pattern (a) in unfiltered phase at G1 to G7; (b) in dissolved (<0.005µm) phase at G2 to G7 and of suspended solid (>0.005µm) at G7; (c) in 0.1µm filtered phase at G2 to G7, when under lower flow condition (flowrate of G5 is 10.03 L/s and of G7 is 586 L/s)

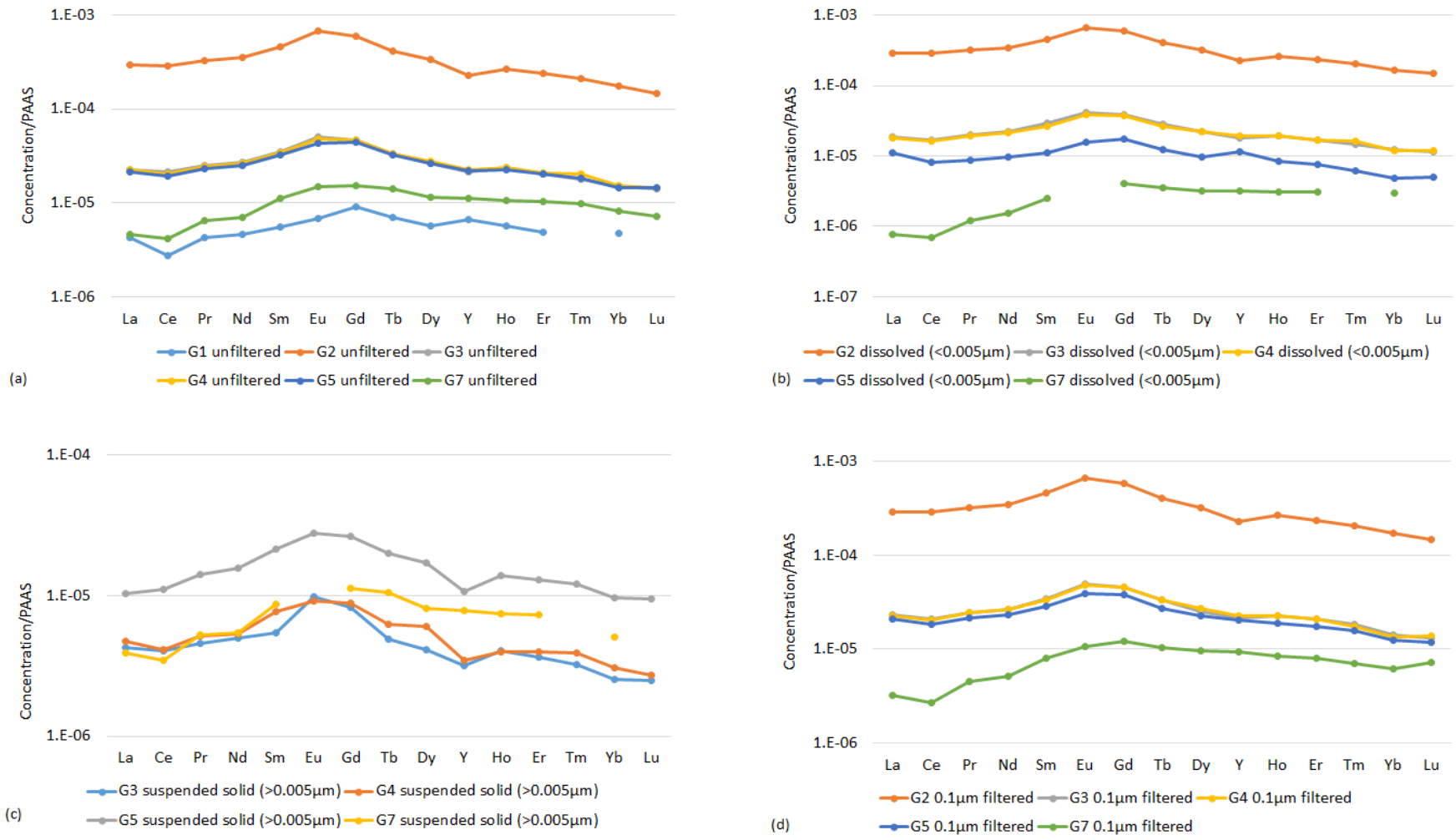

Figure 6.17: PAAS normalized REE concentration distribution pattern (a) in unfiltered phase at G1 to G7; (b) in dissolved (<0.005µm) phase at G2 to G7; (c) in suspended solids (>0.005µm) at G3 to G7; (d) 0.1µm filtered phase at G2 to G7, when under higher flow condition (flowrate of G5 is 100.3 L/s and of G7 is 4480L/s)

Note that some elements in Figure 6.16 and Figure 6.17 (and also Appendix F) do not have a value. This is because the measured concentrations of these elements were below the detection limits of the ICP-MS.

In addition, the REE distribution pattern is exactly the same irrespective of whether the REE load data or REE concentration data are used for the normalization. Therefore, only concentration data are used to demonstrate the spatial variation of normalized REE distribution pattern under each flow condition.

As can be seen from Figure 6.16 and Figure 6.17 (and also Appendix F), MREE enrichment over both LREE and HREE is the common theme on the PAAS normalized distribution patterns for all the displayed phases at G1 to G7. When MREE are ignored, whether LREE or HREE is enriched relative to the other differs between sampling sites. The degree of enrichment of MREE over LREE, compared to the degree of enrichment of MREE over HREE, differs between sampling sites.

The distribution patterns at G1 (upstream Gate Gill mine water) and in the River Glenderamackin (G7) are relatively similar. Specifically, when MREE are ignored some degree of HREE enrichment relative to LREE can be observed on the PAAS normalized distribution pattern. But the mine water discharge (G2) and the Gate Gill downstream of the discharge (G3 to G5) have totally different REE distribution patterns (when MREE are ignored) than G1 and G7. The displayed phases at G2 to G5 all show a similar distribution pattern, in which there is LREE enrichment relative to HREE on the PAAS normalized distribution pattern.

Generally the displayed phases for each of the Gate Gill sites below the mine water discharge have a relatively similar distribution pattern under most flow conditions. This suggests that source-related processes play an important role in the REE fractionation pattern at G3 to G7 under all flow conditions. The fractionation of REE at G3 to G5 is mainly influenced by the Threlkeld mine leachates, which is discussed in Section 6.3.2. But the Threlkeld mine leachates seem to have quite limited influence on the REE distribution pattern at G7, which is shown in Section 6.3.3.

The MREE enrichment over HREE and LREE, and a slight HREE enrichment relative to LREE pattern, can generally be seen on the PAAS normalized distribution pattern for the

unfiltered phases at G1 under most lower (6.88-15.34L/s for G5) and higher flow (87.59-115.1L/s for G5) conditions.

The dissolved (<0.005µm), 0.1µm filtered, suspended solids (>0.005µm) and unfiltered phase at G7 under most lower (6.88-15.34L/s for G5; 253-734L/s for G7) and higher flow (87.59-115.1L/s for G5; 4480-10200L/s for G7) conditions show MREE enrichment pattern over both LREE and HREE, and a general HREE enrichment pattern compared to LREE, after PAAS normalization. But the degree of HREE enrichment relative to LREE for different phases at G7 is not the same. Under most of these flow conditions the HREE enrichment relative to LREE for the suspended solids (>0.005µm) is less obvious, but for the dissolved (<0.005µm) and 0.1µm filtered phase is clearer. This suggests that solution chemistry-related processes induce some degree of REE fractionation at G7 during the REE transformation process. The transformation process includes scavenging of REE from truly dissolved to suspended solids (REE associated with the freshly formed Fe and Al flocs) and removal of REE from water column (REE associated with sediments which are mobilised as flow increases).

Figure 6.18 displays the PAAS normalized distribution pattern in dissolved (<0.005µm) and unfiltered phase at G7 for the one lower flow condition example (10.03L/s at G5; 586L/s at G7) and one higher flow condition example (100.3L/s at G5; 4480L/s at G7) which is respectively shown in Figure 6.16 and Figure 6.17. The solution chemistry-related fractionation across REE group at G7 can be clearly seen in Figure 6.18.

According to Figure 6.18, LREE have a greater affinity for the suspended solid on both the lower (10.03L/s for G5; 586L/s for G7) and higher (100.3L/s for G5; 4480L/s for G7) flows. A similar pattern is seen at G7 under most of the other lower (6.88-15.34L/s for G5; 253-734L/s for G7) and higher flow (87.59-115.1L/s for G5; 4480-10200L/s for G7) conditions. The dissolved and unfiltered PAAS normalized distribution patterns at G7 under these other flow conditions are shown in Appendix F. The reason that leads to the LREE with greater affinity for the suspended solid at G7 is explained in section 6.5.

There is a MREE enrichment over both LREE and HREE, and a LREE enrichment relative to HREE on the PAAS normalized distribution pattern in the dissolved (0.005µm filtered), 0.1µm filtered and unfiltered phases at G2 to G5 under both lower (6.88~15.34L/s for G5) and higher flow (87.59~115.1L/s for G5) conditions. This can be seen from Figure 6.16 and Figure 6.17 (and also Appendix F).

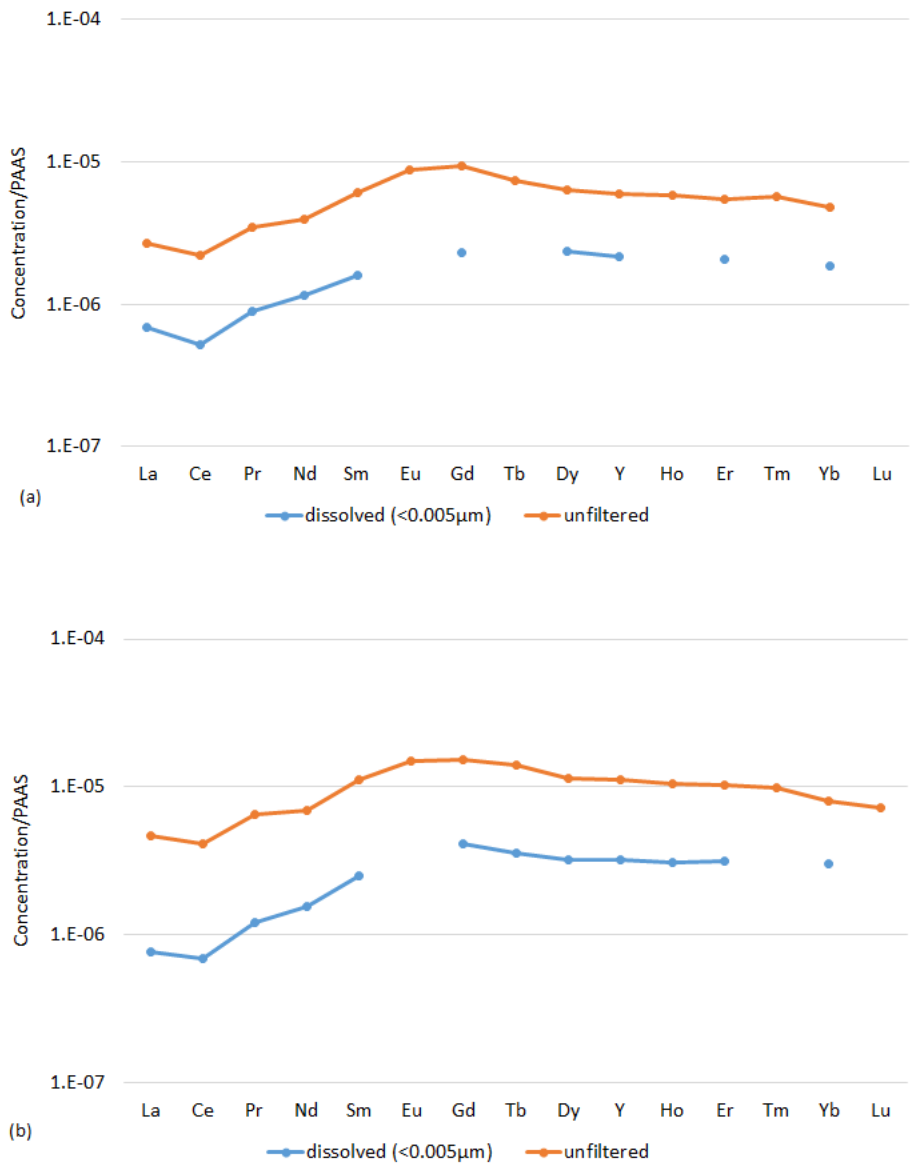

Figure 6.18: PAAS normalized REE distribution pattern in truly dissolved (ultra/ 0.005µm filtered) and unfiltered phase at G7 under (a) lower flow condition (flowrate of G5 is 10.03 L/s and of G7 is 586 L/s, pH of G7 is 5.92); (b) higher flow condition (flowrate of G5 is 100.3 L/s and of G7 is 4480L/s, pH of G7 is 6.31)

According to Figure 6.16 (and also Appendix F), there is little spatial variation of the PAAS normalized REE distribution pattern in either dissolved (<0.005µm) or 0.1µm filtered or unfiltered phase from G2 to G5 under lower flow conditions (6.88-15.34L/s for G5). In addition, since little REE are present in the suspended solid form at G3 to G5 under these lower flow conditions, the PAAS normalized REE distribution patterns in all phases at each sampling site from G2 to G5 are identical under each of these lower flow conditions.

According to Figure 6.17 (and also Appendix F), under each of the higher flow conditions (87.59-115.1L/s for G5), when noticeable REE are present in the suspended solids at G3 to

G5 (15.6%-56.6%), the PAAS normalized REE distribution pattern for dissolved (<0.005µm), 0.1µm filtered and unfiltered phase at G2 to G4 and for unfiltered phase at G5, are nearly identical. But the dissolved (0.005µm filtered) and 0.1µm filtered PAAS normalized REE distribution patterns display a very small variation from G4 to G5. The suspended solids (>0.005µm) at G3 to G5 on these higher flow conditions also show MREE enrichment over LREE and HREE, and LREE enrichment relative to HREE pattern on the PAAS-normalized REE distribution pattern. But the degree of LREE enrichment relative to HREE of suspended solids at G3 and G4 is larger than that at G5 under each of these higher flow conditions.

To clearly show the influence of the solution chemistry on REE fractionation at G3 to G5 when noticeable REE are present in the suspended solids, Figure 6.19 displays the dissolved (<0.005µm) and unfiltered PAAS normalized REE distribution pattern at G3 to G5 for the higher flow condition example (100.5L/s for G5) shown in Figure 6.17. The solution chemistry appears to have little influence on REE fractionation at G3 and G4, according to Figure 6.17 (a) and Figure 6.17 (b). But HREE have a greater affinity for the suspended solid at G5, as can be observed from Figure 6.17 (c). A similar conclusion can be drawn from other higher flow conditions (ultrafiltration was undertaken) when noticeable REE are present in the suspended solids (15.6%-56.6%) at G3 to G5. The PAAS normalized REE distribution pattern in dissolved (<0.005µm) and unfiltered phase at G3 to G5 under these other higher flow conditions are shown in Appendix F. Detailed discussion regards to the influence of solution chemistry on the REE distribution pattern at G3 to G5 when noticeable REE are present in the suspended solids is provided in Section 6.4.

The PAAS normalized REE distribution pattern in the 0.1µm filtered phase is similar to that in the dissolved (<0.005µm) phase at G3 to G7 on each of the sampling occasions (ultrafiltration was undertaken) when noticeable REE are present in the suspended solids. The PAAS normalized REE distribution patterns based on 0.1µm filtered data from sampling occasions when ultrafiltration was not undertaken can therefore cautiously be used to qualitatively show the REE distribution pattern in the truly dissolved phase. This can help to demonstrate the influence of source-related processes on REE fractionation at G3 to G7.

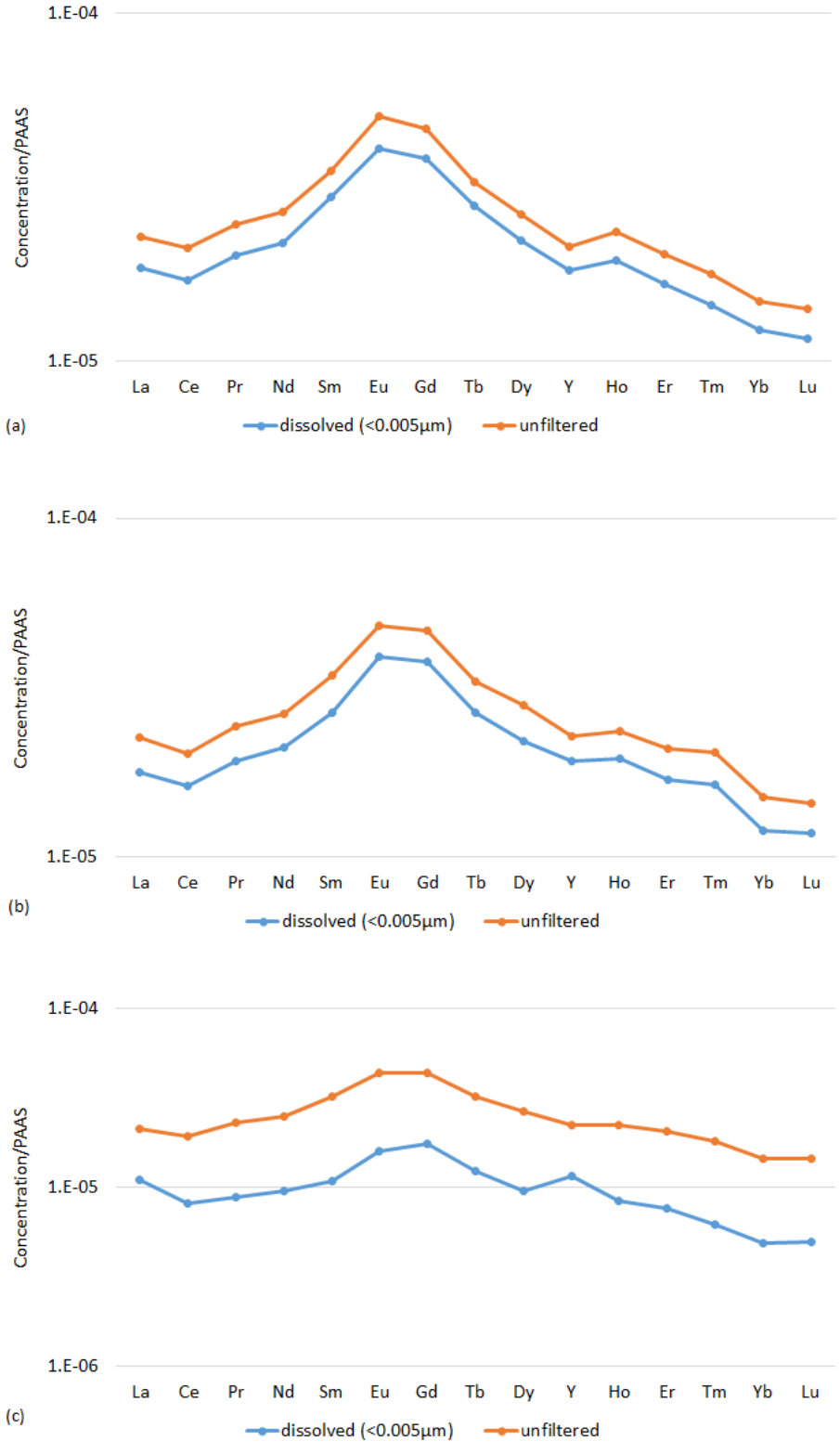

Figure 6.19: PAAS normalized REE distribution pattern in truly dissolved (<0.005µm) and unfiltered phase at (a) G3 (pH=4.49; Q=85.66L/s); (b) G4 (pH=4.76; Q=95.68L/s); (c) G5 (pH=5.23; Q=100.3L/s) on one higher flow condition sampling occasion when ultrafiltration was undertaken

As mentioned in Section 5.2 and 5.3, for sites on the Gate Gill (G3 to G5) below the mine water, on sampling occasions when ultrafiltration was not undertaken, only G5 has some REE (8.71%-14.8%) present in >0.1µm (coarse colloid and particulate fraction) under higher flow conditions (45.42~79.5 L/s at G5). REE (24.9%-44%) present in >0.1µm fraction at G7 under all flow conditions when ultrafiltration (<0.005µm) was not undertaken. The >0.1µm fraction at G5 and at G7 under such flow conditions is expected to contain both REE associated with freshly formed Fe, Al flocs and REE associated with secondary Fe, Al precipitates which are likely remobilised from stream/ river bed.

Figure 6.20: PAAS normalized REE distribution pattern in 0.1µm filtered and unfiltered phase at (a) G5 (G5 Q=45.42 L/s; pH=5.37) (b) G7 (G7 Q=4160 L/s; pH=5.74) on one higher flow condition sampling event when ultrafiltration was not undertaken

The results from sampling occasions when ultrafiltration was not undertaken indicate basically similar patterns to those obtained from sampling occasions when ultrafiltration

(<0.005µm) was undertaken. Therefore, the spatial variation of the PAAS normalized REE concentration distribution pattern from G1 to G7 on sampling events when ultrafiltration (<0.005µm) was not undertaken is only shown in Appendix F.

Figure 6.20 shows the PAAS normalized REE distribution pattern in 0.1µm filtered and unfiltered phases at G5 and G7 from one higher flow condition sampling event (flowrate at G5 of 45.42L/s; at G7 of 4160L/s) when ultrafiltration was not undertaken. Figure 6.20 (a) shows that HREE are preferentially associated with the suspended solids in >0.1µm fraction compared to LREE at G5. As can be seen from Figure 6.20 (b), LREE have the greater affinity for the suspended solids in >0.1µm fraction compared to HREE at G7. Since >0.1µm fraction is the larger size suspended solids, the type of REE with greater affinity for >0.1µm fraction would be preferentially transformed from truly dissolved phase to (suspended) solid phase at suitable pH conditions.

A similar conclusion can generally be obtained at G5 under other higher flow condition (79.5L/s for G5) and at G7 under other lower (5.53-40.1 L/s for G5; 203-1380L/s for G7) and higher (79.5L/s for G5; 5260L/s for G7) flow conditions when noticeable proportions total REE are present in >0.1µm fraction. The 0.1µm filtered and unfiltered PAAS normalized distribution patterns at G5 and G7 under these flow conditions when ultrafiltration was not undertaken are shown in Appendix F. The solution chemistry-related fractionation at G5 and G7 under these flow conditions is detailed in Section 6.4 and Section 6.5.

6.3.2 Source-related fractionation at G3, G4 and G5

As mentioned in Section 6.3.1, the REE distribution pattern in unfiltered phase at G1 differs from that at G2 under all flow conditions. Figure 6.21 shows the PAAS normalized REE concentration distribution pattern for the unfiltered phase at G1 and G2 on all sampling occasions (5.53 - 115.1L/s at G5). Since it was not possible to measure flowrate at G1 in this study (Section 3.2), flowrate at G5 are shown in Figure 6.21 as a representative for the flow condition at G1. As mentioned in Section 5.2.1, the mine water (G2) flow rate is at a consistent 6 L/s, according to Environment Agency. Figure 6.21 shows that there is little temporal variation of both the PAAS normalized REE distribution pattern and the PAAS normalized REE concentration values for the unfiltered phase at either G1 or G2.

The REE distribution pattern at G3, G4 and G5 for the unfiltered phase is very similar to that at G2, but is very different to that at G1 under each flow condition, as noted in Section 6.2.1.

Figure 6.22 shows the temporal variation of PAAS normalized REE load distribution pattern in the unfiltered phase at each individual site of G3, G4 and G5 under all flow conditions (5.53-115.1L/s for G5). The flowrate of G3 and G4 is also shown in Figure 6.22. There is very little temporal variation in the PAAS normalized REE distribution pattern at any of these locations, as shown in Figure 6.22.

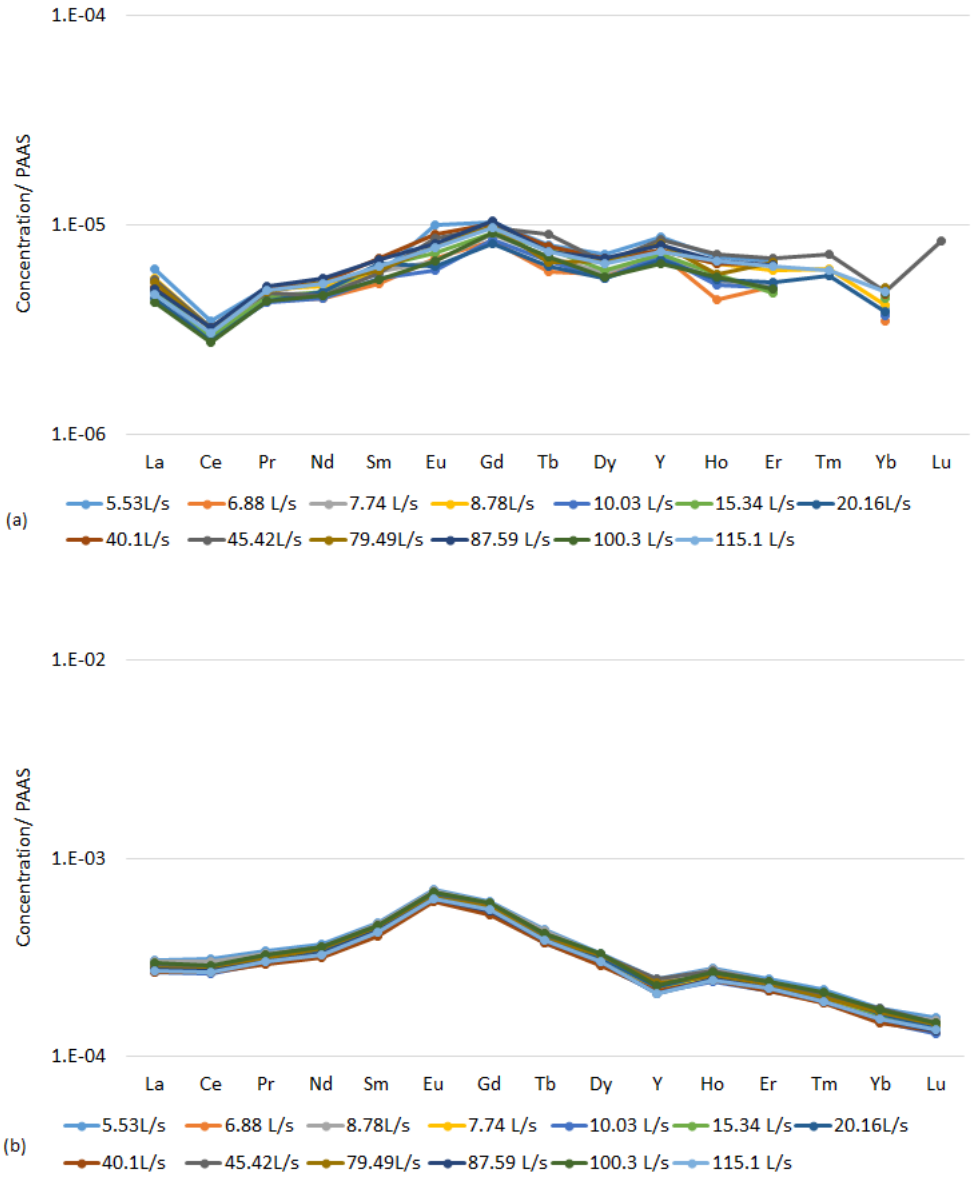

Figure 6.21: PAAS normalized REE concentration distribution pattern for unfiltered phase at (a) G1 and (b) G2 under all flow conditions (5.53-115.1L/s for G5)

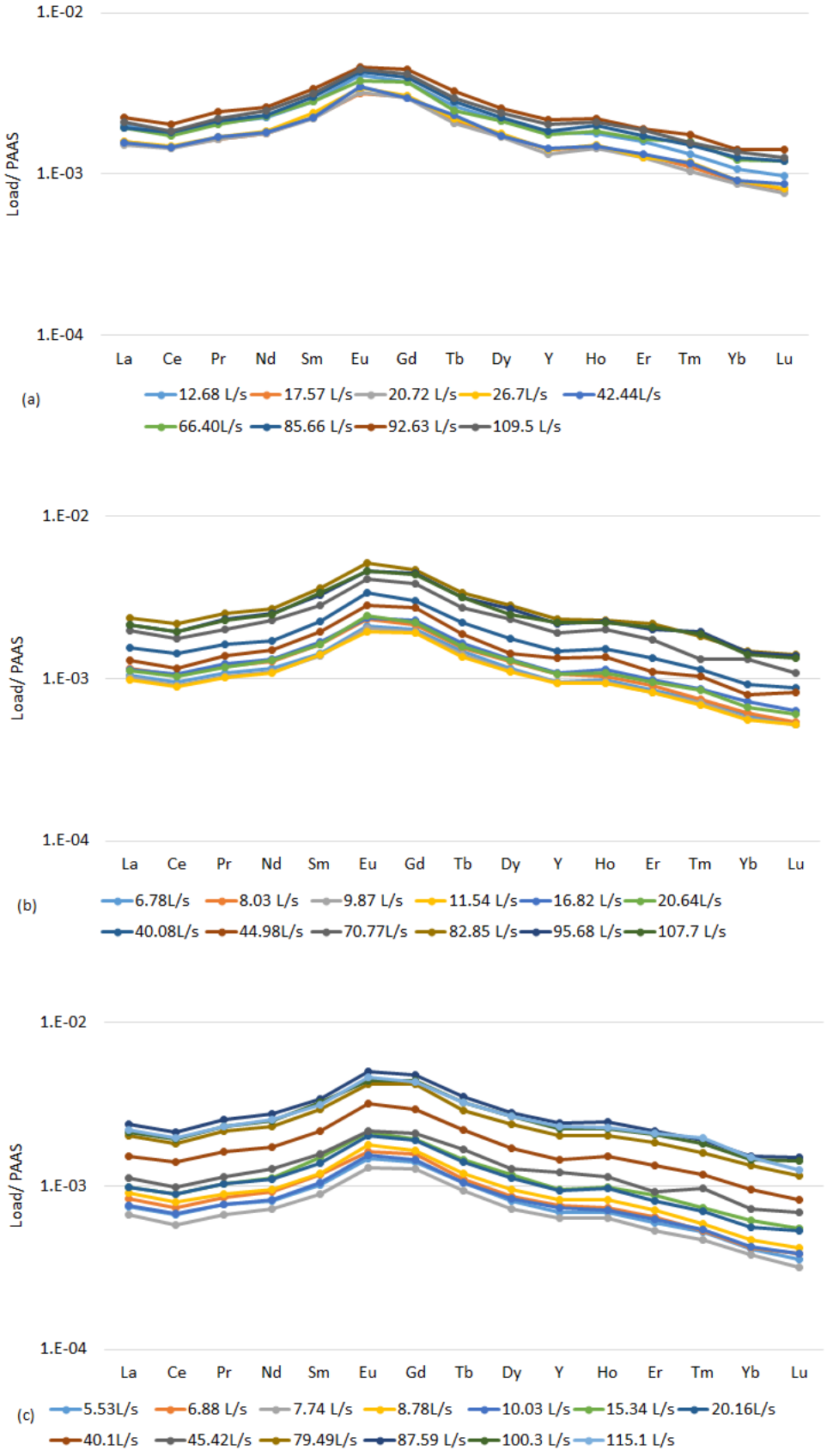

Figure 6.22: PAAS normalized REE load distribution pattern in unfiltered phase at (a) G3; (b) G4; (c) G5 under all flow conditions (12.68-109.5L/s for G3; 6.78-107.7L/s for G4; 5.53-115.1L/s for G5)

Figure 6.22 shows generally the PAAS normalized REE load values in unfiltered phase at G3, G4 and G5 all increase when the flow condition increases from the range of 12.68-42.44L/s to 66.4-109.5L/s for G3, 6.78-44.98L/s to 70.77-107.7L/s for G4, 5.53-45.42L/s to 79.5-115.1L/s for G5. As discussed in Section 5.2.2, this increase of PAAS normalized REE load values is likely due to the dissolution of mine spoils near G3 and the resuspension of REE-containing sediments from stream bed under higher flows.

As shown in Section 5.2.2, G2 is expected to be the only important source of REE at G3, G4 and G5 within the lower flow range (12.68-42.44L/s for G3; 6.78-44.98L/s for G4; 5.53-40.1L/s for G5). Within this lower flow range there is little variation of the PAAS normalized REE load values (unfiltered phase) with increasing flow at G3 and a general increase of the PAAS normalized REE load values (unfiltered phase) as flow rises at G4 and G5, as shown in Figure 6.22. These variations of PAAS normalized REE load values with flow are the same as the variation of ∑REE loads (unfiltered phase) at G3 to G5 as flow rises within the lower flow range (12.68-42.44L/s for G3; 6.78-44.98L/s for G4; 5.53-40.1L/s for G5), which are noted in Section 5.2.2. The reasons for causing these variation of ∑REE loads (unfiltered phase) with flow at G3 to G5 are discussed in Section 5.2.2, which are the same for inducing the variation of PAAS normalized REE load values at G3 to G5 as flow increases within the lower flow range.

As discussed in Section 5.2.2, negligible REE are removed from the water column between G3 and G5 under all flow conditions. Some REE-containing sediments are likely to be brought into the water column at G3 to G5 under higher flow conditions (45.42-115.1L/s for G5). But solution chemistry-related fractionation has little influence on the PAAS normalized REE distribution pattern in suspended solids (>0.005μm) at G3 and G4 under these higher flow conditions (Section 6.3.1). In addition, source-related fractionation has the dominant control on the PAAS normalized REE distribution pattern in suspended solids (>0.005μm) at G5 under these higher flow conditions (Section 6.3.1). Therefore, the unfiltered phase at G3 to G5 under all flow conditions (5.53-115.1L/s for G5) can be regarded as having a source-related REE distribution pattern.

Based on the above results, the following conclusions are drawn:

- The water leached from the mine spoil has a similar PAAS normalized REE distribution pattern to the mine discharge, which is MREE enrichment over both LREE and HREE, and LREE enrichment relative to HREE;

- The fractionation pattern of the REE at G3, G4 and G5 are mainly controlled by the leachates of Threlkeld mine, including the G2 mine discharge and mine spoil leachates under all flow conditions

The PAAS normalized REE distribution pattern at G3 to G5 for all phases (<0.005µm, <0.01µm and unfiltered) under lower flow conditions (5.54-40.1L/s for G5), when little REE are present in suspended solid (>0.005µm) and/ or >0.1µm, entirely inherits the REE fractionation pattern of the Threlkeld mine leachates. No solution chemistry related fractionation occurs at G3, G4 and G5 under such conditions.

Under higher flow conditions (45.42~115.1L/s for G5) when noticeable REE are present in suspended solid (>0.005µm) at G3 and G4, in suspended solid (>0.005µm) and/ or >0.1µm at G5:

(1) PAAS normalized distribution patterns for all phases (<0.005µm, <0.01µm, >0.005µm and unfiltered) at G3 and G4 are entirely controlled by the leachate from Threlkeld mine.

(2) The solution chemistry has some influence on REE distribution pattern for the dissolved (<0.005µm) and/ or 0.1µm filtered phase, suspended solid (>0.005µm) and/ or >0.1µm at G5, but the leachates from Threlkeld mine has the major control on the fractionation at G5.

6.3.3 Source-related fractionation at G7

As noted in Section 6.3.1, the PAAS normalized REE distribution pattern at G7 is very different to that at G2 to G5 under each flow condition. Figure 6.23 shows that temporal variation of PAAS normalized REE load distribution pattern in unfiltered phase at G7 under all flow conditions (203-10200L/s for G7).

According to Figure 6.23, the PAAS normalized REE distribution pattern in unfiltered phase at G7 under all flow conditions are similar, which is MREE enrichment over both LREE and HREE, and HREE enrichment relative to LREE. Since the degree of sediment resuspension at G7 is expected to increase significantly with flow (Section 5.2.2), solution chemistry-related fractionation has some influence on the PAAS normalized REE distribution pattern in unfiltered phase at G7. As mentioned in Section 6.3.1, the source-related fractionation has a great influence on the REE distribution pattern at G7, since the PAAS normalized REE distribution pattern in dissolved (<0.005 µm) and suspended solids (>0.005µm) is generally similar. Although the overall degree of REE transformation from truly dissolved to (suspended) solids at G7 is expected to be relatively high (since the mean pH at G7 under all

flow condition is 6.05, see Section 5.3). Johannesson and Zhou (1997) note that source-related processes can still play an important role on the REE distribution pattern in streams even at neutral pH where the REE attenuation degree is quite high and solution chemistry has a large influence on REE fractionation.

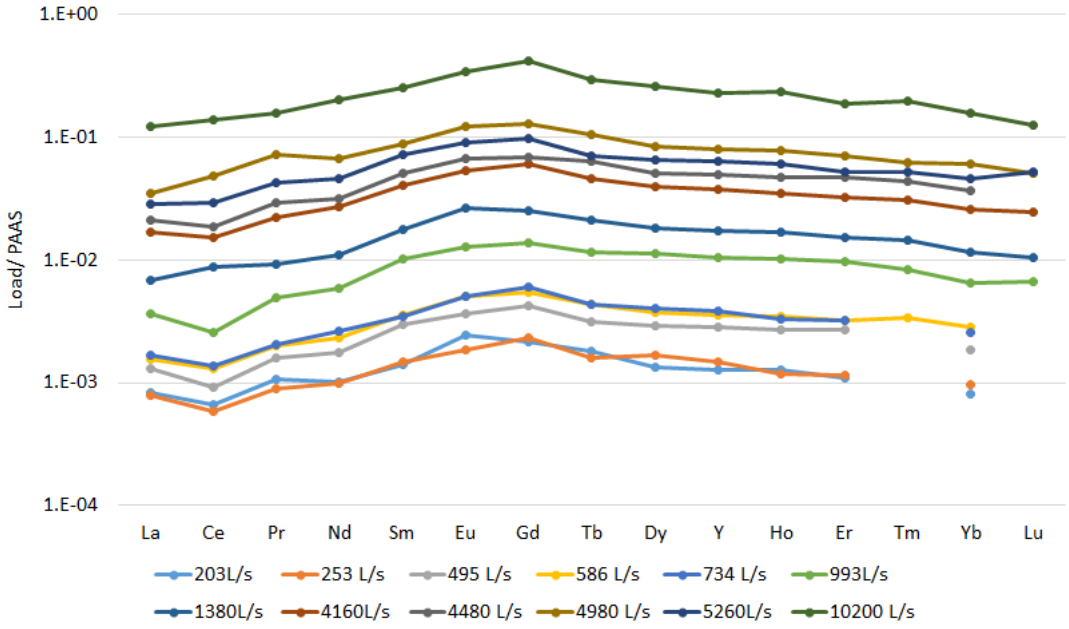

Figure 6.23: PAAS normalized REE distribution pattern in unfiltered phase at G7 under all flow conditions (203-10200L/s for G7; 5.53-115.1L/s for G5)

Figure 6.24 also shows temporal variation in PAAS normalized REE load distribution pattern for dissolved (<0.005 µm) and suspended solids (>0.005µm) at G7 under both lower (253-734L/s for G7) and higher flow (4480-10200L/s for G7) conditions. As can be seen from Figure 6.24, the PAAS normalized REE distribution patterns for dissolved (<0.005 µm) and suspended solids (>0.005µm) are relatively similar at G7 under both these lower and higher flow conditions.

In addition, the unfiltered phase at G7 shown in Figure 6.23 has a relatively similar PAAS normalized REE distribution pattern to that in dissolved and suspended solid shown in Figure 6.24. Therefore, unfiltered phase at G7 is expected to largely inherit the source-related fractionation pattern. The very different PAAS normalized REE distribution pattern in unfiltered phase in the Gate Gill (Section 6.3.2) and at G7 therefore indicates that Gate Gill is not an important source for REE in the River Glenderamackin. This is similar to the conclusion obtained in Section 5.2.2; the overall contribution of REE from Gate Gill at G7 is quite small.

In addition, the PAAS normalized REE load value for dissolved, suspended solid (Figure 6.23) and unfiltered phase (Figure 6.24) increases with the increase of flow, which is same as the variation of ∑REE load in corresponding phase as flow rises (Section 5.2.2). The increase of PAAS normalized REE load value for these phases is likely related to the remobilisation of REE-containing sediments from river bed of Glenderamackin and the dissolution of REE from Bannerdale mine (Section 5.2.2).

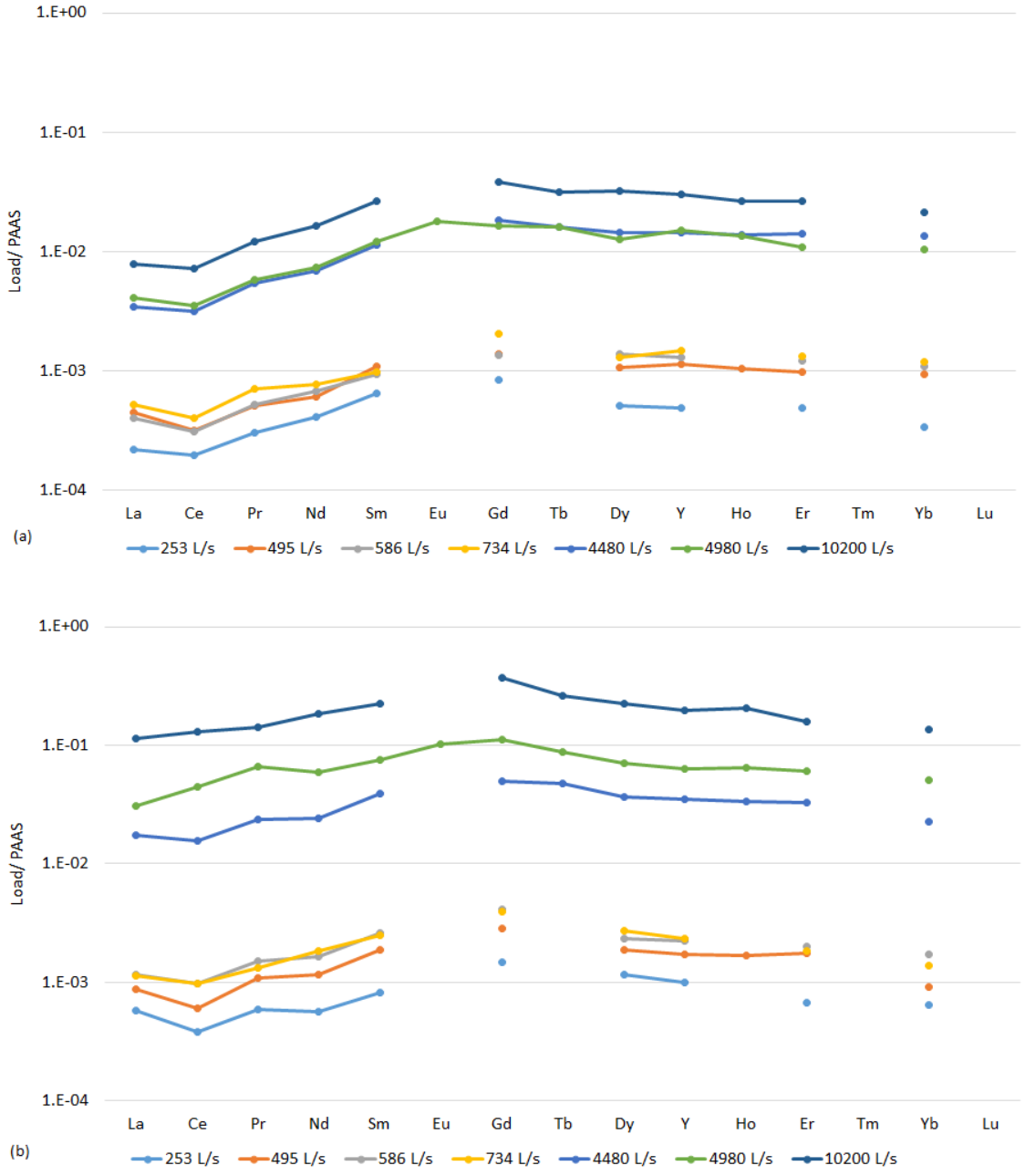

Figure 6.24: PAAS normalized REE load distribution pattern in (a) dissolved (<0.005µm), and (b) suspended solid (>0.005µm) at G7 under all flow conditions when ultrafiltration was undertaken (lower flow conditions:253-734L/s for G7; higher flow conditions: 4480-10200L/s for G7)

The above results suggest that:

(1) REE in the sediments at G7 which are REE associated with secondary Fe and Al precipitates (through the adsorption and/ or co-precipitation process) are expected to also have a MREE enrichment over both LREE and HREE, and HREE enrichment relative to LREE on PAAS normalized REE distribution pattern;

(2) Bannerdale mine leachates may also have this similar PAAS normalized REE distribution pattern of MREE enrichment over both LREE and HREE, and HREE enrichment relative to LREE.

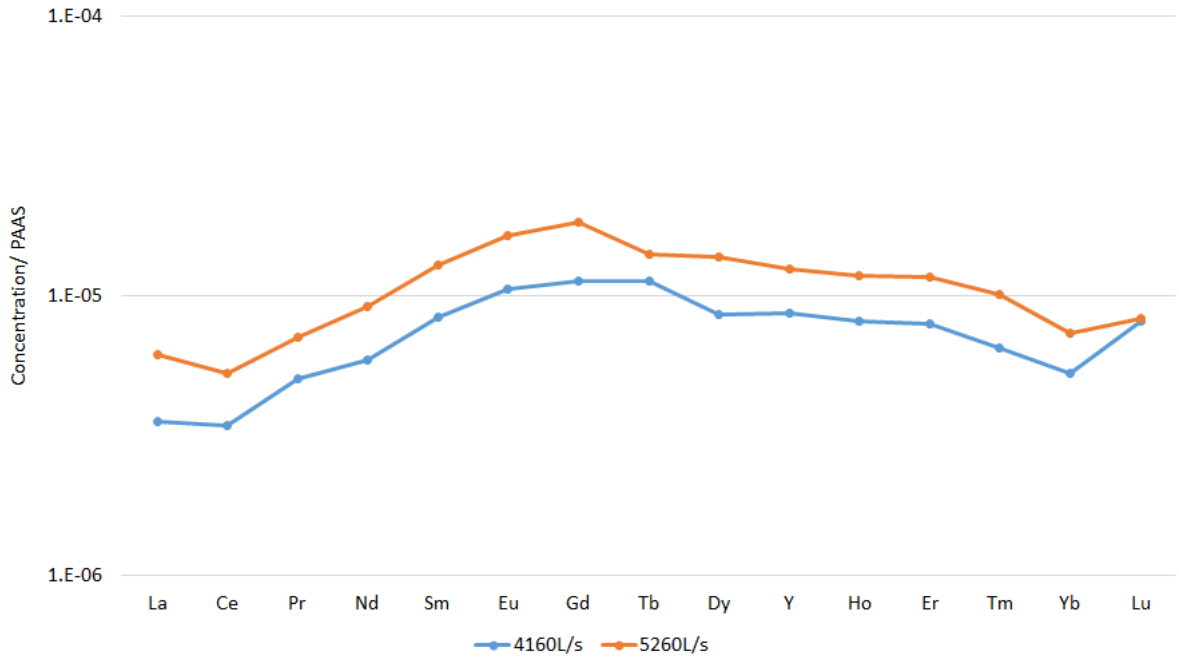

Figure 6.25: PAAS-normalized REE distribution pattern (based on concentration) in the River Glenderamackin upstream (G6) of the confluence with the Gate Gill (flow shown are the flow-rate at G7)

The PAAS normalized REE concentration distribution pattern in unfiltered phase in the River Glenderamackin upstream of the confluence with the Gate Gill (G6) shown in Figure 6.25, is similar to that at G7 i.e. MREE enrichment over both LREE and HREE, and HREE enrichment relative to LREE. Although the sampling of G6 was only undertaken on the first two sampling occasions (under higher flow conditions), it does illustrate the background REE fractionation pattern of River Glenderamackin. The first two sampling occasions are under higher flow condition. Since it is not suitable to perform the flow measurement at G6 (Section

3.2), the flow of G7 is used as the representative to show the flow condition at G6 on these two sampling occasions.

The similar PAAS normalized REE distribution pattern in unfiltered phase at G6 and G7 further indicates that the leachates from the Threlkeld mine have limited influence on the REE fractionation at G7. In addition, the PAAS-normalized REE distribution pattern in unfiltered phase at G1 is approximately similar to that at G7. This suggests that Gate Gill upstream of the mine discharge and the River Glenderamackin may have a similar source rock type, which differs from that of Threlkeld mine.

6.4 Process-related fractionation in acidic waters

This section describes the influence of solution chemistry on the REE fractionation at sampling sites downstream of the mine water discharge (G2) on Gate Gill when noticeable amount of REE are present in suspended solids.

6.4.1 Influence of solution complexation and REE ionic radius on REE distribution pattern

As noted in Section 6.3.1, under higher flow conditions (87.59-115.1L/s for G5) when a noticeable proportion of REE are present in the suspended solids (>0.005µm) at G3 (15.6%-22.7%) and G4 (18.6%-21.4%), solution chemistry-related processes have little influence on the REE fractionation at each sampling site. As noted in Section 5.3, the low pH at G3 (mean value of 4.46; range from 4.28-4.6) and G4 (mean value of 4.63; range from 4.48-4.76) under these flow conditions strongly inhibits the REE adsorption. The low pH at G3 and G4 under these flow conditions is likely to be the reason that solution chemistry-related fractionation has no influence on the REE distribution pattern in dissolved (<0.005µm) and suspended solid (>0.005µm) phases. Before reaching the trigger pH which can induce a relatively high degree of REE adsorption, REE behave conservatively and no solution chemistry-related fractionation occurs during the transformation of REE from dissolved to suspended solid and/ or solid phase (Borrego et al. 2012; Gammons et al. 2005; Verplanck et al. 2004). Therefore, REE in the dissolved phase (<0.005µm), REE associated with freshly formed Fe and Al precipitates and the REE associated with secondary Fe and Al precipitates (through adsorption and co-precipitation) which are remobilised from the stream bed at G3 and G4 entirely inherit the Threlkeld mine leachates.

On the other hand, the degree of REE adsorption at G5 under higher flow conditions (45.42-115.1L/s, noticeable amount of REE are present in >0.005µm and/ or >0.1µm) is expected to

be higher, and the mean pH at G5 under these flow conditions is 5.11 (range from 4.94-5.37). As shown in Section 6.3.1 (Figure 6.19 c and Figure 6.20 a), the solution chemistry is able to fractionate REE during the chemical transformation process and HREE have greater affinity for the freshly formed Fe, Al flocs and secondary Fe, Al precipitates at G5 under these higher flow conditions.

REE species present in water can influence the REE distribution pattern by fractionating REE based on the stability constant of the REE complexes and the ionic radius of free REE. As shown in Section 6.2.1, free REE ions (Ln^{3+}) and REE sulphate complexes ($LnSO_4^+$) are the dominant species at G1 to G5.

$LnSO_4^+$ is not a strong complex and has no obvious variation in stability constant across the REE, which is not able to fractionate REE during the partition of REE onto Fe, Al flocs and precipitates (Verplanck, 2004; Wood, 1990). In the absence of strong complexes, the process-related fractionation is mainly influenced by the ionic radius and electron structure of individual REE. To be more specific, the progressive decrease in ionic radius with increasing atomic number across the REE group leads to a progressive increase in surface reactivity with increasing atomic number (Tertre et al. 2008; Tang and Johannesson, 2005; Tertre et al. 2005;). The preferential removal of HREE relative to MREE and LREE from the truly dissolved phase by the freshly formed Fe, Al flocs and the secondary Fe, Al precipitates in the absence of strong complexes at G5 is similar to the experimental results shown in Tertre et al. (2008, 2005); Verplanck et al. (2004); Coppin et al. (2002) and Kawabe et al. (1999a). These studies all show an increase in the degree of adsorption with increasing REE atomic number in the absence of strong complexes when pH in water reaches the trigger point and the degree of REE adsorption is not very low. However, Tang and Johannesson (2005) mention that in the absence of strong complexes, HREE are still preferentially removed by the scavenging materials even when pH is as low as 4 and the REE adsorption degree is very small. Their findings do not match the results from this study which shows that solution chemistry induced fractionation is strongly suppressed when the REE adsorption degree is quite low, like at G3 and G4 under higher flow conditions (87.59-115.1L/s for G5).

As discussed in Section 5.4, the surface of Fe and Al flocs/ precipitates at G5 is positively charged under higher flow conditions (45.42-115.1L/s) when a noticeable amount of REE are present in >0.005µm and/ or >0.1µm as the pH at G5 ranges from 3.94 to 5.37. No physical sorption induced process-related fractionation across the REE series is expected to occur at

G5 under high flow conditions since the dominant REE species (Ln^{3+} and $LnSO_4^+$) on all sampling occasions are positively charged.

Although an enrichment of HREE relative to LREE is not observed on the PAAS normalized REE distribution pattern in the suspended solid (>0.005µm) at G5 (Figure 6.17 c, Section 6.3.1), the affinity of HREE for Fe, Al flocs/ precipitates at G5 is greater than that for MREE and LREE (Figure 6.19 c, Figure 6.20 a, Section 6.3.1). This suggests that solution chemistry has some influence on the PAAS normalized REE distribution pattern at G5, but the influence is hidden by the source-related fractionation pattern. This further indicates that source-related processes (the distribution pattern of Threlkeld mine leachates) have larger influence on the PAAS normalized REE distribution pattern at G5 compared to the solution chemistry-related process.

6.4.2 Impact of scavenging substances on REE fractionation at G5

In the absence of strong complexes, process-related fractionation is mainly controlled by the surface complexation, since there is no strong competition between solution complexation and surface complexation for dissolved REE. During the surface complexation process, besides the influence of REE ionic radius discussed in Section 6.4.1, the characteristics of scavenging materials can also cause some fractionation (although scavenging materials-related fractionation is fundamentally induced by the electron structure of individual REE) (Quinn, 2006).

The distribution pattern of the REE partition coefficient on (suspended) solid phases is used to show the scavenging material-related fractionation in the absence of strong REE complexes in the adsorption studies (Quinn et al., 2004; Ohta and Kawabe, 2001; 2000; Bau, 1999; Bau, 1996). The partition coefficient equals the REE ion activity in the solid phase divided by the REE ion activity in the corresponding solution phase (Gosselin et al., 1992). The ratio of each individual REE concentration in suspended solids (>0.005µm) to that in the truly dissolved phase (<0.005µm) at G5 under higher flow conditions (87.59-115.1L/s for G5) when a noticeable proportion of REE is present in the suspended solid (31%-56.6%) is used as the "partition coefficient" and plotted against atomic number (Figure 6.26). Although the concentration used is not the activity, rather the ratio of REE concentration in suspended solids (>0.005µm) to that in the dissolved phase (<0.005µm), it can be roughly used as a general guide to show the scavenging material-related fractionation pattern in the absence of strong REE complexes.

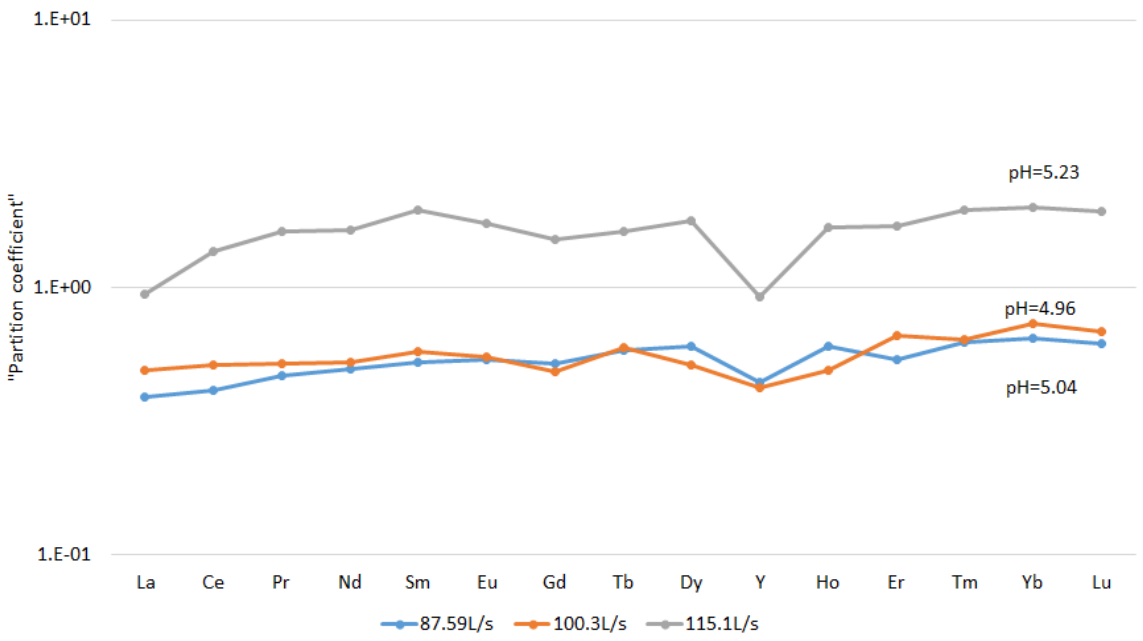

Figure 6.26: The distribution pattern of REE series "partition coefficient" at G5 under higher flow conditions (87.59-115.1L/s for G5) when noticeable amount of REE is present in the suspended solid phase

Even though G5 under higher flow conditions when ultrafiltration was not undertaken (45.42-79.49L/s for G5), a noticeable proportion of REE is present in the >0.1µm fraction (8.9%-14.8%) at G5, these data are not used and discussed in this section since the dissolved REE data under such flow conditions are not available. In addition, since the solution chemistry has little influence on the REE fractionation at G3 and G4 under higher flow conditions when a noticeable proportion of REE is present in the suspended solids, the distribution pattern of the REE group partition coefficient at G3 and G4 is therefore not shown in Figure 6.26.

As mentioned in Section 5.4, Fe and Al oxyhydroxides control the REE transformation from dissolved (<0.005µm) to (suspended) solid phase through the adsorption and/ or co-precipitation process.

According to Quinn et al. (2004); Ohta and Kawabe (2001, 2000); Bau, (1999) and Bau (1996), an M-type lanthanide tetrad pattern can be observed on the distribution pattern of the REE partition coefficient on Fe oxyhydorixdes, in the absence of strong REE complexes in solution. As described in Section 2.4.4, the M-type lanthanide tetrad pattern is four upward-curved segments in the distribution pattern of the REE group partition coefficient, the first from La to Nd, the second from Nd to Gd, the third from Gd to Ho and the last from Ho to Lu. A negative anomaly of La, Y, Gd and Lu is therefore produced on the distribution pattern

of the REE partition coefficient on Fe oxyhydorixdes. Quinn et al. (2004) notes that the partition coefficient of REE increases smoothly and progressively with increasing atomic number across the REE group on the distribution pattern of Al oxyhydroxides, in the absence of strong REE complexes in solution.

As can be seen from Figure 6.26, although an M-type lanthanide tetrad effect is not very obvious, a negative anomaly of Y is the common theme in the distribution pattern of the REE group partition coefficient at G5. The negative anomaly of Y in the distribution pattern of the REE group partition coefficient means a lower affinity of Y relative to its adjacent elements for scavenging materials. REE in the suspended solids used for calculating the "partition coefficient" includes the REE associated with freshly formed Fe and Al flocs and REE associated with secondary Fe and Al oxyhydroxide precipitates which are remobilised from the stream bed. The negative anomaly of Y in the distribution pattern of the REE group partition coefficient suggests that Fe oxyhydroxides is at least one important material scavenging REE from the truly dissolved water phase at G5.

This is because, the bonding between REE with the 4f orbitals (Ce-Lu) and scavenging material surface is influenced by the 4f orbitals of REE. The delocalization of electrons in REE (Ce-Lu) 4f orbitals when interacting with more covalent ligands/ soft ligands induces an enhanced covalency of REE (Ce-Lu). When the interaction between REE and solid phase is comparatively covalent, the enhanced covalency of REE with the 4f orbitals (Ce-Lu) leads to Y behaving as a LREE (Borkowski and Siekierski, 1992; Siekierski, 1981). Quinn et al. (2004) notes that in the absence of strong REE complexes, the comparative covalent interaction between REE and Fe oxyhydroxides leads to the surface reactivity of Y being between that of La and Ce and a negative anomaly of Y in the distribution pattern of the REE group partition coefficient.

On the other hand, when the interaction between REE and solid phase is comparatively ionic, Y has a similar chemical behaviour to Ho and consequently behaves as a HREE (Martell and Hancock, 1996; Liu and Byrne, 1995). While the interaction between Y and Al oxyhydroxides is comparatively ionic, Y then behaves as the HREE, which means Y has a greater partition tendency for the solid phase relative to MREE and LREE, in the absence of strong REE complexes (Quinn et al., 2004). Since no fractionation is induced by the electron structure of REE during their interaction with Al oxyhydroxides, the decrease in REE ionic radius with increasing atomic number then controls the REE fractionation during the

scavenging process in the absence of strong REE complexes. Therefore, in the absence of strong REE complexes in solution, a progressive increase in the REE partition coefficient with increasing atomic number across the REE group can be observed when Al oxyhydroxides is the only important scavenging material (Quinn et al. 2004).

According to Figure 6.26, the negative anomaly of Y in the distribution pattern of the REE group partition coefficient at G5 is more pronounced under a flow of 115.1L/s with higher pH of 5.23 (the proportion of REE present in suspended solid is also higher- 56.6%, as a result of higher pH). Bau (1999) notes that the scavenging substance-related fractionation is pH dependent, the negative Y anomaly in the distribution pattern of the REE group partition coefficient on Fe oxyhydroxides becomes more pronounced as pH increases from 4.64 to 6.2.

6.5 Process-related fractionation in slightly acidic to near neutral water

As shown in Section 6.2.2, $LnCO_3^+$ and Ln^{3+} are the only important species at G7 under all flow conditions (203-10200L/s for G7). The pH ranges from 5.6 and 6.88 at G7 under all flow conditions (Section 5.3). The importance of $LnCO_3^+$ generally increases with the increase of pH, especially for HREE. $LnCO_3^+$ is a less important species compared to Ln^{3+} when pH is $\leq$6.3, and $LnCO_3^+$ becomes a more important species relative to Ln^{3+} when pH is $\geq$6.47 (Section 6.2.2). There is a progressive increase of $LnCO_3^+$ proportion with the increase of atomic number across REE group, as a result of the progressive increase of $LnCO_3^+$ stability constant with increase of REE atomic number. In addition, the difference in proportion of HREE-CO_3^+ and LREE-CO_3^+ under higher pH conditions is generally larger compared to that under lower pH conditions (Section 5.2.2).

The solution chemistry induced REE fractionation is the result of competition between solution complexation and surface complexation (Tang and Johannesson, 2010b; Quinn et al. 2006a, 2006b; Quinn et al., 2004; De Carlo et al., 2000; Benedict et al., 1997). REE can complex with carbonates to form strong solution complexes- $LnCO_3^+$ (Leybourne et al., 2000; Lewis et al., 1998; Takahashi et al., 1997). The formation of $LnCO_3^+$ reduces the partition tendency of those complexed REE for the scavenging solids, like Fe, Al, Mn oxyhydroxides and enhances the mobility of REE (Johannesson & Hendry, 2000; Ohta and Kawabe, 2000; Kawabe et al. 1999b).

Since the stability constant of REE carbonate ($LnCO_3^+$) increases with the increase of REE atomic number, heavier REE-CO_3^+ is essentially more stable than lighter REE-CO_3^+. Stronger

carbonate complexation of heavier REE reduces the surface reactivity of heavier REE relative to lighter REE, which leads to the HREE more difficult to be removed from dissolved phase relative to MREE and LREE (Sun et al., 2011; Luo and Byrne, 2004; Byrne and Kim, 1993; Wood, 1990). When $LnCO_3^+$ is an important species in water, the solution complexation-related fractionation will normally have a dominated control on process-related REE fractionation pattern. This means that a preferential removal of LREE will be observed as a consequence (Quinn et al., 2006b; Kawabe et al., 1999b).

As shown in Section 5.3, a large proportion of REE is present in suspended solid (>0.005µm) and/ or >0.1µm under all flow conditions (203-10200L/s for G7) at G7 due to: (1) the relatively high pH at G7 (mean value of 6.05, ranging from 5.6-6.88); (2) higher flows induced remobilisation of REE-containing sediment. As described in Section 6.3.1 (Figure 6.18 and Figure 6.20 b), LREE have greater affinity for Fe, Al flocs and secondary Fe, Al oxyhydroxides precipitates in suspended solid (>0.005µm) and/ or >0.1µm relative to MREE and HREE at G7 under most of flow conditions (203-10200L/s for G7). Overall speaking, this solution chemistry-related fractionation is likely due to the presence of $LnCO_3^+$ in dissolved phase (<0.005µm) at G7, which leads to HREE being less prone to complex with the freshly formed Fe, Al flocs and the secondary Fe and Al precipitates.

The general decrease in the degree of partitioning to Fe and Al flocs/ precipitates with increasing atomic number across the REE group has been noted in other studies for near neutral (pH>~6) to alkaline waters due to the presence of REE- (di)carbonate complexes (Verplanck, 2013; Sun et al., 2011; Borrego et al. 2012; Quinn et al., 2006a; De Carlo et al., 2000; Johannesson et al. 1996; Johannesson & Lyons, 1994; Johannesson et al., 1994).

This study shows that LREE have greater affinity for Fe and Al flocs/ precipitates in the suspended solids (>0.005µm) and/ or >0.01µm even when pH is slightly acidic (between 5.6-~6) and the mean proportion of $LnCO_3^+$ is ≤ 25%. As mentioned in Section 5.2.2 and 5.3, there is a small decrease of pH at G7 with increasing flow, a large amount of REE associated secondary Fe and Al precipitates are brought into the suspended solids (>0.005µm) and/ or >0.01µm phase under higher flows with lower pH (5.6- ~6). Since the mean pH at G7 is 6.05 (based on the data from all sampling occasions), during the formation of secondary Fe and Al precipitates in the sediments, LREE are expected to be prone to associated with these secondary Fe and Al precipitates. The resuspension of large amount sediments at higher flows (pH between 5.6- ~6) may contribute to the observed greater affinity of LREE for suspended

solids (>0.005μm) and/ or >0.01μm. In addition, the present relative small proportion of $LnCO_3^+$ at G7 under pH of 5.6- ~6 (≤ 25%) may also contribute to the observed greater affinity of LREE for suspended solids (>0.005μm) and/ or >0.01μm in a small degree.

As mentioned in Section 5.4, the surface of Fe and Al flocs/ precipitates at G7 is expected to be positively charged as pH of G7 is ≤6.88 under all flow conditions (203-10200L/s for G7). The dominant REE species (Ln^{3+} and $LnCO_3^+$) at G7 under all flow conditions (203-10200L/s for G7) are positively charged so the physical sorption induced process-related fractionation of REE is not expected to occur.

Although LREE are preferential scavenged by Fe, Al flocs and/ or secondary Fe, Al precipitates. PAAS normalized REE distribution patterns in the dissolved (<0.005μm), suspended solid (>0.005μm) and unfiltered phase all display a MREE enrichment over both LREE and HREE, and a HREE enrichment relative to LREE pattern under most flow conditions (Section 6.3.1, Figure 6.16 and Figure 6.17). Since the displayed PAAS-normalized REE distribution pattern in each phase (<0.005μm and/ or <0.1μm, >0.005μm and unfiltered phase, Figure 6.16 and Figure 6.17) is a combination of both process-related and source-related effects. The source rock has the major control on the overall displayed PAAS-normalized REE distribution pattern in these phases.

6.6 MREE enrichment pattern in waters

As described in Section 6.3.1, MREE enrichment over both LREE and HREE has been noticed on PAAS-normalized REE distribution pattern for all the displayed phases (>0.005μm and/ or >0.1μm, <0.005μm and unfiltered phase) on all sampling occasions.

The MREE enrichment relative to both LREE and HREE on the shale normalized REE distribution pattern in acidic water including acidic river waters (Sholkovitz, 1995; Elderfield et al., 1990), acidic lakes (Johannesson and Lyons, 1995) and acidic brines (Fee et al., 1992; Gosselin et al., 1992) has been reported as the result of chemical weathering/dissolution and/or solid liquid interaction (Johannesson and Lyons, 1995; Fee et al., 1992; Gosselin et al., 1992).

As described in Section 1.5.1, mudstone and siltstone is the bedrock around the study site and quartz is the main gangue mineral for the lead-zinc veins of Threkeld mine. The experiments undertaken by Johannesson and Zhou (1997) show that the leachates of local sandstone,

siltstones and shales have a MREE enrichment on the shale normalized REE distribution pattern. Zhou et al. (1995) also noticed a MREE enrichment on the shale normalized REE distribution pattern for the leachate of sandstone.

Johannesson and Zhou (1997); Johannesson et al. (1996a); Schaltegger et al. (1994) and Zinder et al. (1986) suggest that the acid leachable fraction of local sandstone, siltstones and shales, which are thought to be Fe-Mn oxyhydroxide coatings on the sedimentary mineral grains or apatite within the clastic sedimentary rocks, contributes to the MREE enrichment pattern in natural water. This is because, Fe-Mn oxyhydroxides coatings and secondary minerals in fractures and vugs are known to have a MREE enrichment pattern relative to shale (Banner et al., 1988; Palmer and Elderfield, 1986; Palmer, 1985). The MREE enrichment in Fe-Mn oxyhydroxides coatings and secondary minerals is related to their complex diagenetic history (Conti et al., 1988; Palmer and Elderfield, 1986; Hovorka, 1986). Apatite is one well known MREE enriched phosphate mineral relative to shale (Weber et al., 1995; Gosselin et al., 1992). However, Gosselin et al. (1992) and Banner et al. (1988) mention that the typically low abundance of apatite in many geologic settings leads to a relatively smaller contribution to the overall shale normalized MREE enrichment pattern in natural waters.

The acid leaching experiment and Fe-Mn oxides/ oxyhydroxide extraction experiment operated on the whole source rock by Johannesson and Zhou (1999) also demonstrates the MREE enriched whole rock-normalized signatures from the petrographically identifiable Fe-Mn oxides/oxyhydroxides phase within the source rocks. In addition, Tang and Johannesson (2010a) notes the shale normalized MREE enrichment pattern in groundwater is due to desorption and/or ion exchange reactions between readily released Fe(III) oxides/ oxyhydroxides coatings on sand and the aqueous fluid that interacts with aquifer sand.

Since the source rocks of sampling sites- G2 to G5 are not accessible, as described in Section 3.8. The source rocks of G7 are unknown, since River Glenderamackin is a large scale rivers, and the large scale watersheds will average different bedrocks input, it is therefore difficult to indicate the source rock types of large scale watersheds, according to Leybourne et al. (2000). No leaching experiments were able to undertake on the source rocks of sampling sites. The MREE enrichment pattern on the PAAS normalized REE distribution pattern at sampling sites is due to the dissolution/ desorption/ exchange of the readily soluble or leachable or releasable MREE enrichment minerals/ amorphous phases (relative to shale) within the source-rocks of

this study. But it is unable to know whether the whole source rocks also have the same MREE enrichment pattern (relative to shale) as the readily leachable fraction in the source rocks.

6.7 Source-related positive Eu anomaly at G2, G3, G4 and G5

Positive Eu anomalies have been noticed at G2, G3, G4 and G5 on the PAAS normalized REE distribution pattern for all the displayed phases (<0.005µm, <0.1µm, >0.005µm and unfiltered phase) on most sampling dates (Section 6.3.1, Figure 6.16 and Figure 6.17). This positive Eu anomaly is therefore source-related.

This positive Eu anomaly at G2 to G5 indicates that high content of plagioclase exists in the source rocks (Threlkeld mine) of G2 to G5. Drysdale (2008) notes that positive Eu anomaly is normally noticed in natural water whose host rocks have high content of plagioclase. This is because a positive Eu anomaly is a common figure in plagioclase, as the result of plagioclase ($[Na,Ca]Al_2Si_2O_8$) fractionation during petrogenesis. During the evolution of magma under reduced conditions, Eu can be partially reduced from trivalent state to divalent state, which leads it mobilizing from igneous rocks and then easily substituting for Ca in plagioclase feldspar (Drysdale, 2008; Krauskopf and Bird, 1995; Johannesson & Lyons, 1994; Cullers and Graf, 1984; Henderson, 1984; Hanson, 1980).

6.8 Chapter summary

- A MREE enrichment pattern over both LREE and HREE, and LREE enrichment relative to HREE is noticed on the PAAS-normalized REE distribution pattern at G2 to G5 under all flow conditions (5.53 - 115.1 L/s for G5).

- G1 (Gate Gill upstream of mine discharge) and G7 show a relatively similar PAAS-normalized REE distribution pattern, which is MREE enrichment pattern over both LREE and HREE, and HREE enrichment relative to LREE under all flow conditions (203 – 10200 L/s for G7).

- The REE fractionation pattern in the Gate Gill and River Glendermackin is mainly controlled by their source rocks leachate patterns. The distribution pattern at Gate Gill downstream of the mine discharge (G3 to G5) is expected to mainly reflect those of the discharges from Threlkeld mines (including spoil-related drainage). The source rock type of Gate Gill upstream of the mine discharge (G1) and the River Glenderamackin (G7) is likely to be similar, but differs from that of Threlkeld mine.

- Threlkeld mine is expected to have high content of plagioclase.

- Speciation modelling shows that free REE (Ln^{3+}) and REE sulphate complexes ($LnSO_4^+$) are the dominant species in Gate Gill (G1 to G5), while Ln^{3+} and REE carbonate complexes ($LnCO_3^+$) are the most important species in the River Glenderamackin downstream of Gate Gill (G7), under all flow conditions.

- Solution chemistry has the ability to fractionate REE when the degree of adsorption is higher (pH reaches ~5). In the absence of strong REE complexes ($LnCO_3^+$), solution chemistry-related processes lead to HREE being preferentially scavenged by >0.1µm and / or suspended solid (Fe and/ or Al oxyhydroxides) relative to LREE and MREE. In the presence of $LnCO_3^+$, LREE have a greater affinity for the >0.1µm and/ or suspended solid (Fe and / or Al oxyhydroxides) relative to MREE and HREE.

Chapter 7 Conclusion

7.1 Introduction

This chapter firstly demonstrates the achievements and main conclusions of this project in Section 7.2. Section 7.3 then describes the potential future work which would help to provide further understanding of the controls on rare earth element behaviour in the Gate Gill and other mining-impacted watercourses.

7.2 Thesis achievements

The main achievements of this study are as follows:

7.2.1 Understanding REE source and behaviour in a metal mine polluted stream: the Gate Gill

Comprehensive field sampling was undertaken 13 times, across a range of hydrological conditions, between February 2016 and September 2017. Sampling sites ranged from upstream of the Woodend low level to the River Glenderamackin downstream of its confluence with the Gate Gill. Complete analysis of water samples was undertaken which, in addition to REE, included all variables that may influence the behaviour and fractionation of the REE: pH and other field measurements, metals including Fe and Al, and anions. At each sampling site water was filtered through 0.005µm (for the last 7 sample campaigns), 0.1µm and 0.45µm pore size filter to obtain the REE and other metals concentration in different phases (especially <0.005µm and / or <0.1µm, >0.005µm and / or >0.1µm and >0.45µm) under varying hydrological condition.

Synchronous flow measurement and water quality monitoring enabled REE loads across varying hydrological condition to be determined. REE load data were used to show the sources of REE to the Gate Gill under different flow conditions. The Woodend mine water discharge is the most important source of REE content to Gate Gill under all flow conditions. However, spoil heaps and remobilised REE-containing sediments also appear to contribute to REE content in Gate Gill at higher flows, when the total REE load in the Gate Gill is higher than that of the Woodend Low Level mine water. The overall contribution of Threlkeld mine to REE load in the River Glenderamackin is quite limited though. Re-suspended REE-containing sediment appears to be an important source of REE in the River Glenderamackin under higher flows. The Bannerdale mine, in the upper reaches of the Glenderamackin

catchment, may contribute to the REE content of the River Glenderamackin under higher flow, though this would need further investigation to be confirmed.

7.2.2 Development of a methodology for interference removal during REE analysis

Mathematical correction equations were developed to take account of the potential polyatomic interference(s) on selected isotopes of REE. The influence of each potential polyatomic interference on the accuracy of measured REE results for the samples collected in this study was checked.

LREEO and MREEO interferences were negligible for Gate Gill samples and no corrections for these interferences were required. The errors caused by BaO on Eu for samples from sites G1 and G7 were relatively large, but BaO had a negligible influence on the accuracy of Eu measurement at sites G2, G3, G4 and G5 (Woodend Low Level mine water and Gate Gill downstream of mine water). The correction for BaO interference on Eu was made for all samples collected from 15/09/2016 to 14/09/2017 based on the correction factor (CF) obtained from single Ba solution measurement before sample measurement, followed by application of the correction equation. BaO interference on Eu for all samples was reduced to a negligible level after correction.

7.2.3 A new WATEQ4F database for REE speciation modelling

The calculation of REE speciation for Gategill samples has been performed through PHREEQC. The database used for REE speciation modelling was built using the base data from WATEQ4F and thermodynamic data of REE which includes (1) the infinite dilution stability constants of $LnSO_4^+$, $LnCO_3^+$, $Ln(CO_3)_2^-$, $LnHCO_3^{2+}$, $LnOH^{2+}$, LnF^{2+}, $LnCl_2^+$ obtained from the most recent published papers; (2) The activity coefficients of individual ions using the Davies equation since it is suitable for the ionic strength of Gate Gill samples. The REE speciation calculation for each sampling site's water was performed based on a temperature of 25^{o}C.

7.2.4 Identification of the main controls on REE transformation

pH and the formation of Fe, Al oxyhydroxides are the main factors that control REE transformation from dissolved (<0.005µm) to suspended solid / solid phases in Gate Gill. pH has a master control on REE adsorption; there is an inverse correlation between pH and degree of REE adsorption. The degree of REE adsorption at G3 and G4 under all flow conditions (5.53 - 115.1 L/s for G5) and at G5 under low flow conditions (5.53 - 40.1L/s for

G5) is quite low, as a result of the low pH at G3 to G5 under such flow conditions (mean pH at G3, G4 and G5 was 4.18, 4.4 and 4.44 respectively). The degree of REE adsorption at G5 under higher flow conditions with higher pH (mean value of 5.11) is expected to be relatively higher, and at G7 under all flow conditions (203 – 10200 L/s for G7), with much higher pH (mean value of 6.05), is expected to be quite high. REE in the suspended solids (> 0.005µm) are expected to be mainly associated with freshly formed Fe and Al oxyhydroxides flocs and secondary Fe and Al oxyhydroxides precipitates.

7.2.5 Identification of the main factors influencing REE fractionation under different hydrogeochemical conditions

A source-related pattern (result of interaction between whole source-rocks and aqueous fluids passing the whole source-rocks) has the major control on the REE fractionation pattern at G3 to G5 and G7 under all flow conditions (5.53 - 115.1 L/s for G5). This is because the PAAS normalized REE distribution patterns in dissolved (< 0.005µm), < 0.1µm, suspended solids (> 0.005µm) and unfiltered phase at each of these sampling sites under all flow conditions are similar.

G1 and G7 have a similar PAAS-normalized REE distribution pattern, which is MREE enrichment over both LREE and HREE, and HREE enrichment relative to LREE. The PAAS-normalized REE distribution pattern at G2 to G5 (which differs from that at G1 and G7) is MREE enrichment over both LREE and HREE, and LREE enrichment relative to HREE. The distribution pattern at G2 to G5 is expected to mainly reflect those of the discharges from Threlkeld mines (including spoil-related drainage). The Gate Gill upstream of the mine discharge, and the River Glenderamackin, have a similar source rock type, which differs from that of Threlkeld mine.

MREE enrichment on PAAS normalized REE distribution pattern at all sampling sites is expected to be caused by the dissolution / desorption / exchange of the readily soluble or leachable MREE enriched minerals / amorphous phases within the source-rocks. A positive Eu anomaly on the PAAS-normalized REE distribution pattern at G2 to G5 indicates that plagioclase largely exists in the Threlkeld mine.

Free REE ions and REE sulphate complexes are the main REE species in the Gate Gill downstream of the mine water discharge. Solution chemistry has little influence on REE distribution patterns at G3 to G4 under higher flow conditions (87.59 - 115.1L/s for G5) when

noticeable REE are present as suspended solids (> 0.005µm), as a result of low degree of REE adsorption. The fractionation pattern at G3 and G4 under all flow conditions entirely inherits the patterns of REE fractionation in the leachates from Threlkeld mine.

At G5, under lower flow conditions (5.53-40.1L/s for G5) when little REE are present in suspended solids and / or > 0.1 µm, the distribution pattern of REE entirely inherits the leachates of Threlkeld mine. At G5 under higher flow conditions (45.42 - 115.1 L/s for G5), when the degree of REE adsorption is relatively high compared to that at G3 and G4, HREE have a greater affinity for the > 0.1 µm and / or suspended solid. This is the result of surface complexation-related fractionation in the absence of strong REE complexes. In addition, Y has a weak affinity for the suspended solids compared to the other HREE, which is also the result of surface complexation induced fractionation. This suggests that Fe oxyhydroxide is at least one important substance for scavenging REE from dissolved phase at G5 during higher flow conditions (45.42-115.1L/s for G5). Therefore, the demonstrated PAAS-normalized REE distribution pattern at G5 under higher flow conditions (45.42 - 115.1L/s) is a combination of both process-related and source-related process effects. But source-related processes have the major control on the overall PAAS-normalized REE distribution pattern at G5 under higher flow conditions.

Free REE and REE-carbonate are the dominant species in the River Glenderamackin downstream of Gate Gill under all flow conditions (203 – 10200 L/s for G7). Overall, the presence of strong REE-carbonate complexes at G7 leads to LREE having a greater affinity for the suspended solids. Solution complexation appear to be the main control on process-related fractionation of REE. Both solution chemistry and source-related processes have some influence on the overall PAAS-normalized REE distribution pattern at G7. But the source-related process seems to exert more control on the PAAS-normalized REE distribution pattern.

7.3 Future work

Possible future research avenues are as follows:

(1) Perform thorough dissolution and leaching experiments on spoil samples from heaps located near G3. Compare the PAAS-normalized REE distribution pattern of whole spoil samples and spoil samples leachate with the PAAS-normalized REE distribution pattern at G2 to G5 in order to establish:

- whether the PAAS-normalized REE distribution pattern of spoil samples leachate differs from that of whole spoil samples in order to understand whether solution chemistry fractionates REE during the water-rock interaction and whether leachate has a MREE enrichment pattern relative to whole spoil samples;

- demonstrate whether the PAAS-normalized REE distribution pattern at G2 to G5 is similar to that of spoil sample leachate, but differs from that of whole spoil samples, as this would show whether the PAAS- normalized distribution pattern at G2 to G5 is controlled by source-rock leachates or the whole source-rocks.

(2) Perform complete dissolution of sediments from G5 and G7, and use PAAS-normalized REE distribution patterns of G5 and G7 sediment, as supplementary data to demonstrate the influence that source-related (source rock leachates) and process-related fractionation have on the REE distribution pattern of these sediments.

(3) Extract REE from sediments at G3 to G7 by performing discrete extraction to further understand which materials scavenge REE from water phase.

(4) Measure organic content at sampling sites, and perform REE speciation modelling that includes organic complexes, to demonstrate whether REE organic complexes are a relatively importance species at sampling sites (especially G7). This could indicate whether REE organic complexes also play a role in solution complexation- related fractionation in these waters.

(5) Further research should be conducted in both smaller and larger river catchments to understand the influence of scale on the controlling factors in REE fractionation. In particular, in smaller rivers source rock is widely recognised as a dominant control on REE geochemistry (as in this study), but there is ongoing debate in the scientific literature as to the relative roles of source rock and solution chemistry on REE geochemistry in larger river systems.

(6) Establish the potential for low cost ‘passive’ treatment units for recovery of REE from mine waters. Given the known behaviour of REE, illustrated in this study, lab-scale proof-of principle experiments should be undertaken to evaluate the potential of low cost treatment systems to accumulate REE and simultaneously remove them from riverine environments.

References

Agilent Technologies, 2009. Comparing Collision/Reaction Cell Modes for the Measurement of Interfered Analytes in Complex Matrices using the Agilent 7700 Series ICP-MS. Technical Overview. *Agilent Technologies, USA*.

Agilent Technologies, 2012. Agilent 7700 series ICP-MS Techniques and Operation. *Agilent Technologies, USA*.

Agilent Technologies. 2005. Inductively Coupled Plasma Mass Spectrometry, A Primer. *Agilent Technologies, USA*.

Aide, M.T. and Aide, C. 2012. Rare earth elements: their importance in understanding soil genesis. *International Scholarly Research Network Soil Science*, **2012**, 1-11.

Alpers, C.N., Taylor, H.E. and Domagalski, J.L. 2000. Metals Transport in the Sacramento River, California, 1996–1997. Volume 1: Methods and Data. *US Geological Survey,* Water-Resources Investigations Report 99-4286. Sacramento, California.

Anawar, H.M., Freitas, M.C., Canha, N., Dionisio, I., Dung, H.M., Galinha, C. and Pacheco, A.M.G. 2012. Assessment of bioaccumulation of REEs by plant species in a mining area by INAA. Journal of *Radioanalytical and Nuclear Chemistry*, **294**, 377–381.

Anders, E. and Grevesse, N. 1989. Abundances of the elements: Meteoritic and solar. *Geochimica et Cosmochimica Acta*, **53**, 197-214.

Appelo, C.A.J. Postma, D. 2005. *Geochemistry, Groundwater and Pollution*, 2nd edition. Balkema Publishers, 649 pp.

Aries, S., Valladon, M., Polvé, M. and Dupré, B. 2000. A Routine Method for Oxide and Hydroxide Interference Corrections in ICP-MS Chemical Analysis of Environmental and Geological Samples. *Geostandards Newsletter, Journal of Geostandards and Geoanalysis*, **24** (1), 19-31.

Astrom, M. 2001. Abundance and fractionation patterns of rare earth elements in streams affected by acid sulphate soils. *Chemical Geology*, **175**, 249–258.

Astrom, M.E., Osterholm, P., Gustafsson, J.P., Nystrand, M., Peltola, P., Nordmyr, L. and Boman, A. 2012. Attenuation of rare earth elements in a boreal estuary. *Geochimica et Cosmochimica Acta*, **96**, 105–119.

Bailey, M. 2016. Recovering resources from abandoned metal mine waters: An assessment of the potential options at passive treatment systems. PhD Thesis, Newcastle University.

Banks, D., Hall, G., Reimann, C. and Siewers, U. 1999. Distribution of rare earth elements in crystalline bedrock groundwaters: Oslo and Bergen regions, Norway. *Applied Geochemistry*, **14**, 27–39.

Banner, J.L., Hanson, G.N. and Meyers, W.J. 1988. Rare earth element and Nd isotopic variations in regionally extensive dolomites from the B~adington-Keokuk Formation (Mississippian): Implications for REE mobility during carbonate diagenesis. *Journal of Sedimentary Petrology*, **58**, 415-432.

Banner, J.L., Wasserburg, G.J., Dobson, P.F., Carpenter, A.B. and Moore, C.H. 1989. Isotopic and trace element constraints on the origin and evolution of saline groundwaters from central Missouri. *Geochimica et Cosmochimica Acta*, **53**, 383–398.

Barry, M.J. and Meehan, B.J. 2000. The acute and chronic toxicity of lanthanum to Daphnia carinata. *Chemosphere*, **41**, 1669–1674.

Bau M., Koschinsky A., Dulski P. and Hein J.R. 1996. Comparison of the partitioning behaviours of yttrium, rare earth elements, and titanium between hydrogenetic marine ferromanganese crusts and seawater. *Geochimica et Cosmochimica Acta*, **60**, 1709-1725.

Bau, M. 1991. Rare earth element mobility during hydrothermal and metamorphic fluid-rock interaction and the significance of the oxidation state of europium, *Chemical Geology*, **93**, 219-230.

Bau, M., 1999. Scavenging of dissolved yttrium and rare earths by precipitating iron oxyhydroxide; experimental evidence for Ce oxidation Y-Ho fractionation lanthanide tetrad effect. *Geochimica et Cosmochimica Acta*, **63**, 67–77.

Benischke, R. and Harum, T. 1990. Determination of discharge rates in turbulent streams by salt tracer dilution applying a microcomputer system. Comparison with current meter measuremenu. *International Association of Hydrological Sciences*, **193**, 215-221

Beven, K.J. 1989. Interflow. In: Morel-Seytoux, H.J. (ed.) *Unsaturated flow in hydrologic modeling: theory and practice*, Kluwer, Dordrecht, pp191–219.

Biddau, R., Bensimon, M., Cidu, R. and Parriaux, A. 2009. Rare earth elements in groundwater from different Alpine aquifers. *Chemie der Erde - Geochemistry*, **69**, 327-339.

Bleavins, K., Peron, P., Naik, M., Rehman, M., Aslam, M.N., Dame, M.K., Meshinchi, S., Bhagavathula, N. and Varani, J. 2012. Stimulation of fibroblast proliferation by insoluble gadolinium salts. *Biological Trace Element Research*, **145**, 257–267.

Borkowski, M. and Siekierski, S. 1992. Factors affecting the position of Y and actinides(III) with respect to lanthanides in the NH4SCN - Adogen-464SCN extraction system. *Radiochimica Acta*, **56**, 31-35.

Bowen, H.J.M., 1979. *Environmental Chemistry of the Elements*. Academic Press, London, 330 pp.

Boynton, W.V. 1984. Chapter 3- Cosmochemistry of the rare earth elements: Meteorite studies. *Developments in Geochemistry*, **2**, 63-114.

British Geological Survey, 1992. Regional geochemistry of the Lake District and adjacent areas. *British Geological Survey*, Nottingham.

British Geological Survey, 2011. Rare Earth Elements. *British Geological Survey*.

British Standard 3680-2A, 1995. Liquid Flow Measurement in Open Channels: Dilution Methods- General. *British Standard Institution*, London.

British Standard ISO 10304-1, 2009. Water quality- Determination of dissolved anions by liquid chromatography of ions. Part 1: Determination of bromide, chloride, fluoride, nitrate, nitrite, phosphate and sulfate (ISO 10304-1:2007). *British Standard Institution*, London.

British Standard ISO 11885, 2009. Water quality- Determination of selected elements by inductively coupled plasma optical emission spectrometry (ICP-OES), (ISO 11885:2007). *British Standard Institution*, London.

British Standard ISO 17294-1, 2006. Water quality- Application of inductively coupled plasma mass spectrometry (ICP-MS)- Part 1: General guidelines. *British Standard Institution*, London.

British Standard ISO 17294-2, 2016. Water quality — Application of inductively coupled plasma mass spectrometry (ICP-MS). Part 2: Determination of selected elements including uranium isotopes (ISO 17294-2:2016). *British Standard Institution*, London.

British Standard ISO 5667-1: 2006. Water quality- Sampling- Part 1: Guidance on the design of sampling programmes and sampling techniques. *British Standard Institution*, London.

British Standard ISO 5667-6, 2016. Water quality — Sampling Part 6: Guidance on sampling of rivers and streams (ISO 5667-6:2014). *British Standard Institution*, London.

Brookins, D.G. 1988. *Eh-pH Diagrams for Geochemistry*. Springer-Verlag, New York, 176pp.

Byrne, R.H. and Kim, K.H. 1993, Rare earth precipitation and coprecipitation behavior: The limiting role of PO_4^{3-} on dissolved rare earth concentrations in seawater. *Geochimica et Cosmochimica Acta*, **57**, 519 - 526.

Byrne, R.H. and Sholkovitz, E.R. 1996. Marine chemistry and geochemistry of lanathanides. In: Gschneidner, K.A., Eyring, L. (Eds.). *Handbook on the Physics and Chemistry of Rare Earths*, Elsevier, Amsterdam, pp. 497–593.

Cameron, A. and Withey, L. 2017. *Ore Mining In the Lake District*. Amberley, Gloucestershire, 96 pp.

Cao, X., Yin, M. and Wang, X. 2001. Elimination of the spectral interference from polyatomic ions with rare earth elements in inductively coupled plasma mass spectrometry by combining algebraic correction with chromatographic separation. *Spectrochimica Acta Part B*, **56**, 431-441.

Carlson, L., Bigham, J.M., Schwertmann, U., Kyek, A. and Wagner, F. 2002. Scavenging of As from acid mine drainage by schwertmannite and ferrihydrite: a comparison with synthetic analogues. *Environmental Science and Technology*, **36**, 1712–1719.

Castor, S.B. and Hedrick, J.B. 2006. Rare Earth Elements. In *Industrial Minerals and Rocks*. 769-792pp.

CAT, 2013. The Newsletter of the Cumbria Amenity Trust Mining History Society. No. 113, 1-36.

Chien, N.X., Khai, P. N., Hien, T. D., Nguyen, D., Bot, D.C., Trung, T.V., Cuc, N.T., Minh, L.H., Thuc, N.V., Ngan, B.T. and Thuan, D.V. 2006. The determination of rare earth elements in geological and environmental samples by inductively coupled plasma mass spectrometry. *The Annual Report for 2006, VAEC*, **6** (31), 217-225.

Cidu, R. and Biddau, R. 2007. Transport of trace elements under different seasonal conditions: Effects on the quality of river water in a Mediterranean area. *Applied Geochemistry*, **22**, 2777–2794.

Cobelo-García, A., Filella, M., Croot, P., Frazzoli, C., Du Laing, G., Ospina-Alvarez, N., Rauch, S., Salaun, P., Schäfer, J. and Zimmermann, S. 2015. COSTaction TD1407: network on technology-critical elements (NOTICE)—from environmental processes to human health threats. *Environmental Science and Pollution Research*, **22**, 15188–15194.

Cooper, A.H., Millward, D., Johanson, E.W. and Soper, N.J. 1993. The early Palaeozoic evolution of northwest England. *Geological Magazine*, **130**, 711-724.

Cooper, A.H., Rushton, A.W.A., Molyneux, S.G., Hughes, R.A., Moore, R.M. and Webb, B.C. 1995. The stratigraphy, correlation, provenance and polaeogeography of the Skiddaw Group (Ordovician) in the English Lake District. *Geological Magazine*, **132**, 185-211.

Cooper, D.C. and Read, D. 1983. The distribution of monazite in panned stream sediment concentrates from Britain: palaeogeographic implications. *Report of the British Geological Survey*, No. 84, Vol. 1, 1–4.

Coppin F., Berger G., Bauer A., Castet S. and Loubet M. 2002. Sorption of lanthanides on smectite and kaolinite. *Chemical Geology*. **182**, 57–68.

Coryell, C.D., Chase, J.W. and Winchester, J.W. 1963. A procedure for geochemical interpretation of terrestrial rare-earth abundance patterns. *Journal of Geophysical Research*, **68**, 559–566.

Croot, 2017. The Measurement of Soluble (< 10 kDa) Trace Metals in seawater by the Vivaflow 50. *Sartorius application note*, Publication No.: SL-4065-e170804, Ver. 08.

Cullers, R.L. and Graf, J.L. 1984. Rare earth elements in igneous rocks of the continental crust: Intermediate and silicic rocks--ore petrogenesis. *Rare earth element geochemistry*, **2**, pp 275 – 316.

Dams, R. F. J., Goossens, J. and Moens, L. 1995. Spectral and non-spectral interferences in Inductively Coupled Plasma Mass-Spectrometry. *Microchimica Acta*, **119**, 277-286.

Davranche, M., Pourret, O., Gruau, G. and Dia, A. 2004. Impact of humate complexation on the adsorption of REE onto Fe oxyhydroxide. *Journal of Colloid and Interface Science*, **277**, 271–279.

Day, T.J. 1977. Field procedures and evaluation of a slug dilution gauging method in mountain streams. *Journal of Hydrology (New Zealand)*, **16**, 113–133.

De Baar, H.J.W., Bacon, M.P., Brewer, P.G. and Bruland, K.W. 1985. Rare earth elements in the Atlantic and Pacific Oceans. *Geochimica et Cosmochimica Acta*, **49**, 1943–1959.

De Baar, H.J.W., German, C.R., Elderfield, H. and Gaans, P.V. 1988. Rare earth element distributions in anoxic waters of the Cariaco Trench. *Geochimica et Cosmochimica Acta*, **52**, 1203-1219.

De Boer, J.L.M. 2000. Real-time adjustment of ICP-MS elemental equations. *Journal of Analytical Atomic Spectrometry*, **15**, 1157-1160.

De Carlo, E.H., Wen, X. and Irving, M. 1998. The influence of redox reactions on the uptake of dissolved Ce by suspended Fe and Mn oxide particles. *Aquatic Geochemistry*, **3**, 357-389.

De Carlo, E.H., Wen, X. and Irving, M. 1998. The influence of redox reactions on the uptake of dissolved Ce by suspended Fe and Mn oxide particles. *Aquatic Geochemistry*, **3**, 357-389.

De Carlo, E.H., Wen, X.Y. and Cowen, J.P. 2000. Rare earth element fractionation in hydrogenetic Fe–Mn crusts: the influence of carbonate complexation and phosphatization on Sm/Yb ratios. *Society for Sedimentary Geology Special Publication*, pp. 271–285.

Dia, A., Gruau, G., Olivié-Lauquet, G., Riou, C., Molénat, J. and Curmi, P. 2000. The distribution of rare earth elements in groundwaters: assessing the role of source-rock composition, redoxchanges and colloidal particles. *Geochimica et Cosmochimica Acta*, **64**, 4131–4151.

Dingman, S. L. 1994. *Physical Hydrology*. Prentice-Hall, Inc, New Jersey, 575 pp.

Doherty, W. 1989. An internal standardization procedure for the determination of yttrium and the rare earth elements in geological materials by inductively coupled plasma-mass spectrometry. *Spectrochimica Acta*, **48B** (3), 263-280.

Drysdale, J. 2008. Element mobility as a result of chemical weathering in a granitoid near Valparaiso, Chile. PhD Thesis, Dalhousie University.

Dulski, P. 1994. Interferences of oxide, hydroxide and chloride analyte species in the determination of rare earth elements in geological samples by inductively coupled plasma-mass spectrometry. *Fresenius' Journal of Analytical Chemistry*, **350**, 194-203.

Dzombak, D.A. and Morel, F.M.M. 1990. *Surface Complexation Modelling: Hydrous Ferric Oxide*. John Wiley, 416pp.

Edmunds,W.M., Guendouz, A.H., Mamou, A., Moulla, A., Shand, P. and Zouarid, K. 2003. Groundwater evolution in the continental intercalaire aquifer of southern Algeria and Tunisia: trace element and isotopic indicators. *Applied Geochemistry*, **18**, 805–822.

Edward, M., Quinn, J.A., Burden, A.D., Newton, B.B. and Jardine, A.G. 2010. Effect of different classes of gadolinium-based contrast agents on control and nephrogenic systemic fibrosis-derived fibroblast proliferation. *Radiology*, **256**, 735–743.

Elbaz-Poulichet, F. and Dupuy, C. 1999. Behavior of rare earth elements at the freshwater-seawater interface of two acid mine rivers: the Tinto and Odiel (Andalusia, Spain). *Applied Geochemistry*, **14**, 1063–1072.

Elder, K., Kattelmann, R. and Ferguson, R. 1990. Refinements in dilution gauging for mountain streams. *In Hydrology in mountainous regions. I – Hydrological measurements; the water cycle, International Association for Hydrological Science Publication*. **193**, 247–254.

Elderfield, H. 1988. The oceanic chemistry of the rare-earth elements. *Philosophical Transactions of the Royal Society of London. Series A, Mathematical and Physical Sciences*, **325**, pp. 105-126.

Elderfield, H. and Sholkovitz, E.R. 1987. Rare earth elements in the pore waters of reducing nearshore sediments. *Earth and Planetary Science Letters*, **82**, 280-288.

Elderfield, H., Upstill-Goddard, R. and Sholkovitz, E.R. 1990. The rare earth elements in rivers, estuaries, and coastal seas and their significance to the composition of ocean waters. *Geochimica et Cosmochimica Acta*, **54**, 971–991.

Environment Agency, 1999. Local environment agency plan, west Cumbria action plan. Environment Agency, Bristol.

EPA, 1994. EPA Method 200.8. Revision 5.4: Determination of Trace Elements in Waters and Wastes by Inductively Coupled Plasma – Mass Spectrometry. *U.S. Environmental Protection Agency*, Ohio.

EPA, 1998. EPA method: 6020A- Inductively coupled plasma- mass spectrometry. *U.S. Environmental Protection Agency*, Ohio.

EPA, 2012. Rare Earth Elements: a review of production, processing, recycling, and associated environmental issue. United States Environmental Protection Agency.

European Commission, 2017. List of Critical Raw Materials for the EU. Available online at: https://eur-lex.europa.eu/legal-content/EN/TXT/?uri=CELEX:52017DC0490

Evensen, N.M., Hamilton, P.J. and O'Nions, R.K. 1978. Rare-earth abundances in chondritic meteorites. *Geochimica et Cosmochimica Acta*, **42**, 1199-1212.

Fee, J.A., Gaudette, H.E., Lyons, W.B. and Long, D.T. 1992. Rare-earth element distribution in Lake Tyrrell groundwaters, Victoria, Australia. *Chemical Geology*, **96**, 67-93.

Ferreira da Silva, E., Bobos, I., Matos, J.X., Patinha, C., Reis, A.P. and Fonseca, E.C. 2009. Mineralogy and geochemistry of trace metals and REE in volcanic massive sulfide host rocks, stream sediments, stream waters and acid mine drainage from the Lousal mine area (Iberian Pyrite Belt, Portugal). *Applied Geochemistry*, **24**, 383-401.

Firsching, F.H. and Brune, S.N. 1991. Solubility products of the trivalent rare-earth phosphates. *Journal of Chemical and Engineering Data*, **36**, 93-95.

Fu, Y., Li, F., Xu, T., Cai, S., Chu, W., Qiu, H., Sha, S., Cheng, G. and Xu, Q. 2014. Bioaccumulation, subcellular, and molecular localization and damage to physiology and ultrastructure in Nymphoides peltata (Gmel.) O. Kuntze exposed to yttrium. *Environmental Science and Pollution Research*, **21**, 2935–2942.

Gaillardet, J., Millot, R. and Dupré, B. 2003. Chemical denudation rates of the western Canadian orogenic belt: the Stikine terrane. *Chemical Geology*, **201**, 257-279.

Gammons C.H., Wood S.A., Jonas, J.P., and Madison, J.P. 2003. Geochemistry of the rare-earth elements and uranium in the acidic Berkeley Pit lake, Butte, Montana. *Chemical Geology*, **198**, 269–288.

Gammons, C.H., Wood, S.A., Pedrozo, F., Varekamp, J.C., Nelson, B.J., Shope, C.L. and Baffico, G. 2005. Hydrogeochemistry and rare earth element behavior in a volcanically acidified watershed in Patagonia, Argentina. *Chemical Geology*, **222**, 249–267.

Gao Z. and Zhou Q. 2011. Contamination from rare earth ore strip mining and its impacts on resources and eco-environment. *Chinese Journal of Ecology*, **30**, 2915-2922.

Garbarino, J.R. and Taylor, H.E. 1987. Stable Isotope Dilution Analysis of Hydrologic Samples by Inductively Coupled Plasma Mass Spectrometry. *Analytical Chemistry*, **59** (11), 1568-1575.

Geological society, 2011. Rare earth elements, A briefing note by Geological Society of London. https://www.geolsoc.org.uk/~/media/shared/documents/policy/Rare%20Earth%20Elements%20briefing%20note%20final%20%20%20new%20format.pdf, *Geological Society, London*.

German, C.R., Klinkhammer, G.P., Edmond, J.M., Mitra, A. and Elderfield, H. 1990. Hydrothermal scavenging of rare-earth elements in the ocean. *Nature*, **345**, 516- 518.

Gimeno Serrano, M.J., Auqué Sanz, L.F. and Nordstrom, D.K. 2000. REE speciation in low-temperature acidic waters and the competitive effects of aluminum. *Chemical Geology*, **165**, 167– 180.

Gimeno, M.J., Augue´, L.F., Nordstrom, D.K. and Bruno, J., 1996. Rare earth element (REE) geochemistry and the tetrad effect in the naturally occurring acidic waters of Arroyo Del Val, northeastern Spain. *Geological Society of America Annual Meeting*, A-468.

Goldstein, S. J. and Jacobsen, S. B. 1988b. REE in the Great Whale River estuary, northwest Quebec. *Earth Planet Science Letters.* **88,** 241-252.

Goldstein, S.J. and Jacobsen, S.B. 1987. The Nd and Sr isotopic systematics of river water dissolved material: Implications for sources of Nd and Sr in seawater. *Chemical Geology*, **66**, 245-272.

Goldstein, S.J. and Jacobsen, S.B. 1988a. Rare earth elements in river waters. *Earth and Planetary Science Letters*, **89**, 35-47.

Gonzalez, V. Vignati, D.A.L., Leyval, C. and Giamberini, L. 2014. Environmental fate and ecotoxicity of lanthanides: Are they a uniform group beyond chemistry? *Environment International*, **71**, 148–157.

González, V., Vignati, D.L.A., Pons, M., Montarges-Pelletier, E., Bojic, C. and Giamberini, L. 2015. Lanthanide ecotoxicity: First attempt to measure environmental risk for aquatic organisms. *Environmental Pollution*, **199**, 139-147.

Gosselin, D.G., Smith, M.R., Lepel, E.A. and Laul, J.C. 1992. Rare earth elements in chloride-rich groundwater, Palo Duro Basin, Texas, USA. *Geochimica et Cosmochimica Acta*, **56**, 1495- 1505.

Gromet, L.P., Haskin, L.A., Korotev, R.L. and Dymek, R.F. 1984. The "North American shale composite": its compilation, major and trace element characteristics. *Geochimica et Cosmochimica Acta*, **48**, 2469-2482.

Guo, H., Zhang, B., Wang, G. and Shen, Z. 2010. Geochemical controls on arsenic and rare earth elements approximately along a groundwater flow path in the shallow aquifer of the Hetao Basin, Inner Mongolia. *Chemical Geology*, **270**, 117–125.

Gupta, C.K. and Krishnamurthy, N. 2005. *Extractive Metallurgy of Rare Earths*. CRC Press, 484 pp.

Hall, G.E.M., Vaive, J.E. and McConnell, J.W. 1995. Development and application of a sensitive and rapid analytical method to determine the rare-earth elements in surface waters. *Chemical Geology*, **120**, 91–109.

Hamlin, S.H. 1988. *Depositional and ground-water flow systems of the Carrizo-upper Wilcox, South Texas*. Report of Investigations No.175, Bureau of Economic Geology, 61 pp.

Hanson, G.N. 1980. Rare earth elements in petrogenetic studies of igneous systems. *Annual Review of Earth and Planetary Sciences*, **8**, 371–406.

Harben, P.W. 2002. *Industrial Minerals Handybook: a guide to markets, specifications & prices*. 4th edition, Surrey, 412pp.

Haskin L.A., Frey, F.A., Schmitt, R.A. and Smith, R.H. 1966. Meteoritic, solar, and terrestrial rare earth distributions. *Physics and Chemistry of the Earth*, **7**, 167-321.

Haskin, L. A., Haskin, M. A., Frey, F. A., and Wildeman T. R. 1968. Relative and absolute terrestrial abundances of the rare earths. *Origin and Distribution of the Elements*, volume in International Series of Monographs in Earth Sciences, pp. 889-911.

Haskin, L. and Gehl, M.A. 1962. The rare-earth distribution in sediments. *Journal of Geophysical Research*, **67**, 2537-2541.

Haskin, M.A. and Haskin, L.A. 1966. Rare earths in European shales: A redetermination. *Science*, **154**, 507-509.

Henderson P. 1984. *Rare Earth Element Geochemistry*. Elsevier, Amsterdam, 510 pp.

Henderson, P. 1984. *Rare Earth Element Geochemistry*. Elsevier Science, 510 pp.

Herrmann, H., Nolde, J., Berger, S. and Heise, S. 2016. Aquatic ecotoxicity of lanthanum – A review and an attempt to derive water and sediment quality criteria. *Ecotoxicology and Environmental Safety*, **124**, 213-238.

Herschy, R.W., 2009. *Streamflow Measurement.* (3rd Edition), Taylor & Francis, Abingdon, 507pp.

Hewer, 1984. Bannerdale lead mine. *British mining*, **25**, 26-30.

Hiscock, K. M. 2005. *Hydrogeology Principles and Practice*. Blackwell Science Ltd, Oxford, UK, 389pp.

Hoyle, J., Elderfield, H., Gledhill, A. and Greaves, M. 1984. The behaviour of the rare earth elements during mixing of river and sea waters. *Geochimica et Cosmochimica Acta*, **48**, 143-149.

https://restorerivers.eu/wiki/index.php?title=Case_study%3AGategill_Beck%3A_Abandoned_Metal_Mines

Huang, P.M., Li, Y. and Sumner, M.E. 2011. *Handbook of Soil Sciences: Properties and Processes*, 2nd edition. CRC Press, 1442pp.

Inguaggiato, C., Censi, P., Zuddas, P., Londoño, J.M., Chacón, Z., Alzate, D., Brusca, L. and D'Alessandro, W. 2015. Geochemistry of REE, Zr and Hf in a wide range of pH and water composition: The Nevado del Ruiz volcano-hydrothermal system (Colombia). *Chemical Geology*, **417**, 125–133.

Ixer, R.A. and Stanley, C.J. 1987. A silver-nickel-cobalt mineral association at Tynebottom Mine, Garrigill, near Alston, Cumbria. *Proceedings of the Yorkshire Geological Society*, **46**, 133–139.

Ixer, R.A., Young, B. and Stanley, C.J. 1996. Bismuth- bearing assemblages from the Northern Pennine Orefield. *Mineralogical Magazine*, **60**, 317–324.

Janssen, R.P.T. and Verweij, W. 2003. Geochemistry of some rare earth elements in groundwater, Vierlingsbeek, The Netherlands. *Water Research*, **37**, 1320–1350.

Jarvis, K.E. 1989. Determination of the rare earth elements in geological samples by inductively coupled plasma mass spectrometry. *Journal of Analytical Atomic Spectrometry*, **4**, 563-570.

Jenkins, W., Perone, P., Walker, K., Bhagavathula, N., Aslam, M.N., DaSilva, M., Dame, M.K. and Varani, J. 2011. Fibroblast response to lanthanoid metal ion stimulation: potential contribution to fibrotic tissue injury. *Biological Trace Element Research*, **144**, 621–635.

Johannesson K. H., Lyons W. B. and Bird D. A. 1994. Rare earth element concentrations and speciatlon in alkaline lakes from the western U.S.A. *Geophysical Research Letters*, **21**, 773-776.

Johannesson, K.H. and Hendry, M.J. 2000. Rare earth element geochemistry of groundwaters from a thick till and clay-rich aquitard sequence, Saskatchewan, Canada. *Geochemica et Cosmochimica Acta*, **64**, 1493.

Johannesson, K.H. and Lyons, W.B. 1994. The rare earth element geochemistry of Mono Lake water and the importance of carbonate complexing. *Limnology and Oceanography*, **39**, 1141 - 1154.

Johannesson, K.H. and Lyons, W.B. 1995. Rare-earth element geochemistry of Colour Lake, an acidic fresh water lake on Axel Heiberg Island, Northwest Territories, Canada. *Chemical Geology*, **119**, 209-223.

Johannesson, K.H. and Zhou, X. 1997. Geochemistry of the rare earth elements in natural terrestrial waters: A review of what is currently known. *Chinese Journal of Geochemistry*, **16**, 20-42.

Johannesson, K.H. and Zhou, X.P. 1999. Origin of middle rare earth element enrichments in acid waters of a Canadian High Arctic lake. *Geochimica et Cosmochimica Acta*, **63**, 153–165.

Johannesson, K.H., Lyons, W.B., Fee, J.H., Gaudette, H.E. and John, M.M. 1994a. Geochemical processes affecting the acidic groundwaters of Lake Gilmore, Yilgarn Block, Western Australia: a preliminary study using neodymium, samarium, and dysprosium. *Journal of Hydrology*, **154**, 271-289.

Johannesson, K.H., Lyons, W.B., Stetzenbach, K.J. and Byrne, R.H. 1995. The solubility control of rare earth elements in natural terrestrial waters and the significance of PO_4^- and CO_3^- in limiting dissolved rare earth concentrations: a review of recent information. *Aquatic Geochemistry*, **1**, 157 - 173.

Johannesson, K.H., Lyons, W.B., Yelken, M.A., Gaudette, H.E. and Stetzenbach, K.J. 1996a. Geochemistry of the rare earth elements in hypersaline and dilute acidic natural terrestrial waters: complexation behavior and middle rare earth enrichments. *Chemical Geology*, **133**, 125-144.

Johannesson, K.H., Lyons, W.B., Yelken, M.A., Gaudette, H.E. and Stetzenbach, K.J. 1996a, Geochemistry of the rare earth elements in hypersaline and dilute acidic natural terrestrial waters: complexation behavior and middle rare earth enrichments. *Chemical Geology*, **133**, 125-144.

Johannesson, K.H., Stetzenbach, K.J. and Hodge, V.F. 1997a. Rare earth elements as geochemical tracers of regional groundwater mixing. *Geochimica et Cosmochimica Acta*, **61**, 3605–3618.

Johannesson, K.H., Stetzenbach, K.J., Hodge, V.F. and Lyons, W.B. 1996. Rare earth element complexation behavior in circumneutral pH groundwaters: assessing the role of carbonate and phosphate ions. *Earth and Planetary Science Letters*, **139**, 305-320.

Johannesson, K.H., Stetzenbach, K.J., Hodge, V.F., Kreamer, D.K. and Zhou, X. 1997b. Delineation of groundwater flow systems in the southern Great Basin using aqueous rare earth element distributions. *Ground Water*, **35**, 807–819.

Johannnesson, K.H, Farnham, I.M, Guo, C. and Stetzenbach, K.J. 1999. Rare earth element fractionation and concentration variations along a groundwater flow path within a shallow, basin-fill aquifer, southern Nevada, USA. *Geochimica et Cosmochimica Acta*, **63**, 2697-2708.

Johnston, D. and Rolley, S. 2008. Abandoned mines and the Water Framework Directive in the United Kingdom.

Jonasson, R.G., Bancroft, G.M. and Nesbitt, H.W. 1985. Solubilities of some hydrous REE phosphates with implications for diagenesis and sea water concentrations. *Geochimica et Cosmochimica Acta*, **49**, 2133-2139.

Kajiya, T., Aihara, M. and Hirata, S. 2004. Determination of rare earth elements in seawater by inductively coupled plasma mass spectrometry with on-line column pre-concentration using 8-quinolinole-immobilized fluorinated metal alkoxide glass. *Spectrochimica Acta Part B*, **59**, 543–550.

Kawabe, I., Ohta, A. and Miura, N. 1999b. Distribution coefficients of REE between Fe oxyhydroxide precipitates and NaCl solutions affected by REE-carbonate complexation. *Geochemical Journal*. **33**, 181–197.

Keasler, K. M. and Loveland, W. D. 1982. Rare earth elemental concentrations in some Pacific Northwest rivers. *Earth and Planetary Science Letters*. **61**, 68-72.

Klinkhammer, G., German, C.R., Elderfield, H., Greaves, M.J. and Mitra, A. 1994. Rare earth elements in hydrothermal fluids and plume particulates by inductively coupled plasma mass spectrometry. *Marine Chemistry*, **45**, 179-186.

Klungness, G.D. and Byrne, R.H. 2000. Comparatives hydrolysis behavior of the rare earths and yttrium: the influence of temperature and ionic strength. *Polyhedron*, **19**, 99–107.

Koeppenkastrop, D. and De Carlo, E.H. 1992. Sorption of rare- earth elements from seawater onto synthetic mineral particles: an experimental approach. *Chemical Geology*, **95**, 251– 263.

Köhler, S.J., Harouiya, N., Chaïrat, C. and Oelkers, E.H. 2005. Experimental studies of REE fractionation during water–mineral interactions: REE release rates during apatite dissolution from pH 2.8 to 9.2. *Chemical Geology*, **222**, 168–182.

Korotev R.L. 2009. "Rare Earth Plots" and the Concentrations of Rare Earth Elements Chondritic Meteorites. Available online at: (REE) in http://meteorites.wustl.edu/goodstuff/ree-chon.htm.

Krauskopf, K.B. and Bird, D.K. 1995. *Introduction to Geochemistry*. McGraw-Hill, New York, 452pp.

Kulaksiz, S. and Bau M. 2013. Anthropogenic dissolved and colloid/nanoparticles-bound samarium, lanthanumand gadolinium in the Rhine River and the impeding destruction of the natural rare earth element distribution in rivers. *Earth and Planetary Science Letters*, **362**, 43–50.

Kulaksiz, S. and Bau, M. 2011. Anthropogenic gadolinium as a microcontaminant in tap water used as drinking water in urban areas and megacities. *Applied Geochemistry*, **26**, 1877-1885.

Landa, E.R., Cravotta, C.A., Naftz, D.L., Verplanck, P.L., Nordstrom, D.K. and Zielinski, R.A. 2000. Geochemical investigations by the US Geological Survey on uranium mining, milling, and environmental restoration. *Technology*, **7**, 381–396.

Lee, J.H. and Byrne, R.H. 1992. Examination of comparative rare earth element complexation behavior using linear free-energy relationships. *Geochimica et Cosmochimica Acta*, **56**, 1127-1137.

Lee, J.H. and Byrne, R.H. 1993. Complexation behavior of the trivalent rare earth elements (Ce, Eu, Gd, Tb, Yb) by carbonate ions. *Geochimica et Cosmochimica Acta*, **57**, 295-302.

Lee, K.H., Oshima, M., Takayanagi, T. and Motomizu, S. 2000a. Simultaneous determination of lanthanoids and yttrium in rock reference samples by inductively coupled plasma-mass spectrometry coupled with cation exchange pretreatment. *Bulletin of the Chemical Society of Japan*. **73** (3), 615–622.

Lee, K.H., Shishido, S., Kusachi, I. and Motomizu, S. 2000b. Determination of lanthanoids and yttrium in JGb2 and JR3 by inductively coupled plasma-mass spectrometry after cation-exchange pretreatment. *Geochemical Journal*, **34**, 383- 393.

Lewis A.J., Komninou, A., Yardley, B.W.D. and Palmer, M.R. 1998. Rare earth element speciation in geothermal fluids from Yellowstone National Park, Wyoming, USA. *Geochimica et Cosmochimica Acta*, **62**, 657–663.

Leybourne, M.I. and Johannesson, K.H. 2008. Rare earth elements (REE) and yttrium in stream waters, stream sediments, and Fe-Mn oxyhydroxides: Fractionation, speciation, and controls over REE+ Y patterns in the surface environment. *Geochimica et Cosmochimica Acta*. **72**, 5962-5983.

Leybourne, M.I., Goodfellow, W.D., Boyle, D.R. and Hall, G.M. 2000. Rapid development of negative Ce anomalies in surface waters and contrasting REE patterns in groundwaters associated with Zn-Pb massive sulphide deposits. *Applied Geochemistry*. **15**, 695–723.

Li, J., Hong, M., Yin, X. and Liu, J. 2010. Effects of the accumulation of the rare earth elements on soil macrofauna community. *Journal of Rare Earths*, **28**, 957–964.

Li, X., Chen, Z., Chen, Z. and Zhang, Y. 2013. A human health risk assessment of rare earth elements in soil and vegetables from a mining area in Fujian Province, Southeast China. *Chemosphere*, **93**, 1240-1246.

Lichte, F.E., Meier, A.L. and Crock J.G. 1987. Determination of the rare-earth elements in geological materials by inductively coupled plasma-mass spectrometry. *Analytical Chemistry*, **59**, 1150-1157.

Lide, D.R. ed. 2005. *CRC Handbook of Chemistry and Physics, Internet Version 2005*. <http://www.hbcpnetbase.com>, CRC Press, Boca Raton, FL.

Linnen R.L. and Samson I.M. 2005. Rare Element Geochemistry and mineral deposits. *Geological Association of Canada*, 342 pp.

Liu, D., Zhang, J.,Wang, G., Liu, X.,Wang, S. and Yang, M. 2012. The dual-effects of LaCl3 on the proliferation, osteogenic differentiation, and mineralization of MC3T3- E1 cells. *Biological Trace Element Research*, **150**, 433–440.

Liu, Y., Diwu C., Zhao, Y., Liu, X., Yuan, H. and Wang, J. 2014. Determination of trace and rare-earth elements in Chinese soil and clay reference materials by ICP-MS. *Chinese Journal of Geochemistry*, **33**, 95–102.

Longerich, H.P., Fryer, B.J., Strong, D.F. and Kantipuly, C.J. 1987. Effects of operating conditions on the determination of the rare earth elements by inductively coupled plasma-mass spectrometry (ICP-MS). *Spectrochimica Acta*, **42B**, 75-92.

Luo Y. and Byrne, R.H. 2004. Carbonate complexation of yttrium and the rare earth elements in natural waters. *Geochimica et Cosmochimica Acta*, **68** (4), 691–699.

Luo, Y., and Byrne, R.H. 2000. The ionic strength dependence of rare earth and yttrium fluoride complexation at 25 ^{o}C. *Journal of Solution Chemistry*, **29**, 11, 1089–1099.

Marsac, R., Davranche, M., Gruau, G. and Dia, A. 2010. Metal loading effect on rare earth element binding to humic acid: experimental and modelling evidence. *Geochimica et Cosmochimica Acta*, **74**, 1749–1761.

Martell, A.E. and Hancock, R.D. 1996. *Metal Complexes in Aqueous Solutions*. Plenum Press. 245 pp.

Masuda, A., 1962. Regularities in variations of relative abundance of lanthanide elements and an attempt to analyse separation-index patterns of some minerals. *The Journal of Earth Sciences*, **10**, 173–187.

Masuda, A., Nakamura, N. and Tanaka, T. 1973. Fine structures of mutual normalized rare-earth patterns of chondrites. *Geochimica et Cosmochimica Acta*, 37, 239–248.

May, T.W. and Wiedmeyer, R.H. 1998. A table of polyatimic interferences in ICP-MS. *Atomic Spectroscopy*, **19** (5), 150-155.

Mayes, W.M., Gozzard, E., Potter, H.A.B. and Jarvis, A.P. 2008. Quantifying the importance of diffuse minewater pollution in a historically heavily coal mined catchment. Environmental Pollution, **151**, 165-175.

McLennan, S.M., 1989. Rare earth elements in sedimentary rocks: influence of provenance and sedimentary processes. *Reviews in Mineralogy and Geochemistry*, **21**, 169–200.

Medas, D., Cidu, R., Giudici, G.D. and Podda, F. 2013. Geochemistry of rare earth elements in water and solid materials at abandoned mines in SW Sardinia (Italy). *Journal of Geochemical Exploration*, **133**, 149-159.

Medas, D., Cidu, R., Lattanzi, P., Podda, F., Wanty, R.B. and De Giudici, G. 2012. Hydrozincite seasonal precipitation at Naracauli (Sardinia-Italy): hydrochemical factors and morphological features of the biomineralization process. *Applied Geochemistry*, **27**, 1814–1820.

Merten, D. and Büchel, G. 2004. Determination of Rare Earth Elements in Acid Mine Drainage by Inductively Coupled Plasma Mass Spectrometry. *Microchimica Acta*, **148**, 163–170.

Michard, A., Albarède, F., Michard, G., Minster, J.F. and Charlou, J.L. 1983. Rare-earth elements and uranium in high-temperature solutions from East Pacific Rise hydrothermal vent field (13°N). *Nature*, **303**, 795-797.

Middelburg, J.J., van der Weijden, C.H. and Woittiez, J.R.W. 1988. Chemical processes affecting the mobility of major, minor, and trace elements during weathering of granitic rocks. *Chemical Geology*, **68**, 253-273.

Millero, F.J. 1992. Stability constants for the formation of rare earth inorganic complexes as a function of ionic strength. *Geochimica et Cosmochimica Acta*, **56**, 3123- 3132.

Milodowski, A.E. and Zalasiewicz, J.A. 1991. Redistribution of rare earth elements during diagenesis of turbidite/hemipelagic mudrock sequences of Llandovery age from central Wales. *Geological Society*, **57**, 101–124.

Moeller, T. 1967. Lanthanide elements. *In*: Hampel, C.A. (ed.) *Encyclopedia of Chemical Elements*, Reinhold, New York, pp. 338–349.

Moffett, J.W. 1994a. A radiotracer study of cerium and manganese uptake onto suspended particles in Chesapeake Bay. *Geochimica et Cosmochimica Acta*, **58**, 695–703.

Möller, P. 1986. Rare Earth Mineral Deposits and their Industrial Importance. *In: Lanthanides, Tantalum and Niobium*, Spring-Verlag Berlin Heidelberg GmbH, pp171-188.

Moller, P. and Bau, M. 1993. Rare-earth patterns with positive cerium anomaly in alkaline lake waters from Lake Van, Turkey. *Earth and Planetary Science Letters*, **117**, 671-676.

Moore, R.D. 2004a. Introduction to salt dilution gauging for streamflow measurement: Part I. *Streamline Watershed Management Bulletin*, **7** (4), 20-23.

Moore, R.D. 2004b. Introduction to salt dilution gauging for streamflow measurement Part 2: Constant-rate injection. *Streamline Watershed Management Bulletin*, **8** (1), 11-15.

Moore, R.D., 2005. Introduction to salt dilution gauging for streamflow measurement: Part III: Slug injection using salt in solution. *Streamline Watershed Management Bulletin*, **8** (2), 1-6.

Morel, F.M.M. and Hering, J.G. 1993. *Principles and Applications of Aquatic Chemistry*. Wiley, New York, 588 pp.

Munz, M., Krause, S., Techlenburg, C. and Binley, A. 2011. Reducing monitoring gaps at the aquifer–river interface by modelling groundwater–surface water exchange flow patterns. *Hydrological processes*, **25**, 3547-3562.

Nakamura, N., 1974. Determination of REE, Ba, Fe, Mg, Na and K in carbonaceous and ordinary chondrites. *Geochimica et Cosmochimica Acta*, **38**, 757–775.

Nance W.B. and Taylor S.R. 1976. Rare earth element patterns and crustal evolution I. Australian post-Archean sedimentary rocks. *Geochimica et Cosmochimica Acta*, **40**, 1539-1551.

Nance, W.B. and Taylor, S.R. 1977. Rare earth element patterns and crustal evolution-II. Archean sedimentary rocks from Kalgoorlie, Australia. *Geochimica et Cosmochimica Acta*, **41**, 225-231.

Neal, C. 2007. Rare earth element concentration in dissolved and acid available particulate forms for eastern UK rivers. *Hydrology and Earth System Sciences*, **11**, 313-327.

Neal, C. and Davies, H. 2003. Water quality fluxes for eastern UK rivers entering the North Sea: a summary of information from the Land Ocean Interaction Study (LOIS). Land Ocean Interaction: Processes, Functioning and Environmental Management: a UK Perspective. *Science of the Total Environment*, **314-316**, 821-882.

Nelson, B.J., Wood, S.A. and Osiensky, J.L. 2003. Partitioning of REE between solution and particulate matter in natural waters: a filtration study. *Journal of Solid State Chemistry*, **171**, 51–56.

Nesbitt, H.W. 1979. Mobility and fractionation of rare earth elements during weathering of a granodiorite. *Nature*, **279**, 206-210.

Nordstrom, D.K. and Munoz, J.L. 2006. *Geochemical Thermodynamics*. Blackwell press, 2nd edition, 504 pp.

Ohta, A. and Kawabe, I. 2000. Rare earth element partitioning between Fe oxyhydroxide precipitates and aqueous NaCl solutions doped with NaHCO3: Determinations of rare earth element complexation constants with carbonate ions. *Geochemical Journal*, 34, 439-454.

Ohta, A. and Kawabe, I. 2001. REE (III) adsorption onto Mn dioxide (delta-MnO_2) and Fe oxyhydroxide: Ce(III) oxidation by delta-MnO2. *Geochimica et Cosmochimica Acta*, **65**, 695–703.

Pagano, G., Aliberti, F., Guida, M., Oral, R., Siciliano, A., Trifuoggi, M. and Tommasi, F. 2015b. Rare earth elements in human and animal health: State of art and research priorities. *Environmental Research*, 142, 215-220.

Pagano, G., Guida, M., Tommasi, F. and Oral, R. 2015a. Health effects and toxicity mechanisms of rare earth elements-knowledge gaps and research prospects. *Ecotoxicology and Environmental Safety*, **115**, 40–48.

Palmer, M.R. 1985. Rare earth elements in foraminifera tests. *Earth and Planetary Science Letters*, **73**, 285-298.

Palmer, M.R. and Elderfield, H. 1986. Rare earth elements and neodymium isotopes in ferromanganese oxides coatings of Cenozoic foraminifera from the Atlantic Ocean. *Geochimica et Cosmochimica Acta*, **50**, 409-417.

Palmieri, H.E.L., Knupp, E.A.N., Auler, L.M.L.A., Gomes, L.M.F. and Windmöller, C.C. 2011. Direct quantification of thorium, uranium and rare earth element concentrations in natural waters by ICP-MS. *2011 International Nuclear Atlantic Conference*, Belo Horizonte, MG, Brazil.

Parkhurst, D.L. and Appelo, C.A.J. 2013. Description of input and examples for PHREEQC version 3--A computer program for speciation, batch-reaction, one- dimensional transport, and inverse geochemical calculations. U.S. *Geological Survey Techniques and Methods*, book 6, chap. A43, 497 pp. http://pubs.usgs.gov/tm/06/a43/.

Parks, G.A. 1965. The isoelectric points of solid oxides, solid hydroxides, and aqueous hydroxo complex systems, *Chemical Reviews*, **65**, 177–198.

Pearson, R.G., 1963. Hard and soft acids and bases. *Journal of the American Chemical Society*, **85**, 3533-3539.

Piper, D.Z. 1974a. Rare earth elements in ferromanganese nodules and other marine phases. *Geochimica et Cosmochimica Acta*, **38**, 1007-1022.

Piper, D.Z. 1974b. Rare earth elements in the sedimentary cycle: a summary. *Chemical Geology*, **14**, 285-304.

Piper, D.Z. and Bau, M. 2013. Normalized rare earth elements in water, sediments, and wine: identifying sources and environmental redox conditions. *American Journal of Analytical Chemistry*, **4**, 69-83.

Pokrovsky, O.S., Schott, J. and Dupre, B. 2006. Trace element fractionation and transport in boreal rivers and soil porewaters of permafrost-dominated basaltic terrain in Central Siberia. *Geochimica et Cosmochimica Acta*, **70**, 3239–3260.

Pourret, O., Davranche, M., Gruau, G. and Dia, A., 2007. Rare earth elements complexation with humic acid. *Chemical Geology*. **243**, 128-141.

Prohaska, T., Hann, S., Latkoczy, C. and Stingeder, G. 1999. Determination of rare earth elements U and Th in environmental samples by inductively coupled plasma double focusing sectorfield mass spectrometry (ICP-SMS). *Journal of Analytical Atomic Spectrometry*, **14**, 1-8.

Protano, G. and Riccobono, F. 2002. High contents of rare earth elements (REEs) in stream waters of a Cu-Pb-Zn mining area. *Environmental Pollution*, **117**, 499- 514.

Qu, A., Wang, C. and Bo, J. 2004. Research on the cytotoxic and genotoxic effects of rare-earth element holmium to Vicia faba. *Yi Chuan*, **26**, 195–201.

Quinn, K. A. 2006. Influence of solution and surface chemistry on yttrium and rare earth element sorption. *Graduate Theses and Dissertations*. http://scholarcommons.usf.edu/etd/2665

Quinn, K.A., Byrne R.H. and Schijf, J. 2006a. Sorption of yttrium and rare earth elements by amorphous ferric hydroxide: Influence of pH and ionic strength. *Marine Chemistry*, **99**, 128–150.

Quinn, K.A., Byrne, R.H. and Schijf, J. 2004. Comparative scavenging of yttrium and the rare earth elements in seawater: Competitive influences of solution and surface chemistry. *Aquatic Geochemistry*, **10**, 59–80.

Quinn, K.A., Byrne, R.H. and Schijf, J. 2006b. Sorption of yttrium and rare earth elements by amorphous ferric hydroxide: influence of solution complexation with carbonate. *Geochimica et Cosmochimica Acta*, **70**, 4151–4165.

Restore case study, 2017. Case Study: Gategill Beck: Abandoned Metal Mines. River Restoration Centre, UK. Available online at:

Rico, C.M., Morales, M.I., McCreary, R., Castillo-Michel, H., Barrios, A.C., Hong, J., Tafoya, A., Lee,W.Y., Varela-Ramirez, A., Peralta-Videa, J.R. and Gardea-Torresdey, J. L. 2013. Cerium oxide nanoparticles modify the antioxidative stress enzyme activities and macromolecule composition in rice seedlings. *Environmental Science & Technology*, **47**, 14110–14118.

Rodea-Palomares, I., Gonzalo, S., Santiago-Morales, J., Leganés, F., García-Calvo, E., Rosal, R. and Fernández-Piñas, F. 2012. An insight into the mechanisms of nano- ceria toxicity in aquatic photosynthetic organisms. *Aquatic Toxicology*, **122–123**, 133–143.

Romero, F.M., Prol-Ledesma, R.M., Canet, C., Alvares, L.N. and Pérez-Vázquez, R. 2010. Acid drainage at the inactive Santa Lucia mine, western Cuba: natural attenuation of arsenic, Barium and lead, and geochemical behavior of rare earth elements. *Applied Geochemistry*, **25**, 716-727.

Rudnick, R.L. and Gao, S. 2003. Composition of the Continental Crust. *Treatise on Geochemistry*, 1-64.

Sartorius, 2016. Directions for use Vivaflow 50/50R/200. Publication No.: SLU6097-e160609. Ver. 06.

Schaltegger, U., Stille, P., Rais, N., Pique, A. and Clauer, N. 1994. Neodymium and strontium isotopic dating of diagenesis and low-grade metamorphism of argillaceous sediments. *Geochimica et Cosmochimica Acta*, **58**, 1471-1481.

Schijf, J. and Byrne, R.H. 2004. Determination of $_{SO4}\beta_1$ for yttrium and the rare earth elements at I= 0.66m and t= 25°C—Implications for YREE solution speciation in sulfate-rich waters. *Geochimica et Cosmochimica Acta*, **68** (13), 2825–2837.

Seredin, V.V. and Dai, S. 2012. Coal deposits as potential alternative sources for lanthanides and yttrium. *International Journal of Coal Geology*, **94**, 67–93.

Shaw, M.H. and Gunn, A.G. 1993. Rare earth elements in alkaline intrusions, North-West Scotland. *British Geological Survey WF/MR/93/011*.

Shaw, T.J., Duncan, T. and Schnetger, B. 2003. A preconcentration/matrix reduction method for the analysis of rare earth elements in seawater and groundwaters by isotope dilution ICPMS. *Analytical Chemistry*, **75**, 3396-3403.

Sholkovitz, E.R. 1992. Chemical evolution of rare earth elements; fractionation between colloidal and solution phases of filtered river water. *Earth and Planetary Science Letters*, **114**, 77–84.

Sholkovitz, E.R. 1995. The aquatic geochemistry of the rare earth elements in rivers and estuaries. *Aquatic Geochemistry*, **1**, 1 - 43.

Sholkovitz, E.R., Landing, W.M. and Lewis, B.L. 1994. Ocean particle chemistry: The fractionation of rare earth elements between suspended particles and seawater. *Geochimica et Cosmochimica Acta*, **58**, 1567–1579.

Sklash, M.G. 1990. Environmental isotope studies of storm and snowmelt runoff generation. In: Anderson, M.G. and Burt, T.P. (eds.) *Process studies in hillslope hydrology*, Wiley, Chichester, pp401–435.

Smedley, P.L. 1991. The geochemistry of rare earth elements in groundwater from the Carnmenellis area, southwest England. *Geochimica et Cosmochimica Acta*, **55**, 2767-2779.

Smith, F.W. 1974. Factors governing the development of fluorspar orebodies in the North Pennine orefield. PhD thesis, University of Durham.

Sonke, J.E. and Salters, V.J.M. 2006. Lanthanide-humic substances complexation. I. Experimental evidence for a lanthanide contraction effect. *Geochimica et Cosmochimica Acta*, **70**, 1495–1506.

Sophocleous, M. 2002. Interactions between groundwater and surface water: the state of the science. *Hydrogeology Journal*, **10**, 52–67.

Spedding, F.H. 1978. Prologue. *In*: Gschneidner, Jr. K.A. and Eyring, L. (eds.) *Handbook on the Physics and Chemistry of Rare Earths*, North Holland, Amsterdam, **1**, pp. xv–xxv.

Spitzer, D. W. 1991. *Flow Measurement: Practical Guides for Measurement and Control*. Instrument Society of America, 646 pp.

Stanley, C.J., and Vanghan, D.J. 1982. Copper, lead, zinc and cobalt mineralization in the English Lake District: classification, conditions of formation and genesis. *Journal of the Geological Society*, **139**, 569-579.

Stern, J.C., Sonke, J.E. and Salters, V.J.M. 2007. A capillary electrophoresis-ICP-MS study of rare earth element complexation by humic acids. *Chemical Geology*, **246**, 170–180.

Sugiyama, N. and Woods, G. 2012. Direct measurement of trace rare earth elements (REEs) in high-purity REE oxide using the Agilent 8800 Triple Quadrupole ICP-MS with MS/MS mode. Application note. *Agilent Technologies*, Publication number: 5991-0892EN.

Sun, L., Gui, H. and Chen, S. 2011. Rare earth element geochemistry of groundwater from coal bearing aquifer in Renlou coal mine, northern Anhui Province, China. *Journal of Rare Earths*, **29**, 185-192.

Sverjensky, D.A. 1984. Europium redox equilibria in aqueous solutions. *Earth and Planetary Science Letters*, **67**, 70-78.

Takahashi, Y., Minai, Y., Ambe, S., Makide, Y., Ambe, F. and Tominaga, T. 1997. Simultaneous determination of stability constants of humate complexes with various metal ions using multitracer technique. *Science of The Total Environment*, **198**, 61–71.

Tang, J. and Johannesson, K.H. 2003. Speciation of rare earth elements in natural terrestrial waters: assessing the role of dissolved organic matter from the modeling approach. *Geochimica et Cosmochimica Acta*, **67**, 2321–2339.

Tang, J. and Johannesson, K.H. 2005. Adsorption of rare earth elements onto Carrizo sand: Experimental investigations and modeling with surface complexation. *Geochimica et Cosmochimica Acta*, **69**, 5247-5261.

Tang, J. and Johannesson, K.H. 2010a. Ligand extraction of rare earth elements from aquifer sediments: implications for rare earth element complexation with organic matter in natural waters. *Geochimica et Cosmochimica Acta*, **74**, 6690–6705.

Tang, J. and Johannesson, K.H. 2010b. Rare earth elements adsorption onto Carrizo sand: Influence of strong solution complexation. *Chemical Geology*, **279**, 120–133.

Tang, J.W. and Johannesson, K.J. 2006. Controls on the geochemistry of rare earth elements along a groundwater flow path in the Carrizo Sand aquifer, Texas, USA. *Chemical Geology*, **225**, 156-171.

Taylor, S.R. and McLennan, S.M. 1985. *The Continental Crust: Its composition and evolution*. Blackwell, 312pp.

Tertre, E., Berger, G., Castet, S., Loubet, M. and Giffaut, E. 2005. Experimental study of adsorption of Ni^{2+},Cs^{+} and Ln^{3+} onto Na-montmorillonite up to 150 °C. *Geochimica et Cosmochimica Acta*, **69**, 4937–4948.

Tertre, E., Hofmann, A. and Berger, G. 2008. Rare earth element sorption by basaltic rock: experimental data and modeling results using the "Generalised Composite approach". *Geochimica et Cosmochimica Acta*, **72**, 1043–1056.

Thomas, R. 2008. *Practical Guide to ICP-MS: A tutorial for beginners*, 2nd edition. CRC Press, 324 pp.

Thurman, E.M. 1985. *Organic Geochemistry of Natural Waters*. Nijhoff/Junk, Dordrechtthe, Netherlands, 497pp.

Tipping, E., Rey-Castro, C., Bryan, S.E. and Hamilton-Taylor, J. 2002. Al(III) and Fe(III) binding by humic substances in freshwaters, and implications for trace metal speciation. *Geochimica et Cosmochimica Acta*, **66**, 3211–3224.

Tsuruta, T. 2006. Selective accumulation of light or heavy rare earth elements using gram-positive bacteria. *Colloids and Surfaces B: Biointerfaces*, **52**, 117-122.

URS, 2014. The Coal Authority- Metal mine water treatment review. URS Infrastructure & Environment UK Ltd, Manchester.

Vanhaecke, F., Vanhoe, H. and Dams, R. 1992. The use of internal standards in ICP-MS. *Talanta*, **39** (7), 737-742.

Vaughan M.A. and Horlick G. 1986. Oxide, hydroxide, and doubly charged analyte species in inductively coupled plasma-mass spectrometry. *Applied Spectroscopy*, **40**, 434-445.

Vaughan, M.A. and Horlick, G. 1989. Analysis of steels using inductively coupled plasma mass spectrometry. *Journal of Analytical Atomic Spectrometry*, **4**, 45-50.

Vaughan, M.A. and Horlick, G. 1990b. Correction Procedures for Rare Earth element analyses in Inductively Couplef Plasma-Mass Spectrometry. *Applied Spectroscopy*, **44** (4), 587-593.

Verplanck, P.L. 2013. Partitioning of rare earth elements between dissolved and colloidal phases. *Procedia Earth and Planetary Science,* **7**, 867-870.

Verplanck, P.L., Antweiler, R.C., Nordstrom, D.K. and Taylor, H.E. 2001. Standard reference water samples for rare earth element determinations. *Applied Geochemistry*, **16**, 231-244.

Verplanck, P.L., Nordstrom, D.K. and Taylor, H.E. 1999. Overview of rare earth element investigations in acid waters of U.S. Geological Survery abandoned mine lands watersheds. U.S. Geological Survey Toxic Substances Program: Proceeding of the Technical Meeting. *Water Resources Report of Investigations*, 83-92.

Verplanck, P.L., Nordstrom, D.K., Taylor, H.E. and Kimball, B.A. 2004. Rare earth element partitioning between hydrous ferric oxides and acid mine water during iron oxidation. *Applied Geochemistry,* **19**, 1339-1354.

Walters, A.S., Goodenough, K.M., Hughes, H.S.R., Roberts, N.M.W., Gunn, A.G., Rushton, J. and Lacinska, A. 2013. Enrichment of Rare Earth Elements during magmatic and post-magmatic processes: a case study from the Loch Loyal Syenite Complex, northern Scotland. *Contributions to Mineralogy and Petrology,* **166**, 1177–1202.

Wang, C., He, M., Shi, W., Wong, J., Cheng, T., Wang, X., Hu, L. and Chen, F. 2011. Toxicological effects involved in risk assessment of rare earth lanthanum on roots of Vicia faba L. seedlings. *Journal of Environmental Sciences*, **23**, 1721–1728.

Webster, J.G., Swedlund, P.J., Webster, K.S., 1998. Trace metal adsorption onto an acid mine drainage iron(III) oxy hydroxy sulfate. *Environmental Science and Technology*, **32**, 1361–1368.

Wei, B., Li, Y., Li, H., Yu, J., Ye, B. and Liang, T. 2013. Rare earth elements in human hair from a mining area of China. *Ecotoxicology and Environmental Safety*, **96**, 118-123.

Weltje L., Heidenreich, H., Zhu, W., Wolterbeek, H.T., Korhammer, S., de Goeij, J.J. and Markert, B. 2002. Lanthanide concentrations in freshwater plants and molluscs, related to

those in surface water, pore water and sediment: a case study in the Netherlands. *Science of the Total Environment*, **286**,191–214.

White, D.S. 1993. Perspectives on defining and delineating hyporheic zones. *Journal of the North American Benthological Society*, **12**, 61–69.

Willie, S. and Sturgeon, R. 2001. Determination of transition and rare earth elements in seawater by flow injection inductively coupled plasma time-of-flight mass spectrometry. *Spectrochimica Acta Part B*, **56**, 1707-1716.

Winter, T.C. 1999. Relation of streams, lakes, and wetlands to groundwater flow systems. *Hydrogeology Journal*, **7**, 28–45.

Wolery, T.J. and Jové-Colón, C.F. 2017. Chemical thermodynamic data. 1. The concept of links to the chemical elements and the historical development of key thermodynamic data. *Geochimica et Cosmochimica Acta*, **213**, 635-676.

Wood, E.F., Sivapalan, M. and Beven, K. 1990. Similarity and scale in catchment storm response. *Reviews of Geophysics*, **28**, 1–18.

Wood, S.A. 1990. The aqueous geochemistry of the rare-earth elements and yttrium: 1. Revies of available low-temperature data for inorganic complexes and the inorganic REE speciation of natural waters. *Chemical Geology*, **82**, 159- 186.

Woodhall, D.G. 2000a. Geology of the Keswick district- sheet description of the British Geological Survey. 1:50 000 sheet 29 keswick (England and Wales). *British Geological Survey*, Nottingham.

Woodhall, D.G. 2000b. Geology of the Keswick district- a brief explanation of the geological map. Sheet Explanation of the British Geological Survey. 1:50 000 sheet 29 keswick (England and Wales). *British Geological Survey*, Nottingham.

Worrall, F. 1999. Chemical fingerpringting of acid minewaters: the use of rare earth elements (REE) patterns. *Mine, water & environment, 1999 IMWA Congress*, Sevilla, Spain.

Xia, J., Zhao, H. and Lu, G. 2013. Effects of selected metal oxide nanoparticles on multiple biomarkers in Carassius auratus. *Biomedical and Environmental Sciences*, **26**, 742–749.

Xia, Q., Liu, H. X., Yang, X. D. and Wang, K. 2012. The neural toxicity of lanthanides: An update and interpretations. *Science China Press*, **42**, 1308-1314.

Yamamoto, Y., Takahashi, Y. and Shimizu, H. 2005. Systematics of stability constants of fulvate complexes with rare earth ions. *Chemistry Letters*, **34**, 880–881

Yamamoto, Y., Takahashi, Y. and Shimizu, H. 2010. Systematic change in relative stabilities of REE-humic complexes at various metal loading levels. *Geochemical Journal*, **44**, 39–63.

Yamanaka, K. and Wilbur, S. 2013. Investigations into the use of helium collision mode and aerosol dilution for ultra-trace analysis of metals in mineral reference materials. White Paper. *Agilent Technologies*, Publication number: 5991-2811EN.

Yang, G., Sun, Z., Lv, X., Deng, Y., Zhou, Q. and Huang, X. 2012. Living target of Ce(III) action on horseradish cells: proteins on/in cell membrane. *Biological Trace Element Research*, **150**, 396–402.

Younger, P.L., Banwart, S.A. and Hedin, R.S. 2002. *Mine water: Hydrology, Pollution, Remediation*. Kluwer Academic Publishers, London, 464pp.

Yuan, J., Mao, X., Wang, Y., Deng, Z. and Huang, L. 2014. Geochemistry of rare-earth elements in shallow groundwater, northeastern Guangdong Province, China. *Chinese Journal of Geochemistry*, **33**, 053–064.

Zanker, H., Richter, W. and Huttig, G. 2003. Scavenging and immobilization of trace contaminants by colloids in the waters of abandoned ore mines. *Colloids and Surfaces A: Physicochemical and Engineering Aspects*, **217**, 21–31.

Zhang, J. and Nozaki, Y. 1996. Rare earth elements and yttrium in seawater: ICP-MS determinations in the East Caroline, Coral Sea, and South Fiji basins of the western South Pacific Ocean. *Geochimica et Cosmochimica Acta*, **60**, 4631-4644.

Zhang, S., Wang, L. and Zhang, C. 1994. Neutron activation analysis technology and rare earth elements environmental biogeochemistry: Modern nuclear analysis techniques and their application in environmental science. *Atomic press*, 201-242. (In Chinese)

Zhao, F., Cong, Z., Sun H. and Ren, D. 2007. The geochemistry of rare earth elements (REE) in acid mine drainage from the Sitai coal mine, Shanxi Province, North China. *International Journal of Coal Geology*, **70**, 184-192.

Zhao, W.H., Gou, B.D., Zhang, T.L. and Wang, K. 2012. Lanthanum chloride bidirectionally influences calcification in bovine vascular smooth muscle cells. *Journal of Cellular Biochemistry*, **113**, 1776–1786.

Zhou, X., Johannesson, K.H. and Stetzenbach, K.J. 1995. Batch tests for crushed rocks and pH= 7 distilled water: A first look at rock imparted aqueous rare earth element signatures. *EOS*, **76**, 275.

Zhu, F., Xu, S. and Zhang, H. 1996. The IQ report of children in rare earths area – I: biological effect in jiangxi rare earth area. *Chinese science bulletin*, **41**, 914-916.

Zhu, W., Xu, S., Shao, P., Zhang, H., Wu, D., Yang, W., Feng, J. and Feng, L. 2005. Investigation on liver function among population in high background of rare earth area in South China. *Biological Trace Element Research*, **104**, 1–8.

Zinder, B., Furrer, G. and Stumm, W. 1986. The coordination chemistry of weathering: II. Dissolution of Fe (III) oxides. *Geochimica et Cosmochimica Acta*, **50**, 1861-1869.

Zuddas, P. and Podda, F. 2005. Variations in physico-chemical properties ofwater associated with bioprecipitation of hydrozincite [$Zn_5(CO_3)_2(OH)_6$] in the waters of Rio Naracauli, Sardinia (Italy). *Applied Geochemistry*, **20**, 507–517.

Appendix A BaO intererence related data

Ba concentration, Eu concentration before and after correction of G1 and G7 samples

Sep 2016				15th Nov 2016			
Sample	Ba (ppb)	Eu_{raw} (ppb)	Eu_c (ppb)	Sample	Ba (ppb)	Eu_{raw} (ppb)	Eu_c (ppb)
G1 0.1F	20.7	0.0083	0.0060	G1 ultra	7.75	0.0063	0.0053
G1 0.45F	20.7	0.0101	0.0077	G1 0.1F	9.36	0.0094	0.0082
G1 Tot	20.7	0.0092	0.0068	G1 0.45F	9.20	0.0090	0.0079
G7 0.1F	14.1	0.0137	0.0120	G1 Tot	9.36	0.0095	0.0084
G7 0.45F	14.5	0.0150	0.0134	G7 ultra	5.42	0.0045	0.0039
G7 Tot	14.9	0.0153	0.0137	G7 0.1F	8.38	0.0139	0.0129
13rd Oct 2016				G7 0.45F	8.32	0.0154	0.0144
Sample	Ba (ppb)	Eu_{raw} (ppb)	Eu_c (ppb)	G7 Tot	12.4	0.0277	0.0262
G1 ultra	18.7	0.0078	0.0057	Dec 2016			
G1 0.1F	21.7	0.0087	0.0063	Sample	Ba (ppb)	Eu_{raw} (ppb)	Eu_c (ppb)
G1 0.45F	21.7	0.0089	0.0065	G1 ultra	12.0	0.0050	0.0037
G1 Tot	21.8	0.0097	0.0072	G1 0.1F	14.3	0.0089	0.0074
G7 ultra	12.7	0.0042	0.0028	G1 0.45F	14.3	0.0092	0.0076
G7 0.1F	14.5	0.0079	0.0063	G1 Tot	14.4	0.0095	0.0079
G7 0.45F	15.0	0.0093	0.0076	G7 ultra	12.4	0.0038	0.0024
G7 Tot	15.3	0.0097	0.0080	G7 0.1F	14.9	0.0085	0.0068
27th Oct 2016				G7 0.45F	14.8	0.0090	0.0073
Sample	Ba (ppb)	Eu_{raw} (ppb)	Eu_c (ppb)	G7 Tot	15.3	0.0092	0.0075
G1 ultra	17.1	0.0067	0.0048	June 2017			
G1 0.1F	20.0	0.0090	0.0068	Sample	Ba (ppb)	Eu_{raw} (ppb)	Eu_c (ppb)
G1 0.45F	20.1	0.0088	0.0066	G1 ultra	20.6	0.0044	0.0027
G1 Tot	20.0	0.0088	0.0066	G1 0.1F	24.3	0.0087	0.0066
G7 ultra	12.1	0.0037	0.0024	G1 0.45F	24.9	0.0088	0.0067
G7 0.1F	14.4	0.0083	0.0067	G1 Tot	25.0	0.0097	0.0075
G7 0.45F	14.4	0.0091	0.0075	G7 ultra	12.7	0.0043	0.0032
G7 Tot	14.8	0.0111	0.0094	G7 0.45F	15.3	0.0082	0.0069
10th Nov 2016				G7 Tot	15.7	0.0092	0.0079
Sample	Ba (ppb)	Eu_{raw} (ppb)	Eu_c (ppb)	Sep 2017			
G1 ultra	8.38	0.0078	0.0068	Sample	Ba (ppb)	Eu_{raw} (ppb)	Eu_c (ppb)
G1 0.1F	10.3	0.0100	0.0087	G1 ultra	7.53	0.0048	0.0038
G1 0.45F	10.0	0.0101	0.0088	G1 0.1F	9.60	0.0081	0.0069
G1 Tot	10.2	0.0100	0.0088	G1 0.45F	9.60	0.0085	0.0072
G7 ultra	5.14	0.0038	0.0031	G1 Tot	9.74	0.0086	0.0073
G7 0.1F	7.62	0.0110	0.0101	G7 ultra	7.51	0.0045	0.0035
G7 0.45F	8.14	0.0124	0.0114	G7 0.1F	11.2	0.0129	0.0114
G7 Tot	16.4	0.0378	0.0358	G7 0.45F	11.6	0.0139	0.0125
				G7 Tot	12.7	0.0178	0.0161

Note: Eu_{raw} represent raw Eu data before correction; Eu_c means corrected Eu data

Data relates to BaO interference of G2, G3, G4, G5 samples

Sep 2016					
Sample	Ba (ppb)	Raw Eu data (ppb)	Corrected Eu data (ppb)	%Difference between raw and corrected Eu	Ba/ corrected Eu
G2 0.1F	23.4	0.7107	0.7081	0.37%	33
G2 0.45F	23.6	0.7243	0.7216	0.36%	33
G2 Tot	23.7	0.7101	0.7076	0.37%	33
G3 0.1F	28.0	0.1432	0.1400	2.30%	200
G3 0.45F	28.2	0.1395	0.1363	2.39%	207
G3 Tot	28.4	0.1428	0.1396	2.28%	203
G4 0.1F	30.3	0.1241	0.1207	2.81%	251
G4 0.45F	30.6	0.1267	0.1233	2.78%	248
G4 Tot	30.4	0.1314	0.1280	2.66%	238
G5 0.1F	29.7	0.1070	0.1036	3.21%	286
G5 0.45F	31.0	0.1086	0.1052	3.30%	295
G5 Tot	30.4	0.1117	0.1083	3.15%	281
13rd Oct 2016					
Sample	Ba (ppb)	Raw Eu data (ppb)	Corrected Eu data (ppb)	%Difference between raw and corrected Eu	Ba/ corrected Eu
G2 ultra	22.1	0.6945	0.6921	0.34%	32
G2 0.1F	22.7	0.7003	0.6979	0.35%	33
G2 0.45F	22.3	0.6910	0.6886	0.35%	32
G2 Tot	22.5	0.6985	0.6960	0.35%	32
G3 ultra	32.1	0.2446	0.2410	1.47%	133
G3 0.1F	33.4	0.2564	0.2527	1.46%	132
G3 0.45F	33.5	0.2581	0.2544	1.45%	132
G3 Tot	33.3	0.2554	0.2517	1.46%	132
G4 ultra	31.5	0.2129	0.2094	1.67%	151
G4 0.1F	33.2	0.2261	0.2225	1.65%	149
G4 0.45F	32.9	0.2225	0.2188	1.66%	150
G4 Tot	32.9	0.2258	0.2221	1.64%	148
G5 ultra	31.5	0.1718	0.1683	2.07%	187
G5 0.1F	33.2	0.1766	0.1729	2.13%	192
G5 0.45F	33.3	0.1839	0.1802	2.05%	185
G5 Tot	33.3	0.1847	0.1810	2.04%	184

27th Oct 2016					
Sample	Ba (ppb)	Raw Eu data (ppb)	Corrected Eu data (ppb)	%Difference between raw and corrected Eu	Ba/ corrected Eu
G2 ultra	22.9	0.6567	0.6542	0.38%	35
G2 0.1F	23.0	0.6549	0.6524	0.38%	35
G2 0.45F	23.3	0.6626	0.6601	0.38%	35
G2 Tot	23.2	0.6643	0.6618	0.38%	35
G3 ultra	27.8	0.1975	0.1944	1.58%	143
G3 0.1F	29.0	0.2013	0.1981	1.62%	146
G3 0.45F	28.8	0.2011	0.1980	1.61%	146
G3 Tot	28.9	0.1985	0.1953	1.64%	148
G4 ultra	27.8	0.1859	0.1828	1.68%	152
G4 0.1F	29.1	0.1934	0.1901	1.69%	153
G4 0.45F	28.9	0.1892	0.1860	1.72%	155
G4 Tot	29.1	0.1856	0.1823	1.76%	159
G5 ultra	28.1	0.1565	0.1534	2.03%	183
G5 0.1F	29.7	0.1647	0.1614	2.04%	184
G5 0.45F	29.8	0.1665	0.1632	2.02%	182
G5 Tot	29.5	0.1681	0.1648	1.98%	179
10th Nov 2016					
Sample	Ba (ppb)	Raw Eu data (ppb)	Corrected Eu data (ppb)	%Difference between raw and corrected Eu	Ba/ corrected Eu
G2 ultra	23.4	0.6605	0.6577	0.43%	36
G2 0.1F	23.9	0.6750	0.6721	0.44%	36
G2 0.45F	23.6	0.6795	0.6766	0.43%	35
G2 Tot	23.9	0.6775	0.6746	0.43%	35
G3 ultra	11.7	0.0494	0.0480	3.05%	243
G3 0.1F	12.9	0.0526	0.0510	3.18%	253
G3 0.45F	12.9	0.0548	0.0532	3.04%	242
G3 Tot	12.9	0.0552	0.0536	2.98%	240
G4 ultra	13.7	0.0543	0.0526	3.26%	260
G4 0.1F	15.0	0.0622	0.0603	3.12%	249
G4 0.45F	15.2	0.0622	0.0603	3.15%	251
G4 Tot	15.8	0.0686	0.0667	2.97%	237
G5 ultra	13.7	0.0406	0.0389	4.43%	353
G5 0.1F	15.8	0.0492	0.0472	4.20%	335
G5 0.45F	16.5	0.0494	0.0473	4.37%	348
G5 Tot	16.4	0.0639	0.0619	3.33%	266

15th Nov, 2016					
Sample	Ba (ppb)	Raw Eu data (ppb)	Corrected Eu data (ppb)	%Difference between raw and corrected Eu	Ba/ corrected Eu
G2 ultra	23.9	0.6438	0.6409	0.46%	37
G2 0.1F	24.3	0.6631	0.6601	0.45%	37
G2 0.45F	24.4	0.6665	0.6635	0.45%	37
G2 Tot	24.4	0.6778	0.6748	0.44%	36
G3 ultra	10.5	0.0352	0.0339	3.80%	311
G3 0.1F	11.6	0.0447	0.0433	3.30%	267
G3 0.45F	11.6	0.0451	0.0437	3.23%	266
G3 Tot	11.7	0.0458	0.0443	3.34%	264
G4 ultra	12.7	0.0361	0.0345	4.49%	367
G4 0.1F	13.7	0.0445	0.0428	4.04%	320
G4 0.45F	13.8	0.0449	0.0432	3.91%	320
G4 Tot	14.1	0.0479	0.0462	3.73%	305
G5 ultra	12.3	0.0275	0.0260	5.82%	475
G5 0.1F	14.3	0.0387	0.0370	4.73%	387
G5 0.45F	14.5	0.0393	0.0375	4.72%	386
G5 Tot	14.4	0.0452	0.0434	4.07%	333
Dec 2016					
Sample	Ba (ppb)	Raw Eu data (ppb)	Corrected Eu data (ppb)	%Difference between raw and corrected Eu	Ba/ corrected Eu
G2 ultra	23.4	0.7094	0.7069	0.36%	33
G2 0.1F	23.0	0.7015	0.6990	0.36%	33
G2 0.45F	23.3	0.7082	0.7057	0.36%	33
G2 Tot	23.2	0.7084	0.7058	0.36%	33
G3 ultra	22.0	0.1645	0.1621	1.52%	136
G3 0.1F	22.8	0.1664	0.1638	1.55%	139
G3 0.45F	23.1	0.1671	0.1645	1.53%	140
G3 Tot	23.1	0.1693	0.1668	1.54%	139
G4 ultra	22.8	0.1526	0.1501	1.68%	152
G4 0.1F	23.8	0.1527	0.1501	1.74%	159
G4 0.45F	23.7	0.1539	0.1513	1.77%	157
G4 Tot	23.7	0.1544	0.1517	1.73%	156
G5 ultra	22.5	0.1285	0.1260	1.96%	179
G5 0.1F	23.7	0.1382	0.1356	1.93%	175
G5 0.45F	23.8	0.1353	0.1327	1.97%	179
G5 Tot	25.1	0.1522	0.1492	1.96%	168

June 2017					
Sample	Ba (ppb)	Raw Eu data (ppb)	Corrected Eu data (ppb)	%Difference between raw and corrected Eu	Ba/ corrected Eu
G2 ultra	24.0	0.6783	0.6763	0.30%	35
G2 0.1F	24.1	0.6731	0.6711	0.30%	36
G2 0.45F	24.3	0.6845	0.6824	0.30%	36
G2 Tot	24.4	0.6962	0.6941	0.30%	35
G3 ultra	30.8	0.3421	0.3395	0.77%	91
G3 0.1F	31.5	0.3481	0.3454	0.78%	91
G3 0.45F	31.6	0.3511	0.3484	0.78%	91
G3 Tot	32.0	0.3513	0.3486	0.78%	92
G4 ultra	30.9	0.3062	0.3036	0.88%	102
G4 0.1F	31.0	0.3089	0.3062	0.88%	101
G4 0.45F	31.9	0.3111	0.3083	0.89%	103
G4 Tot	32.3	0.3162	0.3134	0.89%	103
G5 ultra	32.4	0.2488	0.2461	1.10%	132
G5 0.1F	33.2	0.2553	0.2525	1.11%	132
G5 0.45F	33.7	0.2576	0.2547	1.13%	132
G5 Tot	33.6	0.2579	0.2550	1.12%	132
Sep 2017					
Sample	Ba (ppb)	Raw Eu data (ppb)	Corrected Eu data (ppb)	%Difference between raw and corrected Eu	Ba/ corrected Eu
G2 ultra	25.0	0.7205	0.7172	0.46%	35
G2 0.1F	25.5	0.7206	0.7172	0.46%	36
G2 0.45F	25.1	0.7251	0.7218	0.46%	35
G2 Tot	25.7	0.7377	0.7343	0.46%	35
G3 ultra	11.3	0.0455	0.0441	3.35%	256
G3 0.1F	12.8	0.0554	0.0537	3.10%	238
G3 0.45F	12.7	0.0550	0.0534	3.06%	238
G3 Tot	12.6	0.0563	0.0546	3.05%	231
G4 ultra	13.2	0.0438	0.0421	4.15%	314
G4 0.1F	15.3	0.0537	0.0517	3.81%	296
G4 0.45F	15.4	0.0536	0.0516	3.83%	298
G4 Tot	15.4	0.0539	0.0520	3.79%	297
G5 ultra	12.7	0.0175	0.0158	10.50%	800
G5 0.1F	15.7	0.0437	0.0417	4.92%	378
G5 0.45F	15.6	0.0447	0.0427	4.78%	365
G5 Tot	15.6	0.0491	0.0470	4.29%	331

Appendix B LREEO and MREEO interference related data

Correct concentration of interfering REE in samples collected on Sep, 2016

Interfering REE	Pr (ppb)	Nd (ppb)	Sm (ppb)	Eu (ppb)	Gd (ppb)	Tb (ppb)
G1 0.1F	0.0350	0.1449	0.0303	0.0060	0.0371	0.0046
G1 0.45F	0.0380	0.1478	0.0439	0.0077	0.0353	0.0047
G1 Tot	0.0384	0.1618	0.0360	0.0068	0.0381	0.0049
G2 0.1F	2.761	11.59	2.435	0.7081	2.650	0.3034
G2 0.45F	2.804	11.75	2.488	0.7216	2.694	0.3064
G2 Tot	2.765	11.69	2.472	0.7076	2.682	0.3119
G3 0.1F	0.5615	2.330	0.4707	0.1400	0.5412	0.0629
G3 0.45F	0.5588	2.313	0.5120	0.1363	0.5305	0.0620
G3 Tot	0.5620	2.341	0.4975	0.1396	0.5338	0.0641
G4 0.1F	0.5062	2.100	0.4388	0.1207	0.4967	0.0586
G4 0.45F	0.5061	2.110	0.4560	0.1233	0.5011	0.0593
G4 Tot	0.5035	2.138	0.4340	0.1280	0.4991	0.0586
G5 0.1F	0.4419	1.827	0.3620	0.1036	0.4224	0.0501
G5 0.45F	0.4522	1.871	0.4054	0.1052	0.4324	0.0515
G5 Tot	0.4496	1.857	0.3809	0.1083	0.4400	0.0540
G7 0.1F	0.0404	0.1796	0.0512	0.0120	0.0643	0.0086
G7 0.45F	0.0435	0.1968	0.0536	0.0134	0.0679	0.0093
G7 Tot	0.0440	0.2022	0.0567	0.0137	0.0642	0.0091

Interfered REE concentrations before and after correction of samples collected on Sep, 2016

Interfered analyte	Gd (ppb)		Tb (ppb)		Dy (ppb)		Ho (ppb)	
	raw	corrected	raw	corrected	Raw	corrected	raw	corrected
G1 0.1F	0.0370	0.0370	0.0047	0.0046	0.0257	0.0257	0.0050	0.0050
G1 0.45F	0.0354	0.0353	0.0048	0.0047	0.0280	0.0280	0.0061	0.0061
G1 Tot	0.0381	0.0381	0.0050	0.0049	0.0260	0.0260	0.0055	0.0054
G2 0.1F	2.653	2.650	0.3116	0.3034	1.489	1.488	0.2601	0.2597
G2 0.45F	2.697	2.694	0.3148	0.3064	1.498	1.498	0.2658	0.2654
G2 Tot	2.684	2.682	0.3202	0.3119	1.481	1.481	0.2613	0.2609
G3 0.1F	0.5418	0.5412	0.0646	0.0629	0.3097	0.3096	0.0543	0.0543
G3 0.45F	0.5313	0.5305	0.0637	0.0620	0.3051	0.3050	0.0550	0.0549
G3 Tot	0.5346	0.5338	0.0658	0.0641	0.3138	0.3137	0.0560	0.0559
G4 0.1F	0.4970	0.4967	0.0601	0.0586	0.2852	0.2851	0.0519	0.0519
G4 0.45F	0.5012	0.5011	0.0608	0.0593	0.2932	0.2931	0.0526	0.0525
G4 Tot	0.4992	0.4991	0.0602	0.0586	0.2916	0.2916	0.0521	0.0520
G5 0.1F	0.4230	0.4224	0.0514	0.0501	0.2472	0.2472	0.0450	0.0449
G5 0.45F	0.4330	0.4324	0.0528	0.0515	0.2585	0.2584	0.0464	0.0463
G5 Tot	0.4403	0.4400	0.0553	0.0540	0.2584	0.2583	0.0473	0.0473
G7 0.1F	0.0643	0.0643	0.0087	0.0086	0.0481	0.0481	0.0091	0.0091
G7 0.45F	0.0679	0.0679	0.0094	0.0093	0.0489	0.0489	0.0098	0.0098
G7 Tot	0.0642	0.0642	0.0092	0.0091	0.0531	0.0531	0.0101	0.0101
Interfered analyte	Er (ppb)		Tm (ppb)		Yb (ppb)		Lu (ppb)	
	raw	corrected	raw	corrected	Raw	corrected	raw	corrected
G1 0.1F	0.0131	0.0130	0.0017	0.0017	0.0106	0.0105	0.0017	0.0017
G1 0.45F	0.0158	0.0156	0.0020	0.0020	0.0115	0.0114	0.0018	0.0018
G1 Tot	0.0153	0.0151	0.0023	0.0023	0.0109	0.0108	0.0019	0.0019
G2 0.1F	0.6626	0.6511	0.0846	0.0845	0.4669	0.4599	0.0640	0.0627
G2 0.45F	0.6718	0.6602	0.0836	0.0835	0.4826	0.4755	0.0648	0.0634
G2 Tot	0.6665	0.6549	0.0826	0.0826	0.4696	0.4625	0.0620	0.0607
G3 0.1F	0.1384	0.1361	0.0177	0.0176	0.0986	0.0972	0.0142	0.0140
G3 0.45F	0.1368	0.1345	0.0172	0.0172	0.0966	0.0952	0.0137	0.0135
G3 Tot	0.1374	0.1351	0.0179	0.0179	0.0976	0.0962	0.0135	0.0132
G4 0.1F	0.1322	0.1301	0.0169	0.0169	0.0903	0.0890	0.0121	0.0119
G4 0.45F	0.1321	0.1300	0.0164	0.0164	0.0915	0.0901	0.0129	0.0127
G4 Tot	0.1334	0.1313	0.0166	0.0166	0.0921	0.0908	0.0130	0.0127
G5 0.1F	0.1085	0.1067	0.0138	0.0138	0.0748	0.0737	0.0109	0.0107
G5 0.45F	0.1151	0.1133	0.0146	0.0145	0.0796	0.0784	0.0111	0.0109
G5 Tot	0.1153	0.1135	0.0141	0.0141	0.0787	0.0775	0.0117	0.0114
G7 0.1F	0.0263	0.0261	0.0033	0.0033	0.0189	0.0187	0.0031	0.0030
G7 0.45F	0.0257	0.0255	0.0036	0.0035	0.0195	0.0193	0.0030	0.0030
G7 Tot	0.0278	0.0276	0.0034	0.0034	0.0185	0.0184	0.0029	0.0029

Concentration ratio of interfering REE to interfered REE of samples

13/10/16	Pr/Gd	Nd/Tb	Sm/Dy	Sm/Ho	Nd/Er	Sm/Er	Eu/Tm	Gd/Yb	Tb/Lu
G1 ultra	0.9	30	1.1	5.7	8.9	1.8	3.9	2.3	2.5
G1 0.1F	1.0	33	1.1	6.9	10	2.3	3.9	3.5	3.3
G1 0.45F	0.9	34	1.2	6.0	9.9	2.0	3.2	3.9	3.3
G1 Tot	1.0	30	1.2	6.2	11	2.3	4.1	4.0	3.2
G2 ultra	1.1	38	1.7	9.8	18	3.7	8.8	5.7	5.0
G2 0.1F	1.0	37	1.7	9.5	18	3.8	8.0	5.8	4.6
G2 0.45F	1.0	38	1.7	9.8	18	3.8	8.9	5.9	4.9
G2 Tot	1.0	38	1.7	9.6	18	3.8	8.9	5.8	5.0
G3 ultra	1.1	35	1.2	6.4	16	2.5	7.4	5.7	5.1
G3 0.1F	1.0	36	1.2	6.6	16	2.6	7.8	5.7	5.3
G3 0.45F	1.0	36	1.2	6.5	16	2.6	7.8	5.7	5.0
G3 Tot	1.0	36	1.2	6.6	16	2.6	7.9	5.7	4.9
G4 ultra	1.0	35	1.5	8.3	15	3.2	7.1	5.6	4.6
G4 0.1F	1.0	35	1.5	8.6	16	3.3	8.0	5.6	4.8
G4 0.45F	1.0	34	1.5	8.2	16	3.3	7.6	5.7	5.1
G4 Tot	1.0	35	1.5	8.2	16	3.3	7.6	5.7	4.8
G5 ultra	1.0	35	1.5	7.9	15	3.2	7.3	5.9	4.9
G5 0.1F	1.0	37	1.4	7.9	16	3.2	7.4	5.9	5.0
G5 0.45F	1.0	36	1.5	8.3	16	3.3	7.7	5.8	5.0
G5 Tot	1.0	34	1.5	7.9	16	3.3	7.4	5.5	5.3
G7 ultra	0.7	23	1.2	6.0	7.4	2.2	4.2	2.4	2.2
G7 0.1F	0.7	22	1.1	5.9	8.4	2.3	3.9	3.0	3.3
G7 0.45F	0.8	24	1.1	5.9	8.4	2.1	4.8	3.0	3.0
G7 Tot	0.7	24	1.2	6.1	7.7	2.1	4.2	3.8	3.2
27/10/16	Pr/Gd	Nd/Tb	Sm/Dy	Sm/Ho	Nd/Er	Sm/Er	Eu/Tm	Gd/Yb	Tb/Lu
G1 ultra	1.0	32	1.3	5.7	9.6	2.1	4.0	3.4	2.5
G1 0.1F	0.9	30	1.3	5.8	11	2.2	4.5	3.6	3.4
G1 0.45F	0.9	31	1.5	6.9	11	2.6	3.8	5.0	2.9
G1 Tot	1.0	29	1.2	6.0	11	2.2	3.2	3.8	2.8
G2 ultra	1.0	38	1.7	10	18	3.9	8.7	5.9	5.1
G2 0.1F	1.1	38	1.7	10	18	3.9	8.9	6.1	5.0
G2 0.45F	1.0	38	1.7	9.5	18	3.9	8.9	5.9	5.1
G2 Tot	1.0	38	1.7	9.9	18	3.8	8.6	5.9	5.1
G3 ultra	1.0	36	1.5	8.2	16	3.3	7.7	5.9	4.5
G3 0.1F	1.0	36	1.6	8.5	17	3.5	7.8	5.7	4.8
G3 0.45F	1.0	35	1.5	8.5	16	3.4	7.7	5.7	4.7
G3 Tot	1.0	36	1.5	8.6	16	3.3	7.6	5.6	4.8
G4 ultra	1.0	34	1.5	8.2	16	3.3	7.9	5.6	5.3
G4 0.1F	1.0	35	1.5	8.4	16	3.4	7.4	5.6	5.0
G4 0.45F	1.0	34	1.5	8.4	16	3.3	7.7	5.6	4.9
G4 Tot	1.0	35	1.5	8.4	16	3.4	7.5	5.7	4.6
G5 ultra	1.0	35	1.5	8.4	16	3.3	7.4	5.4	4.9
G5 0.1F	1.0	34	1.4	8.0	16	3.2	7.5	5.9	5.0
G5 0.45F	1.0	36	1.5	8.4	16	3.3	7.7	5.7	5.1
G5 Tot	1.0	35	1.5	8.3	16	3.3	7.5	5.6	4.8
G7 ultra	0.7	23	0.8	4.6	6.6	1.5	3.1	2.4	2.9
G7 0.1F	0.7	22	1.2	6.1	7.7	2.1	4.2	2.9	3.4
G7 0.45F	0.7	25	1.0	5.0	7.6	1.6	4.6	3.5	2.8
G7 Tot	0.7	24	1.1	5.8	8.7	2.1	4.1	3.2	3.5

10/11/16	Pr/Gd	Nd/Tb	Sm/Dy	Sm/Ho	Nd/Er	Sm/Er	Eu/Tm	Gd/Yb	Tb/Lu
G1 ultra	0.9	29	1.5	7.8	9.2	2.4	4.3	3.6	2.6
G1 0.1F	1.0	32	1.3	5.9	10	2.1	4.0	3.9	3.1
G1 0.45F	0.9	30	1.3	5.9	12	2.5	4.2	3.8	3.3
G1 Tot	0.9	33	1.2	5.7	10	2.1	4.0	3.6	3.1
G2 ultra	1.1	38	1.7	9.9	18	3.9	8.8	5.9	5.0
G2 0.1F	1.0	39	1.7	9.8	18	3.8	8.9	5.8	5.0
G2 0.45F	1.0	38	1.7	9.8	18	3.8	8.9	5.8	5.0
G2 Tot	1.1	38	1.7	9.8	18	3.8	8.7	5.9	5.1
G3 ultra	1.1	35	1.4	8.2	15	3.1	7.4	4.9	4.0
G3 0.1F	1.0	35	1.5	8.5	15	3.2	7.7	5.2	4.4
G3 0.45F	1.1	35	1.6	9.0	16	3.6	7.5	4.9	4.1
G3 Tot	1.0	35	1.6	8.6	16	3.5	7.0	5.2	4.1
G4 ultra	1.0	35	1.4	8.4	15	3.1	7.2	4.9	4.3
G4 0.1F	1.0	35	1.4	7.8	15	3.1	7.0	5.4	4.9
G4 0.45F	1.0	34	1.5	8.2	15	3.1	7.0	5.1	4.4
G4 Tot	1.0	35	1.5	8.8	15	3.2	8.1	5.2	4.3
G5 ultra	1.1	38	1.5	8.2	16	3.1	6.8	5.3	4.1
G5 0.1F	1.1	37	1.5	7.5	15	2.8	6.6	5.3	4.9
G5 0.45F	1.1	37	1.5	8.5	16	3.1	6.9	5.3	4.1
G5 Tot	1.0	34	1.4	7.8	15	3.1	7.0	5.5	4.4
G7 ultra	0.6	23	1.0	5.6	7.4	2.0	3.1	3.0	2.1
G7 0.1F	0.7	22	1.3	6.5	8.4	2.4	4.2	3.3	4.1
G7 0.45F	0.8	23	1.1	5.7	8.3	2.1	4.4	3.2	3.4
G7 Tot	0.7	30	1.2	6.1	13	2.7	4.6	4.4	4.2
15/11/16	Pr/Gd	Nd/Tb	Sm/Dy	Sm/Ho	Nd/Er	Sm/Er	Eu/Tm	Gd/Yb	Tb/Lu
G1 ultra	0.9	29	1.2	5.6	8.8	1.9	3.2	3.1	2.2
G1 0.1F	1.0	32	1.2	6.2	10	2.1	4.2	3.2	2.9
G1 0.45F	1.0	32	1.3	6.4	10	2.3	3.8	3.4	2.8
G1 Tot	1.0	31	1.1	5.3	10	2.0	3.4	3.3	3.1
G2 ultra	1.1	37	1.7	9.8	18	3.9	8.7	5.8	4.9
G2 0.1F	1.0	38	1.7	9.8	18	3.8	8.8	5.8	5.0
G2 0.45F	1.0	37	1.7	9.7	18	3.8	8.7	5.8	5.0
G2 Tot	1.0	37	1.7	9.8	18	3.8	8.8	5.9	5.0
G3 ultra	1.0	35	1.6	8.4	16	3.4	6.8	5.2	4.0
G3 0.1F	1.1	35	1.5	8.2	15	3.2	7.8	5.1	4.2
G3 0.45F	1.0	36	1.6	8.5	15	3.3	7.8	5.2	4.4
G3 Tot	1.0	37	1.6	8.5	16	3.3	7.6	5.0	4.1
G4 ultra	1.0	35	1.6	8.4	14	3.2	6.4	4.8	3.9
G4 0.1F	1.0	36	1.5	8.2	15	3.0	7.5	5.0	4.2
G4 0.45F	1.0	35	1.5	7.8	15	3.1	6.6	5.2	4.2
G4 Tot	1.0	34	1.6	8.6	14	3.2	6.6	5.1	4.3
G5 ultra	1.0	36	1.3	7.1	16	3.1	6.1	5.1	4.6
G5 0.1F	1.1	39	1.5	8.2	16	3.3	6.8	5.3	4.1
G5 0.45F	1.0	36	1.5	8.0	16	3.2	6.7	5.1	4.3
G5 Tot	1.0	34	1.4	8.1	15	3.0	6.2	4.8	4.6
G7 ultra	0.7	20	1.1	5.0	8.0	2.2	3.9	2.7	3.2
G7 0.1F	0.6	22	1.2	6.4	8.9	2.6	4.5	4.1	4.0
G7 0.45F	0.7	22	1.2	6.6	9.0	2.4	4.6	3.5	3.8
G7 Tot	1.1	28	1.2	6.3	11	2.4	5.2	3.5	3.6

06/12/16	Pr/Gd	Nd/Tb	Sm/Dy	Sm/Ho	Nd/Er	Sm/Er	Eu/Tm	Gd/Yb	Tb/Lu
G1 ultra	0.8	34	1.3	7.1	9.5	2.1	3.5	3.6	2.4
G1 0.1F	0.9	35	1.2	6.1	12	2.3	4.3	4.2	3.5
G1 0.45F	0.9	29	1.1	5.7	11	2.1	4.0	4.2	3.4
G1 Tot	0.9	28	1.2	6.1	12	2.6	3.7	3.4	3.2
G2 ultra	1.1	38	1.7	9.7	18	3.8	8.8	5.8	5.1
G2 0.1F	1.1	38	1.7	9.8	18	3.8	8.7	5.8	5.1
G2 0.45F	1.1	38	1.7	9.5	18	3.7	8.7	5.7	5.0
G2 Tot	1.1	38	1.7	9.7	18	3.7	8.7	5.8	5.1
G3 ultra	1.0	36	1.6	8.8	17	3.5	8.2	5.6	5.0
G3 0.1F	1.0	36	1.6	8.8	17	3.5	8.1	5.5	5.0
G3 0.45F	1.0	37	1.6	8.7	17	3.5	8.1	5.4	4.9
G3 Tot	1.0	38	1.6	8.7	17	3.4	8.2	5.7	4.9
G4 ultra	1.0	34	1.4	8.1	16	3.2	7.6	5.4	4.8
G4 0.1F	1.0	36	1.5	8.7	16	3.4	7.5	5.3	4.6
G4 0.45F	1.0	35	1.5	8.3	16	3.3	7.3	5.3	4.7
G4 Tot	1.0	35	1.5	8.3	16	3.3	7.3	5.3	4.7
G5 ultra	1.0	34	1.5	8.4	15	3.2	7.4	5.7	5.0
G5 0.1F	1.0	35	1.5	8.0	16	3.2	7.4	5.4	4.7
G5 0.45F	1.0	35	1.5	8.5	16	3.3	7.2	5.2	4.7
G5 Tot	1.0	34	1.5	8.4	15	3.3	7.7	5.2	4.7
G7 ultra	0.7	21	0.9	3.9	6.9	1.4	2.7	2.6	2.5
G7 0.1F	0.7	22	1.1	5.7	8.5	1.9	4.0	3.3	3.3
G7 0.45F	0.6	25	1.0	5.5	8.8	1.9	5.3	3.8	3.4
G7 Tot	0.6	26	1.0	5.9	9.7	2.1	4.9	3.9	3.4
01/06/17	Pr/Gd	Nd/Tb	Sm/Dy	Sm/Ho	Nd/Er	Sm/Er	Eu/Tm	Gd/Yb	Tb/Lu
G1 ultra	0.8	32	1.3	6.8	8.1	2.0	4.5	2.8	2.5
G1 0.1F	1.0	33	1.1	6.6	11	2.1	6.0	4.1	3.6
G1 0.45F	1.0	34	1.0	5.7	10	1.7	5.1	3.7	3.6
G1 Tot	1.0	33	1.1	6.7	10	2.0	4.7	4.0	3.2
G2 ultra	1.1	38	1.7	10.3	18	3.9	9.0	5.9	5.1
G2 0.1F	1.1	39	1.7	10.1	18	3.9	8.9	5.9	5.0
G2 0.45F	1.1	39	1.7	10.1	18	3.9	8.9	5.8	4.8
G2 Tot	1.1	39	1.7	10.1	18	3.9	9.2	5.8	4.8
G3 ultra	1.0	37	1.6	8.9	17	3.4	8.4	5.9	4.9
G3 0.1F	1.1	37	1.6	9.1	17	3.5	8.3	5.7	5.0
G3 0.45F	1.1	37	1.5	8.9	17	3.5	8.3	5.7	5.0
G3 Tot	1.1	37	1.6	8.9	17	3.5	8.3	5.8	4.9
G4 ultra	1.1	36	1.5	8.8	17	3.5	8.2	5.8	5.0
G4 0.1F	1.0	36	1.5	8.9	17	3.5	8.2	5.8	5.1
G4 0.45F	1.0	36	1.5	8.9	17	3.4	8.2	5.8	5.1
G4 Tot	1.1	36	1.5	8.9	17	3.5	8.4	5.8	5.1
G5 ultra	1.0	37	1.5	8.6	17	3.3	8.3	5.9	5.1
G5 0.1F	1.1	38	1.5	8.8	17	3.4	8.3	5.8	5.1
G5 0.45F	1.1	37	1.6	9.0	17	3.5	8.3	5.9	5.2
G5 Tot	1.0	37	1.6	8.9	17	3.5	8.1	6.1	5.1
G7 ultra	0.7	43	1.5	14.7	10	2.6	8.3	4.2	3.4
G7 0.45F	0.8	28	1.2	8.4	9.8	2.2	5.6	4.3	5.5
G7 Tot	0.7	27	1.0	6.9	10	2.5	5.6	3.9	3.3

14/09/17	Pr/Gd	Nd/Tb	Sm/Dy	Sm/Ho	Nd/Er	Sm/Er	Eu/Tm	Gd/Yb	Tb/Lu
G1 ultra	0.7	26	1.0	4.4	7.5	1.6	3.3	2.6	1.5
G1 0.1F	1.0	29	1.2	5.9	11	2.2	3.4	3.1	3.1
G1 0.45F	0.9	30	1.2	5.8	9.4	1.9	4.1	3.2	2.5
G1 Tot	0.9	29	1.2	5.5	11	2.2	3.7	3.2	2.8
G2 ultra	1.0	37	1.7	9.7	18	3.8	8.8	5.9	5.0
G2 0.1F	1.0	37	1.7	9.7	18	3.8	8.5	5.7	5.0
G2 0.45F	1.0	38	1.7	9.6	18	3.7	8.5	5.7	4.9
G2 Tot	1.0	38	1.6	9.6	18	3.7	8.6	5.6	5.1
G3 ultra	1.0	34	1.6	8.4	15	3.3	7.1	5.1	4.3
G3 0.1F	1.0	35	1.6	8.5	15	3.2	7.3	5.3	4.6
G3 0.45F	1.0	38	1.6	8.4	16	3.2	7.4	5.3	4.1
G3 Tot	1.0	36	1.6	8.8	16	3.5	7.6	5.2	3.9
G4 ultra	1.0	35	1.4	7.6	14	2.9	6.1	4.9	4.1
G4 0.1F	1.0	35	1.5	8.3	15	3.2	7.3	5.6	4.3
G4 0.45F	1.0	35	1.5	8.3	15	3.2	7.1	5.5	4.3
G4 Tot	1.0	35	1.5	8.2	15	3.2	6.9	5.3	4.1
G5 ultra	1.0	33	1.3	6.6	12	2.3	5.1	5.0	3.3
G5 0.1F	1.1	37	1.5	8.5	16	3.2	6.7	5.1	4.1
G5 0.45F	1.0	38	1.4	7.6	15	2.8	6.3	5.4	4.2
G5 Tot	1.0	34	1.4	8.1	15	3.1	6.0	5.3	4.1
G7 ultra	0.6	19	0.9	4.6	5.9	1.6	3.1	2.3	2.4
G7 0.1F	0.7	22	1.0	5.4	7.7	2.0	4.0	3.2	2.6
G7 0.45F	0.7	23	1.2	6.2	8.2	2.4	3.9	3.5	2.5
G7 Tot	0.8	21	1.2	6.0	8.0	2.1	4.0	3.1	3.5

Appendix C Hydrogeochemical data at Gate Gill

04/02/2016	Unit	G1	G2	G3	G4	G5	G6	G7
Temp	ºC	6.2	12.8	7.3	6.9	7.8	6.3	6.2
Eh	mV	338	410	263	159	113	96	84
pH		4.51	3.54	4	4.52	5.37	5.88	5.74
Cond	µs/cm	43.56	470	133.2	106.2	109.4	68.85	71.75
Alkalinity	mg/L as $CaCO_3$	<1	0	0	<1	2.2	13.3	9.7
Flowrate	L/s				44.98	45.42	5621	4160
Chloride (0.2F)	mg/l	8.1	6.83	8.19	9.15	11.22	11.09	10.47
Sulphate (0.2F)	mg/l	3.93	217.9	44.7	29.42	28.08	2.71	3.36
∑REE (0.1F)	µg/l	0.9601	64.08	12.14	6.464	4.533	0.6650	0.6913
∑REE (0.45F)	µg/l	1.062	63.71	12.61	7.203	4.514	0.7012	0.7688
∑REE (Tot)	µg/l	1.082	64.90	12.70	6.326	5.318	1.141	1.234
Ca (0.1F)	mg/l	0.62	17	3.7	5.64	7.05	5.23	5.38
Ca (0.45F)	mg/l	0.6	17.1	3.66	5.62	7.09	5.22	5.42
Ca (T)	mg/l	0.61	17	3.67	5.65	7.06	5.26	5.44
Mg (0.1F)	mg/l	0.8	11.3	2.74	2.23	2.15	1.43	1.44
Mg (0.45F)	mg/l	0.8	11.3	2.74	2.23	2.16	1.44	1.46
Mg (T)	mg/l	0.79	11.2	2.73	2.24	2.16	1.46	1.48
Na (0.1F)	mg/l	3.544	3.206	3.558	4.051	4.851	4.765	4.918
Na (0.45F)	mg/l	3.534	3.195	3.537	4.057	4.907	4.79	4.986
Na (T)	mg/l	3.505	3.199	3.58	4.004	4.917	4.802	4.966
K (0.1F)	mg/l	0.2	0.6	0.2	0.7	0.7	0.5	0.5
K (0.45F)	mg/l	0.1	0.6	0.2	0.7	0.7	0.5	0.5
K (T)	mg/l	0.2	0.6	0.2	0.7	0.7	0.5	0.6
Zn (0.1F)	µg/l	101.3	41710	7764	4802	4150	6.02	70.8
Zn (0.45F)	µg/l	101.7	41471	7751	4784	4176	5.07	71
Zn (T)	µg/l	97.5	41162	7753	4813	4197	5.89	77.3
Pb (0.1F)	µg/l	31.4	440	108	204	159	0.407	1.53
Pb (0.45F)	µg/l	31	434	110	214	162	0.485	1.84
Pb (T)	µg/l	30.4	435	110	213	177	0.823	2.77
Al (0.1F)	µg/l	261	5887	1362	588	55	41.3	41.3
Al (0.45F)	µg/l	271	5642	1361	587	69.3	52.6	52.2
Al (T)	µg/l	274	6191	1356	618	481	218	367
Fe (0.1F)	µg/l	3.98	3638	534	60.6	43.9	95	97
Fe (0.45F)	µg/l	4.12	3657	533	69.7	42.4	119	120
Fe (T)	µg/l	5.15	3906	573	90	82.6	224	305
Mn (0.1F)	µg/l	58.3	3825	785	479	419	33.3	41.1
Mn (0.45F)	µg/l	57.8	3668	784	478	422	35	41.3
Mn (T)	µg/l	55.3	4027	783	481	422	41	53.1
Si (0.1F)	mg/l	0.64	6.87	1.78	1.72	1.71	1.23	1.24
Si (0.45F)	mg/l	0.65	6.84	1.79	1.73	1.73	1.27	1.28
Si (T)	mg/l	0.64	6.84	1.77	1.73	1.74	1.48	1.8

13/04/2016	Unit	G1	G2	G3	G4	G5	G6	G7
Temp	ºC	7.6	13.4	7.7	7.8	7.7	7.5	7.6
Eh	mV	324	381	247	198	224	197	214
pH		4.60	3.70	4.3	4.3	4.94	6.47	6.15
Cond	µs/cm	46.78	470.1	87.64	88.99	94.56	51.95	54.13
Alkalinity	mg/L as $CaCO_3$	< 1.0	0.0	0	0	< 1.0	12.4	11.7
Flowrate	L/s			66.40	70.77	79.49		5260
Chloride (0.2F)	mg/l	7	6.94	7.52	7.62	10		6.1
Sulphate (0.2F)	mg/l	3.98	219.9	23.86	25.94	23.18		2.6
Fluoride (0.2F)	mg/l	0.28	0.13	0.18	0.14	0.34	3.6	0.29
∑REE (0.1F)	µg/l	0.9859	64.03	6.187	5.782	5.071	1.218	1.158
∑REE (0.45F)	µg/l	1.037	65.79	6.214	5.934	5.127	1.417	1.255
∑REE (Tot)	µg/l	1.077	63.00	6.269	6.020	5.555	1.793	1.725
Ca (0.1F)	mg/l	0.56	16.7	2.93	3.87	5.15	4.73	4.91
Ca (0.45F)	mg/l	0.52	16.7	2.90	3.83	5.12	4.73	4.90
Ca (T)	mg/l	0.52	16.8	2.91	3.86	5.14	4.78	4.95
Mg (0.1F)	mg/l	0.72	11.1	1.77	1.85	1.85	1.13	1.14
Mg (0.45F)	mg/l	0.73	11.1	1.76	1.86	1.86	1.12	1.15
Mg (T)	mg/l	0.73	11.2	1.77	1.87	1.87	1.16	1.18
Na (0.1F)	mg/l	3.513	3.350	3.647	3.709	5.076	3.912	4.013
Na (0.45F)	mg/l	3.497	3.325	3.623	3.711	5.082	3.894	4.026
Na (T)	mg/l	3.517	3.353	3.613	3.705	5.147	3.925	4.061
K (0.1F)	mg/l	0.1	0.6	0.3	0.5	0.5	0.4	0.4
K (0.45F)	mg/l	0.1	0.7	0.3	0.5	0.5	0.4	0.4
K (T)	mg/l	0.1	0.7	0.3	0.5	0.6	0.4	0.4
Zn (0.1F)	µg/l	75.5	39993	3635	3839	3598	9.63	72
Zn (0.45F)	µg/l	101.0	40281	3620	3826	3614	9.60	73
Zn (T)	µg/l	75.3	40788	3635	3873	3631	11.4	77
Pb (0.1F)	µg/l	28.2	416	126	153	140	1.08	2.33
Pb (0.45F)	µg/l	28.2	424	129	157	135	1.35	2.60
Pb (T)	µg/l	28.5	419	127	161	150	1.92	3.73
Al (0.1F)	µg/l	226	6571	734	669	112	96	100
Al (0.45F)	µg/l	242	6671	745	689	137	127	126
Al (T)	µg/l	244	6698	757	707	675	486	484
Fe (0.1F)	µg/l	3.35	3571	159	97	62	206	210
Fe (0.45F)	µg/l	4.35	3573	159	99	64	251	249
Fe (T)	µg/l	3.81	3888	185	120	125	459	462
Mn (0.1F)	µg/l	44.4	4475	435	438	411	26.6	32.5
Mn (0.45F)	µg/l	45.5	4499	434	437	412	29.3	33.3
Mn (T)	µg/l	44.5	4504	435	442	415	40.0	46.5
Si (0.1F)	mg/l	0.56	6.99	1.23	1.35	1.39	0.86	0.90
Si (0.45F)	mg/l	0.56	7.02	1.23	1.36	1.40	0.90	0.94
Si (T)	mg/l	0.56	7.06	1.23	1.38	1.45	1.46	1.46

12/05/2016	Unit	G1	G2	G3	G4	G5
Temp	ºC	14.3	15.2	13.4	18.2	17.7
Eh	mV	371	374	337	188	160
pH		4.33	3.7	3.85	4.55	4.69
Cond	µs/cm	45.54	462.3	227.8	215	204.8
Alkalinity	mg/L as $CaCO_3$	<1	<1	<1	<1	<1
Flowrate	L/s					8.78
Chloride (0.2F)	mg/l	7.00	4.40	5.70	6.10	7.00
Sulphate (0.2F)	mg/l	6.30	203.0	90.80	81.90	74.10
∑REE (0.1F)	µg/l	0.9911	67.25	28.84	24.91	20.94
∑REE (0.45F)	µg/l	1.057	67.46	29.19	25.08	21.08
∑REE (Tot)	µg/l	1.072	66.85	29.13	25.10	21.23
Ca (0.1F)	mg/l	0.84	17.9	10.4	11.6	12.6
Ca (0.45F)	mg/l	0.83	17.9	10.4	11.6	12.5
Ca (T)	mg/l	0.83	17.9	10.4	11.5	12.5
Mg (0.1F)	mg/l	0.94	12.3	6.09	5.79	5.50
Mg (0.45F)	mg/l	0.93	12.2	6.10	5.79	5.47
Mg (T)	mg/l	0.93	12.3	6.11	5.77	5.49
Na (0.1F)	mg/l	3.526	3.198	3.542	3.729	4.325
Na (0.45F)	mg/l	3.521	3.160	3.530	3.762	4.318
Na (T)	mg/l	3.514	3.187	3.541	3.735	4.331
K (0.1F)	mg/l	0.1	0.7	0.6	0.9	0.9
K (0.45F)	mg/l	0.2	0.7	0.6	0.9	0.9
K (T)	mg/l	0.1	0.7	0.6	0.9	0.9
Zn (0.1F)	µg/l	153	41048	19285	17748	16157
Zn (0.45F)	µg/l	152	41082	19332	17727	16119
Zn (T)	µg/l	153	41418	19249	17709	16091
Pb (0.1F)	µg/l	43.6	422	415	650	553
Pb (0.45F)	µg/l	43.4	420	414	646	554
Pb (T)	µg/l	43.8	428	413	647	558
Al (0.1F)	µg/l	231	6538	2768	2086	1322
Al (0.45F)	µg/l	237	6517	2779	2093	1329
Al (T)	µg/l	238	6530	2784	2076	1600
Fe (0.1F)	µg/l	4.53	3835	51.4	34.7	29.4
Fe (0.45F)	µg/l	4.97	3832	51.3	37.7	32.0
Fe (T)	µg/l	8.05	4095	54.0	41.2	36.4
Mn (0.1F)	µg/l	73.9	4401	1881	1684	1478
Mn (0.45F)	µg/l	74.0	4389	1889	1685	1477
Mn (T)	µg/l	71.4	4417	1882	1679	1474
Si (0.1F)	mg/l	0.65	7.26	3.75	3.73	3.61
Si (0.45F)	mg/l	0.64	7.25	3.76	3.73	3.56
Si (T)	mg/l	0.65	7.38	3.78	3.70	3.60

23/06/2016	Unit	G1	G2	G3	G4	G5	G7
Temp	^{o}C	14.8	15.5	15.7	17.2	15.9	16
Eh	mV	386	405	227	212	220	136
pH		4.5	3.68	4.19	4.29	4.11	6.3
Cond	µs/cm	45.19	462.1	269.5	256.2	251.8	100.1
Alkalinity	mg/L as $CaCO_3$	<1	0	0	0	0	16.0
Flowrate	L/s				6.78	5.53	203
Chloride (0.2F)	mg/l	6.6	7.1	2.9	6.9	8.2	7.8
Sulphate (0.2F)	mg/l	7.8	247	102	129	118	8.1
∑REE (0.1F)	µg/l	1.138	68.81	34.85	33.05	28.30	0.7458
∑REE (0.45F)	µg/l	1.147	67.76	34.84	32.96	28.49	0.9059
∑REE (Tot)	µg/l	1.160	68.63	35.45	32.89	28.35	0.9932
Ca (0.1F)	mg/l	1.03	17.7	12.6	14.3	15.2	9.30
Ca (0.45F)	mg/l	1.02	17.6	12.6	14.2	15.3	9.45
Ca (T)	mg/l	1.03	17.8	12.6	14.1	15.4	9.41
Mg (0.1F)	mg/l	1.01	12.2	7.10	7.09	6.89	2.53
Mg (0.45F)	mg/l	1.00	12.2	7.20	7.09	6.93	2.57
Mg (T)	mg/l	1.02	12.3	7.21	7.10	6.90	2.57
Na (0.1F)	mg/l	2.982	3.190	3.234	3.423	4.171	5.526
Na (0.45F)	mg/l	2.960	3.200	3.251	3.391	4.197	5.522
Na (T)	mg/l	3.002	3.236	3.254	3.407	4.220	5.538
K (0.1F)	mg/l	0.2	0.7	0.6	0.9	0.9	0.8
K (0.45F)	mg/l	0.2	0.7	0.7	0.9	1.0	0.8
K (T)	mg/l	0.2	0.7	0.7	0.9	1.0	0.8
Zn (0.1F)	µg/l	250	40525	22183	21577	20437	488
Zn (0.45F)	µg/l	246	40318	22285	21400	20605	500
Zn (T)	µg/l	258	40628	22418	21328	20648	500
Pb (0.1F)	µg/l	55	373	430	692	637	13
Pb (0.45F)	µg/l	57	381	429	686	638	14
Pb (T)	µg/l	57	383	439	692	639	14
Al (0.1F)	µg/l	249	6437	3261	2847	2285	35.9
Al (0.45F)	µg/l	256	6475	3423	2860	2305	56.9
Al (T)	µg/l	259	6531	3479	2856	2308	78.9
Fe (0.1F)	µg/l	4.53	4325	67.5	28.8	27.8	64
Fe (0.45F)	µg/l	4.38	4306	68.5	28.5	28	92
Fe (T)	µg/l	5.34	4533	66.4	29.2	29.4	114
Mn (0.1F)	µg/l	106	4360	2280	2151	1904	80
Mn (0.45F)	µg/l	105	4371	2307	2143	1913	81
Mn (T)	µg/l	108	4390	2291	2133	1912	84
Si (0.1F)	mg/l	0.65	7.16	4.30	4.46	4.39	1.57
Si (0.45F)	mg/l	0.65	7.24	4.35	4.46	4.41	1.59
Si (T)	mg/l	0.68	7.25	4.38	4.48	4.37	1.62

05/07/2016	Unit	G1	G2	G3	G4	G5	G7
Temp	°C	11.4	14.2	11.8	12.1	12.5	13.1
Eh	mV	275	387	298	290	238	203
pH		4.2	3.29	3.9	3.9	4.04	6.03
Cond	µs/cm	353.5	461.5	104.7	109.3	111.3	68.46
Alkalinity	mg/L as $CaCO_3$	0	0	0	0	0	17.0
Flowrate	L/s			42.44	40.08	40.10	1380
Chloride (0.2F)	mg/l	5.90	6.80	6.10	6.20	8.40	5.60
Sulphate (0.2F)	mg/l	5.40	243	39.10	40.60	37.50	6.30
∑REE (0.1F)	µg/l	0.9484	65.62	7.991	8.241	8.052	1.117
∑REE (0.45F)	µg/l	1.022	63.83	8.068	8.338	8.121	1.276
∑REE (Tot)	µg/l	1.059	59.01	8.049	8.334	8.217	1.762
Ca (0.1F)	mg/l	0.57	17.1	4.14	5.04	5.59	6.37
Ca (0.45F)	mg/l	0.57	16.9	4.08	5.05	5.58	6.30
Ca (T)	mg/l	0.57	17.0	4.14	5.03	5.57	6.35
Mg (0.1F)	mg/l	0.69	11.6	2.20	2.38	2.37	1.73
Mg (0.45F)	mg/l	0.68	11.5	2.17	2.40	2.39	1.72
Mg (T)	mg/l	0.68	11.6	2.20	2.38	2.39	1.74
Na (0.1F)	mg/l	2.695	3.110	2.876	2.959	4.094	3.940
Na (0.45F)	mg/l	2.683	3.105	2.855	2.950	4.063	3.925
Na (T)	mg/l	2.701	3.102	2.884	2.947	4.050	3.938
K (0.1F)	mg/l	<D.L.	0.7	0.3	0.4	0.5	0.5
K (0.45F)	mg/l	<D.L.	0.7	0.3	0.5	0.5	0.5
K (T)	mg/l	<D.L.	0.7	0.3	0.5	0.5	0.5
Zn (0.1F)	µg/l	90	41965	5308	5964	5916	171
Zn (0.45F)	µg/l	91	41503	5262	6013	5885	169
Zn (T)	µg/l	101	41569	5354	5981	5906	174
Pb (0.1F)	µg/l	39	369	169	243	240	4
Pb (0.45F)	µg/l	38	366	168	249	234	4
Pb (T)	µg/l	40	371	176	249	246	8
Al (0.1F)	µg/l	189	6236	855	859	822	70.1
Al (0.45F)	µg/l	202	6114	850	880	831	92.3
Al (T)	µg/l	207	6190	867	873	861	228
Fe (0.1F)	µg/l	2.60	4171	212	103	98.1	185
Fe (0.45F)	µg/l	3.03	4161	209	104	99.9	234
Fe (T)	µg/l	3.65	4440	227	108	117	331
Mn (0.1F)	µg/l	68	4392	585	615	599	37
Mn (0.45F)	µg/l	67	4340	581	617	597	37
Mn (T)	µg/l	69	4357	587	615	598	50
Si (0.1F)	mg/l	0.50	7.07	1.50	1.67	1.70	1.30
Si (0.45F)	mg/l	0.49	7.03	1.48	1.69	1.71	1.30
Si (T)	mg/l	0.50	7.09	1.50	1.68	1.73	1.52

15/09/2016	Unit	G1	G2	G3	G4	G5	G7
Temp	°C	15.5	15.5	16.3	16.9	16.1	14.9
Eh	mV	406	410	243	199	210	170
pH		4.65	3.74	4.39	4.65	4.99	6.47
Cond	µs/cm	38.6	454.7	146.8	141.3	132	76.26
Alkalinity	mg/L as $CaCO_3$	<1	0	0	<1	1.1	20.2
Flowrate	L/s			26.70	20.64	20.16	993
Chloride (0.2F)	mg/l	5.36	6.01	5.84	6.30	6.52	6.05
Sulphate (0.2F)	mg/l	4.95	194.5	52.63	50.35	45.91	4.60
Fluoride (0.2F)	mg/l		0.66	0.39	0.38	0.28	
∑REE (0.1F)	µg/l	0.8437	62.41	12.94	11.74	10.14	1.056
∑REE (0.45F)	µg/l	0.9103	63.31	12.88	11.85	10.61	1.126
∑REE (Tot)	µg/l	0.9252	62.71	12.95	11.85	10.45	1.157
Ca (0.1F)	mg/l	0.62	17.2	6.04	7.03	7.78	7.20
Ca (0.45F)	mg/l	0.59	16.5	5.99	7.16	7.72	7.24
Ca (T)	mg/l	0.60	17.5	6.04	7.05	7.76	7.22
Mg (0.1F)	mg/l	0.70	11.4	3.27	3.16	3.01	1.85
Mg (0.45F)	mg/l	0.70	11.0	3.24	3.22	2.99	1.87
Mg (T)	mg/l	0.71	11.5	3.28	3.18	3.00	1.86
Na (0.1F)	mg/l	3.037	3.303	3.244	3.465	3.850	4.393
Na (0.45F)	mg/l	3.028	3.200	3.224	3.528	3.861	4.348
Na (T)	mg/l	3.054	3.370	3.255	3.499	3.846	4.357
K (0.1F)	mg/l	0.1	0.7	0.4	0.7	0.7	0.5
K (0.45F)	mg/l	0.1	0.7	0.5	0.8	0.8	0.5
K (T)	mg/l	0.1	0.7	0.4	0.8	0.7	0.5
Zn (0.1F)	µg/l	111	37497	8277	7976	7561	184
Zn (0.45F)	µg/l	110	37675	8416	8096	7539	187
Zn (T)	µg/l	112	37035	8475	8166	8254	188
Pb (0.1F)	µg/l	39.3	415	237	305	273	3.71
Pb (0.45F)	µg/l	39.6	399	233	315	269	4.68
Pb (T)	µg/l	39.8	414	233	312	269	5.64
Al (0.1F)	µg/l	173	5713	1219	1013	419	49.5
Al (0.45F)	µg/l	187	5710	1206	1030	488	59.0
Al (T)	µg/l	192	5667	1225	1027	810	86.9
Fe (0.1F)	µg/l	2.18	4047	224	57.4	28.0	225
Fe (0.45F)	µg/l	2.23	3914	222	58.3	32.7	294
Fe (T)	µg/l	2.72	4623	254	64.6	58.0	362
Mn (0.1F)	µg/l	60.4	4099	979	888	790	37.0
Mn (0.45F)	µg/l	60.9	4140	973	907	783	37.8
Mn (T)	µg/l	60.7	4054	982	895	788	43.4
Si (0.1F)	mg/l	0.66	6.86	2.31	2.44	2.45	1.77
Si (0.45F)	mg/l	0.66	6.84	2.29	2.44	2.43	1.63
Si (T)	mg/l	0.66	6.85	2.32	2.47	2.43	1.65

13/10/2016	Unit	G1	G2	G3	G4	G5	G7
Temp	^{o}C	9.6	14	11.3	11.2	10.8	10
Eh	mV	236	361	232	220	217	218
pH		4.04	3.11	3.83	3.85	3.94	5.6
Cond	µs/cm	41.78	463.2	228.2	206.2	190	86.01
Alkalinity	mg/L as $CaCO_3$	0	0	0	0	0	23.7
Flowrate	L/s				9.87	7.74	495
Chloride (ultra)	mg/l	5.92	6.19	6.35	6.77	7.10	6.34
Sulphate (ultra)	mg/l	5.51	200.9	75.75	70.66	61.55	4.25
Fluoride (ultra)	mg/l		0.68	0.47	0.55	0.53	
∑REE (ultra F)	µg/l	0.5326	61.85	24.27	20.86	17.11	0.2617
∑REE (0.1F)	µg/l	0.8870	62.30	24.94	21.91	17.45	0.5677
∑REE (0.45F)	µg/l	0.9437	61.72	25.04	21.57	17.78	0.6458
∑REE (Tot)	µg/l	0.9758	62.40	24.93	21.60	18.02	0.7164
Ca (ultra F)	mg/l	0.68	15.8	9.56	10.3	11.0	7.15
Ca (0.1F)	mg/l	0.77	15.9	9.84	10.6	11.4	7.98
Ca (0.45F)	mg/l	0.74	15.9	9.84	10.6	11.4	7.98
Ca (T)	mg/l	0.74	16.0	9.93	10.6	11.4	7.97
Mg (ultra F)	mg/l	0.79	10.9	5.24	4.95	4.58	2.02
Mg (0.1F)	mg/l	0.83	10.9	5.31	5.02	4.67	2.16
Mg (0.45F)	mg/l	0.83	10.9	5.33	5.02	4.67	2.15
Mg (T)	mg/l	0.83	11.0	5.38	5.02	4.67	2.16
Na (ultra F)	mg/l	3.083	3.088	3.269	3.422	3.742	4.556
Na (0.1F)	mg/l	3.217	3.166	3.451	3.602	3.906	4.860
Na (0.45F)	mg/l	3.213	3.175	3.407	3.603	3.909	4.876
Na (T)	mg/l	3.214	3.167	3.382	3.589	3.914	4.847
K (ultra F)	mg/l	0.1	0.6	0.6	0.8	0.8	0.5
K (0.1F)	mg/l	0.1	0.7	0.6	0.9	0.9	0.6
K (0.45F)	mg/l	0.1	0.7	0.6	0.9	0.9	0.6
K (T)	mg/l	0.1	0.7	0.6	0.9	0.9	0.6
Zn (ultra F)	µg/l	138	37260	15171	13806	12168	220
Zn (0.1F)	µg/l	145	37525	15337	14025	12283	253
Zn (0.45F)	µg/l	145	38247	15382	13981	12451	255
Zn (T)	µg/l	146	37223	15414	14148	12503	257
Pb (ultra F)	µg/l	28.3	340	296	373	357	0.584
Pb (0.1F)	µg/l	37.5	348	307	391	369	3.62
Pb (0.45F)	µg/l	37.0	344	311	396	372	4.86
Pb (T)	µg/l	37.3	350	318	388	372	5.68
Al (ultra F)	µg/l	164	5414	2144	1658	663	27.2
Al (0.1F)	µg/l	204	5326	2163	1686	754	27.4
Al (0.45F)	µg/l	211	5286	2186	1681	899	37.6
Al (T)	µg/l	223	5341	2206	1687	1275	50.5
Fe (ultra F)	µg/l	1.63	1604	31.7	23.2	13.9	11.5
Fe (0.1F)	µg/l	1.4	4047	36.7	26.8	15.5	109
Fe (0.45F)	µg/l	1.81	4068	37	26.7	18.3	157

13/10/2016	Unit	G1	G2	G3	G4	G5	G7
Fe (T)	µg/l	3.78	4347	45.9	30.7	36.8	194
Mn (ultra F)	µg/l	68.2	3914	1649	1463	1225	39.8
Mn (0.1F)	µg/l	72.5	3914	1668	1482	1251	44.3
Mn (0.45F)	µg/l	72.4	3915	1669	1479	1253	44.3
Mn (T)	µg/l	72.7	3934	1687	1485	1250	46.6
Si (ultra F)	µg/l	0.73	6.94	3.5	3.55	3.41	1.68
Si (0.1F)	µg/l	0.72	6.93	3.49	3.53	3.4	1.71
Si (0.45F)	µg/l	0.72	6.85	3.51	3.52	3.41	1.71
Si (T)	µg/l	0.73	6.92	3.55	3.52	3.42	1.71

27/10/2016	Unit	G1	G2	G3	G4	G5	G7
Temp	^{o}C	9.4	14	10.8	10.9	10.8	10.7
Eh	mV	319	415	304	260	238	193
pH		4.43	3.27	3.99	4.07	4.06	5.92
Cond	µs/cm	41.29	459.6	194.4	186.4	174.5	84.73
Alkalinity	mg/L as $CaCO_3$	<1	0	0	0	0	22.7
Flowrate	L/s			17.57	11.54	10.03	586
Chloride (ultra)	mg/l	5.52	5.98	6.35	6.63	6.87	6.30
Sulphate (ultra)	mg/l	4.39	186.1	61.61	60.11	56.71	4.06
Fluoride (ultra)	mg/l		0.67	0.50	0.56	0.44	
∑REE (ultra F)	µg/l	0.5503	58.78	18.78	17.58	15.38	0.2296
∑REE (0.1F)	µg/l	0.8539	59.09	19.24	18.19	15.79	0.5759
∑REE (0.45F)	µg/l	0.9192	59.43	19.23	18.11	16.57	0.6618
∑REE (Tot)	µg/l	0.9368	59.25	19.31	18.15	15.98	0.7909
Ca (ultra F)	mg/l	0.65	15.5	8.16	8.97	9.58	6.85
Ca (0.1F)	mg/l	0.75	15.8	8.40	9.27	9.94	7.76
Ca (0.45F)	mg/l	0.72	15.6	8.38	9.30	9.94	7.76
Ca (T)	mg/l	0.72	15.6	8.36	9.29	9.84	7.77
Mg (ultra F)	mg/l	0.78	10.7	4.47	4.33	4.13	1.94
Mg (0.1F)	mg/l	0.81	10.8	4.52	4.41	4.22	2.08
Mg (0.45F)	mg/l	0.82	10.7	4.53	4.44	4.23	2.08
Mg (T)	mg/l	0.81	10.8	4.52	4.43	4.17	2.09
Na (ultra F)	mg/l	3.070	3.106	3.263	3.419	3.623	4.430
Na (0.1F)	mg/l	3.230	3.195	3.377	3.553	3.812	4.801
Na (0.45F)	mg/l	3.205	3.188	3.408	3.565	3.784	4.774
Na (T)	mg/l	3.191	3.159	3.372	3.576	3.798	4.798
K (ultra F)	mg/l	0.1	0.6	0.5	0.8	0.8	0.5
K (0.1F)	mg/l	0.2	0.7	0.6	0.9	0.9	0.7
K (0.45F)	mg/l	0.1	0.7	0.6	0.9	0.9	0.7
K (T)	mg/l	0.1	0.7	0.6	0.8	0.9	0.7
Zn (ultra F)	µg/l	132	35663	12255	11798	10670	195
Zn (0.1F)	µg/l	136	35942	12466	11866	10989	226
Zn (0.45F)	µg/l	136	35977	12466	12086	11030	227
Zn (T)	µg/l	137	36031	12478	11959	10982	232
Pb (ultra F)	µg/l	26.8	344	262	329	321	0.340
Pb (0.1F)	µg/l	35.0	350	273	348	339	3.40
Pb (0.45F)	µg/l	34.9	349	276	347	340	4.46
Pb (T)	µg/l	35.3	351	272	343	334	6.15
Al (ultra F)	µg/l	147	5443	1793	1534	916	25.8
Al (0.1F)	µg/l	197	5528	1797	1546	1025	32.1
Al (0.45F)	µg/l	208	5502	1801	1565	1097	40.7
Al (T)	µg/l	208	5515	1795	1560	1262	69.2
Fe (ultra F)	µg/l	1.60	1658	61.9	32.9	10.9	20.4
Fe (0.1F)	µg/l	1.58	3054	73.0	39.4	28.6	115
Fe (0.45F)	µg/l	1.69	3046	75.2	41.3	38.4	156

27/10/2016	Unit	G1	G2	G3	G4	G5	G7
Fe (T)	µg/l	2.95	3715	90.7	46.3	51.9	240
Mn (ultra F)	µg/l	66.5	3876	1378	1265	1118	37.0
Mn (0.1F)	µg/l	69.1	3910	1396	1290	1142	40.1
Mn (0.45F)	µg/l	69.2	3893	1397	1296	1143	42.2
Mn (T)	µg/l	70.0	3896	1390	1294	1137	44.4
Si (ultra F)	µg/l	0.74	6.77	3.07	3.15	3.09	1.84
Si (0.1F)	µg/l	0.73	6.79	3.07	3.17	3.12	1.83
Si (0.45F)	µg/l	0.74	6.73	3.07	3.19	3.12	1.84
Si (T)	µg/l	0.75	6.80	3.06	3.18	3.08	1.89

10/11/2016	Unit	G1	G2	G3	G4	G5	G7
Temp	°C	5.5	12.6	6	6.3	6.4	5.2
Eh	mV	270	378	272	200	195	222
pH		4.64	3.42	4.28	4.48	5.04	5.69
Cond	µs/cm	34.85	460.4	75.77	82.41	83.69	66.95
Alkalinity	mg/L as $CaCO_3$	<1	0	0	<1	1.5	12.3
Flowrate	L/s			92.63	82.85	87.59	10200
Chloride (ultra)	mg/l	4.83	6.18	5.29	6.06	6.30	7.93
Sulphate (ultra)	mg/l	3.27	212.2	17.40	21.57	19.59	1.44
Fluoride (ultra)	mg/l		0.83	0.16			
∑REE (ultra F)	µg/l	0.6435	59.25	4.455	5.084	4.115	0.3236
∑REE (0.1F)	µg/l	1.022	60.26	5.148	5.868	5.092	0.9816
∑REE (0.45F)	µg/l	1.049	60.48	5.225	5.915	5.283	1.117
∑REE (Tot)	µg/l	1.078	60.49	5.278	6.246	5.955	3.725
Ca (ultra F)	mg/l	0.44	15.6	2.05	3.00	3.90	3.60
Ca (0.1F)	mg/l	0.52	15.7	2.21	3.22	4.38	4.94
Ca (0.45F)	mg/l	0.51	15.6	2.19	3.23	4.37	4.97
Ca (T)	mg/l	0.51	15.8	2.20	3.23	4.38	5.12
Mg (ultra F)	mg/l	0.62	10.7	1.45	1.66	1.64	1.07
Mg (0.1F)	mg/l	0.66	10.7	1.49	1.73	1.76	1.30
Mg (0.45F)	mg/l	0.66	10.7	1.49	1.73	1.75	1.32
Mg (T)	mg/l	0.67	10.8	1.49	1.73	1.76	1.43
Na (ultra F)	mg/l	2.718	3.107	2.831	2.859	3.465	4.280
Na (0.1F)	mg/l	2.850	3.137	2.966	3.037	3.780	4.654
Na (0.45F)	mg/l	2.845	3.137	2.964	3.053	3.774	4.666
Na (T)	mg/l	2.842	3.159	2.965	3.060	3.786	4.765
K (ultra F)	mg/l	<D.L.	0.6	0.2	0.3	0.3	0.9
K (0.1F)	mg/l	0.1	0.7	0.2	0.4	0.4	1.2
K (0.45F)	mg/l	0.1	0.7	0.2	0.4	0.4	1.2
K (T)	mg/l	0.1	0.7	0.2	0.4	0.4	1.5
Zn (ultra F)	µg/l	74.9	35480	2616	3311	3121	22.5
Zn (0.1F)	µg/l	79.2	35523	2709	3459	3377	36.0
Zn (0.45F)	µg/l	80.9	35787	2720	3462	3363	34.8
Zn (T)	µg/l	78.8	35887	2735	3460	3383	44.7
Pb (ultra F)	µg/l	17.2	362	62.6	95.4	80.6	0.282
Pb (0.1F)	µg/l	24.0	368	72.2	115	103	0.899
Pb (0.45F)	µg/l	23.8	364	73.0	119	106	1.17
Pb (T)	µg/l	24.2	374	73.1	123	115	4.70
Al (ultra F)	µg/l	137	5096	554	595	130	40.8
Al (0.1F)	µg/l	197	5058	574	632	201	81.0
Al (0.45F)	µg/l	209	5066	584	636	215	117
Al (T)	µg/l	207	5094	586	682	657	1480
Fe (ultra F)	µg/l	2.46	1587	73.2	34.2	17.0	47.4
Fe (0.1F)	µg/l	2.51	2538	131	99.4	63.1	232
Fe (0.45F)	µg/l	2.98	2542	133	100	65.2	297

10/11/2016	Unit	G1	G2	G3	G4	G5	G7
Fe (T)	µg/l	6.27	3411	182	163	164	1678
Mn (ultra F)	µg/l	47.3	3853	343	404	378	25.3
Mn (0.1F)	µg/l	51.0	3871	352	417	405	40.7
Mn (0.45F)	µg/l	50.8	3862	353	420	404	42.5
Mn (T)	µg/l	50.9	3890	353	422	407	265
Si (ultra F)	µg/l	0.62	6.72	1.13	1.31	1.35	1.33
Si (0.1F)	µg/l	0.63	6.72	1.13	1.31	1.36	1.33
Si (0.45F)	µg/l	0.64	6.74	1.13	1.32	1.36	1.38
Si (T)	µg/l	0.63	6.76	1.13	1.37	1.45	3.75

15/11/2016	Unit	G1	G2	G3	G4	G5	G7
Temp	°C	9.6	13.8	9.8	9.7	9.7	10.3
Eh	mV	242	380	229	196	183	220
pH		4.84	3.64	4.6	4.69	4.96	5.68
Cond	µs/cm	33.77	456.7	63.99	67.14	65.55	59.6
Alkalinity	mg/L as $CaCO_3$	<1	0	<1	<1	0.9	12.7
Flowrate	L/s			109.5	107.7	115.1	4980
Chloride (ultra)	mg/l	4.54	6.26	4.93	5.05	5.64	5.89
Sulphate (ultra)	mg/l	3.21	181.3	12.71	14.88	14.07	1.69
Fluoride (ultra)	mg/l		0.96				
∑REE (ultra F)	µg/l	0.5549	58.26	3.217	3.447	2.778	0.3114
∑REE (0.1F)	µg/l	0.9917	59.23	4.068	4.276	3.907	1.201
∑REE (0.45F)	µg/l	0.9968	59.40	4.106	4.306	3.929	1.329
∑REE (Tot)	µg/l	1.019	59.73	4.161	4.384	4.180	2.602
Ca (ultra F)	mg/l	0.39	15.4	1.57	2.13	2.70	3.66
Ca (0.1F)	mg/l	0.44	15.6	1.70	2.29	3.00	5.08
Ca (0.45F)	mg/l	0.44	15.5	1.71	2.28	3.00	5.11
Ca (T)	mg/l	0.44	15.6	1.72	2.28	3.02	5.16
Mg (ultra F)	mg/l	0.58	10.6	1.17	1.27	1.24	1.03
Mg (0.1F)	mg/l	0.61	10.7	1.20	1.31	1.32	1.26
Mg (0.45F)	mg/l	0.61	10.6	1.21	1.32	1.32	1.28
Mg (T)	mg/l	0.61	10.7	1.22	1.33	1.33	1.33
Na (ultra F)	mg/l	2.657	3.191	2.710	2.763	3.095	3.699
Na (0.1F)	mg/l	2.818	3.255	2.845	2.921	3.327	4.063
Na (0.45F)	mg/l	2.827	3.225	2.853	2.924	3.311	4.054
Na (T)	mg/l	2.842	3.254	2.883	2.940	3.342	4.122
K (ultra F)	mg/l	<D.L.	0.6	0.2	0.2	0.3	0.5
K (0.1F)	mg/l	0.1	0.7	0.2	0.3	0.3	0.7
K (0.45F)	mg/l	0.1	0.7	0.3	0.3	0.3	0.7
K (T)	mg/l	0.1	0.7	0.2	0.3	0.3	0.9
Zn (ultra F)	µg/l	69.8	35038	1886	2200	2048	40.7
Zn (0.1F)	µg/l	74.4	34832	1959	2271	2192	68.7
Zn (0.45F)	µg/l	73.6	34872	1961	2292	2195	70.1
Zn (T)	µg/l	74.4	35198	1979	2296	2200	72.5
Pb (ultra F)	µg/l	16.7	394	61.1	81.9	70.1	0.299
Pb (0.1F)	µg/l	24.0	397	72.0	102	89.9	2.02
Pb (0.45F)	µg/l	24.1	398	72.2	103	90.5	2.24
Pb (T)	µg/l	24.1	404	72.2	105	93.9	3.86
Al (ultra F)	µg/l	116	5086	430	438	182	35.6
Al (0.1F)	µg/l	189	5067	464	476	263	92.7
Al (0.45F)	µg/l	194	5074	467	478	282	116
Al (T)	µg/l	195	5087	473	499	473	993
Fe (ultra F)	µg/l	2.48	1346	57.4	34.1	4.68	38.0
Fe (0.1F)	µg/l	2.59	2552	106	83.8	55.4	257
Fe (0.45F)	µg/l	2.61	2533	106	84.5	56.5	309

15/11/2016	Unit	G1	G2	G3	G4	G5	G7
Fe (T)	µg/l	5.46	3362	137	108	111	944
Mn (ultra F)	µg/l	39.1	3812	252	275	256	20.2
Mn (0.1F)	µg/l	41.3	3847	260	283	271	32.4
Mn (0.45F)	µg/l	41.3	3817	261	285	271	36.0
Mn (T)	µg/l	41.9	3850	263	285	273	73.0
Si (ultra F)	µg/l	0.66	6.79	1.04	1.15	1.17	1.46
Si (0.1F)	µg/l	0.66	6.76	1.04	1.16	1.18	1.45
Si (0.45F)	µg/l	0.66	6.79	1.04	1.15	1.18	1.51
Si (T)	µg/l	0.67	6.79	1.05	1.18	1.21	3.01

06/12/2016	Unit	G1	G2	G3	G4	G5	G7
Temp	^{o}C	4.7	13.2	6.8	6.8	6.4	4.2
Eh	mV	394	422	367	298	216	211
pH		4.58	3.58	4.20	4.51	4.74	5.87
Cond	µs/cm	37.29	467.6	169.0	160.0	146.7	76.2
Alkalinity	mg/L as $CaCO_3$	<1.0	<1.0	<1.0	<1.0	33.0	18.1
Flowrate	L/s			20.72	16.82	15.34	734
Chloride (0.45F)	mg/l	4.7	4.0	4.0	5.4	5.3	6.1
Sulphate (0.45F)	mg/l	4.9	180	51.6	51.1	46.3	6.6
∑REE (ultra F)	µg/l	0.4908	63.41	15.46	14.35	12.53	0.2204
∑REE (0.1F)	µg/l	0.9669	63.37	15.65	14.91	13.09	0.5635
∑REE (0.45F)	µg/l	0.9514	63.31	15.80	14.90	13.15	0.6207
∑REE (Tot)	µg/l	0.9749	63.05	15.99	14.91	13.96	0.6816
Ca (ultra F)	mg/l	0.57	16.2	6.31	7.05	7.66	6.12
Ca (0.1F)	mg/l	0.64	16.4	6.43	7.27	7.93	6.88
Ca (0.45F)	mg/l	0.64	16.4	6.45	7.30	7.92	6.94
Ca (T)	mg/l	0.66	16.4	6.45	7.32	7.99	6.94
Mg (ultra F)	mg/l	0.57	11.2	3.87	3.75	3.54	1.73
Mg (0.1F)	mg/l	0.64	11.2	3.88	3.81	3.59	1.84
Mg (0.45F)	mg/l	0.64	11.3	3.90	3.81	3.58	1.86
Mg (T)	mg/l	0.66	11.4	3.90	3.81	3.61	1.86
Na (ultra F)	mg/l	2.74	3.12	3.04	3.24	3.45	4.06
Na (0.1F)	mg/l	2.88	3.14	3.14	3.40	3.65	4.35
Na (0.45F)	mg/l	2.88	3.11	3.14	3.35	3.65	4.35
Na (T)	mg/l	2.89	3.13	3.15	3.36	3.67	4.35
K (ultra F)	mg/l	<1	<1	<1	<1	<1	<1
K (0.1F)	mg/l	<1	<1	<1	<1	<1	<1
K (0.45F)	mg/l	<1	<1	<1	<1	<1	<1
K (T)	mg/l	<1	<1	<1	<1	<1	<1
Zn (ultra F)	µg/l	118	38250	10560	9910	8910	194
Zn (0.1F)	µg/l	124	38530	10660	10180	9090	220
Zn (0.45F)	µg/l	123	38630	10890	10220	9190	223
Zn (T)	µg/l	124	39340	10900	10420	9480	223
Pb (ultra F)	µg/l	18.8	381	189	244	225	0.500
Pb (0.1F)	µg/l	27.3	386	200	257	237	3.00
Pb (0.45F)	µg/l	27.3	389	202	259	237	3.60
Pb (T)	µg/l	27.2	395	205	260	256	4.10
Al (ultra F)	µg/l	150	5906	1561	1426	892	23.0
Al (0.1F)	µg/l	220	5892	1562	1431	1018	35.0
Al (0.45F)	µg/l	221	5955	1573	1428	1060	42.0
Al (T)	µg/l	226	5979	1574	1439	1575	67.0
Fe (ultra F)	µg/l	1.00	2415	220	74.0	13.0	13.0
Fe (0.1F)	µg/l	1.00	2860	265	98.0	28.0	99.0
Fe (0.45F)	µg/l	1.00	2866	274	96.0	33.0	122
Fe (T)	µg/l	2.00	3646	318	103	241	160

06/12/2016	Unit	G1	G2	G3	G4	G5	G7
Mn (ultra F)	µg/l	59.0	4221	1173	1070	946	41.0
Mn (0.1F)	µg/l	62.0	4251	1178	1086	964	45.0
Mn (0.45F)	µg/l	62.0	4270	1182	1088	964	45.0
Mn (T)	µg/l	63.0	4350	1180	1089	973	46.0
Si (ultra F)	µg/l	0.77	7.1	2.7	2.8	2.7	1.9
Si (0.1F)	µg/l	0.77	7.1	2.7	2.8	2.7	1.9
Si (0.45F)	µg/l	0.77	7.1	2.7	2.8	2.7	1.9
Si (T)	µg/l	0.78	7.2	2.7	2.8	2.8	2.0

01/06/2017	Unit	G1	G2	G3	G4	G5	G7
Temp	oC	13.1	14.3	14.2	14.6	14.7	15.4
Eh	mV	283	421	265	193	174	122
pH		4.73	3.64	4.33	4.72	4.93	6.88
Cond	µs/cm	42.11	461.9	255.7	248.1	241.7	96.55
Alkalinity	mg/L as CaCO3	<1	0	0	<1	<1	25.5
Flowrate	L/s			12.68	8.03	6.88	253
Chloride (ultra)	mg/l	4.76	5.12	5.45	5.56	7.88	5.89
Sulphate (ultra)	mg/l	5.16	181.6	94.55	93.38	88.21	5.95
Fluoride (ultra)	mg/l		0.73	0.40			
∑REE (ultra F)	µg/l	0.3749	60.73	32.74	29.73	24.34	0.2816
∑REE (0.1F)	µg/l	0.8692	60.94	33.32	30.19	24.95	
∑REE (0.45F)	µg/l	0.9249	61.40	33.32	30.24	25.07	0.7079
∑REE (Tot)	µg/l	0.9576	61.63	33.48	30.50	25.34	0.7995
Ca (ultra F)	mg/l	0.77	15.8	11.3	12.5	14.0	7.57
Ca (0.1F)	mg/l	0.87	15.9	11.4	12.9	14.3	
Ca (0.45F)	mg/l	0.84	15.9	11.4	12.9	14.3	8.60
Ca (T)	mg/l	0.85	15.9	11.5	12.9	14.4	8.65
Mg (ultra F)	mg/l	0.73	10.4	5.83	5.66	5.38	1.89
Mg (0.1F)	mg/l	0.76	10.4	5.84	5.75	5.45	
Mg (0.45F)	mg/l	0.76	10.4	5.84	5.77	5.45	2.04
Mg (T)	mg/l	0.77	10.4	5.84	5.78	5.50	2.04
Na (ultra F)	mg/l	1.721	2.180	2.083	2.158	3.224	3.410
Na (0.1F)	mg/l	1.816	2.252	2.179	2.248	3.399	
Na (0.45F)	mg/l	1.808	2.259	2.204	2.266	3.417	3.721
Na (T)	mg/l	1.821	2.232	2.226	2.315	3.439	3.803
K (ultra F)	mg/l	1.4	1.7	1.8	1.9	1.9	1.7
K (0.1F)	mg/l	1.3	1.7	1.8	2.0	2.0	
K (0.45F)	mg/l	1.3	1.8	1.8	2.0	2.0	1.8
K (T)	mg/l	1.3	1.8	1.9	2.0	2.0	1.8
Zn (ultra F)	µg/l	186	36493	18190	17515	16060	273
Zn (0.1F)	µg/l	194	36459	18658	17856	16440	
Zn (0.45F)	µg/l	196	36980	18657	17926	16523	337
Zn (T)	µg/l	197	36802	18539	17784	16494	342
Pb (ultra F)	µg/l	26.2	385	422	421	366	0.741
Pb (0.1F)	µg/l	43.5	395	436	441	377	
Pb (0.45F)	µg/l	43.6	395	431	439	380	4.38
Pb (T)	µg/l	43.7	396	433	442	387	6.06
Al (ultra F)	µg/l	127	5249	2700	2193	1074	29.3
Al (0.1F)	µg/l	174	5184	2701	2206	1175	
Al (0.45F)	µg/l	179	5215	2701	2210	1191	36.9
Al (T)	µg/l	183	5229	2668	2217	1489	59.0
Fe (ultra F)	µg/l	2.50	1752	43.7	26.3	20.4	10.7
Fe (0.1F)	µg/l	1.48	3257	43.1	26.7	22.7	
Fe (0.45F)	µg/l	1.37	3270	43.1	27.2	21.9	105

01/06/2017	Unit	G1	G2	G3	G4	G5	G7
Fe (T)	µg/l	2.94	3858	47.5	28.2	28.7	144
Mn (ultra F)	µg/l	77.8	3862	1993	1864	1596	49.3
Mn (0.1F)	µg/l	80.8	3876	2005	1900	1619	
Mn (0.45F)	µg/l	81.9	3882	2020	1902	1624	66.1
Mn (T)	µg/l	82.7	3881	2024	1910	1628	70.5
Si (ultra F)	µg/l	0.54	6.88	4.09	4.08	3.88	1.19
Si (0.1F)	µg/l	0.54	6.87	4.04	4.07	3.91	
Si (0.45F)	µg/l	0.54	6.89	4.06	4.09	3.94	1.20
Si (T)	µg/l	0.53	6.84	4.04	4.08	3.95	1.24

14/09/2017	Unit	G1	G2	G3	G4	G5	G7
Temp	^{o}C	10.7	13.7	10.9	10.8	10.1	10.4
Eh	mV	272	383	263	208	169	149
pH		4.75	3.62	4.49	4.76	5.23	6.31
Cond	µs/cm	31.19	451.2	68.09	68.37	66.43	54.94
Alkalinity	mg/L as $CaCO_3$	<1	0	0	<1	1.3	12.6
Flowrate	L/s			85.66	95.68	100.3	4480
Chloride (ultra)	mg/l	4.03	5.97	4.60	4.65	4.66	4.76
Sulphate (ultra)	mg/l	3.34	176.8	14.60	16.03	14.14	2.35
∑REE (ultra F)	µg/l	0.3025	63.97	4.128	3.995	2.059	0.3349
∑REE (0.1F)	µg/l	0.8433	64.34	5.007	4.947	4.435	1.083
∑REE (0.45F)	µg/l	0.7702	64.64	5.024	5.062	4.528	1.190
∑REE (Tot)	µg/l	0.9124	65.21	5.033	4.971	4.733	1.468
Ca (ultra F)	mg/l	0.37	15.8	1.75	2.58	2.86	3.95
Ca (0.1F)	mg/l	0.43	15.9	1.94	2.82	3.38	5.12
Ca (0.45F)	mg/l	0.45	15.9	1.94	2.83	3.39	5.12
Ca (T)	mg/l	0.44	16.1	1.96	2.83	3.39	5.16
Mg (ultra F)	mg/l	0.53	10.8	1.29	1.40	1.31	1.10
Mg (0.1F)	mg/l	0.58	10.9	1.34	1.45	1.45	1.28
Mg (0.45F)	mg/l	0.58	10.9	1.34	1.46	1.44	1.29
Mg (T)	mg/l	0.60	10.9	1.35	1.46	1.45	1.29
Na (ultra F)	mg/l	2.622	3.359	2.753	2.902	3.033	3.544
Na (0.1F)	mg/l	2.828	3.432	2.943	3.130	3.350	3.904
Na (0.45F)	mg/l	2.845	3.449	2.959	3.096	3.399	3.915
Na (T)	mg/l	2.851	3.440	3.005	3.122	3.412	3.908
K (ultra F)	mg/l	0.1	0.7	0.3	0.4	0.4	0.5
K (0.1F)	mg/l	0.1	0.7	0.4	0.5	0.5	0.7
K (0.45F)	mg/l	0.1	0.7	0.4	0.5	0.5	0.7
K (T)	mg/l	0.1	0.7	0.4	0.5	0.5	0.7
Zn (ultra F)	µg/l	75.7	38139	2521	2663	2366	52.2
Zn (0.1F)	µg/l	83.9	38226	2627	2797	2647	82.1
Zn (0.45F)	µg/l	84.0	38328	2626	2806	2642	82.4
Zn (T)	µg/l	84.4	38478	2658	2805	2641	83.2
Pb (ultra F)	µg/l	8.45	491	61.6	69.1	45.9	0.139
Pb (0.1F)	µg/l	23.8	500	73.5	84.0	74.1	2.22
Pb (0.45F)	µg/l	23.5	502	72.3	84.4	73.3	2.48
Pb (T)	µg/l	23.8	506	72.8	85.1	78.7	3.02
Al (ultra F)	µg/l	72.4	5863	555	477	112	37.3
Al (0.1F)	µg/l	182	5822	571	537	187	102
Al (0.45F)	µg/l	187	5817	572	542	198	121
Al (T)	µg/l	194	5841	582	551	504	263
Fe (ultra F)	µg/l	1.74	1187	56.6	9.08	41.5	54.6
Fe (0.1F)	µg/l	2.03	3464	181	106	77.9	291
Fe (0.45F)	µg/l	2.06	3456	181	107	79.8	336
Fe (T)	µg/l	3.59	4016	212	126	117	446

14/09/2017	Unit	G1	G2	G3	G4	G5	G7
Mn (ultra F)	µg/l	36.3	3874	300	301	270	20.8
Mn (0.1F)	µg/l	39.5	3893	311	315	299	34.4
Mn (0.45F)	µg/l	39.9	3894	311	316	299	35.6
Mn (T)	µg/l	39.7	3923	314	316	300	44.6
Si (ultra F)	µg/l	0.69	7.11	1.18	1.38	1.38	1.43
Si (0.1F)	µg/l	0.70	7.14	1.18	1.36	1.39	1.43
Si (0.45F)	µg/l	0.70	7.13	1.18	1.36	1.39	1.45
Si (T)	µg/l	0.71	7.16	1.19	1.37	1.40	1.63

Appendix D REE speciation modelling results at G1 to G5

REE speciation results at G1 to G5 from sampling occasions when ultrafiltration was undertaken and the calculations are based on ultra/ 0.005µm filtered cations results.

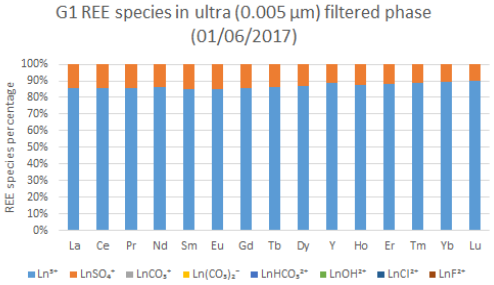

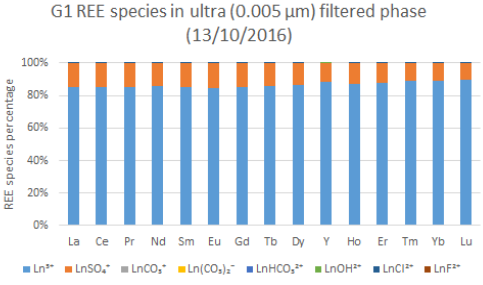

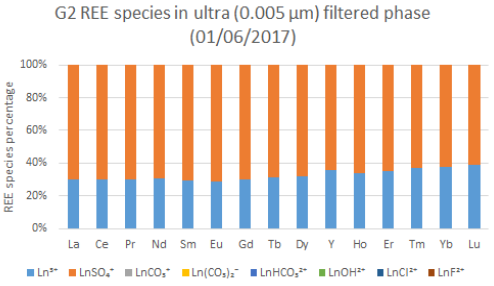

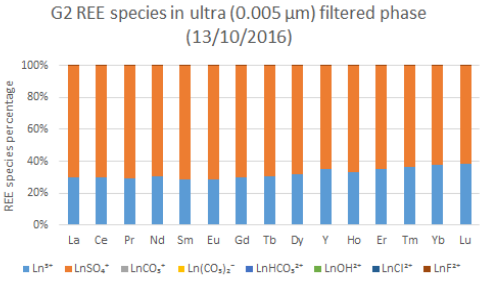

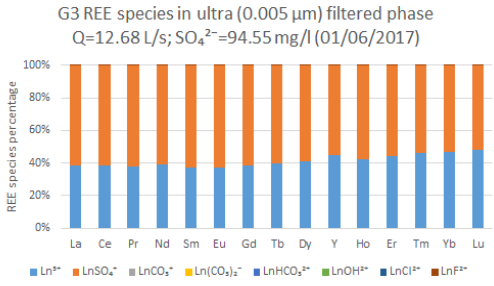

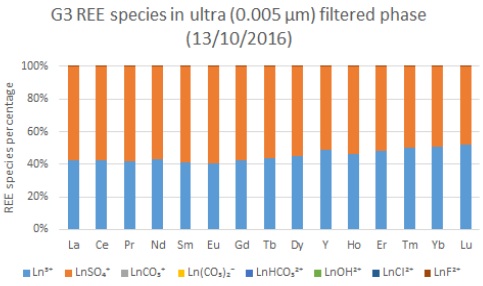

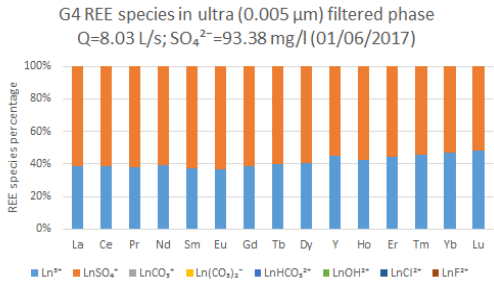

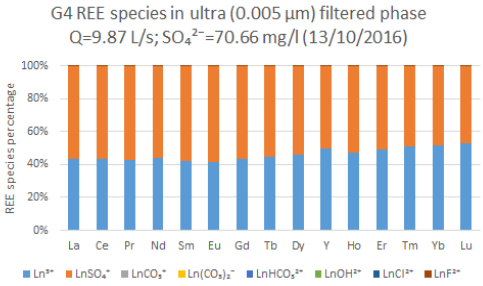

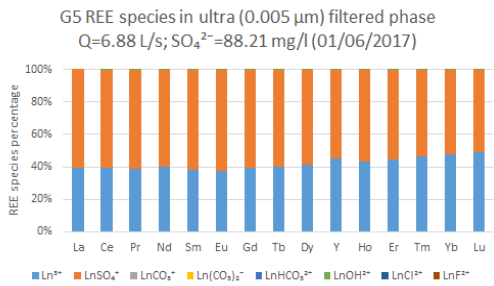

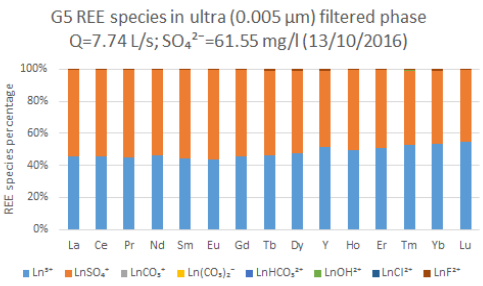

Sampling occasions are displayed in increasing order of the flow condition, and the flowrate of sampling sites where flowrate measurement was undertaken is also shown in graphs.

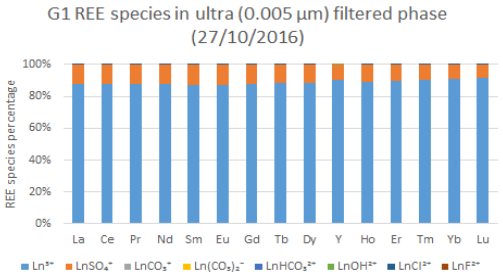

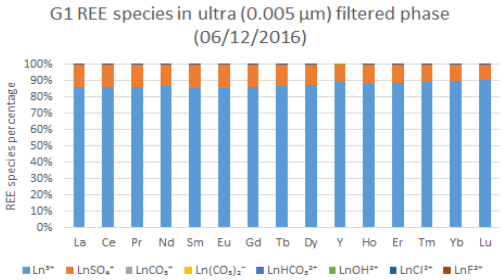

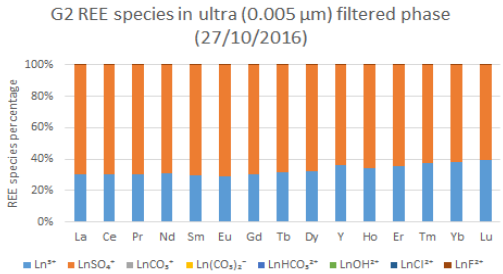

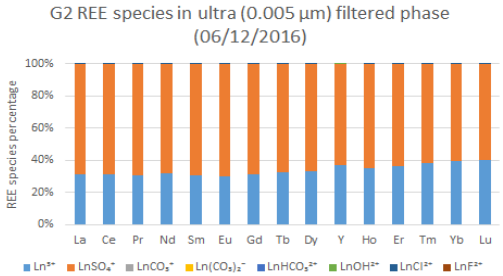

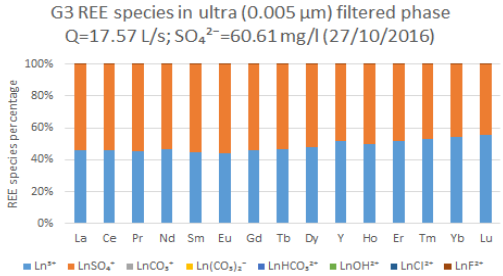

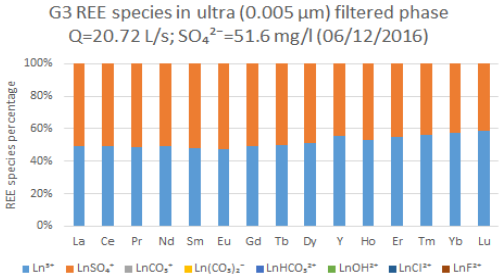

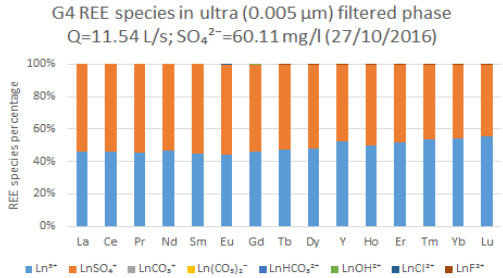

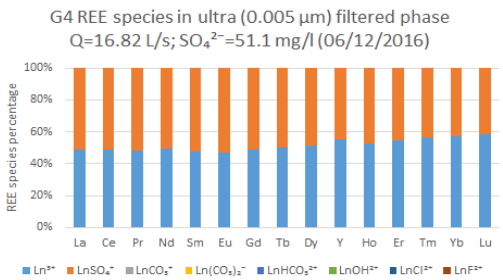

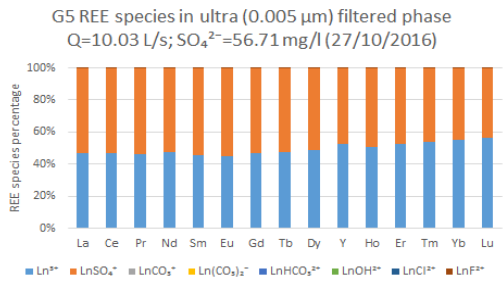

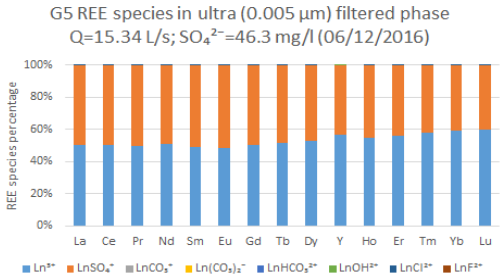

G1 REE species in ultra (0.005 µm) filtered phase (10/11/2016)

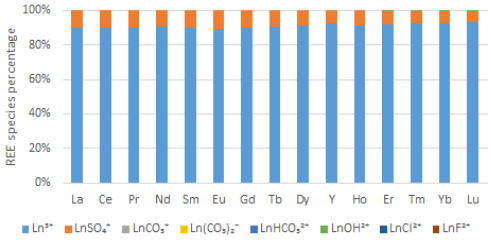

G1 REE species in ultra (0.005 µm) filtered phase (14/09/2017)

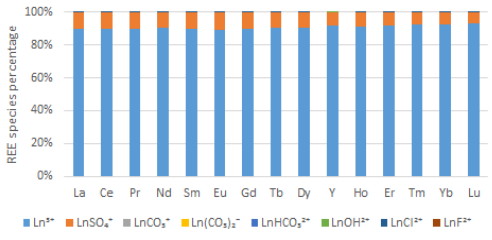

G2 REE species in ultra (0.005 µm) filtered phase (10/11/2016)

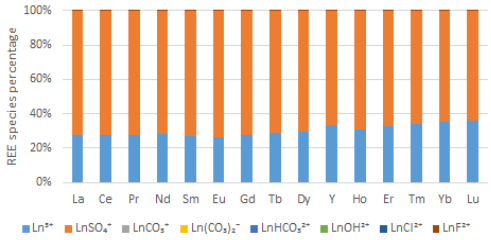

G2 REE species in ultra (0.005 µm) filtered phase (14/09/2017)

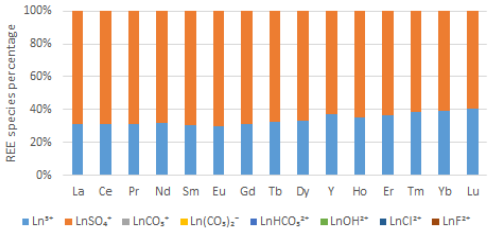

G3 REE species in ultra (0.005 µm) filtered phase Q=92.63 L/s; SO_4^{2-}=17.4 mg/l (10/11/2016)

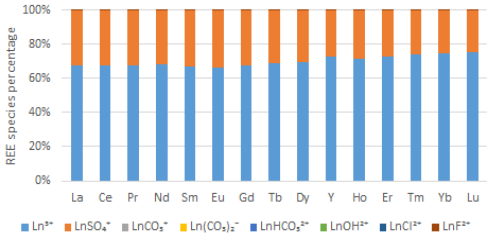

G3 REE species in ultra (0.005 µm) filtered phase Q=85.66 L/s; SO_4^{2-}=14.60 mg/l (14/09/2017)

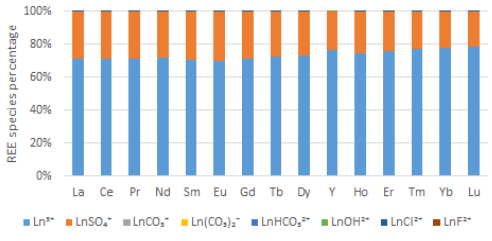

G4 REE species in ultra (0.005 µm) filtered phase Q=82.85 L/s; SO_4^{2-}=21.57 mg/l (10/11/2016)

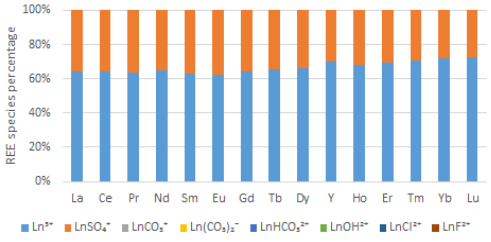

G4 REE species in ultra (0.005 µm) filtered phase Q=95.68 L/s; SO_4^{2-}=16.03 mg/l (14/09/2017)

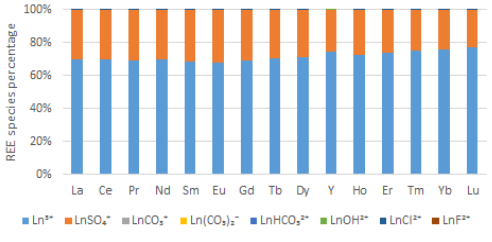

G5 REE species in ultra (0.005 µm) filtered phase Q=87.59 L/s; SO_4^{2-}=19.59 mg/l (10/11/2016)

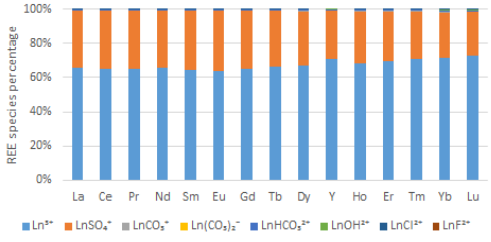

G5 REE species in ultra (0.005 µm) filtered phase Q=100.3 L/s; SO_4^{2-}=14.14 mg/l (14/09/2017)

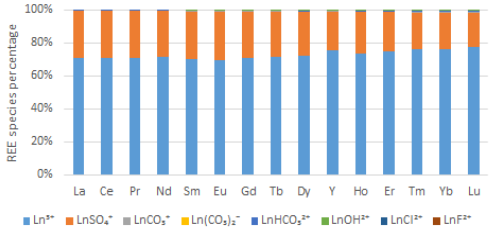

G1 REE species in ultra (0.005 µm) filtered phase (15/11/2016)

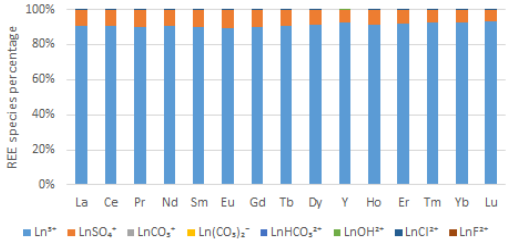

G4 REE species in ultra (0.005 µm) filtered phase Q=107.7 L/s; SO_4^{2-}=14.88 mg/l (15/11/2016)

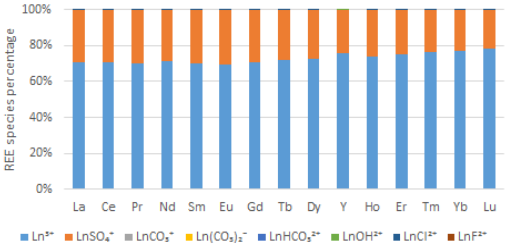

G2 REE species in ultra (0.005 µm) filtered phase (15/11/2016)

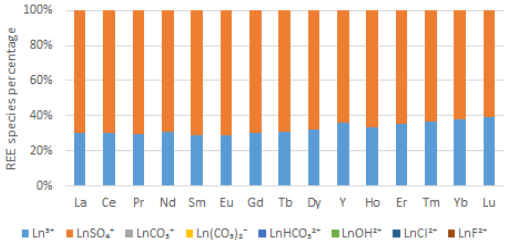

G5 REE species in ultra (0.005 µm) filtered phase Q=115.1 L/s; SO_4^{2-}=14.07 mg/l (15/11/2016)

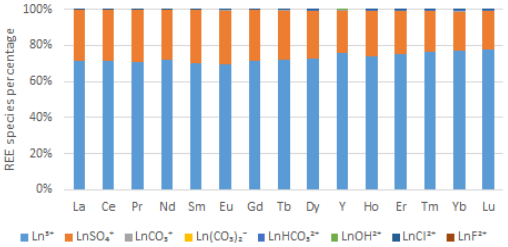

G3 REE species in ultra (0.005 µm) filtered phase Q=109.5 L/s; SO_4^{2-}=12.71 mg/l (15/11/2016)

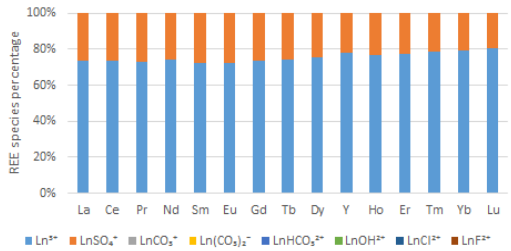

REE speciation results at G1 to G5 from sampling occasions when ultrafiltration was undertaken and the calculations are based on 0.1µm filtered cations results.

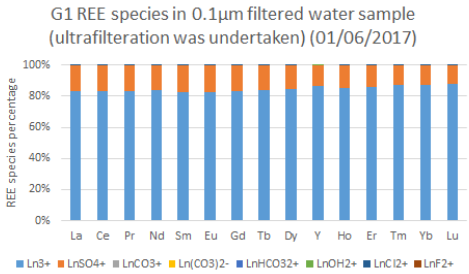

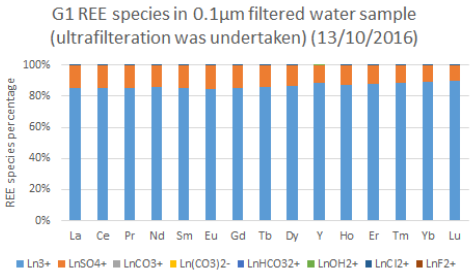

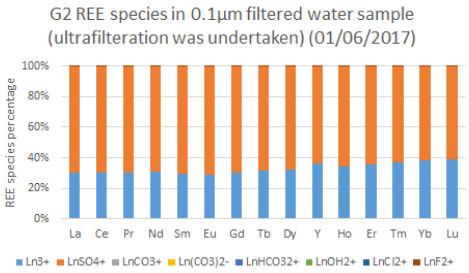

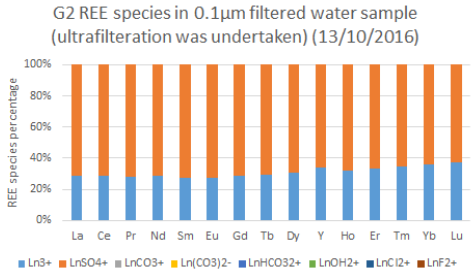

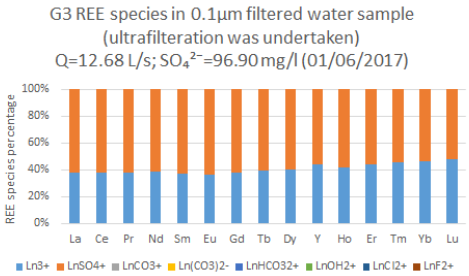

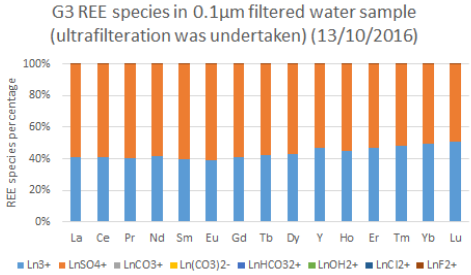

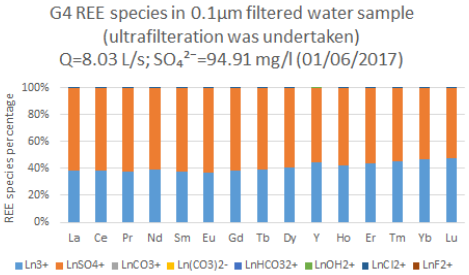

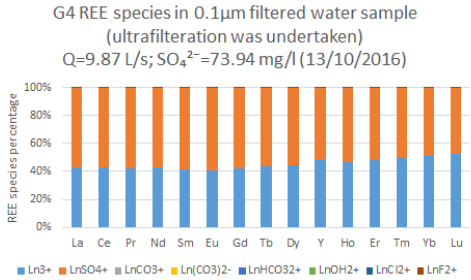

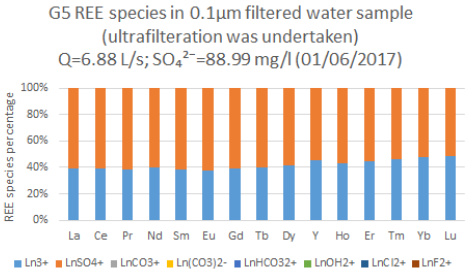

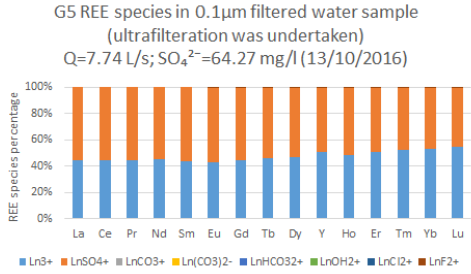

Sampling occasions are displayed in increasing order of the flow condition, and the flowrate of sampling sites where flowrate measurement was undertaken is also shown in graphs.

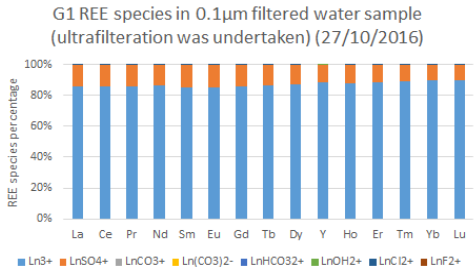

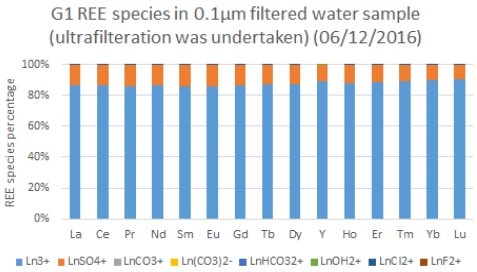

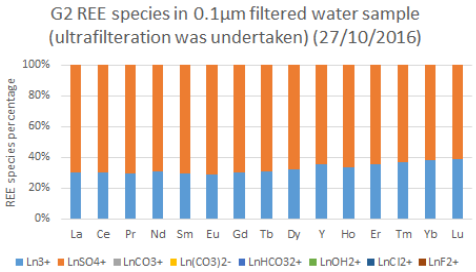

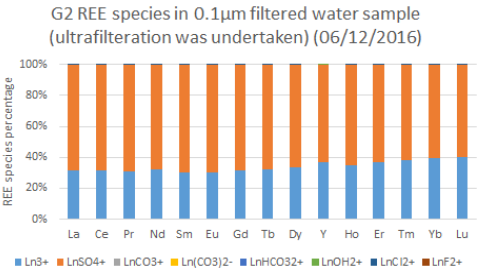

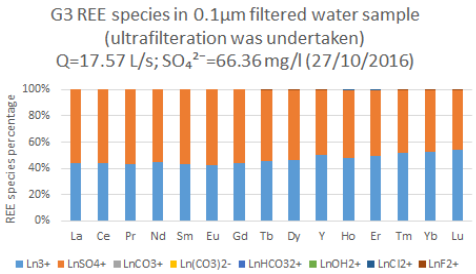

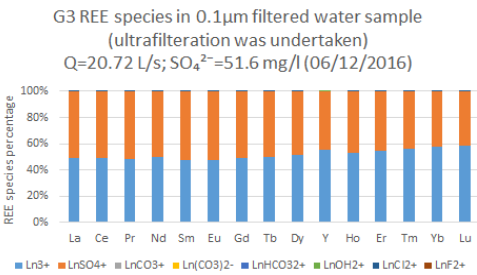

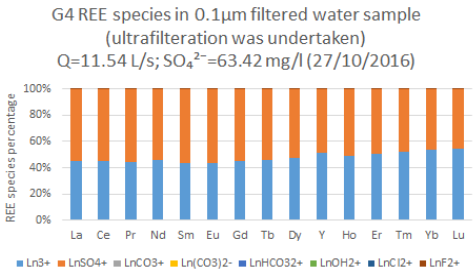

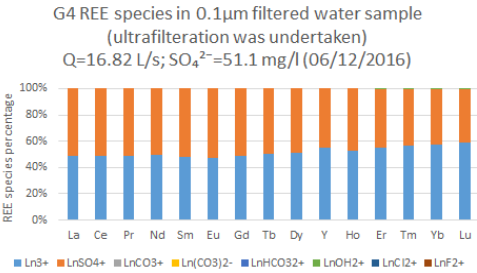

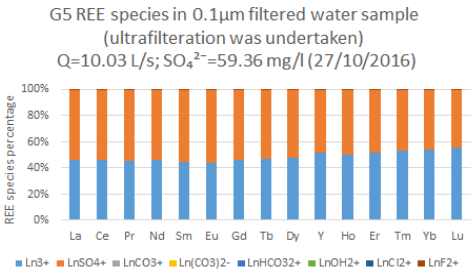

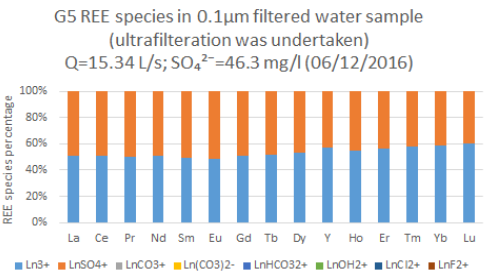

G1 REE species in 0.1µm filtered water sample (ultrafilteration was undertaken) (10/11/2016)

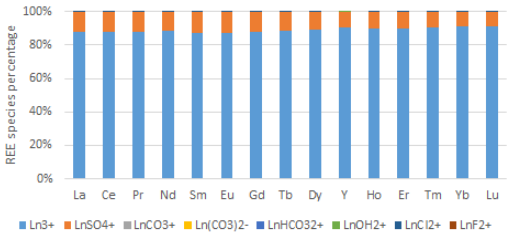

G1 REE species in 0.1µm filtered water sample (ultrafilteration was undertaken) (14/09/2017)

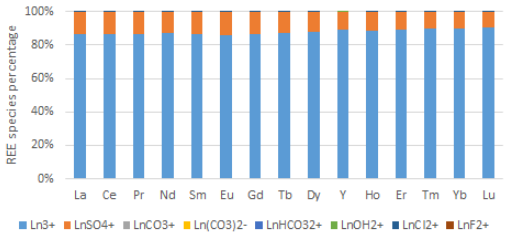

G2 REE species in 0.1µm filtered water sample (ultrafilteration was undertaken) (10/11/2016)

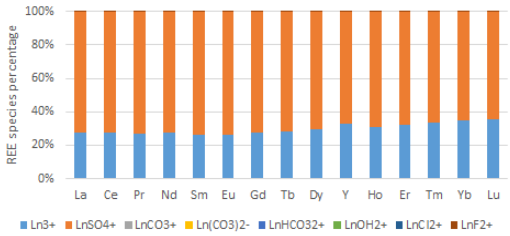

G2 REE species in 0.1µm filtered water sample (ultrafilteration was undertaken) (14/09/2017)

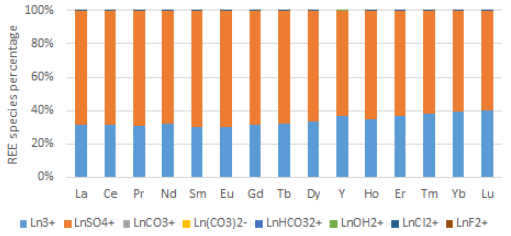

G3 REE species in 0.1µm filtered water sample (ultrafilteration was undertaken) Q=92.63 L/s; SO_4^{2-}=20.62 mg/l (10/11/2016)

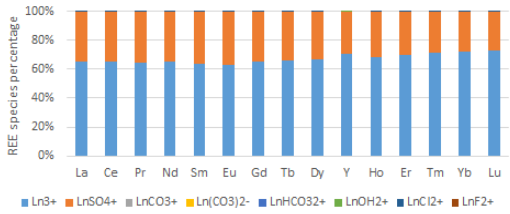

G3 REE species in 0.1µm filtered water sample (ultrafilteration was undertaken) Q=85.66 L/s; SO_4^{2-}=16.91 mg/l (14/09/2017)

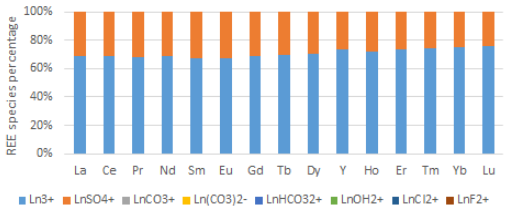

G4 REE species in 0.1µm filtered water sample (ultrafilteration was undertaken) Q=82.85 L/s; SO_4^{2-}=24.95 mg/l (10/11/2016)

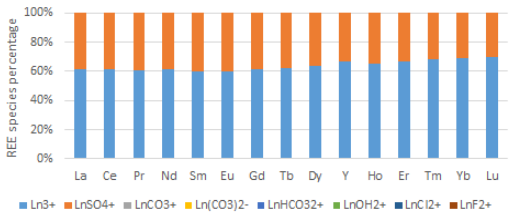

G4 REE species in 0.1µm filtered water sample (ultrafilteration was undertaken) Q=95.68 L/s; SO_4^{2-}=18.23 mg/l (14/09/2017)

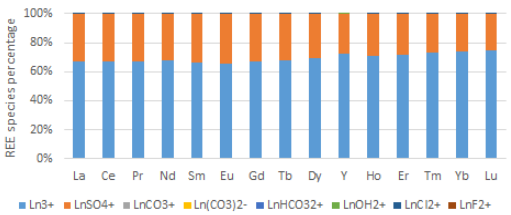

G5 REE species in 0.1µm filtered water sample (ultrafilteration was undertaken) Q=87.59 L/s; SO_4^{2-}=23.86 mg/l (10/11/2016)

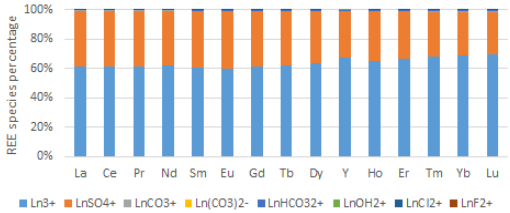

G5 REE species in 0.1µm filtered water sample (ultrafilteration was undertaken) Q=100.3 L/s; SO_4^{2-}=17.56 mg/l (14/09/2017)

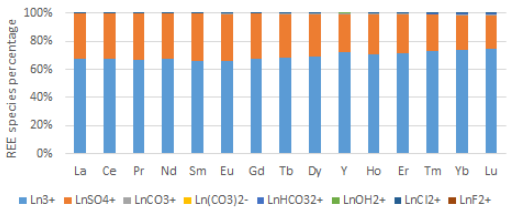

G1 REE species in 0.1µm filtered water sample (ultrafilteration was undertaken) (15/11/2016)

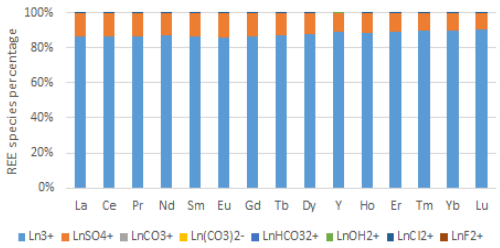

G4 REE species in 0.1µm filtered water sample (ultrafilteration was undertaken) Q=107.7 L/s; SO_4^{2-}=18.09 mg/l (15/11/2016)

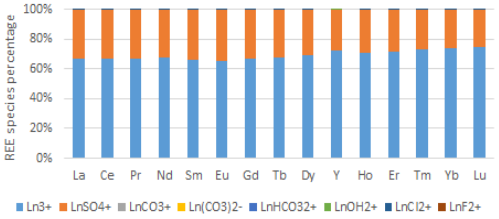

G2 REE species in 0.1µm filtered water sample (ultrafilteration was undertaken) (15/11/2016)

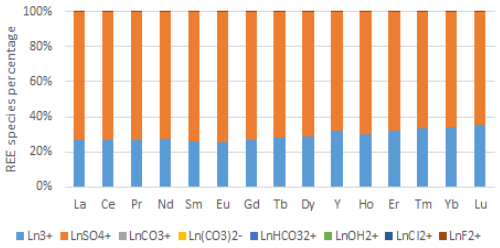

G5 REE species in 0.1µm filtered water sample (ultrafilteration was undertaken) Q=115.1 L/s; SO_4^{2-}=16.91 mg/l (15/11/2016)

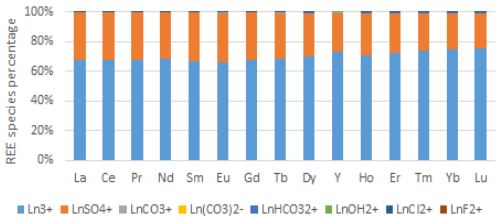

G3 REE species in 0.1µm filtered water sample (ultrafilteration was undertaken) Q=115.1 L/s; SO_4^{2-}=16.11 mg/l (15/10/2016)

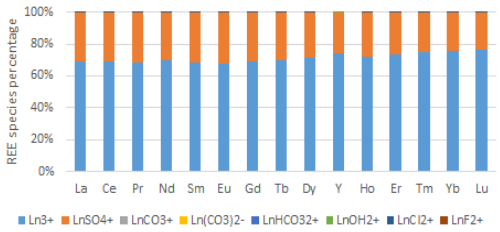

REE speciation results at G1 to G5 from sampling occasions when ultrafiltration was not undertaken and the calculations are based on 0.1µm filtered cations results.

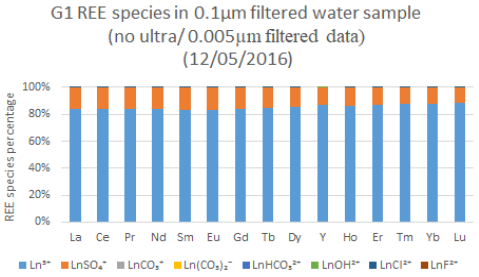

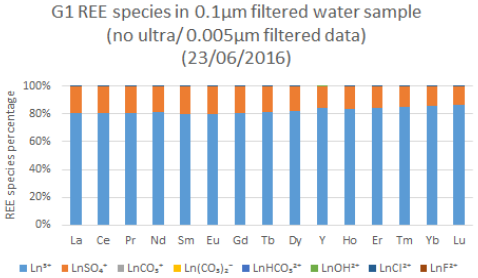

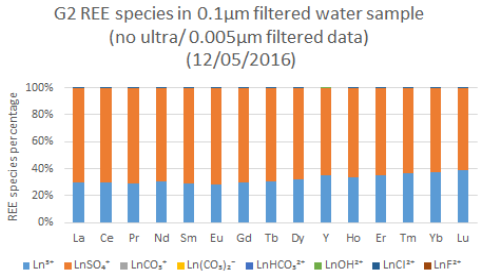

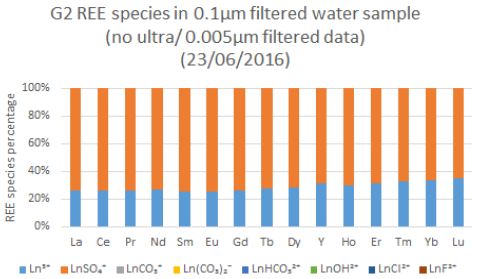

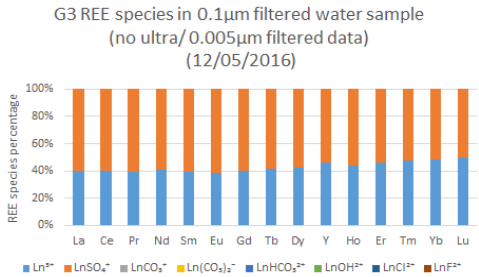

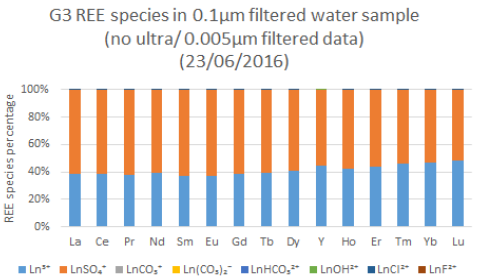

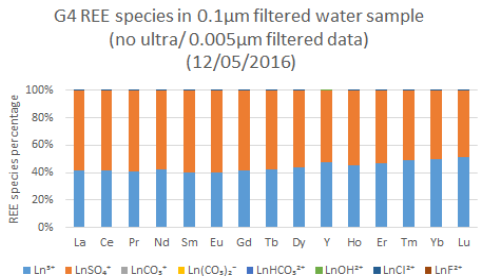

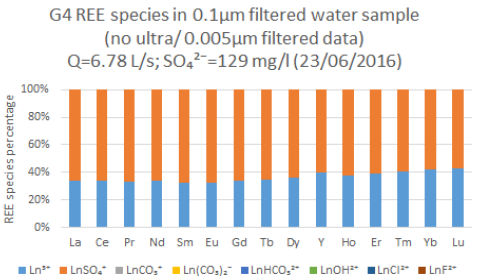

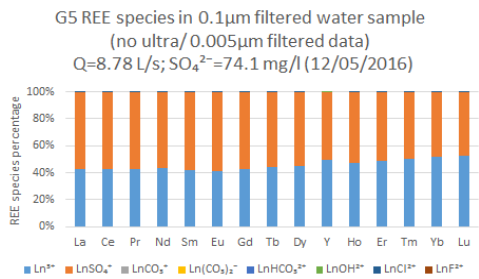

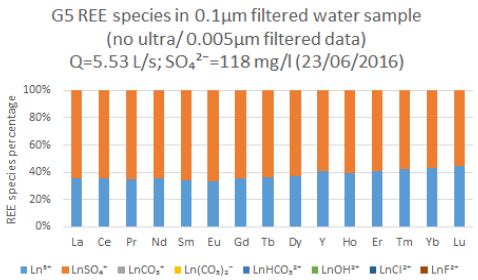

These sampling occasions when ultrafiltration was not undertaken are also displayed in increasing order of the flow condition, and the flowrate of sampling sites where flow measurement was undertaken is also shown in graphs

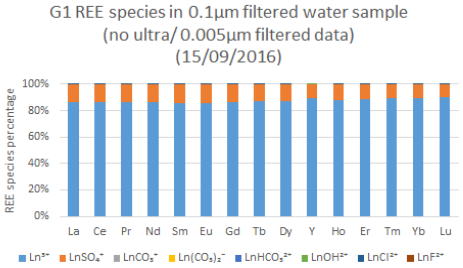

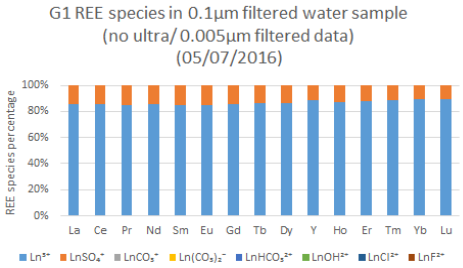

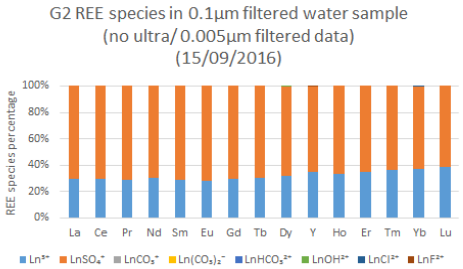

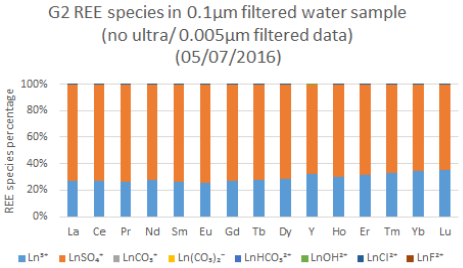

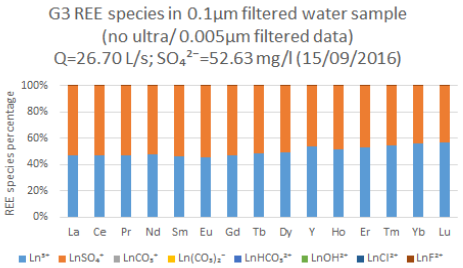

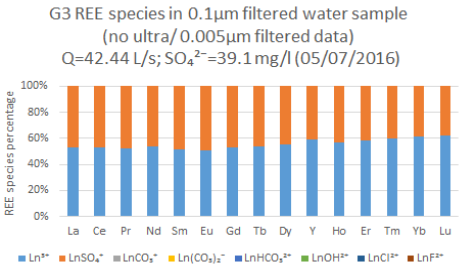

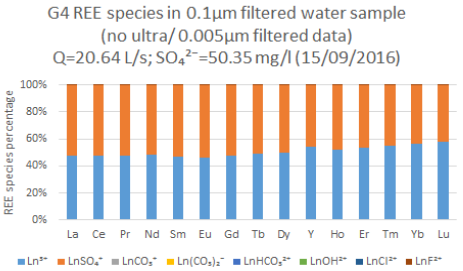

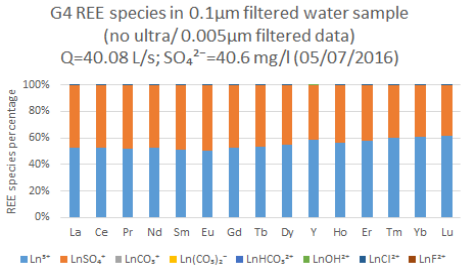

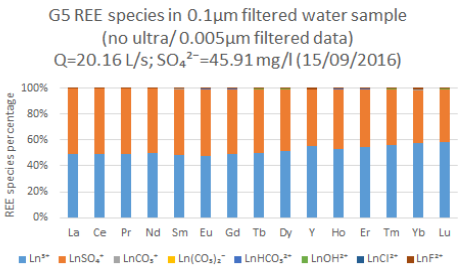

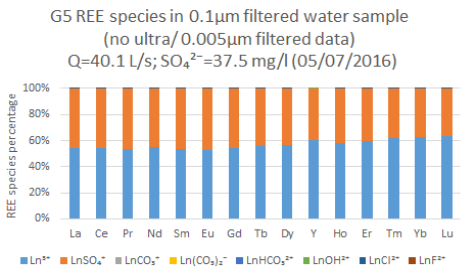

G1 REE species in 0.1µm filtered water sample
(no ultra/ 0.005µm filtered data)
(04/02/2016)

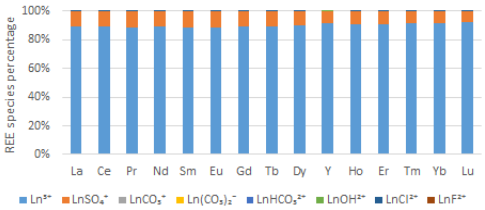

G1 REE species in 0.1µm filtered water sample
(no ultra/ 0.005µm filtered data)
(13/04/2016)

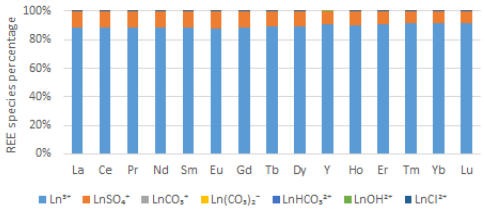

G2 REE species in 0.1µm filtered water sample
(no ultra/ 0.005µm filtered data)
(04/02/2016)

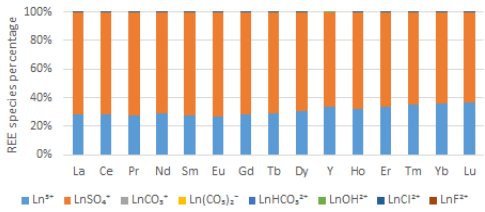

G2 REE species in 0.1µm filtered water sample
(no ultra/ 0.005µm filtered data)
(13/04/2016)

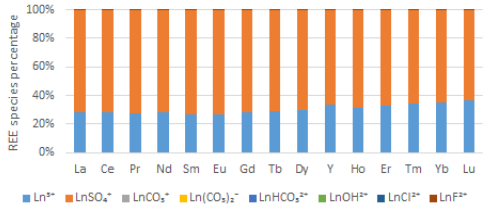

G3 REE species in 0.1µm filtered water sample
(no ultra/ 0.005µm filtered data)
(04/02/2016)

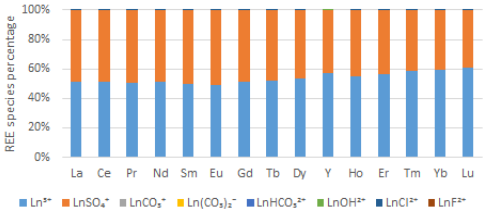

G3 REE species in 0.1µm filtered water sample
(no ultra/ 0.005µm filtered data)
Q=66.40 L/s; SO_4^{2-}=23.86 mg/l (13/04/2016)

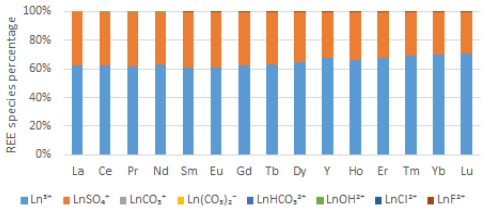

G4 REE species in 0.1µm filtered water sample
(no ultra/ 0.005µm filtered data)
Q=44.98 L/s; SO_4^{2-}=29.42 mg/l (04/02/2016)

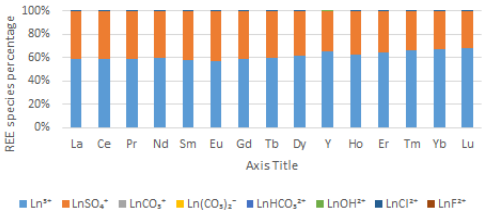

G4 REE species in 0.1µm filtered water sample
(no ultra/ 0.005µm filtered data)
Q=70.77 L/s; SO_4^{2-}=25.94 mg/l (13/04/2016)

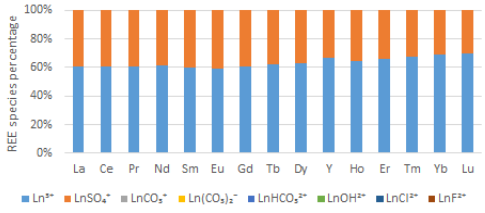

G5 REE species in 0.1µm filtered water sample
(no ultra/ 0.005µm filtered data)
Q=45.42 L/s; SO_4^{2-}=28.08 mg/l (04/02/2016)

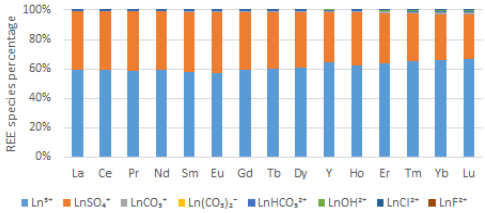

G5 REE species in 0.1µm filtered water sample
(no ultra/ 0.005µm filtered data)
Q=79.49 L/s; SO_4^{2-}=23.18 mg/l (13/04/2016)

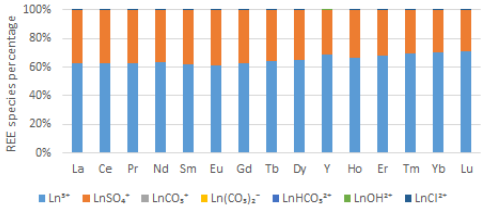

Appendix E REE speciation modelling data at G7

REE speciation results at G7 from sampling occasions when ultrafiltration was undertaken and the calculations are based on 0.1µm filtered cations results.

The results of different sampling occasions are displayed in increasing order of the flow condition, based on flowrate of G7. pH on each sampling occasion is also shown in graphs.

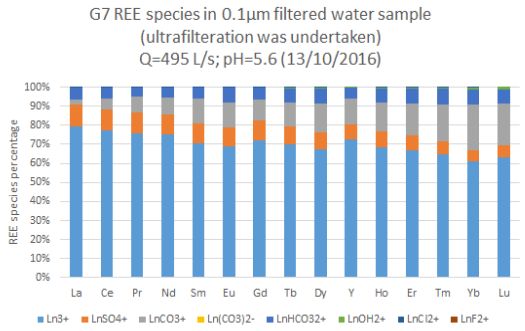

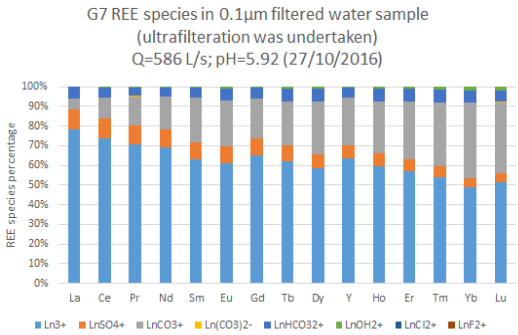

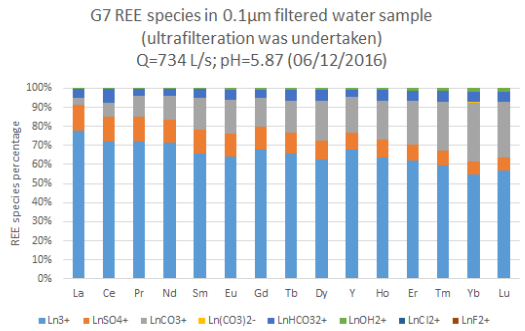

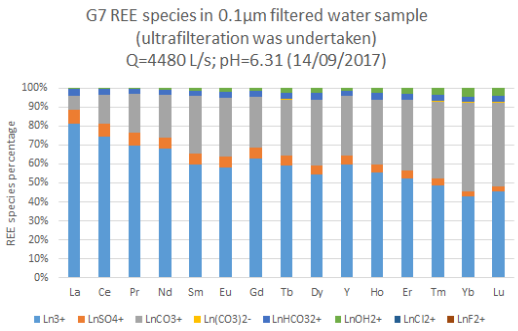

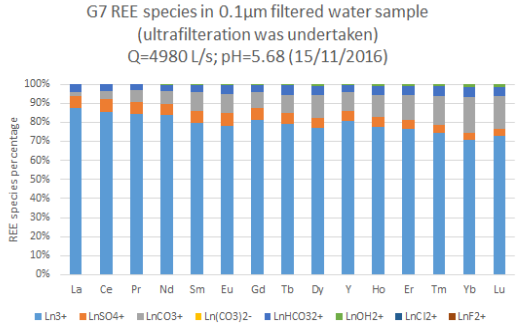

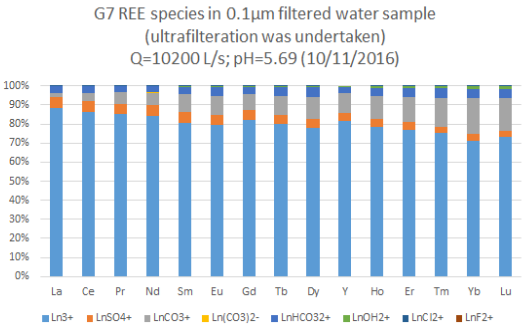

REE speciation results at G7 from sampling occasions when ultrafiltration was not undertaken and the calculations are based on 0.1µm filtered cations results.

The results of different sampling occasions are displayed in increasing order of the flow condition, based on flowrate of G7. pH on each sampling occasion is also shown in graphs.

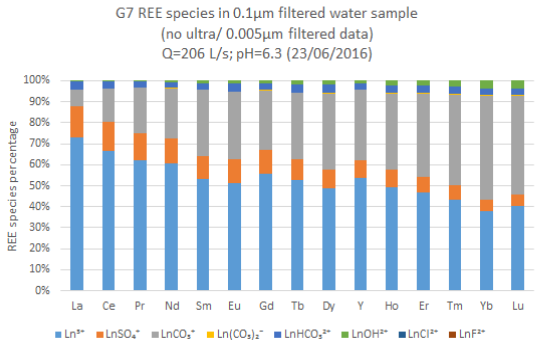

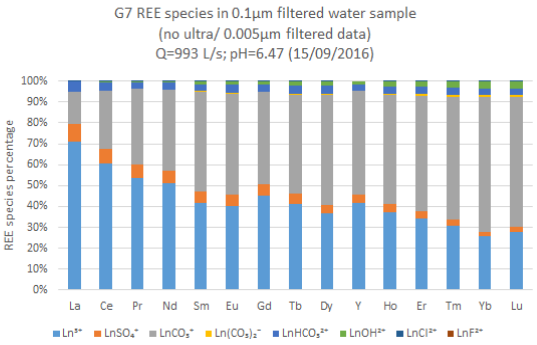

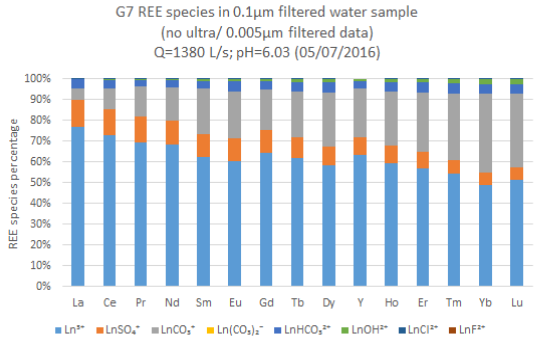

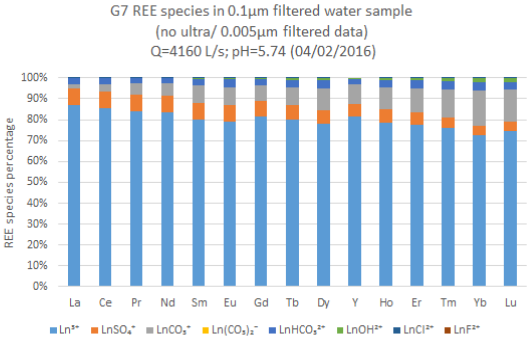

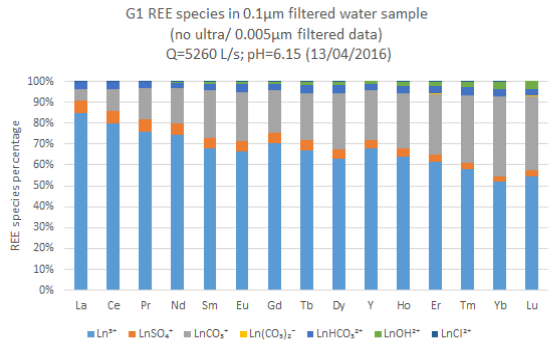

Appendix F PAAS normalized REE distribution pattern at Gategill sampling sites

Spatial variation of PAAS normalized REE distribution pattern in different phases from G1 to G7 under lower flow conditions when ultrafiltration was undertaken and attenuation occurred only at G7. The data are displayed based on the order of flow condition (the flow of G5 and G7 is shown).

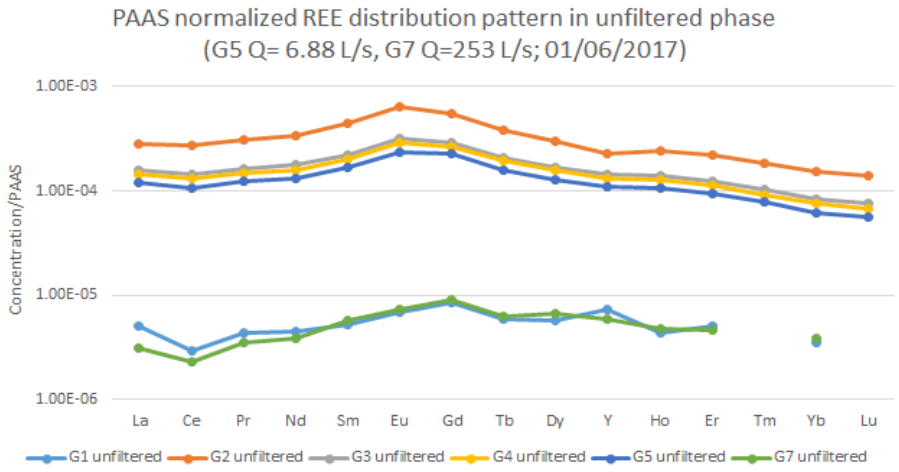

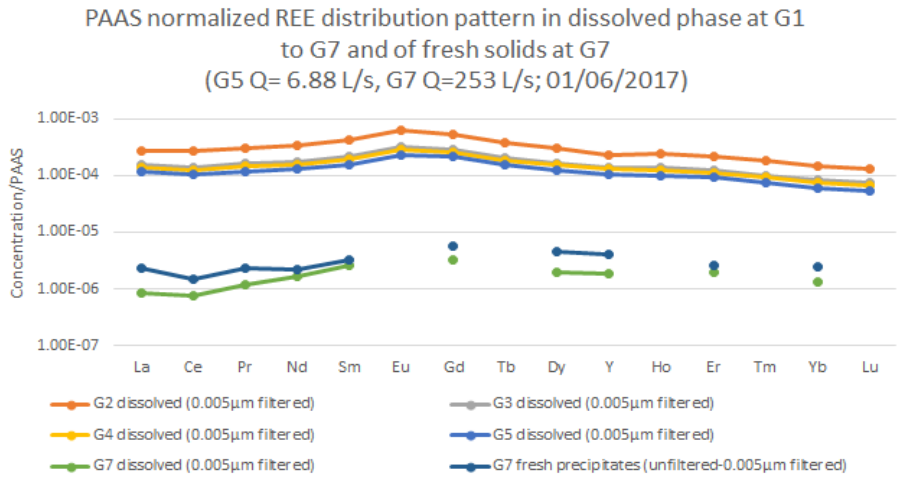

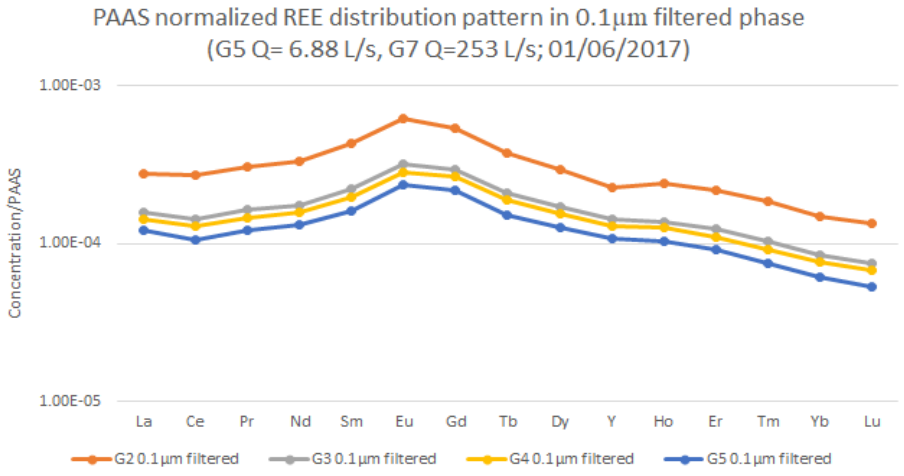

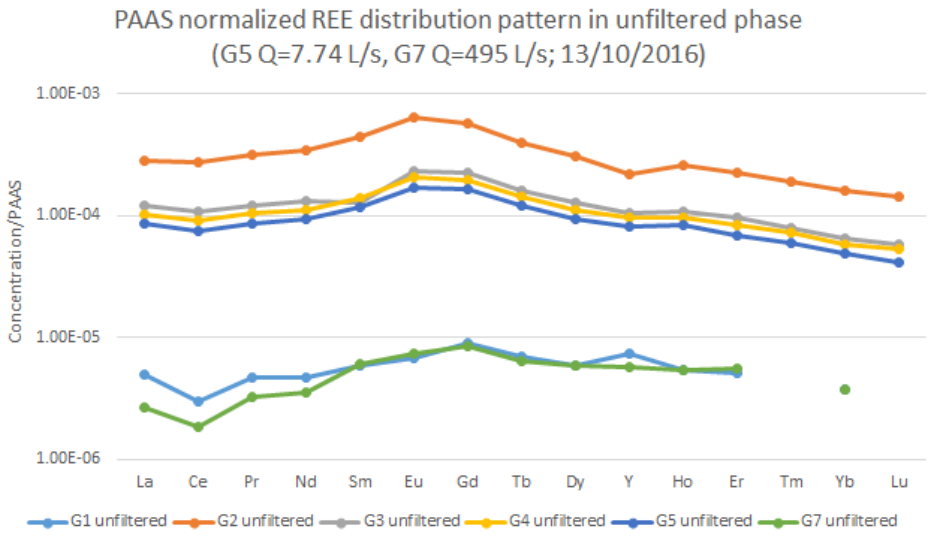
PAAS normalized REE distribution pattern in unfiltered phase
(G5 Q=7.74 L/s, G7 Q=495 L/s; 13/10/2016)
Concentration/PAAS
1.00E-03
1.00E-04
1.00E-05
1.00E-06
La Ce Pr Nd Sm Eu Gd Tb Dy Y Ho Er Tm Yb Lu
G1 unfiltered
G2 unfiltered
G3 unfiltered
G4 unfiltered
G5 unfiltered
G7 unfiltered

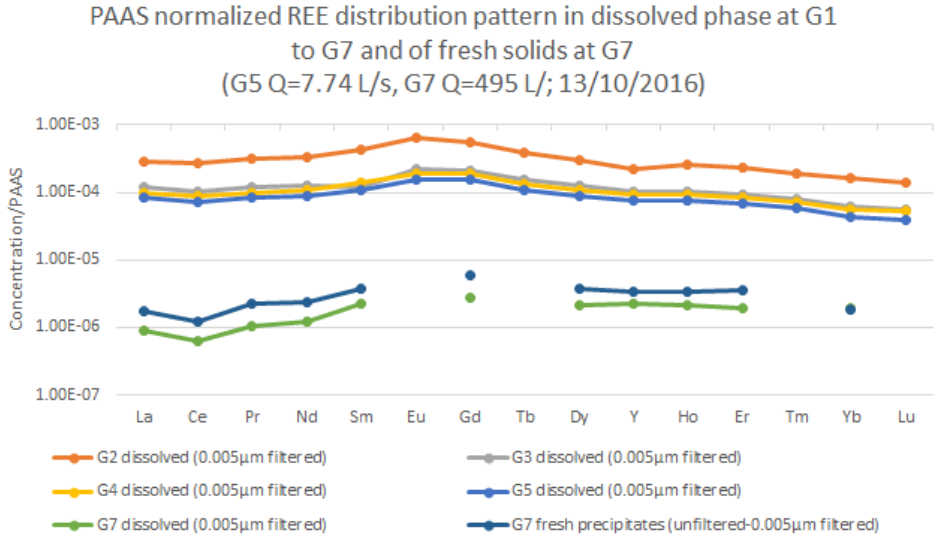
PAAS normalized REE distribution pattern in dissolved phase at G1
to G7 and of fresh solids at G7
(G5 Q=7.74 L/s, G7 Q=495 L/; 13/10/2016)
Concentration/PAAS
1.00E-03
1.00E-04
1.00E-05
1.00E-06
1.00E-07
La Ce Pr Nd Sm Eu Gd Tb Dy Y Ho Er Tm Yb Lu
G2 dissolved (0.005µm filtered)
G3 dissolved (0.005µm filtered)
G4 dissolved (0.005µm filtered)
G5 dissolved (0.005µm filtered)
G7 dissolved (0.005µm filtered)
G7 fresh precipitates (unfiltered-0.005µm filtered)

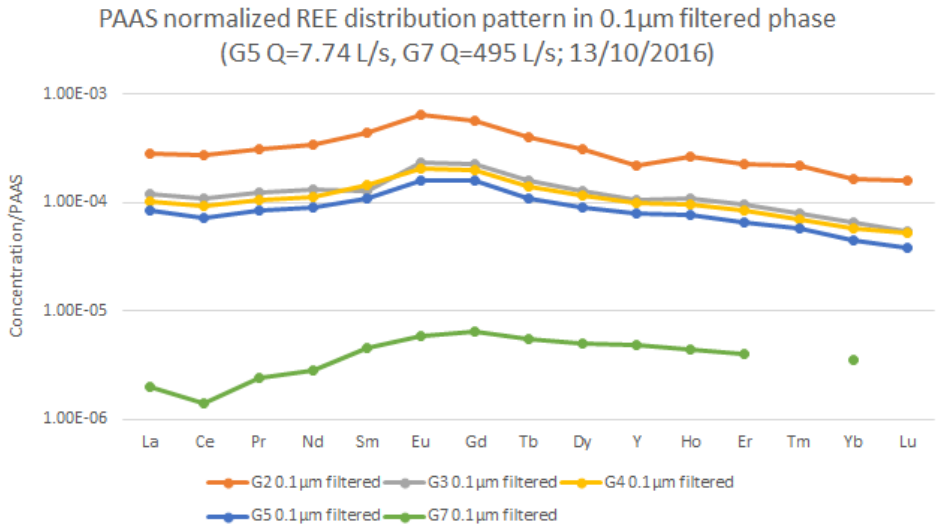
PAAS normalized REE distribution pattern in 0.1µm filtered phase
(G5 Q=7.74 L/s, G7 Q=495 L/s; 13/10/2016)
Concentration/PAAS
1.00E-03
1.00E-04
1.00E-05
1.00E-06
La Ce Pr Nd Sm Eu Gd Tb Dy Y Ho Er Tm Yb Lu
G2 0.1 µm filtered
G3 0.1 µm filtered
G4 0.1 µm filtered
G5 0.1 µm filtered
G7 0.1 µm filtered

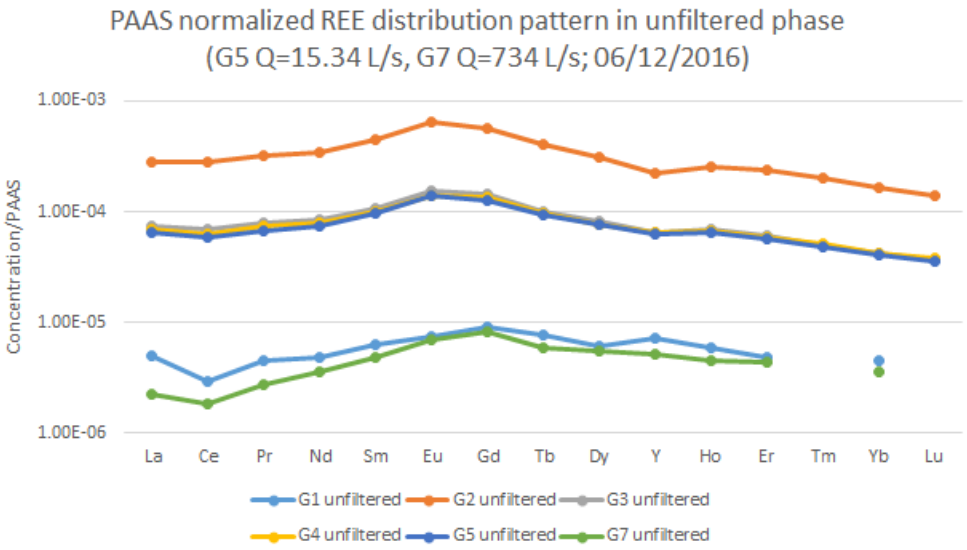
PAAS normalized REE distribution pattern in unfiltered phase
(G5 Q=15.34 L/s, G7 Q=734 L/s; 06/12/2016)
Concentration/PAAS
1.00E-03
1.00E-04
1.00E-05
1.00E-06
La Ce Pr Nd Sm Eu Gd Tb Dy Y Ho Er Tm Yb Lu
G1 unfiltered
G2 unfiltered
G3 unfiltered
G4 unfiltered
G5 unfiltered
G7 unfiltered

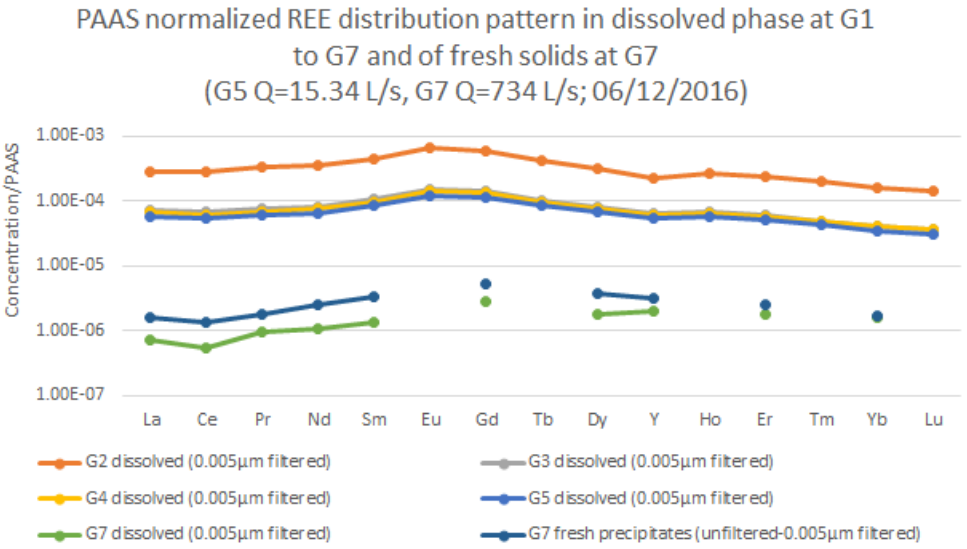
PAAS normalized REE distribution pattern in dissolved phase at G1
to G7 and of fresh solids at G7
(G5 Q=15.34 L/s, G7 Q=734 L/s; 06/12/2016)
Concentration/PAAS
1.00E-03
1.00E-04
1.00E-05
1.00E-06
1.00E-07
La Ce Pr Nd Sm Eu Gd Tb Dy Y Ho Er Tm Yb Lu
G2 dissolved (0.005µm filtered)
G3 dissolved (0.005µm filtered)
G4 dissolved (0.005µm filtered)
G5 dissolved (0.005µm filtered)
G7 dissolved (0.005µm filtered)
G7 fresh precipitates (unfiltered-0.005µm filtered)

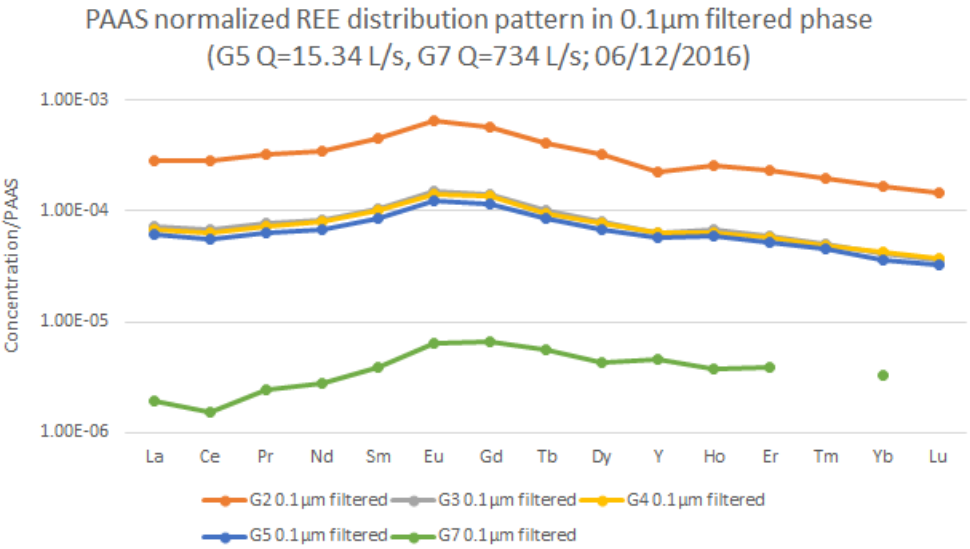
PAAS normalized REE distribution pattern in 0.1µm filtered phase
(G5 Q=15.34 L/s, G7 Q=734 L/s; 06/12/2016)
Concentration/PAAS
1.00E-03
1.00E-04
1.00E-05
1.00E-06
La Ce Pr Nd Sm Eu Gd Tb Dy Y Ho Er Tm Yb Lu
G2 0.1 µm filtered
G3 0.1 µm filtered
G4 0.1 µm filtered
G5 0.1 µm filtered
G7 0.1 µm filtered

Spatial variation of PAAS normalized REE distribution pattern in different phases from G1 to G7 under higher flow conditions when ultrafiltration was undertaken and attenuation of REE occurred at G3 to G7. The data are displayed based on the order of flow condition (the flow of G5 and G7 is shown).

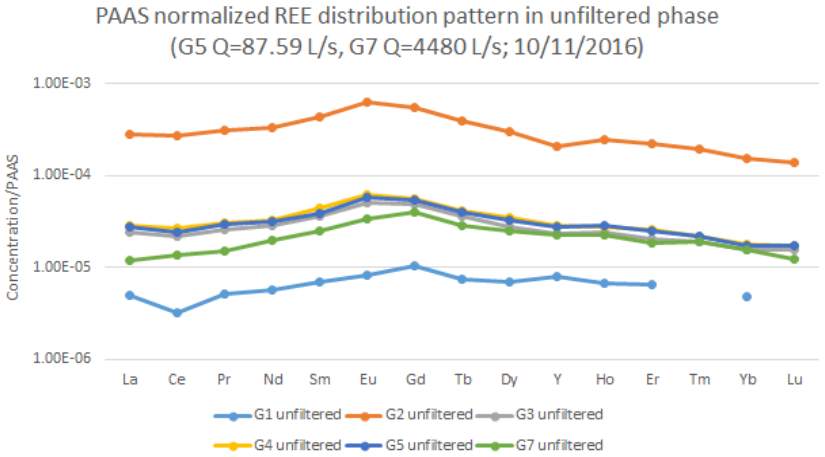

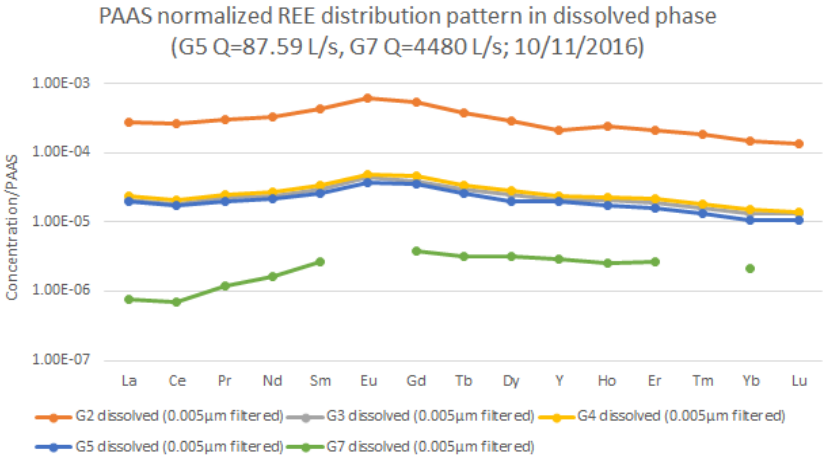

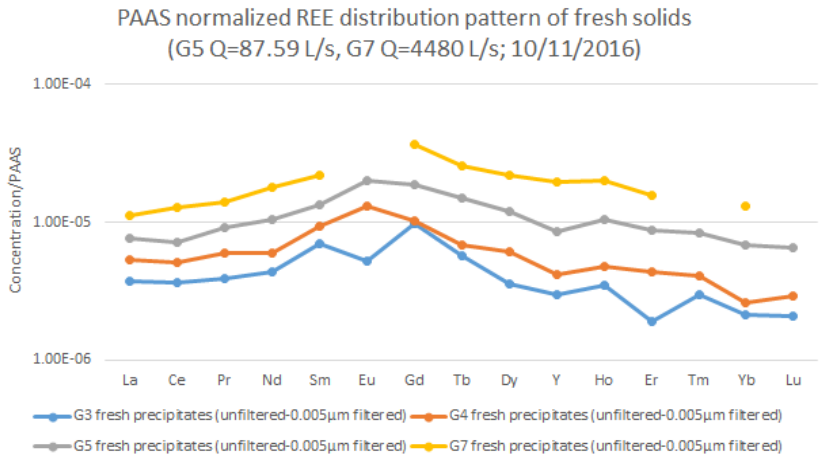

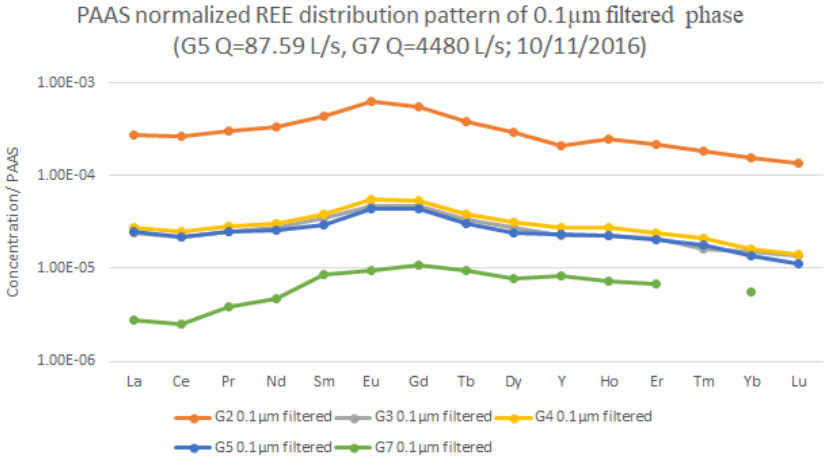

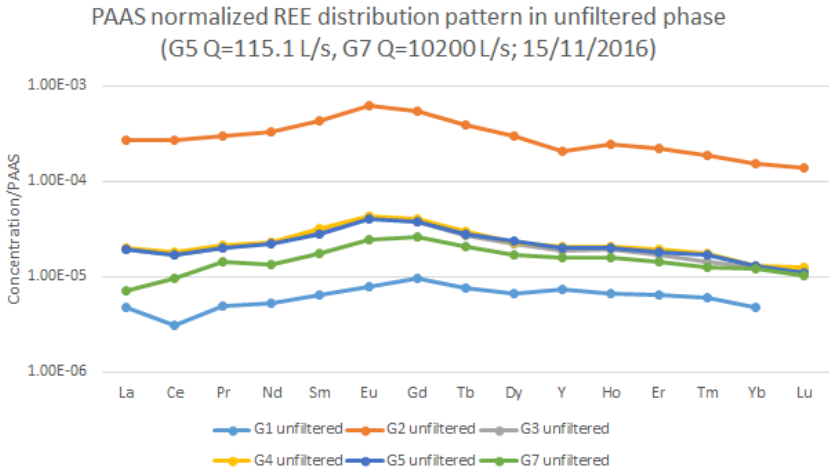
PAAS normalized REE distribution pattern in unfiltered phase
(G5 Q=115.1 L/s, G7 Q=10200 L/s; 15/11/2016)
Concentration/PAAS
1.00E-03
1.00E-04
1.00E-05
1.00E-06
La Ce Pr Nd Sm Eu Gd Tb Dy Y Ho Er Tm Yb Lu
G1 unfiltered
G2 unfiltered
G3 unfiltered
G4 unfiltered
G5 unfiltered
G7 unfiltered

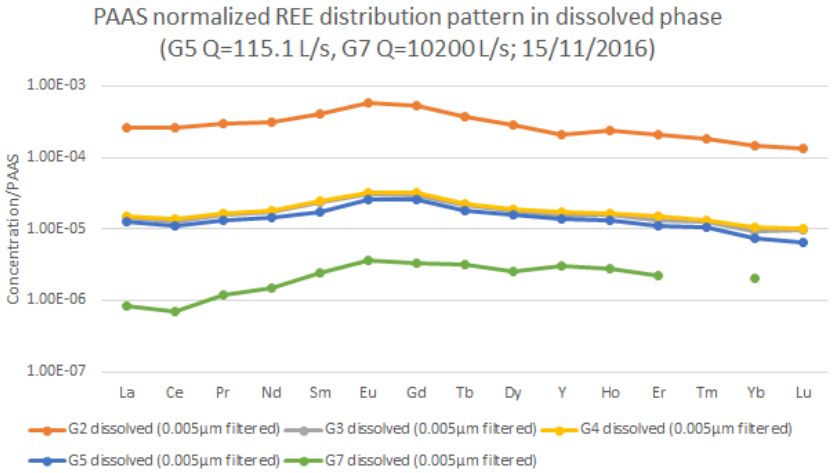
PAAS normalized REE distribution pattern in dissolved phase
(G5 Q=115.1 L/s, G7 Q=10200 L/s; 15/11/2016)
Concentration/PAAS
1.00E-03
1.00E-04
1.00E-05
1.00E-06
1.00E-07
La Ce Pr Nd Sm Eu Gd Tb Dy Y Ho Er Tm Yb Lu
G2 dissolved (0.005µm filtered)
G3 dissolved (0.005µm filtered)
G4 dissolved (0.005µm filtered)
G5 dissolved (0.005µm filtered)
G7 dissolved (0.005µm filtered)

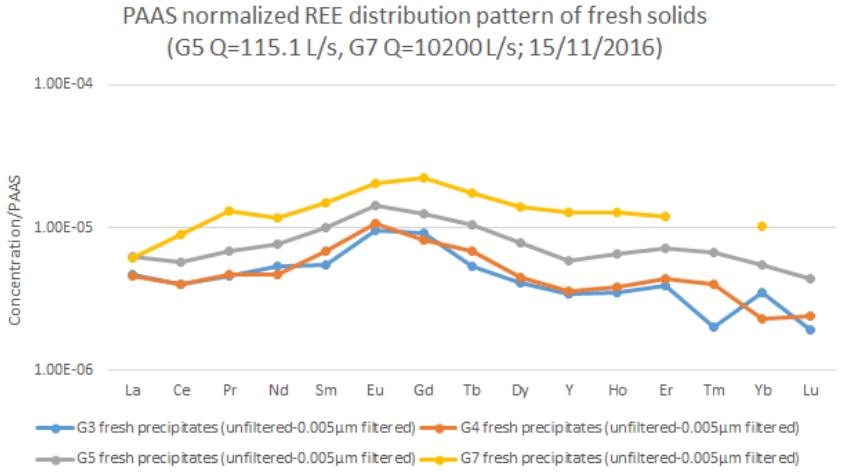
PAAS normalized REE distribution pattern of fresh solids
(G5 Q=115.1 L/s, G7 Q=10200 L/s; 15/11/2016)
Concentration/PAAS
1.00E-04
1.00E-05
1.00E-06
La Ce Pr Nd Sm Eu Gd Tb Dy Y Ho Er Tm Yb Lu
G3 fresh precipitates (unfiltered-0.005µm filtered)
G4 fresh precipitates (unfiltered-0.005µm filtered)
G5 fresh precipitates (unfiltered-0.005µm filtered)
G7 fresh precipitates (unfiltered-0.005µm filtered)

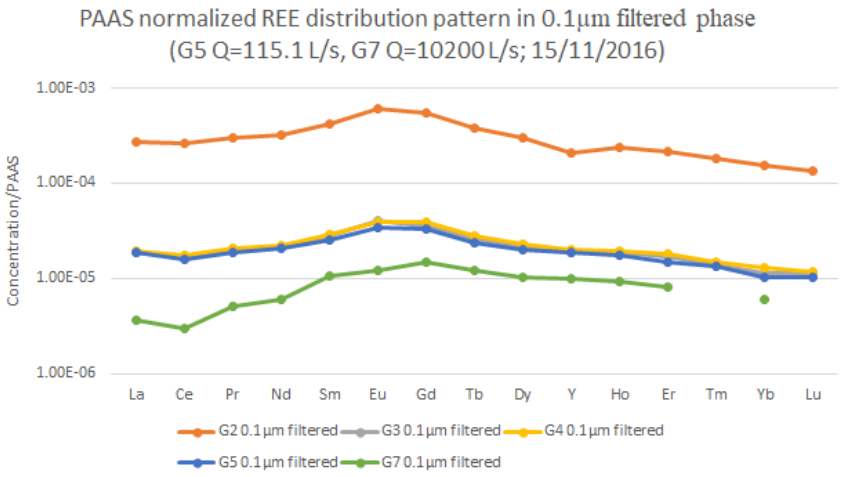
PAAS normalized REE distribution pattern in 0.1µm filtered phase
(G5 Q=115.1 L/s, G7 Q=10200 L/s; 15/11/2016)
Concentration/PAAS
1.00E-03
1.00E-04
1.00E-05
1.00E-06
La Ce Pr Nd Sm Eu Gd Tb Dy Y Ho Er Tm Yb Lu
G2 0.1 µm filtered
G3 0.1 µm filtered
G4 0.1 µm filtered
G5 0.1 µm filtered
G7 0.1 µm filtered

PAAS normalized REE distribution pattern in truly dissolved (0.005µm/ ultra-filtered) and unfiltered phase at G3, G4 and G5 when attenuation of REE occurred and ultrafiltration was undertaken (higher flow conditions). The data are displayed based on the order of flow condition.

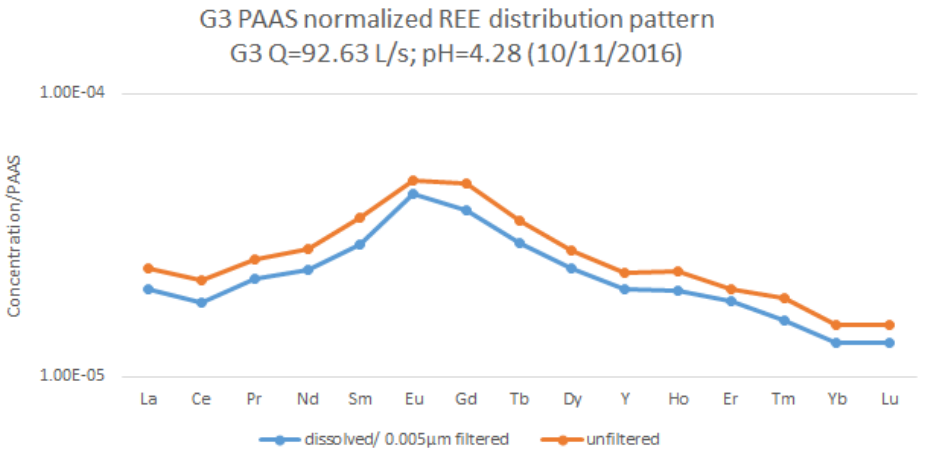

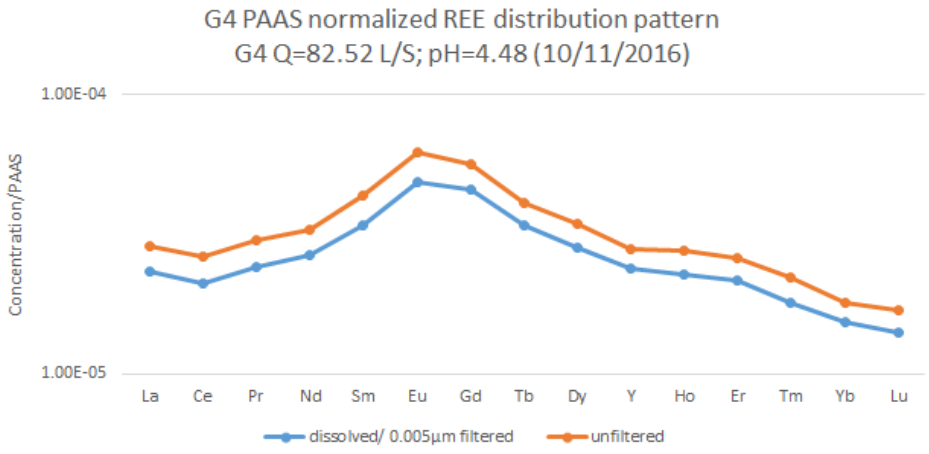

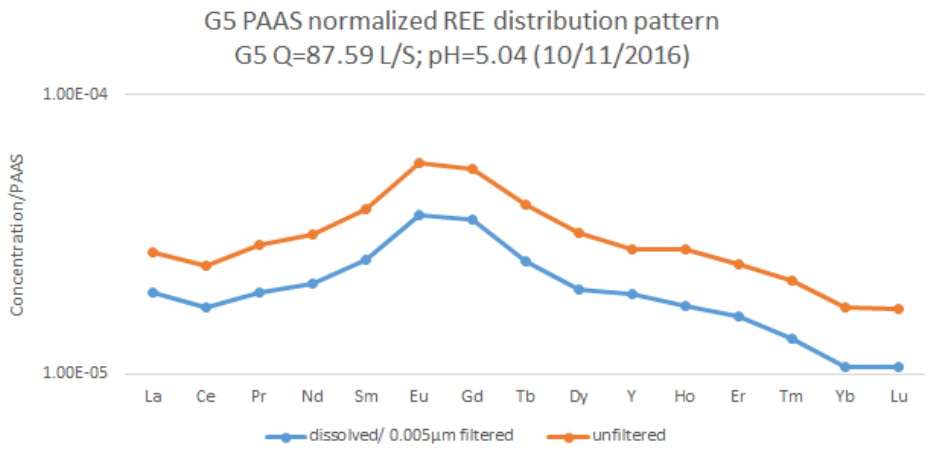

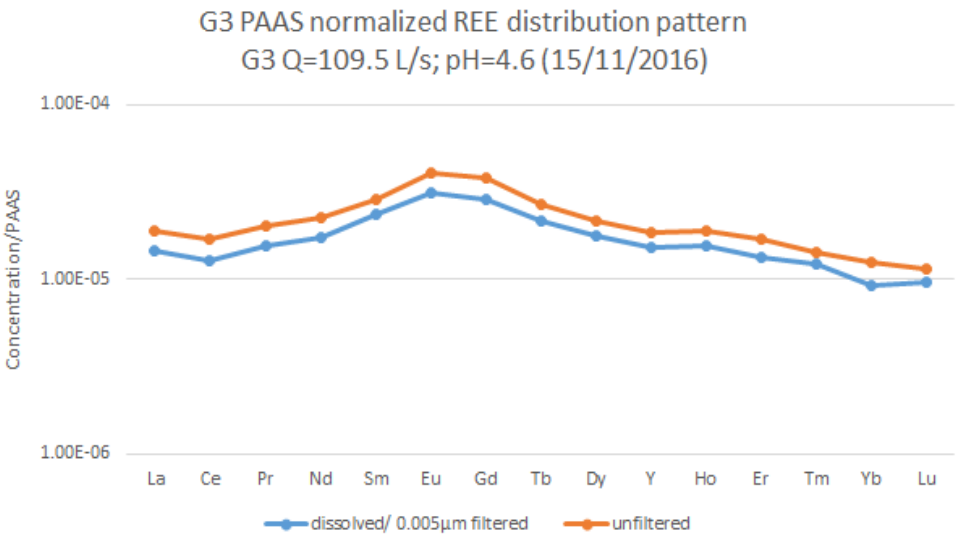
G3 PAAS normalized REE distribution pattern
G3 Q=109.5 L/s; pH=4.6 (15/11/2016)
1.00E-04
1.00E-05
1.00E-06
Concentration/PAAS
La Ce Pr Nd Sm Eu Gd Tb Dy Y Ho Er Tm Yb Lu
dissolved/ 0.005µm filtered
unfiltered

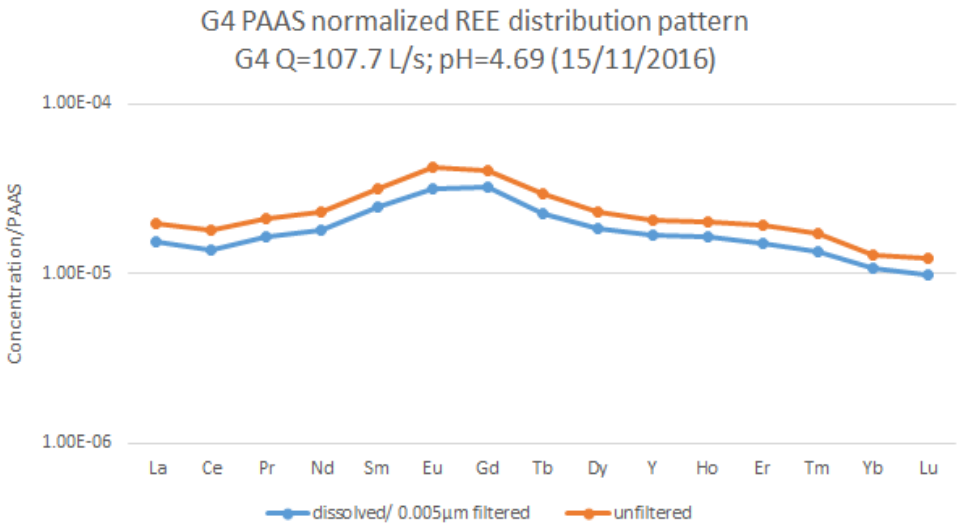
G4 PAAS normalized REE distribution pattern
G4 Q=107.7 L/s; pH=4.69 (15/11/2016)
1.00E-04
1.00E-05
1.00E-06
Concentration/PAAS
La Ce Pr Nd Sm Eu Gd Tb Dy Y Ho Er Tm Yb Lu
dissolved/ 0.005µm filtered
unfiltered

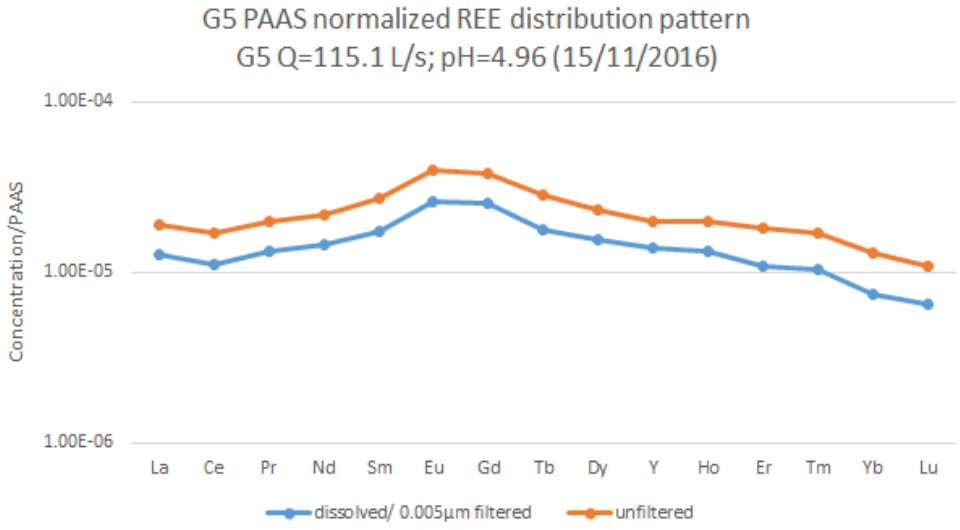
G5 PAAS normalized REE distribution pattern
G5 Q=115.1 L/s; pH=4.96 (15/11/2016)
1.00E-04
1.00E-05
1.00E-06
Concentration/PAAS
La Ce Pr Nd Sm Eu Gd Tb Dy Y Ho Er Tm Yb Lu
dissolved/ 0.005µm filtered
unfiltered

PAAS normalized REE distribution pattern in truly dissolved (0.005µm/ ultra-filtered) and unfiltered phase at G7 under lower flow conditions when ultrafiltration was undertaken. The data are displayed based on the order of flow condition.

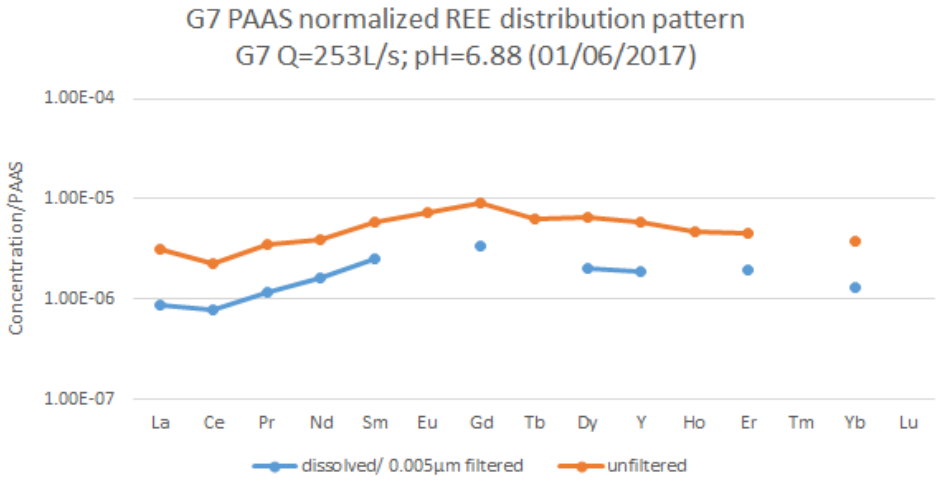

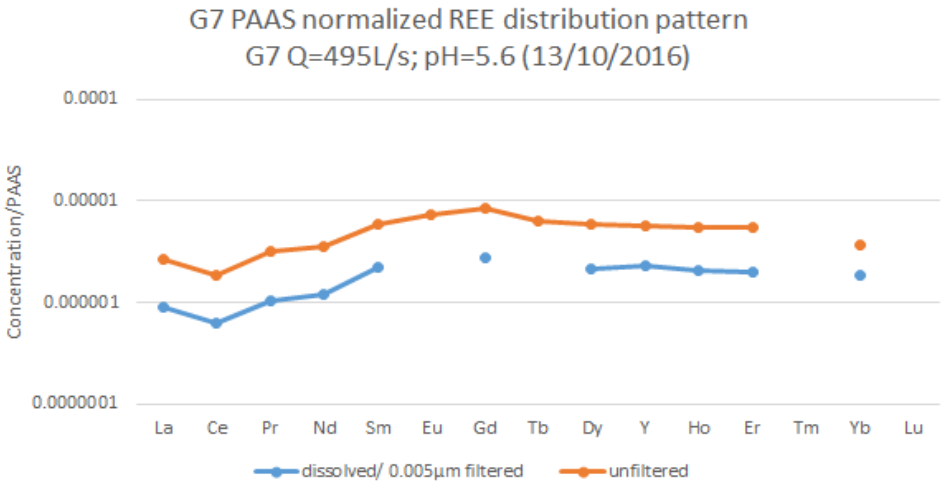

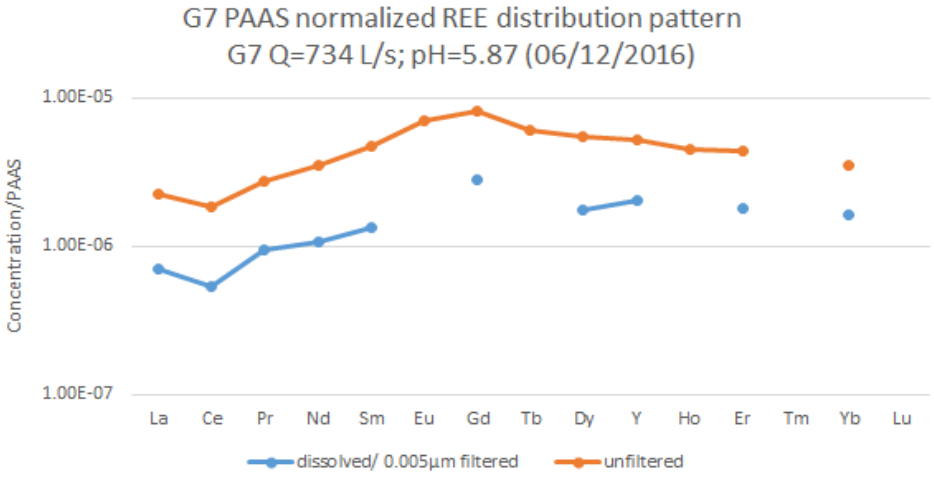

PAAS normalized REE distribution pattern in truly dissolved (0.005µm/ ultra-filtered) and unfiltered phase at G7 under higher flow conditions when ultrafiltration was undertaken. The data are displayed based on the order of flow condition.

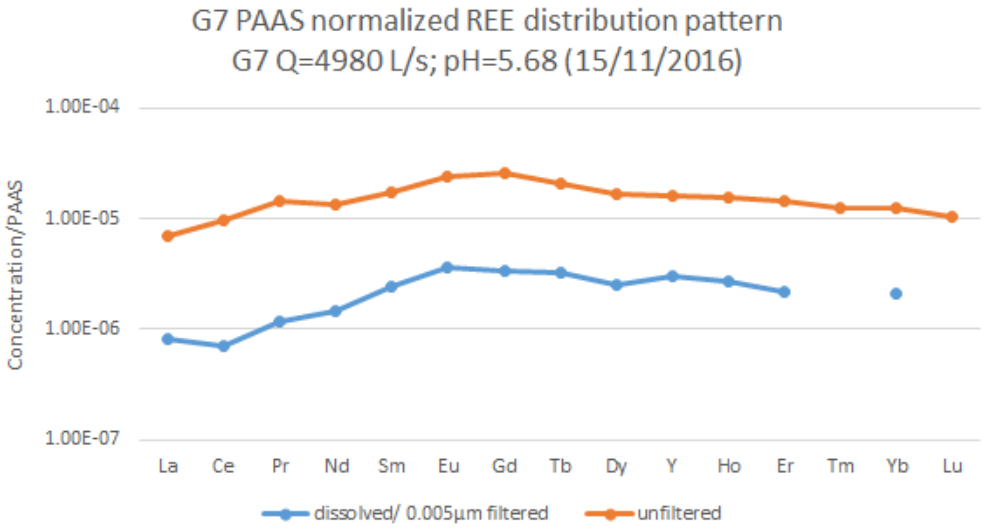

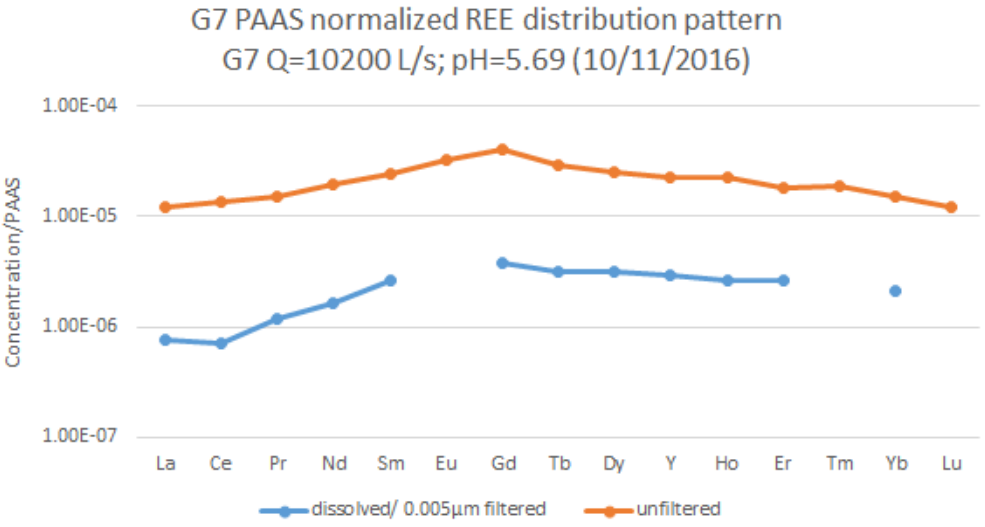

Spatial variation of PAAS normalized REE distribution pattern in different phases from G1 to G7 under lower flow conditions when ultrafiltration was not undertaken and attenuation occurred only at G7. The data are displayed based on the order of flow condition (the flow of G5 and G7 is shown).

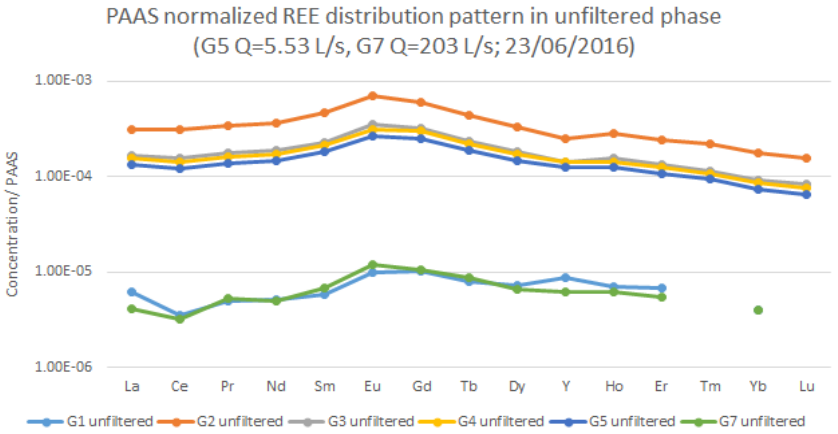

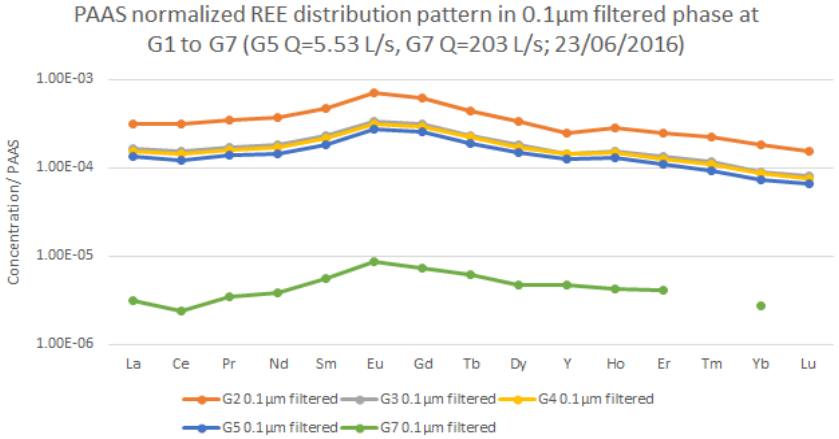

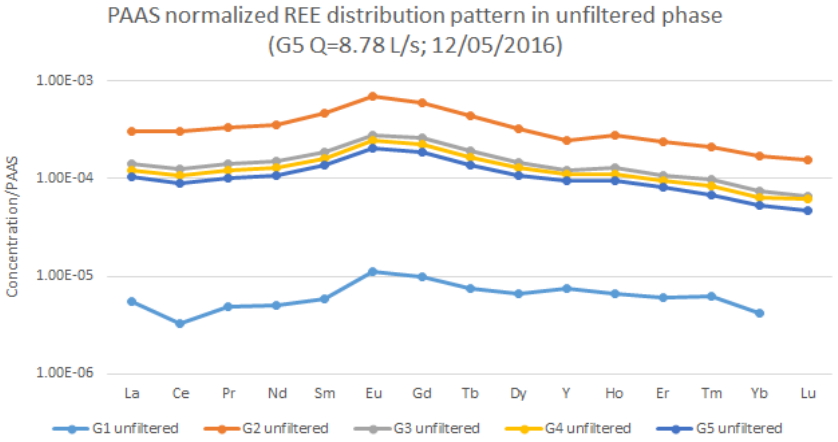

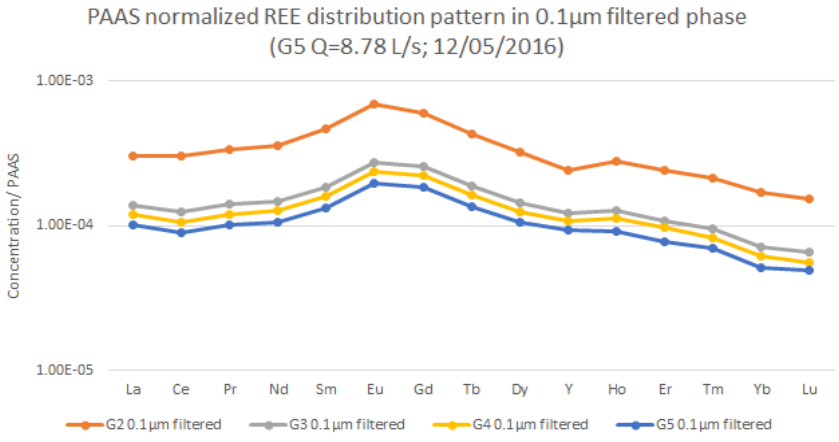

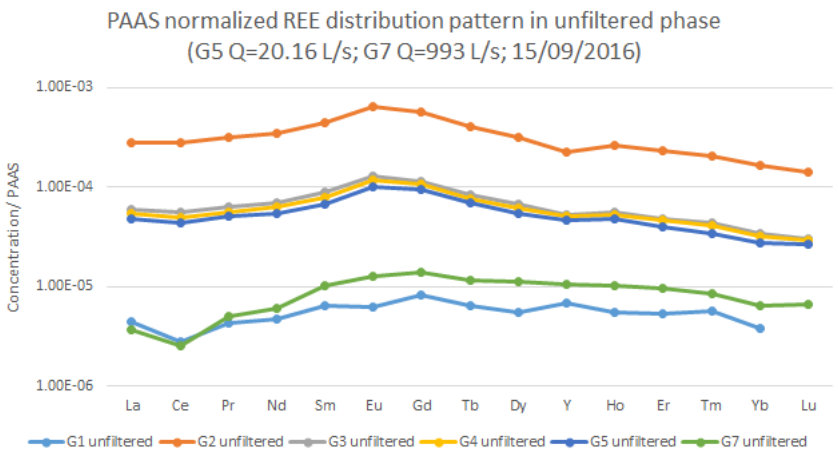
PAAS normalized REE distribution pattern in unfiltered phase
(G5 Q=20.16 L/s; G7 Q=993 L/s; 15/09/2016)
Concentration/ PAAS
1.00E-03
1.00E-04
1.00E-05
1.00E-06
La Ce Pr Nd Sm Eu Gd Tb Dy Y Ho Er Tm Yb Lu
G1 unfiltered G2 unfiltered G3 unfiltered G4 unfiltered G5 unfiltered G7 unfiltered

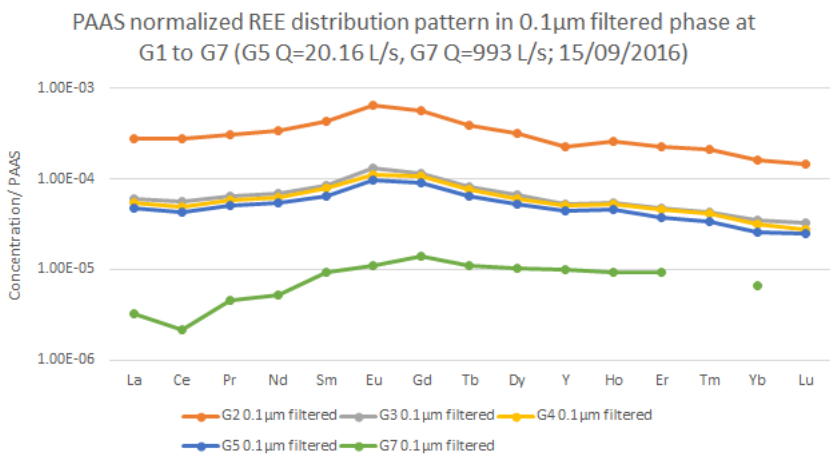
PAAS normalized REE distribution pattern in 0.1µm filtered phase at
G1 to G7 (G5 Q=20.16 L/s, G7 Q=993 L/s; 15/09/2016)
Concentration/ PAAS
1.00E-03
1.00E-04
1.00E-05
1.00E-06
La Ce Pr Nd Sm Eu Gd Tb Dy Y Ho Er Tm Yb Lu
G2 0.1µm filtered G3 0.1µm filtered G4 0.1µm filtered
G5 0.1µm filtered G7 0.1µm filtered

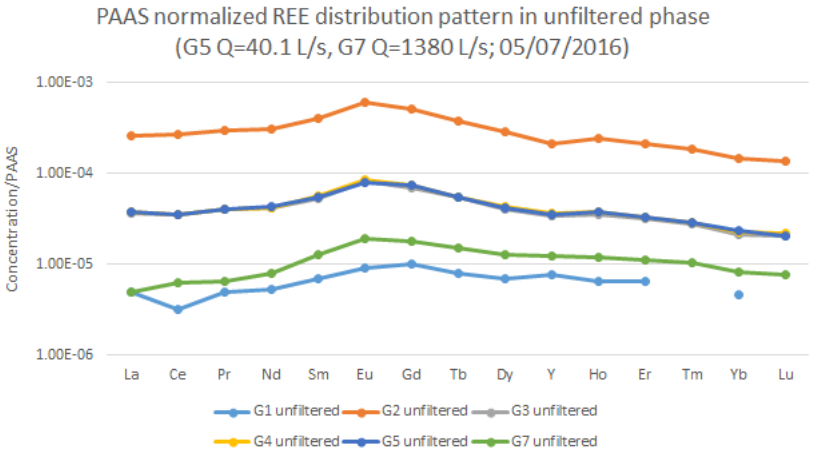
PAAS normalized REE distribution pattern in unfiltered phase
(G5 Q=40.1 L/s, G7 Q=1380 L/s; 05/07/2016)
Concentration/PAAS
1.00E-03
1.00E-04
1.00E-05
1.00E-06
La Ce Pr Nd Sm Eu Gd Tb Dy Y Ho Er Tm Yb Lu
G1 unfiltered G2 unfiltered G3 unfiltered
G4 unfiltered G5 unfiltered G7 unfiltered

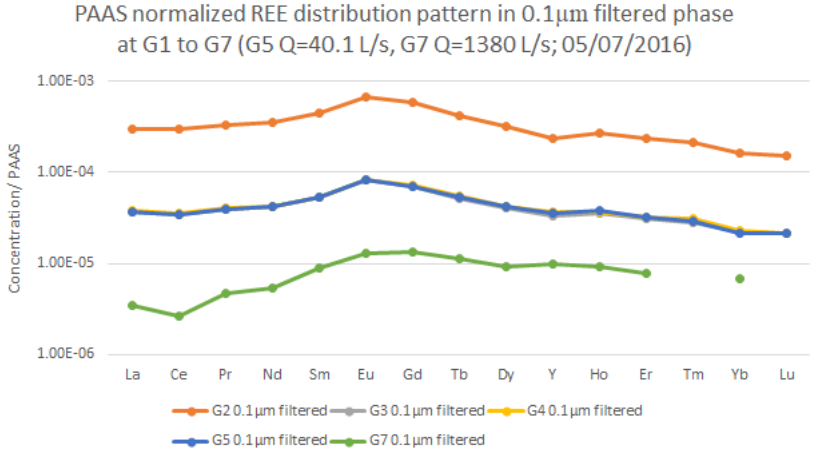
PAAS normalized REE distribution pattern in 0.1µm filtered phase
at G1 to G7 (G5 Q=40.1 L/s, G7 Q=1380 L/s; 05/07/2016)
Concentration/ PAAS
1.00E-03
1.00E-04
1.00E-05
1.00E-06
La Ce Pr Nd Sm Eu Gd Tb Dy Y Ho Er Tm Yb Lu
G2 0.1µm filtered G3 0.1µm filtered G4 0.1µm filtered
G5 0.1µm filtered G7 0.1µm filtered

Spatial variation of PAAS normalized REE distribution pattern in different phases from G1 to G7 under higher flow conditions when ultrafiltration was not undertaken. The attenuation occurred at G5 and G7 on both sampling events (04/02/2016 and 13/04/2016). The data are displayed based on the order of flow condition (the flow of G5 and G7 is shown).

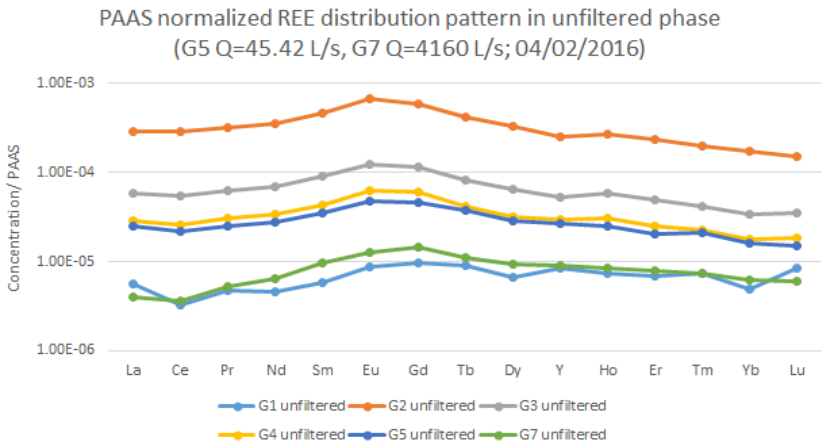

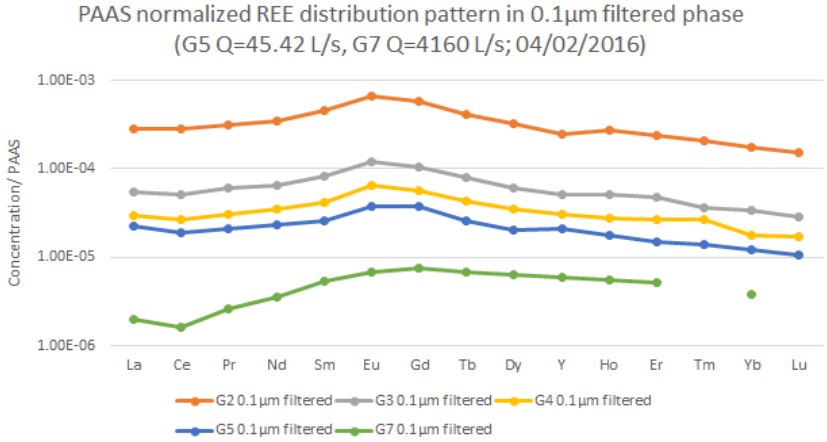

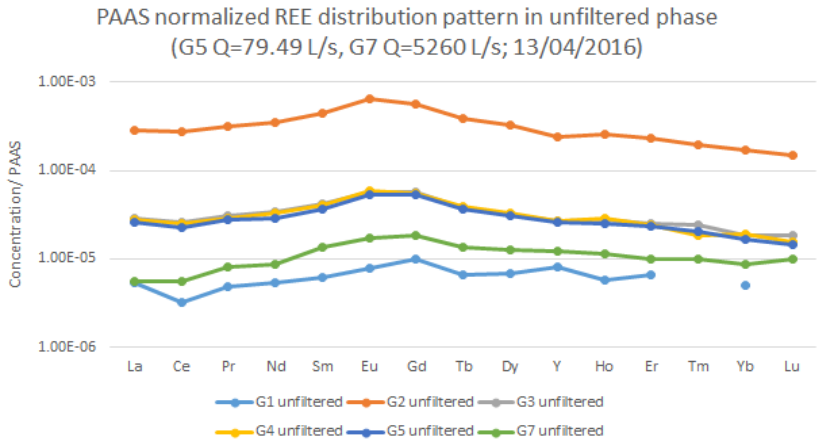

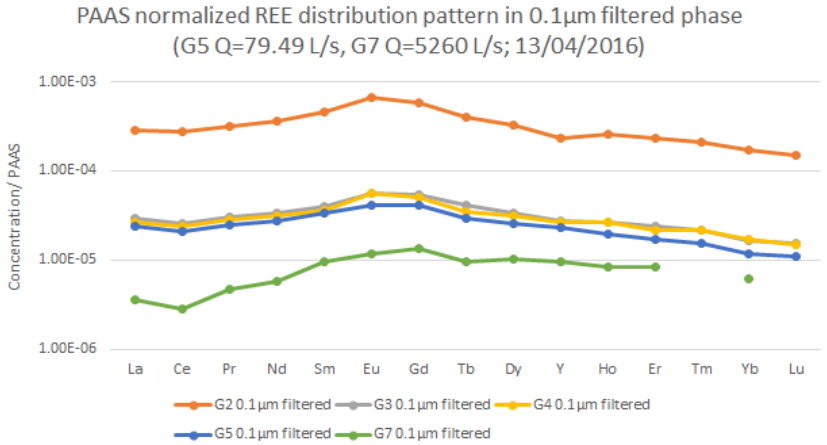

PAAS normalized REE distribution pattern in 0.1µm filtered and unfiltered phase at G5 and G7 under higher flow condition when attenuation of REE occurred and ultrafiltration was not undertaken.

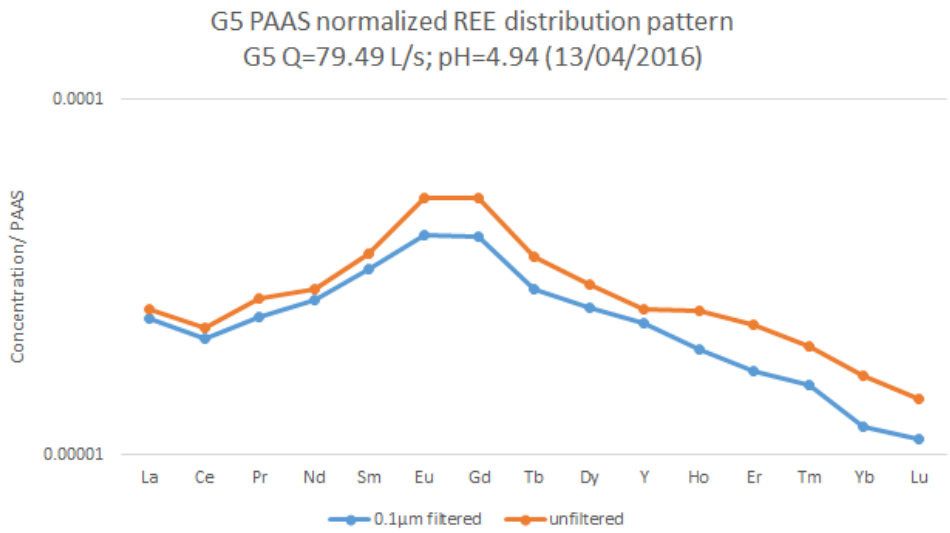

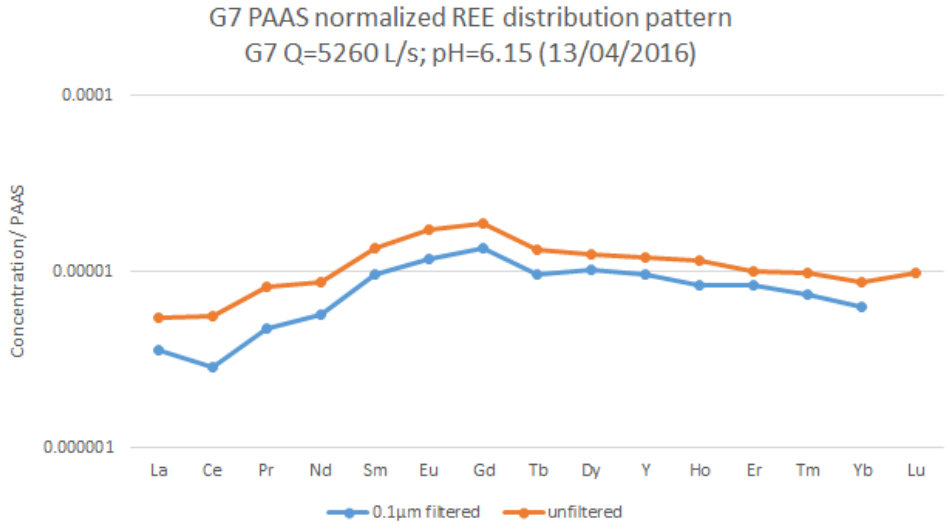

PAAS normalized REE distribution pattern in 0.1µm filtered and unfiltered phase at G7 under lower flow conditions when ultrafiltration was not undertaken. The data are displayed based on the order of flow condition.